

N8512011  


*NASA Conference Publication 2319*

# Wind Tunnel Wall Interference Assessment/Correction 1983

(NASA-CP-2319) WIND TUNNEL WALL  
INTERFERENCE ASSESSMENT AND CORRECTION, 1983  
(NASA) 417 p HC A18/EF A01 CSDL 01A

N85-12011  
THRU  
N85-12035  
Unclas

G3/02 20588

*Edited by*  
Perry A. Newman and  
Richard W. Barnwell  
*Langley Research Center*

Proceedings of a workshop held at  
NASA Langley Research Center  
Hampton, Virginia  
January 25-26, 1983

REPRODUCED BY  
NATIONAL TECHNICAL  
INFORMATION SERVICE  
U.S. DEPARTMENT OF COMMERCE  
SPRINGFIELD, VA. 22161

**NASA**  
National Aeronautics  
and Space Administration

**Scientific and Technical  
Information Branch**

1984

## PREFACE

This workshop on Wind Tunnel Wall Interference Assessment/Correction (WIAC) techniques was an outgrowth of earlier NASA Langley workshops related to the National Transonic Facility (NTF) (High Reynolds Number Research - 1980, NASA CP-2183, 1981, and Wind Tunnel/Flight Correlation - 1981, NASA CP-2225, 1982) and of informal discussions among government, industry, and university personnel during the AIAA 12th Aerodynamics Testing Conference in March 1982. The purpose was to provide an informal technical information exchange focused upon the emerging WIAC techniques applicable to transonic wind tunnels with conventional and passively or partially adapted walls. The possibility of improving the assessment and correction of data taken in conventional transonic wind tunnels by utilizing simultaneously obtained flow field data (generally taken near the walls) appears to offer a larger, nearer-term payoff than the fully adaptive wall concept. Development of WIAC procedures continues, and aspects related to validating the concept needed to be addressed. Thus, the scope of wall interference topics discussed at this workshop was somewhat limited. As analytical/numerical techniques reach the demonstration stage, personnel involved with management, software development, measurement techniques, hardware implementation, facility operation, and data reduction will necessarily become involved.

The 25 informal technical presentations at this workshop consisted of invited talks summarizing the foreign work on WIAC technology and solicited domestic talks concerning data bases suitable for WIAC validation and the status of WIAC strategies, codes, and applications. These talks were grouped into the seven technical sessions indicated in the contents; the material given herein consists of the presentation viewgraphs accompanied by a few words of text. The workshop included brief tours of the NTF and 0.3-Meter Transonic Cryogenic Tunnel and concluded with an open forum discussion of WIAC issues, progress to date, and future directions. A list of attendees is included in this document.

We wish to express our appreciation to all who participated in this workshop: the speakers, coauthors, session chairmen, and attendees. Our only regret is that the workshop was not scheduled to last another day so that smaller group discussions could have been conducted to better assess the progress and recommend future directions. However, we feel that this was more than compensated by the spectrum of papers presented and the good attendance representing almost all groups actively engaged in wind tunnel wall interference research.

Perry A. Newman  
Richard W. Barnwell

**Preceding page blank** NOT FILMED

CONTENTS

PREFACE . . . . . iii  
ATTENDEES . . . . . ix

SESSION I: WIAC OVERVIEW AND WORKSHOP THEME

Chairman: R. W. Barnwell, NASA Langley

AN OVERVIEW OF APPROACHES AND ISSUES FOR WALL INTERFERENCE ASSESSMENT/  
CORRECTION . . . . . 3  
    E. M. Kraft  
WALL INTERFERENCE MEASUREMENTS FOR THREE-DIMENSIONAL MODELS IN TRANSONIC  
WIND TUNNELS: EXPERIMENTAL DIFFICULTIES . . . . . 21  
    R. L. Bengelink and N. J. Zinserling  
SURVEY OF ONERA ACTIVITIES ON ADAPTIVE-WALL APPLICATIONS AND COMPUTATION  
OF RESIDUAL CORRECTIONS . . . . . 43  
    J. P. Chevallier

SESSION II: ADAPTED WALL PROGRESS AND DATA

Chairman: S. R. Pate, Sverdrup Technology

WIND TUNNEL WALL INTERFERENCE IN CLOSED, VENTILATED, AND ADAPTIVE TEST  
SECTIONS . . . . . 61  
    H. Holst  
TWO-AND THREE-DIMENSIONAL MODEL AND WALL DATA FROM A FLEXIBLE-WALLED  
TRANSONIC TEST SECTION . . . . . 79  
    M. J. Goodyer and I. D. Cook  
ASSESSMENT OF LIFT- AND BLOCKAGE-INDUCED WALL INTERFERENCE IN A THREE-  
DIMENSIONAL ADAPTIVE-WALL WIND TUNNEL . . . . . 89  
    Edward T. Schairer  
A DATA BASE FOR THREE-DIMENSIONAL WALL INTERFERENCE CODE EVALUATION . . . . . 101  
    W. L. Sickles

SESSION III: WALL SUCTION EFFECTS AND DATA

Chairman: L. H. Ohman, NAE

INVESTIGATIONS OF FLOW FIELD PERTURBATIONS INDUCED ON SLOTTED TRANSONIC-  
TUNNEL WALLS . . . . . 119  
    J. M. Wu and F. G. Collins

EFFECT OF UPSTREAM SIDEWALL BOUNDARY LAYER REMOVAL ON AN  
 AIRFOIL TEST . . . . . 143 ✓  
 C. B. Johnson, A. V. Murthy, E. J. kay, P. L. Lawing, and  
 J. J. Thibodeaux

PERFORMANCE OF TWO TRANSONIC AIRFOIL WIND TUNNELS UTILIZING  
 LIMITED VENTILATION . . . . . 165 ✓  
 J. D. Lee and G. M. Gregorek

EXPERIMENTS SUITABLE FOR WIND TUNNEL WALL INTERFERENCE  
 ASSESSMENT/CORRECTION . . . . . 171 ✓  
 Joseph G. Marvin

SESSION IV: ANALYTICAL WALL CORRECTION METHODS

Chairman: C. F. Lo, Calspan, AEDC

ASYMPTOTIC METHODS FOR WIND TUNNEL WALL CORRECTIONS AT  
 TRANSONIC SPEED . . . . . 193 ✓  
 N. D. Malmuth, J. D. Cole, and F. Zeigler

EFFECT OF BOUNDARY LAYERS ON SOLID WALLS IN THREE-DIMENSIONAL  
 SUBSONIC WIND TUNNELS . . . . . 205 ✓  
 Jerry B. Adcock and Richard W. Barnwell

SESSION Va: CORRECTION METHODS USING MEASURED BOUNDARY DATA

Chairman: P. A. Newman, NASA Langley

NLR ACTIVITIES IN THE FIELD OF WIND TUNNEL WALL INTERFERENCE . . . . . 221 ✓  
 J. Smith

PROGRESS IN WIND TUNNEL WALL INTERFERENCE ASSESSMENT/CORRECTION  
 PROCEDURES AT THE NAE . . . . . 231 ✓  
 L. H. Ohman, M. Mokry, and Y. Y. Chan

DEVELOPMENT IN UK OF A METHOD FOR CALCULATING TUNNEL WALL  
 CORRECTIONS FROM FLOW MEASUREMENTS . . . . . 254 ✓  
 P. R. Ashill

TUNNEL CONSTRAINT FOR A JET IN CROSSFLOW . . . . . 273 ✓  
 D. J. Wilsden and J. E. Hackett

SESSION Vb: CORRECTION METHODS USING MEASURED BOUNDARY DATA

Chairman: K. L. Kushman, USAF, AEDC

INTERFERENCE FROM SLOTTED WALLS . . . . . 293 ✓  
 Sune B. Berndt

WIND TUNNEL WALL INTERFERENCE CORRECTIONS FOR AIRCRAFT MODELS . . . . .	301
M. H. Rizk, M. G. Smithmeyer, and E. M. Murman	
AN INTERFERENCE ASSESSMENT APPROACH FOR A THREE-DIMENSIONAL SLOTTED TUNNEL WITH SPARSE WALL PRESSURE DATA . . . . .	323
William B. Kemp, Jr.	
DETERMINATION OF EQUIVALENT MODEL GEOMETRY FOR TUNNEL WALL INTERFERENCE ASSESSMENT/CORRECTION . . . . .	335
C. F. Lo	

SESSION Vc: CORRECTION METHODS USING MEASURED BOUNDARY DATA

Chairman: R. L. Bengelink, Boeing

EXPERIENCES WITH A HIGH-BLOCKAGE MODEL TESTED IN THE NASA AMES 12-FOOT PRESSURE WIND TUNNEL . . . . .	345
David W. Coder	
REVIEW OF THE ADVANCED TECHNOLOGY AIRFOIL TEST PROGRAM IN THE 0.3-METER TRANSONIC CRYOGENIC TUNNEL . . . . .	361
E. J. Ray and C. L. Ladson	
SOME EXPERIENCE WITH BARNWELL-SEWALL TYPE CORRECTION TO TWO-DIMENSIONAL AIRFOIL DATA . . . . .	375
Renaldo V. Jenkins	
ADAPTATION OF A FOUR-WALL INTERFERENCE ASSESSMENT/CORRECTION PROCEDURE FOR AIRFOIL TESTS IN THE 0.3-m TCT . . . . .	393
Clyde R. Gumbert, Perry A. Newman, William B. Kemp, Jr., and Jerry B. Adcock	

SESSION VI: OPEN FORUM - ASSESSMENT OF ISSUES

Moderator: P. J. Bobbitt, NASA Langley

DISCUSSION OF WIND TUNNEL WALL INTERFERENCE CORRECTION ISSUES . . . . .	415
P. J. Bobbitt and P. A. Newman	

ATTENDEES

Non-Langley Attendees

ASHILL, Patrick R.  
Royal Aircraft Establishment  
Ministry of Defense, PE  
Aero. Dept. AE 3 Division  
8-Ft. x 8-Ft. Wind Tunnel  
Bedford MK41 6AE  
England

BENGELINK, Ronald L.  
Boeing Commercial Airplane Company  
Mail Stop 1W-82  
P. O. Box 3707  
Seattle, WA 98124

BERNDT, Sune B.  
Royal Institute of Technology  
S-100 44 Stockholm  
Sweden

BLAHA, Bernard J.  
NASA Lewis Research Center  
21000 Brookpark Road  
Cleveland, OH 44135

BLISS, Donald P.  
Princeton University  
Dept. of Mechanical  
and Aerospace Engineering  
Engineering Quadrangle D-207  
Princeton, NJ 08544

BRITCHER, Colin P.  
The University of Southampton  
Langley Research Center  
Mail Stop 287  
Hampton, VA 23669

BROWN, Clinton E.  
Tracor Hydronautics  
7210 Pindell School Road  
Laurel, MD 20707

CHEVALLIER, Jean P.  
Chef de Division  
Experimental Aerodynamics Division  
ONERA  
29 Avenue de la Division Leclerc  
92320 Chatillon  
France

CODER, David W.  
David Taylor Naval Ship Research  
and Development Center  
Code 1543  
Bethesda, MD 20816

COHEN, M. H.  
Rockwell International  
Mail Stop 011-BP02  
P. O. Box 92098  
Los Angeles, CA 90009

COLLINS, Frank G.  
University of Tennessee Space Institute  
Tullahoma, TN 37388

DRESS, David A.  
Kentron  
Langley Research Center  
Mail Stop 287  
Hampton, VA 23665

ELFSTROM, Gary M.  
DSMA International  
10 Park Lawn Road  
Toronto, Ontario M8Y 3H8  
Canada

ERICKSON, John C., Jr.  
Calspan Field Services, Inc.  
AEDC Division  
Mail Stop 600  
Arnold AFS, TN 37389

FANCHER, Michael F.  
Douglas Aircraft Company  
Mail Code 36-81  
3855 Lakewood Boulevard  
Long Beach, CA 90846

GOODYER, M. J.  
The University of Southampton  
Dept. of Aeronautics and Astronautics  
Soton 509 5NH  
Hants  
England

GOTTLIEB, Stanley M.  
David Taylor Naval Ship R&D Center  
Code 166/1  
Bethesda, MD 20084

Preceding page blank

ix

GREGOREK, Gerald M.  
Ohio State University  
Aero. and Astro. Research Lab  
2300 W. Case Road  
Columbus, OH 43220

HAFEZ, Mohamed  
CDI  
NASA Langley Research Center  
Mail Stop 259  
Hampton, VA 23665

HOLST, H.  
DFVLR-AVA  
Bunsenstrasse 10  
D-3400 Gottingen  
West Germany

KEMP, William B., Jr.  
VARC  
Langley Research Center  
Mail Stop 294  
Hampton, Va 23665

KRAFT, Edward M.  
Calspan Field Services, Inc.  
AEDC Division MS 400  
Arnold AFS, TN 37389

KUSHMAN, Keith L.  
Arnold Engineering Development Center  
Directorate of Technology  
Arnold AFS, TN 37389

MASTER, M. L.  
Arnold Engineering Development Center  
Directorate of Technology  
Arnold AFS, TN 37389

LO, Ching F.  
Calspan Field Services, Inc.  
AEDC Division  
Mail Stop 400  
Arnold AFS, TN 37389

MALMUTH, Norman  
Rockwell International  
P. O. Box 1085  
Thousand Oaks, CA 91360

MARVIN, Joseph G.  
NASA Ames Research Center  
Mail Stop 229-1  
Moffett Field, CA 94035

MOKRY, Miroslav  
National Aeronautical Establishment  
National Research Council-Montreal Road  
Ottawa, Ontario K1A 0R6  
Canada

MURTHY, A. V.  
Langley Research Center  
Mail Stop 287  
Hampton, VA 23665

OHMAN, Lars H.  
Head, High-Speed Aerodynamics Laboratory  
National Aeronautical Establishment  
National Research Council-Montreal Road  
Ottawa, Ontario K1A 0R6  
Canada

PAJKOVIC, Dario  
Grumman Aerospace Corporation  
Bethpage, NY 11714

PARIKH, Paresh  
Vigyan Research Associates, Inc.  
28 Research Drive  
Hampton, VA 23666

PARKER, R. Lee, Jr.  
Calspan Field Services, Inc.  
AEDC Division  
Mail Stop 600  
Arnold AFS, TN 37389

PATE, Samuel R.  
Sverdrop Technology, Inc.  
600 William Northern Blvd.  
P. O. Box 884  
Tullahoma, TN 37388

PETRIE, S. L.  
Ohio State University  
Dept. of Aero. and Astro. Eng.  
2036 Neil  
Columbus, OH 43210

PFENNINGER, Werner  
George Washington University  
NASA Langley Research Center  
Mail Stop 339  
Hampton, VA 23665

POLHAMUS, Edward C.  
VARC  
Langley Research Center  
Mail Stop 294  
Hampton, VA 23665

RISK, Magdi  
Flow Research Company  
21414 68th Avenue South  
Kent, WA 98031

SANDERS, Bobby W.  
NASA Lewis Research Center  
Mail Stop 86-7  
21000 Brookpark Road  
Cleveland, OH 44135

SARIC, William S.  
Virginia Polytechnic Institute  
and State University  
Blacksburg, VA 2406

SCHAIRER, Edward T.  
Ames Research Center  
Mail Stop 227-8  
Moffett Field, CA 94035

SHELDON, David W.  
NASA Lewis Research Center  
Mail Stop 86-7  
21000 Brookpark Road  
Cleveland, OH 44135

SICKLES, William L.  
Calspan Field Services, Inc.  
AEDC Division  
Mail Stop 600  
Arnold AFS, TN 37389

SMITH, Jack  
National Aerospace Laboratory-NLR  
Anthony Follerweg 2  
1059 CM Amsterdam  
Holland

SUMMERS, Willard E.  
Sverdrup Technology, Inc.  
600 William Northern Blvd.  
P. O. Box 884  
Tullahoma, TN 37388

WILSDEN, Derek J.  
Lockheed-Georgia Company  
P. O. Box 69  
Smyrna, GA 30080

WITTLIFF, Charles E.  
Calspan Corporation  
P. O. Box 400  
Buffalo, NY 14225

WU, Jain-Ming  
University of Tennessee Space Institute  
Tullahoma, TN 37388

## NASA Langley Attendees

ADCOCK, Jerry B.  
ANDERSON, E. Clay  
ANGLIN, Ernie L.  
BARNWELL, Richard W.  
BENNETT, Robert M.  
BOBBITT, Percy J.  
BOWER, Robert E.  
BOYDEN, Richmond P.  
CARLSON, John R.  
EDWARDS, Clyde L. W.  
ERICKSON, Wayne D.  
EVERHART, Joel L.  
FLECHNER, Stuart G.  
FOX, Charles H., Jr.  
FOUGHNER, Jerome T.  
GLOSS, Blair B.  
GREEN, Lawrence L.  
GUMBERT, Clyde R.  
HAIGLER, Kara J.  
HALL, Robert M.  
HALLISSY, James B.  
HARVEY, William D.  
HOWARD, Floyd G.

HUFFMAN, Jarrett K.  
IGOE, William B.  
JACOBS, Peter F.  
JENKINS, Renaldo V.  
JOHNSON, Charles B.  
LAWING, Pierce L.  
LOVELL, Don  
MANN, Michael J.  
MCKINNEY, L. Wayne  
NEWMAN, Perry A.  
PETERSON, John B.  
PLENTOVICH, Elizabeth B.  
RAY, Edward J.  
ROSE, Lester J.  
SALAS, Manuel D.  
SCHEIMAN, James  
SEWALL, William G.  
SOUTH, Jerry C., Jr.  
STAINBACK, P. Calvin  
STREETT, Craig L.  
THIBODEAUX, Jerry J.  
WHITCOMB, Richard T.  
WHITEHEAD, Allen H., Jr.  
YATES, Carson E. Jr.

SESSION I

WIAC OVERVIEW AND WORKSHOP THEME

Chairman: R. W. Barnwell, NASA Langley

5721  
P. 21

**AN OVERVIEW OF APPROACHES AND ISSUES  
FOR WALL INTERFERENCE ASSESSMENT/CORRECTION**

**E. M. Kraft  
Calspan Field Services, Inc./AEDC Division  
Arnold AFS, Tennessee**

PRECEDING PAGE BLANK NOT FILMED

## THE CHALLENGE

After seven decades of effort, the solution to the wind tunnel wall interference problem now appears on the horizon in the form of adaptive wind tunnel walls, wall interference assessment/correction methods, or combinations of the two. To make this happen will require a concerted effort on the part of the wind tunnel industry. The challenge is to make these techniques practical and routine. In the following discussion, emphasis will be given to the current state of the art in wall interference assessment/correction methods and the issues that have to be addressed in order to meet the challenge.

IF THE CURRENT THRUST IS CONTINUED WALL INTERFERENCE  
WILL BE A SOLVED PROBLEM WITHIN A DECADE. THERE WILL  
BE PRACTICAL AND ROUTINE APPLICATIONS OF

- ADAPTIVE WALLS
- WALL INTERFERENCE ASSESSMENT/CORRECTION METHODS

## **BASIC PREMISES**

The last decade has seen a tremendous development of wall interference assessment/correction techniques. Although many different approaches have been developed all these methods require knowledge of two independent quantities. The accuracy and validity of these independent quantities are therefore measures of the adequacy of any one approach. The nature of these independent quantities will become apparent in the following discussion.

- ALL WALL INTERFERENCE ASSESSMENT/CORRECTION (WIAC) TECHNIQUES REQUIRE KNOWLEDGE OF TWO INDEPENDENT QUANTITIES
- A MEASURE OF MERIT FOR ANY TECHNIQUE IS HOW WELL THE TWO INDEPENDENT QUANTITIES ARE DETERMINED

## DEFINITION

Throughout this presentation reference will be made to an "interface surface". The definition of the interface surface is given in the figure below.

INTERFACE SURFACE IS DEFINED AS THE SURFACE OF A CONTROL VOLUME CONVENIENTLY LOCATED ON OR NEAR THE TUNNEL WALLS. MEASUREMENT OF FLOW VARIABLES AND/OR DEFINITION OF BOUNDARY CONDITIONS FOR WIAC METHODS ARE PERFORMED ON THE INTERFACE SURFACE

## CURRENT APPROACHES

Although not necessarily unique, it is convenient to categorize the current WIAC methods into one of four groups based on what types of measurements are made. As will be shown, within any one category there are various ways of using the same measurements to determine the wall interference. However, this categorization allows an immediate definition of the relative merits of how well the independent quantities are determined. It is also interesting to note that if this workshop were held a decade ago only the classical methods would be discussed.

- CLASSICAL THEORETICAL METHODS
- MEASURED INTERFACE PRESSURE METHODS
- MEASURED INTERFACE AND MODEL PRESSURE METHODS
- MEASURED INTERFACE PRESSURE AND FLOW ANGLE METHODS

## CLASSICAL THEORETICAL METHODS

Classical theoretical methods are herein generalized to include all techniques that analytically or numerically simulate the flow in the tunnel using theoretical boundary conditions on the walls and on the model. This encompasses the spectrum from a simple source between parallel planes to numerical solutions of the Euler equations. Typical examples of some classical methods are given in Refs. 1-3. The independent quantities indicated below are theoretically contrived and hence can be only as good as the theory on which they are based.

As suggested in the figure below, the primary advantages of the classical methods are that they are rapid and easy to apply and are the only method available for a priori estimates. Their inherent weakness is their dependence on theoretical models. However, before strongly discounting these techniques one should recognize that theoretical models of the wall behavior may be calibrated using the more sophisticated techniques to be discussed subsequently. It may be possible to combine the classical approach with some of the more advanced methods to take advantage of the speed of the classical methods in dealing with large quantities of data.

### INDEPENDENT QUANTITIES

1. THEORETICAL SIMULATION OF WALL BEHAVIOR
  - LINEAR, HOMOGENEOUS WALL CHARACTERISTICS

$$U + K \frac{\partial V}{\partial X} + \frac{1}{R} V = 0$$

2. THEORETICAL SIMULATION OF MODEL
  - SUBSONIC - SUPERPOSITION OF SINGULARITIES
  - TRANSONIC - MODEL SURFACE GEOMETRY

### APPROACH

FLOW OVER MODEL IN WIND TUNNEL IS ANALYTICALLY/  
NUMERICALLY SIMULATED

### ADVANTAGES

- RAPID, EASY TO APPLY
- ONLY METHOD FOR "A PRIORI" ESTIMATES

### DISADVANTAGES

- WALL CHARACTERISTICS DEPEND ON PHYSICAL WALL,  $Re$ ,  $M$ , AND MODEL GEOMETRY AND ATTITUDE, HENCE NOT EASILY DETERMINED
- UNKNOWN ADEQUACY OF MODEL SIMULATION

## MEASURED INTERFACE PRESSURE METHODS

To overcome the dependency of the classical theoretical methods on the theoretical wall characteristic, the next level of sophistication is to measure the static pressure at the interface. As seen in the figure below there are at least three ways of using the measured interface pressure to determine the wall interference: 1) as a boundary condition for numerical methods such as in Refs. 4 and 5, 2) to determine the classical theory wall porosity parameters as in Ref. 6, or 3) to determine the strength and distribution of singularities for estimating wall interference in solid-wall tunnels as in Ref. 7.

As shown in the figure below, the measured interface pressure methods retain the convenience of the classical methods but have an improved definition of the wall behavior. The weakness of the method still lies with the model description. Hence, replacement of the model description is the next area of improvement for WIAC methods.

### INDEPENDENT QUANTITIES

1. MEASURED STATIC PRESSURES AT INTERFACE
  - AS BOUNDARY CONDITION FOR NUMERICAL METHODS
  - TO DETERMINE WALL POROSITY
  - TO DETERMINE MODEL SINGULARITY DISTRIBUTIONS
2. SIMULATION OF MODEL

### APPROACH

SIMILAR TO CLASSICAL THEORETICAL METHODS EXCEPT INFORMATION DERIVED FROM PRESSURES MEASURED AT INTERFACE IS USED

### ADVANTAGES

- RELATIVELY RAPID
- IMPROVED DESCRIPTION OF THE TUNNEL WALL BEHAVIOR

### DISADVANTAGES

- UNKNOWN ADEQUACY OF MODEL SIMULATION

## MEASURED INTERFACE AND MODEL PRESSURES METHODS

The most straightforward method for improving the simulation of the model is to directly measure the pressure on the model surface. These measurements can be coupled with the interface pressure measurements to compute an equivalent body including viscous effects using a numerical inverse method (Refs. 8 and 9). This equivalent body can then be used in further numerical computations to determine the corrected Mach number and angle of attack for the measured data.

While measuring the model surface pressures improves the simulation of the model, this may be routinely done only in two-dimensional airfoil tests. For more general three-dimensional production wind tunnel tests, model pressure measurements are not available. Hence, these techniques may be limited in application.

### INDEPENDENT QUANTITIES

1. MEASURED STATIC PRESSURES AT INTERFACE
2. MEASURED STATIC PRESSURES AT MODEL SURFACE

### APPROACH

EFFECTIVE BODY SHAPE DETERMINED FROM MEASURED PRESSURES BY INVERSE CALCULATIONS. EFFECTIVE BODY SHAPE USED FOR AN INFINITE DOMAIN CALCULATION WHICH IS COMPARED WITH THE MEASURED PRESSURES ON THE MODEL

### ADVANTAGES

- ELIMINATES NEED FOR WALL CHARACTERISTIC DESCRIPTION
- IMPROVES SIMULATION OF MODEL

### DISADVANTAGES

- INCREASED COMPUTATIONAL REQUIREMENTS
- MODEL PRESSURE MEASUREMENTS NOT GENERALLY AVAILABLE

## MEASURED INTERFACE PRESSURE AND FLOW ANGLE METHODS

The ideal WIAC technique should have two readily measurable independent quantities that are transparent to any particular model installation. Clearly these measurements should be made at the interface. This approach follows directly from adaptive wall research wherein the pressure and flow angle are measured at the interface. It has been established in Refs. 10 and 11 that use of these two independent quantities avoids simulating the model in addition to the tunnel boundary, at least for subsonic flows.

To illustrate the use of the measured interface pressure and flow angle distributions, consider inviscid, incompressible flow. The perturbation potential in the tunnel,  $\phi_T$ , is governed by the Laplace equation, hence the solution can be written directly from Green's theorem in terms of source and doublet distributions on all the boundaries of the domain. As the tunnel boundary approaches infinity, the integrals on the interface surface vanish, indicating the integrals on the model surface are equivalent to the interference free potential  $\phi_\infty$ . Consequently, the wall interference is solely and uniquely a function of the potential and its normal derivative on the interface surface.

Because the wall interference can be directly determined from the measured pressures and flow angles at the interface, the application of the method can be made completely transparent to any particular model installation. Although it is difficult to measure flow angle near a ventilated wind tunnel wall, use of the differential static pipes discussed in Ref. 12 and multiducer pressure transducers now make it a practical reality. To date, the analysis has only been developed for linear subsonic flows, and although it appears very promising for nonlinear, transonic flows, it remains to be seen if all the advantages of the technique will be realized for transonic flows.

### INDEPENDENT QUANTITIES

1. MEASURED STATIC PRESSURES AT INTERFACE  
TO DETERMINE  $\phi_T$  OR  $\partial\phi_T/\partial X$
2. MEASURED FLOW ANGLES AT INTERFACE TO  
DETERMINE  $\partial\phi_T/\partial n$

### APPROACH

FOR SUBSONIC FLOW THE FLOW VARIABLES  
MEASURED AT THE INTERFACE CAN BE DIRECTLY  
INTEGRATED TO YIELD THE WALL INTERFERENCE

## MEASURED INTERFACE PRESSURE AND FLOW ANGLE METHODS

### APPROACH (CONT.)

FROM GREEN'S THEOREM THE SOLUTION FOR THE PERTURBATION  
IN THE TUNNEL,  $\phi_T$ , IS

$$\phi_T = \int_{\text{INTERFACE}} f(\phi_T, \partial\phi_T/\partial n) ds + \int_{\text{MODEL}} g(\phi_T, \partial\phi_T/\partial n) ds$$

AS THE TUNNEL WALL (AND INTERFACE)  $\rightarrow \infty$

$$\phi_\infty \equiv \lim_{\text{WALL} \rightarrow \infty} \phi_T = \int_{\text{MODEL}} g(\phi_T, \partial\phi_T/\partial n) ds$$

HENCE, BY DEFINITION, THE WALL INTERFERENCE IS

$$\phi_i \equiv \phi_T - \phi_\infty = \int_{\text{INTERFACE}} f(\phi_T, \partial\phi_T/\partial n) ds$$

### ADVANTAGES

- ELIMINATES NEED FOR WALL CHARACTERISTIC DESCRIPTION
- ELIMINATES NEED FOR SIMULATING THE MODEL

### DISADVANTAGES

- MEASUREMENT OF FLOW ANGLE NEAR A VENTILATED WIND TUNNEL WALL IS DIFFICULT
- SOME OF THE ADVANTAGES DETERMINED FOR LINEAR, SUBSONIC FLOW MAY NOT BE EVIDENCED IN NONLINEAR TRANSONIC FLOW

## ISSUES

At a workshop like this we have an excellent opportunity for indicating the direction industry should proceed in developing WIAC techniques. In doing so, however, attention must be paid to the issues enumerated below. Some of these issues are very subtle in nature and not thoroughly understood at this point in time. Part of our challenge is therefore to use the newer WIAC methods to reach a more thorough understanding of these issues.

IN THE DEVELOPMENT OF WIAC SCHEMES, ATTENTION SHOULD BE PAID TO THE FOLLOWING ISSUES

- APPROPRIATENESS OF  $\Delta M$  AND  $\Delta \alpha$  CORRECTIONS VERSUS CORRECTING FORCES AND MOMENTS
- DEFINITIONS OF UNCORRECTABLE DATA
- VISCOUS EFFECTS
- INTERPRETATION OF EQUIVALENT BODIES
- ALLOWABLE MODEL BLOCKAGE
- PRACTICALITY OF APPLICATION IN A PRODUCTION WIND TUNNEL

## APPROPRIATE CORRECTIONS

Traditionally wall interference corrections have been interpreted as incremental corrections to the Mach number,  $\Delta M$ , and angle of attack,  $\Delta\alpha$ . These corrections require the gradient influences of the walls to be negligible, or to be interpreted as a modification to the body shape (i.e., an implied camber). In transonic flows, such a simplification may not be justifiable because of the steep gradients associated with shock waves. The results from all of the WIAC methods presented could alternately be interpreted as corrections to the pressure coefficient,  $C_p$ , or to the force and moment coefficients,  $C_x$ . However, a corrected pressure distribution on an airfoil, for example, does not necessarily coincide with the boundary layer properties measured. It may be feasible, however, to incorporate a simple boundary layer method to simultaneously correct the viscous layer for the corrected pressure distribution. As we develop WIAC techniques we should strive to resolve this issue of how to interpret the wall interference.

- $\Delta M, \Delta\alpha$  CORRECTIONS
  - ASSUMES SMALL GLOBAL CHANGES
  - IMPLIES AN EFFECTIVE CHANGE OF SHAPE OF THE MODEL WHICH MAY NOT BE NEGLIGIBLE FOR CASES OF INTEREST
  
- $\Delta C_p$  OR  $\Delta C_x$  CORRECTIONS
  - UNCLEAR INFLUENCE ON BOUNDARY LAYER INTERPRETATION

## UNCORRECTABLE DATA

It is common terminology in the current WIAC methods to call data uncorrectable if after a  $\Delta M$  and  $\Delta\alpha$  correction the data does not agree with the measured data in some global sense. It is of concern that this oversimplification will categorize an inordinate amount of transonic wind tunnel data as uncorrectable. On the other hand, if corrections are made to the pressures and forces which take into account the gradient effects then it appears that all data is correctable. However, it is not clear at this point in time if there is necessarily a flight condition corresponding to the corrected measurements in the wind tunnel for nonlinear transonic flow. The answer to this question will determine when an adaptive wall tunnel is essential and when a WIAC method is adequate.

- IS THE INABILITY OF  $\Delta M$ ,  $\Delta\alpha$  CORRECTIONS TO MATCH A GIVEN CONDITION AN ADEQUATE MEASURE OF WHETHER THE DATA IS CORRECTABLE OR NOT?
- A DEEPER THEORETICAL QUESTION FOR NONLINEAR TRANSONIC FLOW IS WHETHER THERE IS A CORRESPONDENCE BETWEEN THE FLOW MEASURED IN THE TUNNEL AND FREE FLIGHT

## VISCOUS INTERACTIONS

As mentioned previously, when directly correcting pressure distributions on models one needs to determine if the corrected pressure distribution has a significant effect on the interpretation of the viscous interactions on the model. In the validation of WIAC methods, concern must be given for two other viscous effects, however. First, for any data set used to validate WIAC methods the sensitivity of the model data to Reynolds number effects (as well as other factors such as noise, test installation, etc.) needs to be well documented and understood. Otherwise, comparisons of data from tunnel to tunnel at different Reynolds numbers can produce ambiguous wall interference results. Second, it is possible to alter the level of wall interference with a Reynolds number change as suggested in Ref. 13 and observed in some unpublished results at the Arnold Engineering Development Center. This effect can be erroneously interpreted as a Reynolds number effect.

### IN THE DEVELOPMENT AND VALIDATION OF WIAC METHODS SHOULD CONSIDER:

- WHETHER THE INTERPRETATION OF THE VISCOUS SIMULATION ON THE MODEL IS INFLUENCED BY THE CORRECTIONS (PARTICULARLY  $\Delta C_p$  CORRECTIONS)
- IF ANY DATA SETS USED FOR VALIDATION ARE SENSITIVE TO  $Re$  EFFECTS
- IF THE SENSITIVITY OF A DATA SET TO  $Re$  RESULTS FROM THE MODEL VISCOUS EFFECTS OR TUNNEL WALL VISCOUS EFFECTS

## **EFFECTIVE BODIES**

Several of the WIAC methods, and in particular the measured interface and model pressures methods, use the concept of an equivalent body derived from the measurements in the wind tunnel. Hence, contained in the definition of this effective body are the perturbations caused by the wind tunnel boundaries. Consequently, one must be careful in the interpretation of the results of using this equivalent body in a free air calculation to determine the wall interference effects.

- **ARE THE NONLINEARLY COUPLED MODEL-AND WALL-INDUCED PERTURBATIONS CONTAINED IN THE DEFINITION OF AN EFFECTIVE BODY PROPERLY DELINEATED IN DETERMINING THE WALL INTERFERENCE ?**

### **ALLOWABLE MODEL BLOCKAGE**

The energy savings of testing models in smaller wind tunnels, the use of larger models for increased Reynolds number, or sometimes simply the availability of a wind tunnel, is increasing the frequency of testing models with larger than the 1% blockage ratio commonly accepted as criterion for minimum wall interference. In addition, since a large part of the wall interference can be reduced by using small models, any WIAC method that is restricted to small models will not be practical. A probable upper limit for model blockage ratios should be about 2.5%.

**PRACTICAL WIAC METHODS SHOULD NOT BE RESTRICTED  
TO SMALL BLOCKAGE MODELS. THERE ARE INCREASING  
ECONOMIC AND ENGINEERING REQUIREMENTS TO TEST  
MODELS LARGER THAN 1% BLOCKAGE**

## **GROUND RULES FOR APPLICATIONS**

Returning to the challenge given in the first slides for routine and practical applications of WIAC methods to come about within a decade, the guidelines listed below need to be followed. If these requirements cannot be met in the production wind tunnel environment, then the WIAC methods will be relegated to the role of research tools only.

### **WIAC METHODS SHOULD BE DEVELOPED WITH THE FOLLOWING GENERAL REQUIREMENTS IN MIND**

- 3-D, TRANSONIC
- ONLY GLOBAL MEASUREMENTS ON THE MODEL SUCH AS FORCES AND MOMENTS ARE AVAILABLE
- SYSTEM MUST HAVE MINIMUM IMPACT ON DATA PRODUCTIVITY
- SYSTEM MUST BE ROBUST
- SYSTEM SHOULD BE TRANSPARENT TO THE TEST INSTALLATION

## REFERENCES

1. Garner, H. C., et al. "Subsonic Wind Tunnel Wall Corrections." AGARDograph 109, October 1966.
2. Pindzola, M., and Lo, C. F. "Boundary Interference at Subsonic Speeds in Tunnels with Ventilated Walls," AEDC-TR-69-47 (AD 687440), May 1969.
3. Murman, E. M. "Computation of Wall Effects in Ventilated Transonic Wind Tunnels," AIAA Paper No. 72-1007, AIAA 7th Aerodynamic Testing Conference, September 1972.
4. Rizk, M. H., Hafez, M., Murman, E. M., and Lovell, D. "Transonic Wind Tunnel Wall Interference Corrections for Three Dimensional Models." AIAA Paper No. 82-0588, March 1982.
5. Mokry, M. "Subsonic Wall Interference Corrections for Finite Length Test Sections Using Boundary Pressure Measurements." AGARD-CP-335, 1982.
6. Mokry, M., et al., "Wall Interference on Two Dimensional Supercritical Airfoils, Using Wall Pressure Measurements to Determine the Porosity Factors for Tunnel Floor and Ceiling," NRC (Canada) LR-575, February 1974.
7. Hackett, J. E., Wilsden, D. J., and Lilley, D. E., "Estimation of Tunnel Blockage from Wall Pressure Signatures: A Review and Data Correlation," NASA CR-152251, March 1979.
8. Kemp, W. B., "Transonic Assessment of Two Dimensional Wind Tunnel Wall Interference Using Measured Wall Pressures," NASA CR-2045, 1978, pp 473-486.
9. Murman, E. M. "A Correction Method for Transonic Wind Tunnel Wall Interference," AIAA Paper No. 79-1533, July 1979.
10. Kraft, E. M., and Dahm, W. J. A "Direct Assessment of Wall Interference in a Two-Dimensional Subsonic Wind Tunnel," AIAA Paper 82-0187, January 1982.
11. Smith, J. "Measured Boundary Conditions Methods for 2D Flow" AGARD-CP-335, 1982.
12. Nenni, J. P., Erickson, J. C. Jr., and Wittliff, C. E., "Measurement of Small Normal Velocity Components in Subsonic Flows by Use of a Static Pipe," AIAA Journal, Vol 20, No. 8, August 1982.
13. Aulehla, F., and Eberle, A., "Reynolds Number Effects on Transonic Shock Location." AGARD CP 335, 1982.

N85 12012 D1

WALL INTERFERENCE MEASUREMENTS FOR  
THREE-DIMENSIONAL MODELS IN TRANSONIC WIND TUNNELS:  
EXPERIMENTAL DIFFICULTIES

R. L. Bengelink and N. J. Zinserling  
Boeing Commercial Airplane Company  
Seattle, Washington

PROBLEM: THREE-DIMENSIONAL WALL CORRECTIONS  
TO LIFT REQUIRE VERY ACCURATE  
EXPERIMENTAL METHODS

The purpose of this paper is not to provide a detailed discussion of several wall interference experiments, but rather to use these experiments (recently accomplished in the Boeing Transonic Wind Tunnel (BTWT)) to illustrate the problems associated with many of the measurements required by current wall interference assessment/correction (WIAC) procedures.

This paper will concentrate on the wall correction to lift and will show that, because conventional tunnels and relatively small models will continue to be used, the flow field or flow boundary measurements to be made impose severe requirements on the experiment itself. In some cases, existing instrumentation and test techniques may not be adequate to obtain the data accuracies needed.

Conventional Transonic Tunnels and "Small" Models  
will continue to be used

- Porous Walls necessary to minimize blockage
- 3-D Model size constraints continue  $\left( \frac{A_{model}}{A_{tunnel}} < 1\% \right)$

Proposed 3-D Analytical Correction Schemes all  
Require some Experimental Measurements

- Boundary Pressures
- Flow Field Velocities

Sensitivity of the Measured Forces to the Correction  
Imposes Severe Requirements on the Experiment

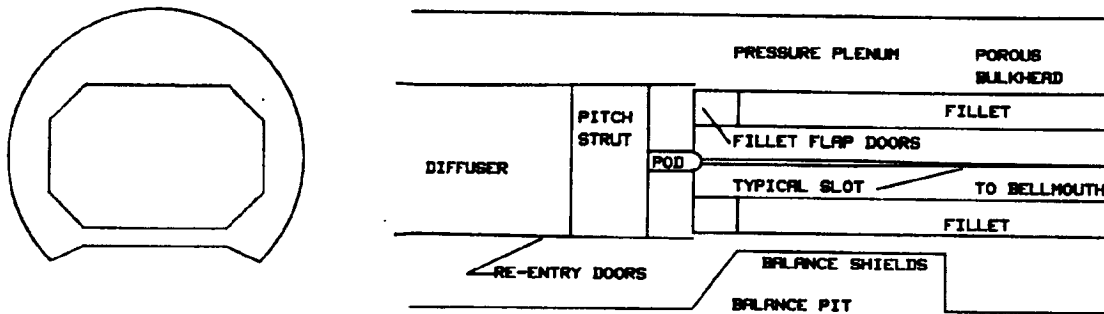
- Test Technique
- Instrumentation: Calibration, Installation and Accuracy

FIGURE 1

BOEING TRANSONIC WIND TUNNEL

The Boeing Transonic Wind Tunnel is an eight by twelve foot rectangular, slotted tunnel with corner fillets and a porosity of 11%. Following are some of the characteristics of the tunnel which are believed to impact wall interference.

1. The fillet flap and re-entry doors are located at the aft end of the test section. These doors control air leaving or entering the test section from the plenum. The doors are calibrated against Mach number to minimize buoyancy and upflow in the tunnel test section.
2. The slots in the test section vary in width longitudinally. There are five in each horizontal wall and three in each vertical wall.
3. The pitch pod and strut are permanent features of the tunnel, although the pod can be "stowed" near the ceiling when not in use.
4. The plenum beneath the floor of the test section is smaller than that above the ceiling due to the presence of the shields surrounding the balance.



CHARACTERISTICS

$P(t) = P(atm)$   
 MACH - 0.4 TO 1.05  
 Re No. per ft. =  $5.7 \times 10^6$  at  $M = 0.8$   
 NORMAL OPERATING TEMPERATURE - 135°F

TEST SECTION SIZE: 8 x 12 ft.  
 NORMAL WALL POROSITY - 11%  
 LONGITUDINAL TURBULENCE  $u/U \sim 0.0\%$  at  $M = 0.8$

FIGURE 2

## RECENT STUDIES ON BTWT WALL INTERFERENCE

Recent studies on wall interference at Boeing began with an analytical analysis of the tunnel using a three-dimensional, subsonic, potential flow computer code (PANAIR). The code included a homogeneous boundary condition at the walls. Various model configurations, mounting systems and wall porosities were evaluated. (Reference 1)

It was deemed necessary to confirm that the PANAIR model was an acceptable representation of the Boeing Transonic Wind Tunnel. Therefore an experiment was done to determine the feasibility of measuring flow velocity through the slots as well as the pressure distribution near the slot. The data were used to compare with mass flux and pressure distributions from the PANAIR model, and to compute K, the slot openness parameter.

At about the same time, a carefully controlled attempt was made to measure the lift interference parameter directly by varying the porosity in BTWT from completely solid walls to 3.5% and 11% openness. A typical transport type model, sting-mounted with an internal six-component balance, was used to measure the interference.

Finally, a feasibility study was performed to evaluate our ability to measure flow field characteristics using static pressure pipes or flow angularity probes.

1. PANAIR
  - Analytical, paneled model of BTWT, assumed homogeneous boundary condition at the walls
  - Various models, mounting systems and porosities
2. Slot Flow Study
  - Measurements of mass flux through the slots and the pressure distribution at the wall
  - Comparison to PANAIR
3. Wall Porosity Variation
  - Constant model, sting mounted
  - Slot openness changes: 0% , 3.5% and 11%
4. Flow Field Measurements
  - Static pipe measurements
  - Flow angularity measurements

FIGURE 3

The Subsonic/Supersonic Advanced Panel Pilot Code, PANAIR, solves for the inviscid, irrotational solution. Boundary conditions are set on the surfaces of the panels upon which either sources, doublets, or both have been distributed. In the example below, the boundary conditions on the wall are based on the homogenous wall boundary condition:

$$\phi_x + Ks \phi_{nx} = 0$$

where K has been based on the Davis and Moore relationship between openness ratio and slot parameter, as well as on the empirical correction of 4 x Davis and Moore (Reference 2). The openness ratio was determined for each wall separately, resulting in different values of K for the walls than for the ceiling and floor. The fillets are solid, as are the pitch strut and pod. The wing/body, based on the BTWT calibration model, is modeled with both sources and doublets to represent a lifting body. The paneling, however, was too coarse to allow comparisons of the force data between PANAIR and experiment. Wakes coming off of the wing and body satisfy the Kutta condition.

All PANAIR runs were made at a Mach number of 0.5.

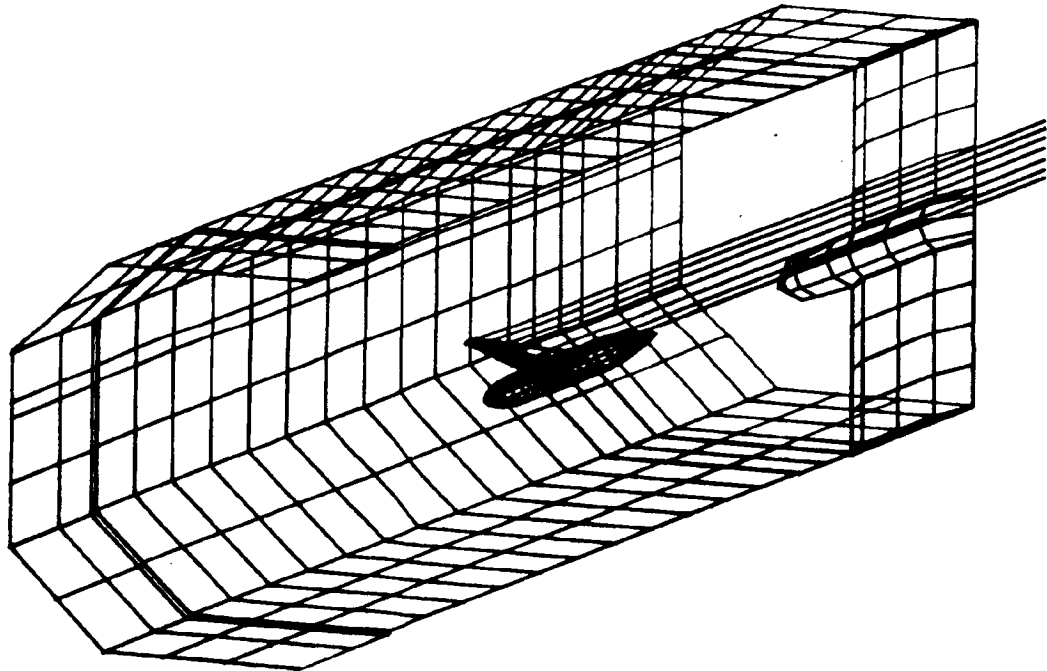


FIGURE 4

## PANAIR - PREDICTIONS OF LIFT INTERFERENCE PARAMETER

Each of the three models tested with PANAIR, a rectangular wing, a swept wing based on the calibration model, and the wing/body, were "flown" first in free air and then in the tunnel environment with various porosities. The lift interference parameter,  $\delta_0$ , was determined from the differences in the lift curves. These values were compared with the curves based on Pindzola and Lo (Reference 3) technique using K factors reflecting both Davis and Moore and 4 x Davis and Moore (Reference 2). Considering that the theoretical predictions of  $\delta_0$  are based on a rectangular tunnel having an average openness of 11%, whereas the PANAIR model included solid fillets and different porosities on the walls and ceiling and floor, agreement is fairly good.

Results also indicate that the lift interference parameter is somewhat model dependent.

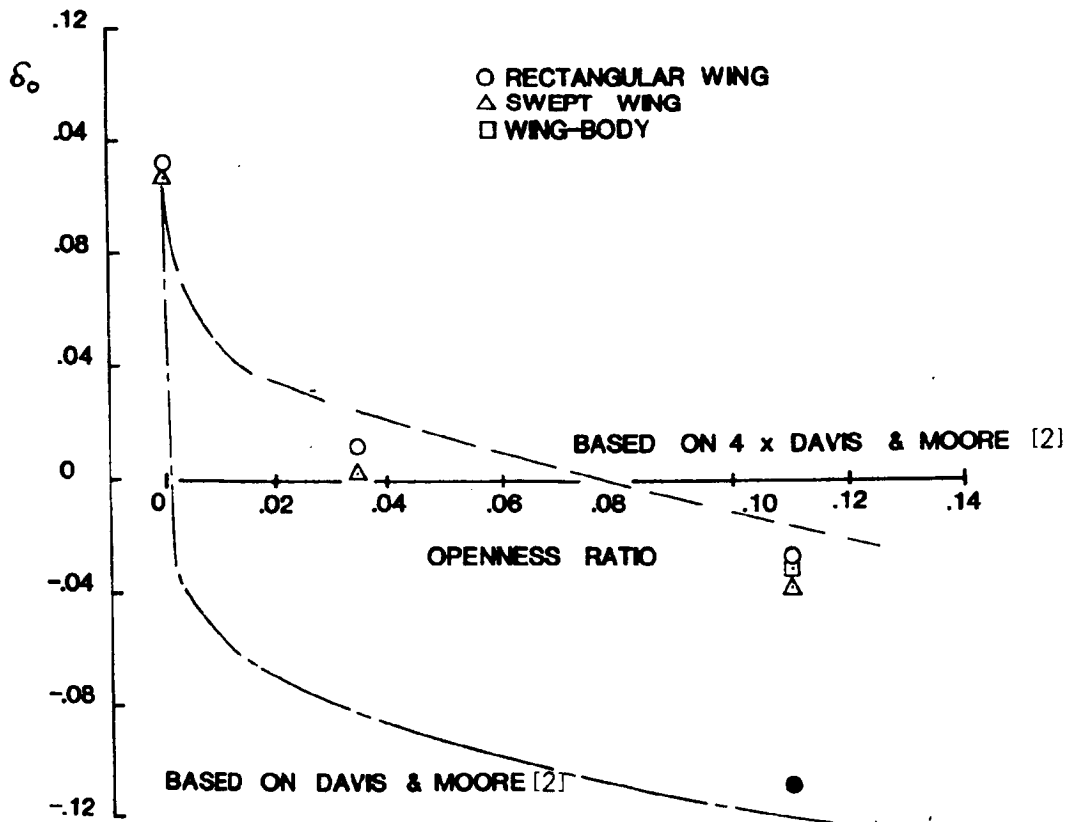


FIGURE 5

## PANAIR - CONCERNS

Among the concerns left from the PANAIR study is the inability of the program to model certain structural components of the tunnel which could affect wall interference. In addition, the selection of K used in PANAIR is based on empiricism and is not confirmed by experiment. Furthermore, a question remains regarding the validity of representing a wall actually having discrete slots as a homogeneous porous boundary.

The results from PANAIR also indicate, by means of a pitching moment change, the presence of other wall effects, predominantly streamline curvature. In order to correct for this condition, the lift interference parameter,  $\delta_0$ , will also have to be adjusted. Currently, no feasible method for measuring or detecting streamline curvature in BTWT has been implemented.

1. Unable to model Re-entry Doors, Fillet Flaps, or Plenum.
2. Used an empirical correction to the Davis and Moore relation between tunnel openness and the slot parameter, K [2].
3. Results gave evidence of streamline curvature effects complicating the determination of the lift interference parameter, and currently not measurable in BTWT.

FIGURE 6

## SLOT FLOW STUDY - PROCEDURE AND APPARATUS

The slot flow study was carried out for a two-fold purpose: first, to determine our ability to measure flow velocity and direction through the slot, thereby allowing the computation of  $K$  directly, and second, to compare the measurements to those predicted with the PANAIR model.

In addition to slot flow velocity and direction, ceiling static pressures were also required. Eight locations on the ceiling slat and in the plenum around the center slot were chosen and measured at five different tunnel stations. The plenum pressures all more or less indicated the same pressure, as expected. One of the pressure taps located 1 inch from the slot was used in the analysis.

The mass flux was determined from a hot film anemometer probe which traversed across the slot measuring flow velocity and angle. An average, normalized mass flux was used.

While the probe was installed at one station location, data was taken at  $M = 0.7$  with the model at  $-4, -2, 0, 2$  and  $4$  degrees angle of attack. Then the probe was moved 6 inches and the series repeated. In all, data was acquired with the probe at 5 tunnel stations at 6-inch intervals.

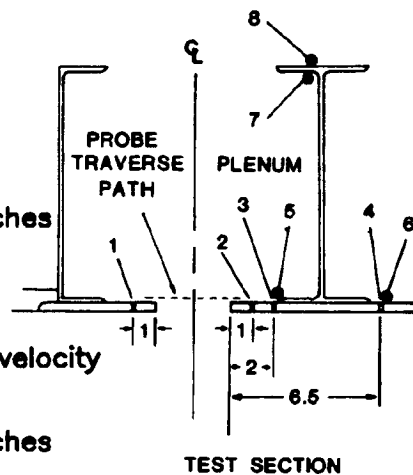
With data for more than one angle of attack of the model, it was possible to analyze the data for both absolute and incremental values. For the incremental analysis, the zero angle of attack was selected as baseline.

### 1. Ceiling Pressure Measurements made

- 1, 2 and 6.5 inches from center slot
- on the plenum side in four locations
- at five tunnel stations spanning 24 inches

### 2. Mass Flux was calculated

- by a hot film anemometer measuring velocity and angle across the center slot
- at five tunnel stations spanning 24 inches



### 3. Tunnel conditions

- Calibration model, sting mounted, at 5 angles of attack
- Mach number of 0.7

### 4. Results analyzed with both absolute values and incremental changes

FIGURE 7

ORIGINAL PAGE IS  
OF POOR QUALITY.

### SLOT VELOCITY AND PRESSURE

The data shows a discouragingly large variation of measured slot velocity as a function of tunnel station. Every effort was made to understand the uncertainty in measured angle due to the repositioning of the probe, but to date no acceptable explanation for either the scatter or the offset in absolute value has been found.

Even so, the gradient of the velocity through the slot matches PANAIR quite well, and as it turns out, so does the variation of that gradient with model  $\alpha$ .

Note too that the variation of measured slot pressure with model  $\alpha$  is similar to that of the PANAIR model, although again an unexplained offset exists.

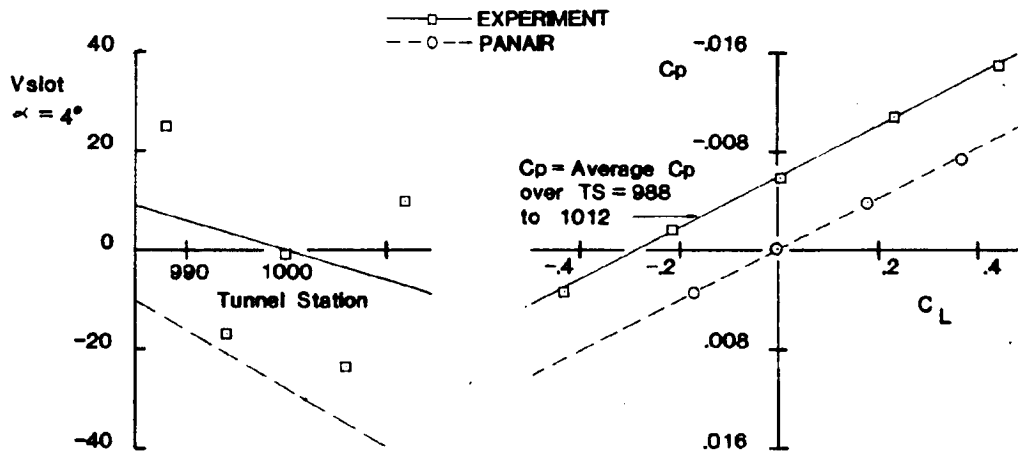


FIGURE 8

## WALL INTERFERENCE FACTOR

Prediction of the wall interference factor,  $K$ , introduces another uncertainty, resolving mass flux through a discrete slot to that through a homogeneous boundary. If the average openness for BTWT, 11%, is used, there is poor agreement between PANAIR and the experimental predictions.

However, if the openness ratio of the ceiling, 15%, is used, as was used in PANIAR, fair agreement is reached with the incremental approach. Note that using the measured values directly (absolute analysis) gives a distinct disagreement with the analytical model.

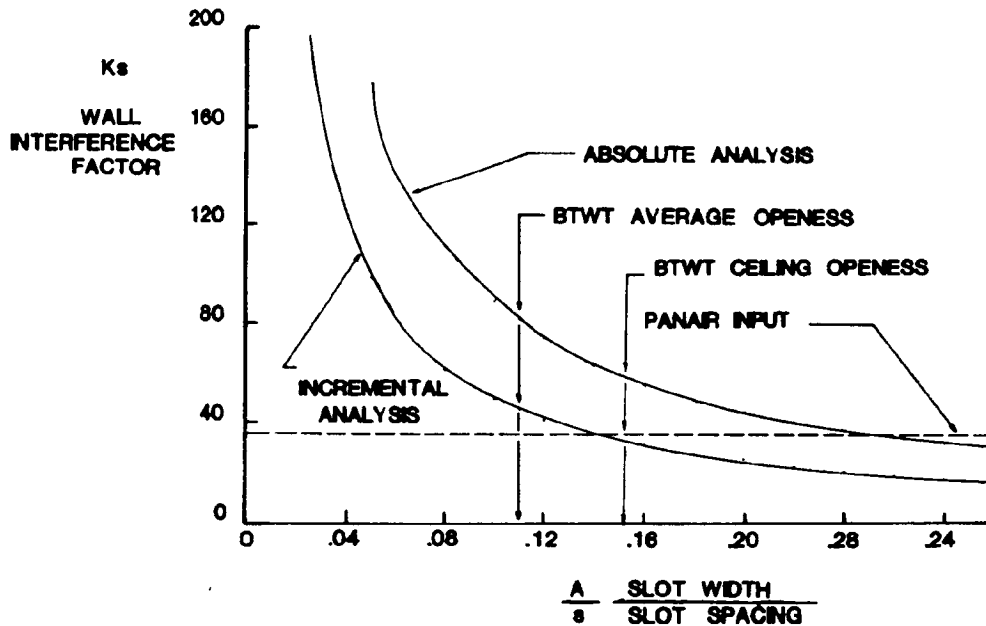


FIGURE 9

## SLOT FLOW STUDY - CONCERNS

It should be kept in mind that the purpose of this paper is not to detail the experiment, but rather to point out the very real problems in applying these techniques to a real tunnel. The local effects near the slot are probably significant. Wu has looked at these effects on the tunnel side of the slot (Ref. 4), and they are probably similarly severe on the plenum side. At any rate, considering the detail with which this type of measurement would have to be taken (i.e., each slot and far upstream and downstream of the model), it does not appear to hold much promise as an experimental method for measuring slot performance.

1. Greatest error was in mass flux, uncertainty on the same order as the measurement
2. Equating flow through discreet slots to flow through a homogeneous boundary
3. For determining wall corrections, measurements must be made over at least one-half the tunnel and the length of the test section

FIGURE 10

## WALL POROSITY VARIATION - PROCEDURE

Lift interference should be directly measurable by varying the porosity in the tunnel and observing the effect on the model lift curve. Recently this experiment was repeated in BTWT using a typical transport model, a developmental model of the 767. Three wall porosities were available, solid walls, 3.5% and 11% openness.

For each of the porosities, the test sections were first calibrated. The fillet flap and re-entry doors schedules were selected for minimal buoyancy and upflow. The centerline static and total pressures were calibrated to the reference sensors. The upflow was determined by flying the model upright and inverted.

In order to insure a high degree of accuracy, each Mach series was repeated three times. The balance used has the best zero stability history, and the laser angle meter system, capable of measuring the angle of attack of the model directly to within  $\pm 0.01$ , was used. The tunnel exhaust doors and cold-air intake doors were held to a constant setting throughout to minimize their effects on the test section flow. The model boundary layer trip was monitored throughout the test for consistency.

Although most emphasis was placed on the force data, model and wall static pressures were also obtained. These will be used for comparisons and/or as input with analytical methods.

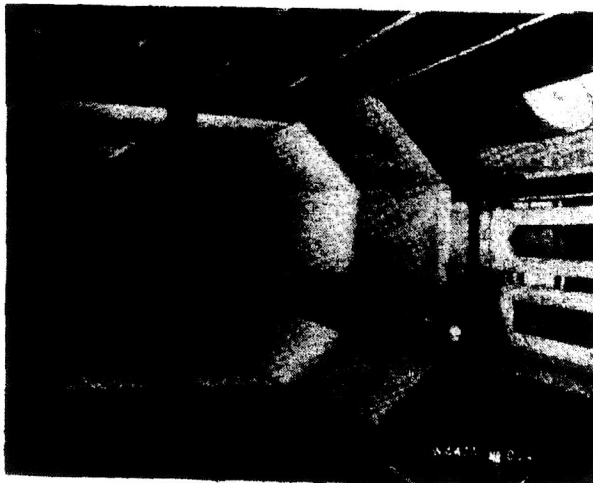
1. Flow Calibration of all three Test Sections
  - Optimized Fillet Flap and Re-entry doors schedules
  - $Q_c$  static and total pressure corrections
  - Measured upflow for model
2. Test Technique for best data accuracy
  - Measured model alpha directly (Laser Angle Meter)
  - Three repeat Mach series
  - Balance selected for zero stability
  - Boundary Layer trip using disks
  - Constant Exhaust Door and Cold Air Intake Door settings
3. Measured Force and Pressure Data over range of  $M = .5$  to  $.88$ 
  - Surface static pressures on wing and body
  - Surface static pressures on Windtunnel walls
4. Analysis emphasized Force Data
  - Model upright and inverted
  - Based on Lift curve and Drag polar

FIGURE 11

TYPICAL MODEL INSTALLATION

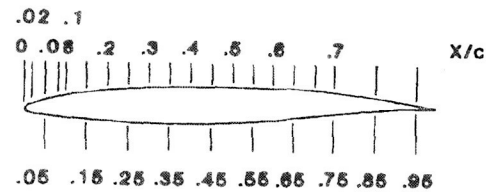
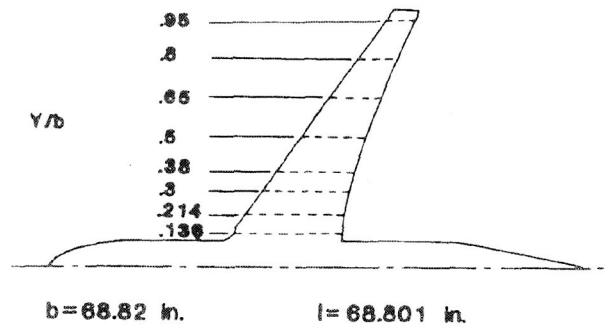
The model used in the study was a 767 development model. The model size is typical of models usually tested in BTWT, with a blockage ratio of near 0.6% and a wing span of almost 69 inches. In all, 240 wing pressures were recorded, 160 on the upper surface and 80 on the lower.

The model mounting system was a straight sting arrangement, depicted using the BTWT calibration model in the photograph.



Calibration Model

(767 Development Model)



$A_{\text{model}}/A_{\text{tunnel}} = 0.58\%$

FIGURE 12

### WALL POROSITY VARIATION - RESULTS

An assumption that has to be made is that the lift interference parameter is known for one of the porosities, and that  $\delta_0$  would not vary with Mach number. The PANAIR value of 0.107 for the solid-wall case was selected. However, since the solid-wall case for BTWT is subject to blockage effects, the classical correction to the data for blockage (Reference 3) was also applied. Blockage effects at 3.5% and 11% porosity are believed to be negligible.

The values for  $\delta_0$  deduced from the measurements are shown for both the upright and inverted model and using both the lift curve and drag polar methods. A 95% confidence band is shown for each deduced value.

In general, a downward trend of  $\delta_0$  with Mach number is indicated, becoming more severe for the higher Mach numbers. The uncertainty of the data also increases at the high Mach numbers. A number of factors could have caused this deviation from the expected. Classical blockage corrections could be insufficient, other forms of wall interference may be affecting the data, or the lift interference parameter may actually vary with Mach number.

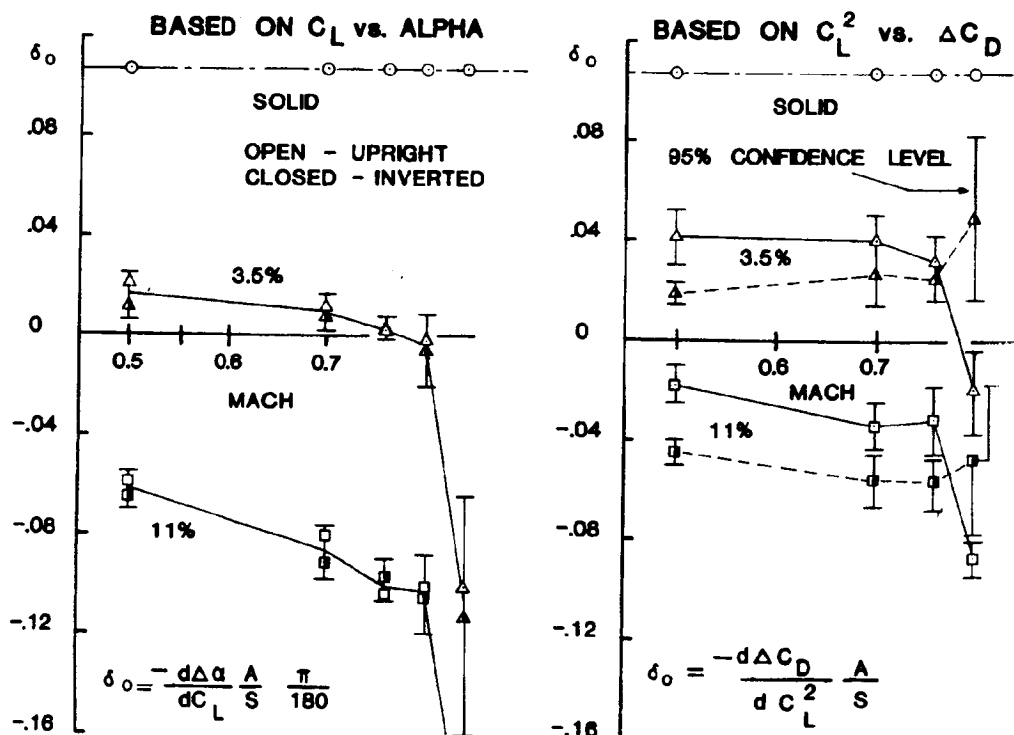


FIGURE 13

## WALL POROSITY VARIATION - CONCERNS

Concern remains primarily with the data acquired with solid walls. In addition to the assumptions made for the solid wall case and the uncertainty of the blockage corrections, questions remain regarding the ability to test with solid walls. The fillet flap and re-entry doors schedules were selected to minimize buoyancy and upflow for both the 3.5% and the 11% case. The schedules result in a static pressure distribution in the test section that could not be duplicated with solid walls. Normal static pressure measurements for the determination of Mach number are made in the plenum. With solid walls, this reference could not be used, and a static pressure tap had to be located in the tunnel.

Furthermore, the accuracy goal in the determination of  $\delta_0$  ( $\pm 0.01$ ), and therefore a correction for lift interference (1% cruise drag), was not met in all cases regardless of the care taken during the experiment. While some areas of doubt can be tested in other ways, generally it is believed that the experiment was conducted with state-of-the-art technique.

1. Correction of Solid Wall to Interference Free
  - Variation with Mach number may be real, but may merely reflect sensitivity to estimated blockage corrections
  - No way to account for blockage buoyancy
  - Model interference on static pressure source
  - Unable to obtain the same pressure distributions with solid walls as with porous walls with existing doors
2. Transonic testing requires determination of  $\delta_0$  to well within  $\pm 0.01$  in order to have confidence in the correction made to drag on the order of  $\pm 1\%$  of cruise drag for a typical transport model

FIGURE 14

## FLOW FIELD MEASUREMENTS - PROCEDURE

Proposals have been made that wall interference, primarily lift interference, can be obtained by measuring flow field characteristics. Among the more common suggestions is the measurement of static pressure distribution or flow angles. An analytical estimation of the feasibility of such an experimental approach was conducted using an infinitesimal horseshoe vortex to represent a lifting body.

The expected distributions of static pressure and flow angle to be measured are sketched in the figure below (referenced to the stationwise location of the vortex). From the standpoint of repeatability and accuracy of the measurement, it must be recognized that severe gradients in these parameters will require close attention to repeatability of the location of the static pipe and flow angle probe.

### 1. Proposed Experiment

- Measure Flow Field Static Pressure with Static Pipe
- Measure Flow Field Angularity with Cone Probe

### 2. First Order Approximation

- Represent lifting body with infinitesimal horseshoe vortex to determine flow field and estimate the changes in flow angle and pressure due to a change in wall porosity

### 3. Selection of the Location of the Probe:

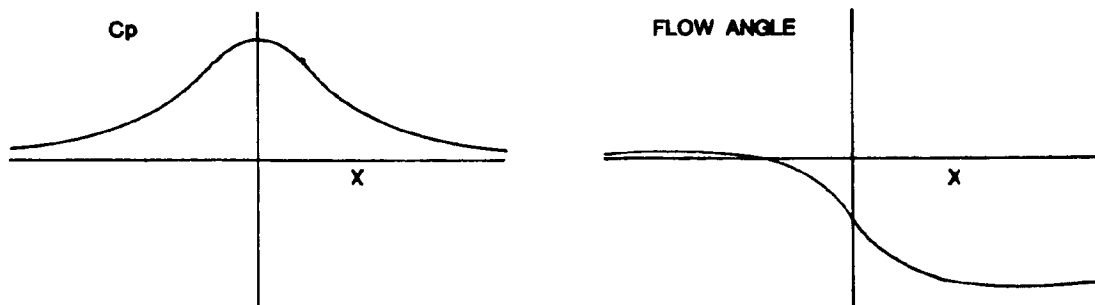


FIGURE 15

## FLOW FIELD MEASUREMENTS - RESULTS

The maximum change in lift interference would occur in going from an open jet to a completely closed tunnel. Using an estimate of the lift interference parameter from Reference 3, the maximum change in lift due to this change in wall configuration was calculated for typical models in BTWT. Since the vortex strength is directly proportional to lift, this provided an easy way to model wall interference.

Results are presented for two model sizes. A maximum deviation of 0.004 psi in static pressure and under 0.05 degrees in flow angle occurs with the larger model. Considering that maximum openness in BTWT is 11%, not 100%, the expected incremental measurements will be even less.

Current state of the art allows measurement of static pressures in a wind tunnel environment to within 0.001 psi. At best, such a pressure measurement would have 25% uncertainty.

For flow angle, the estimate is worse. Cone probe accuracy is 0.02 degrees; error is at least 50% of the expected measurement.

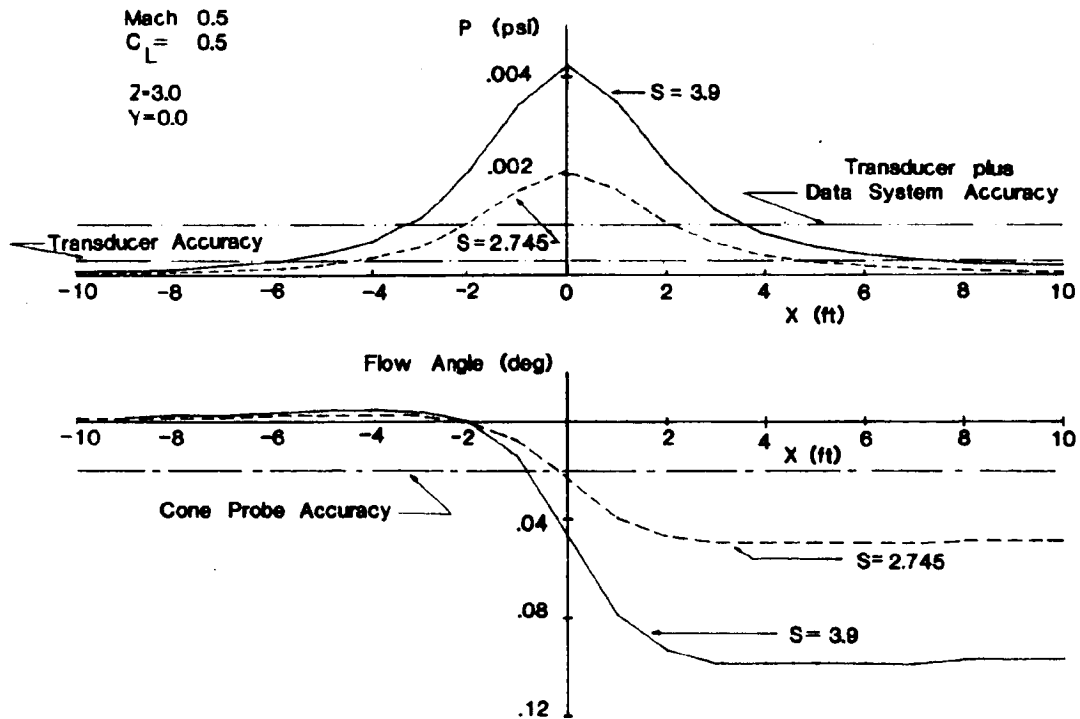


FIGURE 16

## FLOW FIELD MEASUREMENTS - CONCERNS

The small incremental levels to be measured and the accuracy required to obtain meaningful results preclude, at this time, using this technique for determination of wall effects for these relatively small models in a conventional tunnel.

In addition to measurement accuracy, other sources of error would have to be considered, among them variation in local Mach number and local flow angularity. Other forms of wall interference, viscous effects arising from proximity of the probe to the walls or model, and blockage effects would all have to be investigated or eliminated. Extreme care in probe design and placement would have to be insured, so as not to introduce displacement errors, especially in flow angle measurements.

### 1. Measurement Accuracy and the small Magnitude of the data

### 2. Interference

- variation in local Mach number
- variation in local flow angularity
- wall/model effects
- blockage

### 3. Care in Experimental Technique

- rigidity of probe, cannot deflect under load
- alignment of orifice or probe with free stream
- displacement of probe in x, y or z direction

FIGURE 17

## CONCLUSIONS

Classical theory has not been able to predict wall interference in specific wind tunnels to the degree of accuracy necessary for typical transport testing. This is partly due to tunnel characteristics not accountable with current theories, and may also indicate some insufficiencies in theories.

However, direct measurement of lift interference through typical force testing in a tunnel with different porosities, while yielding fair results, has also not attained a level of accuracy required. Attempts to measure flow characteristics have also proven extremely difficult, and those results acquired raise questions regarding their applicability to current theory. The difficulties are due to the small quantities to be measured, the uncertainty of the devices used to make the measurement and the interference from other sources. It can be anticipated that should better quality data be possible, the questions surrounding blockage and streamline curvature will have to be addressed.

As other uncertainties associated with wind tunnel testing continue to improve and the data becomes more accurate, wall interference corrections become more and more important. Experiments to directly or indirectly measure wall effects promise to be very expensive and time consuming, in order to obtain a degree of accuracy currently called for in today's testing. Therefore those working the problem are urged to consider these aspects of three-dimensional reality in their selection of parameters to measure, measurement systems, and the sensitivity of the result to expected inaccuracies in the measurements.

1. Classical theory does not account for physical tunnel characteristics (ie fillets, re-entry doors, etc.) whose effects are likely to influence wall interference.
2. Direct measurement of flow characteristics is expected to be very difficult for the level of accuracy required:
  - small quantities
  - measurement uncertainty
  - other sources of influence, interference
3. Questions regarding relating experimental results to classical theory remain:
  - separating blockage and streamline curvature from lift interference
  - relating discrete slot and wall measurements to a homogeneous boundary
4. Estimates of lift interference corrections have too high a level of uncertainty for transonic transport testing.

FIGURE 18

## SYMBOLS

a	slot width
b	model span
c	model chord
l	model length
s	slot spacing
x	displacement in tunnel longitudinal direction
y	displacement in tunnel lateral direction
z	displacement in tunnel vertical direction
A	cross-sectional area
$C_D$	coefficient of drag
$C_L$	coefficient of lift
$C_p$	coefficient of pressure
K	slot openness parameter
M	Mach number
P	static pressure
P(t)	total pressure
S	model reference area
V <sub>slot</sub>	flow velocity through slot
$\delta_0$	lift interference parameter
$\delta_{nx}$	rate of change as a function of X of the disturbance velocity normal to the wall
$\delta_x$	disturbance velocity in the x-direction

## REFERENCES

1. Lee, K. D., Krynytzky, A. J., Zinserling, N. J. K., and Hill, E. G., "Numerical Simulation of Wall and Model Support Interferences in Wind Tunnel Testing," AGARD Fluid Dynamics Panel Subcommittee on Wind Tunnels and Testing Techniques, September 24-25, 1980.
2. Barnwell, R. W., "Design and Performance Evaluation of Slotted Walls for Two-Dimensional Wind Tunnels," NASA TM-78648, February, 1978.
3. Pindzola, M. and Lo, C. F., "Boundary Interference at Subsonic Speeds in Wind Tunnels with Ventilated Walls," AEDC-TR-69-47, May, 1969.
4. Wu, J. M., Collins, F. G., Bhat, M. K., "Three-Dimensional Flow Studies on a Slotted Transonic Wind Tunnel Wall," AIAA 20th Aerospace Sciences Meeting, AIAA-82-0230, January 11-14, 1982.

N85 12013 <sup>U</sup><sub>2</sub>

SURVEY OF ONERA ACTIVITIES ON ADAPTIVE-WALL APPLICATIONS  
AND COMPUTATION OF RESIDUAL CORRECTIONS

J. P. Chevallier  
ONERA  
Chatillon, France

PRECEDING PAGE BLANK NOT FILLED

Preceding page blank

## INTRODUCTION

The research undertaken at ONERA concerning the computation and/or reduction of wall interference follows two main axes:

1. Improvement of wall correction determinations
2. Use of adaptive flexible walls

Although these two subjects are strongly interconnected, the different topics will be considered in the following order for the sake of clarity:

1. Corrections computed from wall measured data
  - Two-dimensional formulation review
  - Three-dimensional formulation review
2. Model representation
3. Two-dimensional T2 wind tunnel operation
  - Description
  - Adaptation process
  - Validation
4. Three-dimensional future concept

### COMPUTATION OF CORRECTIONS FROM MEASURED WALL DATA: REVIEW OF THE FORMULATIONS

This review of the formulation of the correction procedures based on measured wall data for both two-dimensional and three-dimensional cases is given in detail in reference 1.

#### Two-Dimensional Case

The conventional assumptions of the linear approximation to subsonic compressible flow are used. The perturbation potential  $\phi_m$  is for unbounded flow around the model, which is represented by singularities. These are deduced from measurements made on the model submitted to the flow perturbed by  $\phi_1$ , the tunnel interference potential. In the wind tunnel, the total perturbation potential ( $\phi$ ) yields perturbation speed components  $\frac{\partial \phi}{\partial x}(x, \pm \frac{h}{2})$   $\frac{\partial \phi}{\partial y}(x, \pm \frac{h}{2})$  along the control surface near the wall. Values of these quantities are assumed to have been measured during the test. The perturbation speed components from the model alone (at the same places) may be computed using the volume, lift, pitching moment, and drag of the model. The interference potential

$$\phi_i = \phi - \phi_m \quad (1)$$

may be deduced from

$$\beta^2 \frac{\partial^2 \phi_i}{\partial x^2} + \frac{\partial^2 \phi_i}{\partial y^2} = 0 \quad (2)$$

subject to the conditions that  $\phi_i$  be continuous inside the control surface, since  $\phi$  and  $\phi_m$  have the same singularities, and that  $\phi_i$  derivatives be given along the control surface near or at the wall. That is, distributions of either  $\partial\phi_i/\partial x$ , given by (ref. 1):

$$f(x) = \frac{\partial\phi}{\partial x}\left(x, \pm\frac{h}{2}\right) - \frac{\partial\phi_m}{\partial x}\left(x, \pm\frac{h}{2}\right) \quad (3)$$

or  $\partial\phi_i/\partial y$ , given by (ref. 2):

$$g(x) = \frac{\partial\phi}{\partial y}\left(x, \pm\frac{h}{2}\right) - \frac{\partial\phi_m}{\partial y}\left(x, \pm\frac{h}{2}\right) \quad (4)$$

are known, as indicated above.

By conformal mapping, the problem may be solved analytically to express the speed and the angle-of-attack correction, as well as their corresponding gradients. In particular, for a model at the midheight axis of the test section, we have (ref. 1):

$$\frac{\partial\phi_i}{\partial x}(x) = \frac{1}{\beta h} \int_{-\infty}^{\infty} \frac{f_B(\xi) + f_H(\xi)}{2 \cosh[\pi(\xi-x)/\beta h]} d\xi \quad (5)$$

and

$$\frac{\partial\phi_i}{\partial y}(x) = \frac{1}{h} \int_{-\infty}^{\infty} \frac{f_H(\xi) - f_B(\xi)}{2\pi(\xi-x)/\beta h + 1} d\xi + c \quad (6)$$

where  $f_H$  and  $f_B$  denote the upper (+h/2) and lower (-h/2) walls.

The constant  $c$  is determined by the direction of the far upstream flow. The conjugate formulations (ref. 2)

$$\frac{\partial \phi_i}{\partial x}(x) = \frac{1}{h} \int_{-\infty}^{\infty} \frac{g_H(\xi) - g_B(\xi)}{e^{2\pi(\xi-x)/\beta h} + 1} d\xi + c' \quad (7)$$

and

$$\frac{\partial \phi_i}{\partial y}(x) = \frac{1}{\beta h} \int_{-\infty}^{\infty} \frac{g_H(\xi) + g_B(\xi)}{2 \cosh[\pi(\xi-x)/\beta h]} d\xi \quad (8)$$

are generally difficult to use, since the transverse speed yielding  $g$  is not accurately measured.

Two questions may arise concerning the application of these formulas.

1. Since the functions  $f$  or  $g$  are obtained from  $\partial\phi/\partial x$  or  $\partial\phi/\partial y$ , it is necessary to know not only the speed measured on the control surface but also the "far upstream reference speed" we are seeking.
2. The extrapolation of the functions required to integrate between  $\pm\infty$  also depends on the far upstream and downstream conditions.

It may be easily demonstrated (ref. 1) that any error on the first guess for the Mach number and direction is automatically eliminated by the correction computation through equations (5) and (8).

As concerns the extrapolation, the increase of the denominator with  $\xi$  due to the hyperbolic cosine allowed the truncation of the limits for equations (5) and (8). Equations (6) and (7) must be handled more cautiously for two reasons.

1. They do not demonstrate the same advantage of autoconvergence.
2. Their denominator does not increase without bound in the upstream region of the test section; that is,  $f$  and  $g$  must be accurately known in order that their top and bottom wall differences, which appear in the numerator, produce a negligible contribution to the integral.

It should be pointed out that by using this method, the results of an "empty test section calibration" are eliminated unless some "hole defects" in the wall are detected. These can be taken into account by a corresponding  $\Delta K_p$  before using the wall pressure to obtain  $\partial\phi/\partial x(x)$  for the boundary condition (equation (3)).

### Three-Dimensional Case

The conventional assumptions of the linear approximation to the subsonic compressible flow are made for a rectangular ( $2a \times 2b$ ) test section with two plane solid vertical walls. The total perturbation potential  $\phi$  can be separated into three terms (ref. 1):

$$\phi = \phi_m + \phi_m' + \phi_i \quad (9)$$

where

$\phi_m$  potential for unconfined flow about model yielding same measurements on model

$\phi_m'$  potential of infinite row of model images as a result of vertical solid walls

$\phi_i$  tunnel interference potential of top and bottom walls

The potential  $\phi_i$  is determined to be a solution of

$$\Delta\phi_i = 0 \quad (10)$$

with the boundary conditions given in equations (11) and (13). Thus

$$\frac{\partial\phi_i}{\partial y} = 0 \quad (11)$$

on the lateral vertical solid walls, and

$$\frac{\partial\phi_i}{\partial x} = \frac{\partial\phi}{\partial x} - \left( \frac{\partial\phi_m}{\partial x} + \frac{\partial\phi_m'}{\partial x} \right) \quad (12)$$

which is determined on the control surface  $z = \pm a$  by measuring the pressures yielding  $\frac{\partial\phi}{\partial x}$  and by computing  $\frac{\partial\phi_m}{\partial x} + \frac{\partial\phi_m'}{\partial x}$  from the representation of the model. Thus we have

$$\frac{\partial\phi_i}{\partial x}(x, y, +\beta a) = f_H(x, y) \quad (13a)$$

$$\frac{\partial\phi_i}{\partial x}(x, y, -\beta a) = f_B(x, y) \quad (13b)$$

When  $\phi_i$  is continuous in the band  $|z| < a$  and periodic in  $y$ , the following series are used:

$$\phi_i(x, y, z) = \sum_n \left[ \psi_n(x, z) \cos \frac{2n\pi y}{2\beta b} + \theta_n(x, z) \sin \frac{(2n+1)\pi y}{2\beta b} \right] \quad (14)$$

$$f(x,y) = \sum_n \left[ f_n(x) \cos \frac{2n\pi y}{2\beta b} + g_n(x) \sin \frac{(2n+1)\pi y}{2\beta b} \right] \quad (15)$$

The speed and angle-of-attack corrections based on  $\phi_i$  may be expressed by

$$\frac{\partial \phi_i}{\partial x}(0,0,0) = \frac{1}{2\pi} \sum_n \int_{-\infty}^{\infty} [f_{B,n}(x) + f_{H,n}(x)] I_n(x) dx \quad (16)$$

and

$$\frac{\partial \phi}{\partial z}(0,0,0) = \frac{\beta}{2\pi} \sum_n \int_{-\infty}^{\infty} [f_{H,n}(x) - f_{B,n}(x)] J_n(x) dx \quad (17)$$

where the weighting functions  $I_n$  and  $J_n$  are written as follows:

$$I_n(x) = \int_{-\infty}^{\infty} \frac{e^{-i\omega x}}{2 \cosh\left(\beta a \sqrt{\omega^2 + \left(n^2 \pi^2 / \beta^2 b^2}\right)}\right)} d\omega \quad (18)$$

$$J_n(x) = \int_{-\infty}^{\infty} \frac{e^{-i\omega x} \sqrt{\omega^2 + \left(n^2 \pi^2 / \beta^2 b^2}\right)}}{2i\omega \sinh\left(\beta a \sqrt{\omega^2 + \left(n^2 \pi^2 / \beta^2 b^2}\right)}\right)} d\omega \quad (19)$$

Using the reduced variables  $\xi = \frac{x}{\beta a}$ ,  $\eta = \frac{n\pi a}{b}$ , and  $t = \beta a\omega$ ,  $I_n$  and  $J_n$  are expressed by

$$I_n(\xi) = \frac{1}{\beta a} F(\xi, \eta) \quad (20a)$$

and

$$J_n(\xi) = -\frac{1}{\beta a} G(\xi, \eta) \quad (20b)$$

where

$$F(\xi, \eta) = \int_{-\infty}^{\infty} \frac{\cos \xi t}{2 \cosh \sqrt{t^2 + \eta^2}} dt \quad (21a)$$

and

$$G(\xi, \eta) = \int_{-\infty}^{\infty} \frac{\sqrt{t^2 + \eta^2} \sin \xi t}{2t \sinh \sqrt{t^2 + \eta^2}} dt \quad (21b)$$

As an example, the wall signature weighting functions  $F$  are presented in figure 1 for a square test section. The figure shows the decrease of  $F$  versus  $\xi$  and also versus its order of magnitude. It is necessary to add the terms resulting from  $\phi_m'$  to the corrections based on  $\phi_1$ .

If a crude, uniform, transverse adaptation of the top and bottom walls is made, the residual corrections can be attributed primarily to  $\phi_m'$  because the remaining terms based on  $\phi_1$  are weighted by  $F(\xi, \pi)$ ,  $F(\xi, 2\pi)$ , ..., which are very small.

#### MODEL REPRESENTATION

For both the two- and the three-dimensional cases, the results of the correction computations depend on the accuracy of the model representation (ref. 3). In principle, there are no restrictions as to the number of singularities used in the model representation. In fact, however, the trend is toward a small number of singularities. It is necessary in each case to assess the validity of this representation. Some sample results are given for model representations that are too crude; there are large differences between the measured or computed "signatures" at the wall for both the two-dimensional and the three-dimensional cases (figs. 2 and 3).

It should be pointed out that the good agreement of results obtained with two different boundary conditions at the wall is not a sufficient validation, since the error caused by the defect in the model representation is the same in both cases (ref. 4). Indeed, when shock waves or separations appear on the model but do not extend to the wall, their corresponding fields must be determined by more elaborate methods and assessed by the wall pressure measured with a known boundary condition.

#### ONERA T2 WIND TUNNEL OPERATION

##### Description

The ONERA T2 is a closed-circuit induction-driven blowdown wind tunnel with the following main features (fig. 4 and ref. 5):

1. Stagnation pressure: 5 bars
2. Run duration: 30-60 sec
3. Test section: length = 1.32 m  
height = 0.37 to 0.39 m
4. Two removable blocks for top and bottom flexible adaptive walls, each fitted with 16 jacks (step 0.2 mm, range 25 mm), 16 potentiometers (displacement accuracy 0.05 mm), 91 pressure holes along three lines

5. Data acquisition (1000 points/sec) and reduction, as well as jack and probe displacements, obtained in real time on HP 1000 computer

### Adaptation Process

The well-known iterative process used to adapt the wall is shown in the simplified diagram in figure 5. This process is reduced to one run by the following procedures:

1. Choice of initial shape (computed or adapted during previous test under slightly different conditions)
2. Use of four relaxation coefficients optimized for each term of the set of symmetrical and antisymmetrical parts of test section midline and height
3. Definition of test Mach number during adaptation, consistent with method described for correction computation (see fig. 6)

The time required for one iteration is calculated as follows:

Displacement of walls . . . . .	1 sec
Wall and model pressure measurements . . . . .	5 sec
Virtual external field and new shape computation . . . . .	<u>4 sec</u>
Total . . . . .	10 sec

At the end of the run, a graphic display of the following results is available:

1. Mach number distribution on walls
2. Wall shapes for each iteration
3. Pressure coefficient distribution on model and integration results at each step

These results are used to observe the convergence during the prescribed number of iterations (three to five). After the adaptation run, another run is required to obtain the drag by wake probing.

### Validation

There are several points to be checked in the adaptive-wall operation.

1. According to our experience, with the optimized relaxation coefficients, the convergence of the process is always obtained in one run.
2. All the results depend on the external flow field computation, and a part of the data has to be extrapolated from the control surface measurements. What then is the influence of this extrapolation? By substituting zero for the extrapolated values, we find a difference in the wall shape of only about one jack step (fig. 7).

3. It is not simple to assess the accuracy of the whole process, since the propagation of measurement errors in the functionals given by Green's method is difficult to follow.

Some special tests were made for this purpose in which the same airfoil was placed first on the centerline and then 80 mm below this line (20 percent of the total test section height). The wall shapes and the pressure distributions after the adaptation were quite different in the two cases (fig. 8), but the results on the airfoil (CAST 7;  $c = 200$  mm) were quite similar. The comparison may be made on the very sensitive pressure distribution (fig. 9) or on the lift coefficient obtained by integration (fig. 10). On these last curves, the scale is sufficiently enlarged to show a scatter corresponding to a few thousandths in the Mach number or a few hundredths of a degree in the angle of attack.

Some other tests with systematic changes of the slope or divergence of the test section (yielding nonadapted shapes) assess the influence of the wall shape near the model on the "far upstream references." The latest improvements concern the following points.

1. The small differences between the wall and the plane control surface for both the measured values and the external flow field boundary are now taken into account by the  $\partial/\partial x$  values of the variables at the wall.
2. The vectorization of a part of the code reduces the computation time, despite a decrease in the mesh size.
3. The Mach number determination will be included in the real-time process to obtain a test at given angle-of-attack and Mach number conditions.
4. Operation under cryogenic conditions with a device to precool the special model is planned in the near future.

### THREE-DIMENSIONAL FUTURE CONCEPT

From the two-dimensional experiments on adaptive walls and the three-dimensional interference computation, we can try to formulate some general observations for the orientation of our future work. The perturbation field of a three-dimensional model with the conventional limitation of size is 1 order of magnitude smaller than that for a two-dimensional airfoil such as the CAST 7 in the T2 test section (blockage ratio 6 percent). Just as for the three-dimensional wall interference computation, we can consider the adaptation as the superposition of different terms, the first being, for example, the two-dimensional case with flat parallel vertical walls and adapted top and bottom walls. In theory, the residual corrections in this case can easily be computed from

1. The field of the infinite file of images through the lateral walls
2. The residual corrections arising from the second term of the development

These corrections appear to be an order of magnitude smaller than the part corrected by the adaptation of the top and bottom walls, by which the mean longitudinal gradients are nullified. However, in practice, our experience concerning the wall pressure measurement accuracy has shown that it may be difficult to estimate the

higher order terms, and we have to hope that they are negligible. Moreover, model representation of vortex sheets remains a problem to be solved.

The application of these crude concepts may be useful in showing the possibility and the need to go beyond a two-dimensional adaptation for the sonic 0.8- by 0.8-m<sup>2</sup> S3CH wind tunnel improvement project presently under way. The T2 test section may also be used in the same way, but only with a half model. However, for the industrial tests, the confidence in the corrections computed by the signatures method with improved model representation seems sufficient to render adaptive technologies unnecessary at the present time, as long as the Mach number is significantly under 1.

#### CONCLUSIONS

The use of wall-measured data to compute interference effects is reliable when the model representation is assessed by "signatures with known boundary conditions." When the computed interferences are not easily applicable to correcting the results (especially for gradients in two-dimensional cases), the flexible adaptive walls in operation in T2 are an efficient and assessed means of reducing the boundary effects to a negligible level, if the direction and speed of the flow are accurately measured on the boundary. The extension of the use of adaptive walls to three-dimensional cases may be attempted since the residual corrections are assumed to be small and are computable.

#### REFERENCES

1. Capelier, C.; Chevallier, J. P.; and Bouniol, F.: Nouvelle méthode de correction des effets de parois en courant plan. Presented at 14e Colloque d'Aérodynamique Appliquée, Toulouse, 7-9 Nov. 1977. (Avail. in English as A New Method for Correcting Two-Dimensional Wall Interference. ESA TT-491, European Space Agency, 1978, pp. 1-30.)
2. Paquet, J. B.: Perturbations induites par les parois d'une soufflerie - methods intégrales. Thèse Ing. Doc., Université de Lille, France, 1979.
3. Binion, T.; Vaucheret, K.; and Bouis, X.: Progress in wind tunnel test techniques and in the corrections and analysis of the results. AGARD CP-339, 1983, paper no. 2.
4. Vaucheret, X.: Amélioration des calculs des effets de parois dans les souffleries industrielles de l'ONERA. AGARD CP-335, 1982, paper no. 14. (Available in English as Wall Interference Correction Improvements for the ONERA Main Wind Tunnels. NASA TM-76971, 1982.)
5. Archambaud, J. P.; and Chevallier, J. P.: Utilisation de parois adaptables pour les essais en courant plan. AGARD CP-335, 1982, paper no. 11. (Available in English as Use of Adaptive Walls in 2D Tests. NASA TM-77380, 1984.)

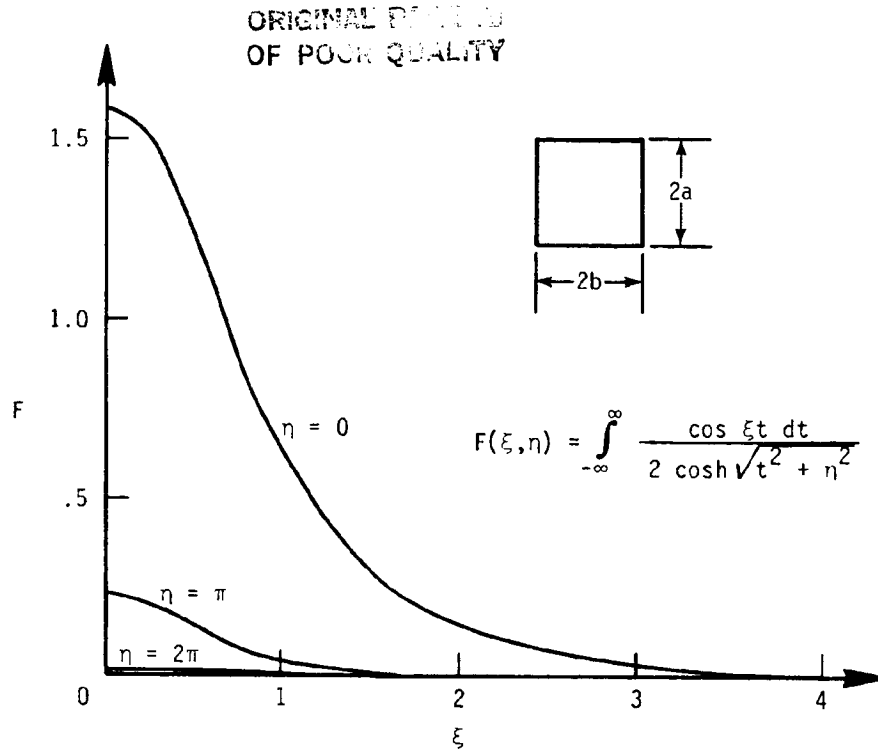


Figure 1. Wall signature weighting functions. Three-dimensional case.

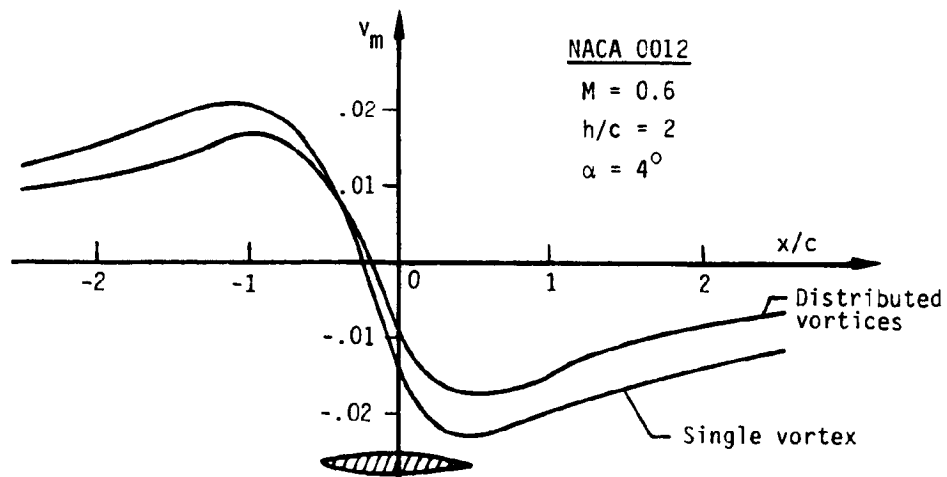


Figure 2. Theoretical assessment of the model representation from the transverse speed component at the wall. Two-dimensional case.

ORIGINAL PAGE IS  
OF POOR QUALITY

ONERA model M2

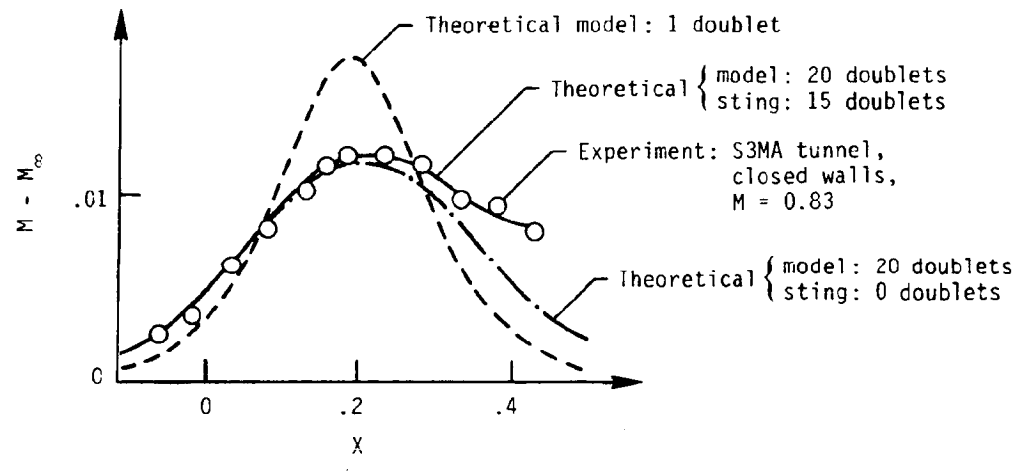
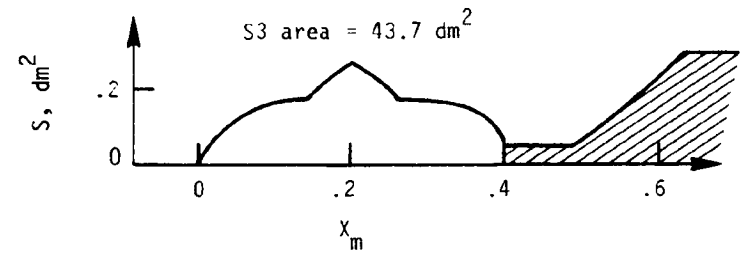


Figure 3. Experimental assessment of the model representation from wall pressure measurements. Three-dimensional case.

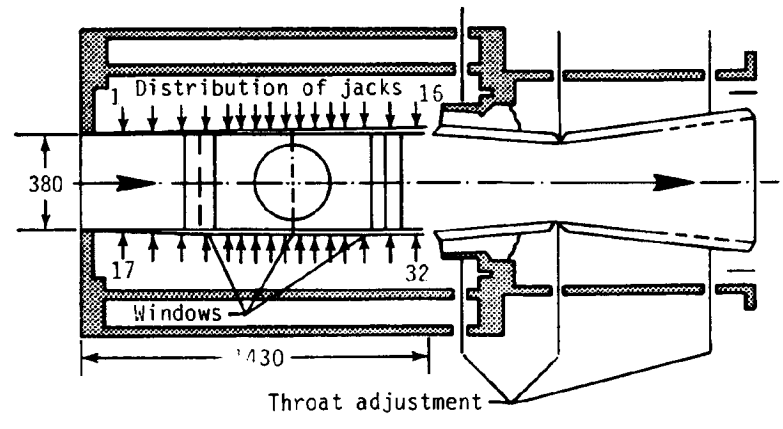


Figure 4. Test section. Dimensions in millimeters.

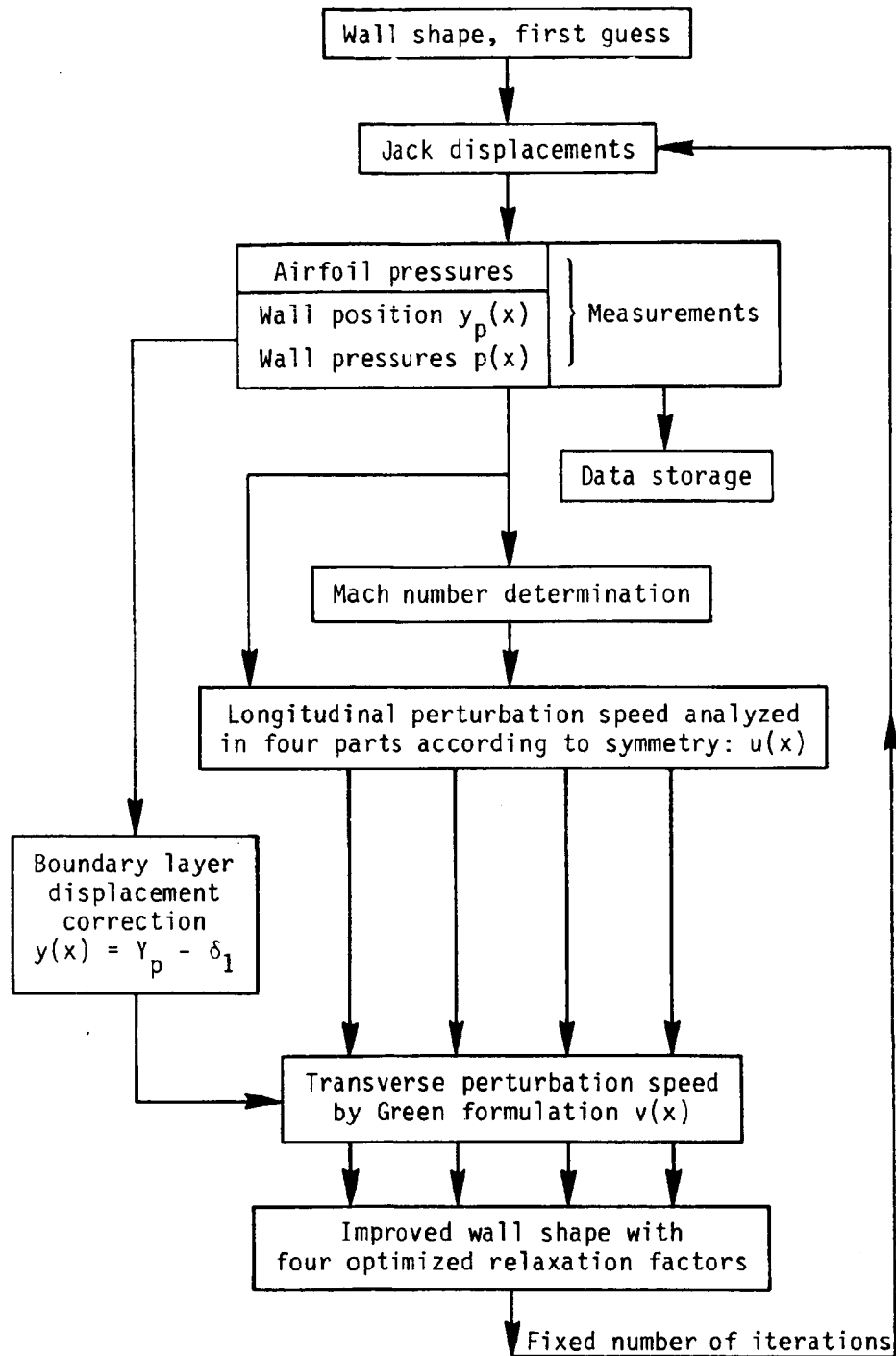


Figure 5. Wall adjustment diagram.

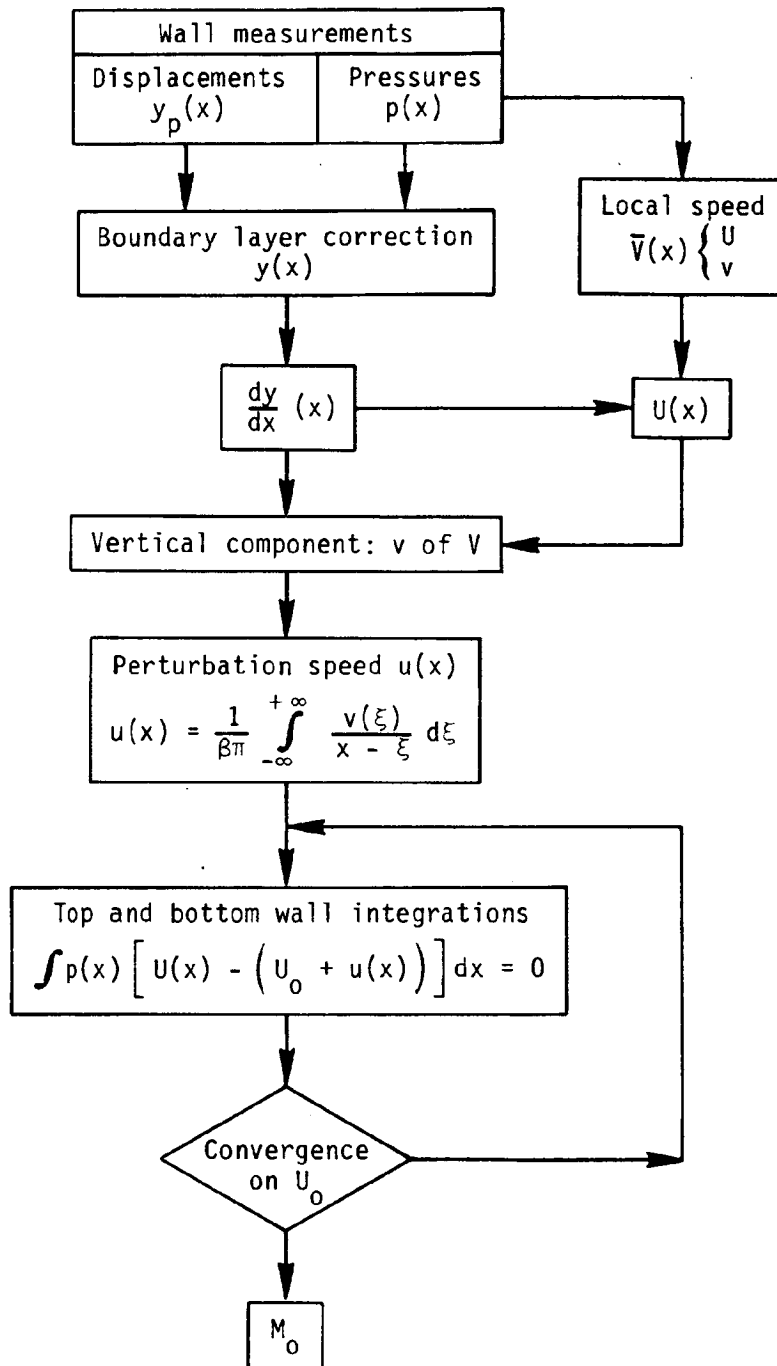
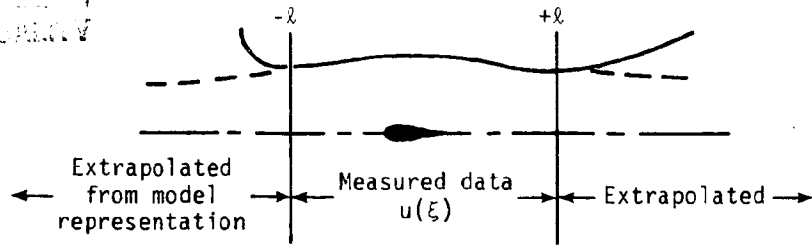


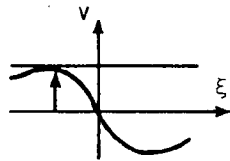
Figure 6. Mach number determination.

OPTIMUM DESIGN OF FOOD QUALITY



$$v_c = \int_{-\infty}^{-l} \frac{u(\xi)}{\xi - x} d\xi + \int_{-l}^{+l} \frac{u(\xi)}{\xi - x} d\xi + \int_{+l}^{+\infty} \frac{u(\xi)}{\xi - x} d\xi$$

$I_1$                        $I_2$                        $I_3$



$$\frac{v_{\max} (I_1 + I_3)}{v_{\max} (I_1 + I_2 + I_3)} \leq 0.15$$

Figure 7. Virtual flow computation.

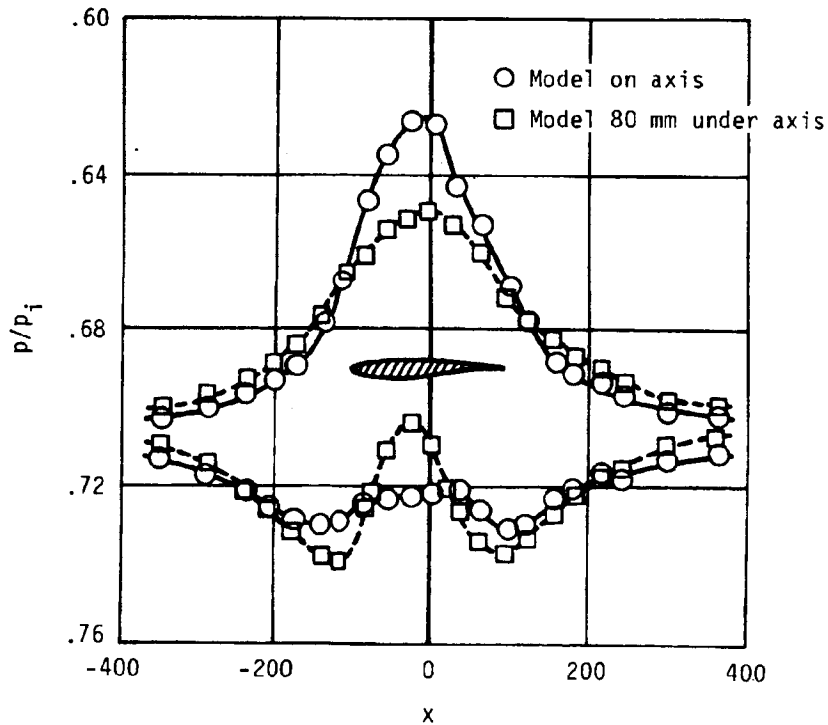


Figure 8. Wall pressure distribution. T2 wind tunnel, CAST 7 profile,  $c = 200$  mm,  $\alpha = 1^\circ$ .

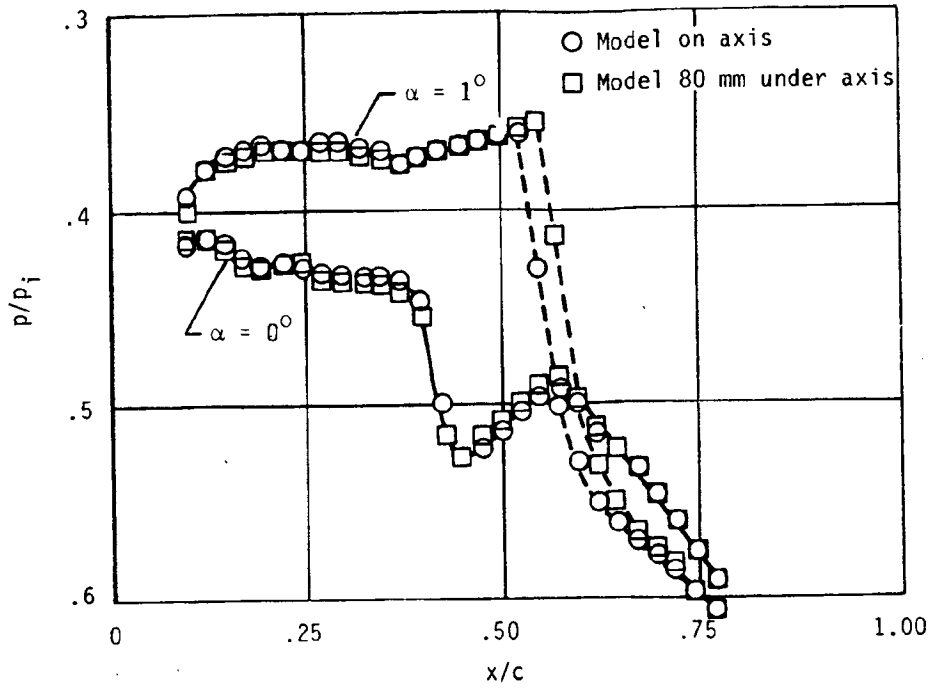


Figure 9. Model pressure distributions. T2 wind tunnel, CAST 7 profile,  $c = 200$  mm.

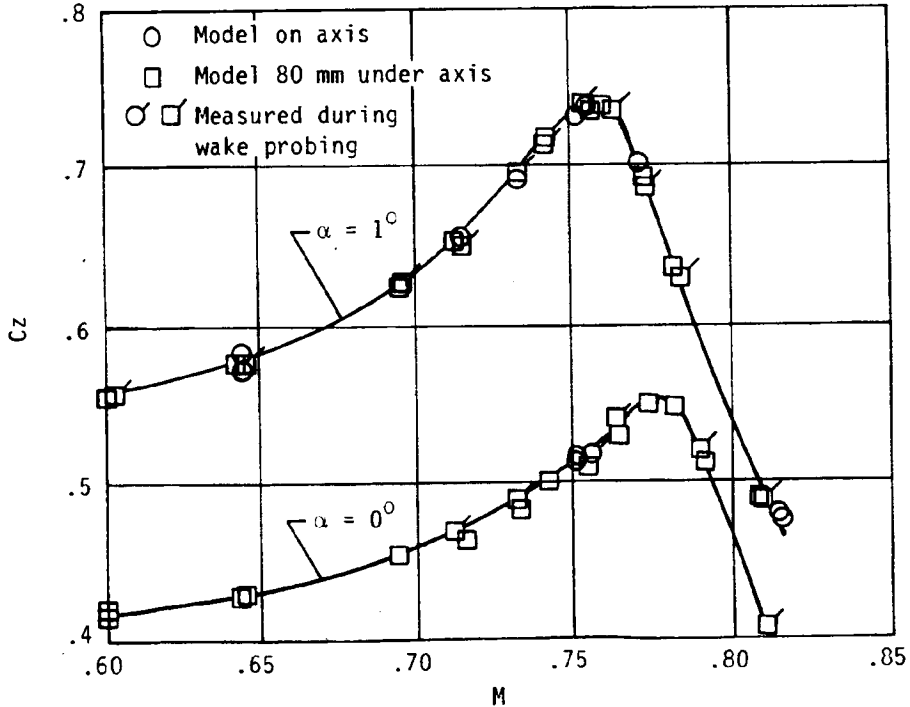


Figure 10. Lift coefficients. T2 wind tunnel, CAST 7 profile,  $c = 200$  mm.

SESSION II

ADAPTED WALL PROGRESS AND DATA

Chairman: S. R. Pate, Sverdrup Technology

N85 12014

43

WIND TUNNEL WALL INTERFERENCE IN CLOSED, VENTILATED,  
AND ADAPTIVE TEST SECTIONS

H. Holst  
DFVLR  
Göttingen, FRG

PRECEDING PAGE(S) NOT FILMED

Preceding page blank

## SUMMARY

A wall interference correction method for closed rectangular test sections has been developed which uses measured wall pressures. Measurements with circular discs for blockage and a rectangular wing as a lift generator in a square closed test section validate this method. These measurements are intended to be a basis of comparison for measurements in the same tunnel using ventilated (in this case, slotted) walls. Using the vortex lattice method and homogeneous boundary conditions, calculations have been performed which show sufficiently high pressure levels at the walls for correction purposes in test sections with porous walls.

In Göttingen, an adaptive test section (which is a deformable rubber tube of 800 mm diameter) has been built and a computer program has been developed which is able to find the necessary wall adaptation for interference-free measurements in a single step. To check the program prior to the first run, the vortex lattice method has been used to calculate wall pressure distributions in the nonadapted test section as input data for the "one-step method." Comparison of the pressure distribution in the adapted test section with "free-flight" data shows nearly perfect agreement. An extension of the computer program can be made to evaluate the remaining interference corrections.

## INTRODUCTION

In many cases the classical wall interference correction methods are not sufficiently accurate because not all model parameters (e.g., extension of the wake) are known. To get rid of this difficulty, a wall pressure method has been developed by G. Schulz, DFVLR Köln (ref. 1). His method is based on the image technique and is restricted to closed rectangular test sections. Measurements in a 1.3-m closed square test section have been carried out at DFVLR Braunschweig and corrected with his method.

Based on calculations with the vortex lattice method and homogeneous boundary conditions, it is shown that in ventilated test sections there is a sufficiently high pressure to apply correction methods using measured wall pressures (ref. 2). The new adaptive test section at Göttingen and the one-step method for wall adaptation (ref. 3) are discussed in the last part of this paper.

## SQUARE TEST SECTIONS WITH SOLID WALLS

Measurements have been carried out in a 1.3-m closed square test section at DFVLR Braunschweig. Circular discs were used for blockage and a rectangular wing was used as a lift generator.

### Blockage

Figure 1 shows the measured wall pressure distribution for a 0.5-m-diameter circular disc. This corresponds to 11.6 percent geometric blockage. The abscissa

indicates the parameter  $2s/H$ , which is the dimensionless circumferential distance, as shown in the sketch below. The symbols (triangle, square, and cross) designate different longitudinal stations. Positive values of  $x$  are upstream of the model,  $x = 0$  is the position of the model, and  $x$  negative is downstream of the model. There exist optimum positions at the walls where the influence coefficients used for correction of the dynamic pressure are independent of model parameters ( $z_{opt}$  in fig. 1). Extensive parametric studies have been done to show this (ref. 1). Comparison with a theoretical result (using a source and a sink) shows that in this case, where the geometric blockage is 11.6 percent and the effective blockage is estimated to be around 30 percent, the results cannot be corrected due to a strong deformation of the wake. The flow has no similarity with the "free-flight" case.

The influence coefficients used are basically the longitudinal velocities induced by the model and the walls (the measured quantity is the wall pressure), divided by the average longitudinal velocity induced by the walls at the position of the model. These influence coefficients or influence functions can be precalculated and can easily be used for the correction procedure.

The correction of the drag coefficients of the circular discs is shown in figure 2. The results can be corrected properly for up to 5 percent geometric blockage. The increasing error for higher blockage ratios is due to the strong deformation of the wake, which the correction procedure cannot account for.

Figure 3 illustrates the optimal positions for the wall pressure measurements. They are situated at the side walls as indicated by  $y_{opt} = \pm H/2$  and  $z_{opt} = \pm 0.348H$ . Both of the longitudinal positions needed are indicated as  $x_{w1}$  and  $x_{w2}$ . At these two positions the wall pressures had to be interpolated. For a given tunnel, the pressure taps can be installed permanently at the optimal positions. Again, negative values of  $x$  are positions downstream of the model.

#### Lift Generator

The model used as a lift generator is shown in figure 4. The quarter-chord line is at  $x = 0$ . The model is supported by a rearward sting. Figure 5 shows the measured wall pressure distribution, which includes lift and blockage influences. The different longitudinal stations are represented by  $x_w$ . It can be seen that there is blockage influence because there is no antisymmetry to  $c_{pw} = 0$ , as one would expect if the model would generate lift alone. By adding top and bottom wall pressure signals and, of course, dividing the results by two, the wall pressure signals (i.e., the pressure coefficients due to blockage) can be extracted. This is possible because pressure signals due to lift differ in sign from top to bottom wall, and those due to blockage have the same sign. Therefore lift signals are cancelled and the blockage signals remain. This is shown in figure 6. The theoretical result has been calculated by representing the volume distributions of fuselage and rectangular wing with a number of doublets in longitudinal and spanwise directions. The strength of the doublets is obviously wrong by a factor of 2.5, but the shape of the theoretical curve compared to the squares looks right, and the correction procedure takes account of the correct strength because it uses the measured wall pressures.

The pressure distribution due to lift alone can be extracted by subtracting bottom wall signals from top wall signals and averaging. This is illustrated in figure 7. For reasons of comparison, theoretical results for two different longitudinal stations have been plotted in the figure. The differences between

experimental data and theoretical results are due to the fact that the calculations were done with a single horseshoe vortex, which means constant lift distribution. The agreement would be better with an elliptical load simulated by a set of horseshoe vortices. The influence coefficients for blockage were mentioned previously. For lift, they are the wall- and model-induced x-velocities at the walls, divided by the vertical velocity  $w$  induced by the wall alone. Thus the measured quantity is the wall pressure, which gives the longitudinal velocity. These velocities and the influence coefficients or influence functions give the vertical velocity  $w$  due to the walls alone; that is, the angle-of-attack correction  $\Delta\alpha$ . Also, for the influence function for angle-of-attack correction,  $f_L$ , optimum positions exist for pressure tap locations. This is illustrated in figure 8. The parameter varied is the relative span,  $f_L$  being independent of this model parameter at a certain spanwise station in this tunnel.

The final results for the corrections are given in table I. The last line illustrates the case discussed in figures 5 to 7. There is a 2.3-percent correction of dynamic pressure, a  $1.8^\circ$  angle-of-attack correction, and a 16-percent change in drag coefficient.

#### PERFORATED WALLS

Figure 9 shows the influence of wall porosity on spanwise distributions of interference. The vortex lattice method was used for the calculation, with homogeneous boundary conditions. The induced velocities at the walls in the main cross section (i.e., at  $x = 0$ ), where the model is located, are presented in figure 10. The parameter varied is the porosity factor  $Q$ , and  $\delta_{x_w}$  is the dimensionless longitudinal velocity induced by the model and the tunnel walls. The calculations indicate a sufficiently high pressure level for application of a Schulz-type wall pressure method even in perforated test sections.

#### ADAPTIVE TEST SECTION

An adaptive test section that is a deformable rubber tube of 800 mm diameter has been built in Göttingen (ref. 3). (See fig. 11.) It will be installed in the high-speed intermittent facility of DFVLR Göttingen (ref. 4) in the near future. It uses a "one-step method" (adaptation in a single step, no iteration necessary). This computer program uses Fourier series and Fourier transforms to find the interference-free contour of the circular test section. The principle of the method is given in appendix A.

To check the one-step method prior to the first run, the vortex lattice method has been used to calculate pressure distributions at the tunnel walls when a model is present, and potential theory gives free-flight data at imaginary walls.

First simulated experimental data were used as input to the computer program, and then calculated free-flight data were input. If the one-step method works as expected, it should give the free-flight pressure distribution after the wall adaptation has been made. Of course, this is just a simulation.

Figure 12 illustrates the principle of the vortex lattice method. The boundary conditions are fulfilled at a set of control points. The case in figure 13 was calculated with a single doublet representing a sphere of 7.5 percent geometric

blockage. Starting from the nonadapted tunnel with cylindrical walls, the free-flight pressure distribution at imaginary walls is reached within an accuracy of 2 percent of the difference. In figure 14 the analytical solution gives the unconfined-flow streamline to be achieved by wall deformation. The differences in this figure and in figure 13 can be explained as follows. Upstream and downstream of the model, the test section diameter was taken to be 800 mm for the analytical calculation. At the beginning of the rubber tube test section, however, the theoretical streamtube already has a diameter of more than 800 mm, whereas the test section hardware is fixed to 800 mm diameter. If a parallel streamline is taken for comparison, the two upper curves in figure 14 fit together exactly. The lower curve shows the influence of compressibility. It should be mentioned that the model is designed for compressible subsonic-flow conditions.

Figure 15 shows another example of checking the one-step method using a wing with elliptic load as a lift generator. The wall pressure distribution calculated by the one-step method after the wall adaptation shows good agreement with "free-flight" imaginary walls. Figure 16 shows the wall displacement for this same case. No data are available presently to compare with such an analytical solution. This figure serves to indicate the order of magnitude of wall displacement. The data used for the calculation were:

Aspect ratio . . . . .	5.0
Lift coefficient . . . . .	2.0
Relative span . . . . .	0.7
Elliptic load	

At the end of the test section, the wall displacement is about 40 mm.

Measurements have not yet been carried out in the deformable rubber tube adaptable test section. The influence of errors in the wall pressure measurement on the wall adaptation is presently being investigated. It will probably be necessary to evaluate the remaining wall interferences if the wall adaptation cannot be performed fully.

#### CONCLUDING REMARKS

A correction method for closed rectangular test sections based on measured wall pressure data and using influence coefficients has been shown. This method appears to be applicable to perforated test sections as well.

Prior to the first run in the deformable rubber tube test section, the computational adaptation procedure (the one-step method) was shown to give accurate results for the cases discussed previously. Experiments will show how good the one-step method and the adaptable test section will be in reality, as well as whether there will be a need to evaluate the remaining wind tunnel wall interference.

## REFERENCES

1. Schulz, G.: Experimentelle Nachprüfung des Mehrebenen-Wanddruckverfahrens für Unterschallwindkanäle. (Experimental Check of the Multi-Plane Wall Pressure Correction Method in Low Speed Wind Tunnels.) WAKO-Exp, DFVLR Köln-Porz, April 1982.
2. Holst, H.: Berechnung von Windkanalinterferenzen nach dem Wirbelgitternetzverfahren. (Calculation of Wind Tunnel Wall Interference Using the Vortex Lattice Method.) DFVLR IB 157-80 A 01, December 1980.
3. Wedemeyer, E.; and Heddergott, A.: Dehnbare Megstrecke für Windkanäle. (Deformable Test Sections for Wind Tunnels.) DFVLR IB 251-80 A 01, February 1981.
4. Ludwig, H.; and Hottner, T.: Hochgeschwindigkeitswindkanal der Aerodynamischen Versuchsanstalt Göttingen. Z. f. Flugwissenschaften 7, pp. 294-299, 1959.

## APPENDIX A

### PRINCIPLE OF THE ONE-STEP METHOD FOR CALCULATION OF THE FINAL WALL CONTOUR IN A SINGLE STEP

The displacement of the wall compared to a cylindrical nondeformed wall is  $\eta(x, \theta)$  in cylindrical coordinates. The calculation starts with an initial preliminary wall setting  $\eta_0(x, \theta)$ . This setting of the wall can be zero, for example, but it is better to choose a wall setting that has been found previously for a neighboring angle of incidence or Mach number.

For the wall setting  $\eta_0$ , the inner flow with the model included has the potential  $\phi_0(r, x, \theta)$ . Normally  $\phi_0$  is not known, but the velocity components at the wall can be determined. The value of  $u_0$  is determined by measuring the wall pressure, and by knowing the wall setting,  $v_0$  is also known:

$$u_0 = \left( \frac{\partial \phi_0}{\partial x} \right)_R \quad \Delta p_0 = -\rho_\infty U_\infty u_0 \quad (1)$$

$$v_0 = \left( \frac{\partial \phi_0}{\partial r} \right)_R \quad v_0 = U_\infty \frac{d\eta_0}{dx} \quad (2)$$

An additional wall displacement  $\Delta\eta = \eta_1 - \eta_0$  generates an additional perturbation of the flow and, accordingly an additional perturbation potential. This unknown additional perturbation potential must be determined; this is done by using Fourier series.

The inner flow region is represented by

$$\phi_{(i)} = \phi_0 + U_\infty \int \sum_n a_{n,k} I_n(\beta kr) e^{i(n\theta + kx)} dk \quad (3)$$

and the fictitious outer flow region is given by:

$$\phi_{(o)} = U_\infty \int \sum_n b_{n,k} K_n(\beta kr) e^{i(n\theta + kx)} dk \quad (4)$$

where

(i) = inner flow region

(o) = outer flow region (fictitious)

The coefficients  $a_{n,k}$  and  $b_{n,k}$  can be determined as follows:

$$v_{(i)} = v_{(o)}$$

and

$$u_{(i)} = u_{(o)}$$

where

$$v_{(i)} = \left( \frac{\partial \Phi_{(i)}}{\partial r} \right)_R \quad v_{(o)} = \left( \frac{\partial \Phi_{(o)}}{\partial r} \right)_R$$

and

$$u_{(i)} = \left( \frac{\partial \Phi_{(i)}}{\partial x} \right)_R \quad u_{(o)} = \left( \frac{\partial \Phi_{(o)}}{\partial x} \right)_R$$

Using equations (3) and (4) we get

$$v_{(i)} = v_0 + U_\infty \int \sum_n a_{n,k} I_n'(\beta k R) \beta k e^{i(n\theta + kx)} dk \quad (5)$$

and

$$v_{(o)} = U_\infty \int \sum_n b_{n,k} K_n'(\beta k R) \beta k e^{i(n\theta + kx)} dk \quad (6)$$

By integration of equations (5) and (6) we find that

$$\eta_{1(i)} = \eta_0 + \int \sum_n \frac{\beta}{i} a_{n,k} I_n'(\beta k R) e^{i(n\theta + kx)} dk \quad (7)$$

and

$$\eta_{1(o)} = \int \sum_n \frac{\beta}{i} b_{n,k} K_n'(\beta k R) e^{i(n\theta + kx)} dk \quad (8)$$

Equations (3) and (4) further give

$$u_{(i)} = u_0 + U_\infty \int \sum_n a_{n,k} i k I_n(\beta k R) e^{i(n\theta + kx)} dk \quad (9)$$

$$u_{(o)} = U_{\infty} \int \sum_n b_{n,k} ikK_n (\beta kR) e^{i(n\theta+kx)} dk \quad (10)$$

By setting  $\eta_{(i)} = \eta_{(o)}$  and  $u_{(i)} = u_{(o)}$ , equations (7) to (10) give

$$\eta_0 = \int \sum_n \frac{\beta}{i} (b_{n,k} K_n' - a_{n,k} I_n') e^{i(n\theta+kx)} dk \quad (11)$$

and

$$\frac{u_0}{U_{\infty}} = \int \sum_n ik(b_{n,k} K_n - a_{n,k} I_n) e^{i(n\theta+kx)} dk \quad (12)$$

Fourier transforms of equations (11) and (12) lead to

$$\frac{\beta}{i} (b_{n,k} K_n' - a_{n,k} I_n') = \frac{1}{(2\pi)^2} \iint \eta_0 e^{-i(n\theta+kx)} d\theta dx \quad (13)$$

and

$$ik(b_{n,k} K_n - a_{n,k} I_n) = \frac{1}{(2\pi)^2} \iint \frac{u_0}{U_{\infty}} e^{-i(n\theta+kx)} d\theta dx \quad (14)$$

From equations (13) and (14)  $a_{n,k}$  and  $b_{n,k}$  can be determined. The expression for  $b_{n,k}$  is

$$b_{n,k} = \frac{I_n' \iint \frac{u_0}{U_{\infty}} e^{-i(n\theta+kx)} d\theta dx + \frac{k}{\beta} I_n \iint \eta_0 e^{-i(n\theta+kx)} d\theta dx}{ik(2\pi)^2 (I_n' K_n - I_n K_n')} \quad (15)$$

The result for the final (additional) wall displacement is obtained from equation (8) using the  $b_{n,k}$  values given in equation (15).

ORIGINAL PAGE IS  
OF POOR QUALITY

TABLE I.- FINAL RESULTS FOR RECTANGULAR WING

$\alpha_g$	$c_L$	$c_D$	$\Delta q/q_\infty$	$c_L$	$c_D$	$\Delta\alpha_m$	$\alpha_m$	$c_{Di}$	$c_D$
$-2,05^\circ$	1,125	0,1200	0,01587	1,107	0,12599	$1,08734^\circ$	$-0,963^\circ$	0,0210	0,1470(0)
$0^\circ$	1,276	0,1571	0,01741	1,254	0,15440	$1,22754^\circ$	$+1,227^\circ$	0,0269	0,1813
$1,12^\circ$	1,360	0,1755	0,01746	1,337	0,17248	$1,30387^\circ$	$2,424^\circ$	0,0304	0,2029
$3,16^\circ$	1,510	0,2125	0,01838	1,483	0,20865	$1,46121^\circ$	$4,621^\circ$	0,0378	0,2465
$4,25^\circ$	1,589	0,2321	0,01996	1,558	0,22754	$1,55156^\circ$	$5,802^\circ$	0,0422	0,2697
$5,18^\circ$	1,659	0,2510	0,02004	1,625	0,24604	$1,60764^\circ$	$6,788^\circ$	0,0456	0,2916
$6,32^\circ$	1,736	0,2724	0,02107	1,700	0,26675	$1,68709^\circ$	$8,007^\circ$	0,0501	0,3168
$7,37^\circ$	1,808	0,2948	0,02113	1,770	0,28867	$1,74473^\circ$	$9,115^\circ$	0,0539	0,3426
$7,80^\circ$	1,834	0,3037	0,02177	1,795	0,29719	$1,78211^\circ$	$9,582^\circ$	0,0558	0,3530
$8,84^\circ$	1,892	0,3244	0,02229	1,851	0,31729	$1,81638^\circ$	$10,656^\circ$	0,0587	0,3760
$10,90^\circ$	1,876	0,3512	0,02334	1,833	0,34314	$1,80704^\circ$	$12,707^\circ$	0,0578	0,4010
uncorr. exp. data			blockage corr.			angle of attack corr. <u>final values</u>			

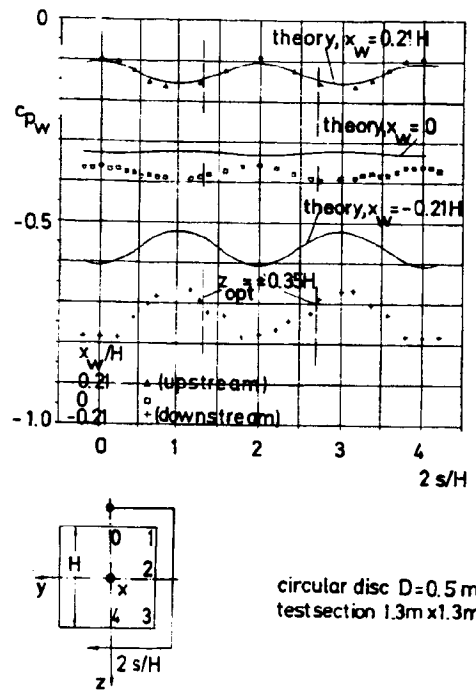


Figure 1.- Wall pressures due to blockage.

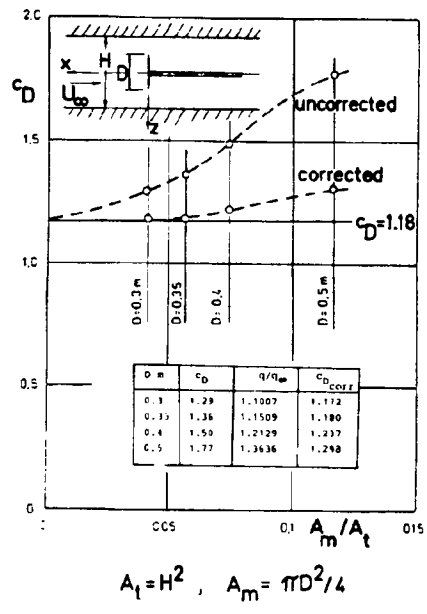


Figure 2.- Results for circular discs.

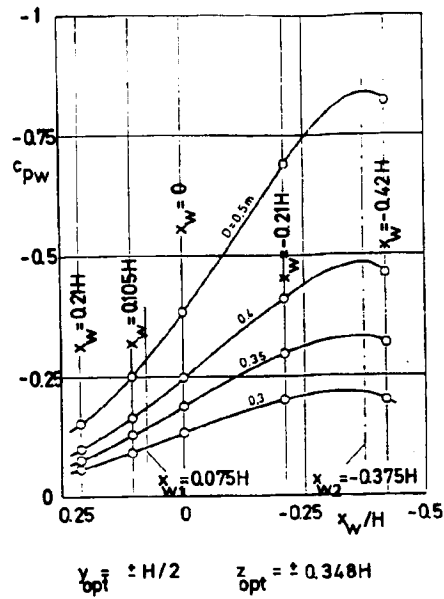
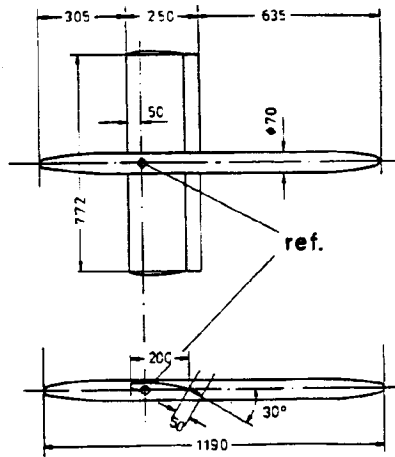


Figure 3.- Using pressures at optimal positions for correction.



Profile: CLARK Y, wing and flap  $d/l=0.117$   
 $S_m = 0.1934 m^2$   
 $l_p = 0.25 m$

Figure 4.- Lift generator.

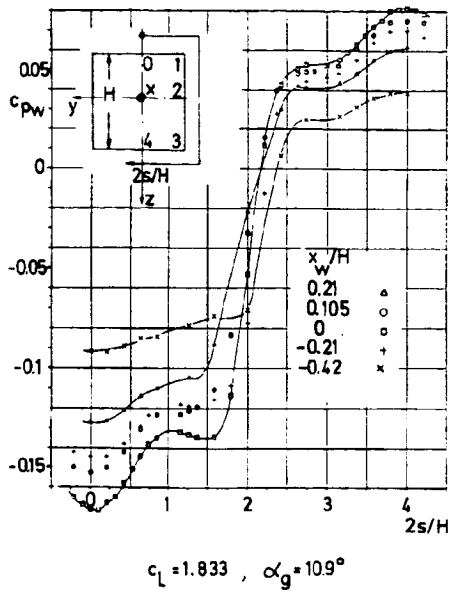


Figure 5.- Experimental wall pressure data include lift and blockage influences.

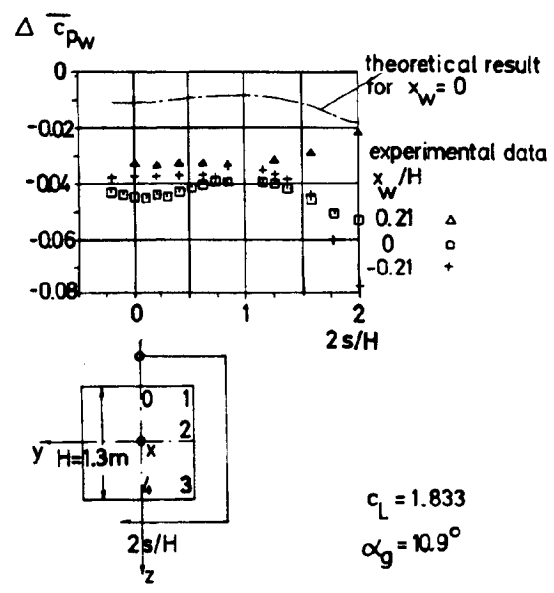


Figure 6.- Wall pressures due to blockage of wing and fuselage.

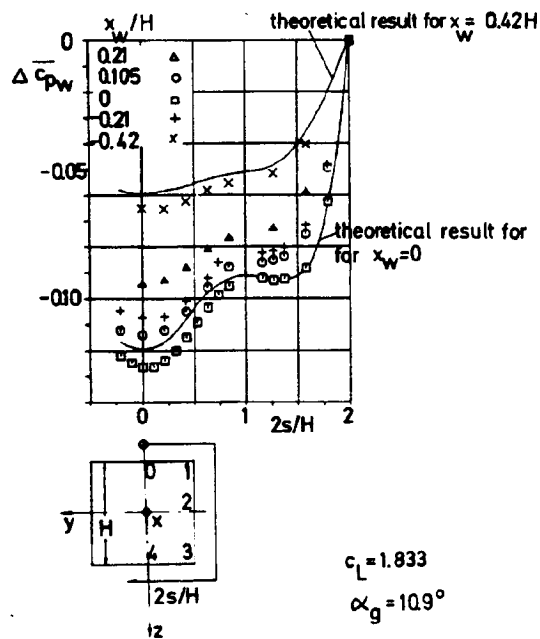


Figure 7.- Wall pressures due to lift (calculations with constant lift distribution).

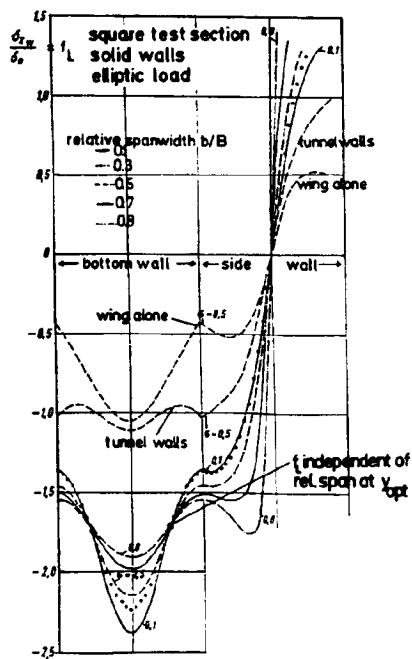


Figure 8.-  $f_L$  as a function of relative span.  $x_w = 0$ .

ORIGINAL QUALITY  
OF POOR QUALITY

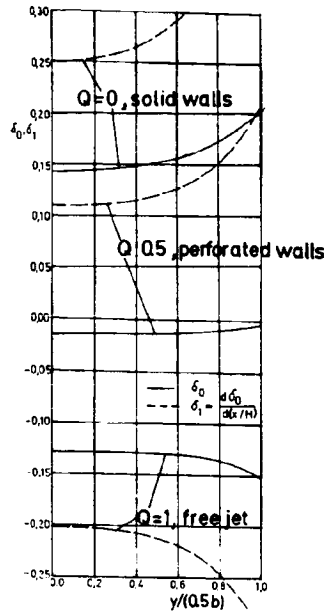


Figure 9.- Spanwise distributions of interference factors for a square test section.

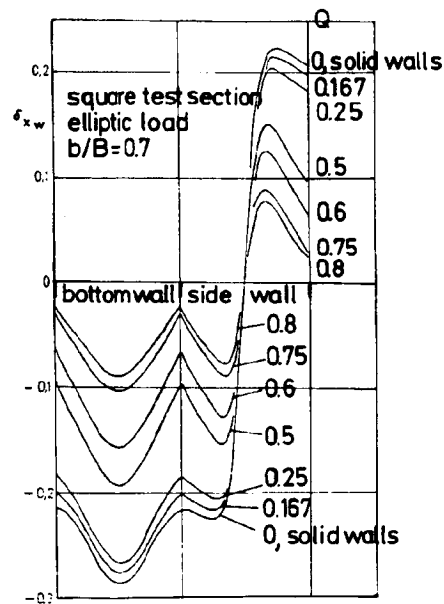


Figure 10.- Influence of porosity factor  $Q$  on  $\delta_{xw}$ ,  $x_w = 0$ .

ORIGINAL PAGE IS  
OF POOR QUALITY

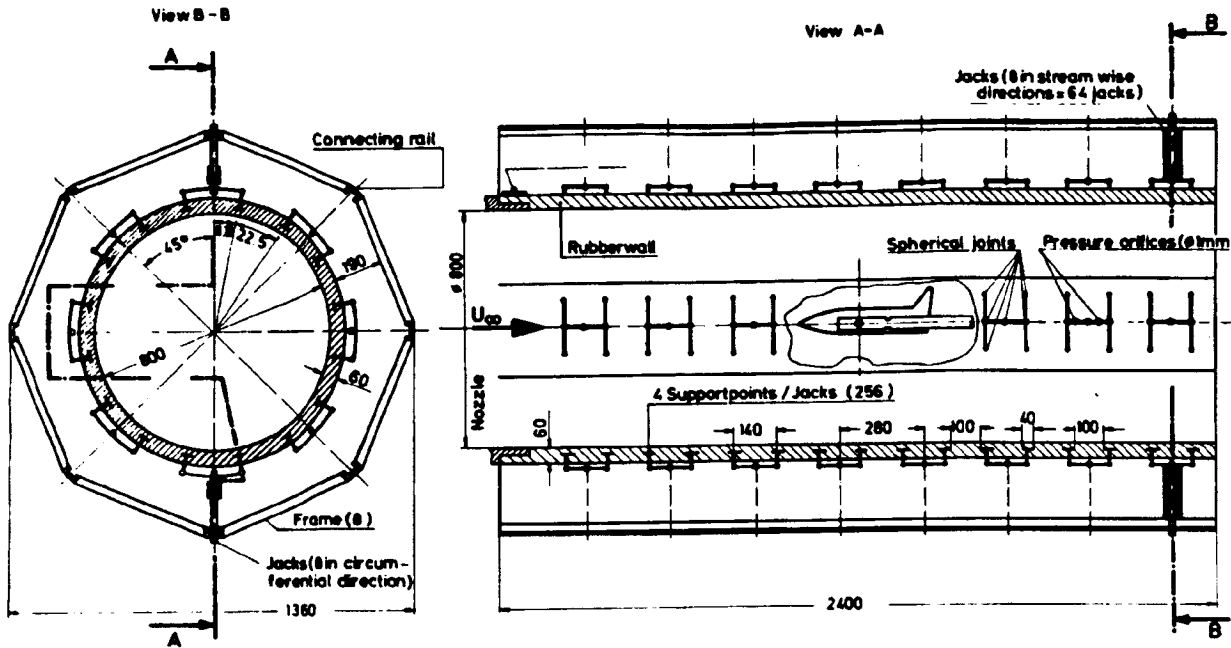


Figure 11.- Three-dimensional deformable rubber tube test section.

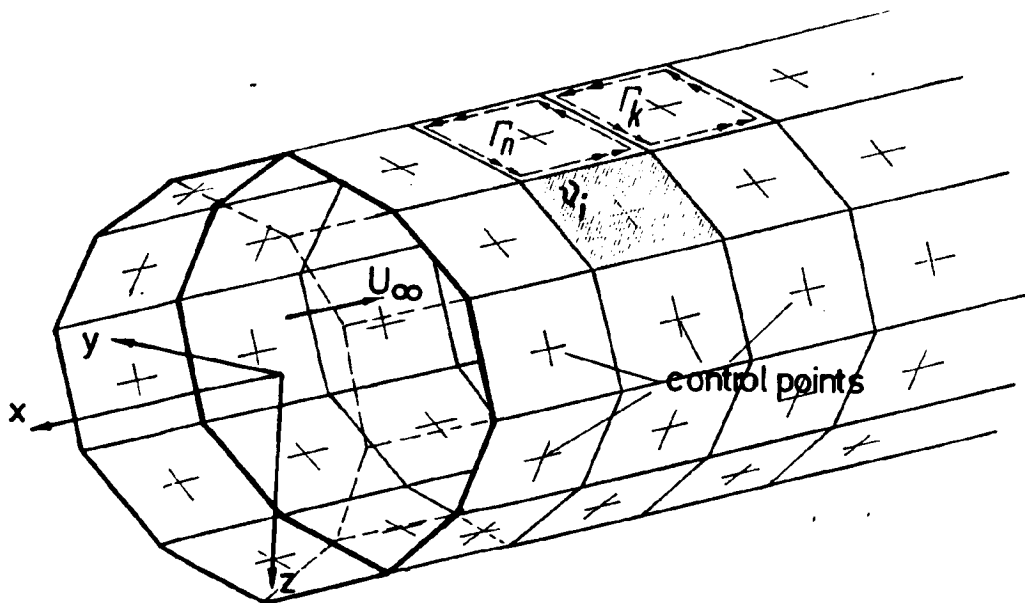


Figure 12.- Representation of tunnel walls by vortex squares.

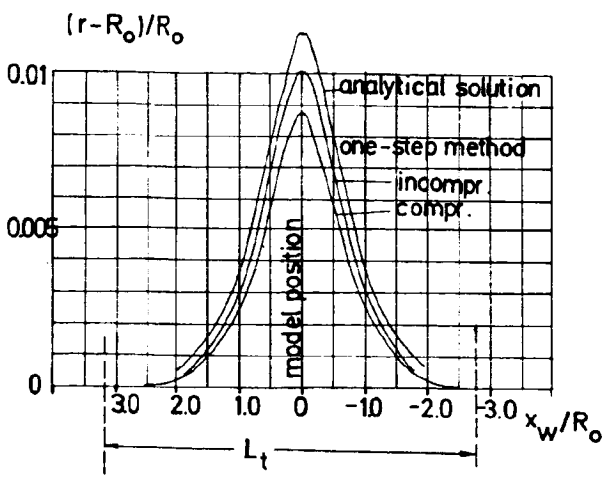


Figure 13.- Model-induced velocities at the wall for a single doublet ( $A_m/A_t = 0.075$ ).

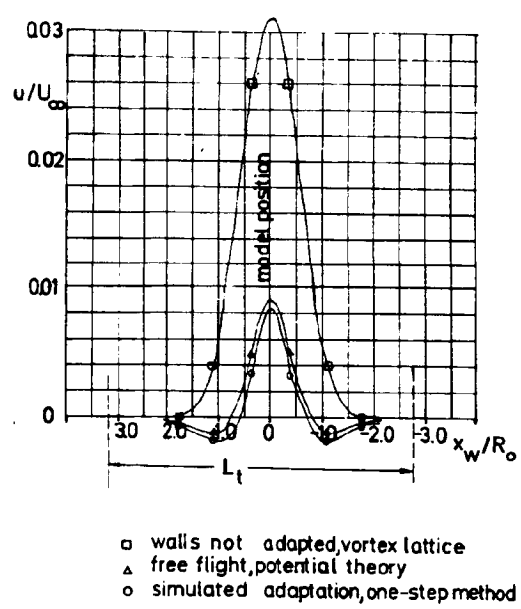


Figure 14.- Wall displacement, single doublet. Compare with figure 13.

ORIGINAL PAGE IS  
OF POOR QUALITY

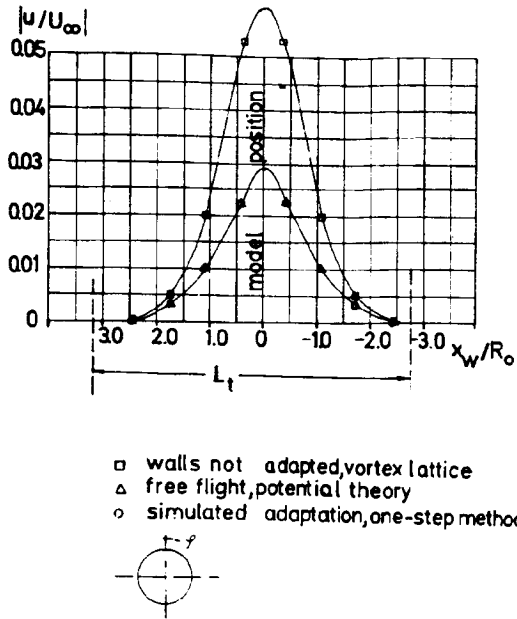


Figure 15.- Model-induced velocities at the wall for a lift generator.  $\zeta = 0$ .

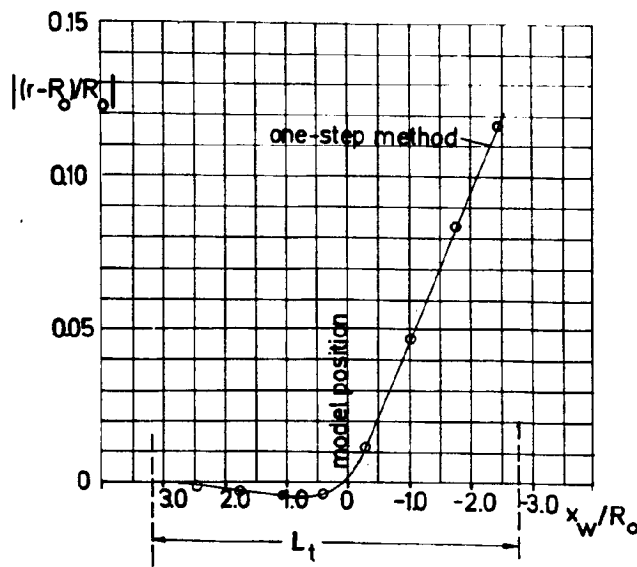


Figure 16.- Wall displacement, lift generator.  $\zeta = 0$ . Compare with figure 15.

N85 12015

24

TWO- AND THREE-DIMENSIONAL MODEL AND WALL DATA  
FROM A FLEXIBLE-WALLED TRANSONIC TEST SECTION\*

M. J. Goodyer and I. D. Cook  
Department of Aeronautics and Astronautics  
University of Southampton  
United Kingdom

\* This work was supported by NASA under grant NSG-7172 and by the British Science and Engineering Research Council.

## INTRODUCTION

The test section has impervious flexible top and bottom walls and therefore has two-dimensional control over the internal flow. With two-dimensional models this allows wall interference to be essentially eliminated at all conditions at least up to the walls becoming supercritical. The practice is to streamline and not to apply corrections, since attempts to apply corrections with our wall-data-based correction method were not reliable. Data bases of wall position, local Mach numbers, and model data are available mostly for walls-streamlined and walls-partially-streamlined cases. Examples are included from recent tests on a CAST-7 airfoil.

The same test section is now being used in three-dimensional testing, where the goal of testing completely free from wall interference is impossible. The philosophy is being adopted of providing the test section with sufficient static pressure tappings around and along its length to allow various measures of interference to be quantified. The principal interferences that the model experiences are wall-induced velocities in the streamwise and vertical directions. This induced velocity field can be manipulated by wall movement and hence the level of interference can be reduced. Information is included which illustrates the levels and types of control over test section flow which are possible by these means. An example of the level of interference experienced by a model in a transonic test with straight test section walls leads in turn to estimates of the wall movements required to eliminate the interference. (See fig. 1.)

2D: INTERFERENCE IS ELIMINATED BY ADJUSTMENTS BASED ON DATA TAKEN AT WALLS. CAST-7 DATA WILL ILLUSTRATE AGREEMENT BETWEEN VARIOUS FLEXIBLE-WALLED TUNNELS.

3D: INTERFERENCE CANNOT BE ELIMINATED BUT WALL ADJUSTMENTS CAN CONTROL & RELIEVE THE PRINCIPAL SOURCES OF WALL-INDUCED ERRORS.

THIS TALK WILL:

- GIVE ESTIMATES OF MAGNITUDES OF THE CONTROL WHICH MAY BE EXERCISED ON FLOW BY MOVEMENT OF ONE WALL JACK
- OUTLINE NEW WALL CONTROL ALGORITHM ( STILL IN ANALYTIC DEVELOPMENT STAGE ) BASED ON USE OF THIS DATA
- GIVE BRIEF EXAMPLES OF CONTROL OF WALL-INDUCED PERTURBATIONS IN REGION OF MODEL

Figure 1

### TRANSONIC FLEXIBLE-WALLED TEST SECTION LAYOUT

Both two- and three-dimensional model testing is being carried out in the transonic flexible-walled test section (fig. 2). The test section has flexible top and bottom walls with rigid sidewalls. It is 6 in. square, runs at atmospheric stagnation conditions, is injector driven, and has a closed circuit. Wall data (pressure and position) are used to automatically streamline the flexible walls. Each wall has 20 motor-driven jacks controlled on-line by a computer. Following streamlining, no corrections are applied to two-dimensional data. The relative sizes of typical models are indicated.

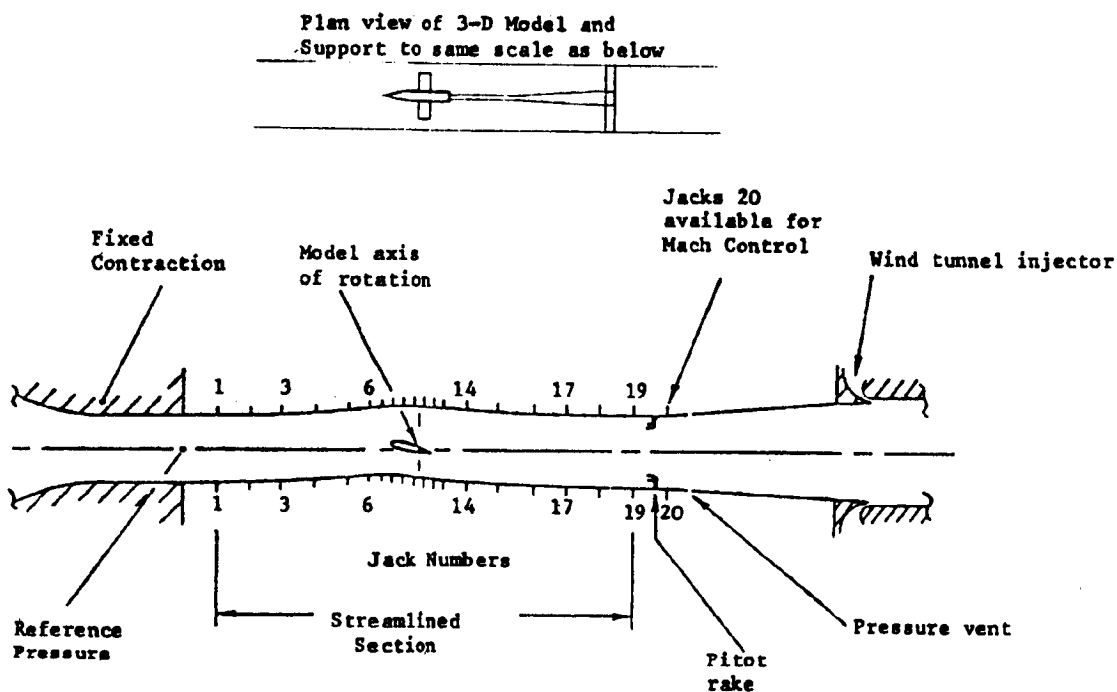


Figure 2

### CAST-7 AIRFOIL DATA COMPARISONS

Recently, eight European tunnels have been used in two-dimensional tests of the CAST-7 airfoil (ref. 1). Figure 3 shows results from five tunnels (Re between  $1.4 \times 10^6$  and  $2.5 \times 10^6$ ). Results from the two adaptive tunnels showed excellent correlation.

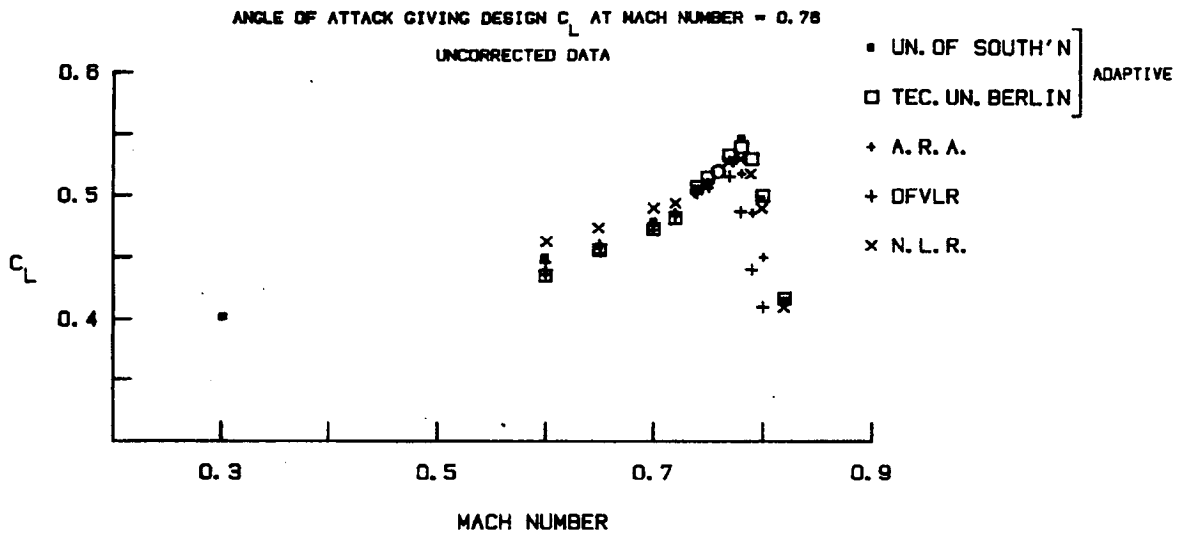


Figure 3

OF POOR QUALITY

# CAST-7 AIRFOIL DATA COMPARISONS

CFR 25.153  
CFR 25.155

Results from three flexible-walled adaptive tunnels show excellent agreement for maximum lift coefficient as a function of Reynolds number. Two trend lines are shown in figure 4, the upper for corrected data (including adaptive), and the lower for uncorrected data. The agreement shown in this unique comparison between results from three flexible-walled adaptive-test-section tunnels is encouraging.

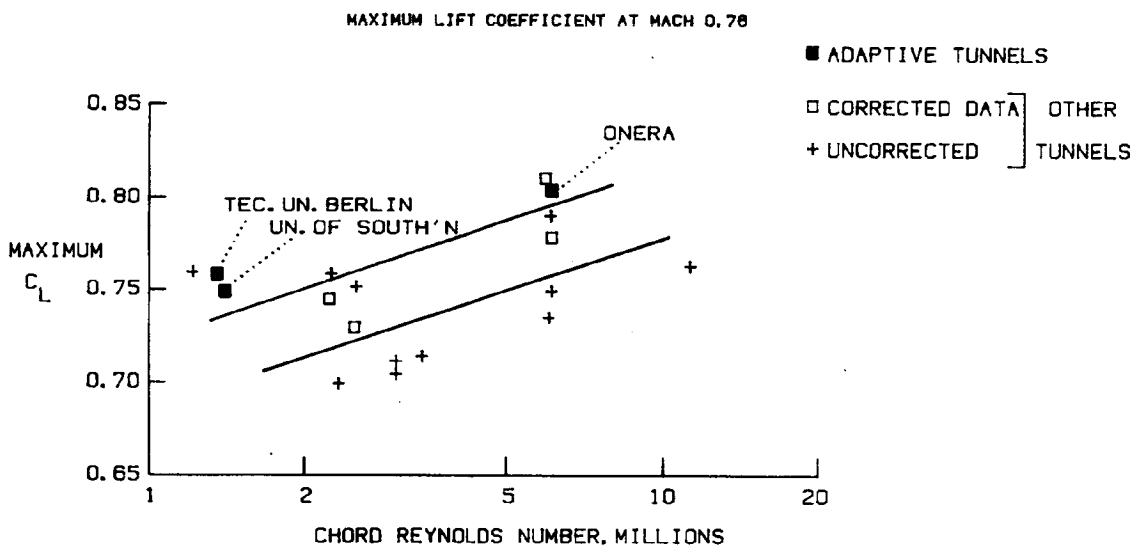


Figure 4

ESTIMATES OF PERTURBATIONS IN MACH NUMBERS  
INDUCED BY MOVEMENT OF A SINGLE JACK

Three-dimensional testing requires a new wall control algorithm. Wall data provide estimates of wall-induced perturbations in the region of the model. Data of the type shown in figure 5 can lead to a solution of the inverse problem, namely, the wall movement required to reduce the principal perturbations. The figure shows computations of perturbations induced near the centerline by moving one jack by a representative amount. The jack spacing corresponds to the closest one shown in figure 2. Information is also required for the other spacings.

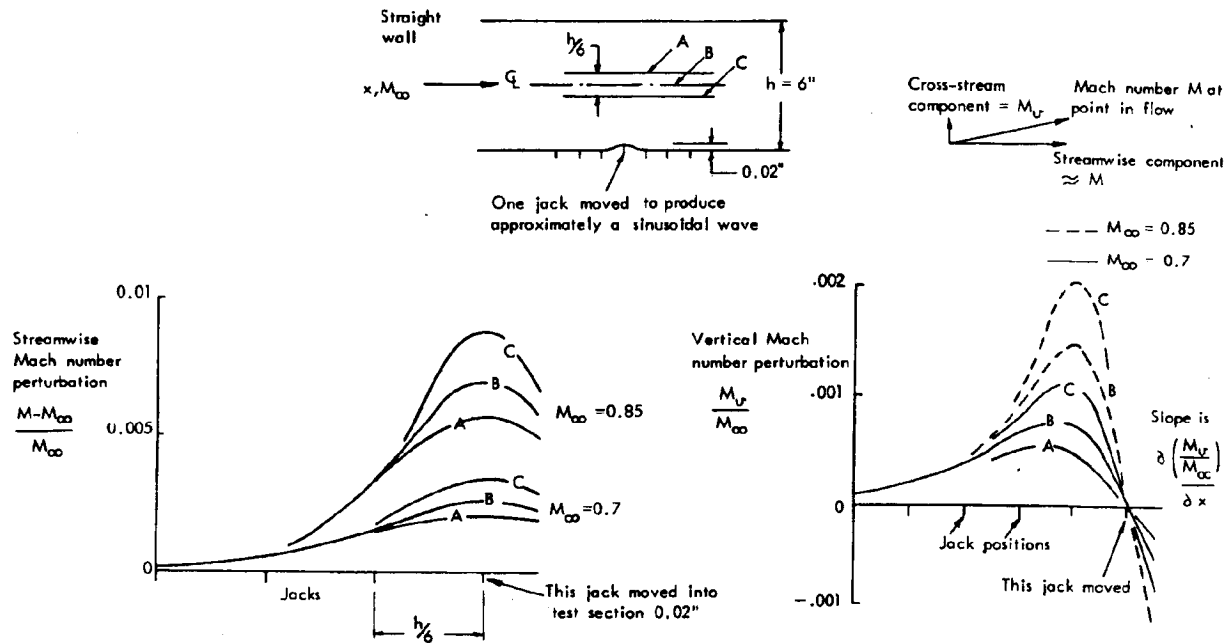


Figure 5

PERTURBATIONS ON CENTERLINE ABOVE SINGLE MOVED JACK

Figure 6 shows perturbations on the centerline as a function of the distance a single jack is moved into the tunnel and shows a strong sensitivity to Mach number. However, at each Mach number a roughly linear variation of perturbation with jack movement results. This linearity suggests that effects due to the movement of multiple jacks may be additive, thus simplifying the application of data in streamlining.

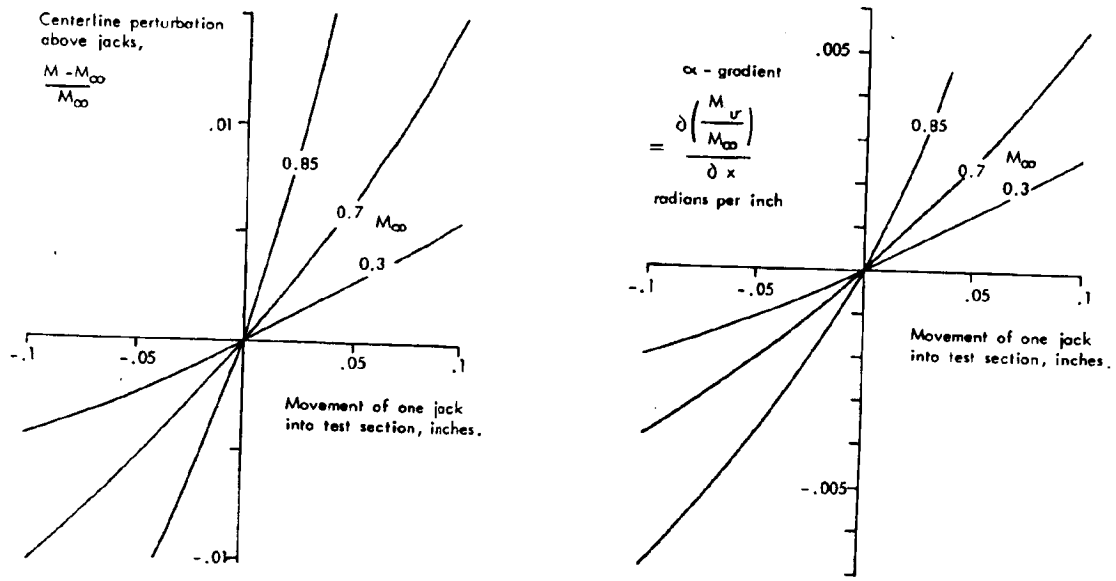
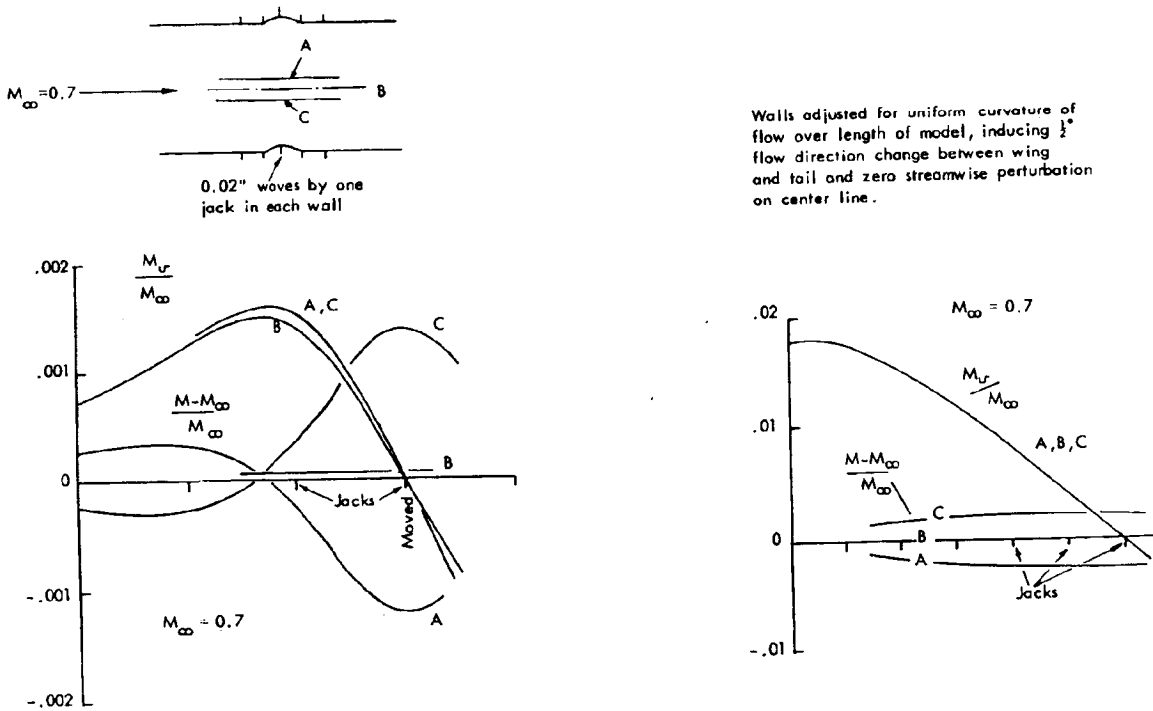


Figure 6

### ADDITIVE EFFECTS OF WALL MOVEMENT: TWO JACKS MOVED

Flexible walls can easily be adjusted to induce uniform velocity or Mach number perturbations in the streamwise ( $u$ ) and cross-stream ( $v$ ) directions as well as to induce a  $u$ -gradient. It is more difficult (but important) to induce a  $v$ -gradient. The example on the left in figure 7 shows results for the simple case in which two jacks have been moved in order to induce a  $v$ -gradient between them. Comparison between these results and those of figure 6 shows that the effects of moving two jacks are additive (i.e., along the centerline the  $u$ -perturbation is near zero). However, the constant  $v$ -gradient does not extend far enough along the test section in this example.

The sketch on the right in figure 7 illustrates a case in which many jacks are moved in order to induce a constant  $v$ -gradient well beyond the axial extent of a model. The maximum wall movement required was quite acceptable at 1/8 in.



Walls adjusted for uniform curvature of flow over length of model, inducing  $\frac{1}{2}^\circ$  flow direction change between wing and tail and zero streamwise perturbation on center line.

Figure 7

ORIGINAL PAGE IS  
OF POOR QUALITY

## SUMMARY

Figure 8 summarizes the current status of the research at the University of Southampton.

- 2D: INTERFERENCES FROM TOP & BOTTOM WALLS ARE ELIMINATED AT MACH NUMBERS TO WHERE THE WALLS BECOME SUPERCRITICAL. CORRECTIONS ARE NOT APPLIED. FACILITY IS AUTOMATED, USING A PREDICTIVE ALGORITHM & HAS RAPID RESPONSE. GOOD AGREEMENT IS SEEN BETWEEN SEVERAL ADAPTIVE FLEX WALL TUNNELS.
- CURRENT RESEARCH IS TOWARD USE OF MACH NUMBERS THROUGH UNITY.
- 3D: A PREDICTIVE ALGORITHM IS IN DEVELOPMENT TO GIVE TOP & BOTTOM WALL CONTOURS TO RELIEVE ALL WALL-INDUCED PERTURBATIONS IN THE STREAMWISE & VERTICAL DIRECTIONS. THE TECHNIQUE IS BEING EXPLORED INITIALLY WITH A CALIBRATED FORCE MODEL.

Figure 8

#### REFERENCES

1. Elsenaar, A.; and Stanewsky, E.: A Report of a Garteur Action Group on Two-Dimensional Transonic Testing Methods. NLR Report No. MP82043U. (Also in AGARD-CP-335, 1982.)
2. Wolf, S. W. D.; Cook, I. D.; and Goodyer, M. J.: The Status of Two- and Three-Dimensional Testing in the University of Southampton Transonic Self-Streamlining Wind Tunnel. Wall Interference in Wind Tunnels, AGARD-CP-335, 1982.

N85 12016

25

ASSESSMENT OF LIFT- AND BLOCKAGE-INDUCED WALL  
INTERFERENCE IN A THREE-DIMENSIONAL  
ADAPTIVE-WALL WIND TUNNEL

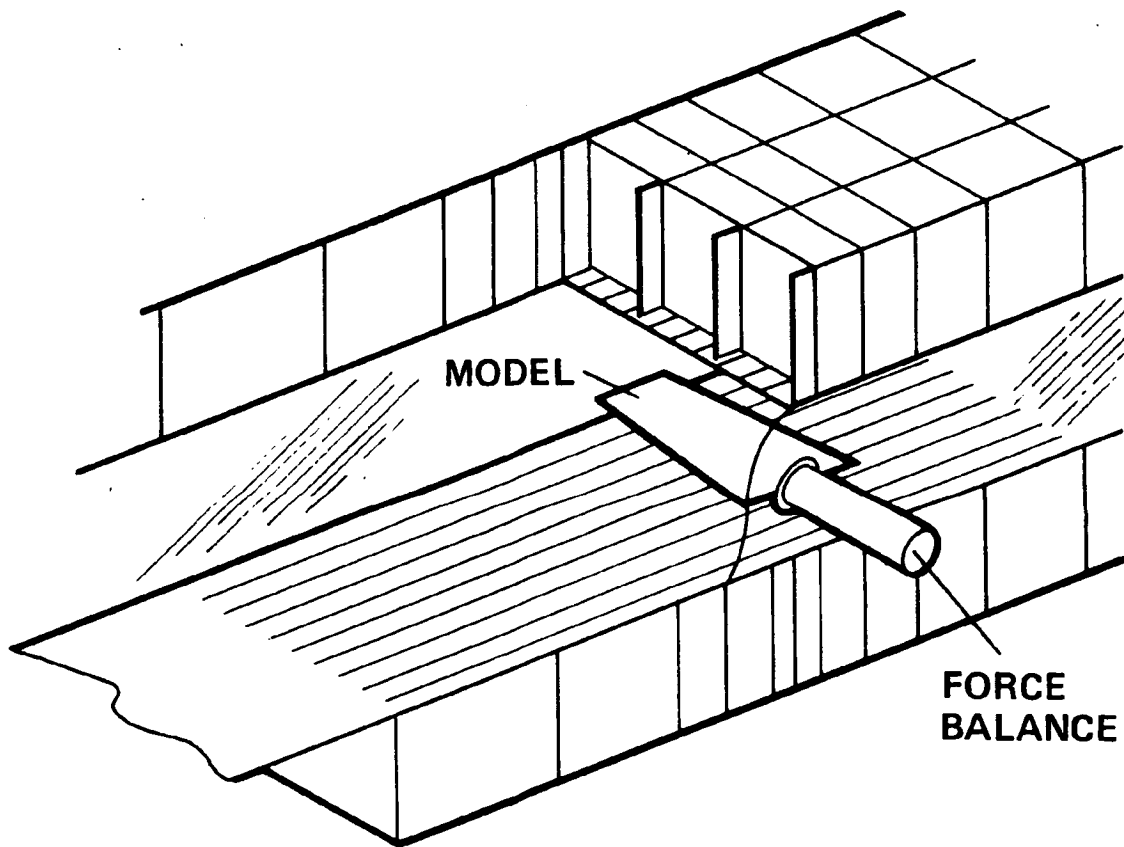
Edward T. Schairer  
NASA Ames Research Center  
Moffett Field, California

## INTRODUCTION

Recently, a three-dimensional adaptive-wall wind tunnel experiment was conducted at Ames Research Center (ref. 1). This experiment demonstrated the effects of wall interference on the upwash distribution on an imaginary surface surrounding a lifting wing. This presentation demonstrates how the interference assessment procedure used in the adaptive-wall experiments to determine the wall adjustments can be used to separately assess lift- and blockage-induced wall interference in a passive-wall wind tunnel. The effects of lift interference on the upwash distribution and on the model lift coefficient are interpreted by a simple horseshoe vortex analysis.

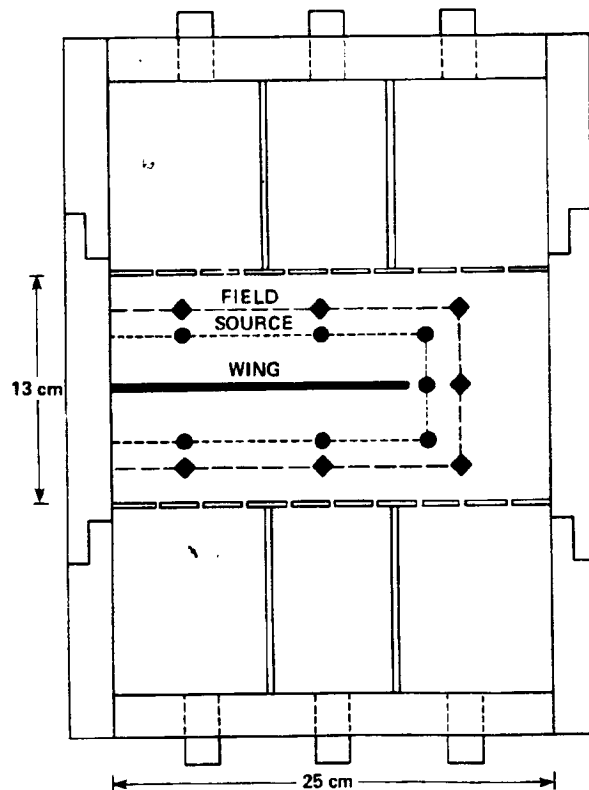
### ADAPTIVE-WALL TEST SECTION

The adaptive-wall experiments were conducted in the Ames 25-by 13-cm atmospheric indraft wind tunnel. The model was a semi-span wing supported by a force balance and was mounted to one sidewall of the test section. The sidewalls were solid plexiglass; the top and bottom walls were slotted. Separate top and bottom plenums were divided into streamwise and cross-stream compartments. Pressures in the compartments were independently adjustable. All the data presented at this workshop, however, were obtained with passive walls (i.e., no net mass flow through the walls). This configuration differs from a conventional passive ventilated wall since the partitions prevent circulation of the air in the plenums.



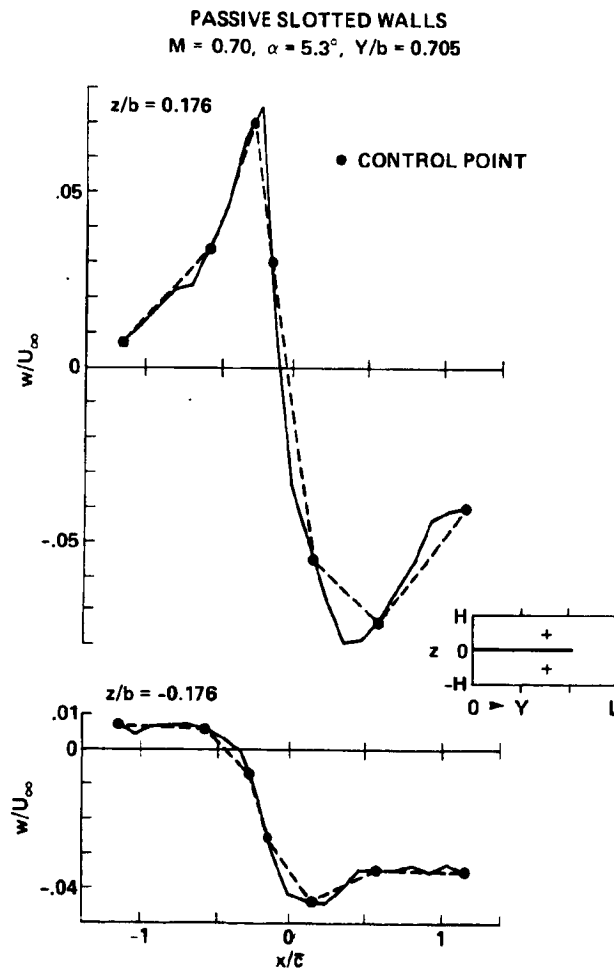
## INTERFERENCE ASSESSMENT PROCEDURE

A two-surface, one-velocity component interference assessment procedure was used (ref. 2). This figure illustrates in cross section the test section, the model, and the interference assessment surfaces. A laser velocimeter was used to measure vertical velocities (upwashes) at control points on the inner (source) and outer (field) interference assessment surfaces. The measured upwash distribution at the source surface was imposed as a near-field boundary condition, and free-air conditions were imposed at a fictitious far-field boundary. The corresponding free-air upwash distribution was computed in the region exterior to the source surface. Interference was assessed by comparing this "outer flow solution" with the measured upwashes at the control points on the field surface. The outer flow solution only approximated the true free-air solution since, for passive walls, the boundary conditions at the source surface included wall effects.



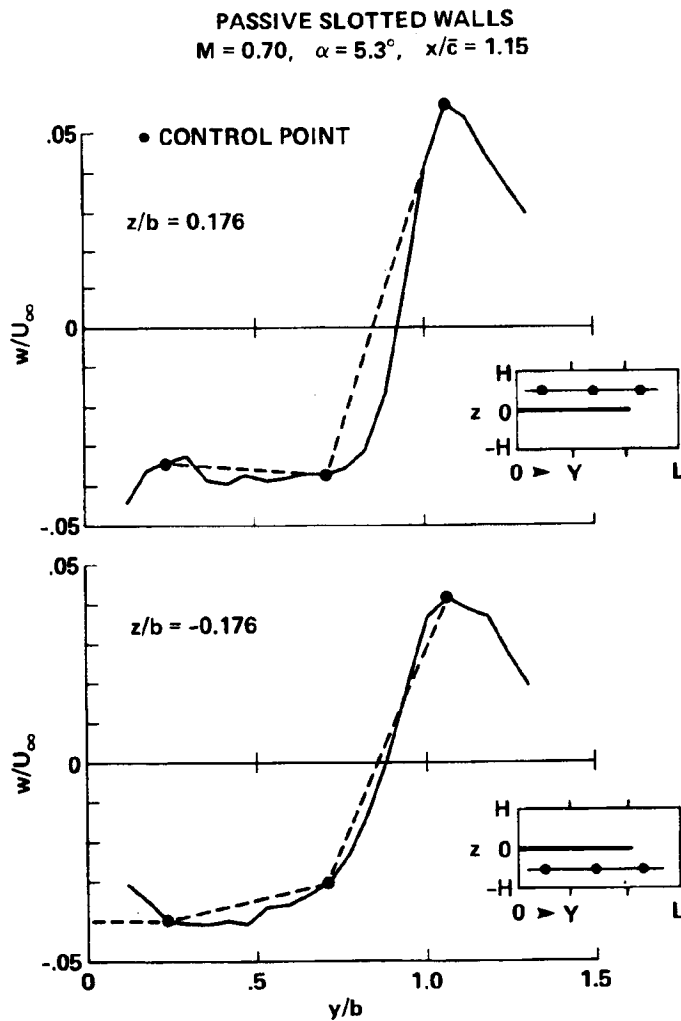
COMPARISONS OF ACTUAL AND INTERPOLATED VERTICAL VELOCITY  
 PROFILES ALONG AXIAL LINES ON THE SOURCE SURFACE

The boundary conditions at the source surface were interpolated from upwash measurements at 49 control points. The control points were located along seven axial lines. On each line, measurements were made at seven points between stations 1.15 mean aerodynamic chords ( $\bar{c}$ ) upstream and downstream of the model quarter chord. This figure compares upwash distributions obtained by linear interpolation between the control points with data obtained at more closely spaced intervals. The inset illustrates in cross section the locations of these measurements.



COMPARISONS OF ACTUAL AND INTERPOLATED VERTICAL VELOCITY  
 PROFILES ALONG SPANWISE LINES ON THE SOURCE SURFACE

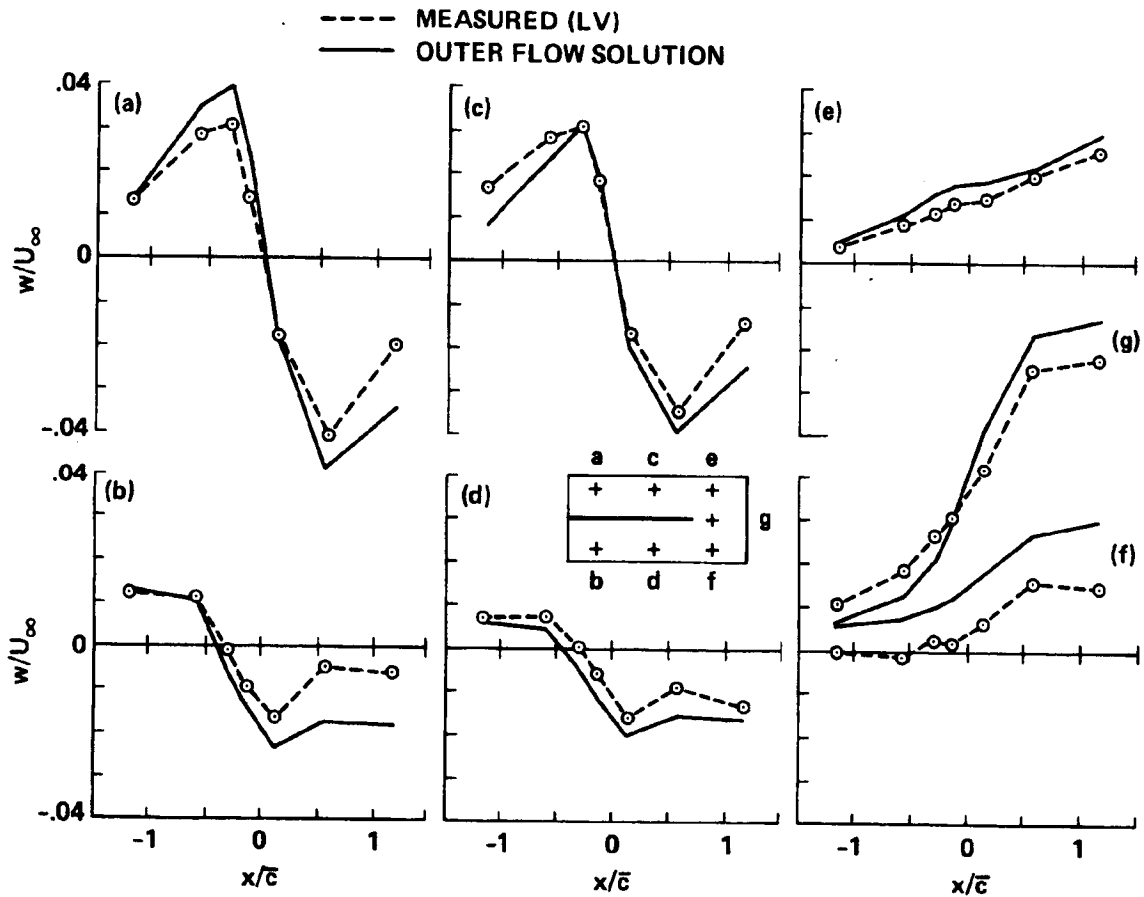
Spanwise upwash distributions at each longitudinal station were approximated by interpolating between measurements at three control points. The figure illustrates measurements made  $1.15 \bar{c}$  downstream of the wing quarter chord. Substantial interpolation errors are evident near the wing tip.



### PASSIVE-WALL INTERFERENCE ASSESSMENT

This figure compares vertical velocities measured at the field surface control points (circles) with the outer flow solution at the same points (solid line). Seven longitudinal upwash distributions are illustrated (see inset). Inboard of the wing tip and downstream of the model the outer flow solution is more negative than the measured downwash. This can be interpreted as a wall-induced upwash. Outboard and downstream of the wing tip the upwash predicted by the outer flow solution exceeds the measured upwash, indicating a wall-induced downwash.

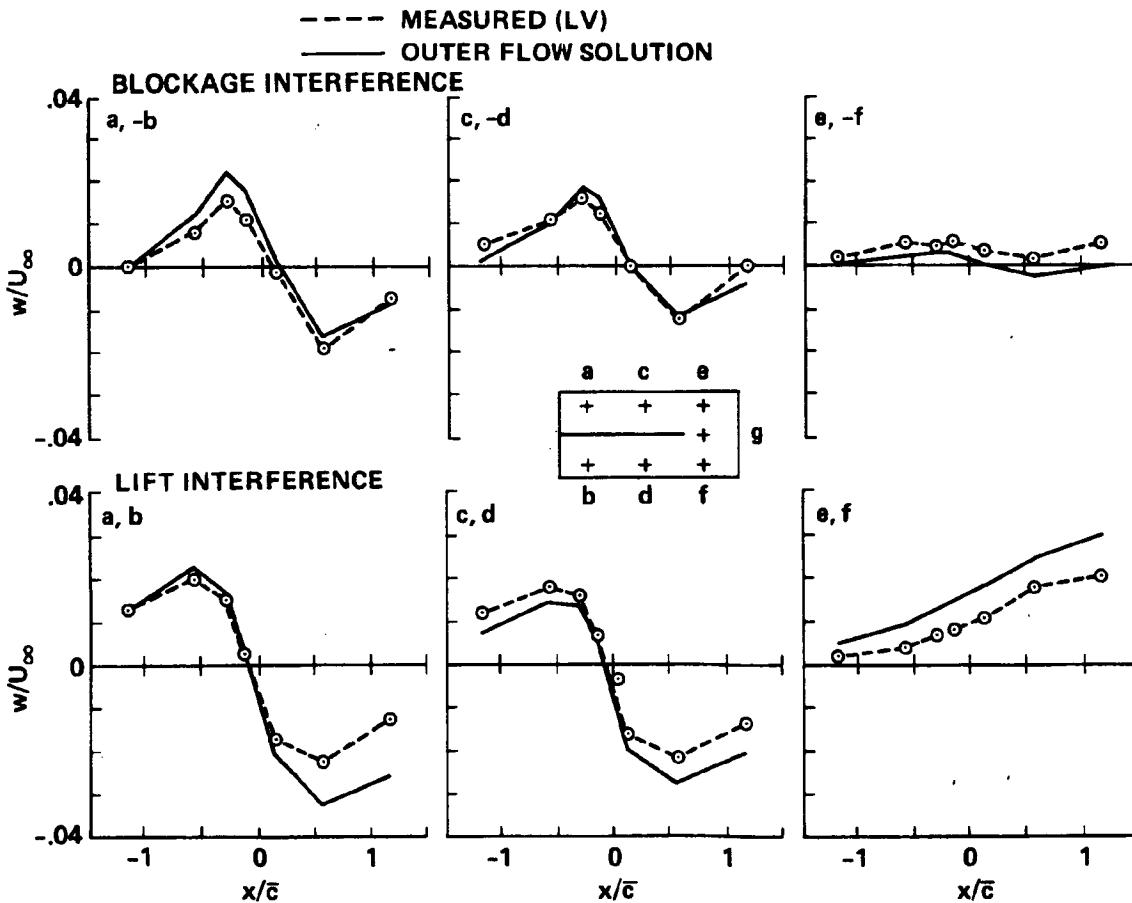
$M = 0.60, \alpha = 5.3^\circ$



## LIFT AND BLOCKAGE INTERFERENCES

The measured upwash distributions were separated into components which were symmetric and antisymmetric with respect to the plane of the wing. These components were associated with lift- and blockage-induced perturbations, respectively. The interference assessment procedure was applied separately to these components to assess lift and blockage interference. The effect of lift interference on the upwash distributions was greater than that of blockage interference. The most pronounced effect of the lift interference was to induce upwash downstream and inboard of the wing tip. Outboard of the tip, the walls induced downwash.

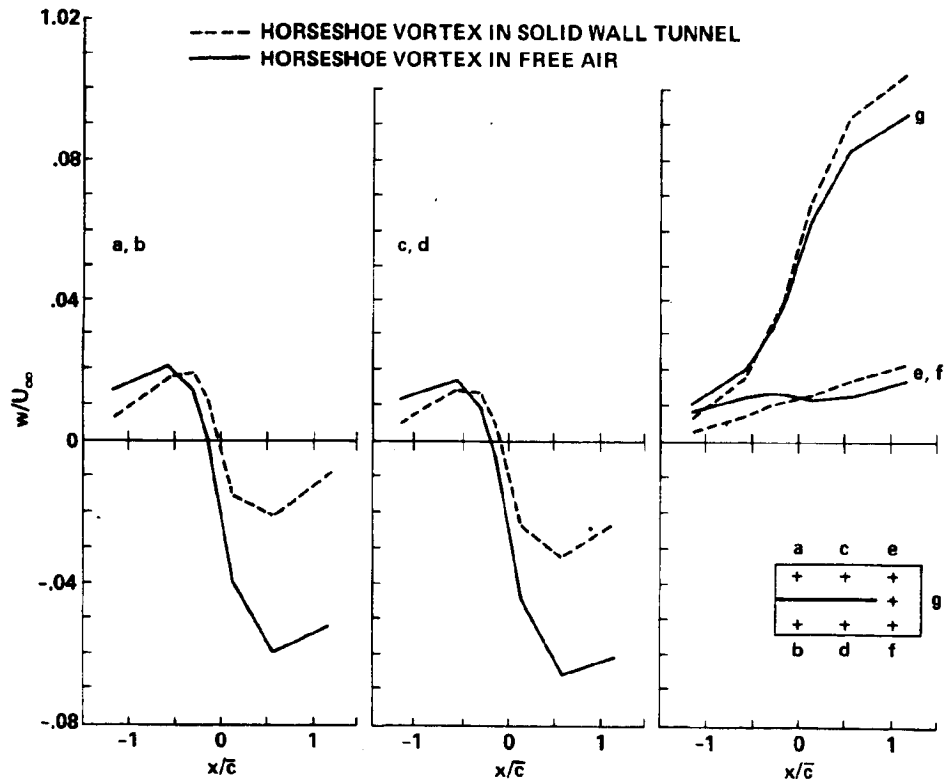
$M = 0.60, \alpha = 5.3^\circ$



### UPWASH DISTRIBUTIONS INDUCED BY A HORSESHOE VORTEX

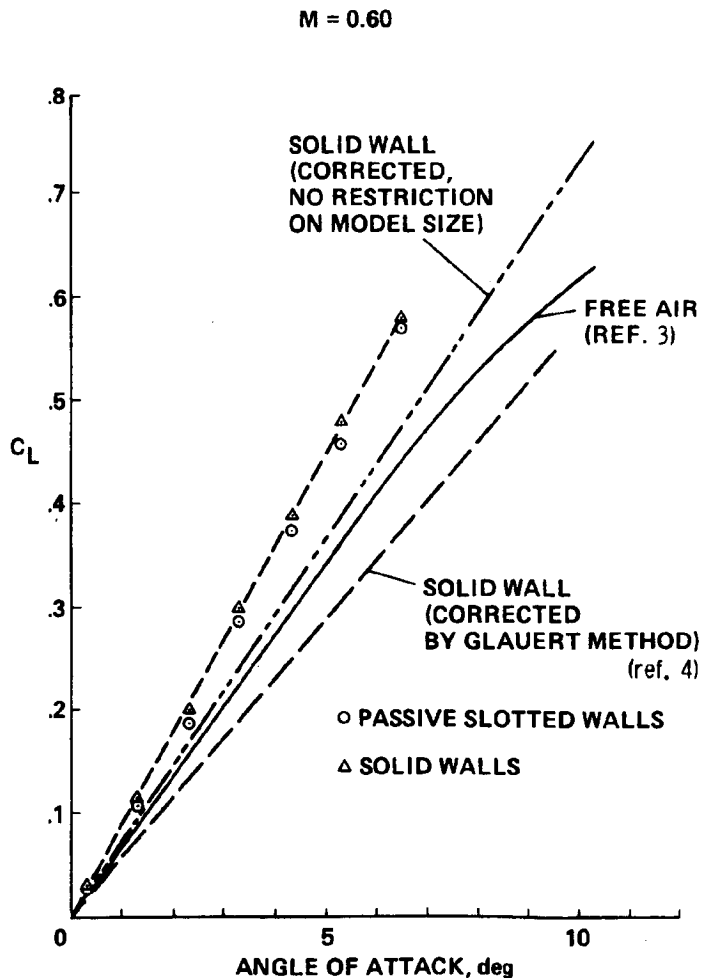
The lift interference was interpreted by comparing upwash distributions due to a horseshoe vortex in free air and a horseshoe vortex in a solid-wall tunnel. Downstream and inboard of the bound vortex the downwash is far greater for the vortex in free air than in the wind tunnel. This is consistent with the lift interference assessment in the previous figure. Outboard and downstream of the bound vortex, the free-air upwash is less than the in-tunnel upwash. Thus the walls induce upwash in this region. This conflicts with the lift interference assessment illustrated in the previous figure. This conflict is due in part to errors in the outer flow solution outboard and downstream of the wing tip. Errors occurred because the interpolated upwash distribution at the source surface did not accurately represent the actual distribution there. Interpolation errors were largest outboard and downstream of the wing tip.

$$\Gamma = 4.25 \text{ m}^2/\text{sec}, \quad U_\infty = 200 \text{ m/sec}$$



### COMPARISON OF LIFT CURVES WITH FREE-AIR DATA

This figure illustrates the passive-wall lift versus angle of attack of the model in the adaptive-wall test section. Passive slotted-wall and solid-wall (taped slots) data are presented. Two classical corrections for lift interference were applied to the taped-wall data, and the corrected lift curves are compared with free-air data (ref. 3). The Glauert method of images (ref. 4) overpredicts the angle-of-attack correction. This is not surprising since in his formulation Glauert assumes that the model span is small compared to the height of the wind tunnel. This condition is clearly violated in this experiment. An alternate correction, also computed by the method of images but without the assumption of a small model, undercorrects for the effects of wall interference.



## SUMMARY

This presentation has shown that data acquired in an adaptive-wall test section for the purpose of adjusting the tunnel walls can be used to qualitatively assess lift- and blockage-induced wall interference. The lift interference was interpreted by a horseshoe vortex analysis. Classical corrections for lift interference were applied to the measured lift coefficients, and the corrected data were compared with experimental free-air data.

## REFERENCES

1. Schairer, E. T. and Mendoza, J. P.: Adaptive-Wall Wind Tunnel Research at Ames Research Center. Wall Interference in Wind Tunnels, AGARD CP 335, 1982.
2. Davis, S. S.: A Compatibility Assessment Method for Adaptive-Wall Wind Tunnels, AIAA Journal, Vol. 19, Sept. 1981, pp 1169-1173.
3. Sleeman, W. C.; Klevatt, P. L.; and Linsley, E. L.: Comparison of Transonic Characteristics of Lifting Wings from Experiments in a Small Slotted Tunnel and the Langley High Speed 7- by 10-foot Tunnel, NACA RM LS1F14, November 5, 1951.
4. Glauert, H.: The Interference of Wind Channel Walls on the Aerodynamic Characteristics of an Airfoil, British ARC R&M No. 867, March 1923.

N85 12017

106

**A DATA BASE FOR THREE-DIMENSIONAL  
WALL INTERFERENCE CODE EVALUATION**

W. L. Sickles  
Calspan Field Services, Inc./AEDC Division  
Arnold AFS, Tennessee

## **NEED FOR EXPERIMENTAL EVALUATION**

A validation of a measured boundary condition technique is the only means to demonstrate the feasibility of a wall interference assessment/correction (WIAC) system. An experimental evaluation is also a means to compare performances of various techniques, to define the number of necessary boundary measurements for accurate assessment/corrections, to define the envelope of test conditions for which accurate assessment/corrections are achieved, and finally, to compare the relative merits of a WIAC system and an adaptive wall tunnel and integrate the two to complement each other.

- TO DEMONSTRATE THE FEASIBILITY OF A WIAC SYSTEM
- TO COMPARE VARIOUS TECHNIQUES
- TO DEFINE MEASUREMENT RESOLUTION
- TO DETERMINE ACCURACY OF THE ASSESSMENT/CORRECTION
- TO DEFINE ENVELOPE OF TEST CONDITIONS FOR ACCURATE A/C
- TO COMPARE AND INTEGRATE WIAC SYSTEM TO ADAPTIVE WALL TUNNEL

## REQUIREMENTS OF A WIAC DATA BASE

A suitable set of three-dimensional data for evaluating and comparing measured boundary conditions techniques should have the following features. Sufficient boundary measurement should be made for good spatial resolution. Measurements should be made far enough upstream and downstream of the model that they can be assumed as the infinity boundary conditions. Another desirable feature of the boundary data would be the measurement of two parameters, such as pressure and flow angle. This would allow evaluation with both one-variable and two-variable techniques.

The model data for this data base should include the following features. Of course, interference must be present and of sufficient amplitude. The model should be instrumented for lifting surface pressures and for forces and moments. The data base should also include interference-free reference data for verification of corrections. Reynolds number sensitivity should be well defined in order to separate wall interference effects from Reynolds number effects.

Simple model geometry would facilitate computational modeling. Data should exist for a variety of test conditions ranging from subcritical to strongly supercritical flows.

### 1. BOUNDARY DATA

- ADEQUATE SPATIAL RESOLUTION
- UPSTREAM AND DOWNSTREAM OF MODEL
- TWO MEASUREMENT PARAMETERS

### 2. MODEL DATA

- INTERFERENCE MUST EXIST
- FORCES AND MOMENTS
- WING SURFACE PRESSURES
- INTERFERENCE-FREE REFERENCE DATA
- VARIETY OF TEST CONDITIONS
- SIMPLE MODEL GEOMETRY
- WELL DEFINED  $Re$  SENSITIVITY

### 3. ADDITIONAL

- AVAILABLE TO WIAC COMMUNITY
- AVAILABLE IN TIME TO MEET DEMAND

## **AEDC WIAC DATA BASE**

As a by-product of the adaptive wall demonstration effort at AEDC, a complete set of experimental data will soon be available. As will be shown, this data will be well suited for WIAC evaluation and meets the aforementioned requirements. This data is being obtained in the AEDC Adaptive Wall Demonstration Tunnel (1T).

- **OBTAINED IN AEDC ADAPTIVE WALL DEMONSTRATION TUNNEL (1T)**
- **MEETS THE AFOREMENTIONED REQUIREMENTS**

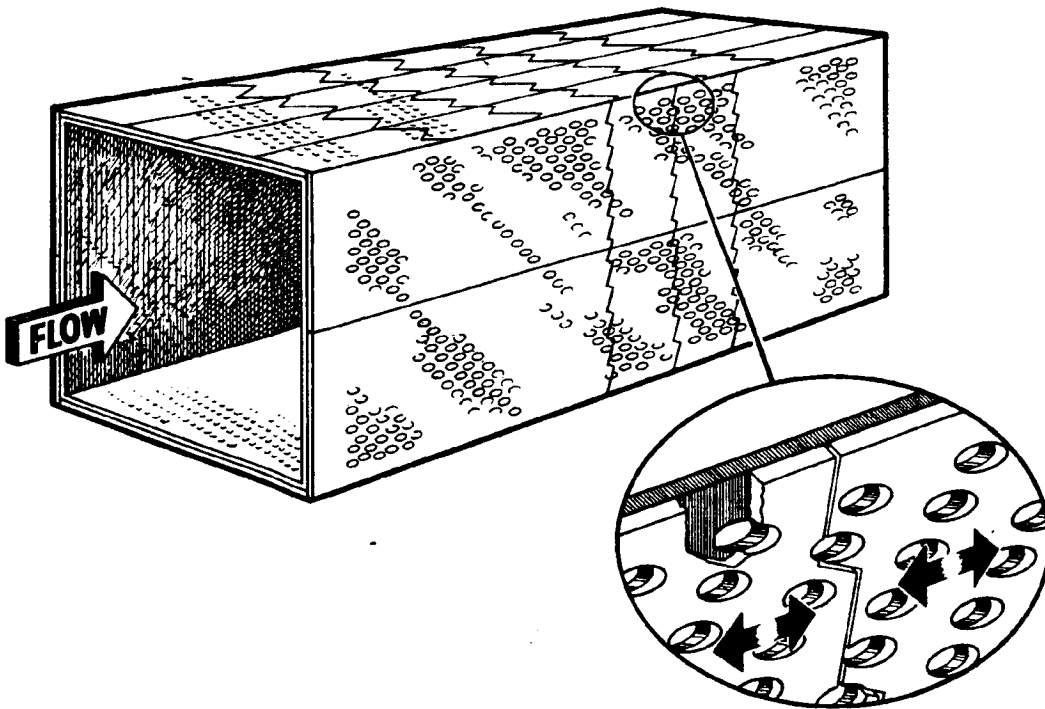
### **AEDC TUNNEL 1T**

Tunnel 1T is a continuous-flow, nonreturn wind tunnel equipped with a two-dimensional, flexible nozzle and an auxiliary plenum evacuation system. The tunnel test section is one foot square and 37.5 inches in length.

## SEGMENTED, VARIABLE-POROSITY TEST SECTION

The AEDC Adaptive Wall Demonstration Tunnel has a one-foot-square test section with segmented, variable-porosity walls for active wall control. There is a total of sixty-four individually controlled segments, twenty-four on the top and bottom and eight on each side. The porosity of each segment can be varied from approximately eight percent to zero percent open-area ratio.

ORIGINAL PHOTO  
OF POOR QUALITY

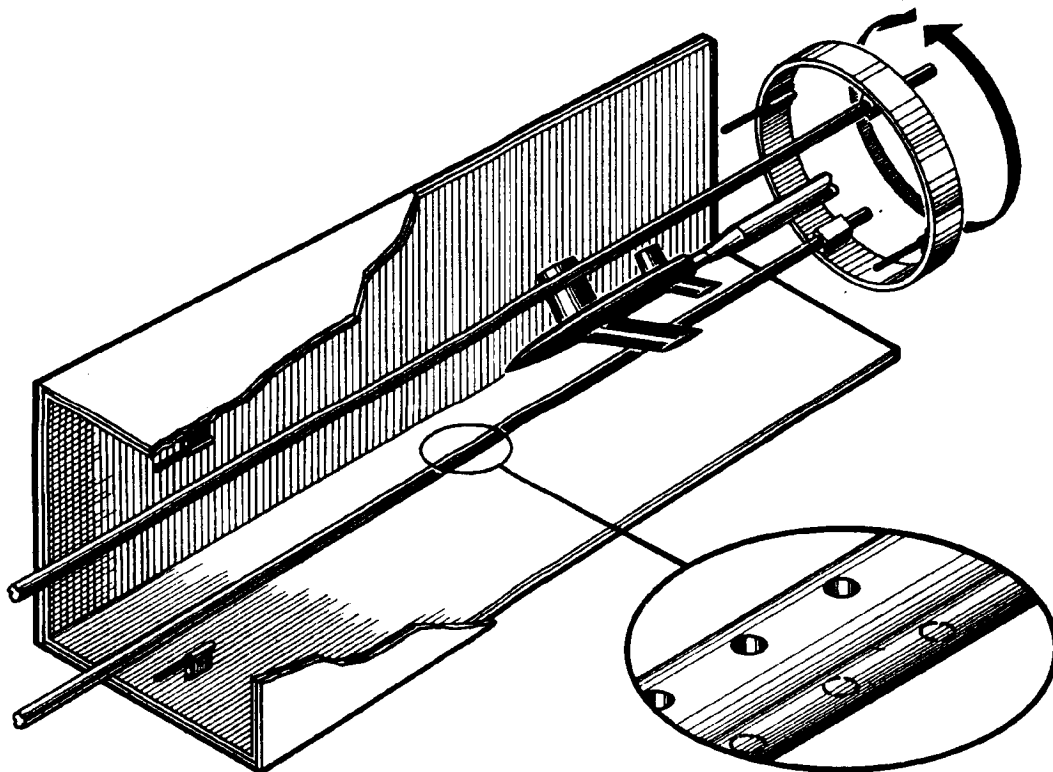


### INTERFACE FLOW VARIABLE MEASUREMENT SYSTEM

The measurement surface boundary data is performed with a system of two rotating pipes. These pipes sweep out a cylindrical measurement surface near the tunnel walls, approximately one inch from the wall at the closest point. Each static pipe is equipped with forty pairs of diametrically opposed orifices. The diameter of the pipe is 5/8 inch. The pressure and the difference in the pressures for each pair are used to determine the components of velocity in the streamwise direction and in the surface normal direction ( $u$  and  $v$ ).

The measurement system offers good resolution of measurements. The longitudinal distribution of measured pressure is well defined by making measurements far upstream and downstream of the model and by making finely spaced measurements in the anticipated regions of large gradients. The rotating pipe system allows one to make measurements at as many azimuthal positions as necessary to adequately define the azimuthal variations.

The flow angle probes at the upstream and downstream are used in the calculation of the  $v$ -velocity distributions.



## DETERMINATION OF TWO VELOCITY COMPONENTS

The two velocity components are determined by the following equations. These equations are derived from potential flow theory for a cylinder in a cross flow. A detailed derivation of these equations can be found in Ref. 1.

The integration to determine the longitudinal distributions of  $v$  is performed in two intervals. First, we determine the peak in the pressure distributions, minimum  $C_p$ . The location of  $C_{p \min}$  segments the region into an upstream region and a downstream region. Integration in the upstream regions is performed from far upstream to the peak, and integration in the downstream region is performed from far downstream back to the peak. The integration constants for the two regions are measured by upstream and downstream flow angle probes.

### 1. EQUATIONS

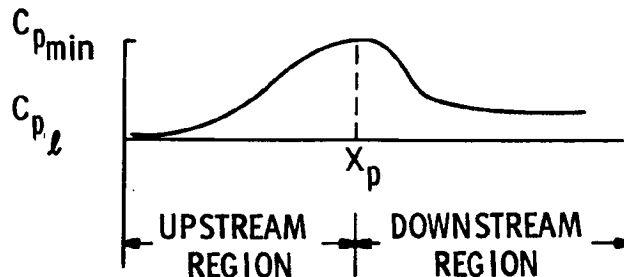
$$u(x) = - \frac{C_{p_l}(x) + C_{p_u}(x)}{4}$$

$$v(x) = v_0(x) + \int_{x_0}^x v'(\xi) d\xi$$

$$\text{where } v'(x) = \frac{C_{p_l}(x) - C_{p_u}(x)}{8\delta}$$

( $\delta$  = RADIUS OF PIPE)

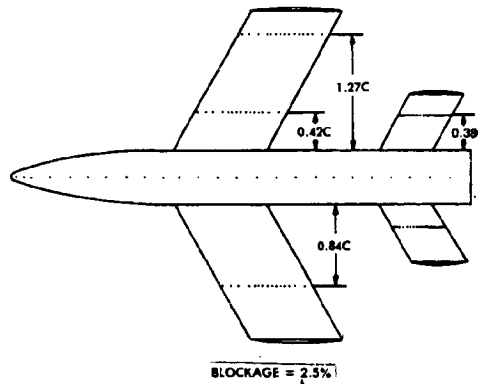
### 2. INTEGRATION



## EXPERIMENTAL MODEL

The experimental model was specially designed and fabricated for the adaptive wall experiments. The model is a wing/tail/body configuration with swept lifting surface. The simple design allows for easy computational modeling. The model has a model-to-tunnel solid blockage ratio of 2.5 percent, which is large enough to generate a significant amount of interference. The lifting surfaces have NACA-0012 airfoil sections with constant chord and are instrumented for chordwise pressure distributions at various span locations on the upper and lower surfaces. The sting support is an integral part of the model and is gauged to measure normal force and pitching moment. Reference data for this model were taken in AEDC Tunnel 4T where the data are assumed to be free of wall interference since the model-to-tunnel solid blockage ratio is 0.156 percent. Model data will be taken in the adaptive-wall tunnel at a variety of test conditions and at a variety of wall porosities including a standard uniform porosity and fully adapted walls. The model data with fully adapted walls constitutes an additional set of reference data which eliminates the questions of uncertainty in the data due to installation, flow uniformity, or Reynolds number effects.

- SWEPT WING/HORIZONTAL TAIL/BODY
- SOLID BLOCKAGE RATIO - 2.5 PERCENT
  - 12 INCH LENGTH
  - 8.4 INCH WING SPAN
  - 2.4 INCH WING CHORD
- NACA-0012 LIFTING SURFACE
- FORCE AND PRESSURE INSTRUMENTED
- REFERENCE DATA OBTAINED IN TUNNEL 4T
  - $0.6 \leq M_{\infty} \leq 1.2$
  - $-8 \leq \alpha \leq 12$  DEG.
  - $0.69 \times 10^6 \leq Re_c \leq 0.99 \times 10^6$
- REFERENCE DATA WILL ALSO BE DETERMINED IN JT WITH FULLY ADAPTED WALLS TO ELIMINATE QUESTIONS OF INSTALLATION, FLOW UNIFORMITY, OR REYNOLDS NUMBER EFFECTS



## **STATUS OF AEDC ADAPTIVE WALL TUNNEL**

The adaptive-wall test section has been installed. All the wall control hardware and software systems have been checked out and are fully operational. The model was installed in January 1983 and baseline data are now being obtained.

- ADAPTIVE WALL TEST SECTION HAS BEEN INSTALLED
- ALL HARDWARE AND SOFTWARE SYSTEMS CHECKED OUT
- MODEL IS INSTALLED
- BASELINE DATA IS NOW BEING OBTAINED

## SUMMARY OF AEDC WIAC DATA BASE

The boundary data taken in Tunnel 1T with the rotating pipe system has been shown to offer several attractive features for WIAC code evaluation. Good spatial resolution of measurements is achieved and measurements are made upstream and downstream of the model. Also, two velocity components are determined.

The completeness of the model data is another strong point of this data set. The model data will include forces and moments, and lifting - surface pressure distributions. Interference-free reference data will exist from Tunnel 4T and from the fully adjusted adaptive wall tunnel.

This data base will soon be obtained and compiled. Requests for this data should be submitted to the address below.

### 1. BOUNDARY DATA TAKEN WITH ROTATING PIPE SYSTEM

- GOOD RESOLUTION
- UPSTREAM AND DOWNSTREAM MEASUREMENTS
- TWO VELOCITY PARAMETERS

### 2. MODEL DATA

- SIMPLIFIED MODEL
- FORCES AND MOMENTS
- WING SURFACE PRESSURES
- INTERFERENCE-FREE REFERENCE DATA (4T AND ADAPTIVE WALL)
- VARIETY OF TEST CONDITIONS

### 3. AVAILABILITY

- SUBMIT REQUEST FOR DATA TO

DR. K. L. KUSHMAN  
AEDC/DOT  
MS 900  
ARNOLD AFS, TN 37389

## **A WIAC MEASUREMENT SYSTEM**

Current conceptual designs of a WIAC measurement system call for a large number of pressure measurements to be made on or near tunnel walls. The conventional method for making multiple pressure measurements uses Scanivalves®. Although these devices are reliable, they are time consuming and there is concern about their impact on productivity. Ideally, one wants a measurement system that keeps pace with the rate at which model data is taken.

A WIAC measurement system that uses electronically scanned pressure measuring (ESPM) modules to rapidly acquire pressures on three fixed static pipes near the tunnel walls was demonstrated in AEDC Tunnel 4T. The acquisition of pipe pressures was able to keep pace with acquisition of model forces and pressures. This demonstrates the feasibility of making large numbers of pressure measurements without impacting productivity.

- **REQUIRES LARGE NUMBER OF PRESSURE MEASUREMENTS**
- **CONCERNED ABOUT IMPACT ON PRODUCTIVITY USING CONVENTIONAL SCANIVALVE®**
- **A WIAC MEASUREMENT SYSTEM THAT USES ELECTRONICALLY SCANNED PRESSURE MEASURING (ESPM) MODULES WAS DEMONSTRATED IN AEDC TUNNEL 4T**
- **DEMONSTRATES THE FEASIBILITY OF MAKING LARGE NUMBER OF PRESSURE MEASUREMENTS WITHOUT IMPACTING PRODUCTIVITY**

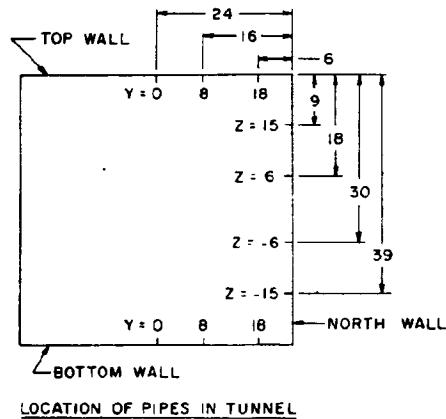
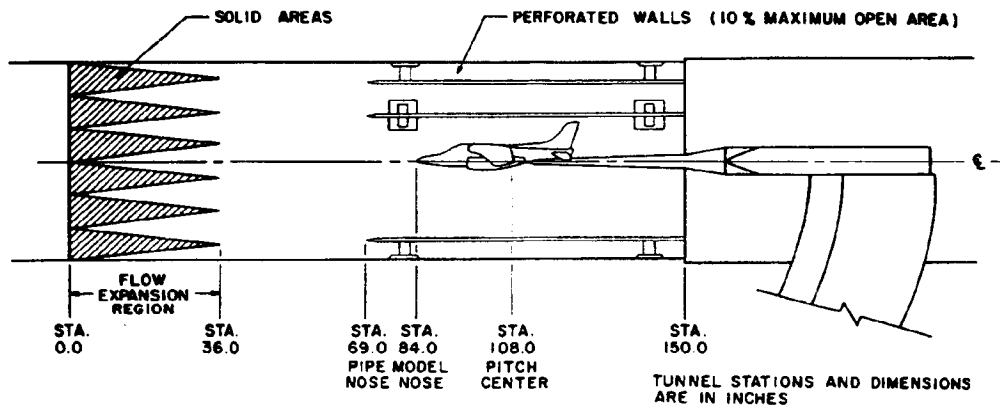
## AEDC 4T EXPERIMENT

The purpose of this test was to obtain wind tunnel data with probable wall interference effects. The model data is to be compared with both flight test data and reference data obtained in Tunnel 16T. The boundary data was obtained for the purpose of assessing wall interference.

- OBTAINED MODEL DATA FOR TUNNEL-TO-TUNNEL CORRELATION
- OBTAINED BOUNDARY DATA FOR INTERFERENCE ASSESSEMENT

## TUNNEL 4T WIAC INSTALLATION

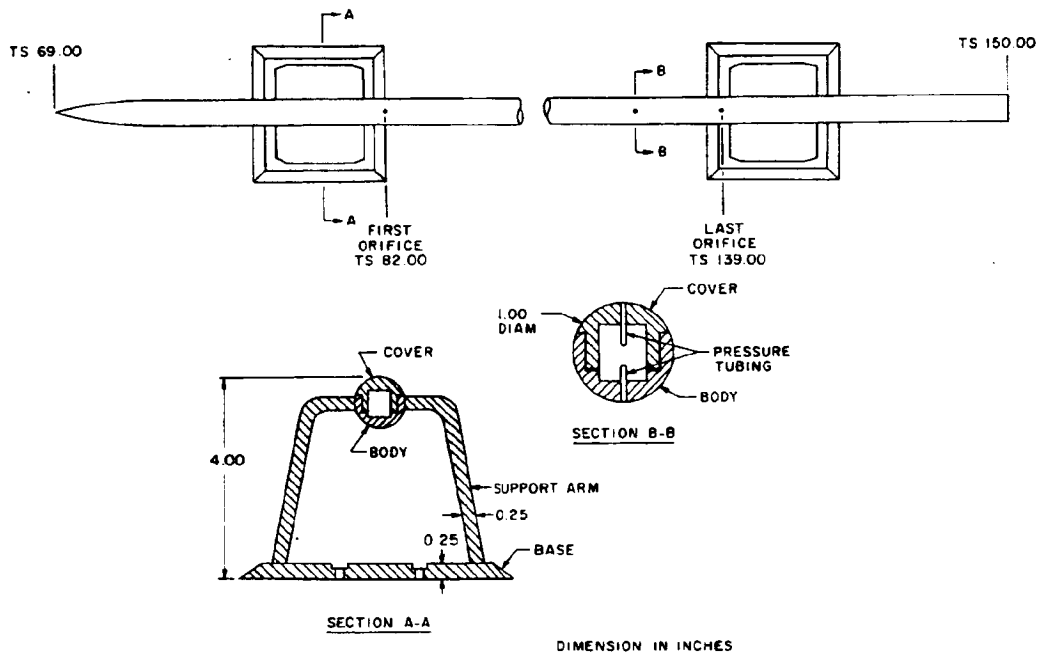
A schematic of the Tunnel 4T installation is shown below. The relative location of the pipes and model are illustrated. The pipes are mounted on the top, bottom, and side walls. The test matrix was run with the pipes located at three different locations on the top and bottom walls and four locations on the side wall. Lateral symmetry is assumed so that the boundary data is only obtained on one side of the tunnel.



ORIGINAL FILED IN  
OF FOUR QUARTERS.

### TUNNEL 4T STATIC PRESSURE PIPES

The construction of the static pressure pipes and mounting brackets is shown below. The three pipes are one inch in diameter and each contains thirty pairs of diametrically opposed orifices. The pipes are constructed with a removable cover for repairing damaged tubing. The pipes are mounted to the wall by a fore and aft plate and are suspended four inches from the wall by support arms.



## REFERENCE

1. Nenni, J. P., Erickson, J. C. Jr., and Wittliff, C. E., "Measurement of Small Normal Velocity Components in Subsonic Flows by Use of a Static Pipe." AIAA Journal, Vol. 20, No. 8, August 1982.

SESSION III

WALL SUCTION EFFECTS AND DATA

Chairman: L. H. Ohman, NAE

N85 12018

D7

INVESTIGATIONS OF FLOW FIELD PERTURBATIONS  
INDUCED ON SLOTTED TRANSONIC-TUNNEL WALLS

J. M. Wu and F. G. Collins  
Gas Dynamics Division  
The University of Tennessee Space Institute  
Tullahoma, TN

APPROVED FOR RELEASE 1987 BY NSA

Preceding page blank

## ABSTRACT

The free-stream interference caused by the flow through the slotted walls of the test sections of transonic wind tunnels has continuously presented a problem in transonic tunnel testing. The problem of wall interference appears in the imposing constraints presented by the partially ventilated walls, which take the form of a resistance to the flow normal to the walls. The adaptive-wall transonic tunnel is designed to actively control the near-wall boundary conditions by sucking or blowing through the wall. This may introduce even larger near-wall flow field perturbations.

In order to make the adaptive-wall concept work, one must know two flow parameters for computational boundary conditions. These parameters must be measured with sufficient accuracy to allow numerical convergence of the flow field computations and must be measured in an inviscid region away from the model that is placed inside the wind tunnel. We have been engaged in the measurement of the near-wall flow field perturbations for the past two and one-half years with the support of the NASA Ames Research Center. The near-wall flow field was mapped in detail using a five-port cone probe that was traversed in a plane transverse to the free-stream flow. The initial experiments were made using a single slot and recent measurements used multiple slots, all with the tunnel empty. The projection of the flow field velocity vectors on the transverse plane revealed the presence of a vortex-like flow with vorticity in the free stream. These results were discussed in the presentation. Our current research involves the measurement of the flow field above a multislot system with segmented plenums behind it, in which the flow is controlled through several plenums simultaneously. This system would be used to control a three-dimensional flow field. Research to be performed on this configuration was also discussed.

### UTSI TRANSONIC WIND TUNNEL

Three-dimensional flow field measurements were made near a single-slotted and multislotted transonic wind tunnel wall. Velocity and static pressure distributions were obtained above the wall for Mach numbers ranging from 0.6 to 0.9 and wall suction strengths varying from zero (natural flow into the plenum chamber) to 0.25 standard  $\text{m}^3/\text{s}$  (530 SCFM). The measurements were made in the UTSI transonic wind tunnel. The tunnel is of the blow-down type with a test section measuring 0.34 m wide by 0.28 m high and 2.66 m long. The test section is topped along its entire length with a plenum chamber which is connected to the test section through a porous plate having about a 30% open area. No external suction or blowing was applied to the upper plenum. Figure 1 shows the UTSI transonic wind tunnel test section with the model wall on the tunnel floor.

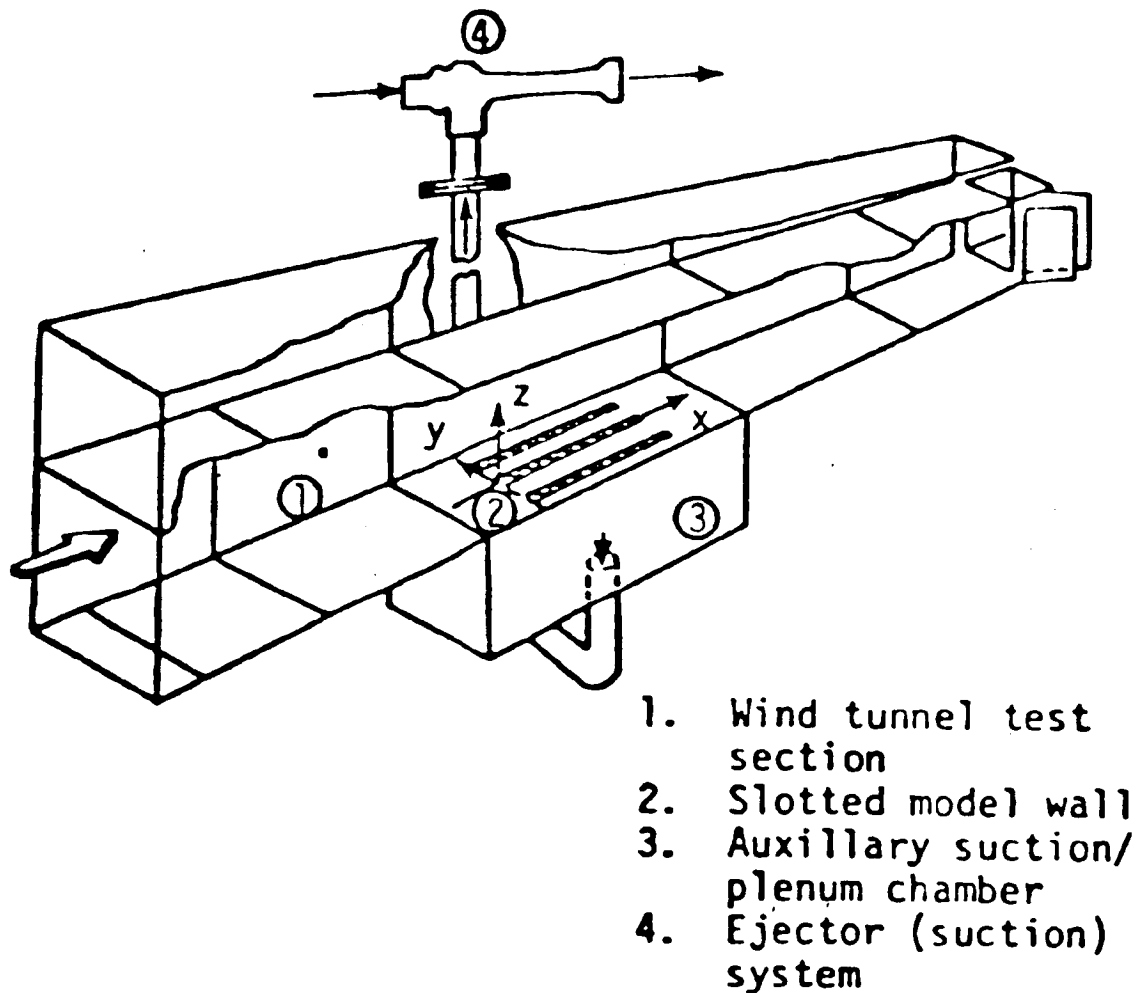


Figure 1.

### WALL MODEL

A model of a section of a slotted-wall test section similar to that which exists in the 11 x 11 ft. transonic tunnel at NASA Ames Research Center was constructed and mounted on the test section wall. The model contained three slots, one on the tunnel centerline and one on each side, separated from the centerline by 0.051 m. Inserts could be placed in the slots to vary the width, upstream geometry and edge geometry. The first measurements were performed on a single slot on the tunnel centerline measuring 0.0066 m wide and 0.36 m long (ref. 1). The leading edge was perpendicular to the flow direction. Zigzag baffles with  $14^\circ$  slant angle were used to direct the flow in the slots (fig. 2).

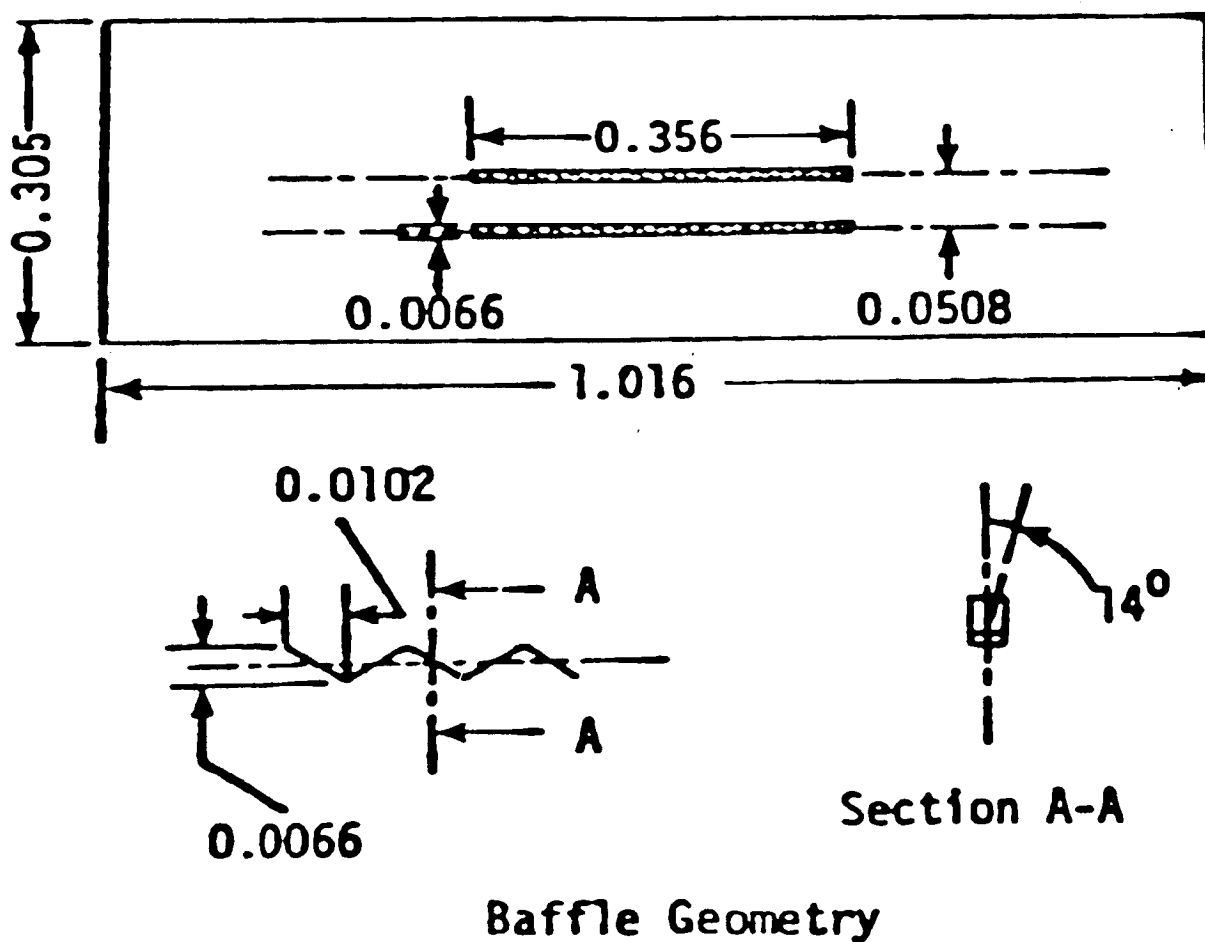


Figure 2.

### WALL SLOT GEOMETRY

The present measurements were performed on a single slot on the tunnel centerline and on three slots. The slots were 0.66 m long, 0.0065 m wide and had a tapered upstream end with  $6^\circ$  included angle (fig. 3). All edges were sharp.

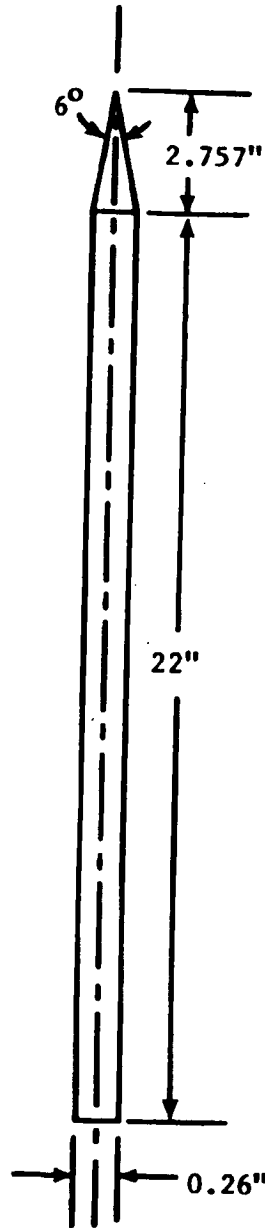


Figure 3.

## WALL PLENUM CHAMBER

A separate plenum chamber was provided below the slotted-wall model. Suction to the chamber was provided by two air-operated ejector pumps. The suction rate was measured by a sharp-edge orifice plate flow meter that was placed in the pipe. Four rows of static pressure orifices were installed on the plenum chamber plate. They ran longitudinally at the center of the solid portion between the slots and outside the slots, each at a distance of 2.54 cm from a slot centerline. (See fig. 4.)

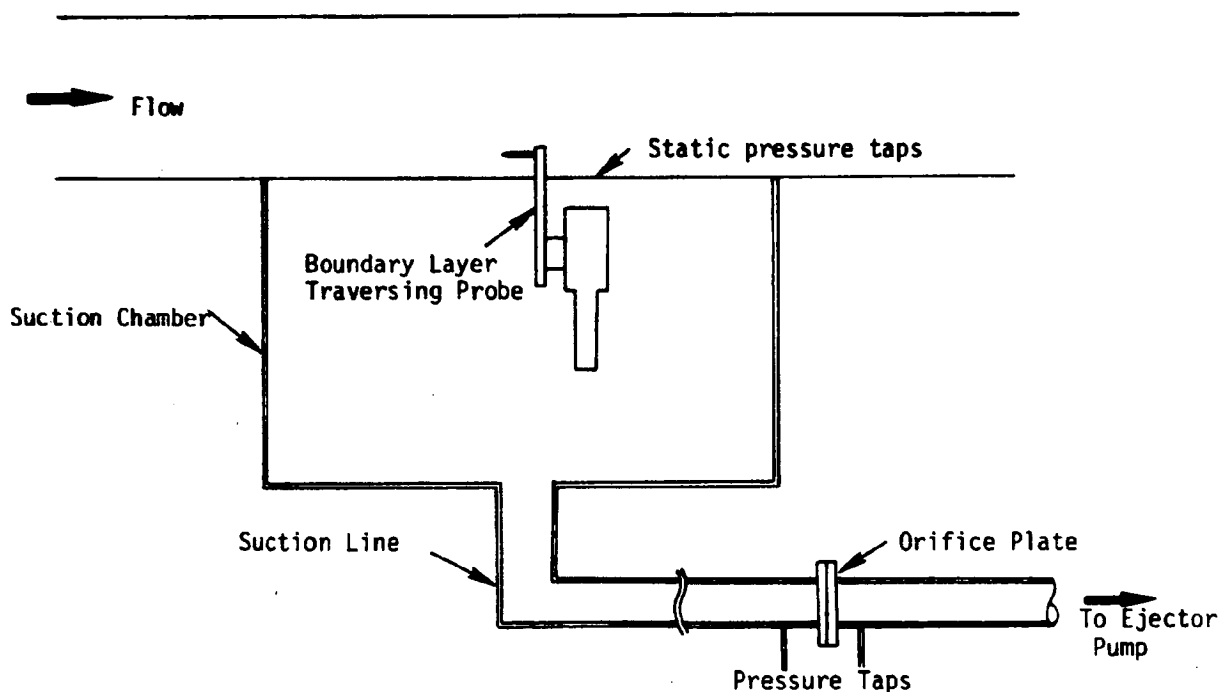


Figure 4.

In the present investigation a detailed study of the viscous flow phenomena over a slotted wind tunnel wall was made. Due to the fact that the flow over a slotted wall is semi-three-dimensional in nature, a five-port cone probe (fig. 5) was used to measure the flow velocity through the wall boundary layer. The boundary layer traverses were made above the single slot on an outside slot and at three stations 1.3, 2.5, or 3.8 cm transversely away from the slot (toward the center slot for the three-slotted model). Previous measurements were made 0.19 m downstream from the slot leading edge (ref. 1); present measurements were 0.05 m, 0.15 m and 0.25 m downstream from the end of the tapered section of the slots (Figure 3). The small perturbation analysis of Wu and Lock (ref. 2) and supersonic small perturbation theory were applied to the cone-cylinder configuration of the cone probe to estimate its performance. From each reading of the probe the local Mach number, static pressure, stagnation pressure and flow direction were determined. Then, using an assumed form of the velocity-temperature relation for an equilibrium turbulent boundary layer, the flow velocity components were determined.

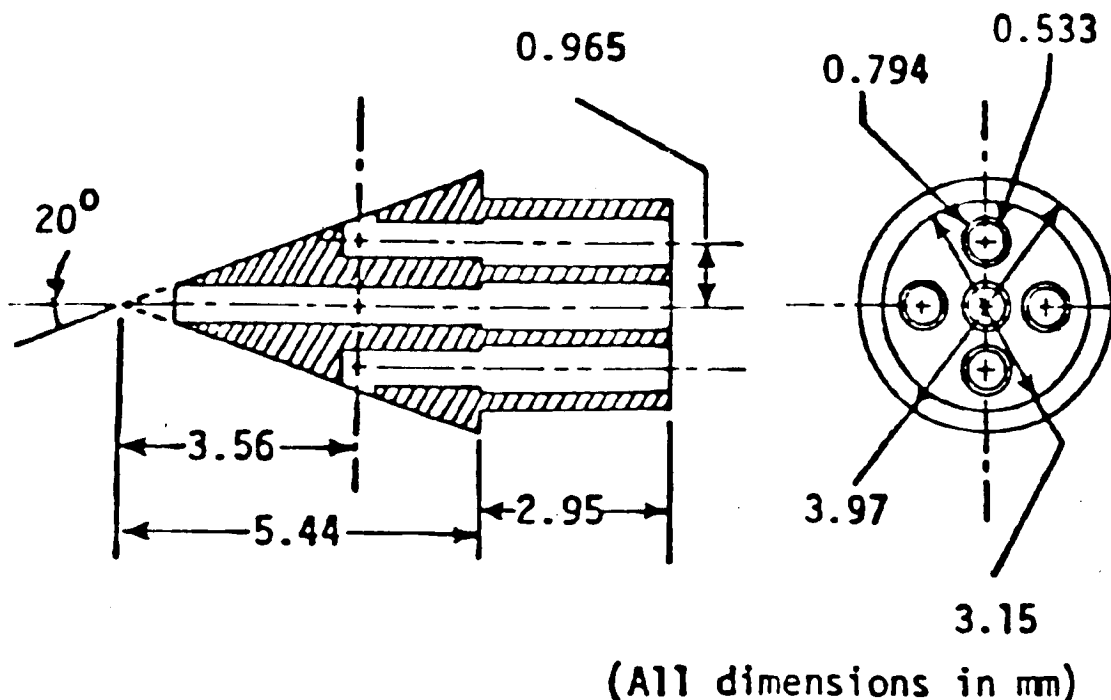


Figure 5.

## SLOT FLOW AND MEASUREMENT PLANE

The tests were performed at Mach numbers of approximately 0.6, 0.76 and 0.9. The unit Reynolds number varied from  $1.6 \times 10^7$  to  $3.1 \times 10^7$  per meter. The applied suction through the slots varied from zero to 0.25 standard  $\text{m}^3/\text{s}$  (530 SCFM). For all the tests the cone probe was traversed in the  $z$ -direction for various  $x$ -stations and  $y = 0, 1.3, 2.5$  and  $3.8$  cm. (See fig. 6.)

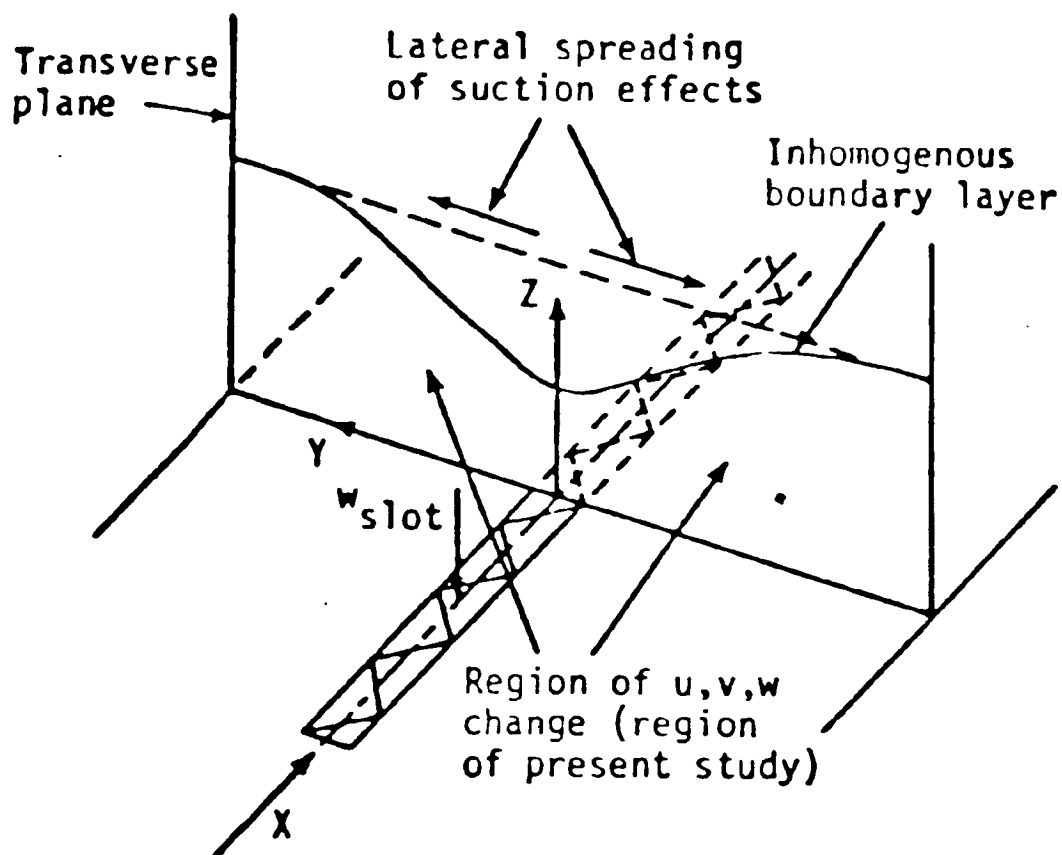


Figure 6.

VELOCITY COMPONENT DISTRIBUTION

The velocity components  $u$ ,  $v$ ,  $w$  in the  $x$ ,  $y$ ,  $z$ -directions, respectively, were obtained from the cone probe measurements. A typical result for one cone probe traverse is given in figure 7 (ref. 1). These results were obtained for the single, short, slotted-wall model at  $M_\infty = 0.81$ ,  $Re/m = 2.67 \times 10^7$ ,  $Q = 1.65 \text{ m}^3/\text{min}$  and  $y = 1.27 \text{ cm}$ . The nature of the wall shear layer and the near region external to the shear layer was analyzed using these measured velocity components. In the immediate neighborhood of the wall (approximately 1.5 probe diameters) the cone probe results become spurious due to the probe-wall interference.

$M = 0.812$ ,  $RE/FT. = 8.14E+06$ ,  $Q = 56 \text{ CFM}$ ,  $Y = -0.5 \text{ IN.}$

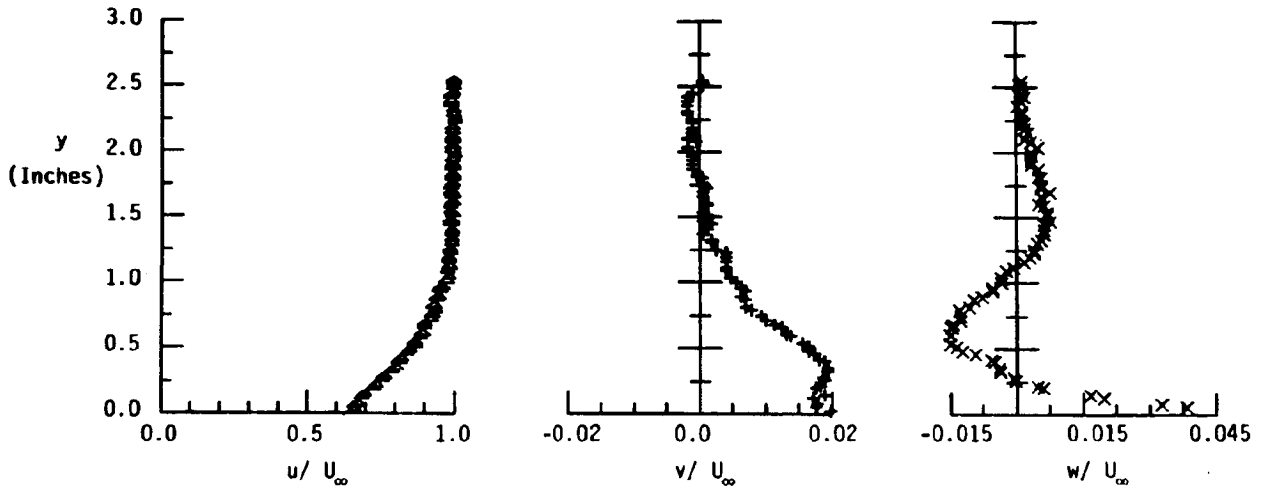


Figure 7.

### THREE-DIMENSIONAL VELOCITY PROFILES

Figure 8 is an example of the three-dimensional velocity profiles that were measured at the four transverse planes for one test condition. They were obtained using the short one-slot wall model for  $M_\infty = 0.76$ ,  $Re/m = 3.4 \times 10^7$  and no applied suction (ref. 1). This plot exhibits the three-dimensional nature of the flow field on the single slotted-wall model in a qualitative sense. From this result it can be seen that the transverse and normal velocity components were skewed toward the slot for measurement stations away from the slot. The extent of the skewness decreased with a distance away from the slot. There was flow outward from the test section through the slot to the plenum chamber at this longitudinal measuring station ( $x = 0.19$  m) for all the measurements, even without applied suction (i.e., natural ventilation only). At the slot itself the flow was directed into the slot by the baffles. The baffle angle was  $14^\circ$  and the measured flow angle on the slot was slightly greater than  $14^\circ$ .

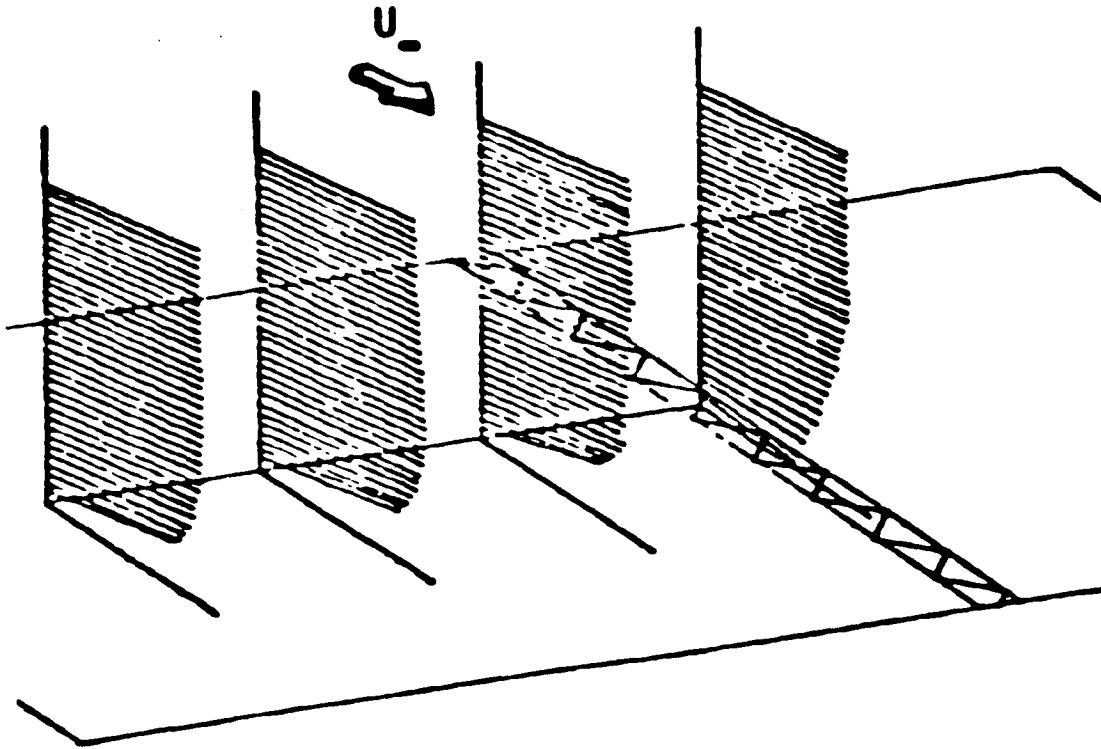


Figure 8.

ORIGINAL FIGURE  
OF POOR QUALITY

BOUNDARY LAYER THICKNESS DISTRIBUTION  
IN TRANSVERSE PLANE

The boundary layer thickness was defined as the  $z$ -location where the  $u$ -component of the velocity was equal to  $0.99 U_e$ , where  $U_e$  is the  $u$ -component of the velocity at the edge of the boundary layer. The distribution of the boundary layer thickness in the transverse measurement plane on the one-slot wall model is shown in figure 9 (ref. 1). The boundary layer thickness remained relatively constant with no applied suction through the slot but decreased in the vicinity of the slot with applied suction and almost disappeared above the slot at the highest suction rate.

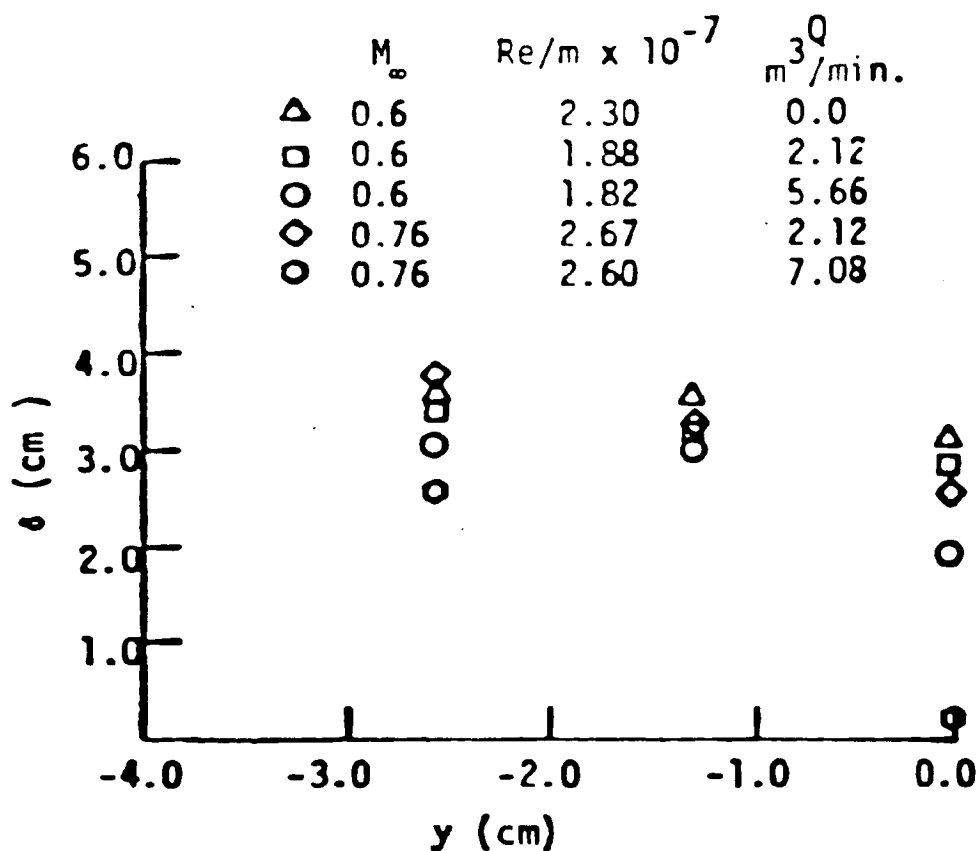


Figure 9.

BOUNDARY LAYER DISPLACEMENT THICKNESS  
DISTRIBUTION IN TRANSVERSE PLANE

The displacement thickness was defined as

$$\delta^* = \int_0^{z^e} \left(1 - \frac{\rho u}{\rho_e U_e}\right) dz$$

where  $\rho$  and  $u$  are the density and velocity, respectively, at a distance  $z$  above the wall and  $\rho_e$  and  $U_e$  are the density and velocity, respectively, at the edge of the boundary layer ( $z^e$ ). This is only an approximation to the actual displacement thickness for the three-dimensional flow (ref. 3). The boundary layer displacement thickness distributions in the transverse plane are shown for various Mach numbers and suction rates (fig. 10). The measurements are for the short one-slot wall model (ref. 1). For no auxiliary suction,  $\delta^*$  decreased monotonically with increase in distance away from the slot axis except at the lowest Mach number. At  $M_\infty = 0.6$  the natural suction velocity ( $Q = 0.0$ ) is larger than at higher Mach numbers and this results in a lower downstream test section pressure with a consequently larger outflow from the test section into the plenum upstream on the slot at the measuring station. The increase in  $\delta^*$  for no applied suction can be explained as follows. For  $Q = 0$  the flow entering the plenum chamber was mostly drawn from the low-momentum slotted-wall boundary layer and very little came in from the outer stream. Also,  $\delta$  varied only slightly away from the slot (fig. 9). The drawing of mass from the boundary layer together with only a slight change in  $\delta$  (from zero to a moderate amount of applied suction through the slot) resulted in an increased velocity defect in the shear layer and consequently an increase in  $\delta^*$ . With applied suction the displacement thickness above the slot was reduced and the influence of the suction spread laterally as the suction rate was increased.

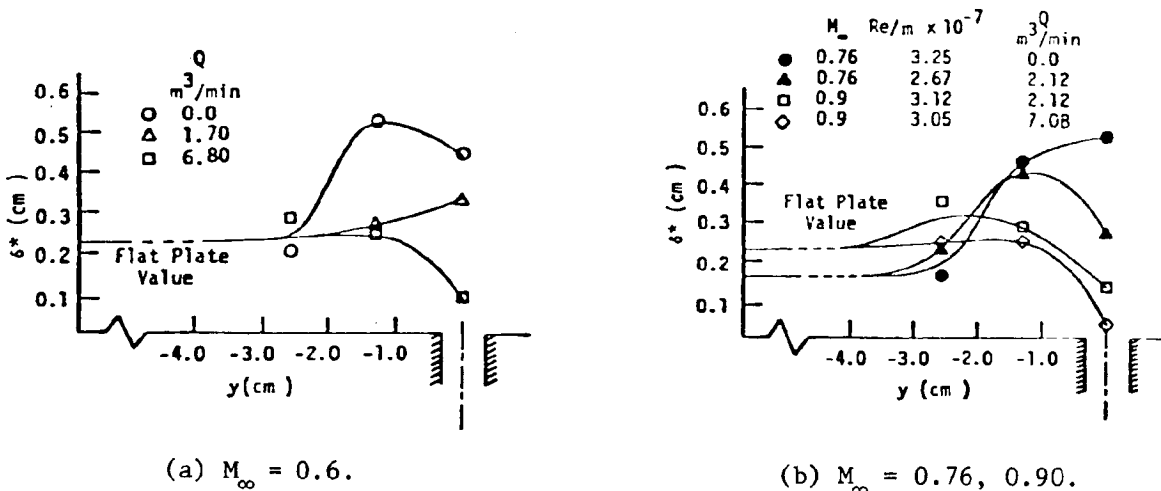


Figure 10.

VELOCITY VECTOR DISTRIBUTION ON TRANSVERSE PLANE

$$Q = 0.0, M_{\infty} = 0.6, Re/m = 2.4 \times 10^7$$

The behavior of the flow field is better visualized by considering the projection of the resultant of the  $v$  and  $w$  velocity components onto the traverse plane (figures 11, 12, 13). In these figures the main flow direction is out of the plane of the paper. These measurements were made on the short one-slot wall model (ref. 1). The flow pattern in the transverse plane indicated the existence of a vortex-like secondary flow. For no applied suction (only with natural ventilation), the vortex-like flow is strong and spread to the outer regions of the measurement plane which are outside the wall shear layer. Close to the slotted wall the flow is directed toward and into the slot. At moderate suction the vortex-like tendency of the outer flow is rather decreased (figure 12) and at high suction this phenomenon has almost disappeared (figure 13). Secondary flow can arise in turbulent flows from mean flow skewing (secondary flow of the first kind) and from anisotropy of the wall turbulence in the presence of a boundary layer which is nonuniform in the transverse direction (secondary flow of the second kind) (ref. 4). Following the analysis of ref. 4 it is possible to explain the formation and the subsequent attenuation with increased applied suction of the secondary vortex flow observed in these experiments. Details of the argument are given in ref. 1. For natural ventilation into the slot the mean flow skewing leads to the generation of a pair of vortices which expel fluid from the shear layer out into the mean flow.

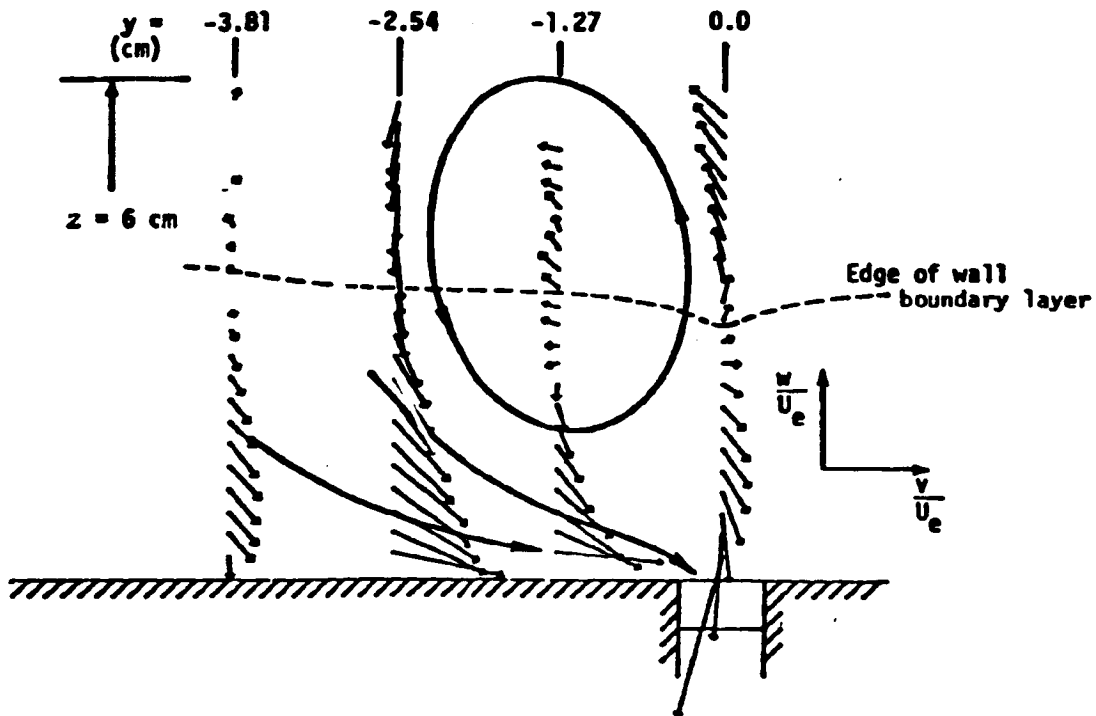


Figure 11.

VELOCITY VECTOR DISTRIBUTION ON TRANSVERSE PLANE

$$Q = 2.01 \text{ m}^3/\text{min}, M_\infty = 0.6, Re/m = 1.89 \times 10^7$$

At moderate suction the vortex-like tendency of the outer flow is rather decreased (fig. 12). It can be argued (ref. 1) that the only stress-induced streamwise vorticity production term leads in this case to a secondary motion in a sense opposite to that produced by mean flow skewing. At moderate suction this term balances the mean flow skewing and the secondary motion disappears. Another plausible explanation for the disappearance of secondary motion with moderate suction is that the upward movement along the centerline from the secondary motion caused by mean flow skewing (Figure 11) was balanced by the downward movement toward the slot caused by the increased suction. Only further experimentation can unambiguously determine the source of the streamwise vorticity that is observed and its change with amount of applied suction.

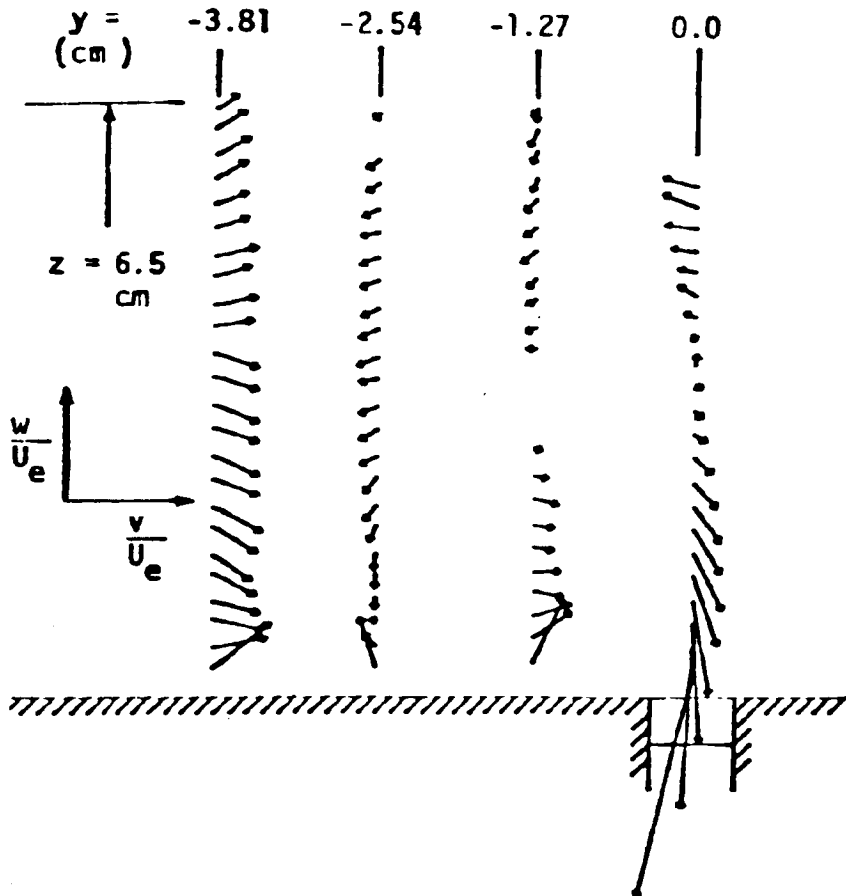


Figure 12.

VELOCITY VECTOR DISTRIBUTION ON TRANSVERSE PLANE

$$Q = 7.1 \text{ m}^3/\text{min}, M_\infty = 0.6, Re/m = 1.78 \times 10^7$$

At high suction rate the secondary motion has almost disappeared (fig. 13). The conclusion is that the two sources of streamwise vorticity generate secondary motions of the opposite rotation sense, for the present geometry, which tend to counter-balance each other. At no applied suction, since there is only a slight variation of  $\delta$  with  $y$ , the contribution to the secondary flow is mainly from the mean flow skewing (Figure 11). With moderate applied suction the influence of the inhomogeneous boundary layer is strong and the two secondary flow sources tend to cancel one another. Then no secondary pattern is discernable (Figure 12). At the highest applied suction rate the suction effect overrides the secondary motion and the velocity vectors are directed toward the slot.

CONTINUOUS  
OF POSITION

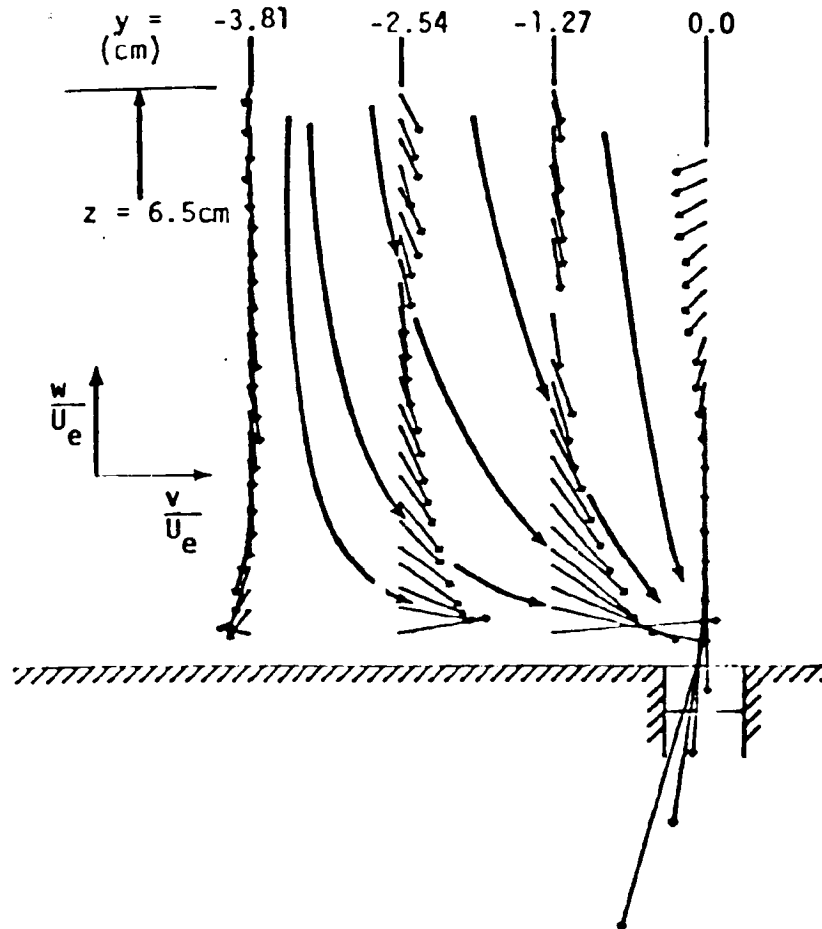


Figure 13.

## LONGITUDINAL DISPLACEMENT THICKNESS DISTRIBUTION

The results given in Figures 14 to 18 were obtained using the long one-slot wall model (Figure 3). The longitudinal displacement thickness distribution is shown for  $y = 0.0$  and  $1.3$  cm for  $M_\infty = 0.76$  for various amounts of suction through the slot. The displacement thickness  $\delta^*$  decreased at all longitudinal stations with increased suction. There was natural flow into the plenum chamber at the first and last longitudinal measurement stations but not at the middle station and the displacement thickness was influenced little until large amounts of suction were applied.

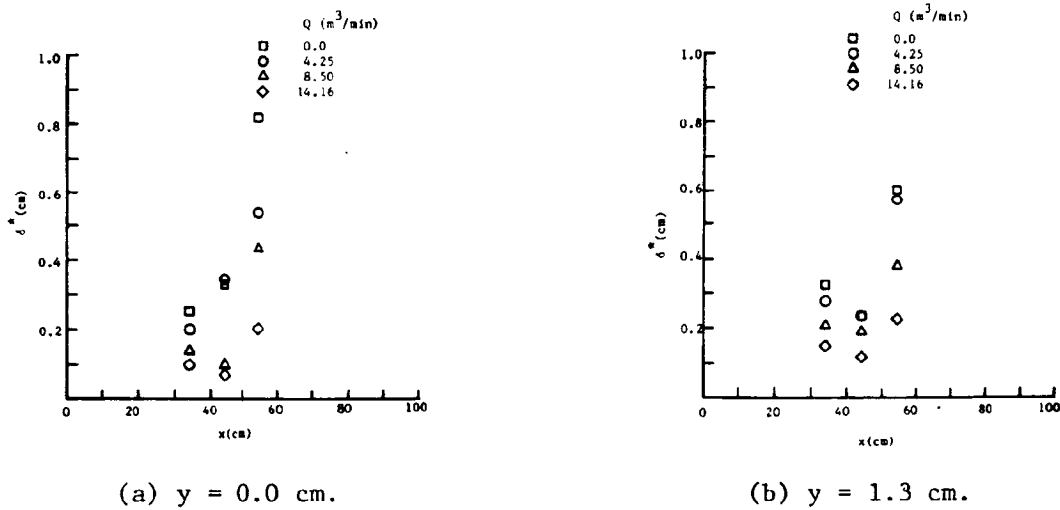


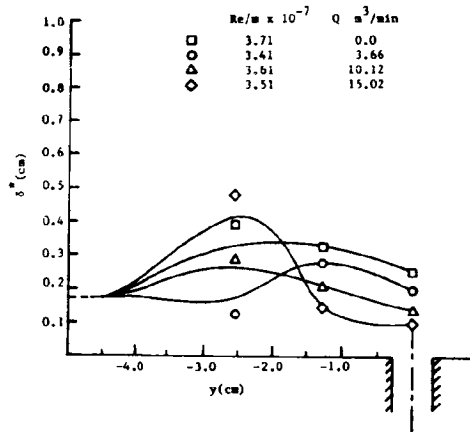
Figure 14.

ORIGINAL PAGE IS  
OF POOR QUALITY

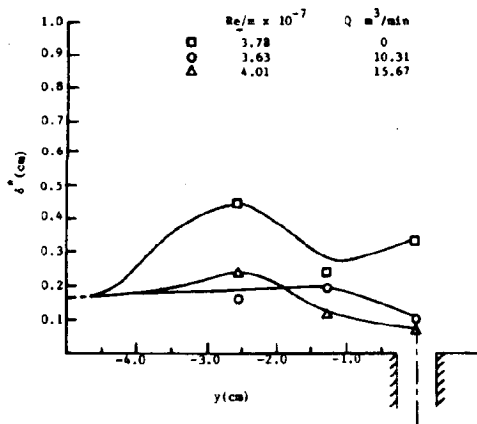
## BOUNDARY LAYER DISPLACEMENT THICKNESS DISTRIBUTION IN TRANSVERSE PLANES

The displacement thickness distributions at three transverse planes measured on the long one-slot tunnel wall at  $M_\infty = 0.76$  are shown. They can be explained in the same way as the distributions shown in Figure 10.

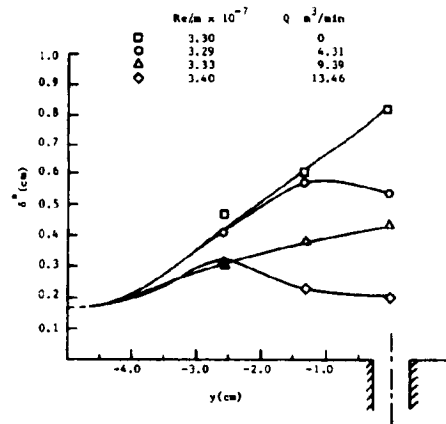
ORIGINAL  
OF POOR QUALITY



(a)  $x = 5.1 \text{ cm.}$



(b)  $x = 15.2 \text{ cm.}$



(c)  $x = 25.4 \text{ cm.}$

Figure 15.

VELOCITY VECTOR DISTRIBUTIONS IN TRANSVERSE PLANE  
 $M_\infty = 0.76, x = 5.1 \text{ cm}, Re/m = 3.6 \times 10^7$

The velocity vector distributions in the transverse plane  $x = 5.1 \text{ cm}$  downstream from the end of the tapered section of the one-slot wall model for zero and low suction rates are shown. For no suction there is no significant variation of the boundary layer thickness across the transverse plane. The main contribution to the secondary vortex motion is due to the skewing of the mean flow as a result of the flow into the plenum through the slot. Close to the wall the flow is directed by the wall and the slot. There is an increased variation in the boundary layer thickness at increased suction with slightly increased local suction and somewhat attenuated vortex motion. The flow is mostly directed towards the slot.

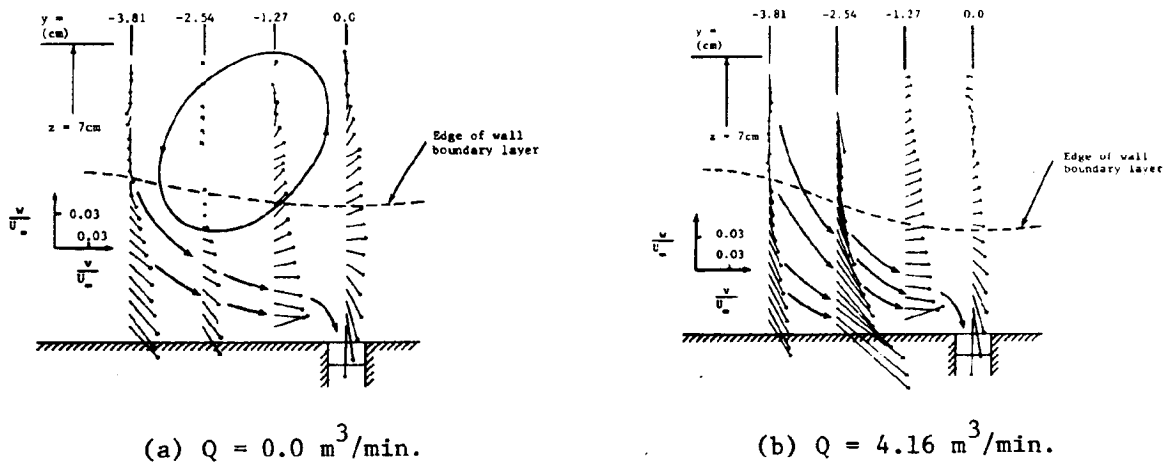
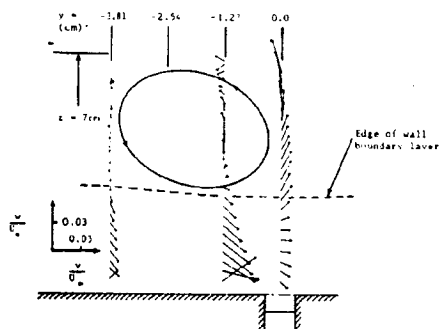


Figure 16.

ORIGINAL PHOTOCOPIES  
 OF POOR QUALITY

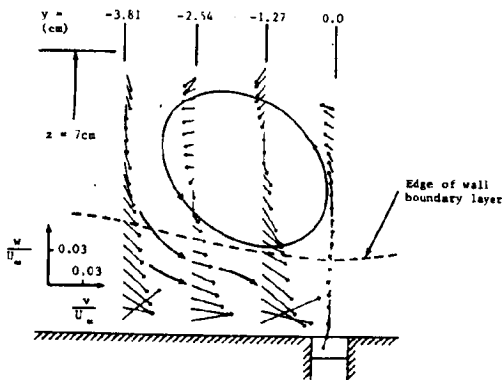
VELOCITY VECTOR DISTRIBUTIONS IN TRANSVERSE PLANE  
 $M_\infty = 0.76$ ,  $x = 15.2$  cm,  $Re/m = 3.6 \times 10^7$

The velocity vector distributions in the transverse plane  $x = 15.2$  cm downstream from the end of the tapered section of the one-slot wall model for zero, moderate and large suction rates are shown. For  $Q = 0.0$ , there is no variation of the boundary layer thickness across the plane and there is very little natural ventilation at this station. A weak vortex-like motion exists outside the conventional wall shear layer. In the wall shear layer the flow moves toward the slot and is constrained by the wall. Mean flow skewing is possibly the source of outside vortex motion. At  $Q = 9.91$  m<sup>3</sup>/min there is greater variation of the boundary layer thickness with  $y$  but little suction at the slot. Mean flow skewing generates outside vortex motion. Similar remarks apply at the highest suction.

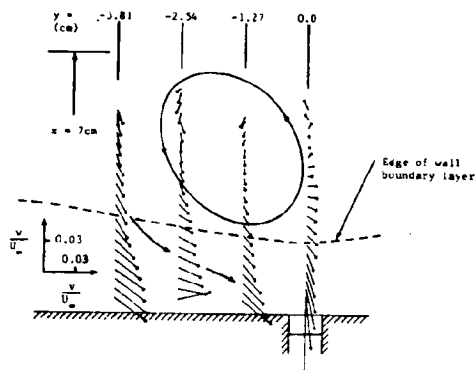


ORIGINAL FIGURE  
 OF POOR QUALITY

(a)  $Q = 0.0$  m<sup>3</sup>/min.



(b)  $Q = 9.91$  m<sup>3</sup>/min.



(c)  $Q = 14.16$  m<sup>3</sup>/min.

Figure 17.

VELOCITY VECTOR DISTRIBUTION IN TRANSVERSE PLANE

$M_\infty = 0.76, x = 25.4 \text{ cm}$

The velocity vector distributions in the transverse plane  $x = 25.4 \text{ cm}$  downstream from the end of the tapered section of the one-slot wall model for two suction rates are shown. The boundary layer thickness variations are small and of the type that enhances vortex motion produced by mean flow skewing. In this case the vortex motion is closer to the normally defined shear layer than for those stations upstream.

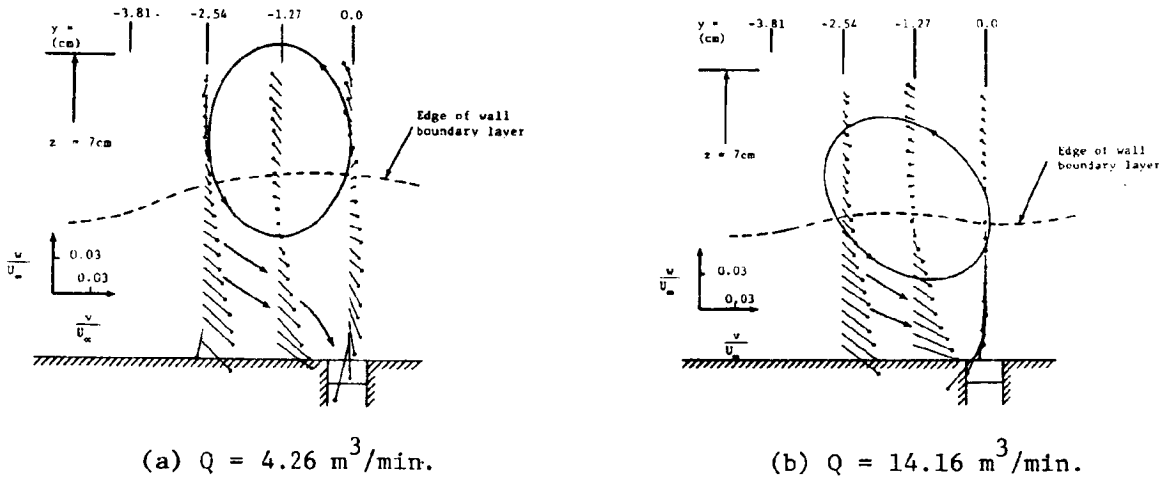


Figure 18.

ORIGINAL PAGE IS  
OF POOR QUALITY

TRIPLE-SLOTTED WALL MODEL

ORIGINAL...  
OF FOUR...

The triple-slotted wall model is shown in figure 20. The probe holder moved upward through one of the side slots and measured the velocity about the center slot. The presence of the probe holder interfered with the suction through the side slot. A new probe holder is being constructed that will move the probe from the wall above the slotted-wall model and eliminate this interference.

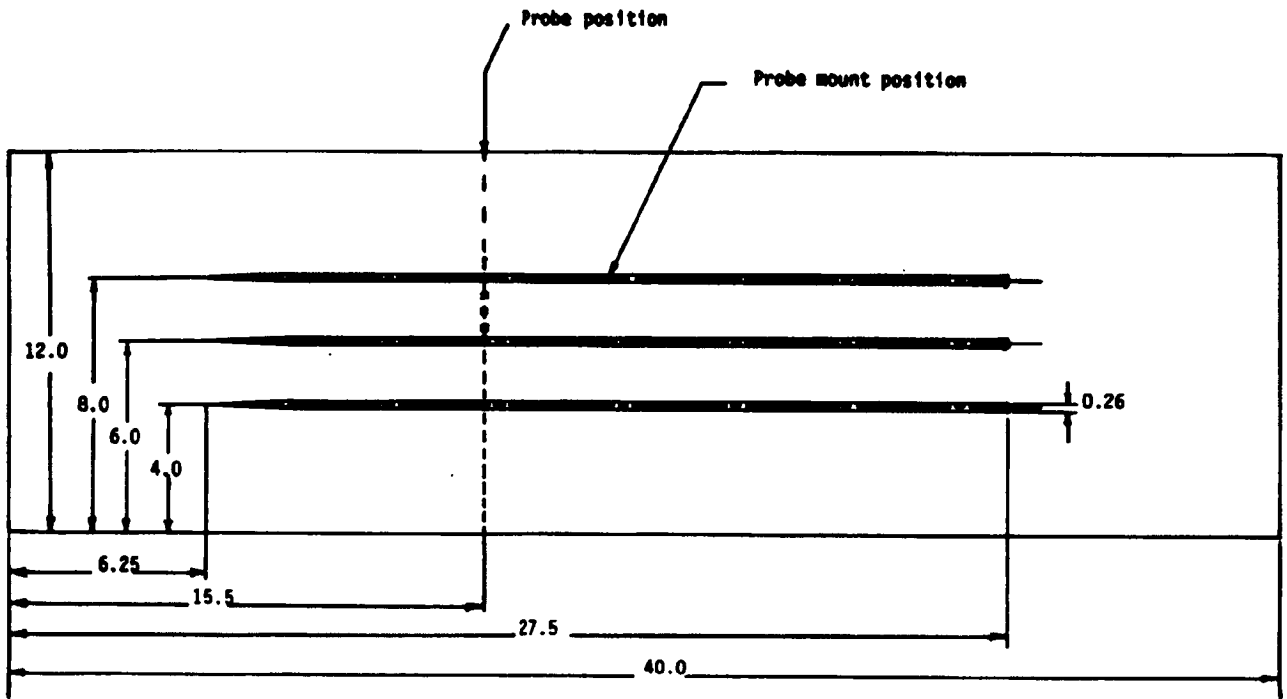


Figure 19.

DISPLACEMENT THICKNESS DISTRIBUTION IN  
TRANSVERSE PLANE

$M_\infty = 0.6$ ,  $x = 15.2$  cm, three slots

The displacement thickness distribution in the transverse plane, with and without suction, is given in figure 20. The displacement thickness is reduced across most of the plate as a result of the suction. The increase above the slot for zero suction was previously explained (see fig. 10).

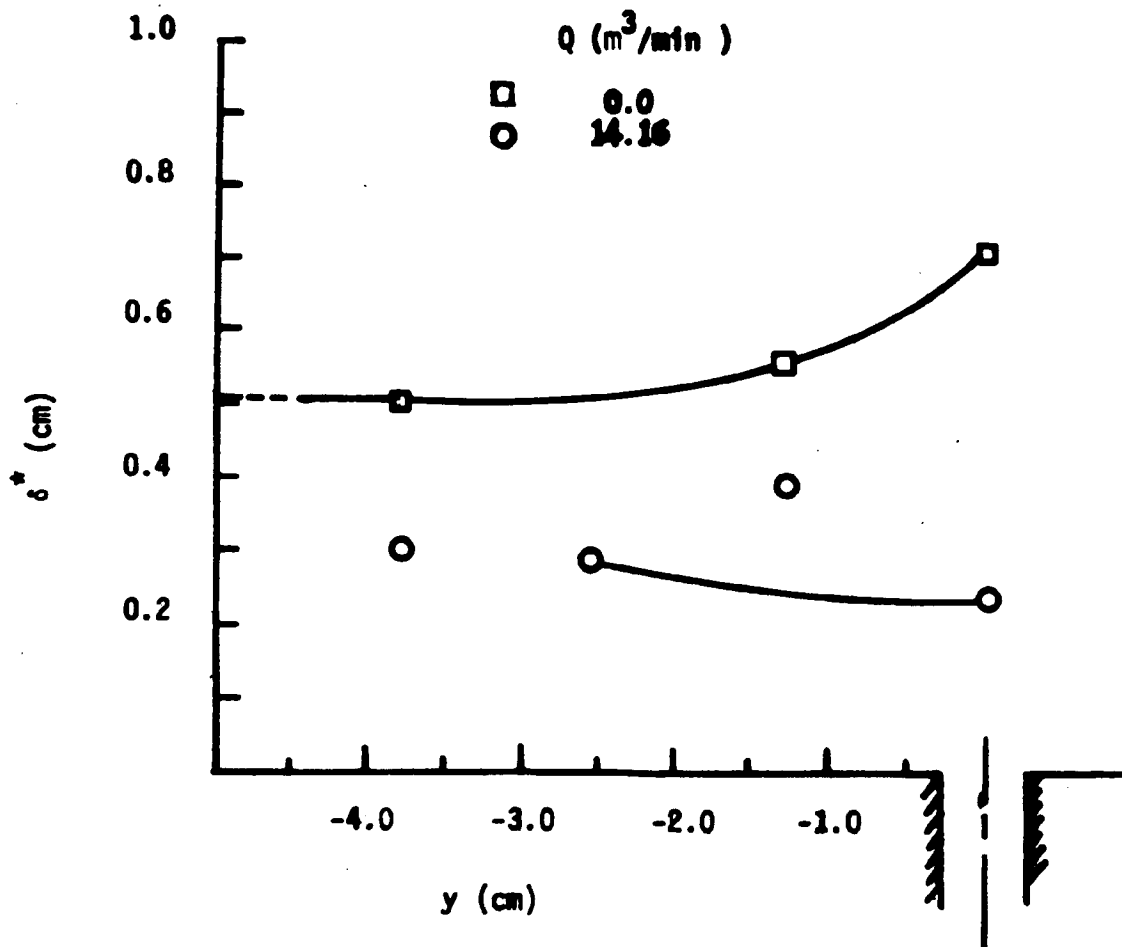


Figure 20.

VELOCITY VECTOR DISTRIBUTION ON TRANSVERSE PLANE

$M_\infty = 0.6, x = 15.2 \text{ cm}$

The velocity vector distribution on the transverse plane was measured at four positions away from the center slot. Symmetry was prevented because the probe holder proceeded up from the left hand slot. The vortex-like motion does not appear to exist for the conditions shown but the suction continues to influence the flow beyond the edge of the normally-defined shear layer (fig. 21).

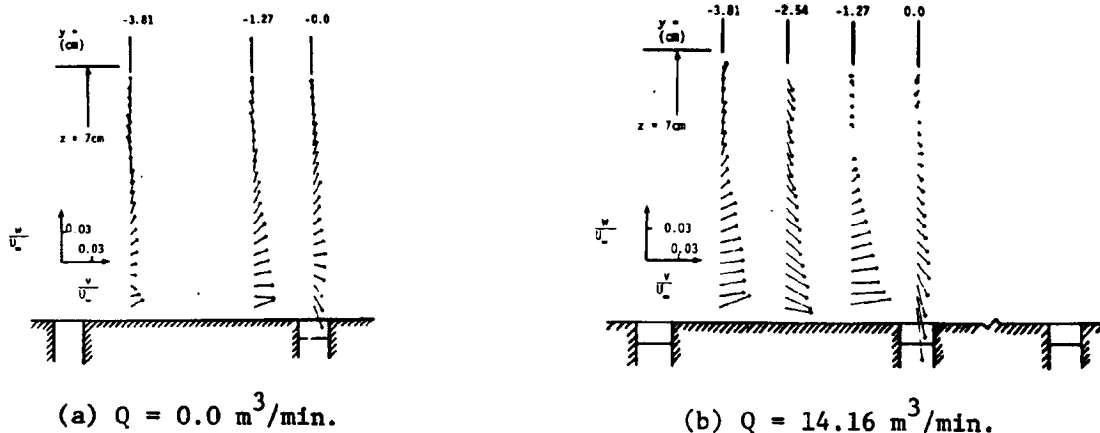


Figure 21.

#### REFERENCES

1. Wu, J. M.; Collins, F. G.; and Bhat, M. K.: Three-Dimensional Flow Studies on a Slotted Transonic Wind Tunnel Wall. AIAA Paper No. 82-0230, 1982.
2. Wu, J. M.; and Lock, R. C.: A Theory for Subsonic and Transonic Flow Over a Cone -- With Small Yaw Angle. U. S. Army Missile Command, Technical Report RD-74-2, December, 1973.
3. Lighthill, M. J.: On Displacement Thickness. J. Fluid Mech., vol. 4, part 4, August, 1958, pp. 383-392.
4. Perkins, H. H.: The Formation of Streamwise Vorticity in Turbulent Flow. J. Fluid Mech., vol. 44, part 4, December 1970, pp. 721-740.

N85 12019

Dg

EFFECT OF UPSTREAM SIDEWALL BOUNDARY LAYER REMOVAL  
ON AN AIRFOIL TEST

C. B. Johnson, A. V. Murthy, E. J. Ray,  
P. L. Lawing, and J. J. Thibodeaux  
NASA Langley Research Center  
Hampton, Virginia

## ABSTRACT

Sidewall boundary layer effects have been investigated by applying partial upstream sidewall boundary layer removal in the Langley 0.3-m Transonic Cryogenic Tunnel. Over the range of sidewall boundary layer displacement thickness ( $2\delta^*/b = 0.02$  to  $0.01$ ) of these tests the influence on pressure distribution was found to be small for subcritical conditions; however, for supercritical conditions the shock position was affected by the sidewall boundary layer. For these tests, with and without boundary layer removal, comparisons with predictions of the GRUMFOIL computer code indicated that Mach number corrections due to the sidewall boundary layer improve the agreement for both subcritical and supercritical conditions. The results also show that sidewall boundary layer removal reduces the magnitude of the sidewall correction; however, a suitable correction must still be made.

## INTRODUCTION

With the development of advanced technology airfoils in the past decade, there has been a need to generate reliable wind tunnel data at transonic speeds and high Reynolds numbers, both for practical applications and also to assess the merits of the sophisticated computer codes developed for airfoil analysis. This has led to a renewed interest in the understanding and evaluation of the tunnel wall interference effects. Considerable work has been reported in the literature (refs. 1, 2 and 3) on the top and bottom wall corrections which use measured data near or on the wall to assess the interference effects which are primarily inviscid in nature. The sidewall interference, which is primarily viscous in nature, has received considerable attention after a lapse of about 30 years. In the past, the general practice was to use as high an aspect ratio as possible and assume that the sidewall boundary layer effect can be ignored on the large aspect ratio models. However, systematic investigations conducted at ONERA (ref. 4) recently demonstrated the sidewall effects to be nearly independent of the aspect ratio, at least for subsonic flows, and if anything, the sidewall effects were slightly higher for small chord airfoils due to the increased pressure gradients over the chord. Following this study, Barnwell (ref. 5), and Winter and Smith (ref. 6) with independent but somewhat similar approaches showed that for the case of an attached sidewall boundary layer, change in normal force coefficient was directly proportional to the ratio of boundary layer displacement thickness to the semispan and was independent of aspect ratio.

The purpose of this paper is to present some of the observed effects of the sidewall boundary layer on a 12% supercritical advanced technology airfoil at transonic speeds and also to assess the importance of sidewall corrections in relation to top and bottom wall interference. These results are from tests conducted in the Langley 0.3-m Transonic Cryogenic Tunnel.

## NOMENCLATURE

b	span of tunnel, 8 inches
c	chord of airfoil, 6 inches
$c_l$	section lift coefficient from airfoil pressures
$c_n$	section normal-force coefficient from airfoil pressures
$C_p$	pressure coefficient
M	Mach number
$M_c$	corrected Mach number
$M_\infty$	nominal Mach number upstream of perforated plates
$\dot{m}$	mass flow rate
p	pressure
R	Reynolds number per meter
$R_c$	Reynolds number based on airfoil chord
SW	sidewall
T&B	top and bottom wall
x	chordwise distance from leading edge of airfoil
y	spanwise distance from centerline of tunnel and model
z	vertical distance normal to upstream flow vector
$\alpha$	uncorrected angle of attack, deg
$\alpha_G$	angle of attack obtained from GRUMFOIL code
$\delta^*$	displacement thickness
$\Delta M$	change in Mach number for the wall corrections ( $\Delta M = M_c - M$ )

### Subscripts

b1	boundary layer removal
t	total value
ts	test section
w	wake trailing airfoil
$\infty$	free-stream condition upstream of perforated plates

## SIDEWALL BOUNDARY LAYER GROWTH WITH AN AIRFOIL

The interaction of the sidewall boundary layer with the airfoil pressure fields (shown schematically in Figure 1), gives rise to a locally three-dimensional flow field at the junction of the model and wall, and also causes variations in the width of the flow passage above and below the airfoil because of different pressure fields. This introduces a blockage type of interference and can be viewed as a global correction to the free-stream Mach number. To account for this type of effect, a flow similarity correction procedure was developed by Barnwell (ref. 5) and later extended to transonic speeds by Sewall (ref. 7).

The Barnwell-Sewall similarity rules, in addition to providing a first approximation to correct for the sidewall boundary layer effects, demonstrate the importance of keeping the value of the ratio of boundary layer thickness to semispan ( $2\delta^*/b$ ) small. At transonic speeds, with relatively thin sidewall boundary layer (1 - 2% of tunnel width), the corrections to the overall force coefficients may not be appreciable; however, the shock location and pressure distribution on the airfoil under supercritical conditions can be altered. Also, in addition to the blockage type of interference, the shock wave boundary layer effects on the sidewall can introduce spanwise nonuniformities. In order to study these effects, an investigation was conducted in the Langley 0.3-m Transonic Cryogenic Tunnel (TCT) (described in ref. 8) with and without sidewall boundary layer removal ahead of the model.

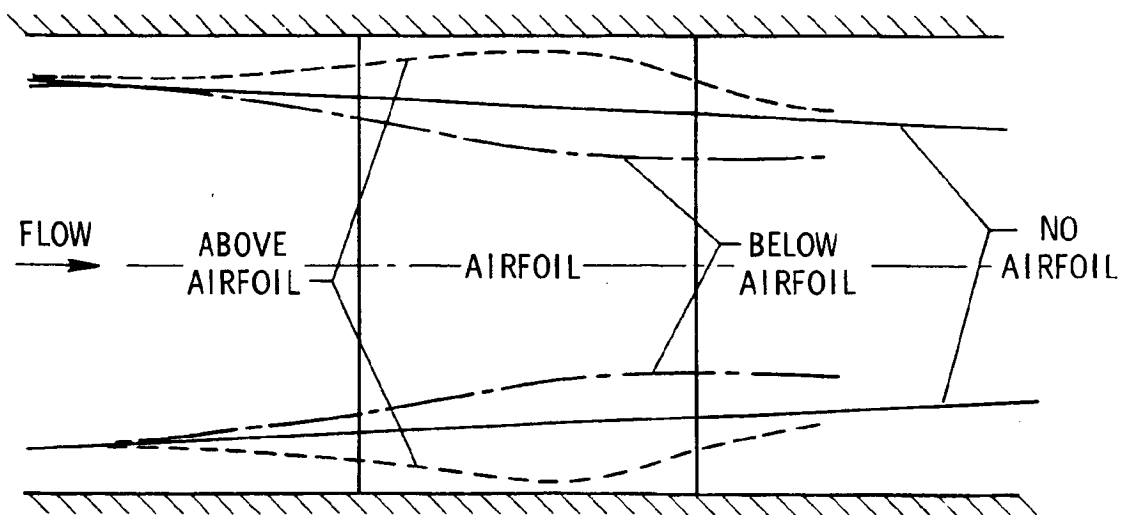


Figure 1.- Typical sidewall boundary layer growth due to lifting airfoil flow field.

## 0.3-METER TRANSONIC CRYOGENIC TUNNEL

A top view of the Langley 0.3-meter TCT test section is shown in Figure 2. In this photograph, the top of the plenum chamber and the top tunnel slotted wall have been removed. Visible in the photograph are the airfoil model, boundary layer bleed ducting, one of the four boundary layer sidewall rakes, and one of the two perforated plates. The electron-beam-drilled perforated plates are fitted upstream of the model location on both sidewalls in order to remove the boundary layer. The perforated plates (0.726 mm thick), used for "boundary layer mass removal" in the sidewall boundary layer bleed system, have a nominal porosity of 20 percent, with electron-beam-drilled holes 0.25 mm in diameter and 0.5 mm apart. It should be noted that "boundary layer mass removal" has often been referred to in engineering terms as "boundary layer bleed", thus throughout this paper the colloquialism "bleed" will be used to depict the sidewall boundary layer mass removal. The perforated plate was etched to obtain a smooth surface on the side exposed to the flow.

The amount of the boundary layer mass flow removed from either of the sidewalls is controlled independently by two digital valves and discharged directly to the atmosphere. With this arrangement, the maximum mass flow that can be removed is equal to the mass flow of liquid nitrogen that is being injected into the tunnel for cooling purposes.

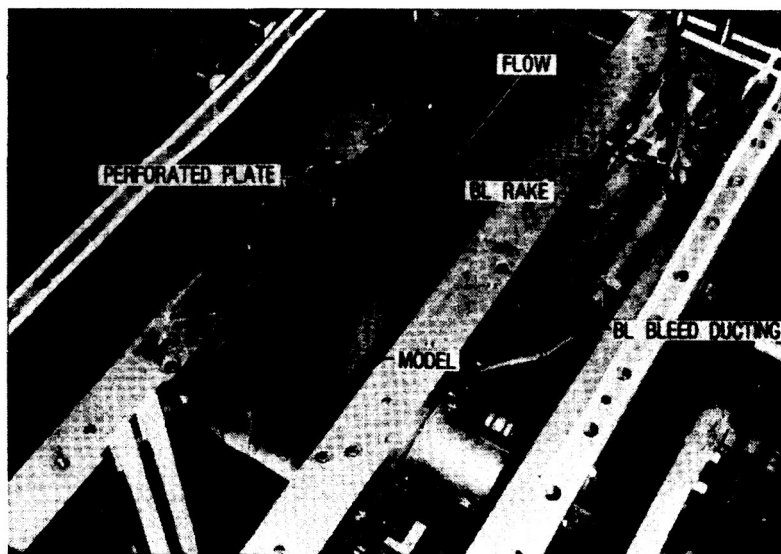


Figure 2.- 0.3-Meter Transonic Cryogenic Tunnel 2-D test section.

## SIDEWALL DISPLACEMENT THICKNESS WITH BLEED

Initially, tests were conducted to determine the sidewall boundary layer thickness and also to obtain the Mach number calibration under different bleed conditions. The details and analysis of the sidewall boundary layer are reported in ref. 9. Shown in Figure 3 is the variation of the sidewall boundary layer bleed at the model location for the tunnel empty condition. It may be noted that the ratio of the displacement thickness to the tunnel width ( $2\delta^*/b$ ) is reduced from about 0.02 with no bleed to about 0.01 with bleed. These tests also indicated approximately the same thickening of the boundary layer growth when there was no bleed through the perforated plates as was observed with the solid walls. A calibration factor relating the upstream reference Mach number and the test Mach number at the model location was also established for different bleed rates in order to arrive at the correct test Mach number with the model in the tunnel.

These passive bleed tests without the model showed that a thin sidewall boundary layer displacement thickness ( $2\delta^*/b \sim 0.01$  is generally considered to be low enough for the sidewall boundary layer effects to be small) could be obtained by bleeding about 2 percent of the test section mass flow.

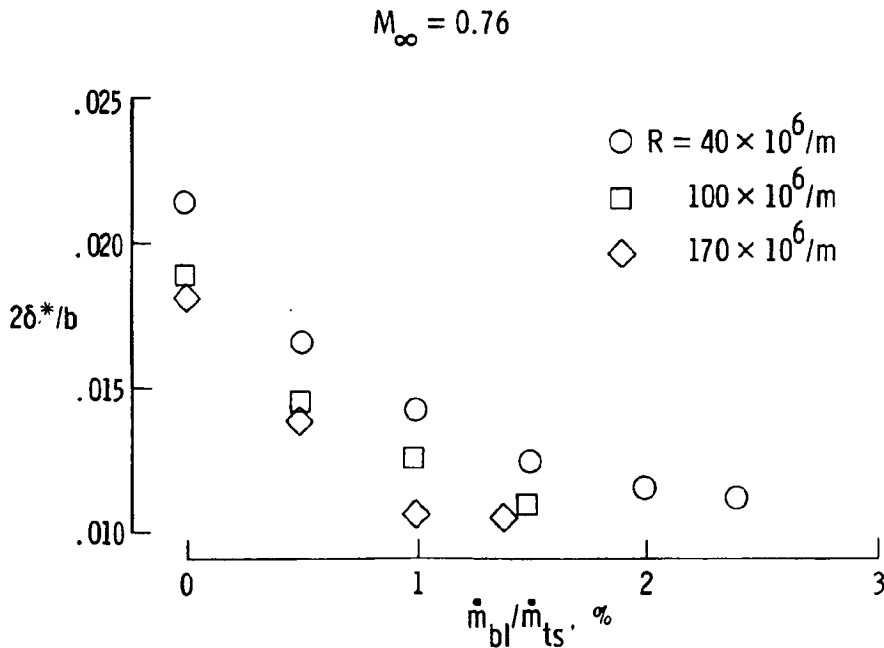


Figure 3.- Variation of sidewall boundary layer displacement thickness with sidewall bleed at location of airfoil.

AIRFOIL PRESSURE DISTRIBUTION WITH BLEED

In contrast to other studies, the present investigation is in the regime of relatively thin boundary layer displacement thicknesses (1 to 2 percent of tunnel width); therefore, the influence of bleed (at least for attached sidewall boundary layers) on global parameters such as  $c_n$  was not significant and hence direct comparison of the mid-span pressure distribution is made. Shown in Figure 4 is the effect of bleed on mid-span pressure distribution for angles of attack of  $0^\circ$  and  $2^\circ$  at a nominal upstream Mach number of 0.76 and Reynolds number of  $6 \times 10^6$ . For the shock-free, baseline case at  $\alpha = 0^\circ$ , corresponding to a  $c_n$  of about 0.56 (near the design  $c_n$  of 0.70), the effect of reducing  $2\delta^*/b$  from 0.022 to 0.012 is not significant. However, at  $\alpha = 2^\circ$  ( $c_n = 0.88$ ), there is a forward movement of the shock with increasing sidewall boundary layer bleed. This effect is associated both with the slight drop in the test Mach number,  $M$ , due to bleed and with the reduction in the sidewall boundary layer displacement thickness. In all figures the Mach number,  $M$ , associated with specific data refers to the calibrated Mach number obtained with and without bleed. In this figure and in the next 6 figures, the solid lines are simply a fairing of the data. The change in Mach number and in  $\delta^*$  when bleed is applied is not a significant problem in applying the correction since the Barnwell-Sewall flow similarity correction procedure (refs. 5 and 7) takes into account both Mach number and  $\delta^*$ .

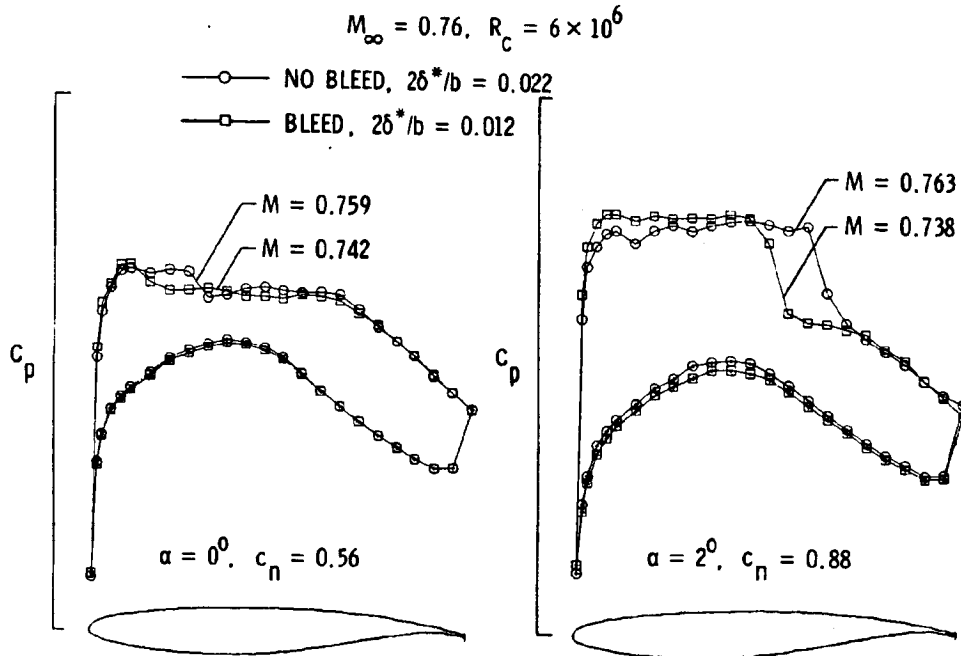


Figure 4.- Effect of sidewall boundary layer bleed on airfoil pressure distribution.

## AIRFOIL WAKE WITH BLEED

The total head pressure distribution in the wake of the airfoil ratioed to the total pressure upstream of the perforated plates is shown in Figure 5 for three spanwise locations ( $2y/b$  of  $-0.75$ ,  $-0.50$  and  $0.0$ ). The results for this shock-free baseline case at  $\alpha = 0^\circ$  indicates that the effect of reducing the boundary layer displacement thickness is not significant. The shift in the wake distribution is due to the change in Mach number due to the bleed. The right hand portion (with respect to  $z$ ) of the wake distribution above the airfoil indicates no entropy change thus indicating that the flow is shock free.

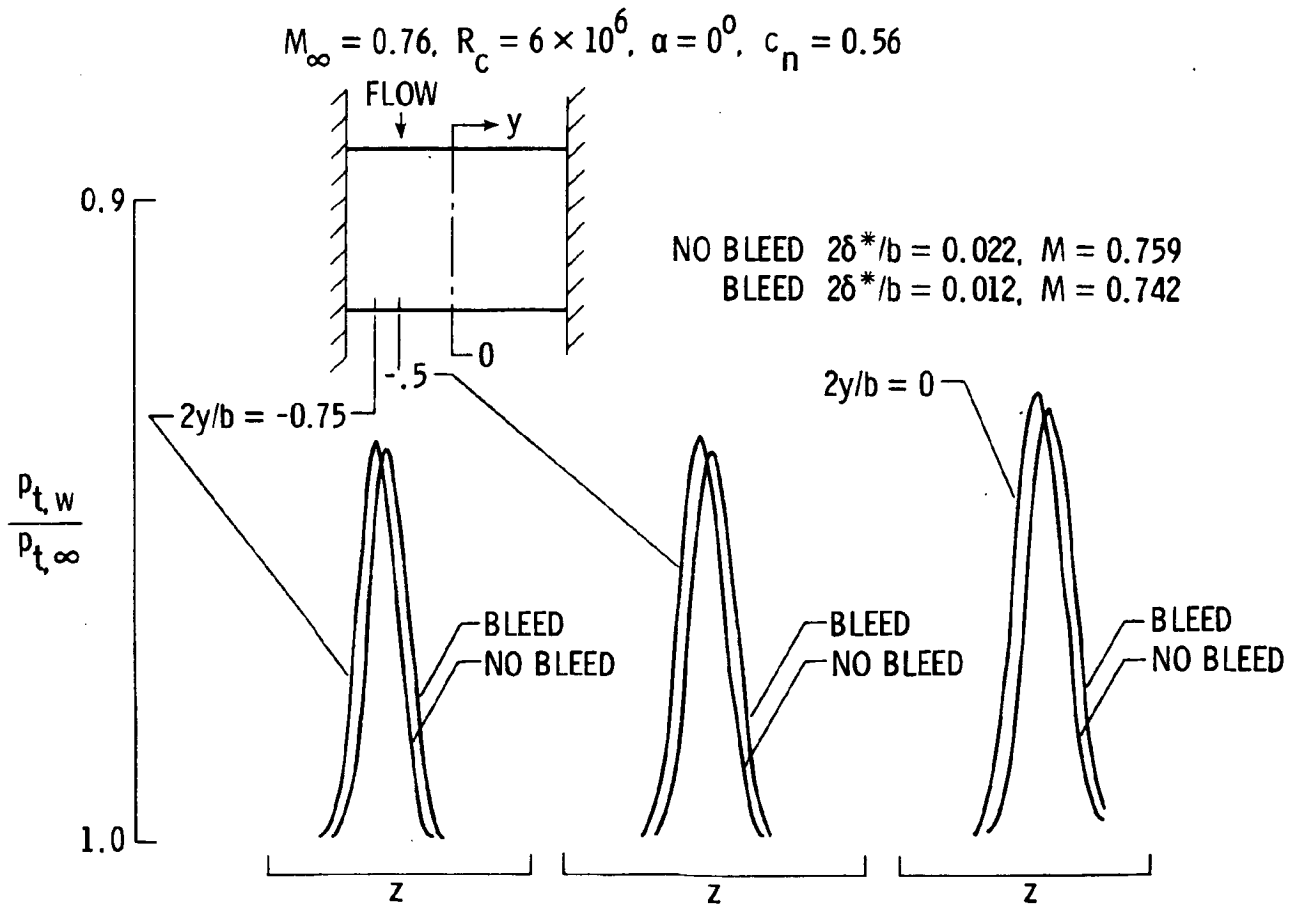


Figure 5.- Effect of sidewall boundary layer bleed on airfoil wake at various spanwise locations.

AIRFOIL WAKE WITH BLEED

ORIGINAL PAPER OF POOR QUALITY

The total head pressure distribution in the wake of the airfoil ratioed to the total pressure upstream of the perforated plates is shown in Figure 6 for three spanwise locations ( $2y/b$  of  $-0.75$ ,  $-0.50$  and  $0.0$ ). The results for this high lift case at  $\alpha = 2^\circ$  indicate that the effect of reducing the sidewall boundary layer displacement thickness is to smooth the wake distributions, especially the outer portion of the wake from the flow over the upper surface of the airfoil. The change in the level of the upper (shock related) portion of the wake is due to the combined change in displacement thickness and Mach number when bleed is applied.

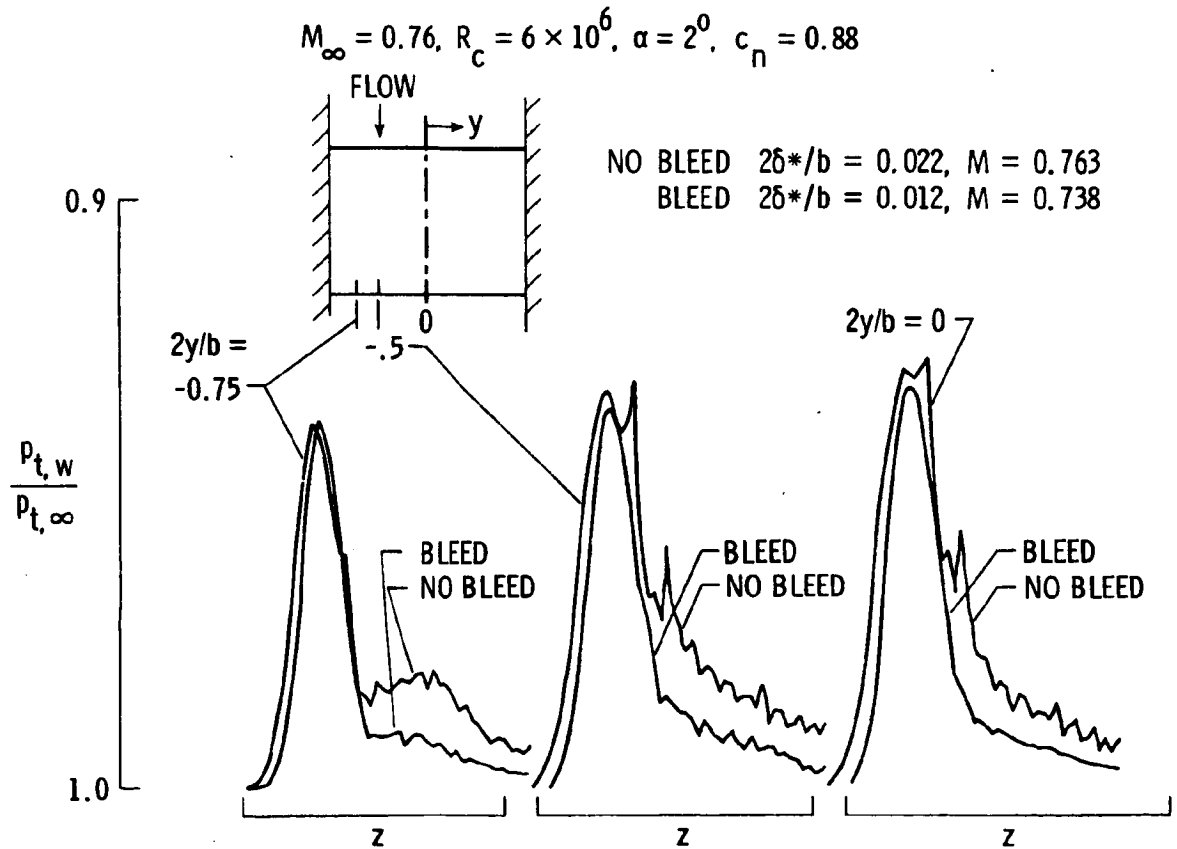


Figure 6.- Effect of sidewall boundary layer bleed on airfoil wake at various spanwise locations.

## SPANWISE PRESSURE DISTRIBUTION WITH BLEED

Spanwise pressure distributions are shown in Figure 7 at three chordwise locations ( $x/c$ 's of 0.15, 0.5, and 0.8) for the shock-free baseline case at  $\alpha = 0^\circ$ . For this shock-free case the distributions are nearly uniform in the spanwise direction. The upstream spanwise distribution ( $x/c = 0.15$ ) suggests possible wave disturbances emanating from the interaction region at the junction of the airfoil leading edge and the sidewall. However, in general, for these flow conditions the effect of sidewall bleed does not have a significant effect on the spanwise pressure distributions.

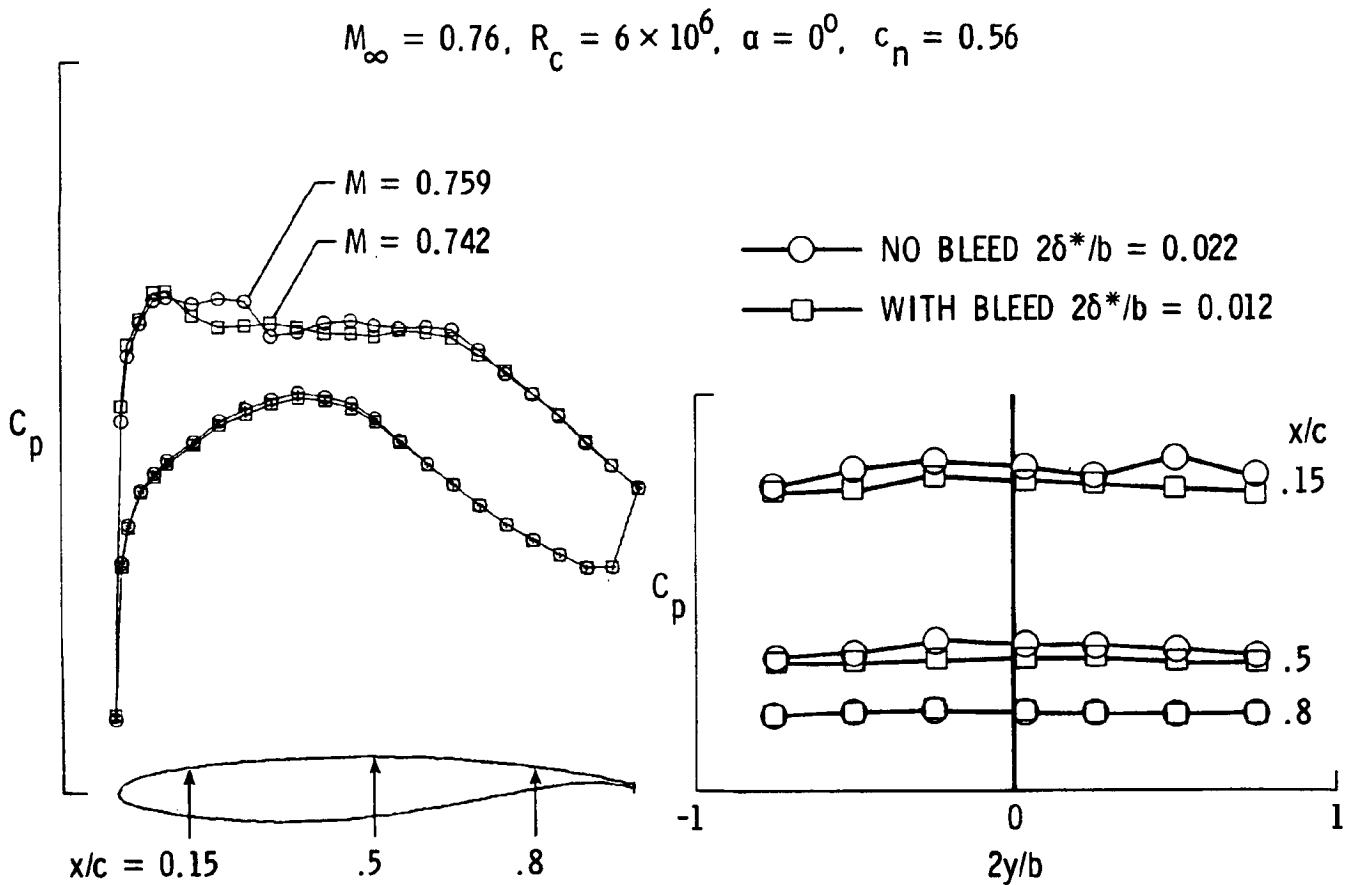


Figure 7.- Effect of sidewall boundary layer bleed on spanwise pressure distribution.

## SPANWISE PRESSURE DISTRIBUTION WITH BLEED

The effect of bleed is shown in Figure 8 for the mid-span chordwise pressure distribution and for three spanwise pressure distributions ( $x/c$ 's of 0.15, 0.5 and 0.8) for a high lift and moderately high angle of attack ( $\alpha = 4^\circ$ ) condition. When bleed is applied there is a significant improvement of the mid span pressure recovery on the upper surface near the trailing edge of the airfoil. This suggests that with bleed the separation on the upper surface is significantly reduced, and in turn, the supersonic region becomes larger, and thus moving the shock downstream despite the fact that there is a decrease in Mach number when bleed is applied. In addition, reducing the sidewall boundary layer displacement thickness with bleed for this moderately high angle of attack case improves the spanwise uniformity at the 50 percent chord station. It is interesting to note at 80 percent chord where the flow is subsonic and possibly separated that the spanwise distribution is uniform. At the 15 percent chord station, the spanwise distribution again suggests possible wave disturbances emanating from the region at the junction of the airfoil leading edge and sidewall.

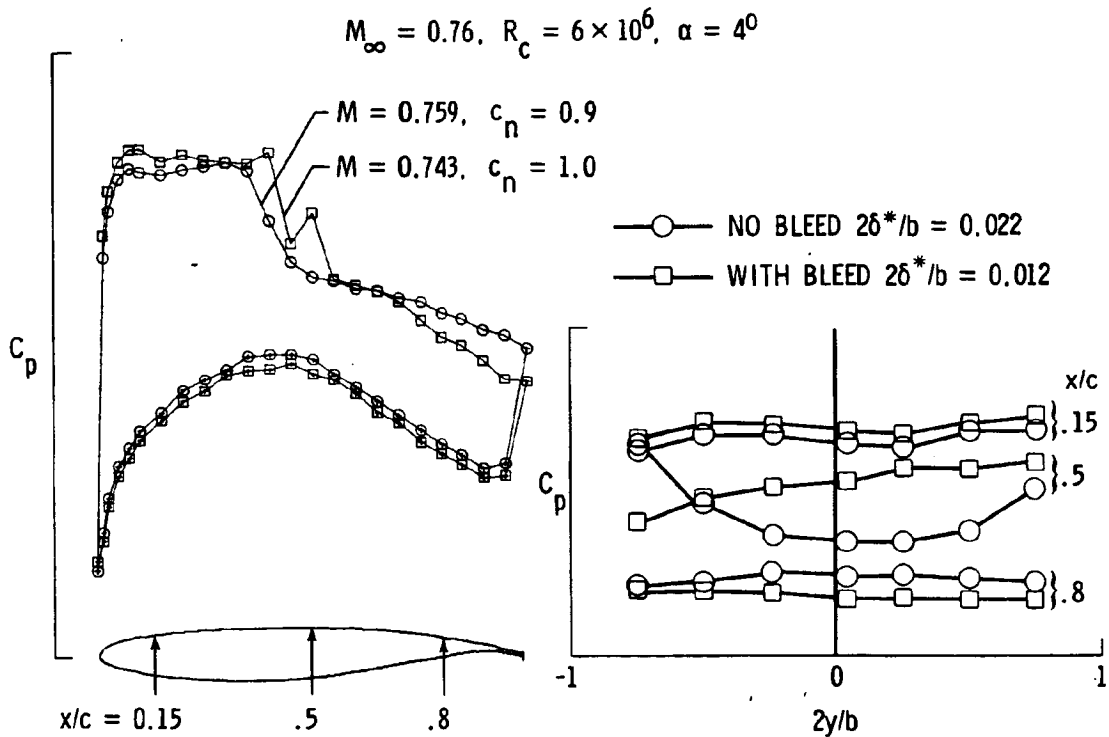


Figure 8.- Effect of sidewall boundary layer bleed on spanwise pressure distribution.

## EFFECT OF REYNOLDS NUMBER

The effect of Reynolds number with and without bleed is shown in Figure 9 for a high angle of attack ( $\alpha = 6^\circ$ ) high lift case. For this high angle of attack condition the flow over the airfoil tends to be somewhat three-dimensional and the analysis of the flow becomes quite difficult and complex. As was noted previously for  $\alpha = 4^\circ$ , when bleed is applied for the  $R_c = 6 \times 10^6$  condition there is an increase in the pressure recovery on the trailing edge of the upper surface of the airfoil indicating that bleed decreases the boundary layer separation on the upper surface of the airfoil. Again the region of supersonic flow increases when bleed is applied and the shock location moves downstream despite the decrease in Mach number. When the Reynolds number is increased to  $25 \times 10^6$  the effect of bleed is not nearly as pronounced as it was for the lower Reynolds number of  $6 \times 10^6$ . For the rest of the figures the data will be at  $R_c = 25 \times 10^6$  (with one exception for the shock-free baseline case at  $\alpha = 0^\circ$  and  $R_c = 6 \times 10^6$ , which will be shown in a subsequent figure). This value of Reynolds number ( $R_c = 25 \times 10^6$ ) is near the design and flight conditions for this class of airfoil and also eliminates the uncertainties in the location of transition.

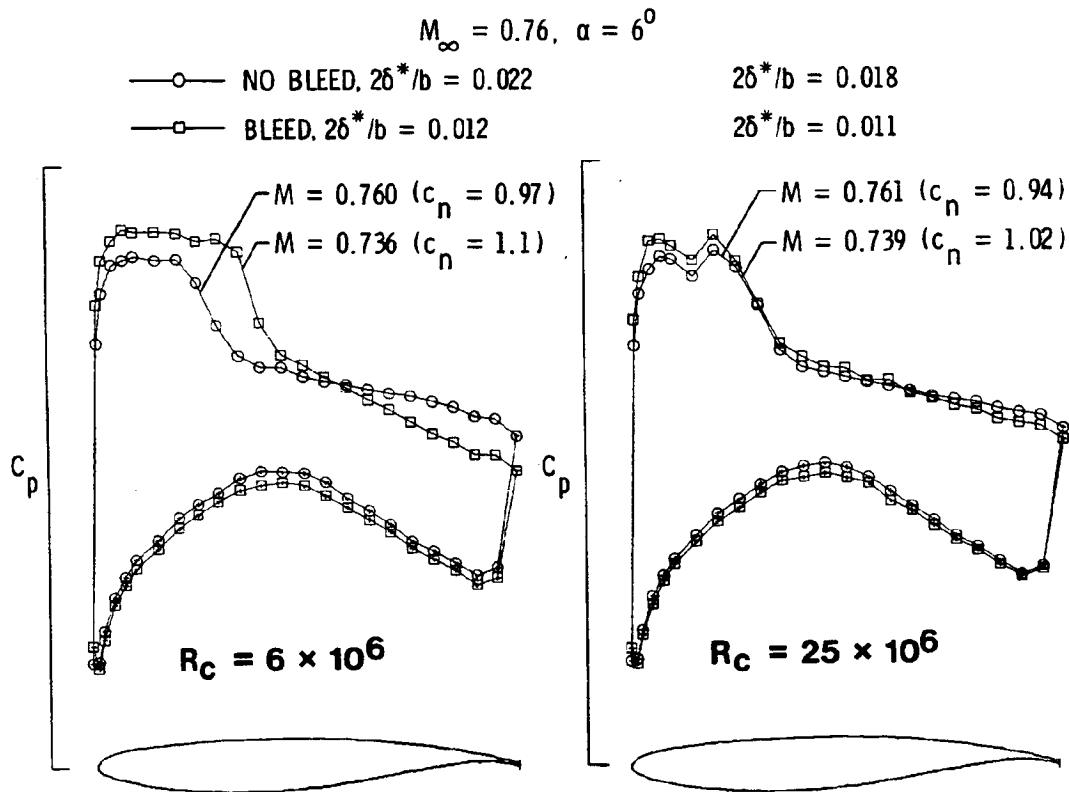


Figure 9.- Effect of Reynolds number with and without bleed.

## AIRFOIL PRESSURE DISTRIBUTION WITH BLEED

The effect of sidewall boundary layer bleed on the pressure distribution at a nominal free stream Mach number of 0.70 is shown in Figure 10. Up to this point all the data shown have been at a nominal free stream Mach number of 0.76 and all the flow on the upper surface of the airfoil has been predominately supercritical. In Figure 10 at  $\alpha = 0^\circ$  the flow is subcritical and when bleed is applied there is no change in the pressure distribution. However, at  $\alpha = 2^\circ$  when the flow becomes supercritical and there are strong shocks on the upper surface, the effect of bleed is to cause an upstream movement in shock position. The movement of the shock for this condition again is a combined effect of Mach number and the change in the sidewall  $\delta^*$ ; however, this combined effect is accounted for by the Barnwell-Sewall flow similarity correction (refs. 5 and 7).

The data thus far indicate that the effect of bleed on the pressure distributions for shock free supercritical and subcritical flow is not significant. However, when the flow is supercritical, with strong shocks, the position of the shock can change depending on the combined influence of the change in Mach number and the change in sidewall  $\delta^*$ .

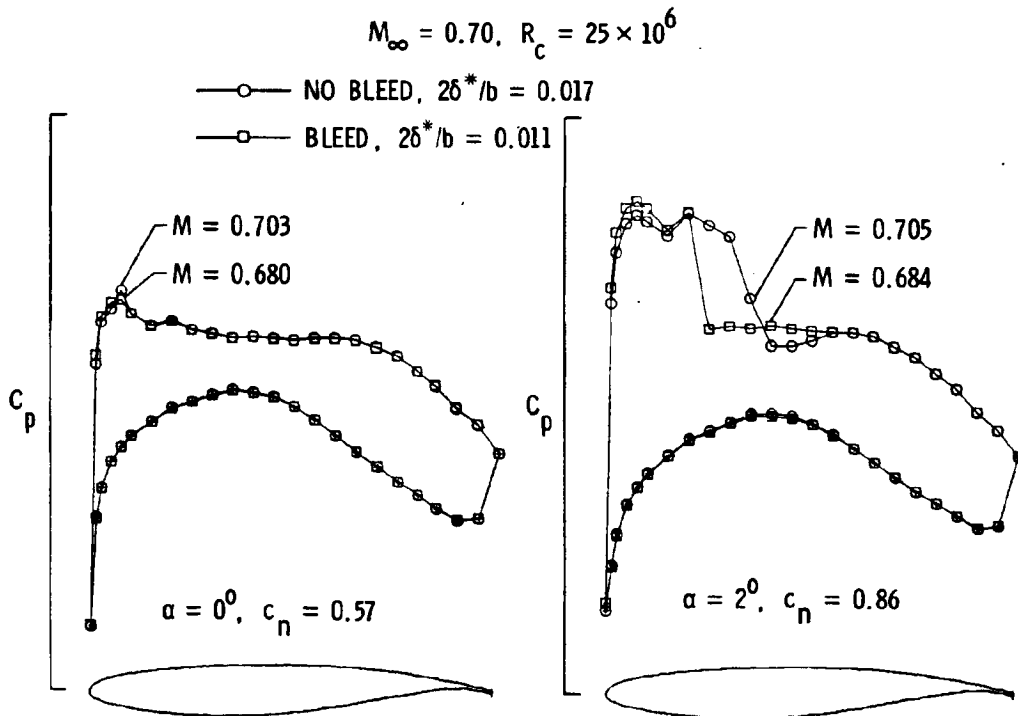


Figure 10.- Effect of sidewall boundary layer bleed on airfoil pressure distribution.

## DATA-THEORY COMPARISON

The effects on airfoil data with and without bleed are examined in Figures 11 through 16 by comparing the uncorrected and corrected experimental pressure distributions with the GRUMFOIL (refs. 10, 11 and 12) 2-D transonic airfoil code. The corrections to the experimental data consist of (1) only sidewall corrections, and (2) combined top and bottom wall and sidewall corrections. The sidewall correction is based on the procedures suggested by Barnwell (ref. 5) and Sewall (ref. 7) and consists of making global corrections to the measured Mach number, pressure coefficients, and lift coefficient. The top and bottom wall interference assessment and correction have been made using the transonic flow computations developed by Kemp (refs. 2 and 13). To correct for both sidewall boundary layer and top and bottom wall effects, two procedures, sequential and unified, either of which can be considered to be equally valid, have been suggested recently by Kemp and Adcock (ref. 14). In the present calculations, for purposes of convenience, the sequential procedure has been adopted.

### SUBCRITICAL CASE-NO BLEED

A comparison of data with GRUMFOIL is shown in Figure 11 for a subcritical case at a nominal free stream Mach number of 0.70 with no bleed. For the uncorrected data the agreement between the data and theory is fairly good. This indicates, at this high Reynolds number, which results in 1.7 percent  $\delta^*$  (on both walls--in relation to the total span), that the corrections for the subcritical case are quite small. When the sidewall correction is applied to the data, there is a 0.016 decrease in the Mach number at the airfoil and the agreement between the data and theory improves, particularly on the lower surface.

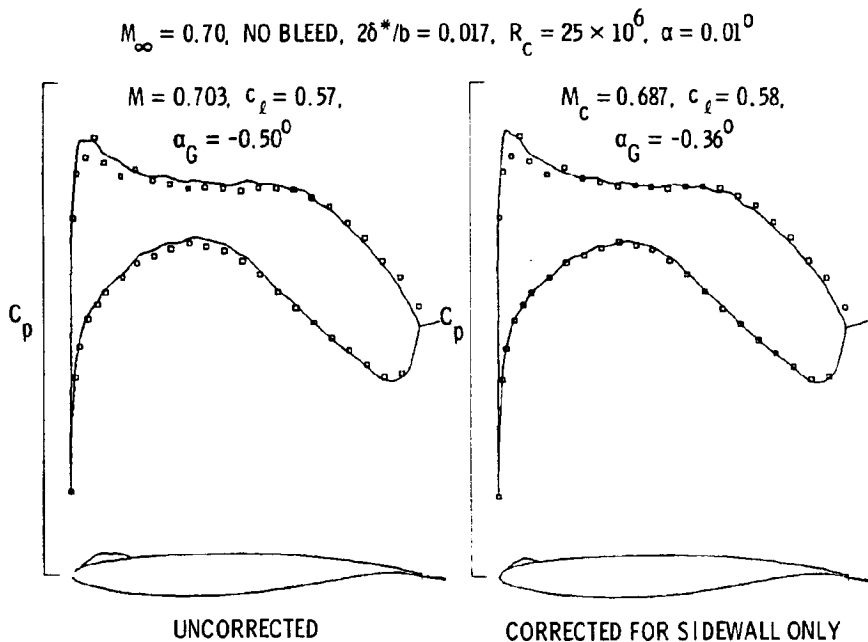


Figure 11.- Comparison of data with GRUMFOIL for a subcritical case.

SUBCRITICAL CASE-WITH BLEED

A comparison of data with GRUMFOIL is shown in Figure 12 for a subcritical case with sidewall boundary layer bleed. When the bleed is applied the  $\delta^*$  reduces to 1.1 percent of the span and the agreement between the uncorrected data and theory is quite good. When the sidewall correction is made the Mach number correction is about 0.010 and the agreement between the data and theory is further improved. In general, the effect of bleed on the data-theory comparison was not significant; however, it is interesting to note that even with boundary layer bleed a sidewall correction was needed to get the best agreement with theory and data. It is felt that the comparison of the corrected and uncorrected data with GRUMFOIL will serve as a guide to check the validity of state of the art wall corrections to the 2-D airfoil data, primarily because the GRUMFOIL computer code is considered to represent the present state of the art for making 2-D transonic airfoil flow field calculations.

ORIGINAL PAGE IS  
OF POOR QUALITY

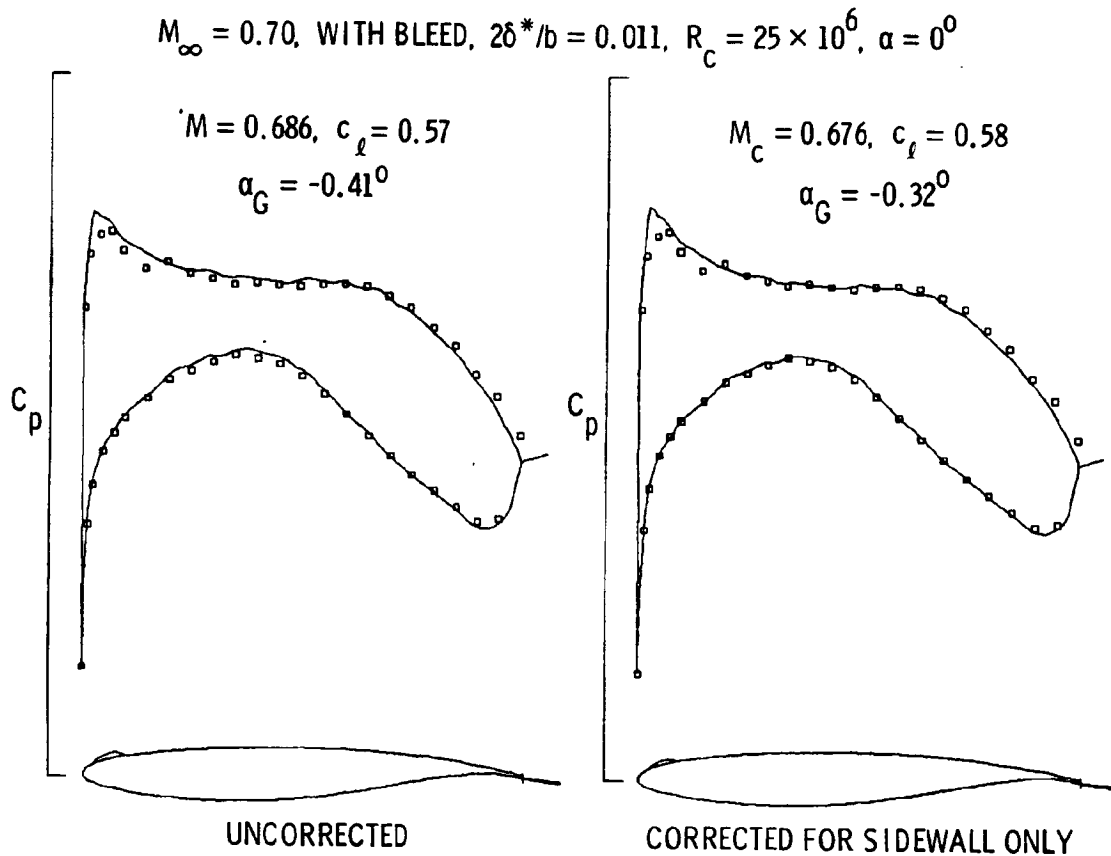


Figure 12.- Comparison of data with GRUMFOIL for a subcritical case.

NEAR DESIGN LIFT CASE - NO BLEED

A comparison of data with GRUMFOIL at near the design lift is shown in Figure 13 for the baseline, supercritical shock-free case (see Figures 4, 5, and 7) with no bleed at  $R_c = 6 \times 10^6$ . This is the only data-theory comparison at the lower Reynolds number which has a sidewall  $\delta^*$  of 2.2 percent of the span. The comparison between the uncorrected data and theory shows a noticeable discrepancy in the supersonic region on the upper surface and some discrepancy on the lower surface. When the sequential procedure is used for the combined sidewall and top and bottom wall correction there is a net 0.010 decrease in Mach number at the model (top and bottom wall has  $\Delta M = +0.009$ , and the sidewall has a  $\Delta M = -0.019$ ). The correction results in some improvement in the agreement on the upper surface, particularly in the supercritical region, with not much change on the lower surface. When the corrections are made for the sidewall only ( $\Delta M = -0.019$ ) the agreement is excellent on the lower surface and is considerably improved on the upper surface. Thus it appears that the sidewall similarity correction procedure may provide a quick and simple method that accounts for most of the blockage effects. These results were quite surprising considering the importance normally attributed to the top and bottom wall effects in contrast to the sidewall effects which are often ignored.

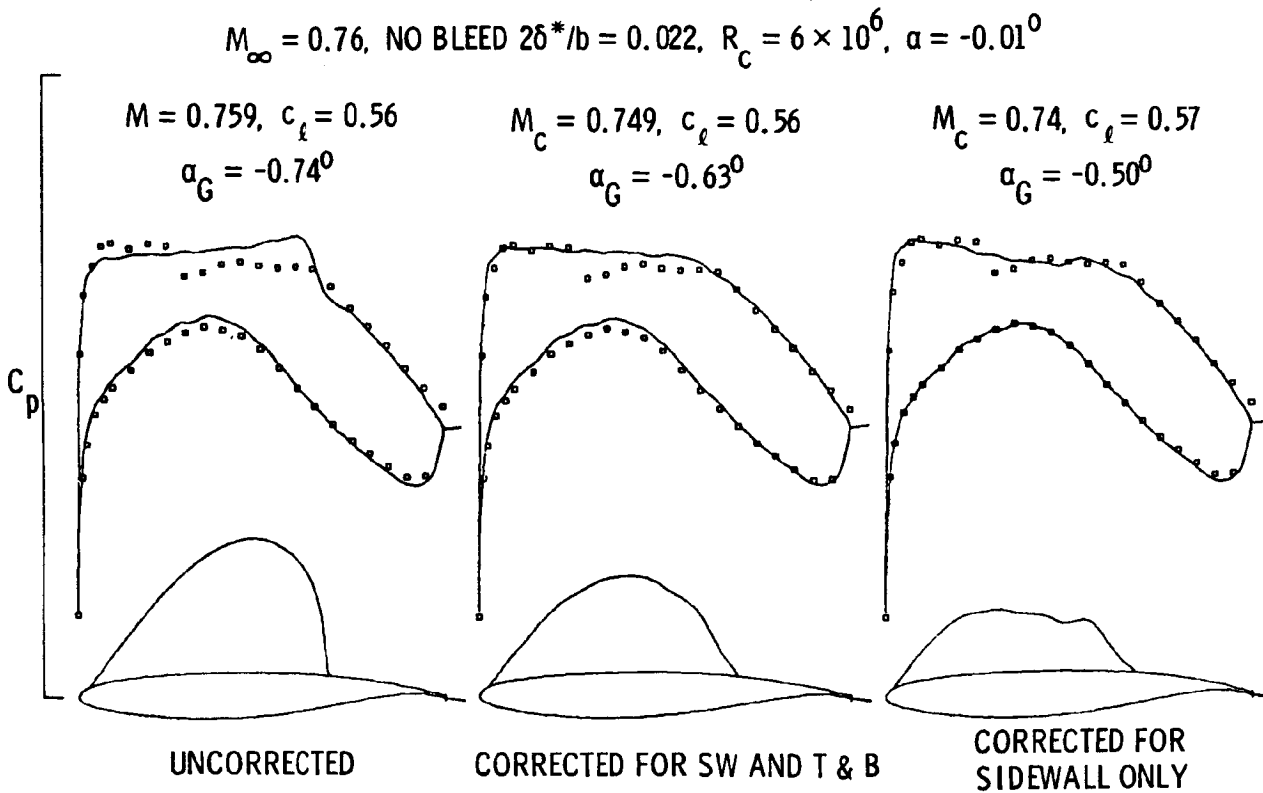


Figure 13.- Comparison of data with GRUMFOIL at near design lift.

### NEAR DESIGN LIFT CASE WITH BLEED

A comparison of data with GRUMFOIL is shown in Figure 14 for a case near the design lift with bleed applied at a Reynolds number of  $25 \times 10^6$ . When bleed is applied and the Reynolds number is increased to  $25 \times 10^6$  the  $\delta^*$  on the sidewall reduces by a factor of 2 from the previous data in Figure 13 to 1.1 percent of the span. The agreement between the uncorrected data and theory is much improved as a result of the combined effect of bleed and increasing Reynolds number. When the sidewall correction ( $\Delta M = -0.010$ ) is applied to the data, the agreement with GRUMFOIL is again improved. The agreement on the lower surface is excellent; however, the upper surface expansions and compression in the supersonic region are not completely predicted by the theory. Again it can be seen that even when sidewall bleed is applied, a sidewall correction is needed to get good agreement between data and GRUMFOIL.

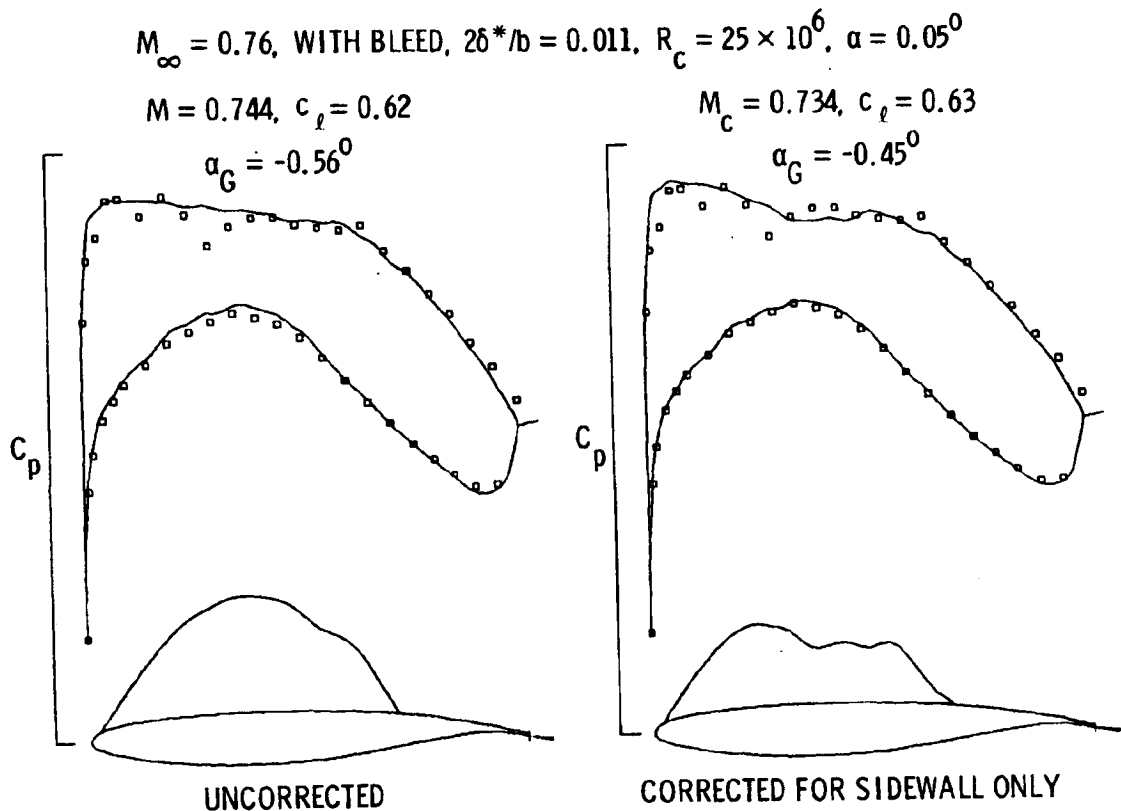


Figure 14.- Comparison of data with GRUMFOIL at near design lift.

## HIGH LIFT CASE - NO BLEED

A comparison of data with GRUMFOIL for a high lift case ( $\alpha \sim 2^\circ$ ) with a strong shock is shown in Figure 15 with no sidewall bleed and sidewall  $\delta^*$  that is 1.8 percent of the span. With no corrections there is considerable disparity between data and theory particularly on the upper surface of the airfoil. When the sequential procedure is used the sidewall correction to Mach number is  $-0.016$  and the top and bottom wall correction is  $+0.018$ , which results in a net  $\Delta M = +0.002$ . The sequential procedure correction improves the agreement on the upper surface; however, on the lower surface the agreement is not as good as it was with the uncorrected data. When the sidewall correction is applied there is good agreement on the lower surface, good agreement in the supercritical region, and good prediction of the shock location; however, downstream of the shock on the upper surface the measured pressures are much lower than the predictions of GRUMFOIL. A possible explanation of the low pressure near the trailing edge of the upper surface is that there is considerable thickening of the sidewall boundary layer downstream of the shock wave which tends to accelerate the subsonic flow in this region.

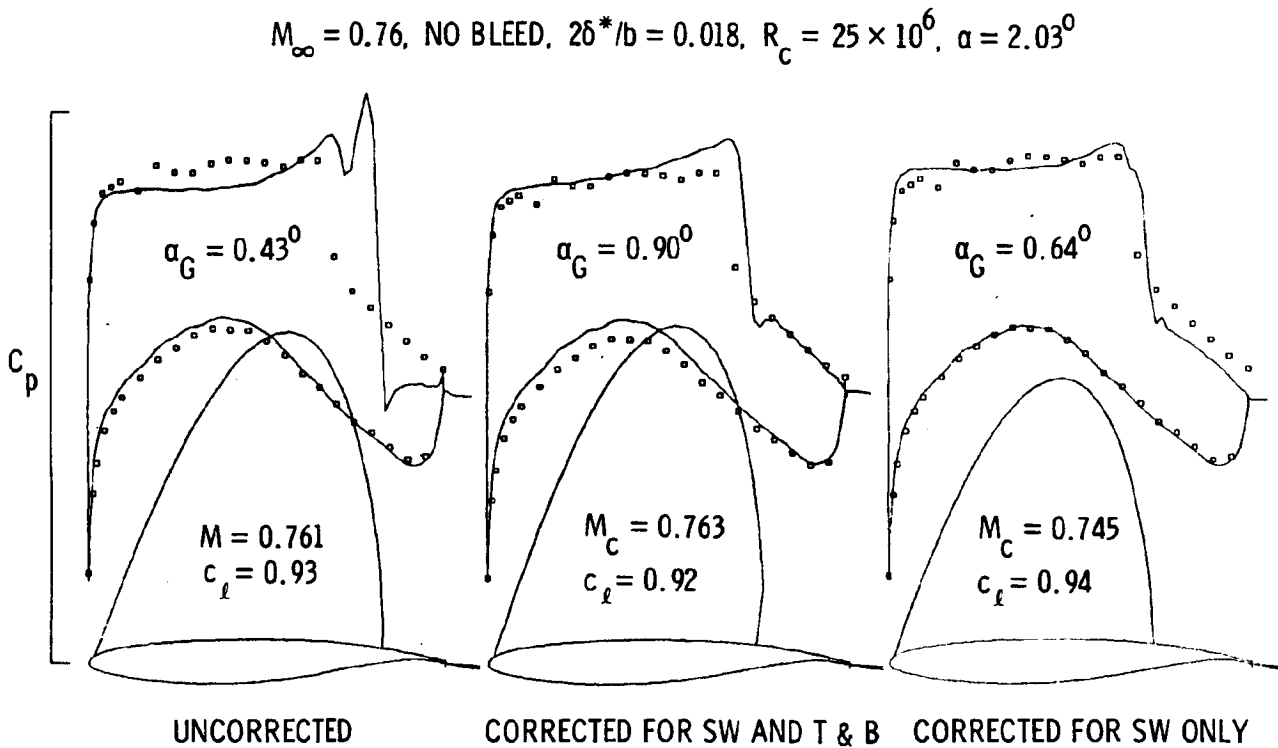


Figure 15.- Comparison of data with GRUMFOIL for a high lift case.

## HIGH LIFT CASE WITH BLEED

A comparison of data with GRUMFOIL is shown in Figure 16 for a high lift case with sidewall bleed which reduces the sidewall  $\delta^*$  to 1.1 percent of the span. When the bleed is applied, the data-theory agreement for the uncorrected data is greatly improved over the no bleed condition shown on Figure 15; however, with no sidewall correction, the shock position is not correctly predicted. When the sidewall correction is made ( $\Delta M = -0.010$ ) the data and GRUMFOIL indicate excellent agreement on the lower surface and improved agreement on the upper surface, and a correct prediction of the shock location. Thus even with sidewall bleed, an appropriate sidewall correction must be made. In general, it was observed in Figures 11 through 16 that with the measured Mach number corrected for only sidewall effects, the shock location and the pressure distribution are remarkably well predicted. This result was surprising in view of the first-order global treatment of the model-induced sidewall boundary layer effects.

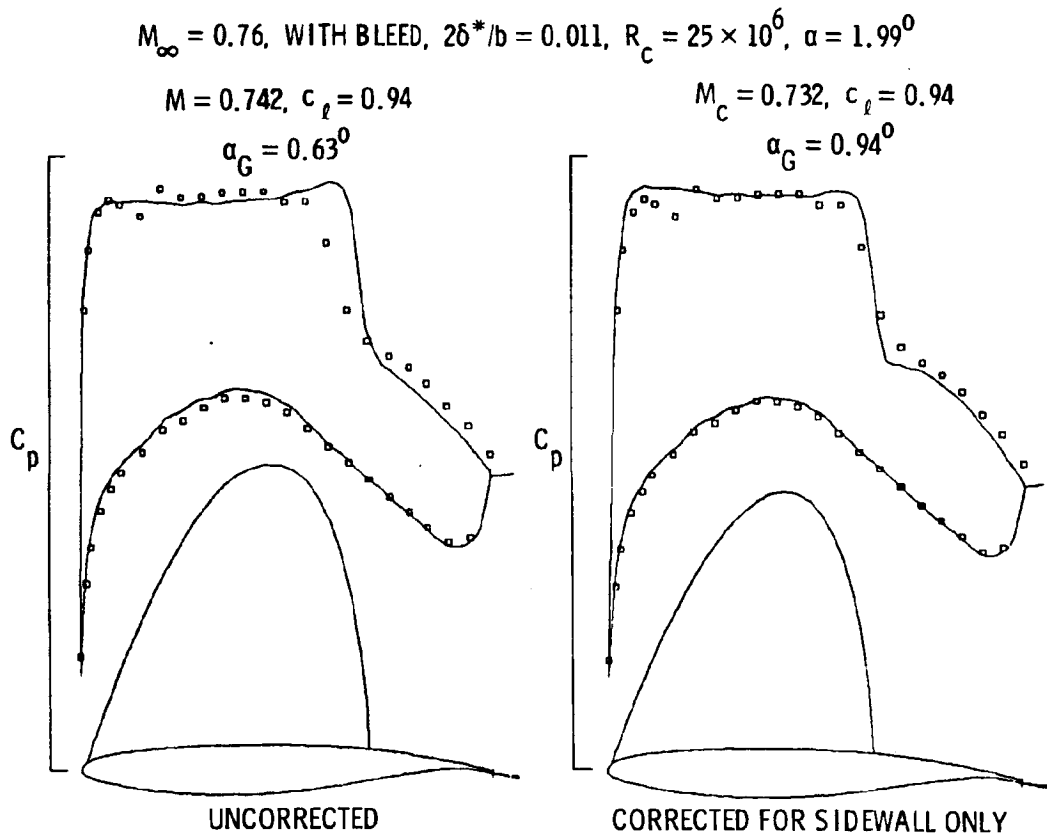


Figure 16.- Comparison of data with GRUMFOIL for a high lift case.

## CONCLUDING REMARKS

Wind tunnel tests conducted on an advanced-technology 12-percent supercritical airfoil with and without upstream sidewall boundary layer bleed over the range of sidewall boundary layer displacement thicknesses of  $2\delta^*/b \sim 0.02$  to 0.01 indicated the following:

1. The effects of bleed on mid-span pressure distributions are not significant for subcritical conditions.
2. For supercritical conditions, the shock position is affected by bleed.
3. At a high lift condition, sidewall boundary layer bleed has a significantly larger effect on the low Reynolds number pressure distributions than on the high Reynolds number distributions.
4. Sidewall boundary layer bleed tends to improve the spanwise uniformity of the pressure distribution at increased angles of attack.
5. For supercritical conditions sidewall boundary layer bleed smooths the shape of the total head wake behind the airfoil.
6. For supercritical flows in this tunnel the shock position and pressure distribution compare well with GRUMFOIL predictions when the sidewall similarity rule is used to correct for sidewall boundary layer effects.
7. The sidewall boundary layer removal reduces the magnitude of the sidewall corrections. However, suitable corrections must still be made.

## REFERENCES

1. Mokry, M. and Ohman, L. H.: Application of the Fast Fourier Transform to Two-Dimensional Wind Tunnel Wall Interference. Journal of Aircraft, Vol. 17, No. 6, pp. 402-408, June 1980.
2. Kemp, W. B.: Transonic Assessment of Two-Dimensional Wind Tunnel Wall Interference Using Measured Wall Pressures. Advanced Technology Airfoil Research, Vol. I, NASA CP-2045, 1979, pp. 473-486.
3. Murman, E. M.: A Correction Method for Transonic Wind Tunnel Wall Interference. AIAA Paper 79-1533, July 1979.
4. Bernard-Guelle, Rene: Influence of Wind Tunnel Wall Boundary-Layers on Two-Dimensional Transonic Tests. NASA TT F-17255, October 1976.
5. Barnwell, R. W.: Similarity Rule for Sidewall Boundary Layer Effect in Two-Dimensional Wind Tunnels. AIAA Journal, Vol. 18, Sept. 1980, pp. 1149-1151.
6. Winter, K. G. and Smith, J. H. B.: A Comment on the Origin of Endwall Interference in Wind Tunnel Tests of Aerofoils. RAE Tech Memo. Aero 1816, August 1979.
7. Sewall, W. G.: The Effects of Sidewall Boundary Layer in Two-Dimensional Subsonic and Transonic Wind Tunnels. AIAA Journal, Vol. 20, Sept. 1982, pp. 1253-1256.
8. Ray, E. J., Ladson, C. L., Adcock, J. B., Lawing, P. L., and Hall, R. M.: Review of Design and Operational Characteristics of the 0.3-Meter Transonic Cryogenic Tunnel. NASA TM-80123, Sept. 1979.
9. Murthy, A. V., Johnson, C. B., Ray, E. J., and Lawing, P. L.: Recent Sidewall Boundary Layer Investigations with Suction in the Langley 0.3-m Transonic Cryogenic Tunnel. AIAA Paper No. 82-0234, January 1982.
10. Melnik, R. E., Chow, R., and Mead, H. R.: Theory of Viscous Transonic Flow Over Airfoils at High Reynolds Number. AIAA Paper No. 77-680, June 1977.
11. Melnik, R. E.: Wake Curvature and Trailing-Edge Interaction Effects in Viscous Flow over Airfoils. Advanced Technology Airfoil Research, NASA CP-2045, pp. 255-270, 1979.
12. Melnik, R. E.: Turbulent Interactions on Airfoils at Transonic Speeds--Recent Developments. Computations of Viscous-Inviscid Interactions. AGARD CP-291, 1981.
13. Kemp, W. B.: TWINTAN; A Program for Transonic Wall Interference Assessment in Two-Dimensional Wind Tunnels. NASA TM-81819, May 1980.
14. Kemp, W. B. and Adcock, J. B.: Combined Four-Wall Interference Assessment in Two-Dimensional Airfoil Tests. AIAA Paper No. 82-0586, March 1982.

N85 12020

49

PERFORMANCE OF TWO TRANSONIC AIRFOIL WIND  
TUNNELS UTILIZING LIMITED VENTILATION

J. D. Lee and G. M. Gregorek  
The Ohio State University  
Columbus, Ohio

PRECEDING PAGE BLANK NOT REPRODUCED

Preceding page blank

## ABSTRACT

A limited-zone ventilated wall panel was developed for a closed-wall icing tunnel which permitted correct simulation of transonic flow over model rotor airfoil sections with and without ice accretions. Candidate porous panels were tested in the OSU 6- × 12-inch transonic airfoil tunnel and result in essentially interference-free flow, as evidenced by pressure distributions over a NACA 0012 airfoil for Mach numbers up to 0.75. Application to the NRC 12- × 12-inch icing tunnel showed a similar result, which allowed proper transonic flow simulation in that tunnel over its full speed range.

ORIGINAL PAGE IS  
OF POOR QUALITY

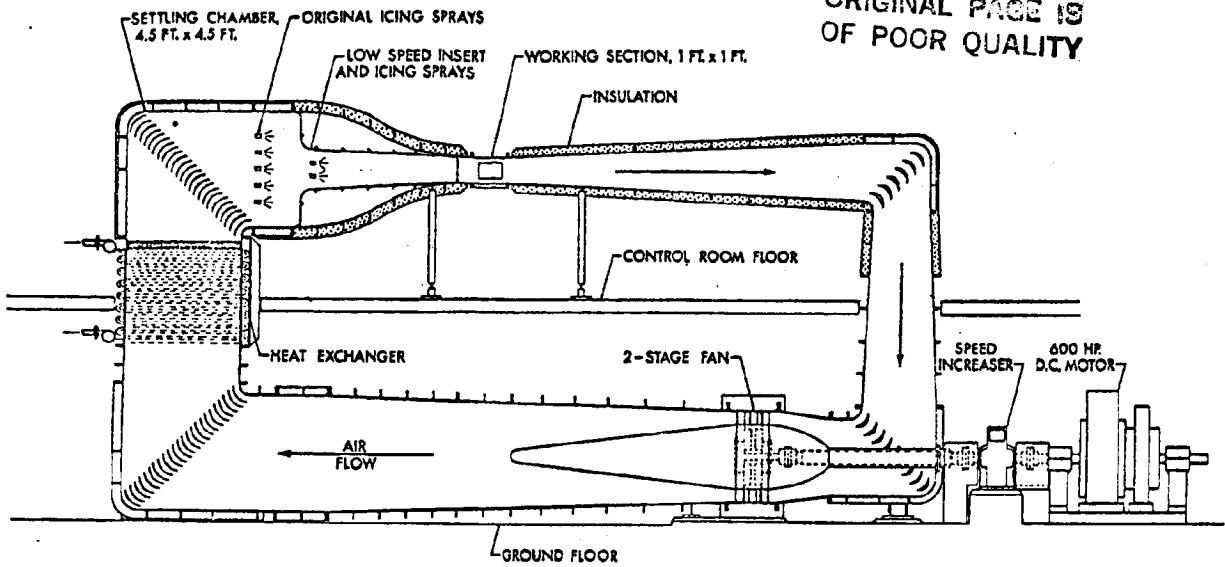


Figure 1. - High-speed icing wind tunnel.

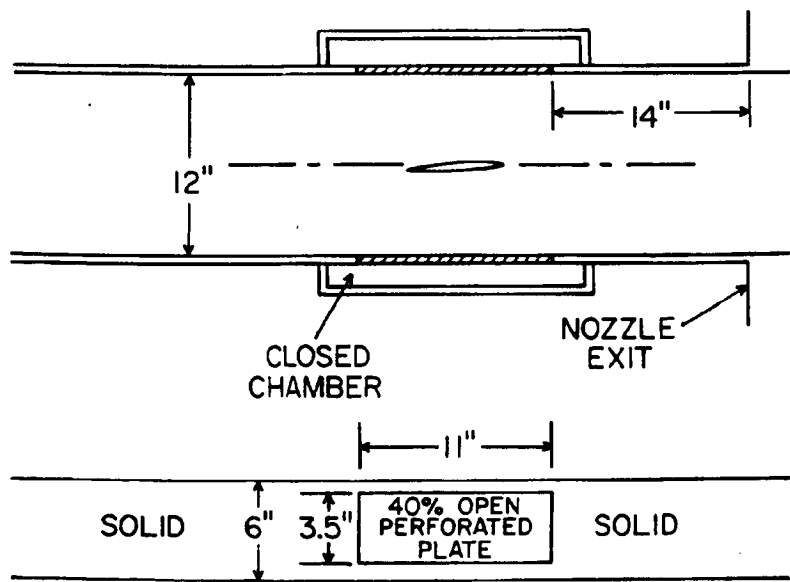


Figure 2. - Configuration tested in the OSU 6- x 12-in. high Reynolds number transonic wind tunnel as a simulation of proposed modification to NRC high-speed icing tunnel.

ORIGINAL PAGE IS  
OF POOR QUALITY

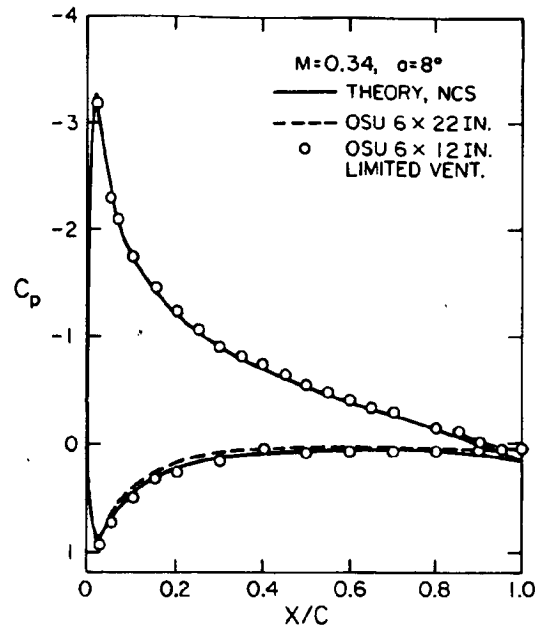


Figure 3. - Comparison of subcritical data from OSU 6- x 12-in. tunnel with limited ventilation panel with other data and theory.

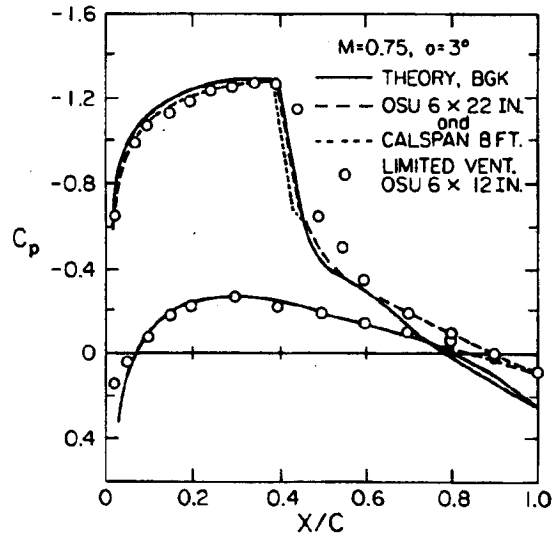


Figure 4. - Comparison of supercritical data from OSU 6- x 12-in. tunnel with limited ventilation panel with other data and theory.

ORIGINAL LOCATION  
OF PHOTOGRAPH

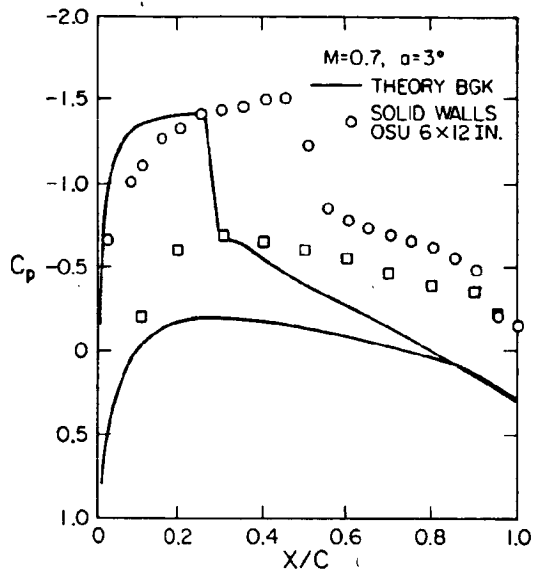


Figure 5. - Comparison of supercritical flow theory with experiment showing interference from solid wall. NACA 0012;  $C = 6$  in.

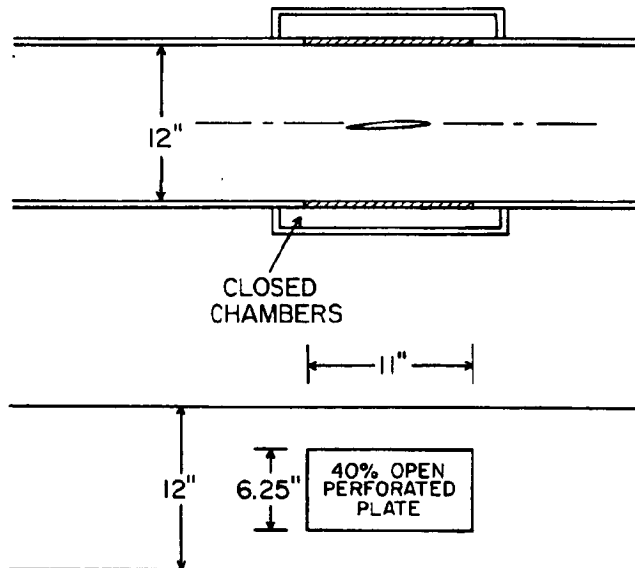


Figure 6. - Dimensions of NRC high-speed icing tunnel with ventilated panels proposed and tested.

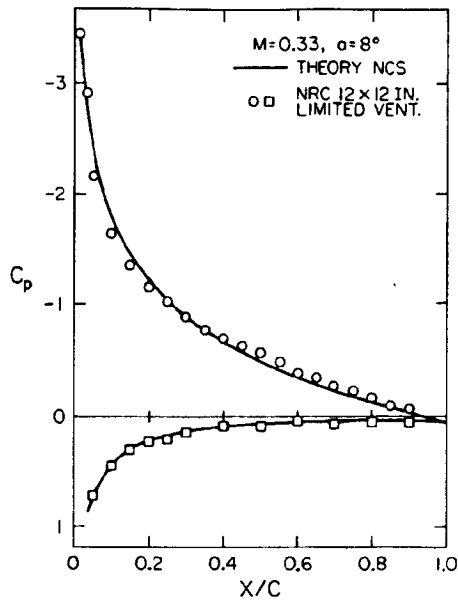
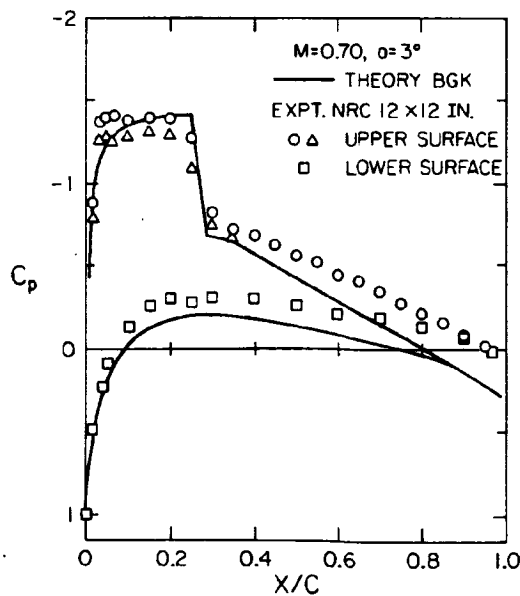


Figure 7. - Comparison of subcritical data from NRC 12- x 12-in. icing tunnel having limited ventilation panels with theory. NACA 0012;  $C = 6$  in.



UNCLASSIFIED  
OF POOR QUALITY

Figure 8. - Comparison of supercritical data from NRC 12- x 12-in. icing tunnel having limited ventilation panels with theory. NACA profile;  $C = 6$  in. (Compare with figs. 4 and 5.)

N85 12021 210

EXPERIMENTS SUITABLE FOR WIND TUNNEL WALL  
INTERFERENCE ASSESSMENT/CORRECTION

Joseph G. Marvin  
NASA Ames Research Center  
Moffett Field, California

## INTRODUCTION

The Experimental Fluid Dynamics Branch has been conducting careful experiments intended to verify advanced computer codes being developed at Ames Research Center. Part of that effort is directed toward verification experiments at transonic speeds and high Reynolds numbers. The purpose of this paper will be to report on three experiments that contain information suitable for assessing wind tunnel wall interference and verifying techniques used to correct for interference effects. The experiments are: (1) a series of airfoil tests using a newly designed transonic flow facility that employs side-wall boundary layer suction and upper- and lower-wall shaping; (2) tests on a swept airfoil section spanning a solid-wall wind tunnel with fixed contouring on all four walls; and (3) tests on a swept wing of aspect ratio 3 mounted in a solid-wall wind tunnel with fixed flat walls. Each of the experiments provides data on the airfoil sections as well as on the wind tunnel walls.

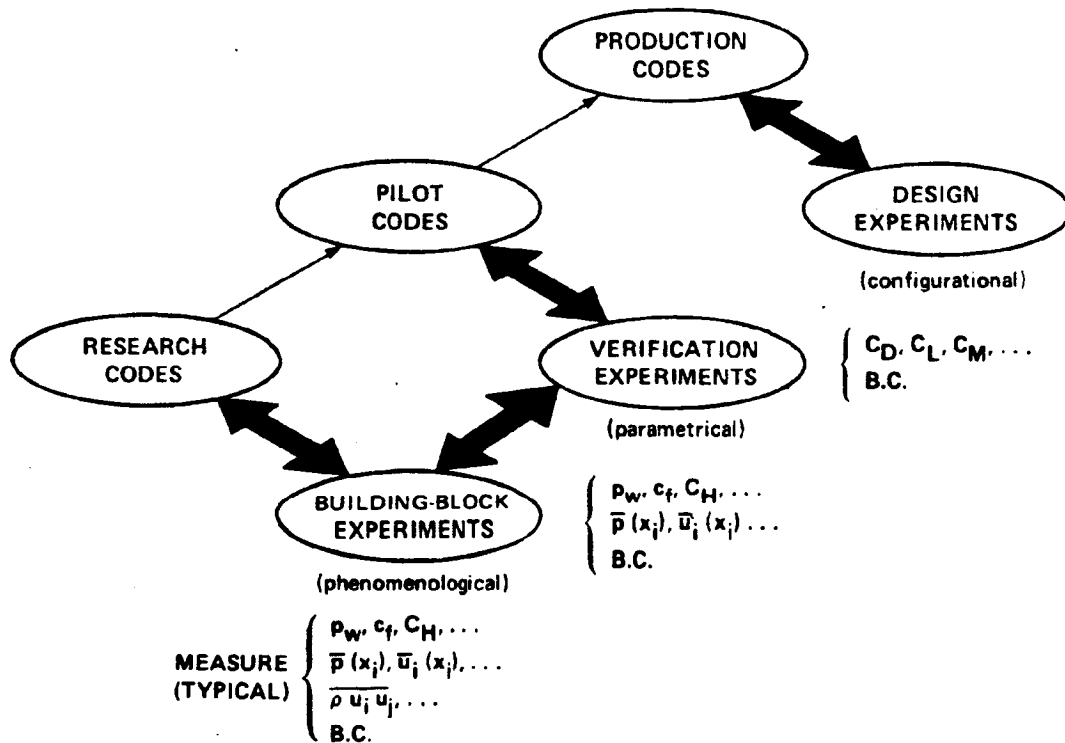
- o INTRODUCTION
  - MOTIVATION
  - FACILITIES
  
- o EXPERIMENTS SUITABLE FOR WIAC
  - AIRFOILS
  - SWEPT AIRFOIL
  - SEMI-SPAN WING
  
- o SUMMARY OF EXPERIMENTAL RESULTS
  - AIRFOILS
  - SWEPT AIRFOIL
  - SEMI-SPAN WING

December 1984

SYNERGISTIC FRAMEWORK FOR ADVANCING COMPUTATIONAL AERODYNAMICS

The primary motivation for our experiments is to provide support for the development of computational aerodynamics. The experiments are keyed directly to three stages of development: research codes, pilot codes, and production codes. Experiments supporting each stage require different measurement information.

The experiments discussed herein are verification experiments and they are intended primarily to provide benchmark data to assess the transonic codes being developed at the Ames Research Center. However, since our data requirements include simultaneous measurements on wind tunnel wall surfaces as well as model surfaces, they may be suitable for evaluating methods for assessing and/or correcting wind tunnel wall interference.



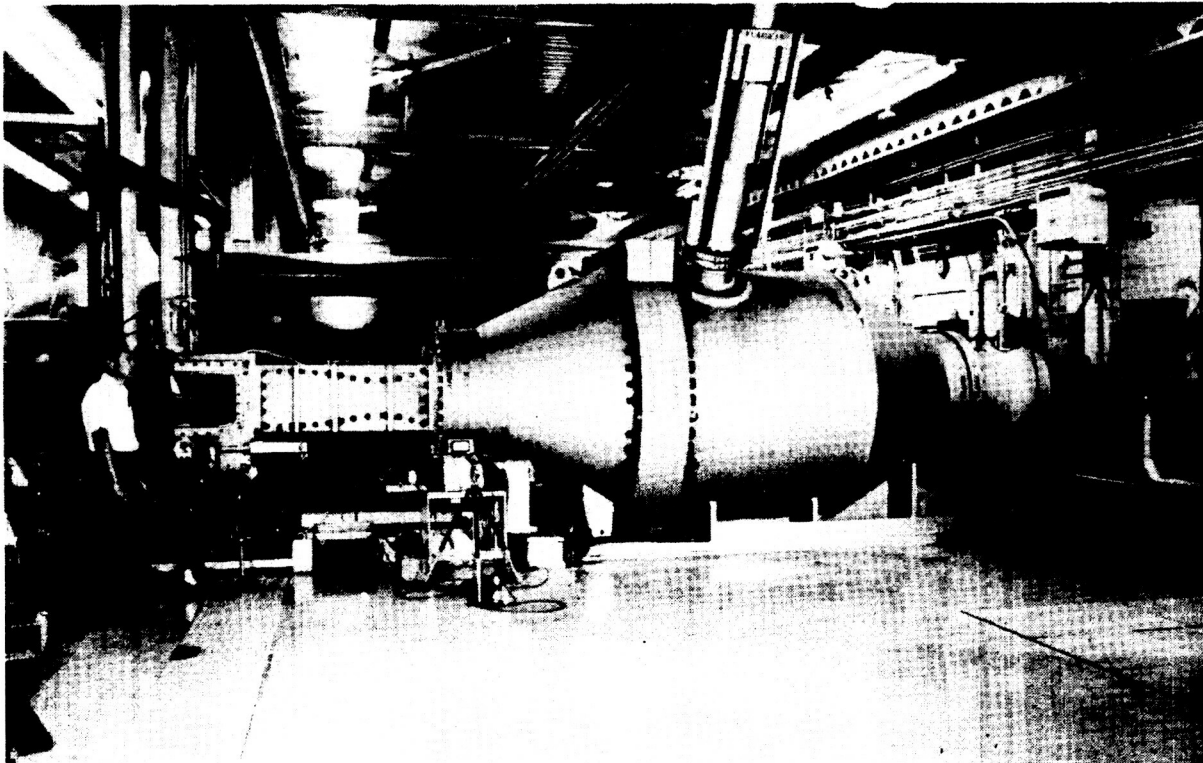
ORIGINAL TEST  
OF POOR QUALITY

## AMES HIGH REYNOLDS NUMBER FACILITY

### TUNNEL 1

A photograph of one of the test facilities used in these experiments is shown. It is a blowdown tunnel that can operate subsonically between Mach numbers of 0.4 and 0.9 for Reynolds numbers up to  $40 \times 10^6$  per foot. The Mach number is fixed by choking inserts at the downstream end of the solid-wall test section, which is rectangular with cross section dimensions of 10x15 inches and a length of 60 inches. It can also operate supersonically at Mach numbers of 2 and 3 with the rectangular test section by inserting nozzle blocks between the entrance section and the test section. The photograph was taken with the facility configured for supersonic flow. The settling chamber is fitted with a combination of screens, honeycomb and acoustic absorbing material to provide a low disturbance test stream.

The swept-airfoil and low-aspect-ratio-wing experiments were tested in this facility.

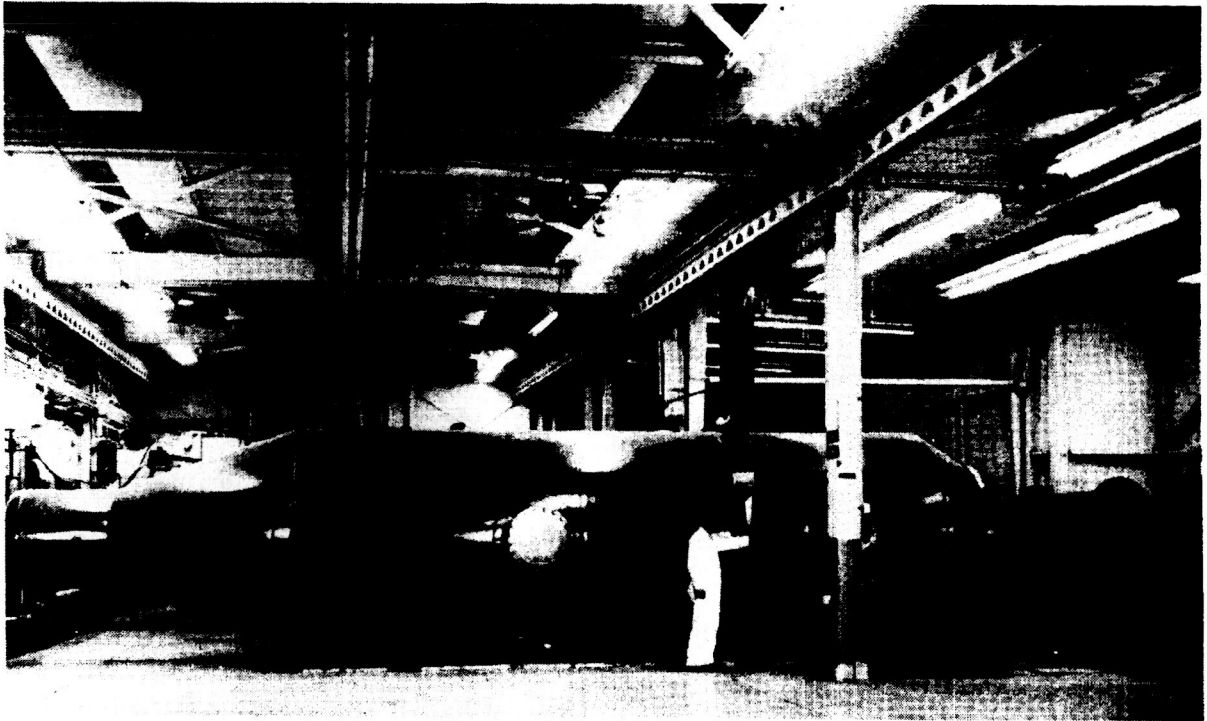


ORIGINAL DOCUMENT  
OF POOR QUALITY

## AMES HIGH REYNOLDS NUMBER FACILITY

### TUNNEL 2

A description of the design and operational characteristics of this test leg for the Ames High Reynolds Number Facility is given in reference 1.



## AIRFOIL EXPERIMENTS

The airfoil experiments are being conducted under the direction of John B. McDevitt. Two airfoil sections are being investigated. Wall and model pressures are measured simultaneously and the tests have several unique features. The NACA 0012 tests are in progress and the supercritical tests will begin later this year.

### PRINCIPAL INVESTIGATOR

JOHN McDEVITT, MAIL STOP 229-1

### AIRFOIL SECTIONS

NACA 0012 (8 INCH CHORD)

KORN-GARABEDIAN SUPERCRITICAL (8 INCH CHORD)

### MEASUREMENTS

AIRFOIL PRESSURES

TUNNEL WALL PRESSURES

LASER VELOCIMETER SURVEYS

### UNIQUE FEATURES

HIGH REYNOLDS NUMBER

SHAPED UPPER/LOWER WALLS

SIDE WALL MASS REMOVAL

ACCURATE TEST VARIABLE SETTINGS

BUFFETT ONSET DETERMINATION

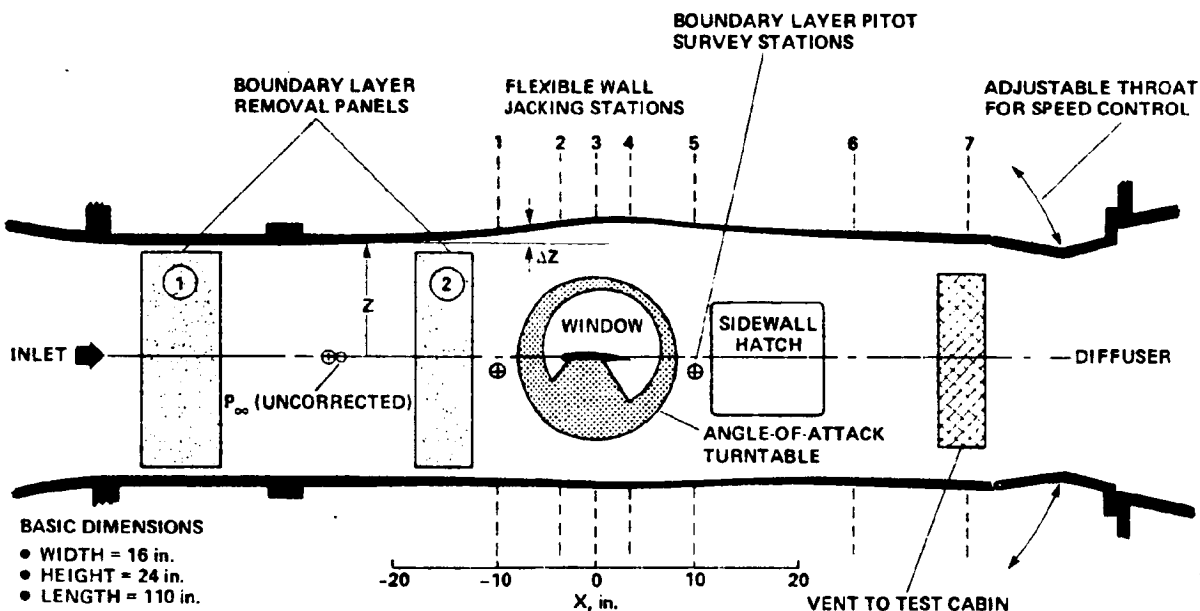
### STATUS

NACA 0012 TESTS IN PROGRESS

SUPERCRITICAL TESTS TO BEGIN FEB '83

AIRFOIL TEST SECTION

A sketch of the test section used in the airfoil tests is shown. All walls are solid. The top and bottom have flexible jacking stations to provide shaping to eliminate wall interference. On the sides, two boundary layer mass removal panels are provided. For these tests wall shapes are set to correspond to streamlines at one and a half chords from the model as computed from a Reynolds averaged Navier-Stokes code (refs. 2 and 3). Sidewall pressures are measured at various locations up to 11 inches above the tunnel centerline. It is assumed that topwall pressures are uniform across the test section and equivalent to those measured at the 11-inch sidewall stations.

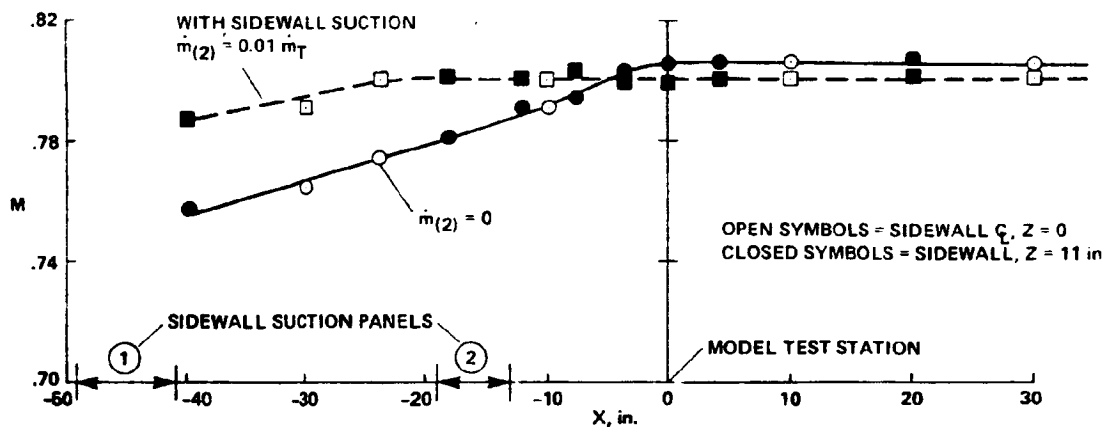
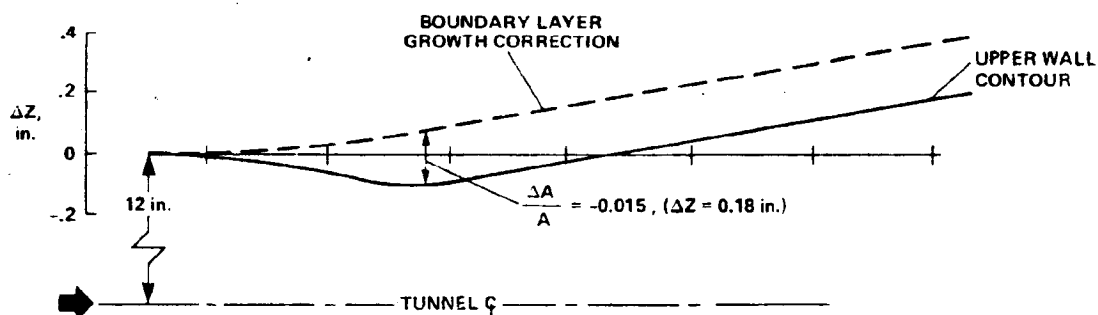


MINOR EFFECTS  
OF POOR QUALITY

### CORRECTIONS FOR WALL BOUNDARY LAYER DISPLACEMENT AND MASS REMOVAL

Wall boundary layer growth and sidewall mass removal both affect the Mach number distribution in the test section and corrections must be provided. The upper portion of the figure illustrates the tunnel empty wall corrections for the boundary layer (dashed curve) and for the combined effects of boundary layer and mass removal (solid curve).

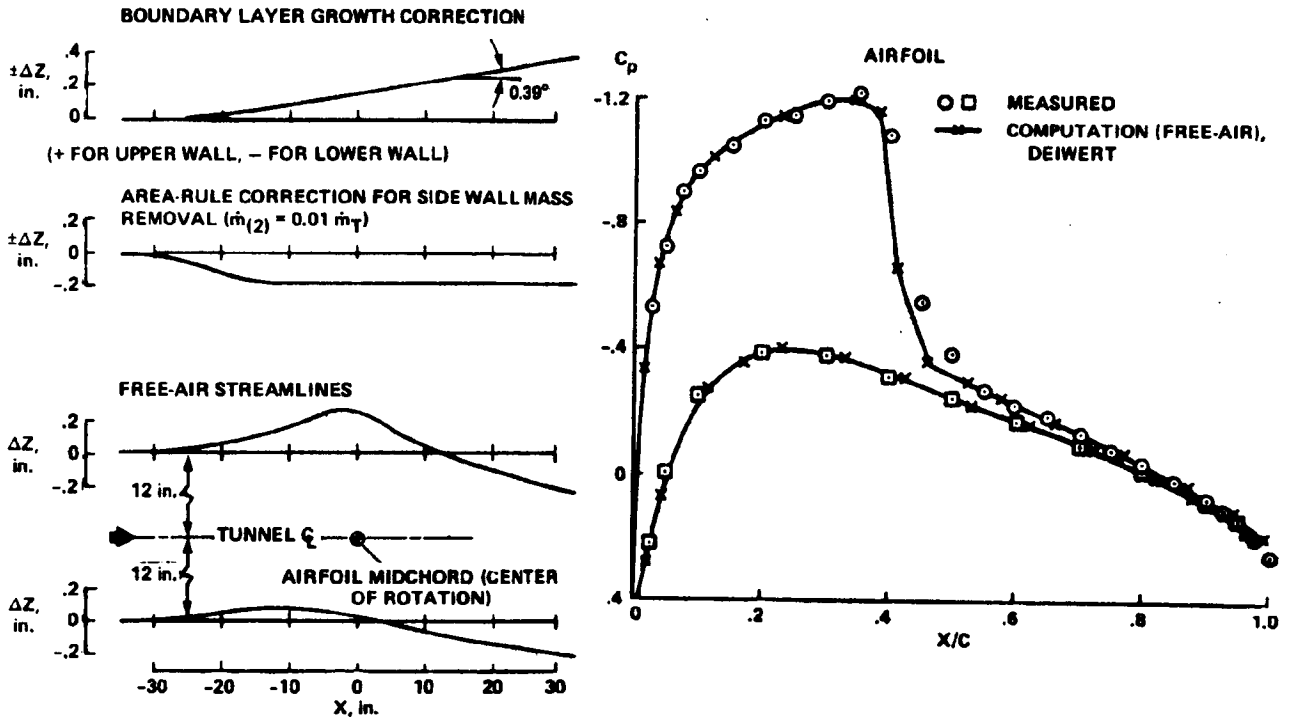
The Mach number distribution achieved in the empty tunnel with the wall corrections for mass removal and boundary layer is shown in the lower portion of the figure. The square symbols represent the distribution with mass removal and illustrate that uniform free stream Mach number can be achieved about 3 chords ahead of the model station ( $x = 0$ ). The circle symbols represent the distribution with the same contour, but for no mass removal, and a significant influence of mass removal on Mach number distribution is illustrated. Also, the difference in Mach number level for the two cases is a result of the influence of mass removal on the effectiveness of the speed control.



# NACA 0012 AIRFOIL EXPERIMENT

Additional wall shaping is employed for the airfoil tests. The separate effects of boundary layer growth correction (tunnel empty), side wall mass removal correction (tunnel empty), and the airfoil free-air streamlining to account for the airfoil are combined. The resulting airfoil pressure distribution compares well with the computation used to determine the free air streamline shapes (refs. 2 and 3).

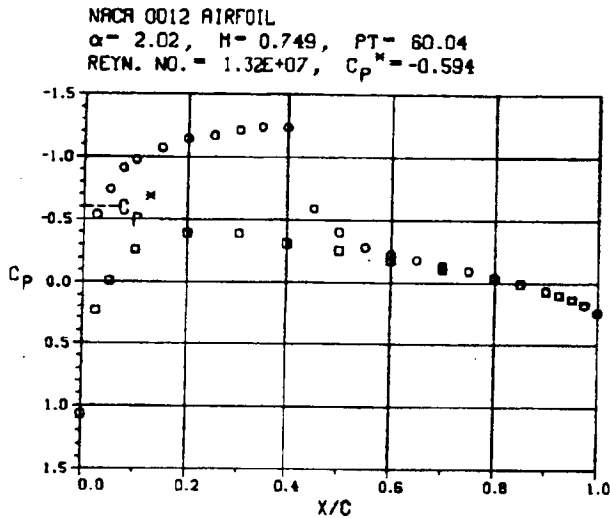
$$M_\infty = 0.75, RE_{c,w} = 10^7, \alpha = 2^\circ$$



TYPICAL TEST DATA

The data from the airfoil tests will be available in the format shown here. Wall shape settings will accompany these data which will be acquired over a range of Mach number, Reynolds number, and angle of attack. Such data will provide the opportunity to assess methods of determining and/or correcting wall interference effects.

TEST-204, RUN-73, FRAME-17



o - AIRFOIL UPPER SURFACE

X/C	C <sub>p</sub>	P/PT	M
0.000	1.061	0.976	0.185
0.025	-0.536	0.544	0.975
0.050	-0.743	0.488	1.066
0.075	-0.911	0.442	1.145
0.100	-0.979	0.424	1.178
0.150	-1.070	0.400	1.224
0.200	-1.144	0.380	1.263
0.250	-1.172	0.372	1.278
0.300	-1.215	0.360	1.301
0.350	-1.241	0.353	1.316
0.400	-1.237	0.354	1.313
0.450	-0.591	0.529	0.999
0.500	-0.405	0.580	0.918
0.550	-0.283	0.613	0.867
0.600	-0.227	0.628	0.844
0.650	-0.187	0.639	0.827
0.700	-0.142	0.651	0.808
0.750	-0.098	0.663	0.790
0.800	-0.046	0.677	0.768
0.850	0.005	0.691	0.747
0.900	0.059	0.705	0.725
0.925	0.095	0.715	0.709
0.950	0.129	0.724	0.695
0.975	0.187	0.740	0.671
1.000	0.251	0.757	0.643

□ - AIRFOIL LOWER SURFACE

X/C	C <sub>p</sub>	P/PT	M
0.025	0.237	0.753	0.650
0.050	-0.015	0.685	0.755
0.100	-0.261	0.619	0.858
0.200	-0.392	0.583	0.914
0.300	-0.389	0.584	0.912
0.400	-0.311	0.604	0.880
0.500	-0.259	0.619	0.857
0.600	-0.181	0.640	0.825
0.700	-0.113	0.658	0.796
0.800	-0.039	0.678	0.766
0.850	0.006	0.691	0.747
0.900	0.066	0.707	0.722
0.925	0.094	0.715	0.710
0.950	0.130	0.724	0.696
0.975	0.178	0.737	0.674

SIDEWALL, Z=0

X̄	C <sub>p</sub>	P/PT	M
-30.0	0.054	0.704	0.727
-24.0	0.003	0.690	0.748
-10.0	0.056	0.704	0.726
10.0	0.033	0.698	0.736
30.0	0.024	0.696	0.739

SIDEWALL, Z=11

X̄	C <sub>p</sub>	P/PT	M
-30.0	0.034	0.698	0.736
-20.0	-0.018	0.684	0.757
-16.0	-0.016	0.685	0.756
-12.0	-0.013	0.685	0.755
-8.0	-0.055	0.674	0.773
-4.0	-0.103	0.661	0.793
0.0	-0.057	0.673	0.773
4.0	-0.079	0.667	0.783
8.0	-0.021	0.683	0.759
12.0	-0.001	0.688	0.750
16.0	-0.013	0.685	0.755
20.0	-0.005	0.687	0.752
30.0	0.024	0.695	0.740

SIDEWALL, Z=-11

X̄	C <sub>p</sub>	P/PT	M
-30.0	0.043	0.700	0.732
-8.0	-0.009	0.686	0.753
-4.0	0.016	0.693	0.743
0.0	0.001	0.689	0.749
4.0	-0.008	0.686	0.753
8.0	-0.009	0.686	0.753
12.0	0.019	0.694	0.742
16.0	0.012	0.692	0.745
20.0	0.027	0.696	0.738
30.0	0.033	0.698	0.736

## SWEPT AIRFOIL EXPERIMENT

The swept airfoil experiments are being conducted under the direction of George Mateer in tunnel 1 of the High Reynolds No. Facility. When swept across the tunnel the airfoil has a NACA 0012 section in the streamwise direction. Pressures are measured simultaneously on the model and all four tunnel walls. Skin friction will also be measured on the airfoil. The tests are performed with the airfoil at zero incidence. All four tunnel walls are uniquely shaped to minimize the wall interference and establish a flow simulating infinite sweep for subcritical flow conditions. The pressure tests are complete (ref. 4) and skin friction tests are planned.

### PRINCIPAL INVESTIGATOR:

GEORGE MATEER, MAIL STOP 229-1

### AIRFOIL SECTION

NACA 0012 (STREAMWISE)

### MEASUREMENTS

AIRFOIL PRESSURES

TUNNEL WALL PRESSURES

SKIN FRICTION

### UNIQUE FEATURES

HIGH REYNOLDS NUMBER

SHAPING ON FOUR WALLS

ACCURATE TEST VARIABLE SETTINGS

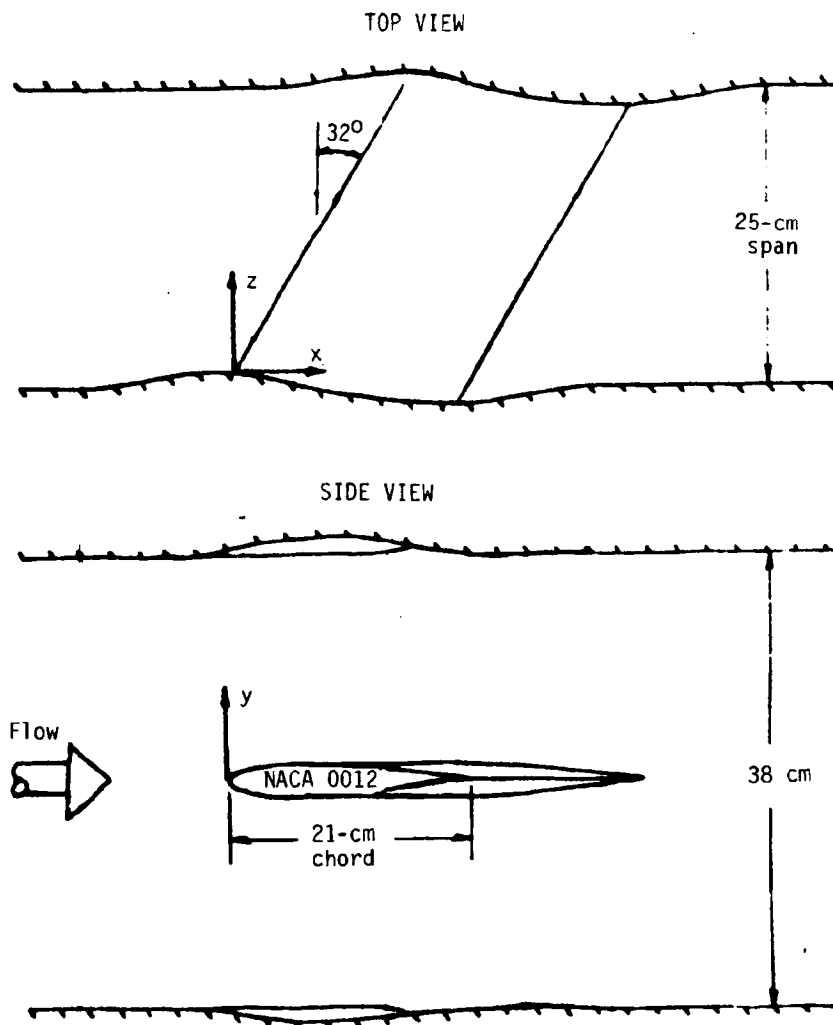
### STATUS

AIRFOIL AND WALL PRESSURE TESTS COMPLETE

SKIN FRICTION TO BEGIN SEPT 1983

## SWEPT AIRFOIL EXPERIMENTAL ARRANGEMENT

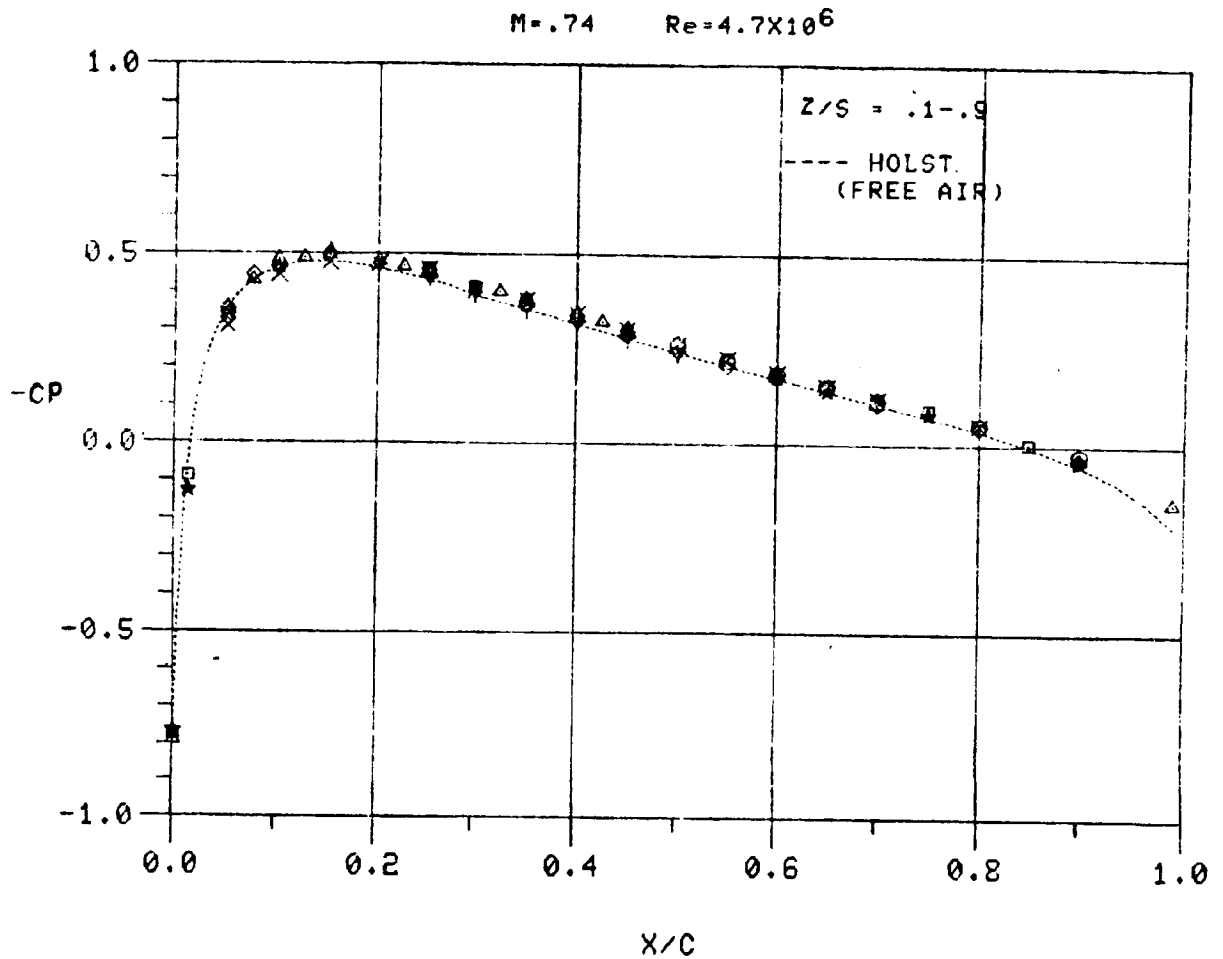
A sketch of the model installation is shown to illustrate the wall shaping. It should be noted that the sketched wall shaping is not to scale. The side and top wall shaping was determined by calculations using the inviscid transonic small disturbance code developed by Ballhaus and Bailey (ref. 5) and Bailey and Ballhaus (ref. 6) for a free stream Mach number of 0.8. Essentially, the shapes represent the inviscid free air streamlines from the calculations. The sidewalls were manufactured on a programmable milling machine. The upper and lower walls were diverged to account for sidewall boundary layer displacement effects from all four walls.



UNITED STATES  
OF POST OFFICE

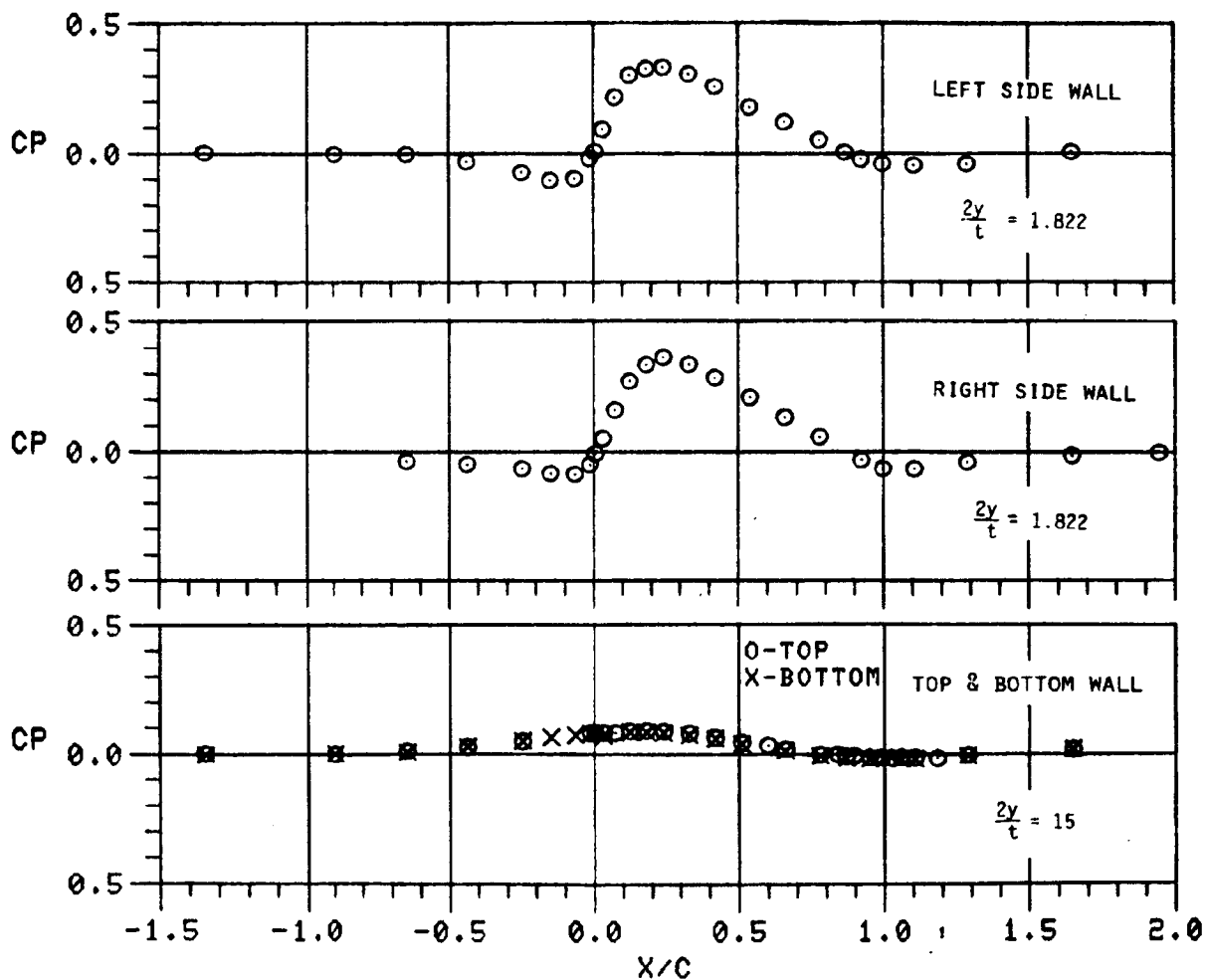
### SWEPT AIRFOIL PRESSURES

A condition of infinite sweep was achieved as illustrated here. Pressures over the span of the airfoil are shown to illustrate the results. They were achieved at a Mach number slightly different from the design value, i.e., 0.74 versus 0.8, and that may be due to the use of the small disturbance code. A prediction using Holst's full potential code (ref. 7) shows good agreement.



### TUNNEL WALL PRESSURES

Data were also obtained simultaneously on the tunnel walls. Pressures on the left and right sidewalls along a single line above the airfoil and along the centerline of the top and bottom walls are shown here. Data on the sidewalls are available along nine lines above the model. Data along the side walls and along the top and bottom walls compare favorably, illustrating that wall interference has been eliminated. The data will also be compared with predictions from the Holst code (ref. 7).



QUALITY OF PAPER QUALITY

## SEMISPAN WING EXPERIMENT

The wing experiments were conducted in tunnel 1 of the High Reynolds Number Facility under the direction of William Lockman (ref. 8). A wing with aspect ratio 3 was mounted on the tunnel sidewall and swept 20°. The streamwise wing section was an NACA 0012 section. The chord-to-tunnel half-height ratio was 1.875. The tunnel walls were flat and the top and bottom walls were tapered to allow for boundary layer displacement effects. Mach number was varied between 0.5 and 0.84,  $\alpha$  between 0° and 2° and Reynolds number between  $2 \times 10^6$  and  $8 \times 10^6$ , based on chord. Wing and wall pressures were measured simultaneously. Some velocity profiles over the wing at several span stations, obtained with a laser velocimeter, are also available for the higher Mach number tests.

### PRINCIPAL INVESTIGATOR

WILLIAM LOCKMAN, MAIL STOP 229-1

### AIRFOIL SECTIONS

NACA 0012 (STREAMWISE)

### MEASUREMENTS

WING PRESSURES

TUNNEL WALL PRESSURES

VELOCITY PROFILES FROM LDV

### UNIQUE FEATURES

HIGH REYNOLDS NUMBER

SUBCRITICAL THRU SUPERCRITICAL FLOWS

FLAT WALLS

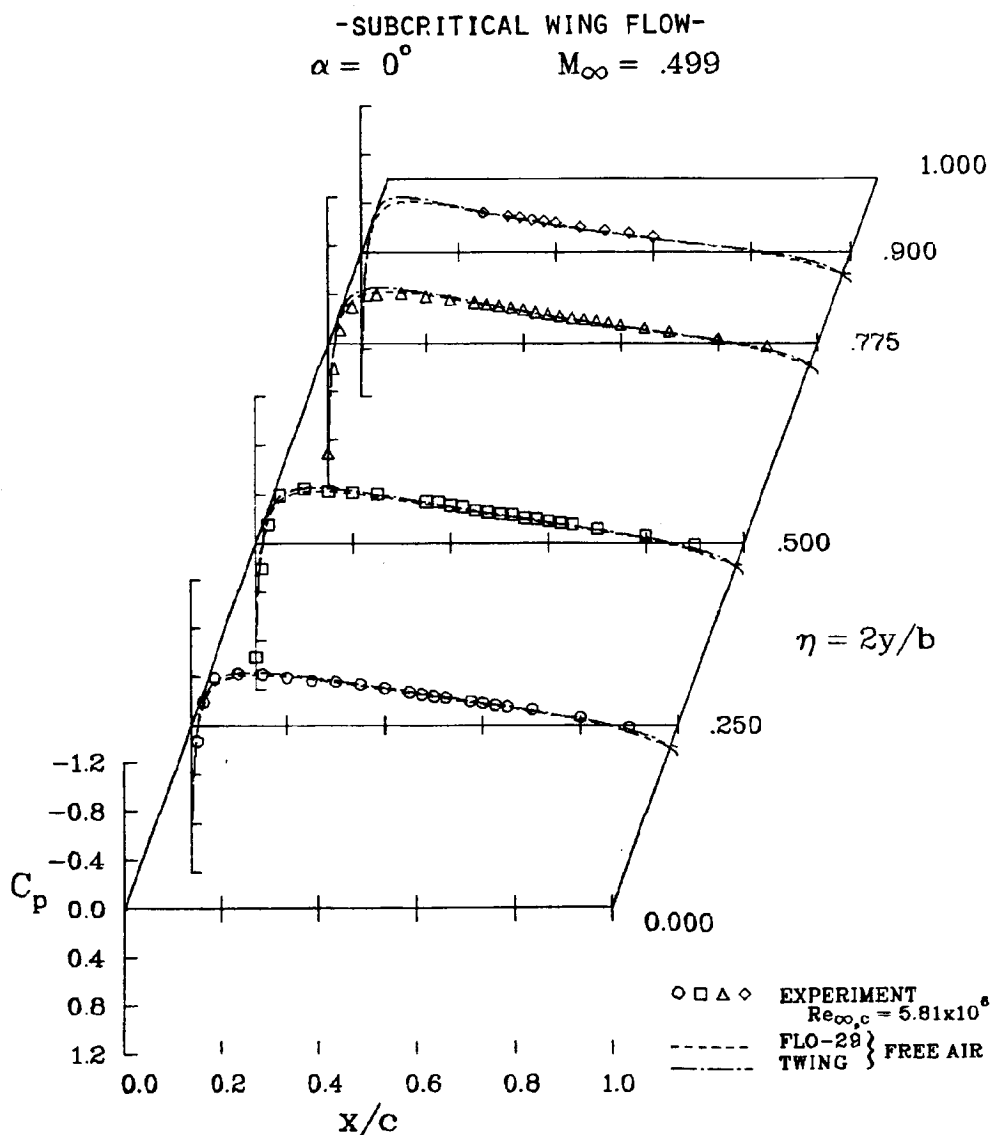
ACCURATE TEST VARIABLE SETTINGS

### STATUS

COMPLETED

### WING SURFACE PRESSURES

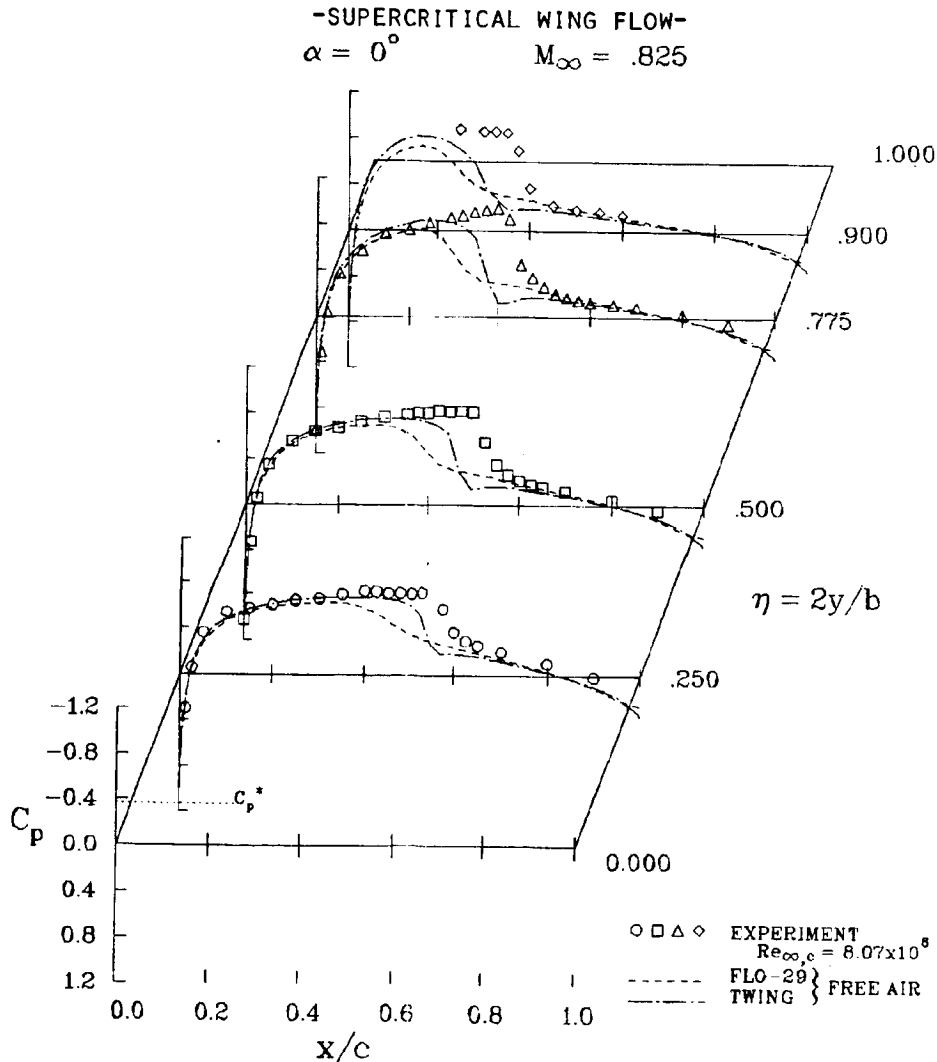
Data for a subcritical flow condition are illustrated here. They are compared with two full potential transonic codes, FLO-29 prepared by Flow Research Corp. (refs. 9 to 11) and TWING prepared by Holst (ref. 12) at ARC. The FLO-29 code was developed to include solid wall boundary conditions. The agreement of the predictions employing free air boundary conditions and the data indicates minimal wall interference.



ORIGINAL PAGE IS  
OF POOR QUALITY

WING PRESSURES

Data for a supercritical flow condition are illustrated here. In this case there is significant influence of the tunnel walls and the data should provide an excellent test case for assessing interference correction methods. The data are compared with the two potential code predictions with free air boundary conditions and the disagreement is a measure of the wall interference effects. The two predictions, which use essentially the same number of grid points, do not agree with one another and the reasons for the differences are not understood at this time. However, our experiences with the FLO-29 code (refs. 9 to 11) have shown anomalies and indicate the code is not performing adequately. For that reason, solutions using the exact wall boundary conditions in that code are not presented at this time. Wall boundary conditions have not yet been added to the TWING code (ref. 12).

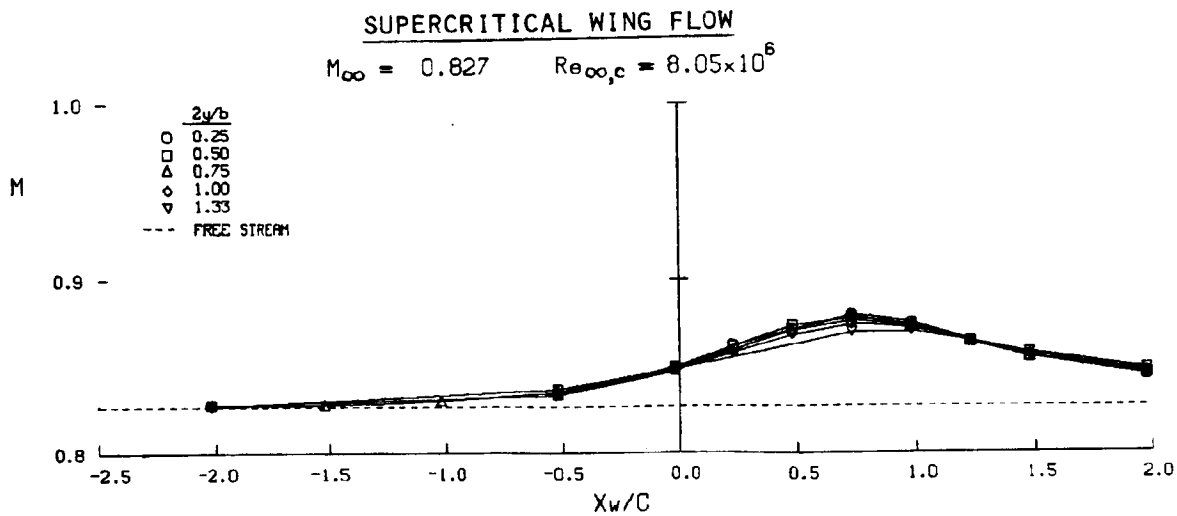
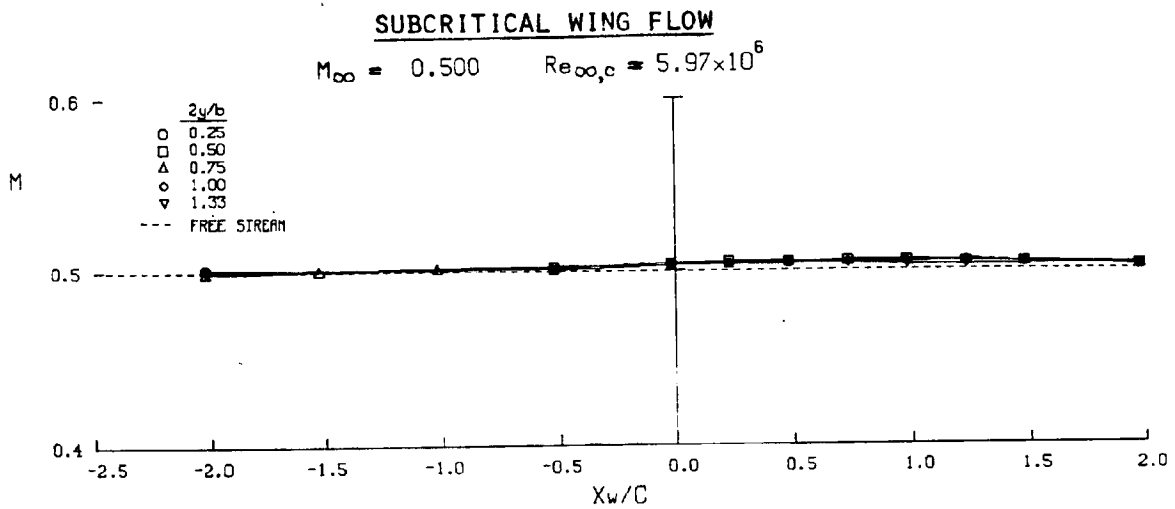


CRITICAL POINTS  
OF POOR QUALITY

CHANNEL TOP-WALL MACH NUMBERS

Data were taken on the tunnel side and top and bottom walls. Here data along the top wall for the subcritical and supercritical wing flows shown previously are presented. For the subcritical flow case the Mach number across the tunnel wall is essentially the same at all wall span locations  $y$ ; this further illustrates the presence of minimal wall interference. In contrast, the data for the supercritical flow case show a spanwise variation and hence the presence of wall effects.

$$\alpha = 0^\circ$$



## SUMMARY

Three experiments suitable for wall interference assessment and evaluation of proposed correction methods have been presented. All the experiments were performed in solid wall wind tunnels corrected for boundary layer displacement effects. Simultaneous model and wall pressure data are available. Although the experiments were performed primarily to evaluate computer code performance, it is believed that they also provide information that can be used to evaluate methods for assessing and correcting wall interference effects. The principal investigators may be contacted for further information and will provide any data presently available.

- o THREE EXPERIMENTS DESCRIBED
  - o AIRFOIL
  - o SWEPT AIRFOIL
  - o SEMISPAN SWEPT WING
- o UNIQUE FEATURES OF EXPERIMENT
  - o HIGH REYNOLDS NUMBER
  - o PERFORMED IN SOLID WALL FACILITIES
  - o UPPER/LOWER WALLS DIVERGED FOR DISPLACEMENT CORRECTIONS
  - o WALL SHAPING (SWEPT/UNSWEPT AIRFOILS)
  - o SIDEWALL MASS REMOVAL (UNSWEPT AIRFOIL)
- o AIRFOIL AND WALL PRESSURE DATA FOR WIAC STUDIES
  - o SUBCRITICAL AND SUPERCRITICAL FLOWS
  - o DATA AVAILABLE THRU PRINCIPAL INVESTIGATORS

## REFERENCES

1. McDevitt, J. B.; Polek, T. E.; and Hand, L. A.: A New Facility and Technique for Two-Dimensional Aerodynamic Testing. AIAA Paper 82-0608, March 1982.
2. Deiwert, George S.: Numerical Simulation of High Reynolds Number Transonic Flow. AIAA J., vol. 13, no. 10, 1975, pp. 1354-1359.
3. Deiwert, George S.: Computation of Separated Transonic Turbulent Flows. AIAA J., vol. 14, no. 6, 1976, pp. 735-740.
4. Mateer, G. G.; and Bertelrude, A.: Contouring Tunnel Walls to Achieve Free-Air Flow Over a Transonic Swept Wing. AIAA Paper 83-1725, July 1983.
5. Ballhaus, W. F.; and Bailey, F. R.: Numerical Calculation of Transonic Flow About Swept Wings. AIAA Paper 72-677, June 1972.
6. Bailey, F. R.; and Ballhaus, W. F.: Comparisons of Computed and Experimental Pressures for Transonic Flows About Isolated Wings and Wing-Fuselage Configurations. NASA SP-347, March 1975, pp. 1213-1231.
7. Holst, T. L.: A Fast, Conservative Algorithm for Solving the Transonic Full-Potential Equation. AIAA Paper 79-1456, July 1979. (Also, AIAA J., vol. 18, no. 12, 1980, pp. 1431-1439.)
8. Lockman, W. K.; and Seegmiller, H. L.: An Experimental Investigation of the Subcritical and Supercritical Flow About a Swept Semi-Span Wing. NASA TM-84367, June 1983.
9. Mercer, J. E.; Geller, E. W.; Johnson, M. L.; and Jameson, A.: A Computer Code to Model Swept Wings in an Adaptive Wall Transonic Wind Tunnel. AIAA Paper 80-0156, January 1980.
10. Mercer, J. E.; Geller, E. W.; and Johnson, M. L.: Calculation of Transonic Flow About a Wing in an Adaptive Wall Wind Tunnel. Flow Research Company, Kent, Washington, Flow Research Report No. 164, May 1980.
11. Mercer, J. E.; and Murman, E. M.: Application of Transonic Potential Calculations to Aircraft and Wind Tunnel Configurations. AGARD CP-285, May 1980, pp. 1-1 to 1-15.
12. Holst, T. L.; and Thomas, S. D.: Numerical Solution of Transonic Wing Flow Fields. AIAA Paper 82-0105, January 1982.

*omit*

SESSION IV

ANALYTICAL WALL CORRECTION METHODS

Chairman: C. F. Lo, Calspan, AEDC

N85 12022

D11

ASYMPTOTIC METHODS FOR WIND TUNNEL WALL  
CORRECTIONS AT TRANSONIC SPEED

N. D. Malmuth, J. D. Cole, and F. Zeigler  
Rockwell International Science Center  
Thousand Oaks, California

PRECEDING PAGE BLANK NC

**Preceding page blank**

ASYMPTOTIC METHODS FOR WIND TUNNEL WALL CORRECTIONS AT TRANSONIC SPEED

This talk will be an outline of our effort in developing classical methods to compute wall interference at transonic speeds. To be discussed are the two-dimensional theory and three-dimensional developments. Also, some numerical application of the two-dimensional work will be indicated.

## ASYMPTOTIC METHODS FOR TRANSONIC WIND TUNNEL WALL CORRECTIONS

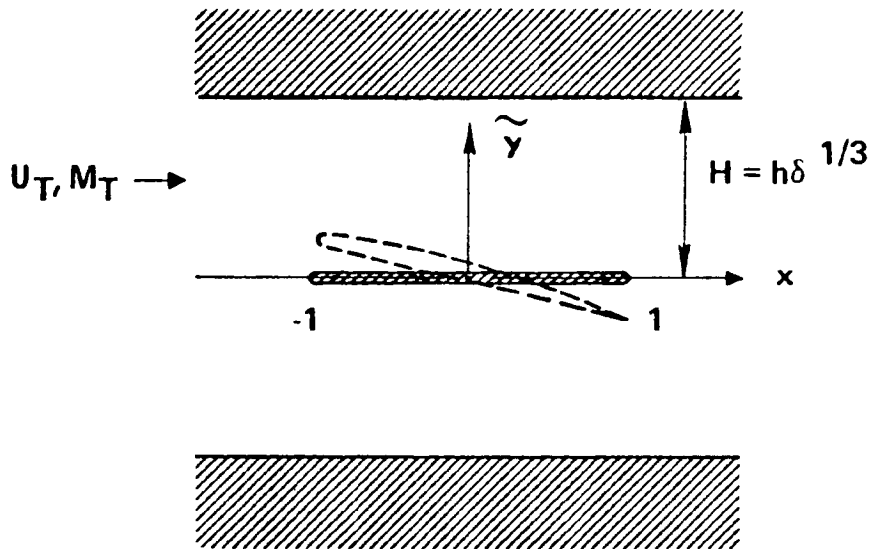
The basic meaning of the asymptotic procedure is to compute the flow field in the limit as some parameter takes on extreme values. In our analyses, this limit is that the height-to-chord ratio becomes large. This will lead to important simplifications of the analysis which will reduce the number of parameters necessary to describe the corrections as well as the associated computational effort. In addition, the results should provide insight into adaptive applications.

### GOALS

- **STUDY STRUCTURE OF CONFINED FLOWS AT TRANSONIC SPEEDS USING ASYMPTOTIC THEORY**
- **REDUCE NUMBER OF PARAMETERS NECESSARY TO DESCRIBE CORRECTIONS**
- **REDUCE COMPUTATIONAL EFFORT IN CORRECTION AND ASSESSMENT EVALUATION**
- **PROVIDE INSIGHT RELEVANT TO ADAPTIVE APPLICATIONS**

### CONFINED AIRFOIL

This figure shows a schematic of a two-dimensional problem involving an airfoil confined between walls. The walls are assumed (without excessive loss of generality) to be solid. For large height-to-chord ratio, a singular perturbation problem occurs in which the walls weakly and linearly perturb the near field from its nonlinear behavior in the corresponding unconfined flow. Near these walls, the approximation becomes invalid, and a different one idealizing the flow as a reflected potential vortex must be used. Matching between both domains determines unknown elements in both approximations.



ORIGINAL PAGE IS  
OF POOR QUALITY

## INNER FORMULATION

These ideas can be made more precise by using so-called "limit process expansions" in which the flow quantities are written as perturbation series for the velocity potential  $\Phi$  which become more accurate as the parameters  $\delta$  (characteristic flow deflection) and  $H$  (height) take on the indicated limiting values. These series are substituted into the exact equations to obtain equations of motion for the approximate quantities. For the inner (near-field region), the dominant equation is the Karman-Guderley (KG) small-disturbance equation. The perturbation equation is a linearized form of the KG equation. Matching with the outer approximation (valid near the walls) gives the necessary far-field boundary condition to solve this equation.

### AIRFOIL SHAPE

$$\gamma = \delta F_{u,l}(x) - a_T(x), |F_{u,l} \text{ MAX}| = 1$$

### KARMAN-GUDERLEY (KG) EXPANSION

$$\phi = U_T \left\{ x + \delta^{2/3} \phi(x, \tilde{y}; K_T, A_T, H) + \dots \right\}$$

$$x, \tilde{y} = \delta^{1/3} y, K_T = \frac{1 - M_T^2}{\delta^{2/3}}, A = \frac{a_T}{\delta}, H = h \delta^{1/3} \text{ fixed as } \delta \rightarrow 0$$

### INNER EXPANSIONS

$$\phi = \phi_0(x, \tilde{y}) + \frac{\ell n H}{H^2} \phi_{1/2} + \frac{1}{H^2} \phi_1 + \dots$$

$$K_T = K_F + \frac{\ell n H}{H^2} K_S + \frac{1}{H^2} K_c + \dots$$

(1/2 SUBSCRIPT TERMS ARE "SWITCHBACKS" INTRODUCED FOR MATCHING)

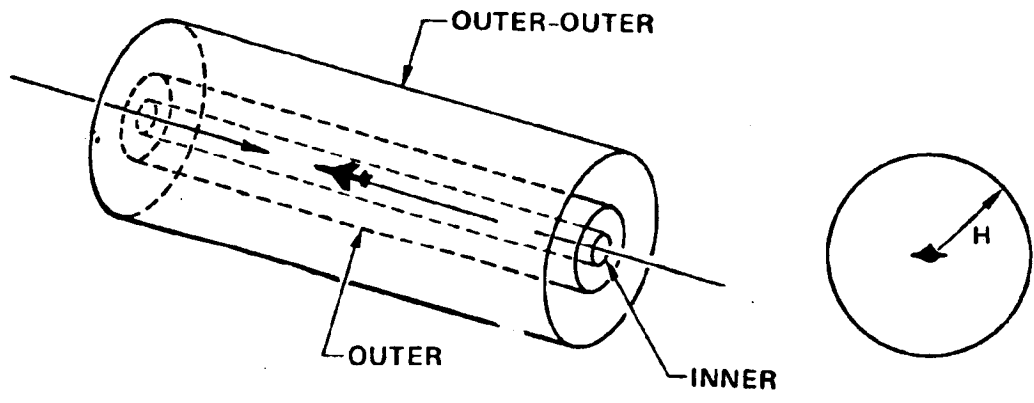
### INNER LIMIT:

$$x, \tilde{y} \text{ FIXED AS } H \rightarrow \infty$$

REPRODUCED FROM  
A COPY OF POOR QUALITY

### BASIC STRUCTURE OF FLOW OVER CONFINED SLENDER VEHICLE

For the three-dimensional case of a fighter shape that can be approximated by a slender body, three rather than two regions are necessary to properly describe the confined flow. If the body's transverse dimensions are small compared to those of the wall, an inner region near the body has dominant cross-flow gradients which lead to the flow being harmonic in cross planes. In an "outer" region, the flow is representable as a nonlinear line source. Near the walls, in an "outer-outer" region, we obtain a linear line source representation for the flow in which the influence of the walls is to introduce image reflections. The behavior of this solution in the outer region provides a far-field boundary condition for the determination of the nonlinear line source flow.

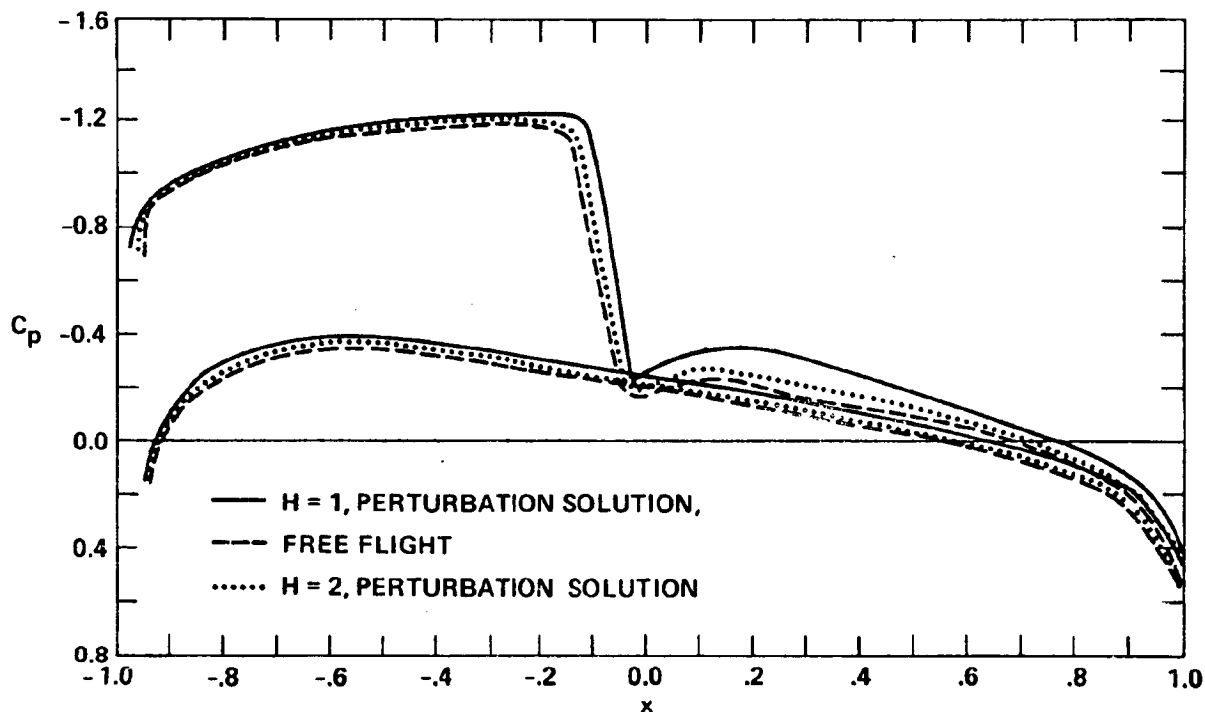


H → ∞ LIMIT

- INNER - DOMINANTLY UNCONFINED SLENDER-BODY THEORY
- OUTER - WALL-INDUCED LINEAR PERTURBATIONS ON DOMINANT UNCONFINED LINE SOURCE
  - DOMINANT FLOW GIVEN BY EQUIVALENCE RULE
- OUTER-OUTER - FOR LOCALLY SUBSONIC CONDITIONS IS LINE SOURCE OR DOUBLET IMAGED IN WALLS

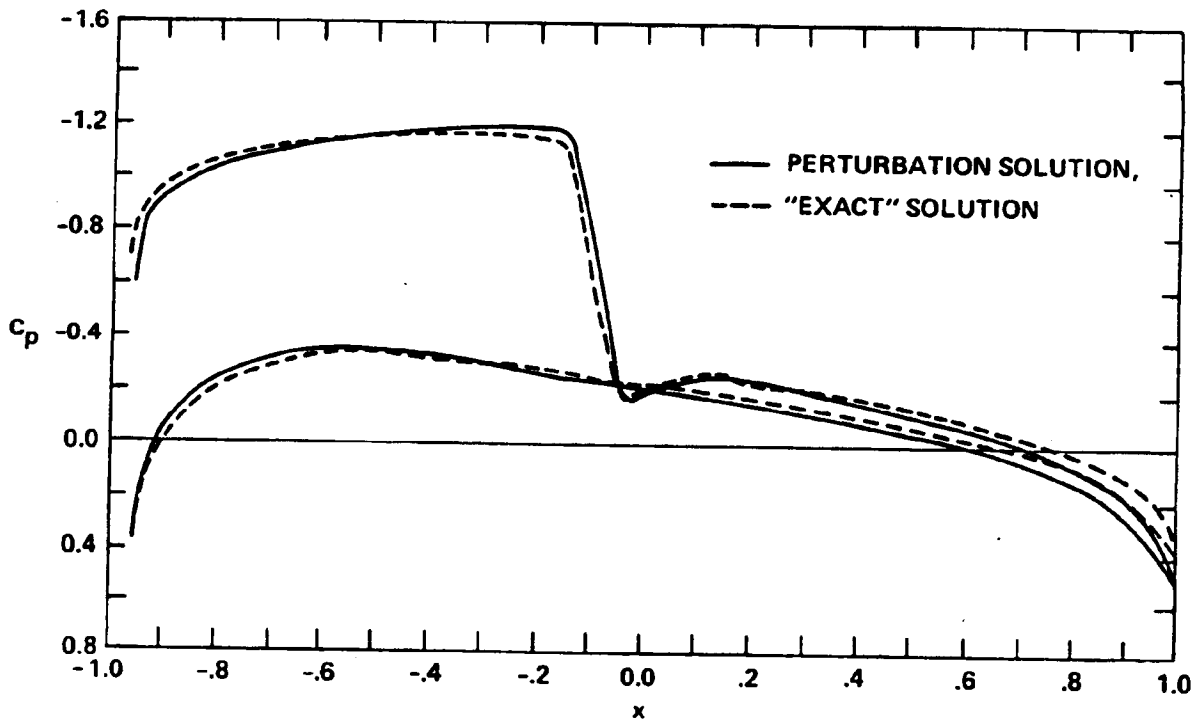
FREE AND CONFINED CHORDWISE PRESSURES - NACA 0012 AIRFOIL

Returning to the two-dimensional problem, results will be presented from the computational solution of the perturbed near field near the model using successive line overrelaxation solvers with proper attention to the treatment of the perturbed shocks. Chordwise pressures for a NACA 0012 airfoil at a tunnel Mach number  $M_f$  of 0.75 and angle of attack  $\alpha_c$  of  $2^\circ$  are depicted in the plot for various values of the height parameter  $H$  as compared to the free-field values. Strikingly and surprisingly small effects are shown upstream of the shock for the rather low values of  $H$  used. Important numerical issues are the treatment of the perturbed Kutta conditions and the proper treatment of the shock waves in these calculations.



COMPARISON BETWEEN EXACT AND APPROXIMATE CHORDWISE PRESSURES  
ON CONFINED NACA 0012 AIRFOIL

This is an example of one validation of the solution against a so-called exact approach in which the confined flow is a solution of the small-disturbance equation required to satisfy the exact boundary conditions. The agreement is quite reasonable. However, further effort is required to reduce the discrepancies to be substantially below the magnitude of the basic interference effect. This is related to the numerical issues described previously.



COMPARISON OF LIFT COEFFICIENTS FOR CONFINED AIRFOIL AT VARIOUS WALL HEIGHTS

Corresponding to the validation of the chordwise pressures shown previously, other validations were performed for the confined lift using the exact and perturbation theories. The results show very good comparisons down to fairly low values of the height parameter. In spite of this, more effort is required to properly treat the Kutta condition in the perturbed problem.

$$M_F = 0.7, \alpha_F = 3.5^\circ$$

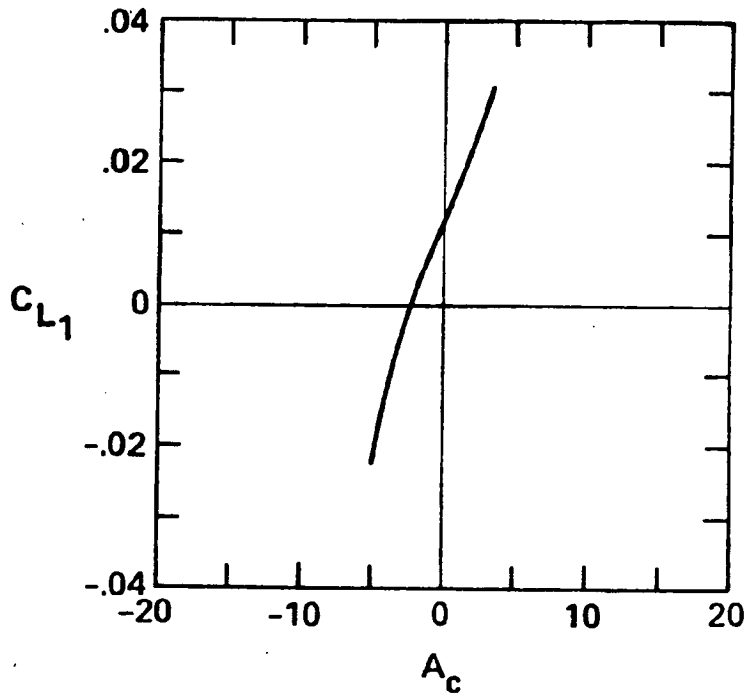
METHOD \ H	1	2	3	4	5
EXACT	.3655	.3653	.3652	.3652	.3652
ASYMPTOTIC SOLUTION	.3662	.3654	.3653	.3652	.3652

$$M_F = 0.75, \alpha_F = 2^\circ$$

METHOD \ H	1	2	3	4	5	6
EXACT	.4322	.4266	.4234	.4234	.4233	.4234
ASYMPTOTIC SOLUTION	.4356	.4264	.4248	.4242	.4238	.4237

# INTERFERENCE LIFT VERSUS REDUCED ANGLE OF ATTACK - NACA 0012 AIRFOIL

The total lift  $C_L$  is equal to  $C_{L_F} + \frac{1}{H^2} C_{L_I}$ . Here,  $C_{L_I}$  is the interference lift coefficient. If  $A_c$  is the tunnel angle of attack in units of the thickness ratio  $\delta$ , the curve shows a universal variation of  $C_{L_I}$  with  $A_c$ , with the height parameter separated out. Also indicated is the necessary adjustment of  $A_c$  to provide interference-free lift ( $C_{L_I} = 0$ ) independent of  $H$ , demonstrating the utility of the theory in extrapolations down to zero model size in the transonic regime.



## SUMMARY AND CONCLUSIONS

The basic advantages of the asymptotic theory are indicated. In the future, three-dimensional generalizations of the two-dimensional model will be developed.

### ASYMPTOTIC THEORY OF SOLID TUNNEL WALL INTERFERENCE ON TRANSONIC AIRFOILS:

- LEADS TO SINGULAR PERTURBATION PROBLEM FOR LARGE  $H$ 
  - NEAR FIELD – WEAK LINEAR PERTURBATIONS ON KG THEORY
  - FAR FIELD – REFLECTED MULTIPOLE DOMINATED BY VORTEX
  - SWITCHBACK TERMS REQUIRED FOR MATCHING, ALTERING SIMILARITY PARAMETER
- GIVES PERTURBATIONS OF NEAR-FIELD PRESSURES AND FORCES  $O((\ln H)/H^2)$
- PROVIDES GOOD AGREEMENT WITH THE EXACT KG MODEL FOR LARGE TO MODERATE  $H$  FOR LIFT CORRECTIONS
- UTILITY OF THEORY
  - SEPARATES  $H$  OUT OF PROBLEM
  - INVOLVES A NONLINEAR AND LINEAR UNIVERSAL PROBLEM AS COMPARED TO TWO NONLINEAR PROBLEMS IN EXACT CASE

3-D EXTENSION TO SLENDER MODEL CONFINED BETWEEN SOLID WALLS SHOWS 3-LAYER STRUCTURE

N85 12023

012

EFFECT OF BOUNDARY LAYERS ON SOLID WALLS  
IN THREE-DIMENSIONAL SUBSONIC WIND TUNNELS

Jerry B. Adcock and Richard W. Barnwell  
NASA Langley Research Center  
Hampton, Virginia

PRECEDING PAGE BLANK NOT REPRODUCED

Preceding page blank

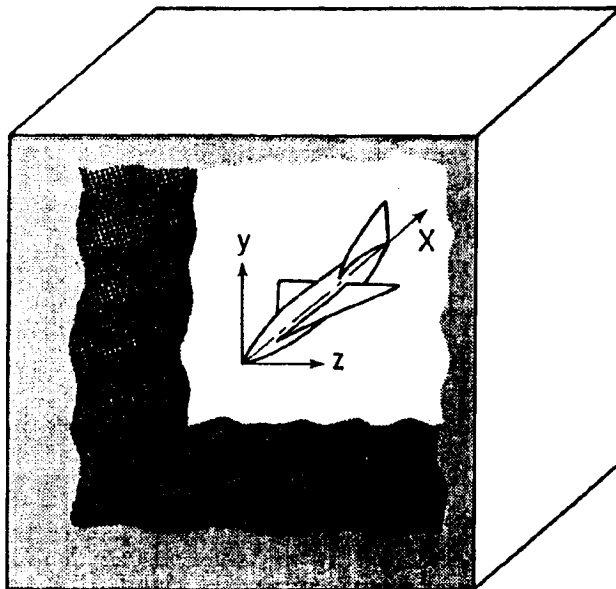
## Introduction

A number of linear methods have been developed for predicting the interference of open, closed, and ventilated walls in two- and three-dimensional subsonic wind tunnels. Summaries of these methods are given in references 1 and 2. In general, the ventilated walls are assumed to be homogeneous and are either perforated with small holes or are slotted longitudinally. The purpose of the present paper is to present a linear method which accounts for the effects of boundary layers on solid walls in subsonic three-dimensional wind tunnels. As will be shown, the numerical method and the nature of the results bear a striking resemblance to those for subsonic wind tunnels with slotted walls.

The critical feature of the present method is the manner in which the boundary condition for solid wind tunnel walls is handled. The present method is based on a theory developed recently by Barnwell (ref. 3) and Sewall (ref. 4) which predicts the effects of boundary layers on solid sidewalls in two-dimensional subsonic and transonic wind tunnels. The present solution for three-dimensional flow is substantially different from the two-dimensional solutions of references 3 and 4 in that the two-dimensional solutions result in similarity rules relating compressibility and sidewall boundary layer effects. No such similarity exists for the three-dimensional problem.

### Three Dimensional Subsonic Wind Tunnel With Wall Boundary Layers

Consider steady subsonic, small-perturbation flow in a wind tunnel with a rectangular cross section of width  $2b$  and height  $2h$ . Let the Cartesian coordinates in the freestream, horizontal, and vertical directions be  $x$ ,  $y$ , and  $z$ , respectively, and let the perturbation velocity potential be  $\phi$ . The flow is governed by the small disturbance condition and the viscous solid-wall boundary condition.



#### SMALL DISTURBANCE EQUATION

$$(1 - M_{\infty}^2) \frac{\partial^2 \phi}{\partial x^2} + \frac{\partial^2 \phi}{\partial y^2} + \frac{\partial^2 \phi}{\partial z^2} = 0$$

#### VISCOUS SOLID-WALL BOUNDARY CONDITION

$$\frac{\partial \phi}{\partial n} = -U \frac{\partial \delta^*}{\partial x}$$

## Tunnel Wall Boundary Layer Analysis

In the present treatment, the dynamics of the sidewall boundary layer are modeled with the von Karman momentum integral, which can be written as shown. This equation can be simplified because the sidewall boundary layer in most wind tunnels can be approximated as a flat-plate boundary layer with a large Reynolds number and an equivalent length on the order of  $\delta^*/(\tau_w/\rho U^2)$ . In general, the model length scale  $c$  is much smaller than the boundary layer equivalent length so that the inequality shown pertains.

As shown in reference 5, the shape factor for boundary layers with constant total temperatures can be approximated as shown in the third expression where  $\bar{H}$  is the transformed shape factor and  $\gamma$  is the ratio of specific heats. Because  $\bar{H}$  approaches 1 as the Reynolds number becomes large, this equation can be written as

$$H = 1 + (\gamma - 1)M^2$$

for the present problem. From this equation and the small perturbation energy equation, it follows that the streamwise gradient of  $H$  is given by the fourth expression.

With the inequality and the shape factor gradient derived above, the von Karman momentum integral can be simplified as indicated. This simplified expression can then be used to evaluate the viscous solid-wall boundary condition as indicated. Note that this is a linear boundary condition for the function  $\phi$ .

### VON KARMAN MOMENTUM INTEGRAL

$$\frac{\partial \delta^*}{\partial x} + \frac{\delta^*}{U} (2 + H - M^2) \frac{\partial U}{\partial x} = \frac{H \tau_w}{\rho U^2} + \frac{\delta^*}{H} \frac{\partial H}{\partial x}$$

### BOUNDARY LAYER LENGTH SCALE APPROXIMATION

$$\text{LENGTH SCALE} \approx \frac{\delta^*}{\tau_w/\rho U^2} \gg c = \text{MODEL LENGTH}$$

### SHAPE FACTOR APPROXIMATION

$$H = (\bar{H} + 1) \left\{ 1 + \frac{\gamma - 1}{2} M^2 \right\} - 1 \approx 1 + (\gamma - 1)M^2$$

$$\frac{\partial H}{\partial x} = \frac{(H - 1)(H + 1)}{U} \frac{\partial U}{\partial x}$$

### SIMPLIFIED MOMENTUM INTEGRAL

$$\frac{\partial \delta^*}{\partial x} = -\frac{\delta^*}{U} \left( 2 + \frac{1}{H} - M^2 \right) \frac{\partial U}{\partial x}$$

### VISCOUS SOLID-WALL BOUNDARY CONDITION

$$\frac{\partial \phi}{\partial n} = \delta^* \left( 2 + \frac{1}{H} - M^2 \right) \frac{\partial^2 \phi}{\partial x^2}$$

### Comparison of Tunnel Wall Boundary Conditions

The viscous solid-wall boundary condition is similar in form to the conventional linear boundary conditions for slotted and porous walls. The quantities  $F$  and  $R$  are nondimensional constraints, and

$$\beta = 1 - M_{\infty}^2$$

As in reference 1, Fourier transforms are used to account for dependence on the streamwise coordinate in the present treatment. The present solutions for the viscous solid-wall boundary condition are very similar to those for the slotted-wall boundary condition.

VISCOUS SOLID WALL

$$\frac{\partial \phi}{\partial n} = \delta^* \left( 2 + \frac{1}{H} - M_{\infty}^2 \right) \frac{\partial^2 \phi}{\partial x^2}$$

SLOTTED WALL

$$\frac{\partial \phi}{\partial n} = -\frac{1}{Fb} \phi$$

POROUS WALL

$$\frac{\partial \phi}{\partial n} = -\frac{R}{\beta} \frac{\partial \phi}{\partial x}$$

## Analysis Parameters

The results for the viscous solid-wall boundary condition are expressed in terms of the viscous parameter  $N$ . This parameter has a value of 1 for a wall with a zero-thickness free-stream velocity. The results for the slotted-wall boundary condition are presented in terms of the parameter  $P$  of reference 1, which is related to the slotted-wall coefficient  $F$  as indicated. This parameter has values of 0 and 1 for closed and open walls, respectively. As a study of the boundary conditions will show, the blockage for a solid wall with  $N = 1$  and a slotted wall with  $P = 0$  must be identical because both are simply a solid wall with no boundary layer. Although it is not as obvious, the boundary conditions require that the blockage for a solid wall with  $N = 0$  be identical to that of a slotted wall with  $P = 1$ .

### ● VISCIOUS SOLID-WALL BOUNDARY CONDITION

$$\frac{\partial \phi}{\partial \bar{n}} = \frac{\delta^*}{b} \left( 1 + \frac{1+H}{\beta^2 H} \right) \frac{\partial^2 \phi}{\partial \bar{x}^2}$$

$$\text{VISCIOUS PARAMETER: } N = \frac{1}{1 + \frac{\delta^*}{b} \left( 1 + \frac{1+H}{\beta^2 H} \right)}$$

$$\text{LIMITS } N = 1, \delta^* = 0$$

$$N \rightarrow 0, M \rightarrow 1.0$$

### ● SLOTTED-WALL BOUNDARY CONDITION

$$\frac{\partial \phi}{\partial \bar{n}} = -\frac{1}{F} \phi$$

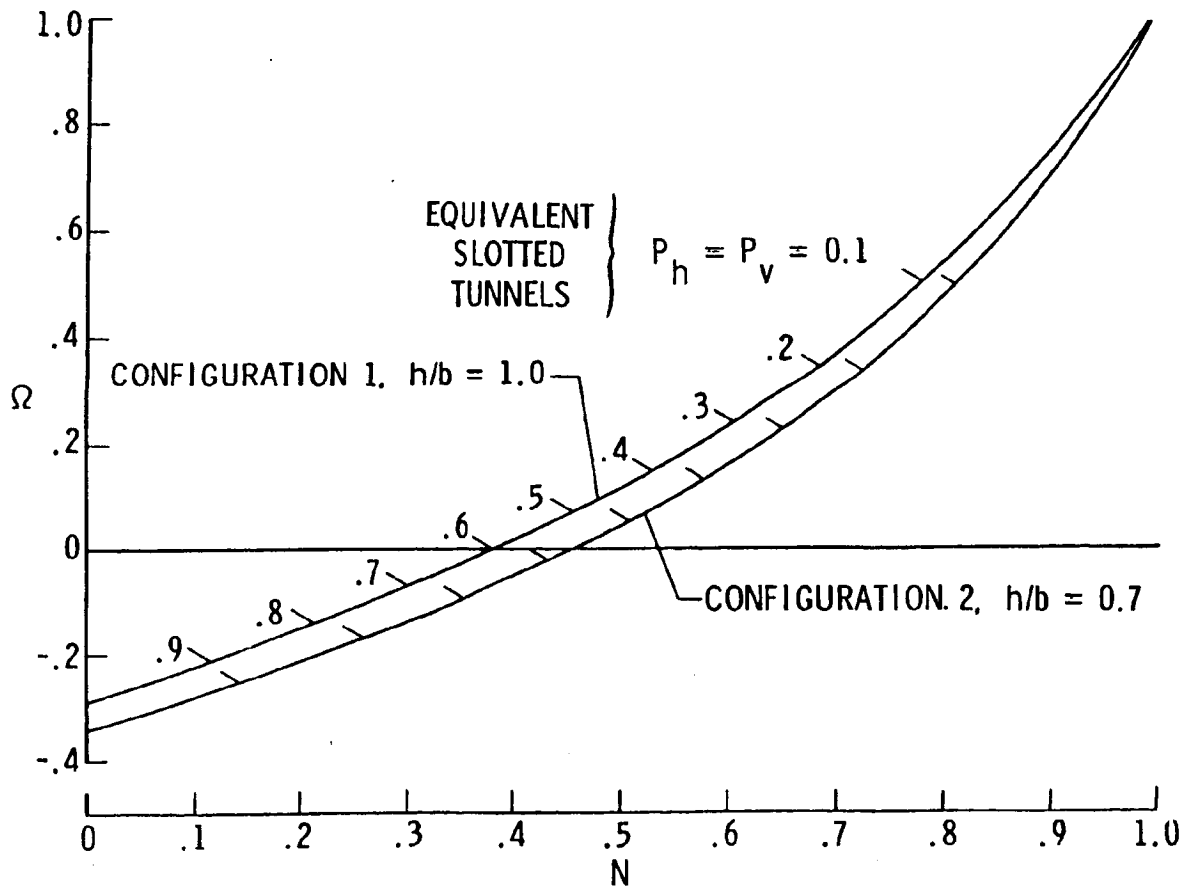
$$\text{SLOT PARAMETER: } P = \frac{1}{1+F}$$

$$\text{LIMITS } P \rightarrow 0, F \rightarrow \infty, \text{ SOLID WALL}$$

$$P = 1, F = 0, \text{ OPEN WALL}$$

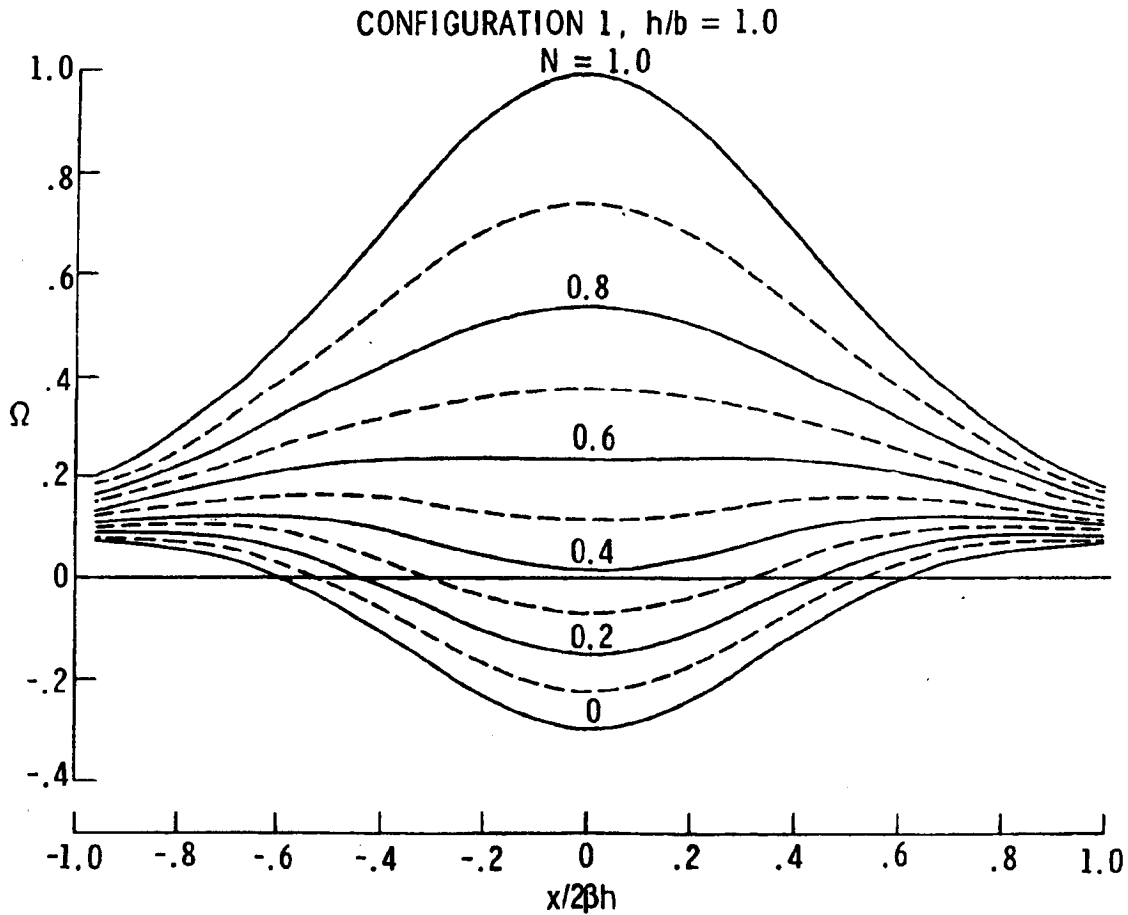
Solid Blockage Ratios for Solid-Wall Tunnels

The model-induced wall boundary layer effects on the solid blockage for the solid-wall configurations 1 and 2, which have height-to-width ratios of 1 and 0.7, respectively, are presented. These blockage ratios,  $\Omega$ , are at the model position ( $x=0$ ) and for values of the boundary layer parameter,  $N$ , from 0.0 to 1.0. In reality, values of  $N$  less than about 2/3 are largely academic because they can be obtained only with excessively thick boundary layers or with near-sonic free-stream Mach numbers; in both cases, this linear procedure would be less than adequate for the problem. The model-induced wall boundary layer effect reduces the blockage factor from the closed-wall zero-thickness value ( $N=1, \Omega=1$ ) and is similar to the blockage relief that is obtained when the walls are slotted. As a matter of interest, the tick marks indicate the slot parameter values for an equivalent slotted tunnel ( $P=P_h=P_v$  on horizontal and vertical walls) that would produce the same blockage factors. For the square tunnel, a boundary layer parameter,  $N$ , of 0.780 produced a blockage ratio of 0.5 as does the slotted tunnel with a  $P$  factor of 0.1. For given boundary layer parameter values, the blockage relief is greater for configuration 2 ( $h/b=0.7$ ) than for the square tunnel.



### Solid Blockage Ratios Along Tunnel Centerline

The wall boundary layer effect on the solid blockage distribution along the longitudinal axis of tunnel configuration 1 has been evaluated and is shown. The blockage factor varies symmetrically about the model position, with  $N$  values from 0.4 to 0.6 producing fairly constant values of blockage along the axis.

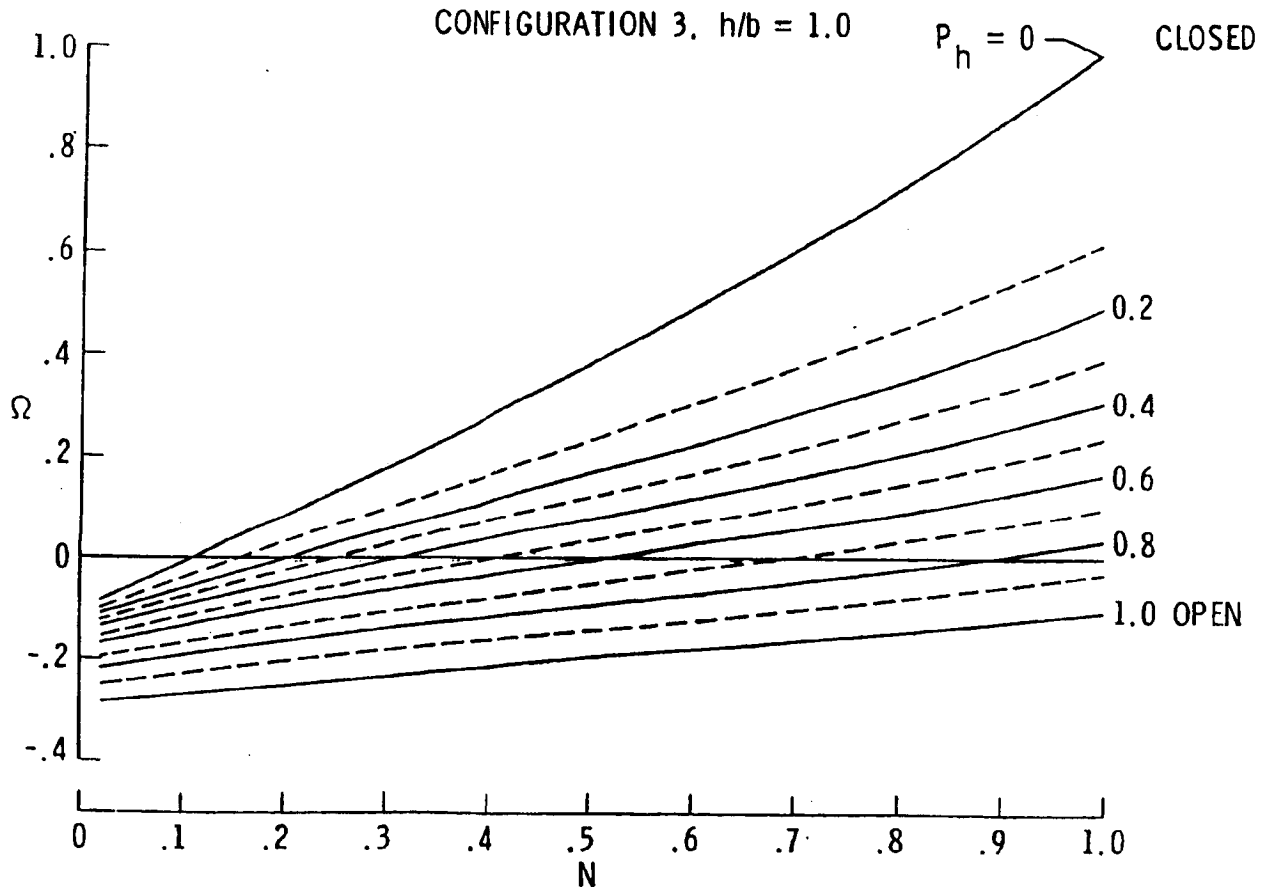


ORIGINAL PAGE IS  
OF POOR QUALITY

### Solid Blockage Ratios for Combination Wall Tunnel

The blockage ratio at the model station for the combination wall configuration, which has slotted top and bottom walls and solid sidewalls, is presented. It is assumed that the horizontal wall boundary condition is dominated by the slot effects; no attempt has been made to combine slot and boundary layer conditions on the same wall.

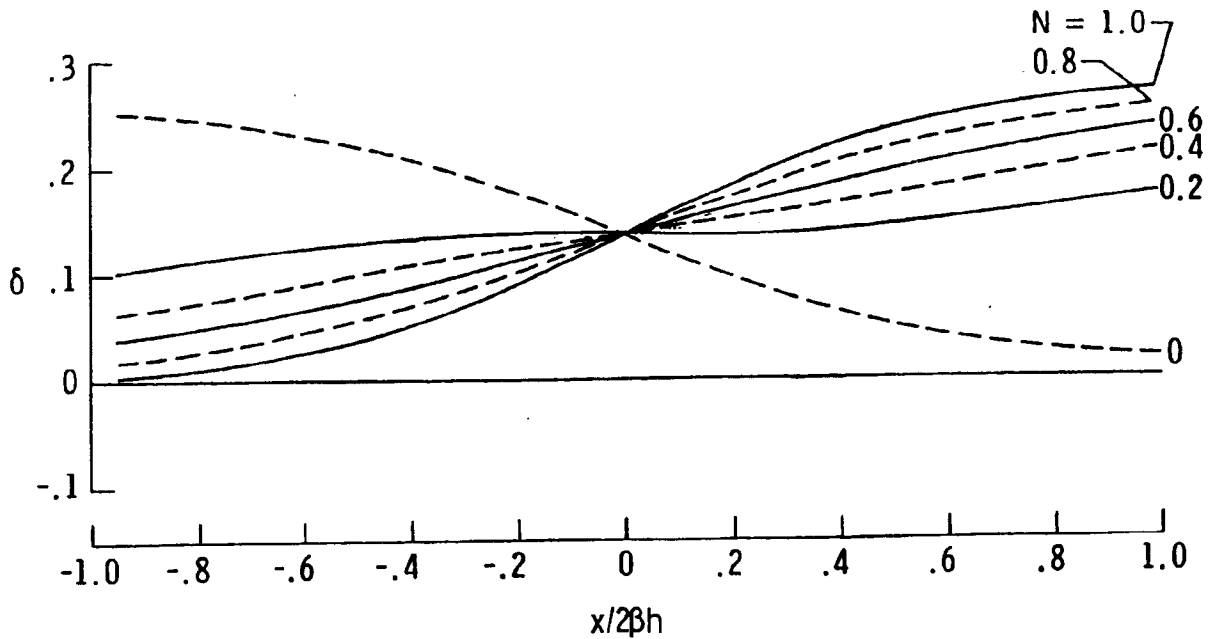
At  $N$  equals 1.0 (no sidewall boundary layers), the blockage factors for the various horizontal slot parameter values are the same as those of Pindzola and Lo (ref. 1). As the boundary layer on the sidewall builds up (decreasing  $N$ ), additional blockage ratio reductions occur. This effect is more pronounced for the more closed horizontal slots. As the horizontal slots go toward fully open ( $P_h=1.0$ ) it is anticipated that the sidewall boundary layer effect should diminish.



## Lift Interference Factors Along Tunnel Centerline

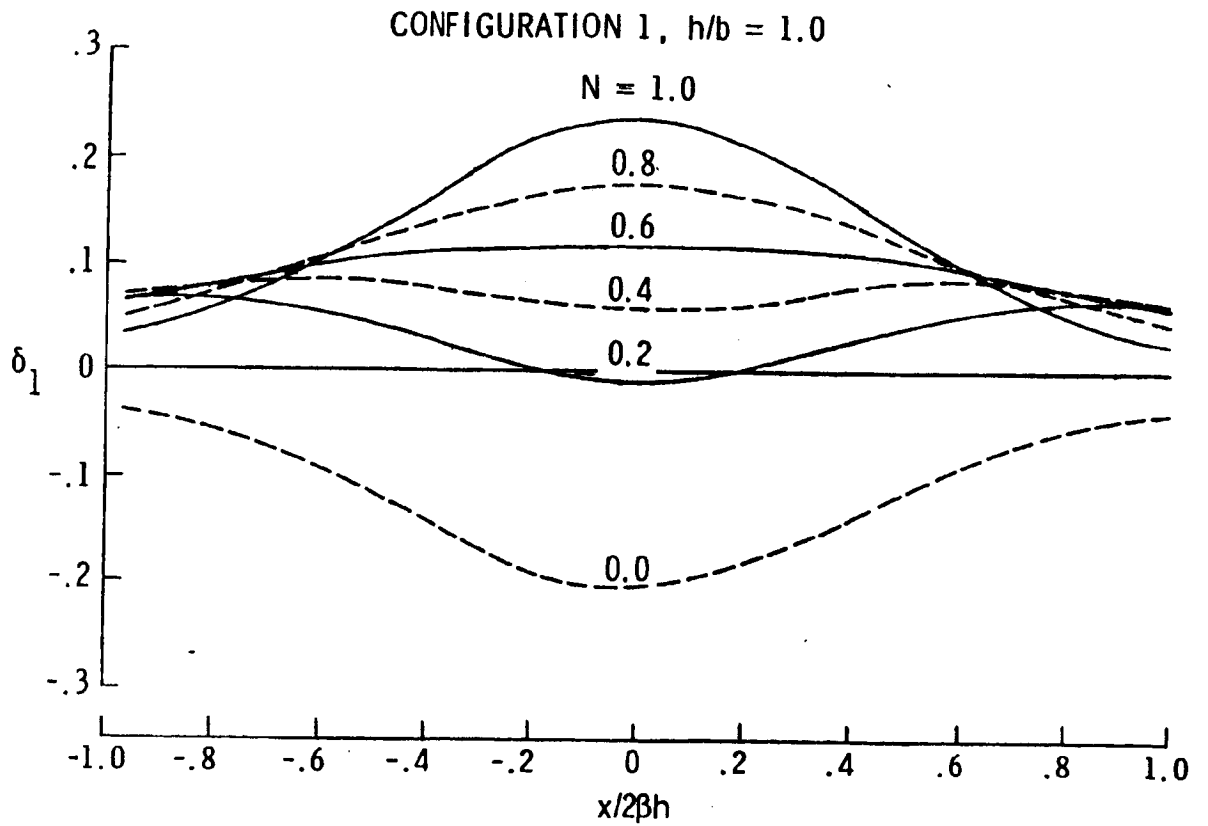
The lift interference,  $\delta$ , contains two terms, one of which is independent of  $x$  (two-dimensional lift) and the second of which is  $x$ -dependent (three-dimensional lift). An examination of the two-dimensional-lift boundary condition reveals that the wall boundary layer parameter,  $N$ , has no effect on the two-dimensional-lift interference term. The value for this term is just the closed-wall value. The three-dimensional-lift term is affected by the wall boundary layer; the longitudinal distributions of this term for the solid-wall tunnel configurations are shown in the figure. The lift interference values for the no-boundary-layer case ( $N=1$ ) are the same as those of reference 1. It is apparent that the effect of the wall boundary layer is smaller for the lift interference factor than for the solid blockage ratio.

CONFIGURATION 1,  $h/b = 1.0$



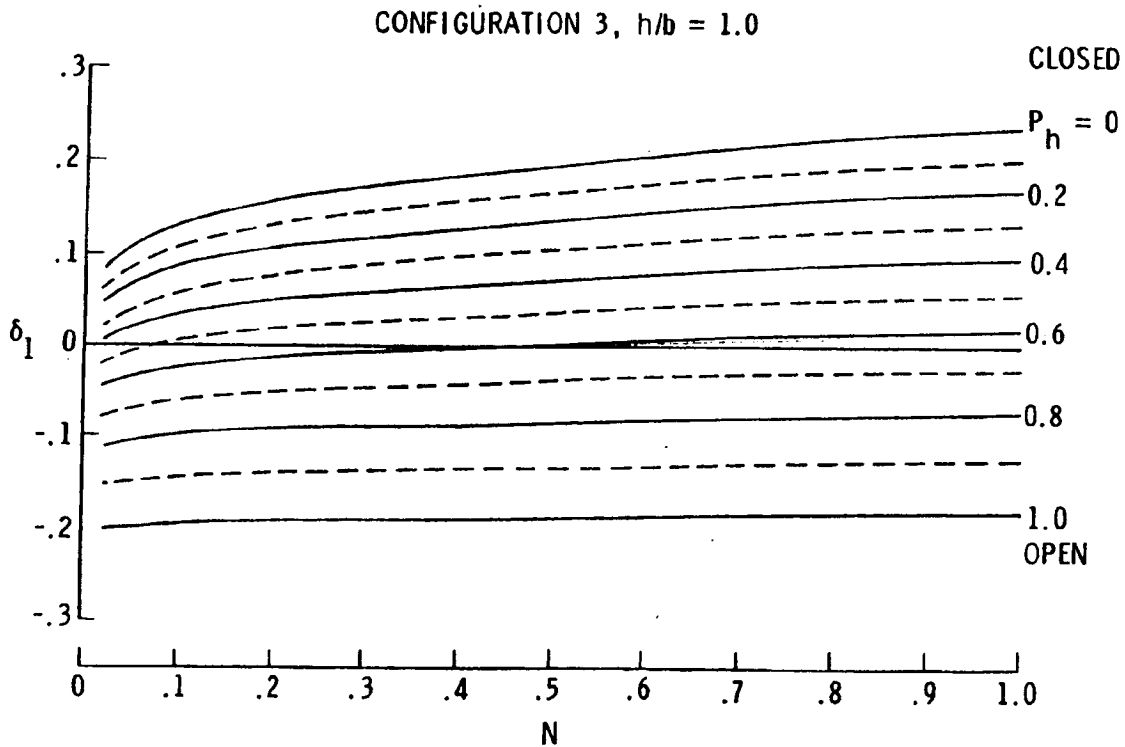
### Streamline Curvature Factors Along Tunnel Centerline

The model-induced wall boundary layer effects on the streamline curvature factor  $\delta_1$  are presented for a solid-wall configuration. The streamline curvature factors near the model station ( $x=0$ ) are reduced by the wall boundary layer effect. This effect is similar to opening slots in the horizontal walls.



### Streamline Curvature Factors for Combination-Wall Tunnel

The streamline curvature factor  $\delta_1$  at the model station ( $x=0$ ) for a square combination-wall tunnel with slotted horizontal walls and solid sidewalls is presented. It is seen that the slotted horizontal wall effects are dominant with only slight changes in the streamline curvature factor for practical values of the boundary layer parameter  $N$ .



## Summary

A solution for the tunnel wall boundary layer effects for three-dimensional subsonic tunnels has been presented. The fundamentals and methodology of the procedure are the same as the Pindzola and Lo treatment of the ventilated wall problem (ref. 1). The model potentials are represented with simple singularities placed on the centerline of the tunnel and Laplace's equation in cylindrical coordinates is solved for either the conventional homogeneous slotted-wall boundary condition, the solid-wall viscous boundary condition (refs. 3 and 4), or a combination of them. The Fourier transform and point-matching techniques of reference 1 are used.

This analysis of the model-induced boundary layer effects on the solid walls of several three-dimensional wind tunnel configurations leads to several observations.

The most pronounced wall boundary layer effect is on solid blockage for completely closed wind tunnels. Boundary layers on the wall reduce the blockage from the solid-wall, no-boundary-layer case in a manner similar to opening slots in a solid wall. Additionally, for solid-wall tunnel configurations, the streamline curvature interference factor is reduced by a significant amount, whereas the lift interference factor at the model station does not depend on the boundary layer parameter.

For combination wall configurations, the slot effect of the horizontal walls dominates the viscous effect of the solid sidewalls. This is true not only for solid blockage but for lift and streamline curvature interference as well.

- MODEL-INDUCED, VISCOUS; SOLID-WALL BOUNDARY CONDITION HAS BEEN DEVELOPED AND LINEAR POTENTIAL-FLOW SOLUTIONS FOR 3-D SUBSONIC WIND TUNNELS HAVE BEEN OBTAINED
- SOLID-WALL TUNNELS – SOLID BLOCKAGE AND STREAMLINE CURVATURE INTERFERENCE FACTORS ARE INFLUENCED MOST BY WALL BOUNDARY LAYER EFFECT
- COMBINATION-WALL TUNNELS – TYPICAL SLOT OPENINGS IN THE HORIZONTAL WALLS; THE SLOT EFFECTS DOMINATE THE SIDE-WALL BOUNDARY LAYER EFFECTS

## References

1. Pindzola, M.; and Lo, C. F.: Boundary Interference at Subsonic Speeds in Wind Tunnels with Ventilated Walls. AEDC-TR-69-47, May 1969.
2. Garner, H. C.; Rogers, E. W. E.; Acum, W. E. A.; and Maskell, E. C.: Subsonic Wind-Tunnel Wall Corrections. AGARDograph 109, October 1966.
3. Barnwell, R. W.: Similarity Rule for Sidewall Boundary-Layer Effect in Two-Dimensional Wind Tunnels. AIAA Journal, Vol. 18, No. 9, pp. 1149-1151, September 1980.
4. Sewall, William G.: Effects of Sidewall Boundary Layers in Two-Dimensional Subsonic and Transonic Wind Tunnels. AIAA Journal, Vol. 20, No. 9, pp. 1253-1256, September 1982.
5. Green, J. E.: Interactions Between Shock Waves and Turbulent Boundary Layers. Progress in Aeronautical Sciences, Vol. II, Pergamon Press, New York, 1970.

07717

SESSION Va

CORRECTION METHODS USING MEASURED BOUNDARY DATA

Chairman: P. A. Newman, NASA Langley

N85 12024 D13

NLR ACTIVITIES IN THE FIELD OF  
WIND TUNNEL WALL INTERFERENCE

J. Smith  
National Aerospace Laboratory NLR  
The Netherlands

PRECEDING PAGE IS Preceding page blank

## BASIC WIAC OPTIONS

Modern WIAC methods apply some form of measured field data as a boundary condition for calculating the interference flow field. They can be roughly divided into two categories. For the first category, the field data must consist of distributions of a single velocity component, but in addition, an accurate estimate of the hypothetical free-air contribution of the model to this component is required. The differences between measured values and estimated model contributions are attributed to wall interference (after appropriate corrections for disturbances already present are made in absence of the model), and they establish the aforementioned boundary condition. The associated field data measurements can be rather simple, but the necessary "model representation" generally is a serious drawback.

The second category requires field data consisting of velocity vector distributions at the price of multicomponent measurements, but at the profit that no information at all is required about the model. In solid-wall test sections (where  $v = 0$  or, for compliant walls,  $v$  is known anyhow), the price is reduced to virtually zero but the profit remains (ref. 1). (See fig. 1.)

**SINGLE COMPONENT:**  
(2D: "Schwarz" type)

- Model representation
- + Limited field data
- + Simple measurement of field data

**MULTICOMPONENT:**  
(2D: "Cauchy" type)

- + No model representation
- (-) More extensive field data
- More complicated measurement of field data

Figure 1

NLR WIAC STRATEGY

NLR initially chose the single-component approach because our main interest was in ventilated-wall test sections, and the available instrumentation for multicomponent velocity measurements did not seem attractive for routine testing. The experience gained with the 2-D "Schwarz" type method has given us enough confidence in the field data approach to attack the 3-D problem. However, the necessary model representation is considered to be a very serious obstruction; it will have to depend on the type of model and thus be a recurrent problem and wipe out the possibility to attain a compact computer program. On the contrary, the problem of multicomponent velocity measurements could have a very general solution, i.e., a solution applicable to a very wide variety of models. Besides, the so-called "Calspan pipe" proposed by Wittliff (ref. 2) seems a very promising solution already. Therefore, NLR is now aiming at the more versatile multicomponent approach and is presently exploring the merits of the Calspan pipe. The evolution of this strategy is reflected in figure 2, which summarizes the 2-D field data now available at NLR. The complete set of data should be sufficient for 2-D WIAC procedure evaluations, but the Calspan pipe results are still being analyzed. Several parts of the data set include the test program shown in the section concerning the experimental 2-D data base.

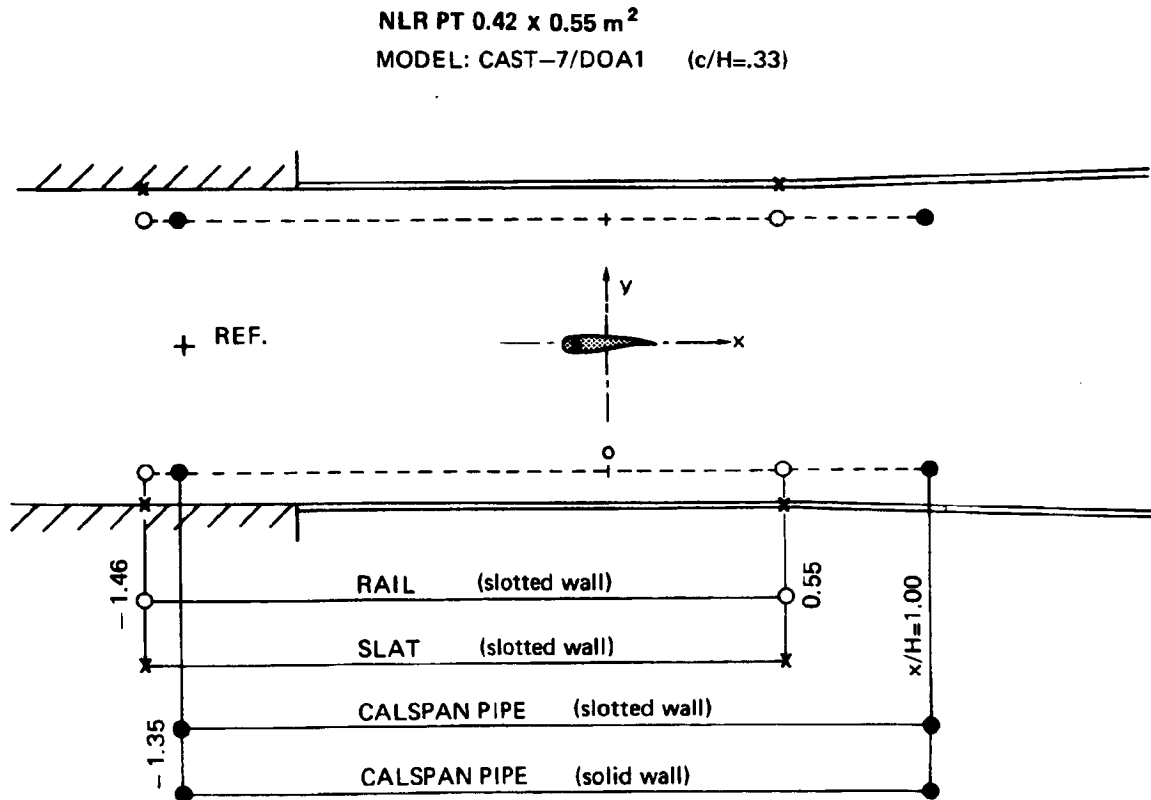


Figure 2

PLANNED THREE-DIMENSIONAL EVALUATIONS

In accordance with our present strategy, a 3-D WIAC procedure that requires multicomponent field data measurements has been developed, and models are being defined in behalf of its experimental evaluation. The models will be tested in both a small and a relatively large test section. Field data will be measured in, at least, the smaller test section, and the larger one should provide a nominally interference-free environment (or one requiring sufficiently small corrections that can be applied with great confidence). In order to obtain the wall velocity vector, it seems convenient to measure two of its components and, from these, to calculate the third one. Since the solid-wall test sections present the minor instrumentation problem (zero velocity normal to the walls, hence only wall pressure measurements required), the low-speed tests will be performed first. This will leave some time to evaluate properly the 2-D tests with Calspan pipes (fig. 2) before possibly using those in the subsequent 3-D transonic-speed tests. (See fig. 3.)

A basic drawback of this approach is that, together with the fact that the wind tunnels involved (except for the HST) operate at atmospheric conditions, the small model sizes lead to low Reynolds numbers (300 000 for the low-speed model). In spite of that, NLR will try to simulate low-speed high-lift conditions ( $C_{L_{max}} > 2$ ).

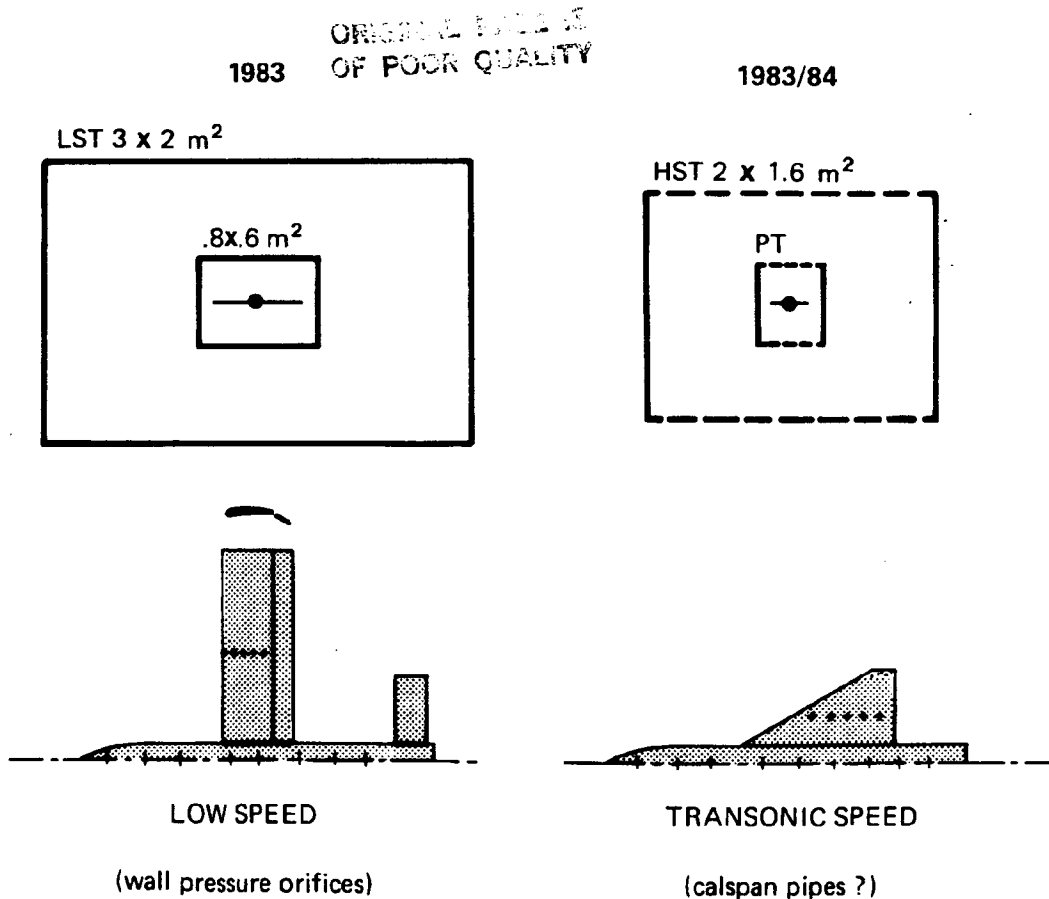


Figure 3

ORIGINAL PAGE IS  
OF POOR QUALITY

PRELIMINARY CALSPAN PIPE RESULTS

The Calspan pipe results obtained in the NLR PT are still being analyzed, so they are preliminary in nature but may be of some interest. The data obtained in the slotted-wall test section look rather promising although some possibly minor problems were encountered. Examples of the repeatability of the  $v$ -component are shown in figure 4. It is noted that  $v$  is determined from the actually measured  $\partial v/\partial x$  by simple integration, assuming  $v$  to be zero at the most upstream pressure stations. Remarkably, the repeatability of  $v/U_{REF}$  may be as bad as  $0.30^\circ$  in terms of flow angle, but in spite of that, the corresponding repeatability of the wall corrections turns out to be (almost) acceptable.

It was found that the pressures on the pipe fluctuate by about  $\pm 0.002$  in  $C_p$  with a frequency of roughly 3 Hz. Since  $\partial v/\partial x$  is related to a pressure difference, this may well be the cause of the poor repeatability: These fluctuations occurred both with and without the model installed, but they were not present in the tunnel reference pressure. Therefore, a possible cause could be the upstream pipe support.

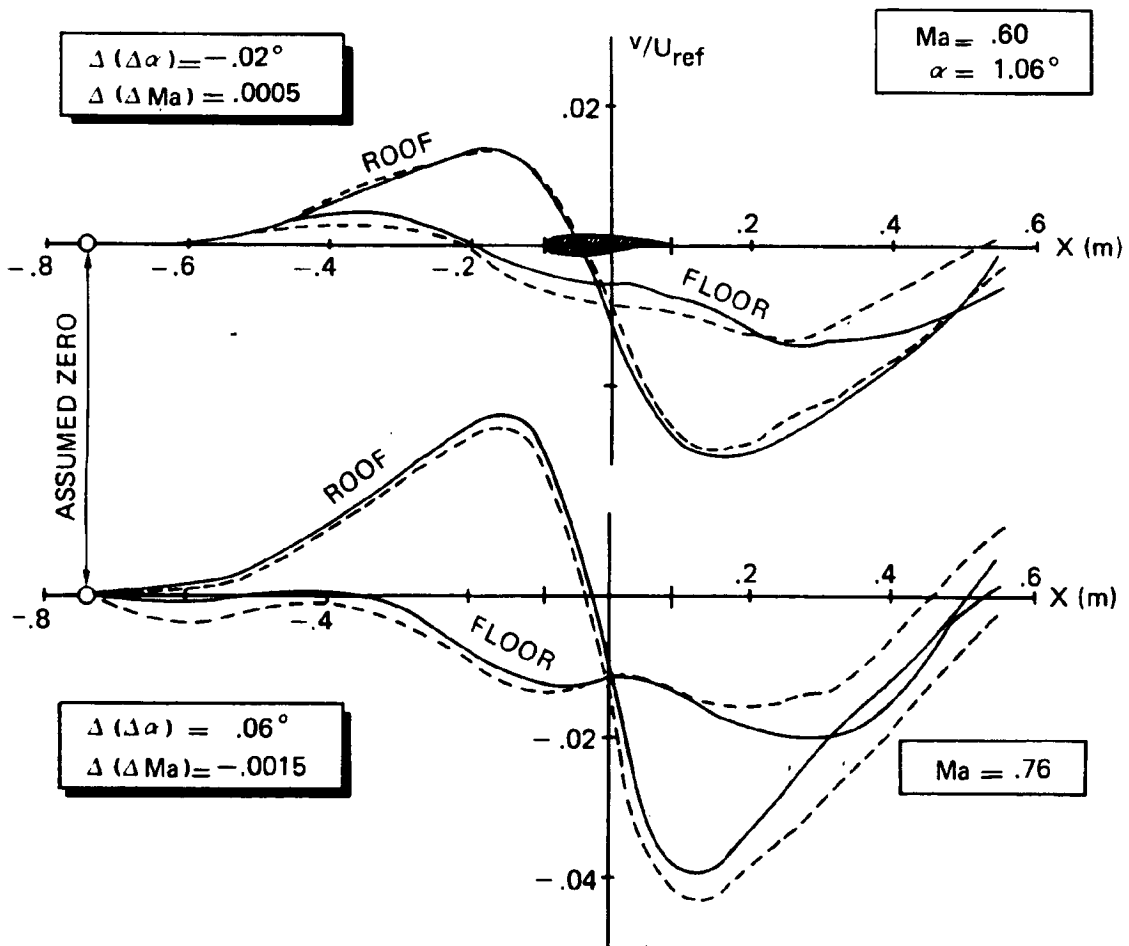


Figure 4

## EXPERIMENTAL TWO-DIMENSIONAL DATA BASE

NLR participates in the Group for Aeronautical Research and Technology in Europe (GARTEur) Action Group (AG 02), which is mainly concerned with a "validation of 2-D transonic testing." To this purpose, measurements were performed in seven European wind tunnels, each using its own model of the same airfoil (CAST-7/D0 A1) and its own measurement system. A summary of wind tunnel characteristics is shown in figure 5, together with the common test program. Extensive field data measurements were performed in the ONERA T2 and S3MA, TU-Berlin, and NLR PT wind tunnels. The field data consist of wall and/or rail pressures and, in the compliant-wall wind tunnels, also of wall shape. These data are being used for WIAC evaluation studies.

The group's final report is expected to appear in 1983. A progress report, however, has been published by Elsenaar and Stanewsky (ref. 3) with ample references to the separate data reports.

No	Tunnel	bxH (m <sup>2</sup> )	Type	$\sigma$ (%)	NS <sup>1)</sup>	b/c	H/c	$\delta^*/b$	Remarks
1	S3Ma	0.56 x 0.78	Perforated	9.7	—	2.8	3.9	0.010	Straight holes; solid side walls
2	TWB	0.34 x 0.60	Slotted	2.35	4	2.3 1.7	4.0 3.0	—	Solid side walls
3	ARA	0.20 x 0.46	Slotted	3.2	6	1.6	3.6	0.015	Solid side walls
4	TKG	0.99 x 0.98	Slotted <sup>2)</sup>	3.4 <sup>3)</sup>	4	5	4.9	0.011	Solid side walls
5	T-2	0.40 x 0.38	Solid	—	—	3.3 2.0	3.2 1.9	0.005	Parallel side walls; flexible top and bottom walls
6	NLR	0.42 x 0.55	Slotted	10	7	2.3	3.1	0.007	Solid side walls
7	TU-B	0.15 x 0.15	Solid	—	—	1.5	1.5	—	Parallel side walls; flexible top and bottom walls

1) No. of slots (excluding slots at intersection of vertical and horizontal walls)

2) Aluminium bars of 10 mm thickness mounted on perforated walls

3) Based on slot width only

### CHARACTERISTICS OF WIND TUNNELS INVOLVED

#### A. Angle-of-attack sweeps

$\alpha$	-2	-1	0	1	1.5	2	2.5	3	3.5	4	4.5	5	5.5	6	6.5	7	7.5	8	
$M_\infty$																			
0.60	•	•	•	•		•		•		•		•	•	•	•	•	•	•	•
0.70	•	•	•	•		•		•	•	•	•	•	•						
0.76	•	•	•	•	•	•	•	•	•										

#### B. Mach number sweeps

$M_\infty$	0.60	0.65	0.70	0.72	0.74	0.75	0.76	0.77	0.78	0.79	0.80	0.82	at angles of attack	
------------	------	------	------	------	------	------	------	------	------	------	------	------	---------------------	--

giving at  $M_\infty=0.76$  lift coefficients of  $C_L=0.52$  and  $C_L=0.73$ , respectively

### TEST PROGRAM

Figure 5

ORIGINAL  
OF POOR QUALITY

## NEED FOR A THEORETICAL DATA BASE

The ultimate goal of WIAC methods is, of course, to attain an improved accuracy of measured data. Consequently, an experimental data base should provide the ultimate test for the applicability and reliability of a WIAC method. However, experiments are all too often poor guides to improvements of the methods. The amount of information from an experiment is generally rather limited. On the contrary, theoretical data can be as extensive as desired at relatively low cost. Besides, theoretical wind tunnel and corresponding unbounded flow data can both be obtained with the same accuracy. Therefore, a theoretical data base seems an ideal source of information for detailed WIAC studies. However, a first attempt to create a set of theoretical data for 2-D transonic flow did not quite succeed because the generated field data seemed questionable although the calculated model pressure distributions looked quite reliable. This may be related to the fact that many computation methods focus on the model and have relaxed accuracy requirements for the "far field." It also suggests that the creation of a theoretical WIAC data base may be of some benefit to theoreticians also.

An example of a theoretical data base for 2-D flow and some possible applications are shown in figure 6. Similar considerations should also apply to 3-D flow.

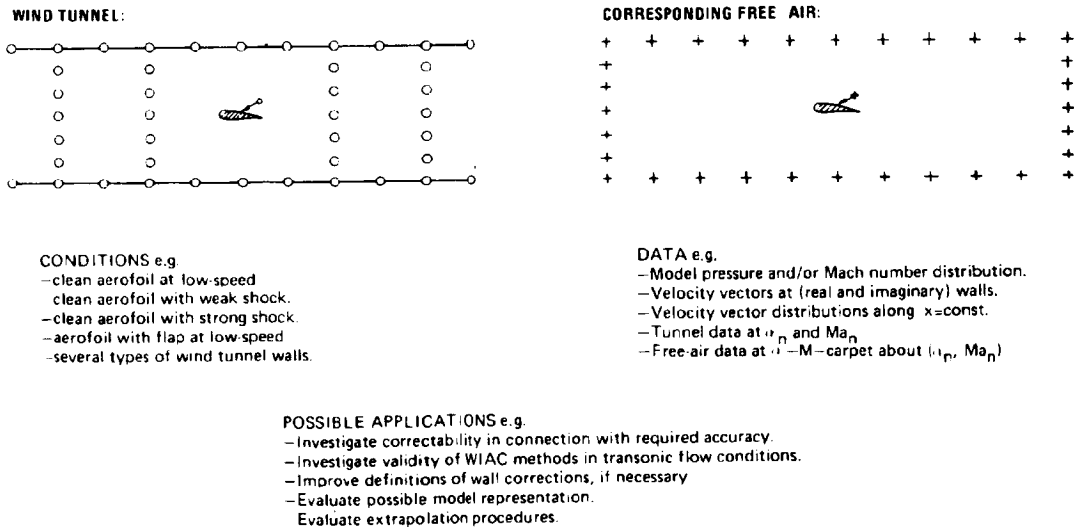


Figure 6

## FUTURE WORK AND POTENTIAL PROBLEM AREAS

At present, the principles and possibilities of WIAC methods using "measured boundary conditions" are becoming well established. However, for routine testing, it is desirable to reduce the amount and the complexity of required field data. On the other hand, applying appropriate theoretical means to achieve this may endanger the feasibility of the often expressed desire to apply the corrections on-line. Probably, some optimum will have to be established for the somewhat conflicting requirements 1 and 2 of figure 7. Another aspect that will need more attention is the connection between required accuracy and "correctability." Resulting quantitative correctability criteria may then be used as a "target" for the design and operation of "correctable-interference" test sections. As part of this process, it may be desirable to reconsider definitions of wall interference corrections, especially for complicated models. Appropriate theoretical data bases, in a sense as shown in figure 5, may be the most efficient tools for this job.

Beyond the scope of WIAC, other interference effects can be of comparable importance to the experimental aerodynamicist with model support interference (especially in connection with strut supports) as the most obvious example.

### 1. REDUCTION OF NECESSARY AMOUNT OF FIELD DATA AND SAMPLING TIME

- Accurate, fast-response instrumentation
- Simultaneous readings
- Efficient theoretical use of measured data

### 2. ON-LINE WIAC CALCULATIONS

- Fast algorithms

### 3. IMPROVED WIAC DEFINITIONS

- Fundamental research in order to
  - define correctability in terms of required accuracy
  - define corrections for complicated models  
(such as: propellers, TPS, 3-D aircraft)

### 4. DESIGN AND OPERATION OF CORRECTABLE-INTERFERENCE TEST SECTIONS

### 5. OTHER INTERFERENCES (E.G. MODEL SUPPORTS)

Figure 7

#### REFERENCES

1. Smith, J.: Measured Boundary Conditions Methods for 2-D Flow. AGARD CP-335, Paper No. 9, May 1982, pp. 9-1 to 9-15.
2. Nenni, J. P., Erickson, J. C., Jr., and Wittliff, C. E.: Measurement of Small Normal Velocity Components in Subsonic Flows by Use of a Static Pipe. AIAA Journal, vol. 20, no. 8, August 1982, pp. 1077-1083.
3. Elsenaar, A., and Stanewsky, E.: A Report of a GARTEur Action Group on "Two-Dimensional Transonic Testing Methods." AGARD CP-335, Paper No. 5, May 1982, pp. 5-1 to 5-16.

PROGRESS IN WIND TUNNEL WALL INTERFERENCE  
ASSESSMENT/CORRECTION PROCEDURES AT THE NAE

L. H. Ohman, M. Mokry, and Y. Y. Chan  
National Research Council Canada  
National Aeronautical Establishment  
Ottawa, Canada

REPRODUCED FROM ORIGINAL DOCUMENT

Preceding page blank

## INTRODUCTION

The initial approach to the transonic wall interference problem at the NAE was to assess wall corrections as a function of wall porosity. Considerable efforts were thus directed towards establishing effective porosities primarily for the two-dimensional case.

1. Through comparison of experimental data for two geometrically similar models of different chord/height ratio, an overall value of wall porosity could be deduced (ref. 1).
2. Through theoretical development allowing for unequal porosity for the floor and ceiling and wall boundary pressure measurements, porosities for floor and ceiling could be deduced. Various schemes were developed to obtain porosity values via best fit procedures (ref. 2).
3. Following point 2 above, a scheme was also developed which allowed not only for unequal porosity of floor and ceiling but also for streamwise varying porosity (ref. 3).

In an experiment performed to determine the boundary layer development along the perforated floor and ceiling under the influence of the model pressure field (ref. 4), substantial variations in boundary layer thickness were measured, underlining the difficulties in deducing meaningful values of wall porosity. Since 1980 the concept of wall porosity, in the aerodynamic sense, was dropped and an entirely new approach was adopted (ref. 5). Wall boundary pressure measurement, in combination with singularity modelling of the airfoil, was then sufficient to yield required information on the wall interference flow without first having to establish some value for wall porosity. This new method has been used routinely at NAE for two-dimensional investigations since 1980 and has proven to be very effective and consistent. The singularity modelling of the airfoil initially covered only lift and volume but has been extended to include drag (wake) and pitching moment (unpublished results), and second-order volume term (ref. 6). A good collection of simultaneously measured model data and wall boundary pressure data exists at NAE for a variety of airfoils and a good range of Mach numbers.

Although the methods discussed above are all based on subsonic compressible flow analysis, it has been shown by asymptotic transonic small disturbance analysis (ref. 7) that the derived corrections to angle of attack and free-stream Mach number are correct to the first order. The asymptotic analysis further shows that the second-order term for the angle-of-attack correction is insignificant.

### SAMPLE DATA AND CORRECTIONS FOR BGK1 AIRFOIL

Samples of data and wall interference corrections for the BGK1 airfoil are given in figures 1 through 10 as corrections to Mach number ( $\Delta M$ ) and angle of attack ( $\Delta \alpha$ ). Figures 1 to 7 show results according to the method described in reference 5, which accounts for lift and solid blockage. The data for the case shown in figure 4 have also been corrected using the extended methods. Figure 8 shows calculated corrections based upon the method of Mokry (unpublished results), which accounts for lift, solid blockage, pitching moment, and wake drag. Figure 9 shows similar results when the volume doublet due to lift is also included (ref. 6). The case shown in figure 7 has been circulated among a number of researchers as a test case to obtain their assessment of the wall interference corrections to Mach number and angle of attack. The results are summarized in figure 10.

ORIGINAL PRINT  
OF POOR QUALITY

RUN 23893/1

$R_c = 20.28 \times 10^6$

$M = 0.7826$

$\alpha = -3.639^\circ$

$C_N = -0.2194$

$C_D = 0.0000$

$C_M = 0.0000$

$A = 0.0754$

$c/h = 0.1667$

$\Delta M = -0.0021$

$\Delta \alpha = 0.243^\circ$

$c \times \delta \Delta M / \delta x = 0.0024$

$c \times \delta \Delta \alpha / \delta x = 0.015^\circ$

$M_{cor} = 0.7805$

$\alpha_{cor} = -3.397^\circ$

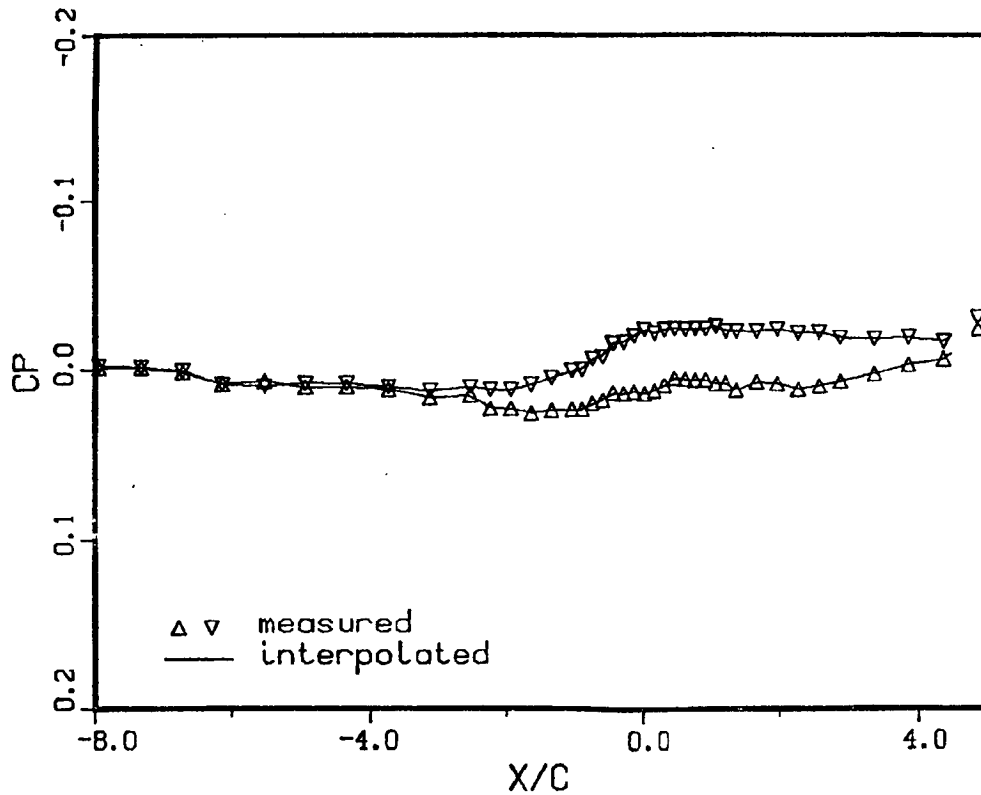


Figure 1.- Data for BGK1 airfoil, run no. 23893/1. Calculated corrections  $\Delta M$  and  $\Delta \alpha$  account for lift and solid blockage (ref. 5).

ORIGINAL PAGE IS  
OF POOR QUALITY

RUN 23893/2

$R_c = 20.49 \times 10^6$

$M = 0.7824$

$\alpha = -0.397^\circ$

$C_N = 0.2936$

$C_D = 0.0000$

$C_M = 0.0000$

$A = 0.0754$

$c/h = 0.1667$

$\Delta M = -0.0034$

$\Delta \alpha = -0.490^\circ$

$c \times \delta \Delta M / \delta x = 0.0011$

$c \times \delta \Delta \alpha / \delta x = -0.042^\circ$

$M_{cor} = 0.7790$

$\alpha_{cor} = -0.888^\circ$

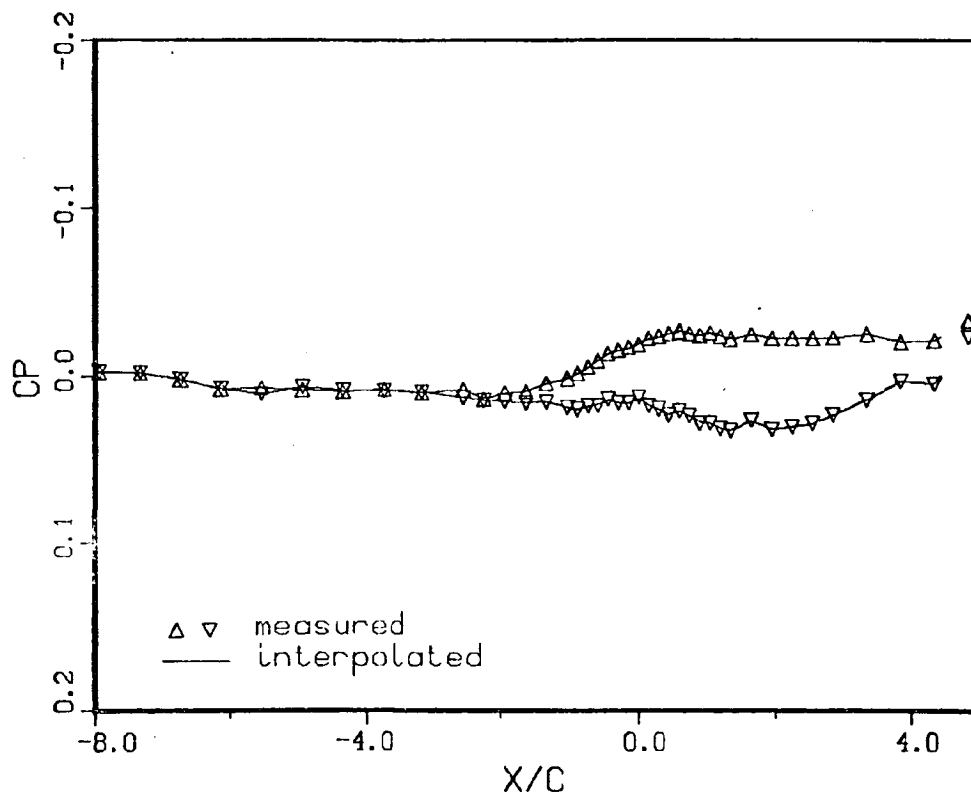


Figure 2.- Data for BGK1 airfoil, run no. 23893/2. Calculated corrections  $\Delta M$  and  $\Delta \alpha$  account for lift and solid blockage (ref. 5).

RUN 23893/3

$R_c = 20.57 \times 10^6$

$M = 0.7826$

$\alpha = 1.486^\circ$

$C_N = 0.6154$

$C_D = 0.0000$

$C_M = 0.0000$

$R = 0.0754$

$c/h = 0.1667$

$\Delta M = -0.0103$

$\Delta \alpha = -0.814^\circ$

$c \times \delta \Delta M / \delta x = 0.0015$

$c \times \delta \Delta \alpha / \delta x = -0.029^\circ$

$M_{cor} = 0.7723$

$\alpha_{cor} = 0.672^\circ$

DATA POINTS  
OF POOR QUALITY

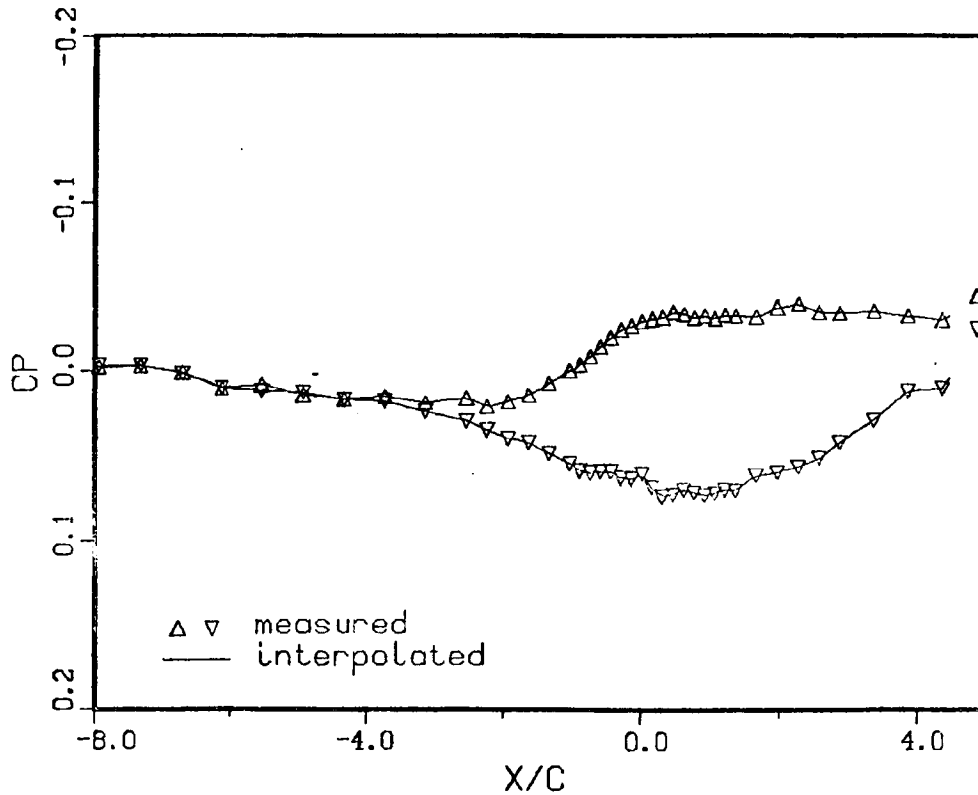


Figure 3.- Data for BGK1 airfoil, run no. 23893/3. Calculated corrections  $\Delta M$  and  $\Delta \alpha$  account for lift and solid blockage (ref. 5).

RUN 23893/4

$R_c - 20.62 \times 10^6$   
 $M - 0.7825$   
 $\alpha - 2.497^\circ$   
 $C_N - 0.7697$   
 $C_D - 0.0000$   
 $C_M - 0.0000$   
 $A - 0.0754$   
 $c/h - 0.1667$

$\Delta M - -0.0136$   
 $\Delta \alpha - -0.965^\circ$   
 $c \times \delta \Delta M / \delta x - 0.0022$   
 $c \times \delta \Delta \alpha / \delta x - -0.030^\circ$   
 $M_{cor} - 0.7690$   
 $\alpha_{cor} - 1.533^\circ$

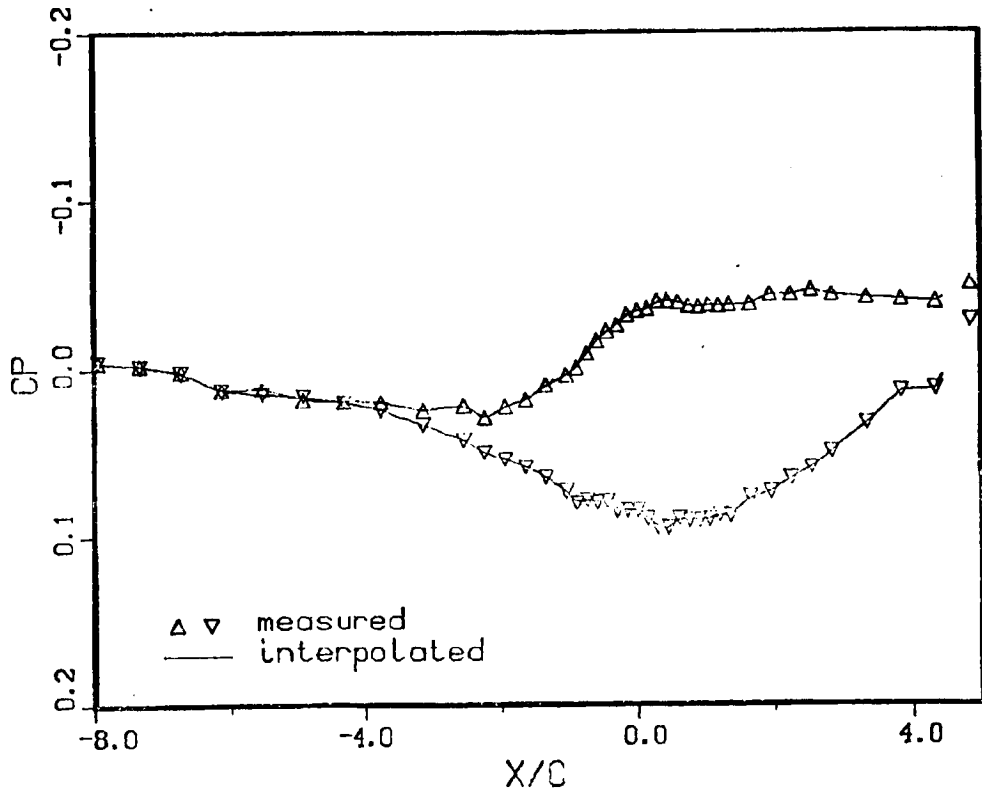


Figure 4.- Data for BGK1 airfoil, run no. 23893/4. Calculated corrections  $\Delta M$  and  $\Delta \alpha$  account for lift and solid blockage (ref. 5).

RUN 23893/5

$R_c = 20.66 \times 10^6$

$M = 0.7824$

$\alpha = 3.518^\circ$

$C_N = 0.8167$

$C_D = 0.0000$

$C_M = 0.0000$

$A = 0.0754$

$c/h = 0.1667$

$\Delta M = -0.0146$

$\Delta \alpha = -1.006^\circ$

$c \times \delta \Delta M / \delta x = 0.0027$

$c \times \delta \Delta \alpha / \delta x = -0.027^\circ$

$M_{cor} = 0.7678$

$\alpha_{cor} = 2.513^\circ$

OF FOUR QUARTERS

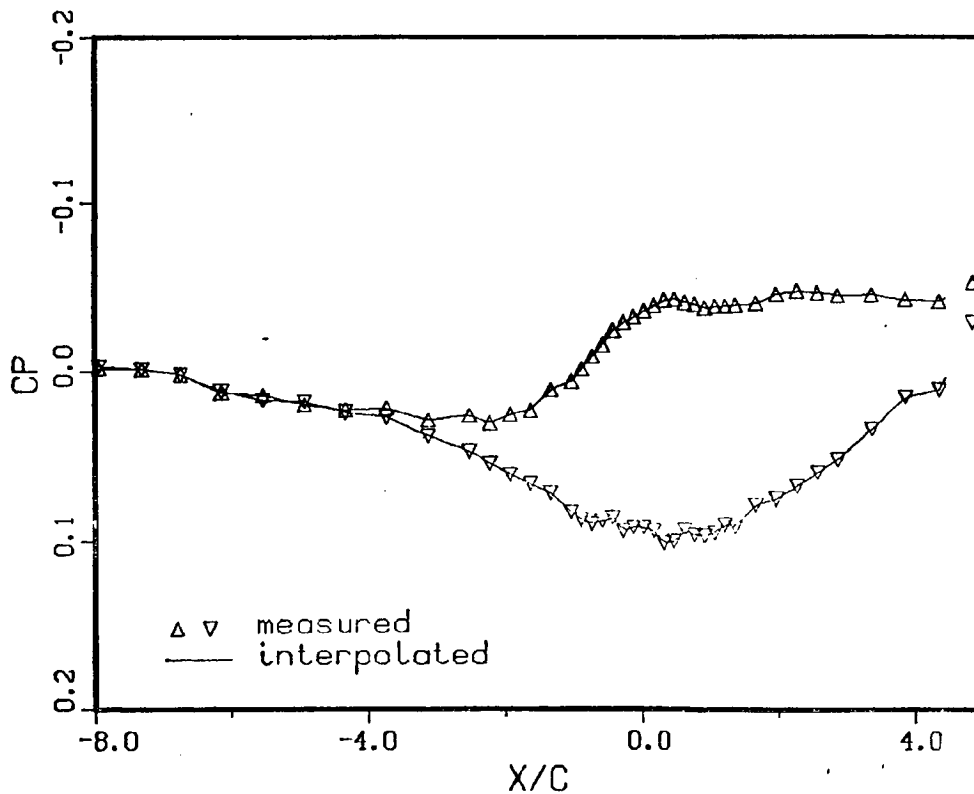


Figure 5.- Data for BGK1 airfoil, run no. 23893/5. Calculated corrections  $\Delta M$  and  $\Delta \alpha$  account for lift and solid blockage (ref. 5).

RUN 23893/6

$R_c - 20.70 \times 10^6$   
 $M - 0.7827$   
 $\alpha - 4.524^\circ$   
 $C_N - 0.8291$   
 $C_D - 0.0000$   
 $C_M - 0.0000$   
 $A - 0.0754$   
 $c/h - 0.1667$

$\Delta M - -0.0150$   
 $\Delta \alpha - -1.006^\circ$   
 $c \times \delta \Delta M / \delta x - 0.0031$   
 $c \times \delta \Delta \alpha / \delta x - -0.025^\circ$   
 $M_{cor} - 0.7677$   
 $\alpha_{cor} - 3.518^\circ$

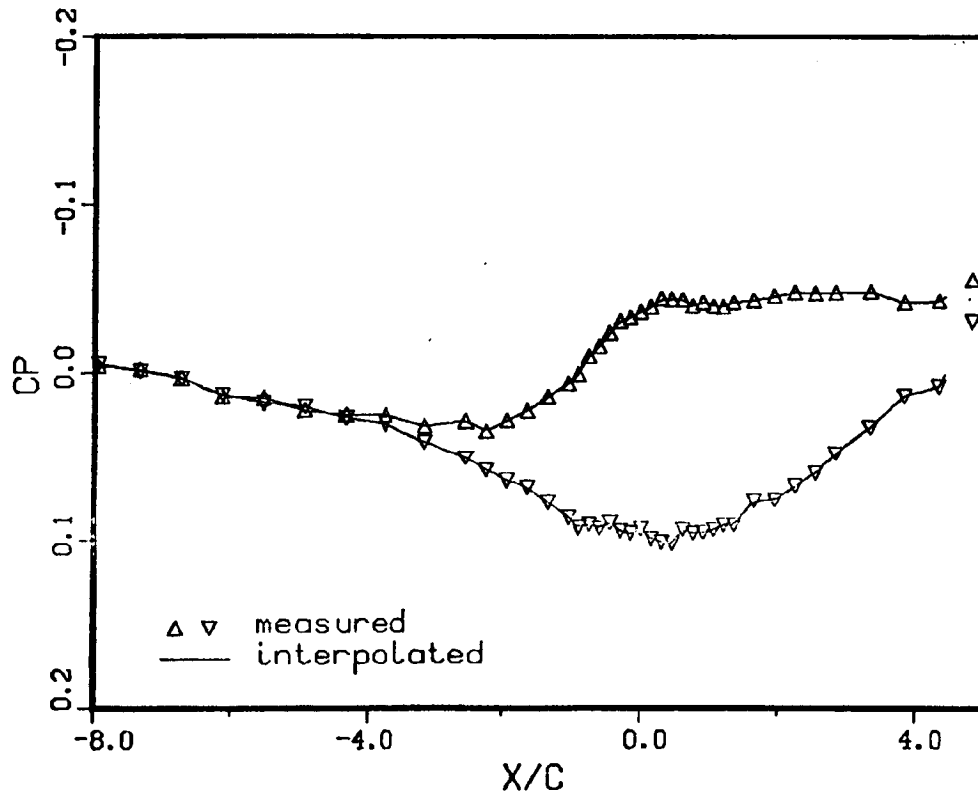


Figure 6.- Data for BGK1 airfoil, run no. 23893/6. Calculated corrections  $\Delta M$  and  $\Delta \alpha$  account for lift and solid blockage (ref. 5).

RUN 20914/4

$R_c - 21.03 \times 10^6$

$M - 0.7839$

$\alpha - 2.560^\circ$

$C_N - 0.7641$

$C_D - 0.0000$

$C_M - 0.0000$

$A - 0.0754$

$c/h - 0.1667$

$\Delta M - -0.0150$

$\Delta \alpha - -0.669^\circ$

$c \times \delta \Delta M / \delta x - 0.0003$

$c \times \delta \Delta \alpha / \delta x - -0.053^\circ$

$M_{cor} - 0.7689$

$\alpha_{cor} - 1.891^\circ$

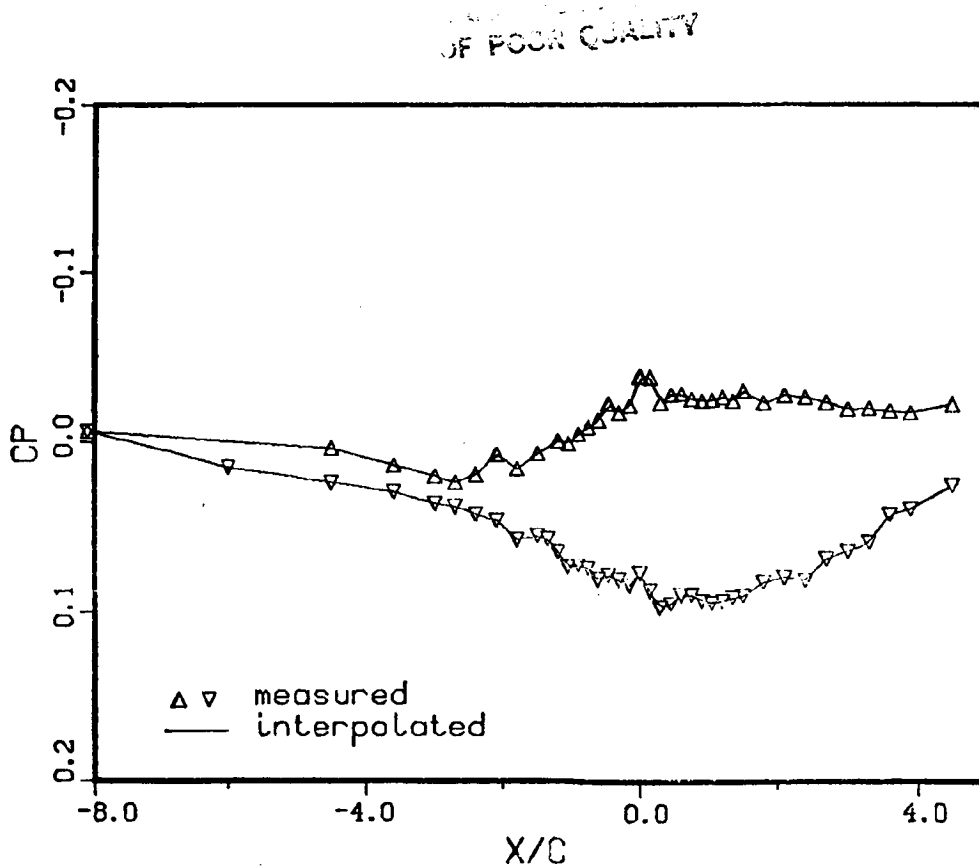


Figure 7.- Data for BGK1 airfoil, run no. 20914/4. Calculated corrections  $\Delta M$  and  $\Delta \alpha$  account for lift and solid blockage (ref. 5).

CP vs X/C  
 CP vs X/C

RUN 23893/4

$R_c$ - $20.62 \times 10^6$	$\Delta M$ - $-0.0136$
$M$ - $0.7825$	$\Delta \alpha$ - $-1.065^\circ$
$\alpha$ - $2.497^\circ$	$c \times \delta \Delta M / \delta x$ - $0.0019$
$C_N$ - $0.7697$	$c \times \delta \Delta \alpha / \delta x$ - $-0.030^\circ$
$C_D$ - $0.0187$	$M_{cor}$ - $0.7690$
$C_M$ - $-0.1395$	$\alpha_{cor}$ - $1.433^\circ$
$R$ - $0.0754$	
$c/h$ - $0.1667$	

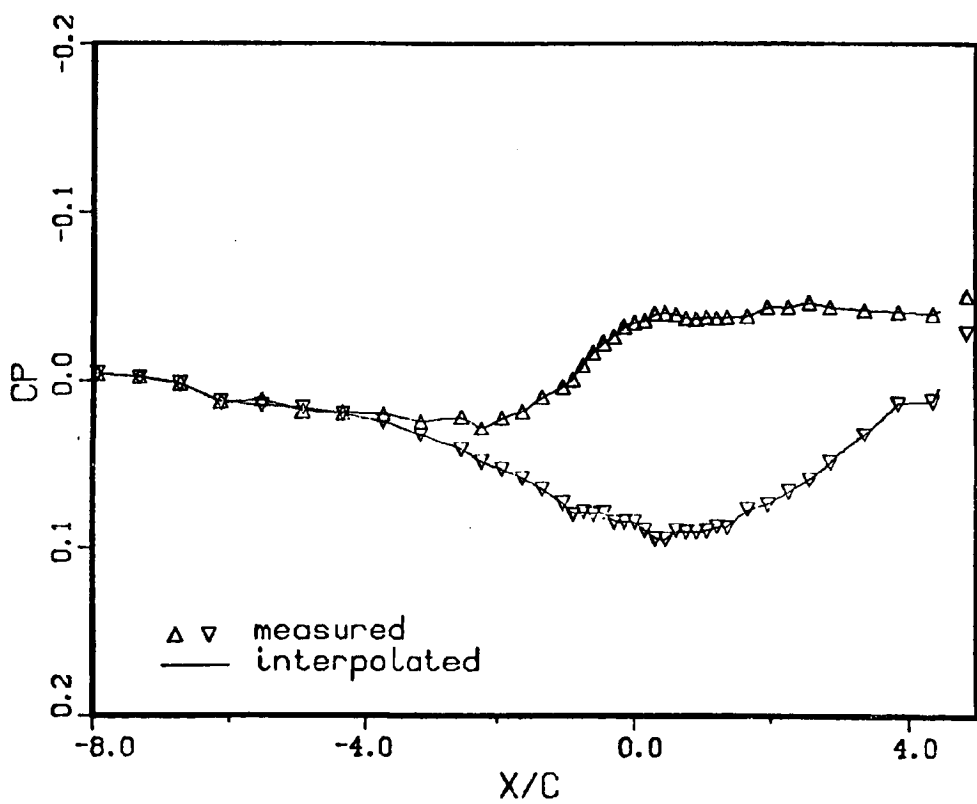


Figure 8.- Data for BGK1 airfoil, run no. 23893/4. Calculated corrections  $\Delta M$  and  $\Delta \alpha$  account for lift, solid blockage, pitching moment, and wake drag. (M. Mokry, unpublished results, 1983).

RUN 23893/4

$R_c - 20.62 \times 10^6$

$M - 0.7825$

$\alpha - 2.497^\circ$

$C_N - 0.7697$

$C_D - 0.0187$

$C_M - -0.1395$

$A - 0.0754$

$c/h - 0.1667$

$\Delta M - -0.0144$

$\Delta \alpha - -1.065^\circ$

$c \times \delta \Delta M / \delta x - 0.0019$

$c \times \delta \Delta \alpha / \delta x - -0.030^\circ$

$M_{cor} - 0.7681$

$\alpha_{cor} - 1.433^\circ$

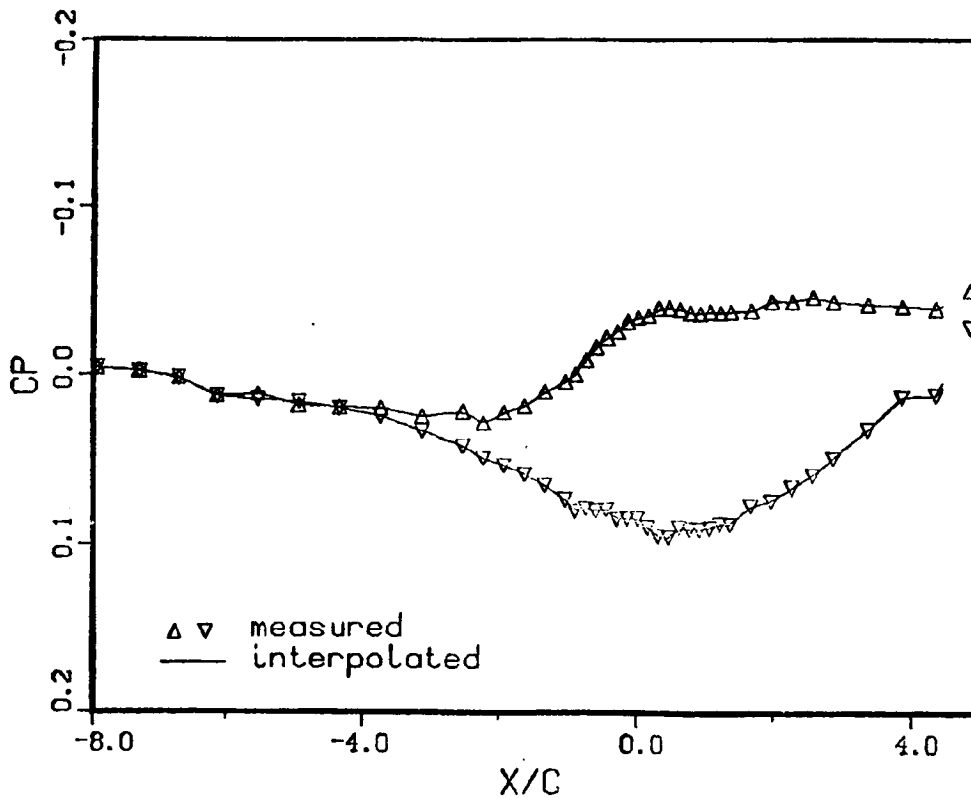


Figure 9.- Data for BGK1 airfoil, run no. 23893/4. Calculated corrections  $\Delta M$  and  $\Delta \alpha$  account for lift, solid blockage, pitching moment, wake drag, and the "Chan" doublet (ref. 6).

	$\Delta M$	$\Delta \alpha$
ONERA, France Capelier, Chevallier and Bouniol	-0.015	-0.67°
NAE, Canada Mokry and Ohman	-0.015	-0.67°
NLR, The Netherlands Smith	-0.015	-0.56°
NAL, Japan Sawada	---	-0.58°
NASA Langley, USA Kemp	-0.017	-0.64° -0.89°

Figure 10.- Comparison of corrections for the BGK1 airfoil test case.

NAE TWO-DIMENSIONAL HIGH LIFT AIRFOIL

Wall pressure data were obtained in the NAE 15- x 60-in. high Reynolds number 2-D test facility for a 21-percent-thick simple slotted airfoil (fig. 11). Note that in spite of a fairly large correction to angle of attack, there are no significant wall-induced gradients (velocity and flow curvature) at the position of the model. This latter fact implies that correction of the measured data for wall interference effects is indeed meaningful.

Test Conditions	Calc. Corrections	Corrected Results
$Rc = 10.29 \times 10^6$	$\Delta M = -0.0087$	$Rc = 9.81 \times 10^6$
$M_\infty = 0.2253$	$\Delta \alpha = -4.24^\circ$	$M_{\infty c} = 0.2166$
$\alpha_g = 17.85^\circ$		$\alpha_c = 13.61$
$c/h = 0.2$	$c \frac{\delta \Delta M}{\delta x} = 0.0005$	$C_{Lc} = 3.7524$
$A = 0.1390$	$c \frac{\delta \Delta \alpha}{\delta x} = -0.009^\circ$	$C_{Dc} = 0.1152$
$C_L = 3.4643$		$C_{m_c} = -0.6003$
$C_D = 0.3647$		
$C_m(c/4) = -0.5570$		

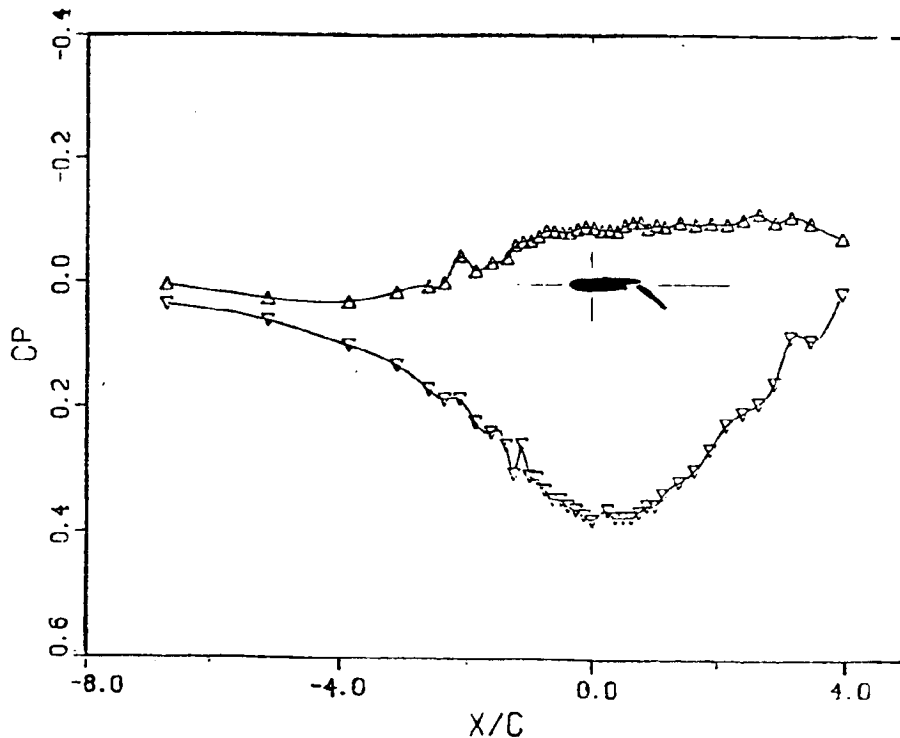
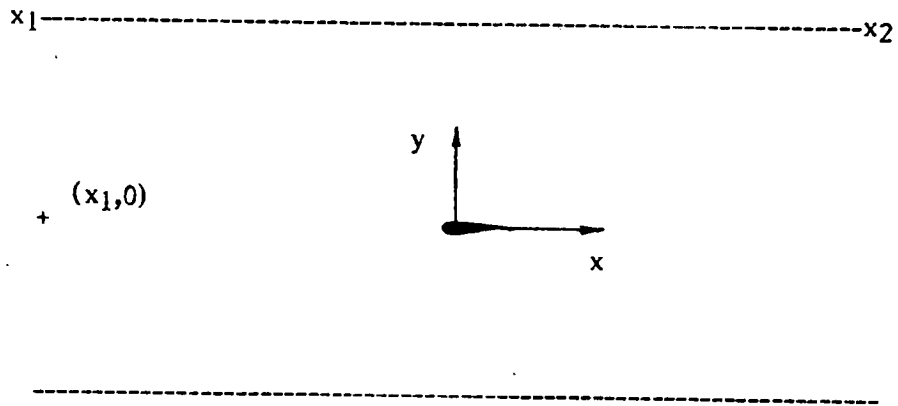


Figure 11.- Wall pressure data for high-lift airfoil.

EFFECT OF TRUNCATION OF WALL PRESSURE DATA ON WIND TUNNEL CORRECTIONS

The Mach number and angle-of-attack corrections,  $\Delta M$  and  $\Delta\alpha$ , are the corrections to the corresponding free-stream flow quantities at the position of the model (fig. 12). It appears that  $\Delta M$  is not excessively sensitive to the length over which the wall pressures are measured. To obtain a meaningful  $\Delta\alpha$ , however, the reference point  $(x_1, 0)$ , where the flow is assumed parallel to the tunnel axis, must be sufficiently far from the model so that the pressures at  $x = x_1$  are not influenced by model incidence.



$x_1/c$	$x_2/c$	RUN 20914/4		RUN 23893/4	
		$\Delta M$	$\Delta\alpha^\circ$	$\Delta M$	$\Delta\alpha^\circ$
-8	4.5	-0.0150	-0.669	-0.0136	-0.965
-6	4.5	-0.0151	-0.843	-0.0123	-1.095
-4	4.5	-0.0139	-1.080	-0.0095	-1.129
-4	2.5	-0.0170	-1.387	-0.0156	-1.530
-2.5	2.5	-0.0170	-1.749	-0.0143	-1.716

Figure 12.- Effect of truncation of wall pressure data on  $\Delta M$  and  $\Delta\alpha$ . NAE two-dimensional data.

### EDGETONE NOISE EFFECT ON NAE SUPERCRITICAL AIRFOIL DATA

Wall boundary and airfoil pressure data were obtained in the NAE 15- x 60-in. high Reynolds number 2-D test facility for the BGK1 supercritical airfoil with and without edgetone noise suppression. The data tabulated in figure 13 relate to those presented in figure 14. The noise suppression is obtained by overlaying the 20-percent perforated floor and ceiling with a fine mesh screen of 40 percent open area (ref. 8).

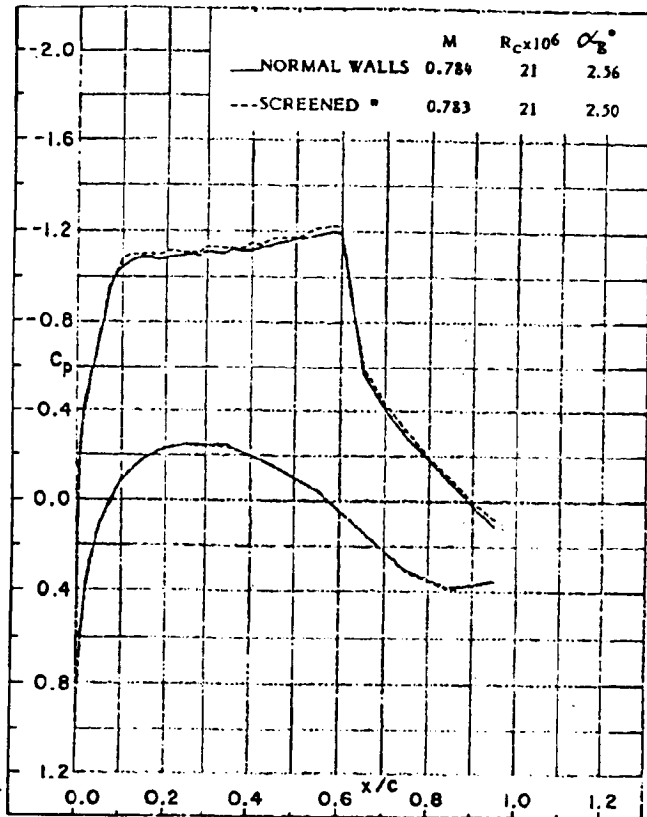
Although the elimination of edgetone noise significantly reduces the overall free-stream noise level (by 50 percent or more), the effect of this noise reduction is hardly discernible on the airfoil pressure data (figs. 14(a) and 15). There is some evidence (fig. 15) that shock position is influenced by the noise level when the shock is located over the "flat" portion of the airfoil surface.

The data plotted in figure 14(b) show that the use of a fine mesh screen for edgetone suppression has a negligible effect on the wall interference characteristics. This is further emphasized by the tabulated results in figure 13. Note, however, the appreciable difference in  $\Delta\alpha$  and consequently in  $\alpha_c$ . This difference,  $0.30^\circ$  in  $\Delta\alpha$ , is believed to be due to a small measuring error, or bias, in the 1978 wall data, which primarily affected the  $\alpha$ -correction results. Only solid blockage and lift effects are accounted for in both of these calculated wall correction examples.

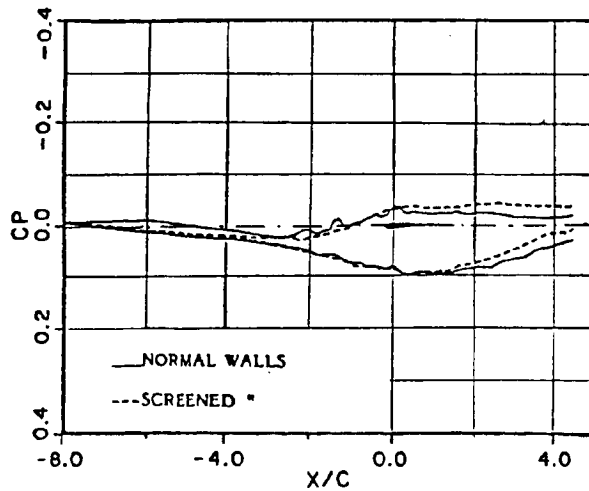
NORMAL WALLS (1978)		RUN 20914/4
Test Conditions	Calc. Corrections	Corrected Results
$R_C = 21.03 \times 10^6$	$\Delta M = -0.015$	$R_C = 20.78 \times 10^6$
$M_\infty = 0.7839$	$\Delta\alpha = -0.67^\circ$	$M_{\infty C} = 0.769$
$\alpha_g = 2.56^\circ$	$c \frac{\partial \Delta M}{\partial x} = -0.0003$	$\alpha_c = 1.89^\circ$
$C_{Np} = 0.757$		$C_{Nc} = 0.775$
$C_{m(c/4)} = 0.1401$	$c \frac{\partial \Delta\alpha}{\partial x} = -0.053^\circ$	$C_{m_c} = -0.1435$
$C_{D_W(\xi)} = 0.0186$		$C_{D_{Wc}} = 0.0187$
"SCREENED" WALLS (1981)		RUN 23893/4
Test Conditions	Calc. Corrections	Corrected Results
$R_C = 20.62 \times 10^6$	$\Delta M = -0.014$	$R_C = 20.42 \times 10^6$
$M_\infty = 0.7825$	$\Delta\alpha = -0.97^\circ$	$M_{\infty C} = 0.769$
$\alpha_g = 2.50^\circ$	$c \frac{\partial \Delta M}{\partial x} = 0.0022$	$\alpha_c = 1.53^\circ$
$C_{Np} = 0.780$		$C_{Nc} = 0.798$
$C_{m(c/4)} = -0.1480$	$c \frac{\partial \Delta\alpha}{\partial x} = -0.030^\circ$	$C_{m_c} = -0.1512$
$C_{D_W(\xi)} = 0.0187$		$C_{D_{Wc}} = 0.0192$

Figure 13.- Edgetone noise effect on supercritical airfoil data and wall correction data.

CHARACTERISTICS OF POOR QUALITY



(a) Airfoil pressure distributions.



(b) Wall pressure distributions.

Figure 14.- Sample data from edgetone noise study (ref. 8).

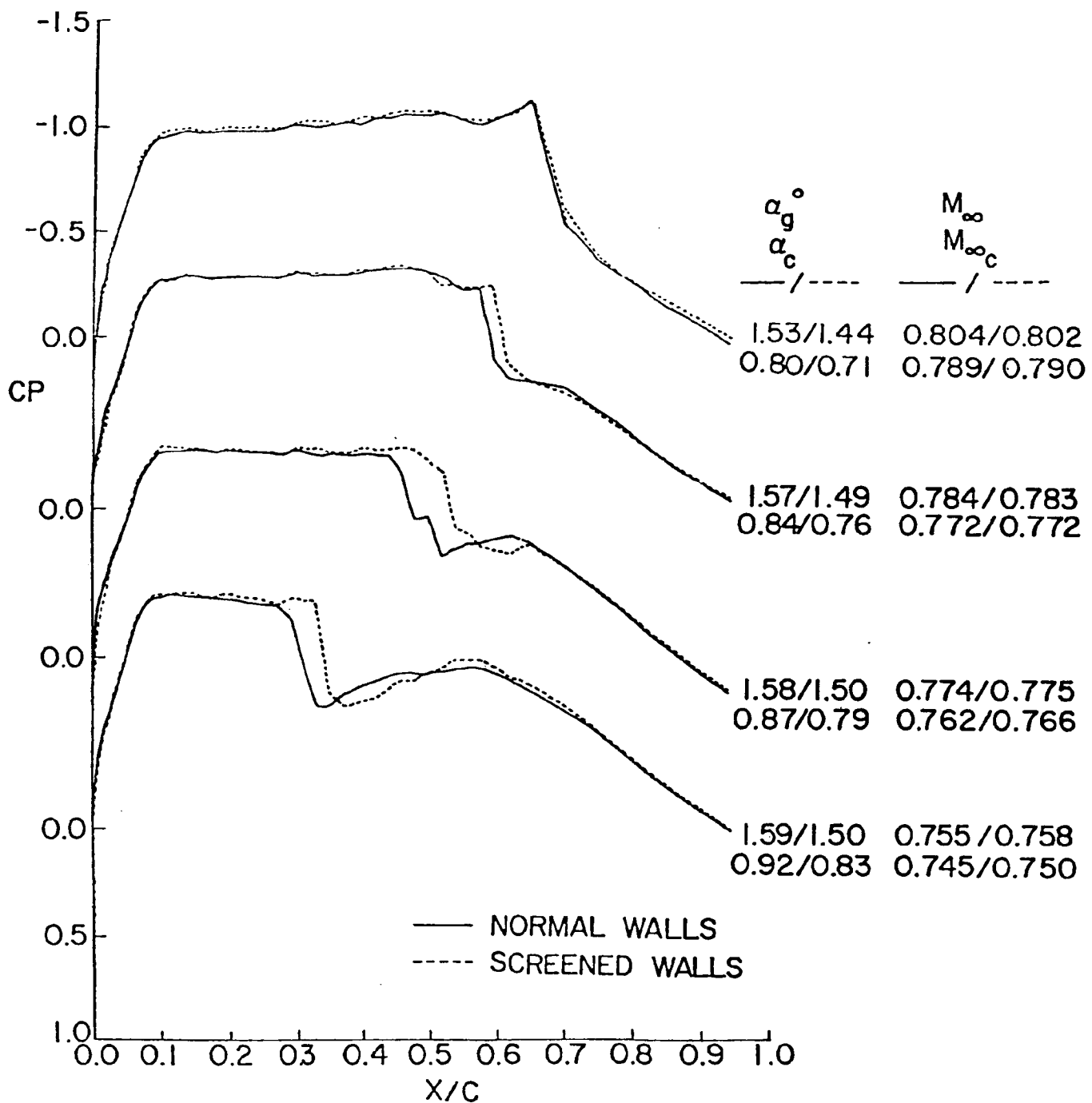


Figure 15.- BGK1 airfoil upper surface pressure distributions.  
 $R_C = 21 \times 10^6$  (ref. 8).

### NAE APPROACH TO THREE-DIMENSIONAL WALL INTERFERENCE CORRECTIONS

The approach to three-dimensional wall interference has basically followed the same pattern as for the two-dimensional case (ref. 9). The theoretical development has also in this case progressed to the stage (ref. 10) equivalent to that reported for the two-dimensional case (ref. 5). Figure 16 illustrates tunnel cross section shapes for three-dimensional testing with four static pressure pipes installed near the walls (ref. 11). Subsonic wall interference corrections are evaluated using the Fourier solution for the Dirichlet problem in the circular cylinder interior to a three-dimensional test section, with the required wall boundary values obtained from static pressure measurements along four generators of the cylinder. Figure 17 depicts the three-dimensional model and outlines the correction procedure. The feasibility and accuracy of the method have been demonstrated on a theoretical example, as indicated in figure 18.

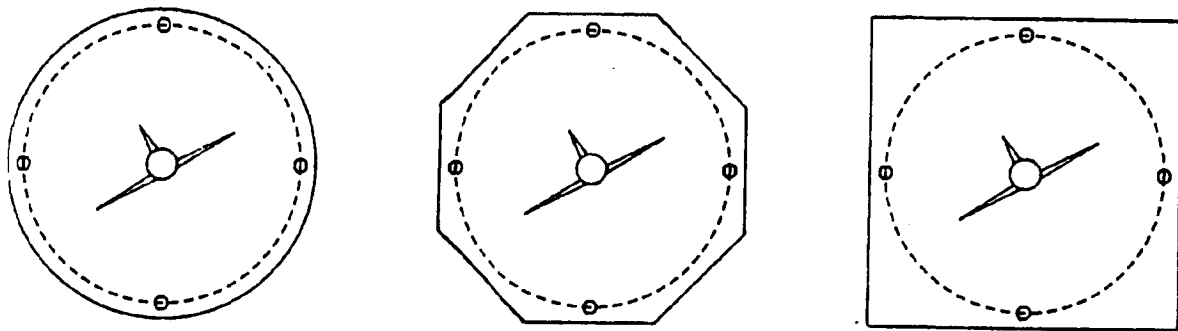
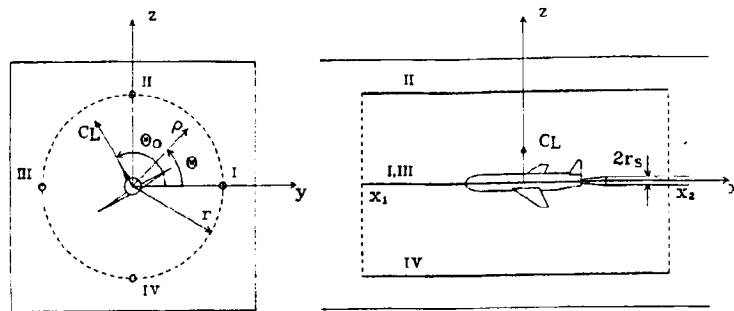


Figure 16.- Tunnel cross section shapes with four static pressure pipes. (From ref. 11.)



$$\phi = \phi_p + \phi_w \longrightarrow u = \partial\phi_w/\partial x = -C_p/2 - \partial\phi_p/\partial x$$

$$u = a_0(x, \rho) + \sum_{n=1}^{\infty} a_n(x, \rho) \cos n\theta + b_n(x, \rho) \sin n\theta$$

2 tubes :  $a_0(x, r), b_1(x, r)$

4 tubes :  $a_0(x, r), a_1(x, r), b_1(x, r), a_2(x, r)$

$a_0(0,0)$  ..... Mach number correction  $\Delta M_m$

$a_1(0,0)$  ..... sideslip correction  $\Delta\alpha_y$

$b_1(0,0)$  ..... incidence correction  $\Delta\alpha_z$

Figure 17.- NAE three-dimensional geometry and correction procedure. (From ref. 11.)

	exact	present method	
		-1.6 < x < 1.6	-3.2 < x < 3.2
		m=32	m=128
		/Table 2/	
$\Delta M$	0.00724	0.00715	0.00722
$\Delta\alpha_y$ (deg)	-0.05900	-0.05420	-0.05892
$\Delta\alpha_z$ (deg)	0.22020	0.20228	0.21989
$\partial\Delta M/\partial x$ (1/L)	0.00210	0.00207	0.00209
$\partial\Delta\alpha_y/\partial x$ (deg/L)	-0.08254	-0.08123	-0.08221
$\partial\Delta\alpha_z/\partial x$ (deg/L)	0.30803	0.30315	0.30680

Figure 18.- Three-dimensional wall interference corrections, theoretical example. (From ref. 11.)

### NAE THREE-DIMENSIONAL WALL INTERFERENCE DATA

No good experimental data base exists for the three-dimensional case because of inadequate data discrimination. Because of the much lower pressure signature at the wall boundary, it is extremely difficult to obtain well-defined wall pressure data. A typical example, taken from an early test (ref. 9) is given in figure 19. Improvements have been made to the flow quality in the 5-ft wind tunnel since those data were obtained, and some initial samples of data were given in reference 11. Figure 20 is a typical example from this latter study, and, as can be seen, the field pressure signals are small and so too are the corrections  $\Delta M$  and  $\Delta \alpha$ . In this case, the model was located too far downstream in the test section to obtain a reasonably complete wall pressure signature.

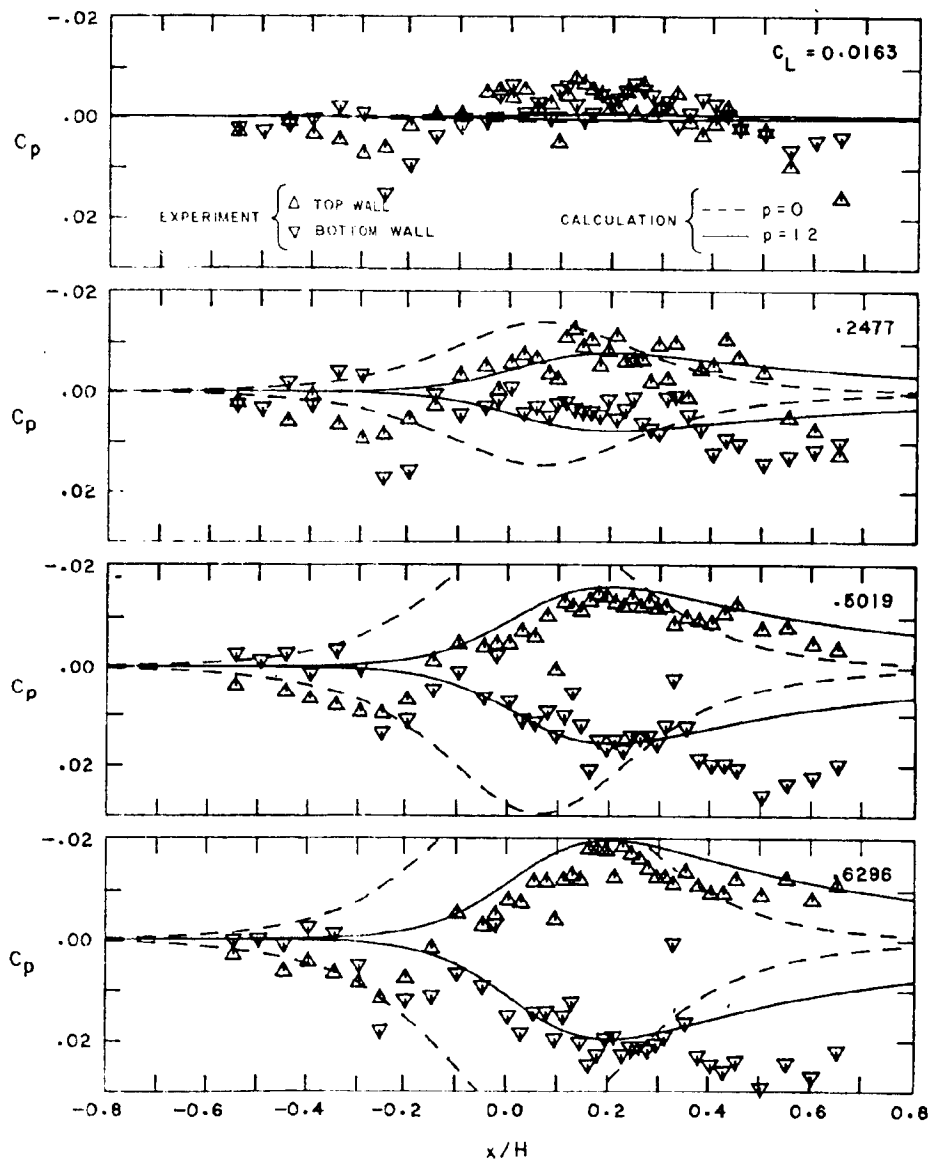


Figure 19.- Samples of early three-dimensional wall pressure data (ref. 9).

ORIGINAL REPORT  
OF POOR QUALITY

RUN 23310/2

M - 0.7538  
 $\alpha$  - 4.441°  
CY - 0.0022  
CZ - 0.5029

$\Delta M$  - -0.0051  
 $\Delta \alpha$  - -0.100°

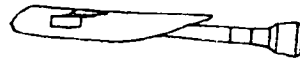
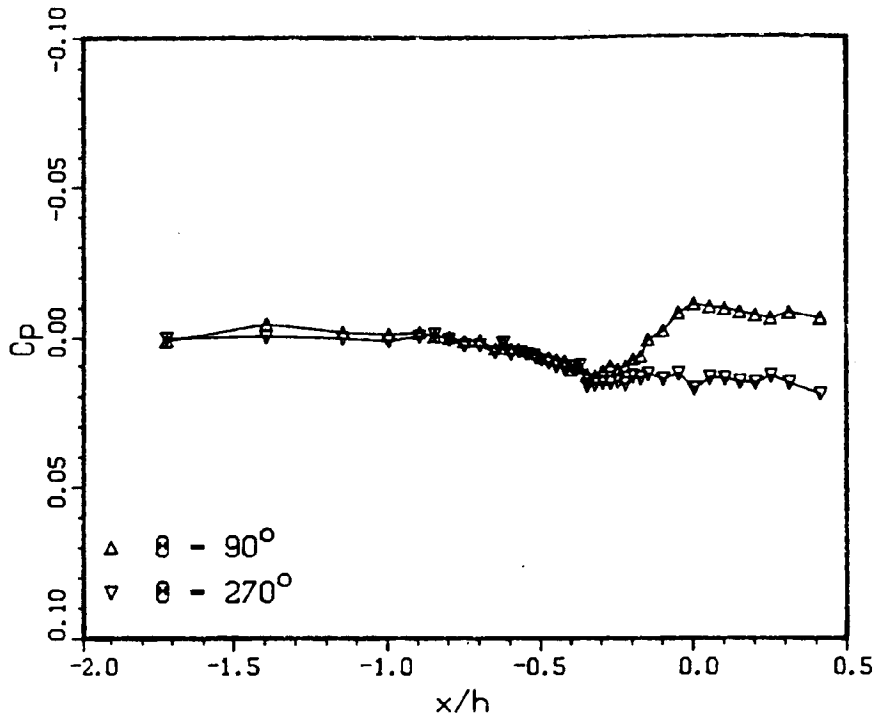
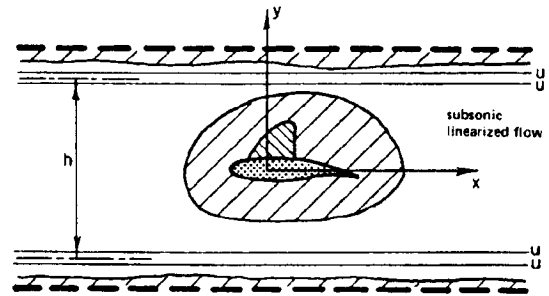
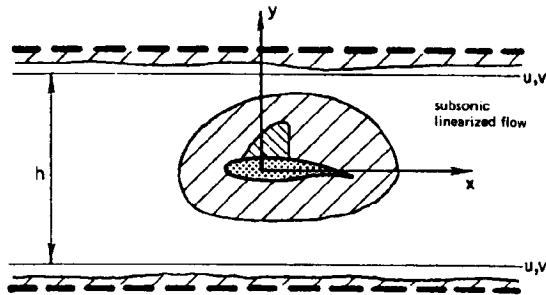


Figure 20.- Sample of more recent three-dimensional wall pressure data.

PROPOSED SCHEME FOR TWO-DIMENSIONAL WALL CORRECTIONS  
BASED UPON TWO MEASURED DATA ARRAYS

Mach number and angle-of-attack correction schemes for two-dimensional wind tunnel flows based upon two measured quantity arrays are shown in figure 21. Figure 21(a) depicts a scheme for u and v arrays measured along a single boundary and figure 21(b) depicts a scheme for u arrays measured along double boundaries. Measurements are not required at the model and the flow around it as well as at the wall need not be potential. However, it is assumed that in the region where measurements are made the flow can be described by subsonic linearized equations.



$$\Delta M_\infty = \left(1 + \frac{\kappa - 1}{2} M_\infty^2\right) M_\infty \left\{ \frac{\beta \frac{h}{2}}{2\pi} \int_{-\infty}^{\infty} \frac{u\left(x, \frac{h}{2}\right) + u\left(x, -\frac{h}{2}\right)}{x^2 + \left(\frac{\beta \frac{h}{2}}{2}\right)^2} dx \right.$$

$$\left. + \frac{1}{2\pi\beta} \int_{-\infty}^{\infty} \left[ v\left(x, \frac{h}{2}\right) - v\left(x, -\frac{h}{2}\right) \right] \frac{x}{x^2 + \left(\frac{\beta \frac{h}{2}}{2}\right)^2} dx \right\}$$

$$\Delta \alpha = \frac{\beta \frac{h}{2}}{2\pi} \int_{-\infty}^{\infty} \frac{v\left(x, \frac{h}{2}\right) + v\left(x, -\frac{h}{2}\right)}{x^2 + \left(\frac{\beta \frac{h}{2}}{2}\right)^2} dx$$

$$- \frac{\beta}{2\pi} \int_{-\infty}^{\infty} \left[ u\left(x, \frac{h}{2}\right) - u\left(x, -\frac{h}{2}\right) \right] \frac{x}{x^2 + \left(\frac{\beta \frac{h}{2}}{2}\right)^2} dx$$

(a) u and v measured along single boundary.

CORRECTIONS OBTAINED FROM THE PRECEDING FORMULAE USING

(1)  $\frac{\partial v(x,y)}{\partial x} = \frac{\partial u(x,y)}{\partial y}$

AND INTEGRATING BY PARTS OR

(2) DIRECTLY SUBSTITUTING

$$v(x,y) = \int_{-\infty}^x \frac{\partial u(\xi,y)}{\partial y} d\xi$$

(b) u measured along double boundary.

Figure 21.- Mach number and angle of attack corrections based on two measured data arrays.

ORIGINAL REPORT  
OF POOR QUALITY

### SIDEWALL BOUNDARY LAYER AND SUCTION EFFECTS

In an airfoil test facility, the sidewall boundary layer thickness varies in a three-dimensional fashion due to the "two-dimensional" airfoil pressure field superimposed upon it. This effect is particularly severe for high-speed transonic flows since the strength and location of the shock on the model are sensitive to the perturbed boundary layer shape. To lessen the sidewall boundary layer effect, a common practice is to control the growth of the boundary layer by applying suction at an area of the wall where the model is mounted. This method is employed in the NAE two-dimensional test facility (refs. 1 and 12). The effectiveness of the control is demonstrated by comparing measured airfoil pressure distributions and the boundary layer developments without and with surface suction.

Figure 22 is sample data showing the effect of sidewall suction level (CDW) on the airfoil surface pressure distribution for a supercritical airfoil. The shock wave has been shifted appreciably.

Calculations of the sidewall boundary layer development for a typical transonic airfoil test case were reported recently in reference 13. Figure 23 and 24, taken from reference 13, show the three-dimensional nature and relative size of the sidewall boundary layer displacement effects, respectively.

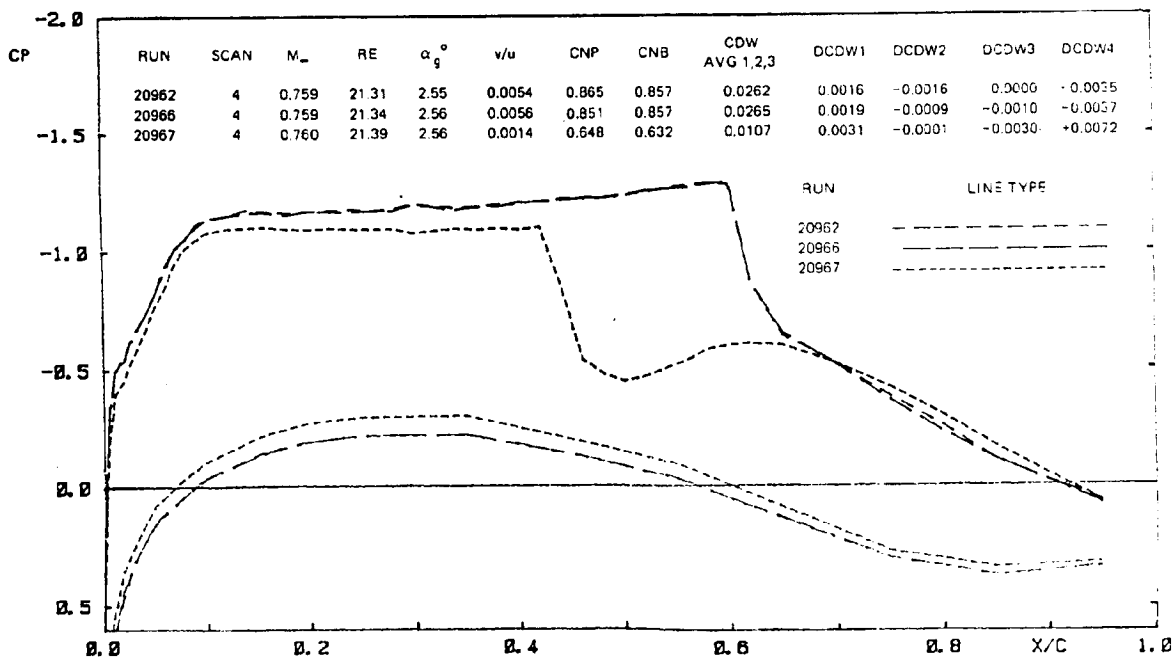
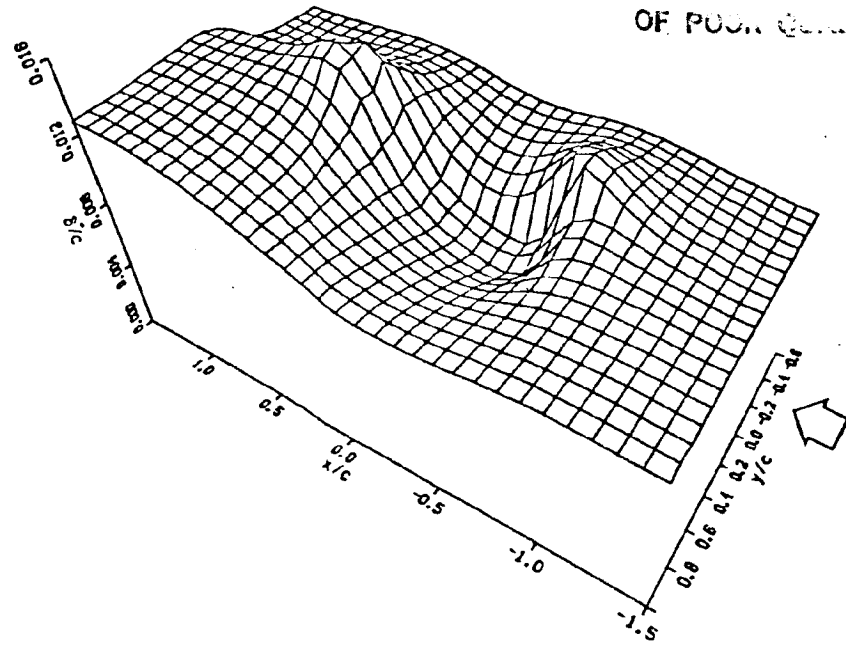
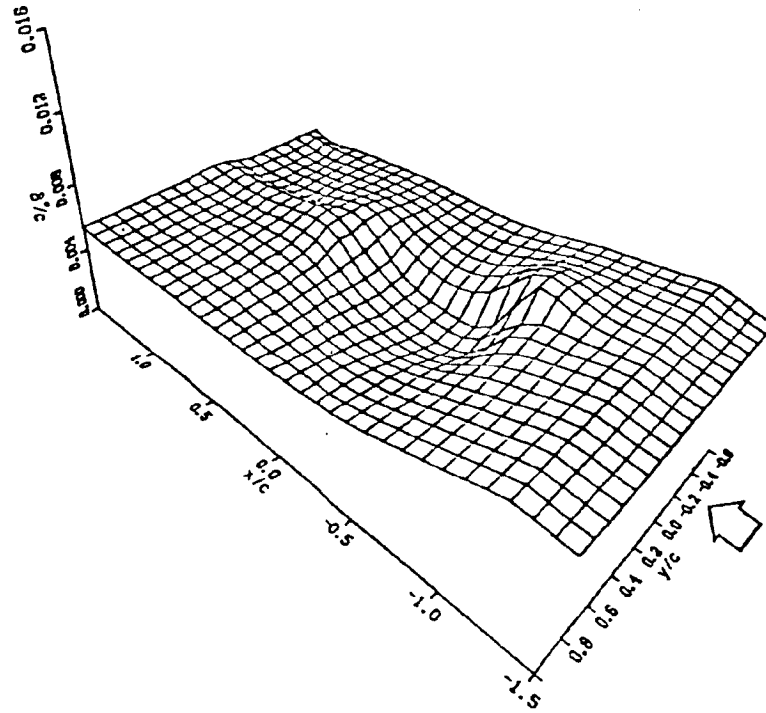


Figure 22.- Effect of sidewall suction on airfoil pressure distribution.  
M = 0.76, Re = 21 × 10<sup>6</sup>.

ORDER OF PUCK QUANTITY



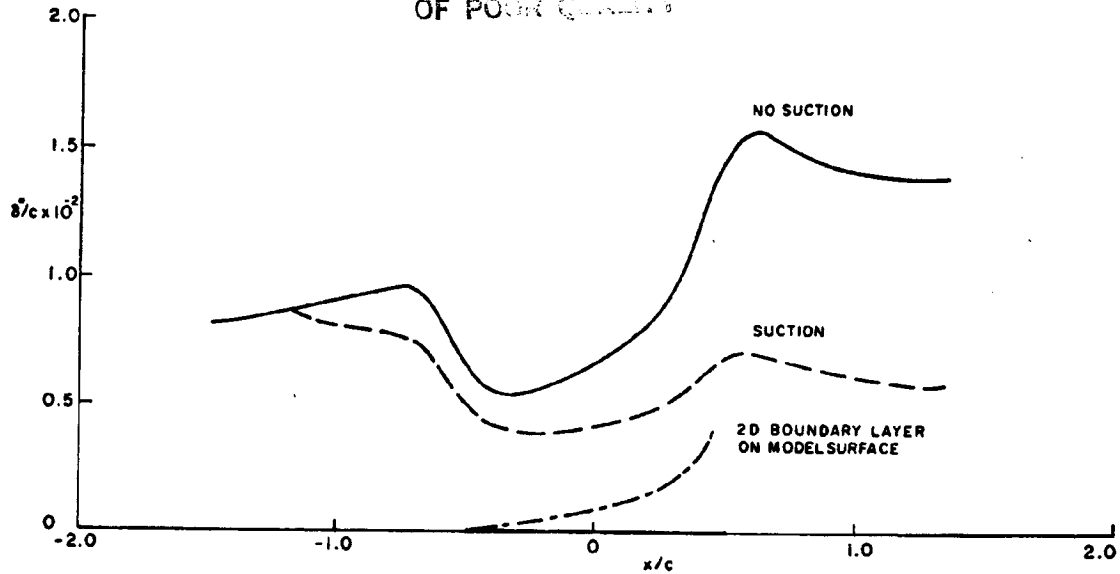
(a) No suction.



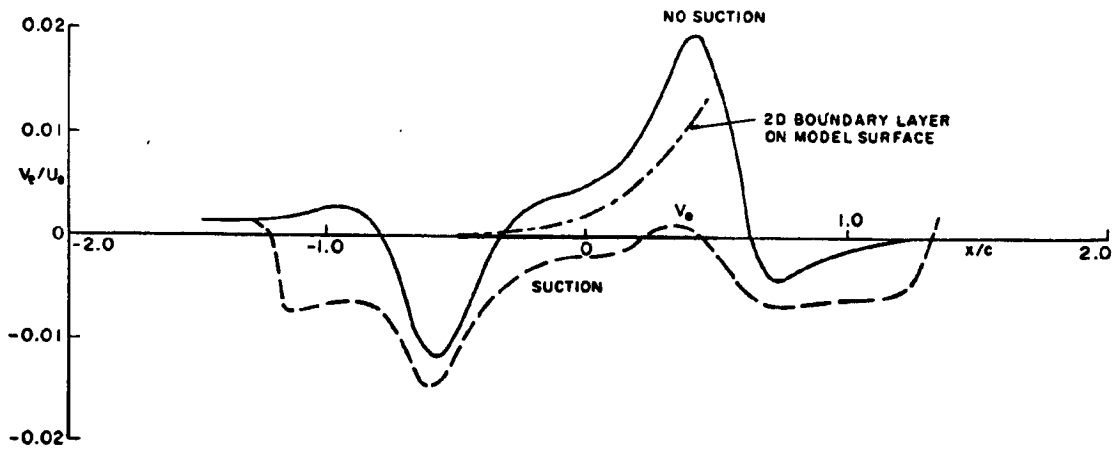
(b) With suction.

Figure 23.- Effect of suction on sidewall boundary layer development. (From ref. 13.)

ORIGINAL SOURCE  
OF POOR QUALITY



(a) Displacement thickness.



(b) Effective normal velocities.

Figure 24.- Effect of suction on sidewall boundary layer development and comparison with data from two-dimensional boundary layer on model surface. (From ref. 13.)

## REFERENCES

1. Ohman, L. H.; and Brown, D.: The NAE High Reynolds Number 15" x 60" Two-dimensional Test Facility: Operating Experiences and Some Representative Results. AIAA Paper No. 71-293, March 1971.
2. Mokry, M.; Peake, D. J.; and Bowker, A. J.: Wall Interference on Two-Dimensional Supercritical Airfoils Using Wall Pressure Measurements to Determine the Porosity Factors for Tunnel Floor and Ceiling. NRC Aeronautical Report LR-575, February 1974.
3. Jones, D. J.: A Method for Computing 2-D Wind Tunnel Wall Interference Effects Allowing for Variable Porosity Along Floor and Ceiling. NAE LTR-HA-37, February 1979.
4. Chan, Y. Y.: Analysis of Boundary Layers on Perforated Walls of Transonic Wind Tunnels. AIAA Paper No. 81-4186, June 1981.
5. Mokry, M.; and Ohman, L. H.: Application of the Fast Fourier Transform to Two-Dimensional Windtunnel Wall Interference. AIAA Paper No. 80-4059, June 1980.
6. Chan, Y. Y.: Lift Effect on Transonic Windtunnel Blockage. AIAA J. Aircraft, Eng. Note, vol. 17, no. 12, December 1980.
7. Chan, Y. Y.: A Singular Perturbation Analysis of Two-Dimensional Windtunnel Interferences. ZAMP, vol. 31, no. 5, 1980.
8. Ohman, L. H.: Investigation of the Effect of Edgetone Noise on 2-D Test Data for the BGK No. 1 Airfoil. NAE/NRC LTR-HA-64, June 1982.
9. Mokry, M.; and Galway, R. D.: Analysis of Wall Interference Effects on ONERA Calibration Models in the NAE 5 ft x 5 ft Windtunnel. NRC Aeronautical Report LR-594, March 1977.
10. Mokry, M.: Evaluation of Three-Dimensional Wall Interference Corrections From Boundary Pressure Measurements. NAE LTR-HA-51, November 1980.
11. Mokry, M.: Subsonic Wall Interference Corrections for Finite Length Test Sections Using Boundary Pressure Measurements. AGARD CP-335, September 1982, pp. 10-1 - 10-15.
12. Chan, Y. Y.: Boundary Layer Controls on the Sidewalls on Wind Tunnels for Two-Dimensional Tests. J. Aircraft, vol. 17, no. 5, May 1980, pp. 380-382.
13. Chan, Y. Y.: Wall Boundary Layer Effects in Transonic Wind Tunnels. AGARD CP-335, September 1982, pp. 7-1 - 7-15.

N85 12026

D15

DEVELOPMENT IN UK OF A METHOD FOR  
CALCULATING TUNNEL WALL CORRECTIONS FROM  
FLOW MEASUREMENTS

P.R. Ashill  
Royal Aircraft Establishment  
Bedford, England

PRECEDING PAGE BLANK NOT REPRODUCED

Preceding page blank

#### CURRENT UK WORK

It is generally agreed that the classical methods of calculating wall corrections are not satisfactory for a number of flows of interest. To meet these objections, a number of methods have been developed which use measurements of the flow at or close to the tunnel walls as an outer boundary condition to define wall interference. Work currently in progress in the UK on the development, assessment and application of one such method is summarized in fig. 1.

- DEVELOPMENT OF WALL - CORRECTION METHOD AT RAE
- ASSESSMENT OF RAE METHOD FOR TRANSONIC FLOWS (ARA)
- APPLICATION OF RAE METHOD TO POROUS - WALL TUNNELS (CITY UNIVERSITY, LONDON)

Figure 1

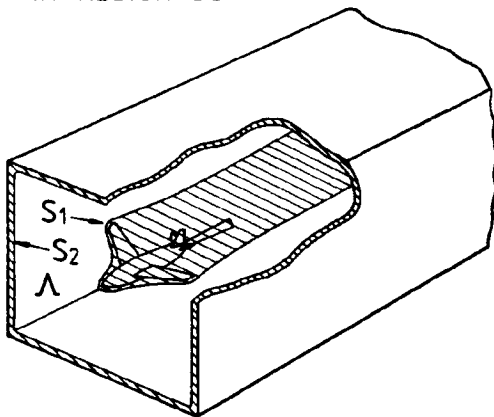
RAE WALL-CORRECTION METHOD : BASIC ASSUMPTION

The method relies on one main assumption, namely that there is a region  $\Lambda$  (fig. 2) between the model and the tunnel where the flow satisfies the small-perturbation equation (1). As shown in fig. 2, this region is bounded by the surface  $S_1$  surrounding the model and its associated regions of transonic flow and shear and a cylindrical surface  $S_2$  adjacent to the tunnel walls. By using the transformation (2) (fig. 2) the small-perturbation equation may be transformed to Laplace's equation (3) (ref. 1).

FLOW SATISFIES SMALL  
PERTURBATION EQUATION

$$\beta^2 \phi_{xx} + \phi_{yy} + \phi_{zz} = 0 \quad (1)$$

IN REGION  $\Lambda$



BY USING TRANSFORMATION

$$(X, Y, Z) = (x, \beta y, \beta z) \quad (2)$$

SMALL PERTURBATION EQUATION  
TRANSFORMED TO LAPLACE'S  
EQUATION

$$\phi_{xx} + \phi_{yy} + \phi_{zz} = 0 \quad (3)$$

Figure 2

### APPLICATION OF GREEN'S THEOREM

The formal solution to Laplace's equation in the transformed space is obtained by using Green's theorem (ref. 2). The solution is written in terms of integrals over the surfaces  $S_1$  and  $S_2$  (equation 1, fig. 3), the integral over the latter surface being the wall interference velocity potential (equation 2). The further assumption is made that the wall interference velocity may be continued analytically within the shaded region close to the model. This is a reasonable basis on which to proceed for flows in which the wall interference velocity varies slowly in the region of the model; e.g., 'correctable' flows.

$$\phi(X,Y,Z) = \Delta\phi - \frac{1}{4\pi} \iint_{S_1} \left\{ \frac{\partial\phi}{\partial N} \frac{1}{R} - \phi \frac{\partial}{\partial N} \left( \frac{1}{R} \right) \right\} dS^1 \quad (1)$$

WHERE

$$\Delta\phi = - \frac{1}{4\pi} \iint_{S_2} \left\{ \frac{\partial\phi}{\partial N} \frac{1}{R} - \phi \frac{\partial}{\partial N} \left( \frac{1}{R} \right) \right\} dS^1 \quad (2)$$

IS WALL INTERFERENCE POTENTIAL

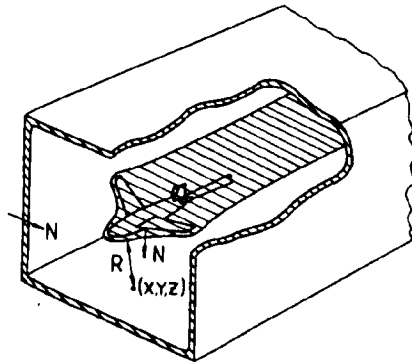


Figure 3

INTERPRETATION OF WALL INTERFERENCE VELOCITY POTENTIAL

Fig. 4 shows an interpretation of the expression for the wall interference velocity potential. The first term under the integral sign is the contribution of a distribution over  $S_2$  of sources, the local strength of which is equal to the normal velocity increment at the surface  $S_2$ . For tunnels with solid, though possibly adaptive, walls (ref. 3) this velocity component is essentially defined by the condition of no flow through the tunnel walls. Unfortunately, the situation is less straightforward for tunnels with porous or slotted walls which need special techniques to determine the normal-velocity increment, as will be shown later. The second term is associated with doublets with axes normal to the surface  $S_2$ ; this distribution is mathematically equivalent to a distribution of elementary horseshoe vortices of strength equal to the local increment in streamwise velocity. This velocity increment may be deduced from measurements of static pressure at or close to the walls by using the linearised version of Bernoulli's equation.

	$\Delta\phi = -\frac{1}{4\pi} \iint_{S_2} \frac{\partial\phi}{\partial N} \frac{1}{R} dS' + \frac{1}{4\pi} \iint_{S_2} \phi \frac{\partial}{\partial N} \left(\frac{1}{R}\right) dS'$	
TYPE OF SINGULARITY	POINT SOURCES, STRENGTH $\partial\phi/\partial N$	DOUBLET, STRENGTH $\phi$ OR HORSESHOE VORTICES, STRENGTH $\partial\phi/\partial x$
REPRESENTS CHANGE IN — AT $S_2$ RELATIVE TO CALIBRATED EMPTY TUNNEL	<p>FLOW PITCH ANGLE</p> 	<p>STREAMWISE VELOCITY</p> $\partial\phi/\partial x = u = -U_\infty C_p/2$ 

Figure 4

WALL INTERFERENCE I. AIRFOIL TESTS IN RAE 8 FT X 8 FT TUNNEL

A series of airfoil sections has been tested in the 8 ft x 8 ft Tunnel at RAE Bedford with the aim of providing a better understanding of the boundary layers of 'advanced' airfoil sections. The 8 ft x 8 ft Tunnel is equipped with solid walls that, for subsonic tests, are maintained in an essentially straight configuration, and static pressures are measured on the walls over the interval shown in fig. 5. Also shown in this figure is one of the sections studied, RAE 5225; the size of the model is decided primarily by the need to make boundary-layer measurements over a range of Reynolds numbers (up to  $20 \times 10^6$ ). As a consequence, the model is relatively large for tests at high subsonic speeds in a solid-wall tunnel, and some of the flows examined are not strictly correctable (ref. 4). Calculations by the present method indicate that, while the chordwise variation of blockage may be ignored, the variation along the model chord line of wall-induced upwash cannot be neglected for a number of cases of interest.

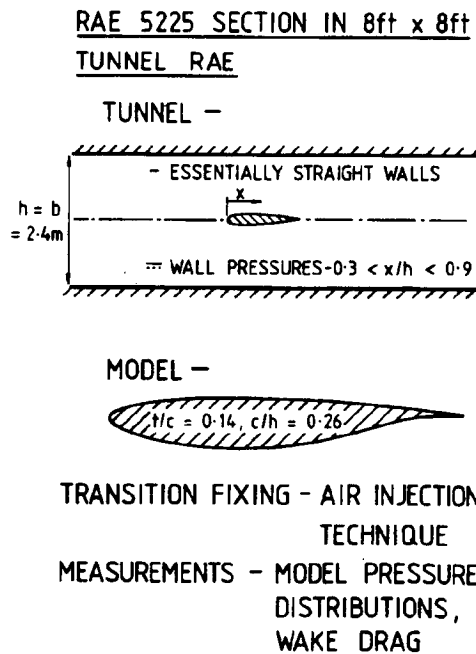


Figure 5

GENERAL PRINCIPLES  
OF POOR QUALITY

CALCULATION OF BLOCKAGE INCREMENT IN 8 FT X 8 FT AIRFOIL TESTS

Since the chordwise variation of blockage increment in Mach number is small, it is reasonable to define a mean value along the chord  $\overline{\Delta M}$ . Calculations of this increment are shown in fig. 6 plotted against normal-force coefficient for an effective free-stream Mach number,  $M_e$ , of 0.73. Results are shown for various methods including those of the present method, Smith's method (ref. 5), Göthert's technique (ref. 6) and classical linear theory (ref. 7). Agreement between the first three methods, which all use wall-pressure measurements; is reasonable, the variation with normal-force coefficient of the present method being closely matched by that of Göthert's method. The linear theory, on the other hand, gives values that are consistently lower than those of the other methods. Göthert's method and the present approach are found to give blockage increments that are in good agreement over the range of Mach numbers and angles of incidence tested.

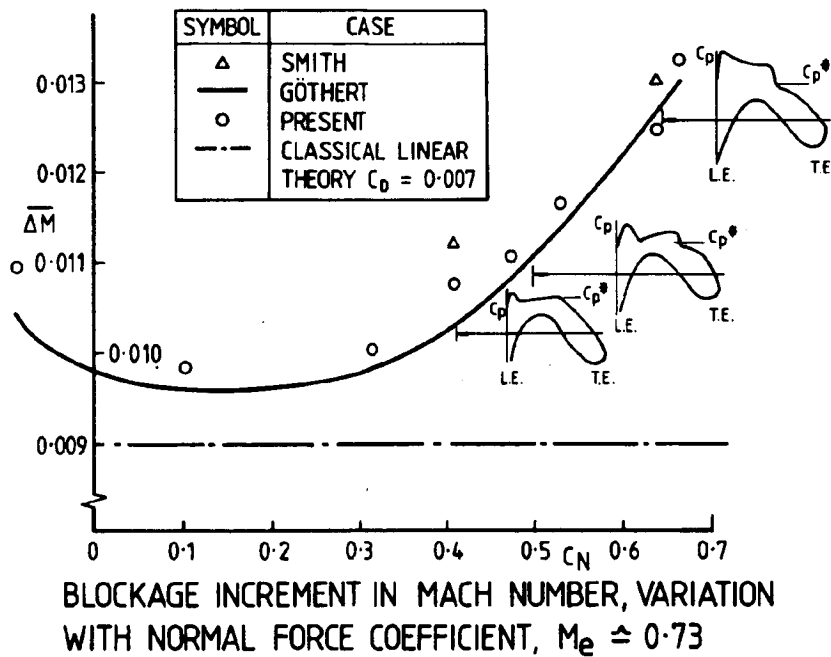
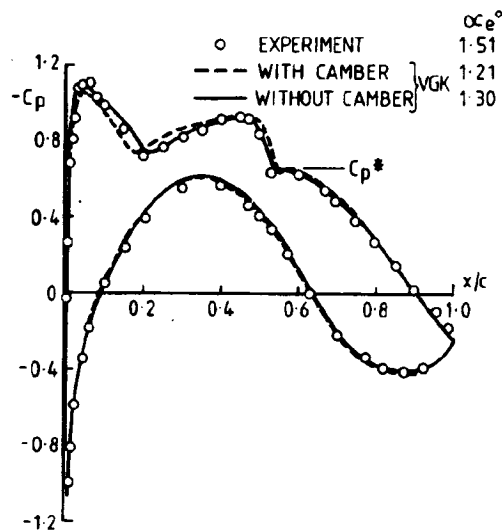


Figure 6

ASSESSMENT OF PRESENT METHOD : 1. COMPARISON BETWEEN  
 VISCOUS FREE-AIR THEORY AND MEASUREMENT

Although the flows studied are not strictly 'correctable', comparisons have been made between measurement and calculation of equivalent free-air flows with the object of assessing the accuracy of the wall corrections by the present method. The calculations have been made with a viscous version of the Garabedian and Korn program (ref. 8), and airfoil pressure distributions are shown in fig. 7 for one of the cases examined ( $M_e = 0.736$ ,  $C_L = 0.54$ ,  $R = 20 \times 10^6$ ). The chordal Reynolds number  $20 \times 10^6$  was deliberately chosen to minimise differences between theory and measurement arising from the failure of the former to represent viscous effects accurately. Two types of calculation are shown, one with a camber correction to allow for the chordwise variation in upwash (the dashed line), and the other without (the full line). Broadly, the agreement with either type of calculation and measurement is reasonable but the effect of camber is to worsen the agreement with measurement in the region of the shock. However, the lack of agreement in this region may be due to extraneous viscous effects (e.g., due to sidewall boundary layers (ref. 9)), although the effect of these layers would be expected to be small because of the relatively large aspect ratio of the model.



PRESSURE DISTRIBUTIONS —  
 COMPARISON BETWEEN VGK &  
 MEASUREMENT,  $M_e = 0.735$ ,  
 $C_L = 0.536$ ,  $R_c = 20 \times 10^6$

Figure 7

ASSESSMENT OF PRESENT METHOD:  
 2. USE OF TRANSONIC FLOWFIELD METHOD

CARR  
 OF PRESENT METHOD

In order to avoid the extraneous viscous effects referred to previously, Carr and Morrison of Aircraft Research Association (Bedford) have performed some numerical experiments, under contract to RAE, using a potential-flow method for calculating inviscid transonic flows around airfoils. Fig. 8 shows the Mach number distributions calculated for two airfoils, each in wind tunnels with porous walls designed to minimise the wall camber effect. The calculations are also used to provide the flow data needed by the present method to calculate the wall corrections. In turn, the corrections are used to define free-stream conditions for an equivalent free-air flow which is calculated by the same potential-flow method that is used to calculate the wind-tunnel flow. The airfoil Mach-number distributions for the equivalent free-air flows are shown in fig. 8 to be in reasonably good agreement with those of the corresponding tunnel flows, indicating that, for these cases, the correction method is of acceptable accuracy.

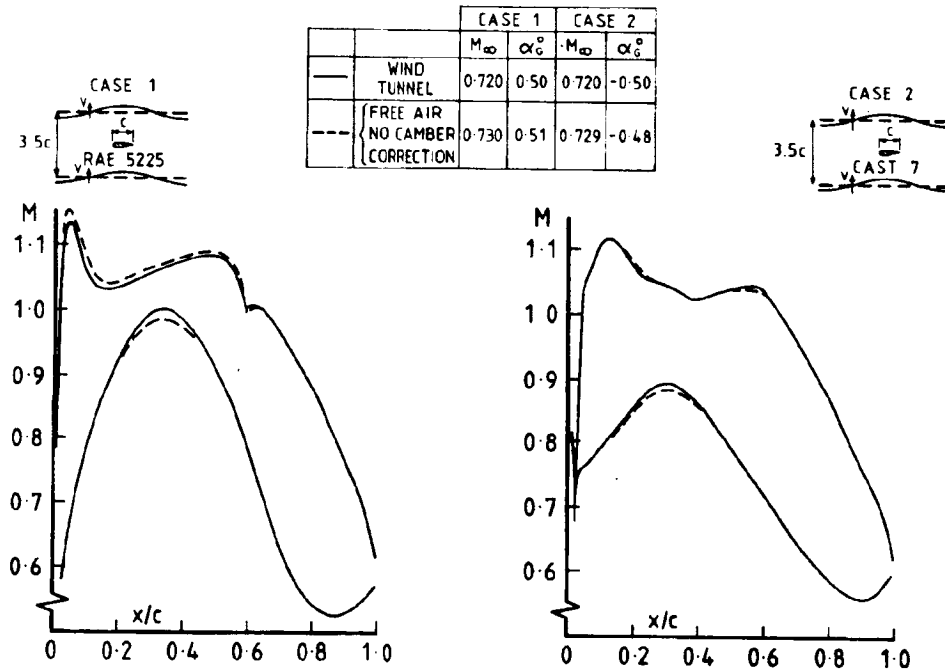


Figure 8

ASSESSMENT OF PRESENT METHOD : 3 . APPLICATION TO THREE-  
DIMENSIONAL, WALL INTERFERENCE

The present method will be used to correct three-dimensional flows only if it does not need an unacceptably large number of measurements to achieve the desired accuracy. In order to provide a check, some calculations have been made for a solid-wall tunnel with a working section that is cylindrical and is of square cross section (fig. 9). The classical image method has been used to provide static pressures at a number of streamwise rows of holes spaced at equal intervals around the working section. Each row consists of 11 wall holes distributed in the way shown in fig. 9. A number of different flows have been examined (ref. 4), all with a vertical plane of symmetry so that the wall-pressure data only needs to be specified in one half of the working section, and, in each case, results for wall-induced velocities at the axis of symmetry are compared with those of the image method. Results for the wall-induced upwash for one of the cases studied (a horseshoe vortex on the horizontal plane of symmetry) are shown in fig. 9. With 5 streamwise rows or 55 wall holes, the present method gives values within 5% of those of the image method. An increase in the number of wall holes to 99 reduces the discrepancy to within 1%.

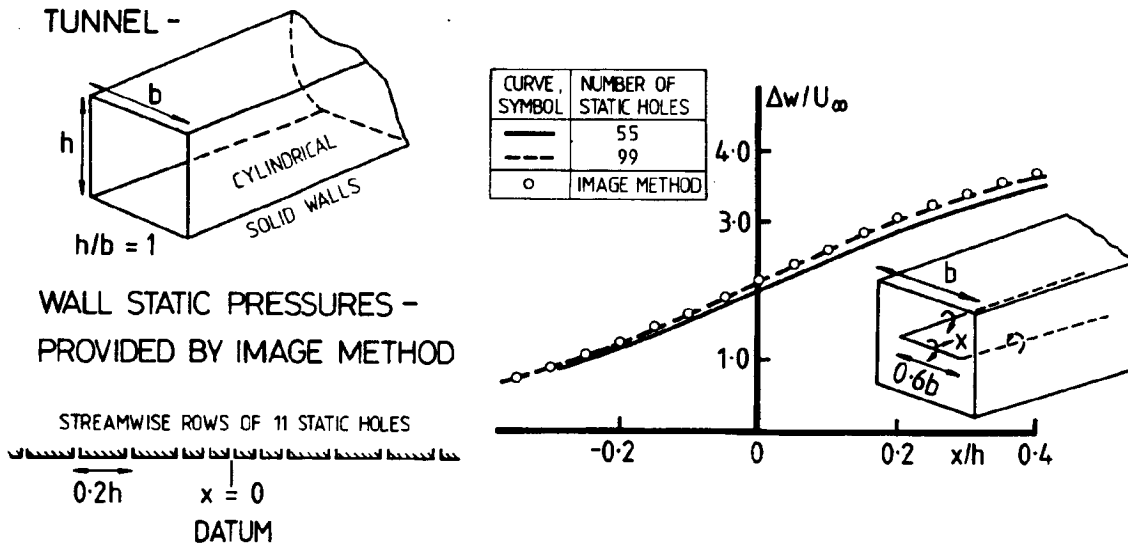


Figure 9

BOUNDARY CONDITIONS FOR PERFORATED-WALL WIND TUNNELS:  
1. CORRELATION OF WALL TRANSPIRATION

As already noted, the normal velocity increment at the boundary surface  $S_2$  (fig. 2) is not readily determined for tunnels with either perforated or slotted walls. In the former case, Freestone and Henington (refs. 10 and 11) have proposed a model of the flow close to the walls consisting of two interacting components, namely the wall boundary layer and the mass transfer through the perforations. Under contract to USAF, they have attempted to establish experimentally a correlation of the mass transfer in the form given in equation (1) of fig. 10. The experiments have consisted of measurements of the streamwise distribution of wall boundary-layer, displacement thickness and flow angle at the outer edge of the wall boundary layer,  $\theta_e$ , for various working-section flows. On the assumption that the flow near the wall is a transpiring, two-dimensional, boundary layer, they have then calculated the wall transpiration using the mass balance equation (2). Recently, in work under contract to RAE, Freestone and Henington have considered an alternative method of determining wall transpiration by measuring mass flow through a perforation directly with a mass-flow cell. This promises to be more accurate than the original method, and offers the possibility of extending the method to three-dimensional flows.

$$f \left( \frac{\Delta p}{q_e}, \theta_w, M_e, \delta^* \right) = 0 \quad (1)$$

$\Delta p$  = PRESSURE DIFFERENCE ACROSS LINER

$q_e$  = DYNAMIC PRESSURE AT EDGE OF BOUNDARY LAYER

$\theta_w = \rho_w V_w / \rho_e U_e$ , WALL TRANSPIRATION PARAMETER

$M_e$  = MACH NUMBER AT EDGE OF BOUNDARY LAYER

$\delta^*$  = BOUNDARY LAYER DISPLACEMENT THICKNESS

$$\theta_w = \theta_e + \frac{1}{\rho_e U_e} \frac{d}{dx} \left\{ \rho_e U_e (\delta - \delta^*) \right\} \quad (2)$$

Figure 10

BOUNDARY CONDITIONS FOR PERFORATED-WALL  
WIND TUNNELS: 2. APPLICATION OF METHOD

The procedure used to calculate the normal-velocity increment is outlined in fig. 11. Stage 2 has been programmed and Stage 3 follows once Stage 2 is complete. It is planned to assess the procedure in tests on a series of airfoils in the transonic wind tunnel at City University, London in the near future under contract to RAE.

The prospects for an analogous procedure for slotted-wall tunnels seem remote, at present, and the only feasible scheme for determining normal-velocity increment in this case would seem to be by direct measurement of flow angle. It is interesting to note, in this respect, the development by Calspan (ref. 12) of a two-velocity-component static pipe. In the view of the author, further work in this area is justified by the considerable gain in simplicity in the wall-correction method that follows from not needing a representation of the flow in the region of the model.

- (1) MEASURE STATIC PRESSURE DISTRIBUTION  
AT OR CLOSE TO TUNNEL WALLS
- (2) CALCULATE BOUNDARY - LAYER DEVELOPMENT  
ITERATIVELY WITH WALL TRANSPIRATION EQUATION
- (3) DETERMINE NORMAL VELOCITY INCREMENT AT  
BOUNDARY OF INVISCID FLOW

$$\frac{\partial \phi}{\partial n} = U_e \theta_w + \frac{1}{\rho_e} \frac{d}{dx} (\rho_e U_e \delta^*)$$

Figure 11

#### REFERENCES

1. Goldstein, S.; Young, A. D.: The linear perturbation theory of compressible flow with applications to wind tunnel interference. Aeronautics Research Committee Reports and Memoranda 1909, 1943.
2. Robinson, A.; Laurmann, J. A.: Wing Theory. Cambridge University Press (p. 22-23), 1956.
3. Chevallier, J.-P.: Soufflerie transsonique a parois auto-adaptables. Paper 12, AGARD CP 174, 1976, pp. 12-1 - 12-8.
4. Ashill, P. R.; Weeks, D. J.: A method for determining wall interference corrections in solid wall tunnels from measurements of static pressures at the walls. RAE TR 82091, 1982.
5. Smith, J.: A method for determining 2D wall interference on an aerofoil from measured pressure distributions near the walls and on the model. NLR TR 81016U, 1981.
6. Göthert, B.: Windkanalkorrekturen bei hohen unterschallgeschwindigkeiten unter besonderer berücksichtigung des geschlossenen kreiskanals. Deutsche Luftfahrtforschung Forschungsbericht 1216, 1940 (translated as NACA Tech Memo 1300), Feb. 1952.
7. Garner, H. C.; Rogers, E. W. E.; Acum, W. E. A.; Maskell, E. C.: Subsonic wind tunnel wall corrections. AGARDograph 109, 1966.
8. Locke, R. C.: A review of methods for predicting viscous effects on aerofoils and wings at transonic speeds. AGARD CP 291, Feb. 1981, pp. 2-1 - 2-32.
9. Barnwell, R. W.: Similarity rule for sidewall boundary layers in two-dimensional wind tunnels. AIAA Journal, Vol. 18, No. 1, 1980, pp. 1149-1151.
10. Freestone, M. M.; Henington, P.: A scheme for incorporating the viscous effects of perforated windtunnel walls in two-dimensional flow calculations. The City University Research Memo Aero 78/7, City University London, 1979.
11. Freestone, M. M.; Henington, P.: Incorporation of viscous effects of perforated windtunnel walls in two-dimensional flow calculations. The City University Research Memo Aero 81/1, City University London, 1981.
12. Parker, R. L., Jr.; Erickson, J. C., Jr.: Development of a three-dimensional adaptive wall test section with perforated walls. Paper 17, AGARD CP No. 335, 1982, pp. 17-1 - 17-14.

N85 12027 D16

TUNNEL CONSTRAINT FOR A JET IN CROSSFLOW

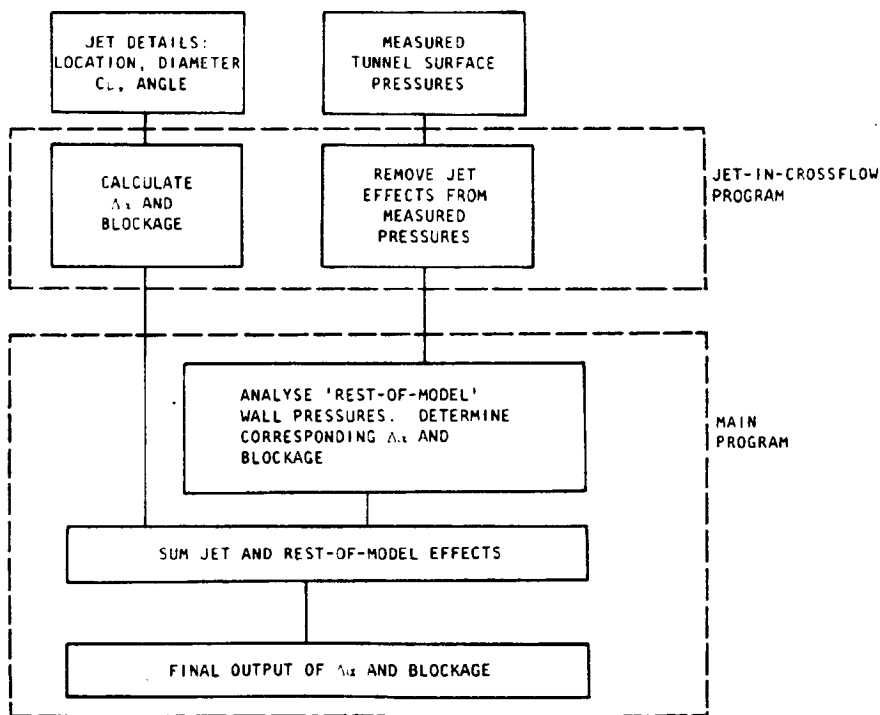
D. J. Wilsden and J. E. Hackett  
Lockheed-Georgia Company  
Marietta, Georgia

CONFIDENTIAL

Preceding page blank

RELATIONSHIP OF JET-IN-CROSSFLOW PROCEDURES TO  
REMAINDER OF TUNNEL CORRECTION SCHEME

This paper describes one facet of a unified tunnel correction scheme which uses wall pressures to determine tunnel-induced blockage and upwash. With this method, there is usually no need to use data concerning model forces or power settings to find the interference; it follows directly from the pressures and tunnel dimensions. However, highly inclined jets do not produce good pressure signatures and are highly three dimensional, so they must be treated differently (fig. 1). The remainder of this paper will be devoted to "filling in the boxes" concerning flow modeling. Jet impingement cases will be discussed later in this paper.



Relationship between jet-in-crossflow and the main, wall-pressure-analysis programs.

ORIGINAL PRESENTED  
OF POOR QUALITY

Figure 1

RIG FOR JET-IN-CROSSFLOW EXPERIMENTS

Though a wealth of jet-in-crossflow experimental data exists, no data could be found on wall pressure measurements or on the effects of tunnel constraint on jet trajectory, so new tests were conducted (fig. 2). Jets of two alternative sizes (3- and 1-in. in diameter) were used and were tested at various inclinations and velocity ratios. The large jet was used predominantly for getting wall pressure data and for impingement studies. The small jet was used to check the large jet trajectory for tunnel-induced distortion and to provide a check on the wall pressures predicted by the present method.

Instrumentation at the positions indicated in figure 2 was via a rake of 5-holed pneumatic probes. Boundary layer blowing was applied, as shown, to control flow breakdown when the jet impinged. Feedback for the boundary layer control was on the basis of measured tunnel surface pressures.

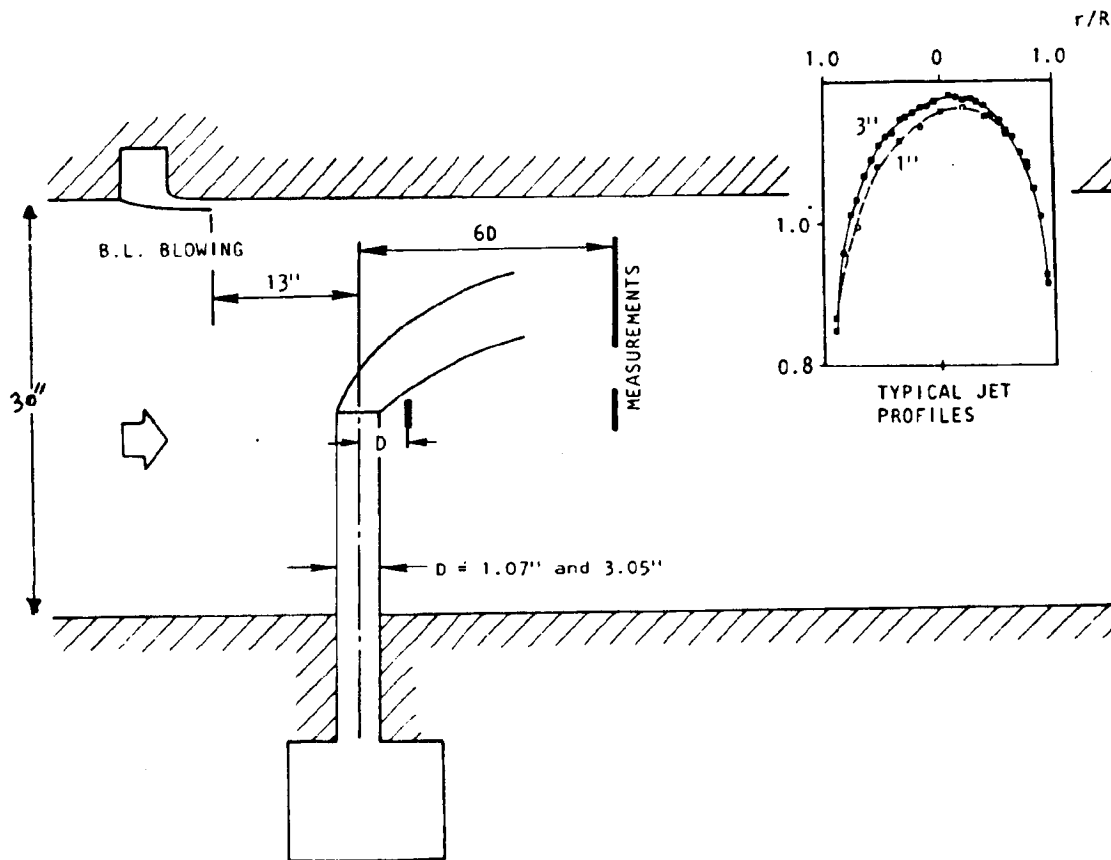


Figure 2

ORIGINAL QUALITY  
OF POOR QUALITY

IMPINGEMENT AND FREE-AIR STREAMLINES (R = 6)

Streamlines were calculated from measured crossflows at  $X/D = 6.0$  (fig. 2). These streamlines gave a very clear indication of vortex trajectory and of the effects of the tunnel upon it, particularly at impingement (fig. 3).

Additional plots were made of total pressure contours to define the maximum energy centerline.

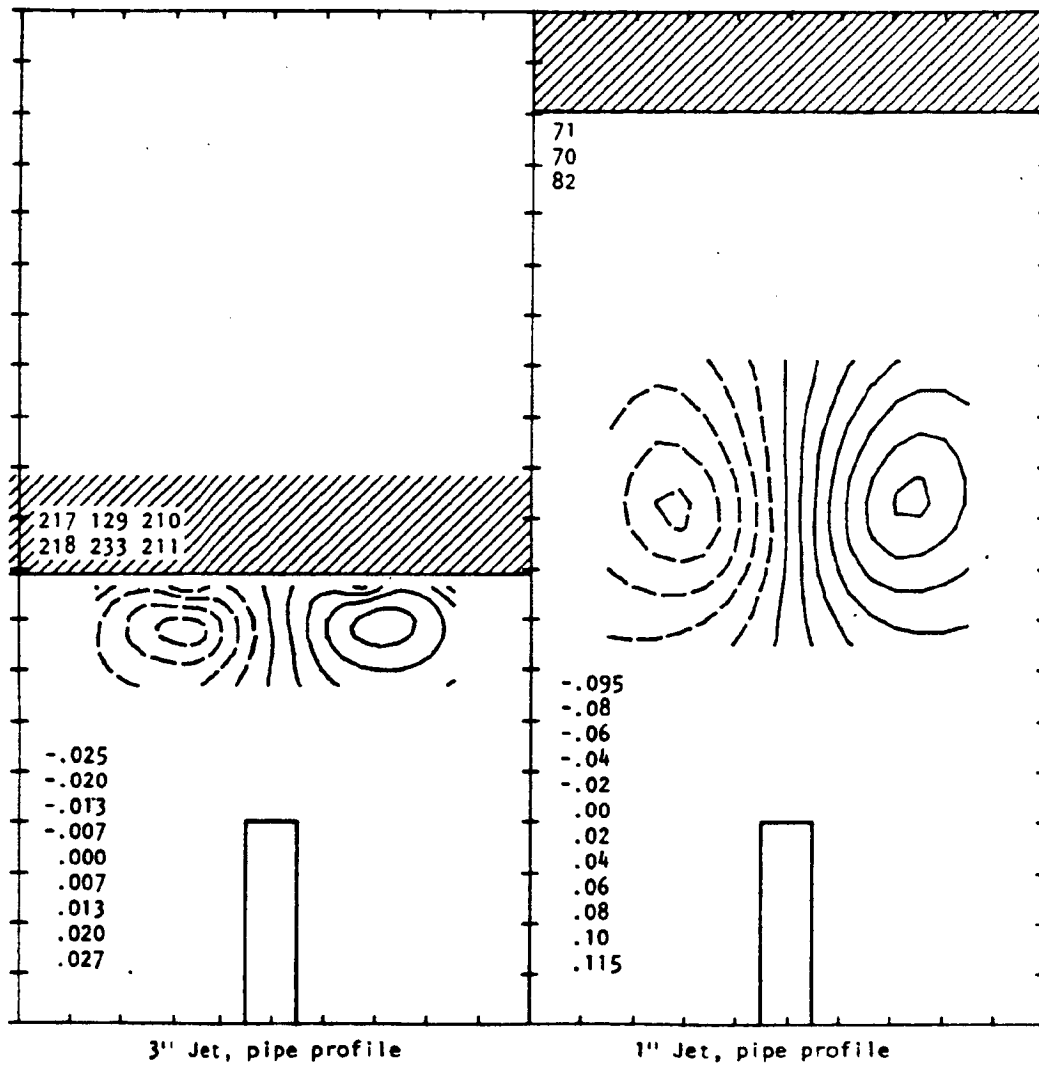


Figure 3

VORTEX PENETRATION AS A FUNCTION OF JET VELOCITY RATIO, R

Figure 4 shows a compilation of vortex center locations as a function of  $R (\equiv V_j/V_\infty)$  taken from plots of which figure 3 is an example. The 1-in. jet, which should be affected very little by the tunnel, penetrates slightly farther than the data reported by Weston (ref. 1); however, Weston's jets emerged from a flat surface. A pipe was chosen in the present experiments as being more representative of typical powered models.

Trajectories of 1- and 3-in. jets disagree only beyond  $R = 3$ , and the difference is not large at  $R = 4$ . Figure 4 shows that the large jet holds its trajectory in impinging cases until the plume is within a diameter of the tunnel roof. This gives a useful clue for modeling the impinged cases; the free-air shape can be "cut off" at the impingement point and can approximate the real situation reasonably well.

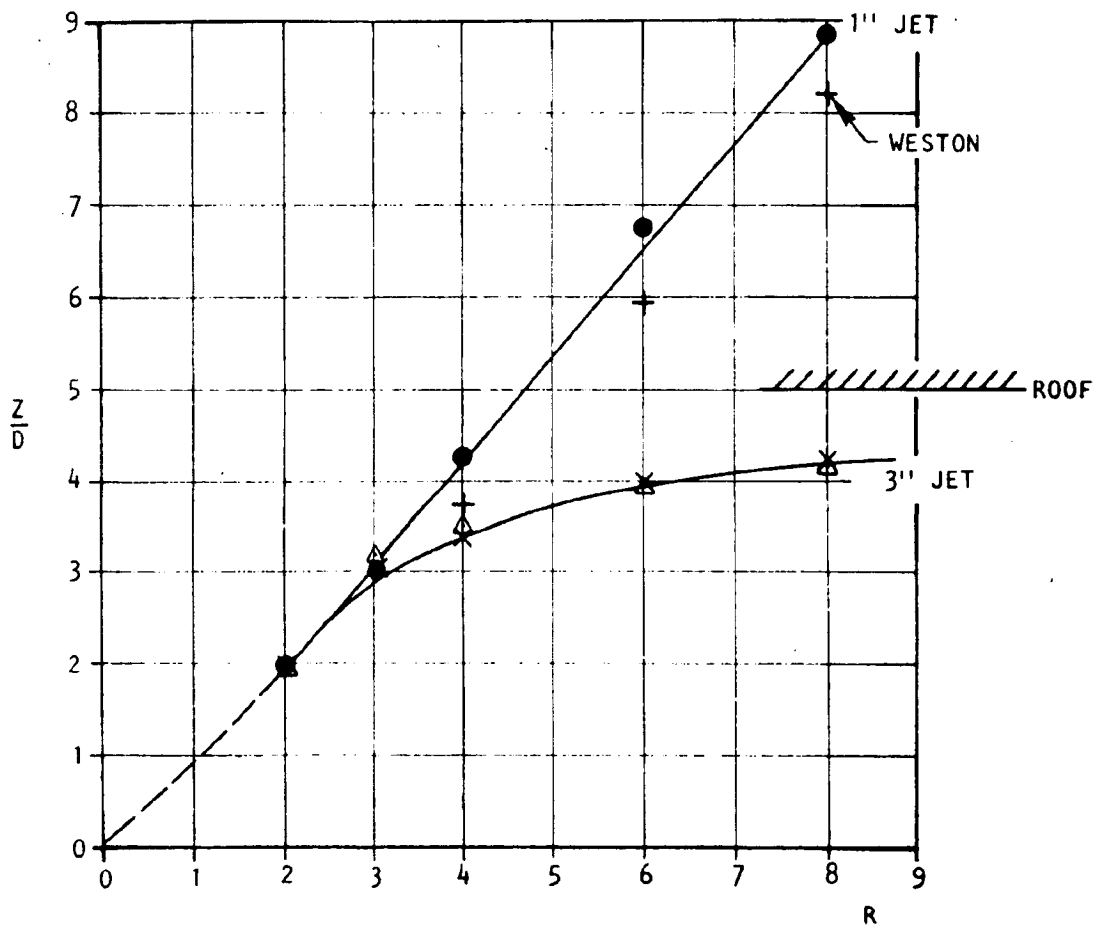


Figure 4

U-4

VORTEX AND JET CENTER PENETRATION AS A FUNCTION  
OF JET VELOCITY RATIO

Figure 5 shows jet center and vortex center penetration from the present tests (jet from pipe) and as quoted by Williams and Wood (ref. 2) (jet from surface). The greater penetration of the jet center is evident and was accommodated in the flow model that was developed.

Similar plots were prepared for lateral vortex spacing and plume width.

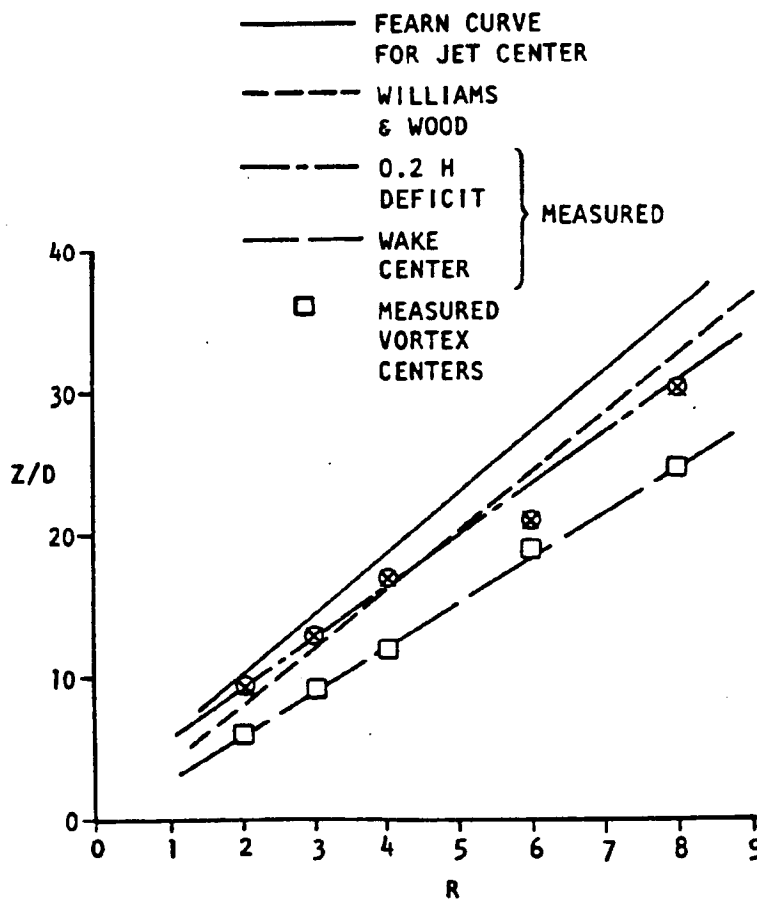


Figure 5

FEATURES OF THE VORTEX SOURCE DOUBLET (VSD) JET-IN-CROSSFLOW  
THEORETICAL MODEL

The theoretical model shown in figure 6 was developed using trajectory information developed previously. Trajectory equations developed by Fearn (ref. 1) were used, but the constants were revised. Originally, only vortices were included, but these did not produce enough pressure perturbation at the tunnel walls. Only when both source and doublet lines were added as indicated below was the flow model good enough to predict wall pressures properly. Further details are given in figure 7.

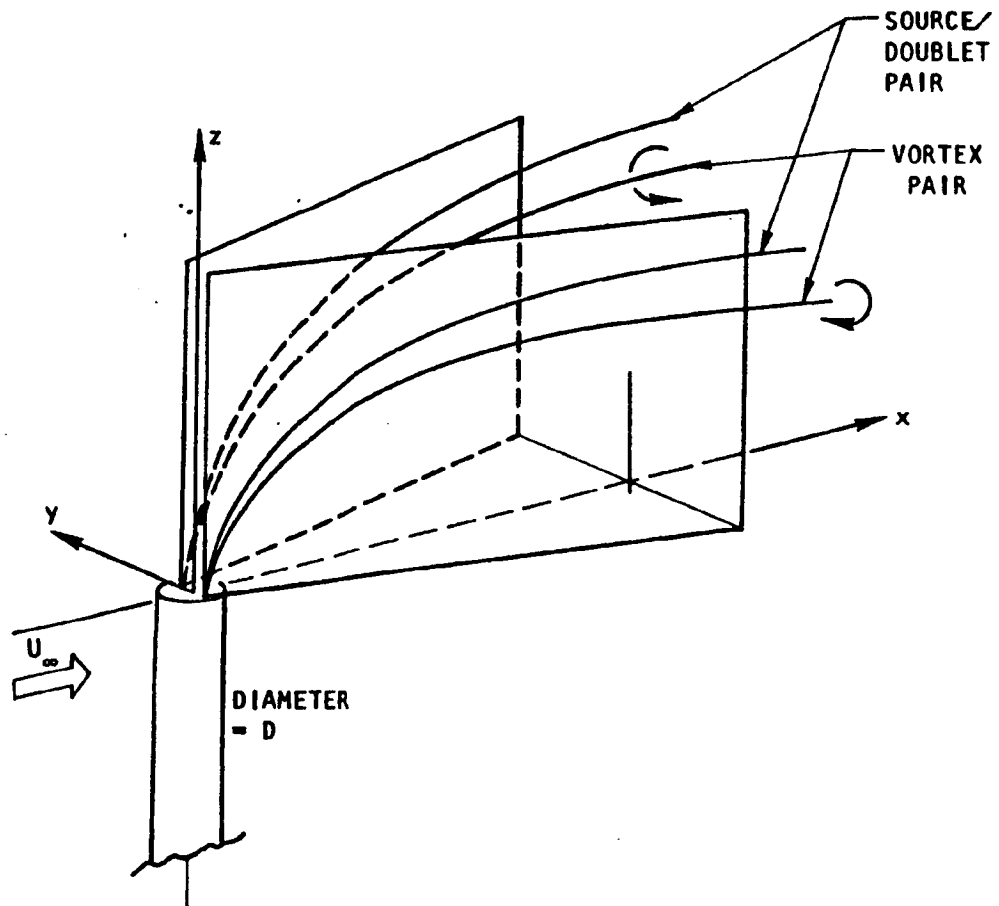


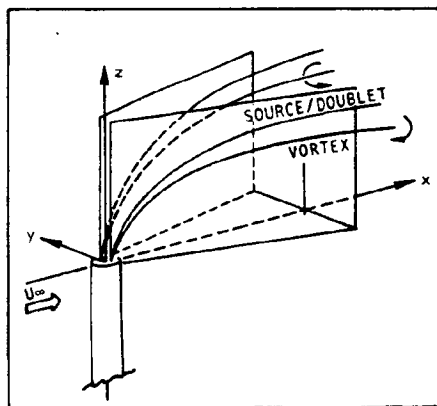
Figure 6

LINE SINGULARITY PROFILE AND STRENGTH  
EQUATIONS FOR THE VSD MODEL

Vortex trajectories closely followed the measured paths. However, it was found that wall pressures were not sensitive to source and doublet line spacing, so the vortex value was used for convenience.

Vortex strength distribution again rested upon Fearn's work, again with appropriately revised constants. Source and doublet strengths were assigned using simple mixing and blockage considerations respectively (fig. 7). Wall pressures could then be matched without the need for further adjustment.

Broadly speaking, it may be stated that the source and doublet lines affect u-component interference (and hence wall pressures) while the vortex system causes upwash interference.



LINE SINGULARITY	STRENGTH	TRAJECTORY
VORTEX	$\frac{\Gamma}{U_\infty D} = 0.600 \frac{R^2}{(X/D)} (1 - e^{-0.035(X/D)^2}) + 0.084 \tanh(X/D)$	$Z/D = 0.352 (X/D)^{0.429} R^{1.122}$
SOURCE	$Q_{12} = U_\infty D (Z_2 - Z_1) \sqrt{(1+0.23 S_{12}/D)}$ $\nu_{12} = -\frac{\Gamma}{2} U_\infty D^2 \sqrt{(1+0.23 S_{12}/D)}$	$Z/D = 0.758 (X/D)^{0.333} R^{1.000}$
DOUBLET		$Y/D = 0.0769 (X/D)^{0.440} R^{1.000}$ for all

Figure 7

ORIGINAL COPY  
OF POOR QUALITY

TYPICAL LINE SINGULARITY STRENGTHS  
FOR THE VSD FLOW MODEL

The broken line (fig. 8) shows vortex strength buildup (as per Fearn) as the round jet rolls up to a vortex pair. The line source strength buildup is as needed to provide the mass flow augmentation caused by entrainment. The doublet distribution (not shown) has the same form as for the source strength, but it is sized to match the jet diameter at the jet exit plane, thus giving the proper solid blockage effect. Only upstream-directed doublets are included.

Total source strength includes not only the line sources mentioned but also point sources implied where the straight lengths of line doublet join. These point sources cause the steps that occur in the total source strength curve.

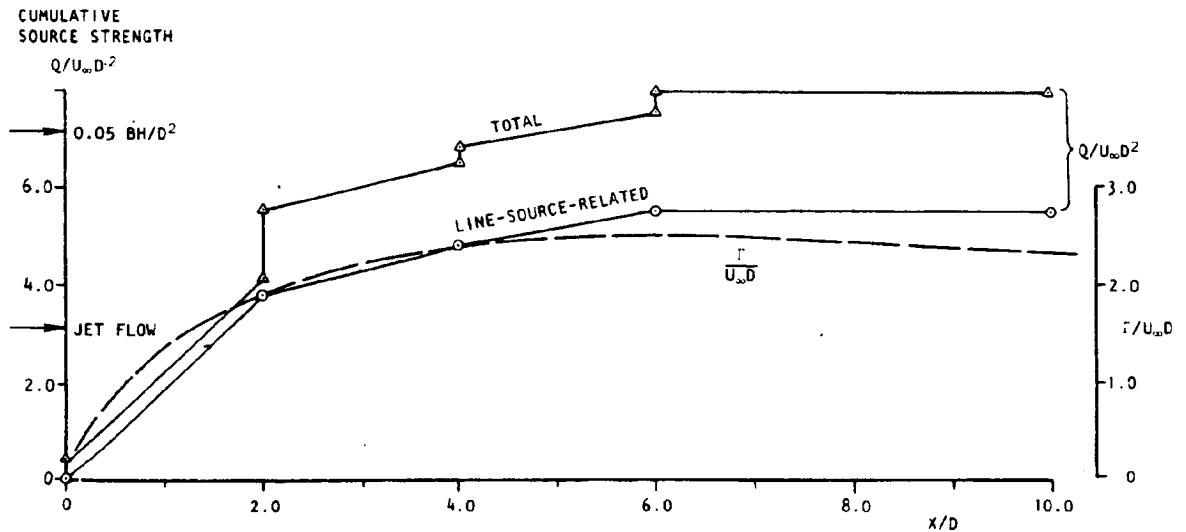


Figure 8

### THE EFFECTS OF POWERED-FLOW IMPINGEMENT

Any jet-in-crossflow model for use in tunnel constraint calculations is incomplete if it is unable to accommodate impingement cases. We shall therefore digress temporarily to consider this subject.

Figure 9 shows floor impingement beneath a 3-D jet flap model at high  $C_u$ . This example has been selected because the laser velocimeter provides the best illustration. Forward-moving jet air causes a massive floor separation that straightens the flow approaching the wing. Because of this distortion, it is not considered reasonable to try to model the flow unless the separation is suppressed. For this reason, a blowing slot is provided as shown. The question is how hard should the blowing be?

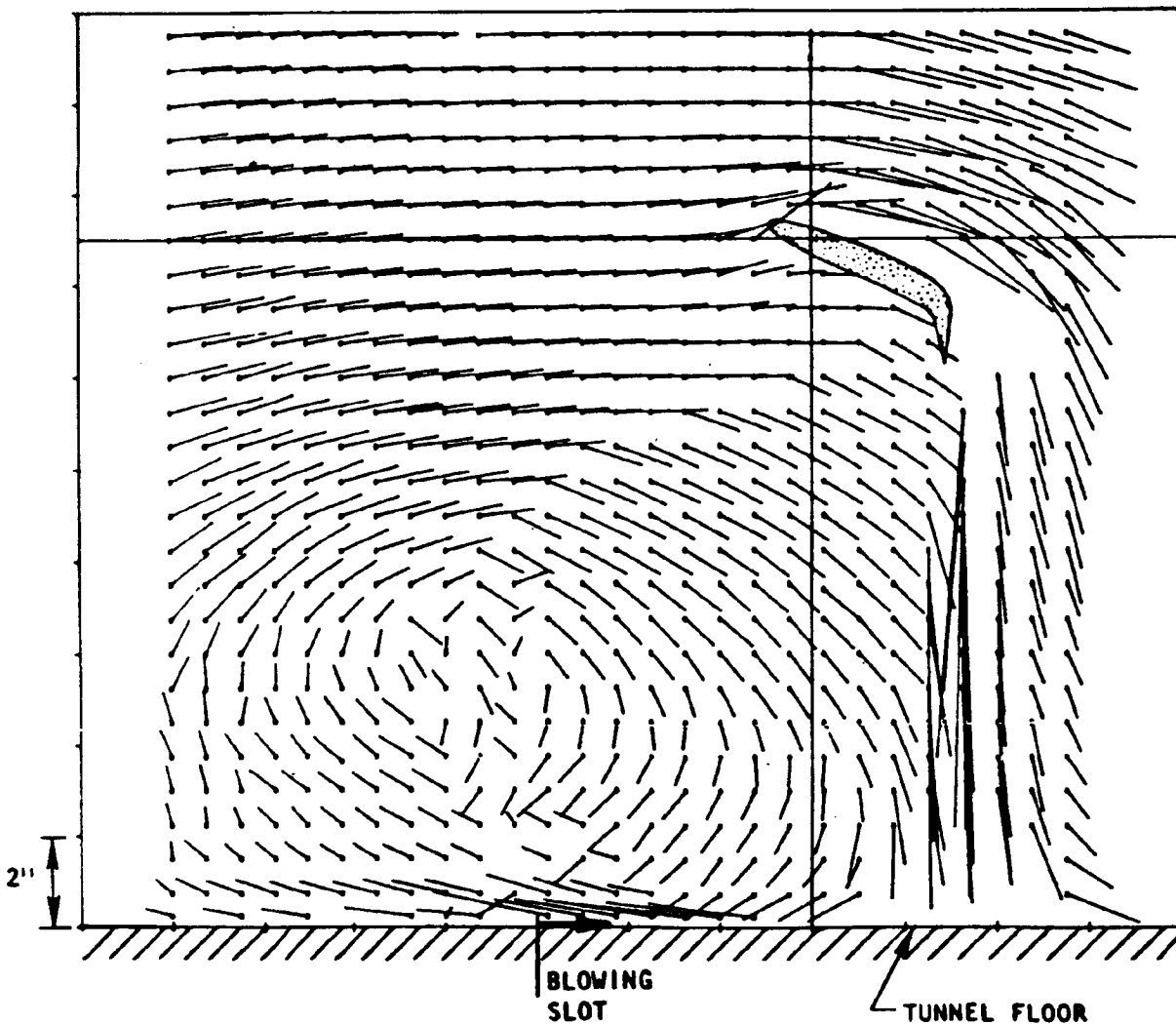


Figure 9

SELECTION OF FLOOR BLOWING STRENGTH

ORIGINAL  
OF PAPER

The floor separation vortex produces an unmistakable peaked suction signature, as shown in figure 10. As blowing is increased along the floor, the peak height and width diminish and eventually they disappear. This was used, somewhat arbitrarily, as a criterion, and it was found that a significant deficit in model lift relative to large tunnel data was removed. It will also be noted (as shown in the lower plot below) that floor blowing almost cuts in half the magnitude of wall signature. This is a sure indication of a substantial reduction in blockage.

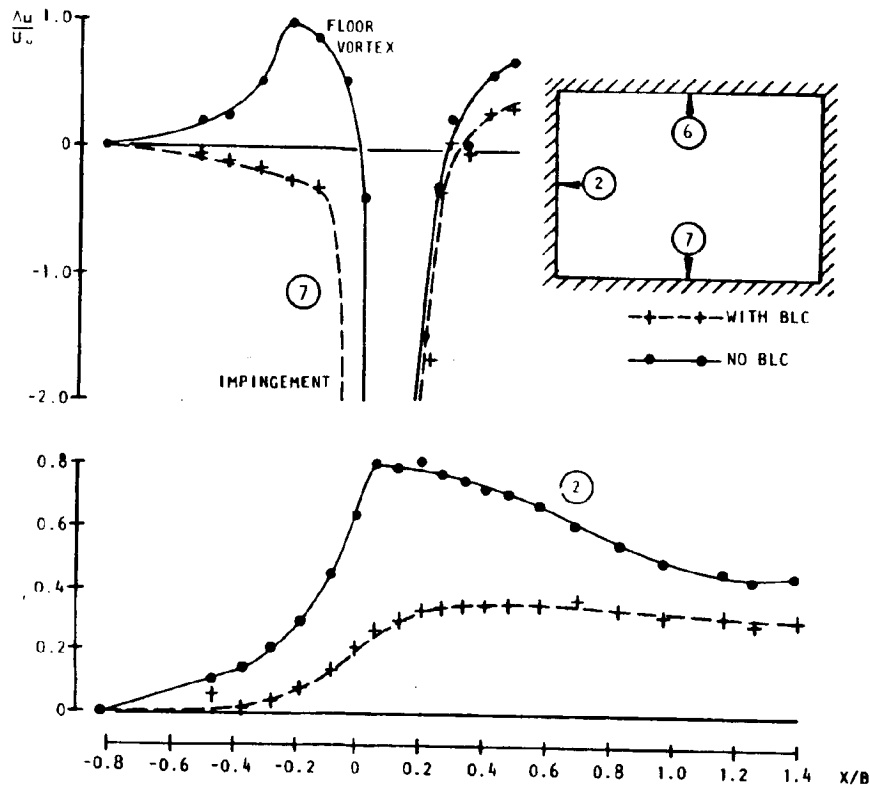


Figure 10

ORIGINAL PAGE 3  
OF FOUR QUALITY

### LV MEASUREMENTS WITH FLOOR BLOWING APPLIED

Having set the floor blowing entirely on the basis of removing the suction peak (fig. 10), new LV measurements showed a dramatic reduction in floor vortex size and a large increase in upwash at the model. This confirms the need to remove or at least minimize the vortex whenever possible. The fact that the flow gave good force corrections shows that a small residual vortex is permissible (fig. 11).

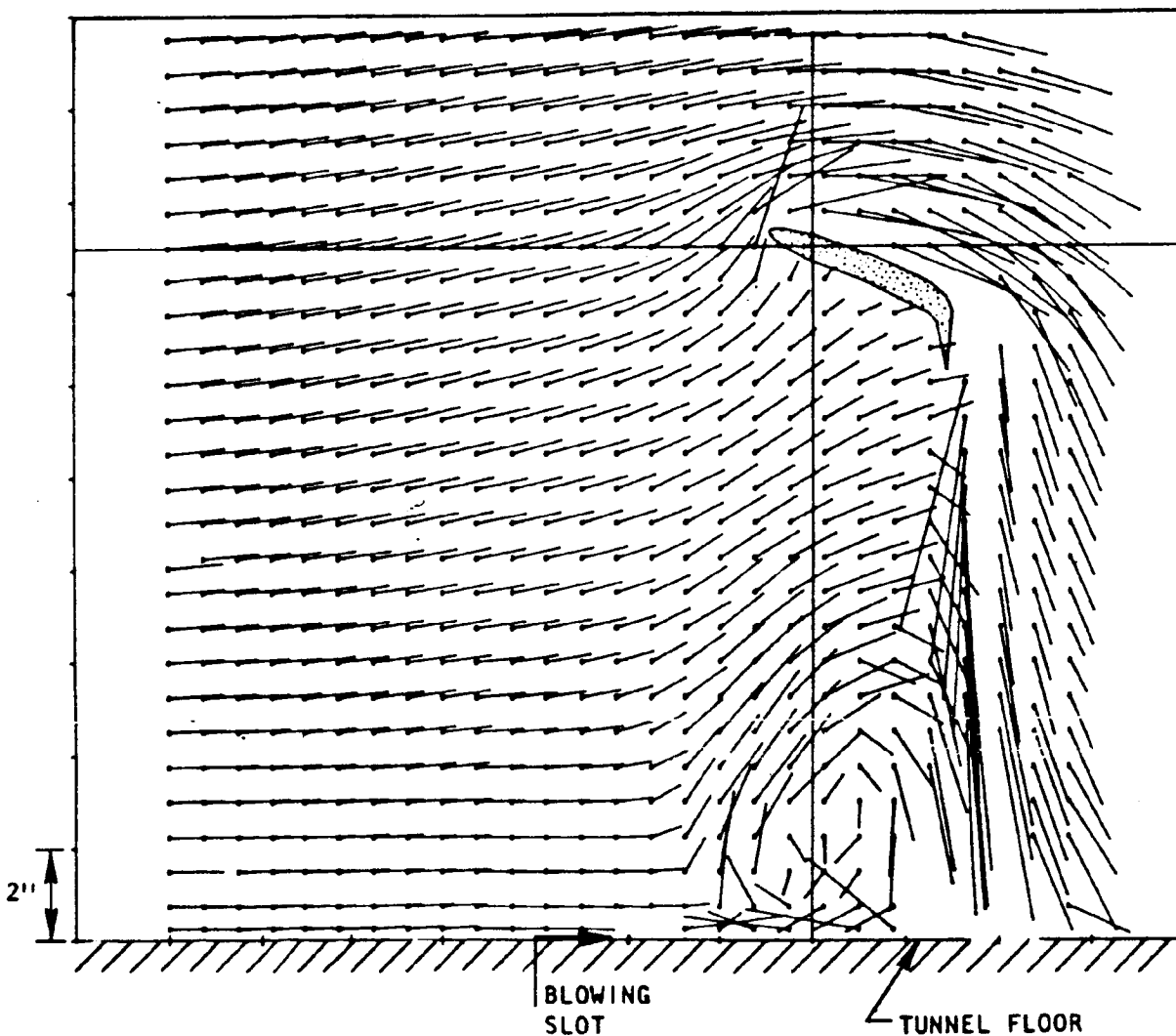


Figure 11

FLOW MODELING FOR IMPINGEMENT CASES

CHAPMAN  
OF FLOW

Provided floor separation is controlled as just described, figure 4 suggests that one may approximate the impinged flow by truncating the free-air plume where it intersects the floor, thus allowing the vortices to trail downstream along the tunnel surface as shown in the left sketch in figure 12. These vortices split into the jet legs (a) and the trailing part (b) as illustrated. In doing the correction, however, it is obvious that (b) is totally unrealistic since the real jet continues to penetrate into the flow. What is needed is a correction which, after performing the usual imaging operations, redirects the trajectories from the "kinked plume" configuration to a "flowing plume" condition. The "redirection term" sketched in (c) does this and has been included in this VSD correction scheme.

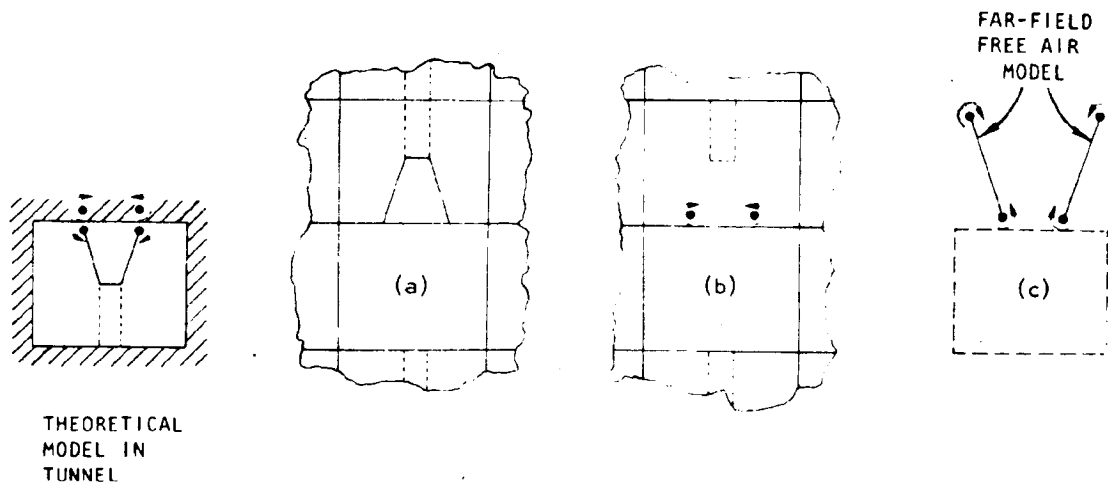


Figure 12

INTERFERENCE ANALYSIS FOR AN IMPINGED CASE

The plots in figure 13 show the tunnel centerline distributions of blockage and upwash interference due to the impinged 3-in. jet at  $R = 6$ . The cumulative effects of components (a), (b), and (c) in figure 12 are shown. Though blockage is sufficiently well represented without the redirection term (c), upwash interference cannot be predicted successfully without it. This is because the image of the kinked part of the trailing plume produces a large excess of interference (compare (a) + (b) with (a) in the lower figure). On redirecting the plume (i.e., (a) + (b) + (c)), a more realistic upwash distribution is obtained.

The effects described are more noticeable aft of the jet and should be expected to be particularly significant at tailplane locations.

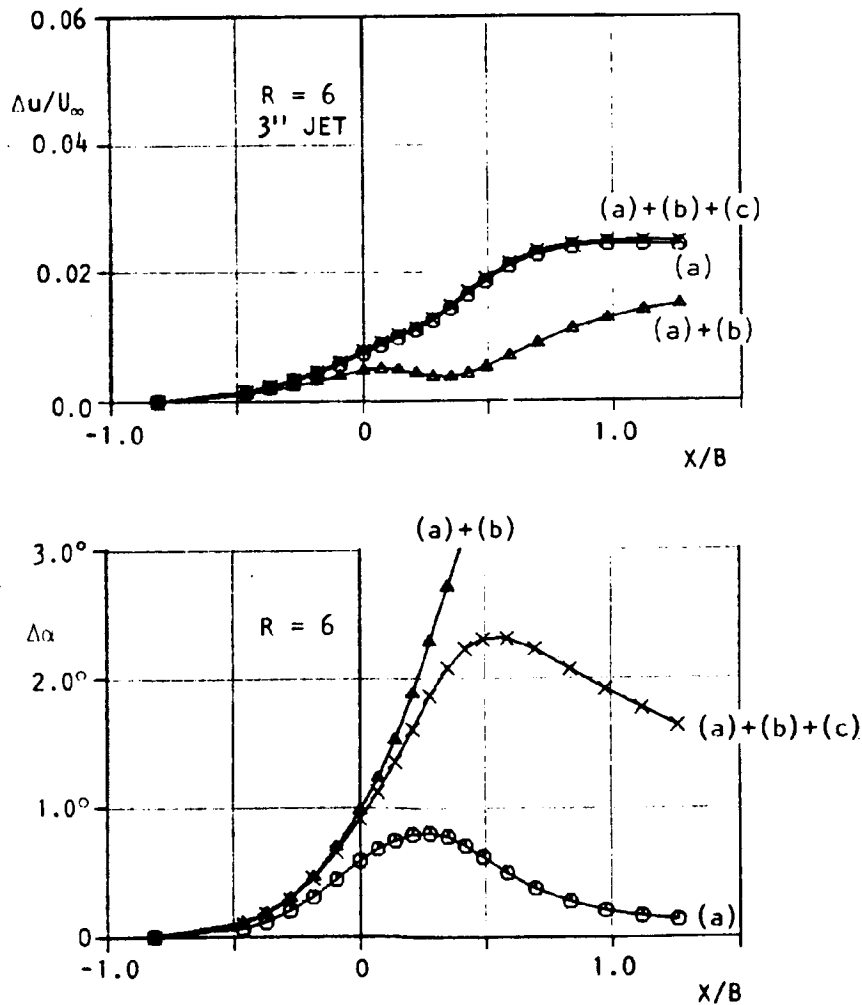


Figure 13

## DISCUSSION

It should be emphasized that this work stops short of a direct checkout involving powered-model comparisons between large and small wind tunnels. Nonetheless, several factors suggest the potential for more accurate tunnel corrections than are possible via existing methods. The most compelling of these factors is the fact that this adaptation of the unified tunnel correction scheme method can predict wall pressures for a large jet in crossflow which contemporary methods cannot. This shows that the VSD model has superior far-field prediction capability and so should give better interference estimates.

Though currently entirely theoretical, the treatment of impingement cases has already answered a number of questions qualitatively, particularly concerning previous difficulties with pitching moment interference for tailed models. Nonetheless, detailed validation of the method is obviously highly desirable (ref. 3).

## CONCLUSIONS

### PREIMPINGEMENT CASES

- o Effects on wall pressures are weak; upwash effects predominate
- o Existing flow models predict wall pressures poorly
- o Improved flow model adds source and doublet lines to Fearn's curved-vortex model
- o Recommended procedure:
  - a) Characterize jet by CMU, DIA, ANGLE
  - b) Remove jet effects from wall pressures
  - c) Calculate jet effects
  - d) Calculate rest-of-model effects from wall pressures

### POSTIMPINGEMENT CASES

- o Floor blowing to remove standing vortex reduces flow distortion and improves chance for successful correction
- o Redirection term needed to "unkink" the impinged plume to an estimated free-air trajectory
- o Recommended procedure:
  - a) (As before)
  - b) (As before)
  - c) Calculate jet effects, including redirection
  - d) (As before)

## LIVING WITH SOLID-WALLED TUNNELS

Upgrading existing tunnels may be accomplished by

- o Measuring, interpreting, and sometimes reacting to test section conditions
- o Exploiting the latest data recording and computer advances when doing this

The payoff:

- o Reliable corrections for models several times larger than before
- o Tunnel flow breakdown point pushed back substantially

## REFERENCES

1. Fearn, R. L., and Weston, R. P.: Induced Velocity Field of a Jet in a Crossflow. NASA TP-1087, May 1978.
2. Williams, J., and Wood, M. N.: Aerodynamic Interference Effects With Jet-Lift V/STOL Aircraft Under Static and Forward-Speed Conditions. Zeitschrift für Flugwissenschaften, vol. 15, sec. 7, pp. 237-256, July 1967.
3. Hackett, J. E.: Living With Solid-Walled Tunnels. AIAA Paper No. 82-0583, March 1982.

## BIBLIOGRAPHY

1. Hackett, J. E., and Wilsden, D. J.: Determination of Low Speed Wake-Blockage Corrections Via Tunnel-Wall Static Pressure Measurements. AGARD CP-174, Paper No. 22, October 1975, pp. 22.1-22.9.
2. Hackett, J. E., Wilsden, D. J., and Stevens, W. A.: A Review of the "Wall Pressure Signature and Other Tunnel Constraint Correction Methods for High Angle-of-Attack Tests." AGARD Report No. 692, February 1981.
3. Hackett, J. E., Boles, R. A., and Lilley, D. E.: Ground Simulation and Tunnel Blockage for a Jet-Flapped, Basic STOL Model Tested to Very High Lift Coefficients. NASA CR-137857, March 1976.
4. Hackett, J. E., and Boles, R. A.: Ground Simulation and Tunnel Blockage for a Swept, Jet-Flapped Wing Tested to Very High Lift Coefficients. NASA CR-152032, June 1977.
5. Hackett, J. E., Wilsden, D. J., and Lilley, D. E.: Estimation of Tunnel Blockage From Wall Pressure Signatures: A Review and Data Correlation. NASA CR-152241, March 1979.
6. Hackett, J. E., Sampath, S., and Phillips, C. G.: Determination of Wind Tunnel Constraint Effects by a Unified Wall Pressure Signature Method: Part I, Applications to Winged Configurations. NASA CR-166186, June 1981.
7. Hackett, J. E., Sampath, S., Phillips, C. G., and White, R. B.: Determination of Wind Tunnel Constraint Effects by a Unified Wall Pressure Signature Method: Part II, Application to Jet-in-Crossflow Cases. NASA CR-166187, November 1981.

omit

SESSION Vb

CORRECTION METHODS USING MEASURED BOUNDARY DATA

Chairman: K. L. Kushman, USAF, AEDC

N85 12028

D17

INTERFERENCE FROM SLOTTED WALLS

Sune B. Berndt  
Aeronautical Research of Sweden  
Royal Institute of Technology  
Stockholm, Sweden

PRECEDING PAGE BLANK

Preceding page blank

DATA BASES FROM FFA SLOTTED TRANSONIC WIND TUNNELS

Three data bases are mentioned here. They were obtained in the tunnels shown in Fig. 1. The models and wall geometries used were not defined to minimize wall interference but rather to make the wall interference predominant so as to facilitate study of the slot flow itself.

(i) Plane flow (Ref. 1)

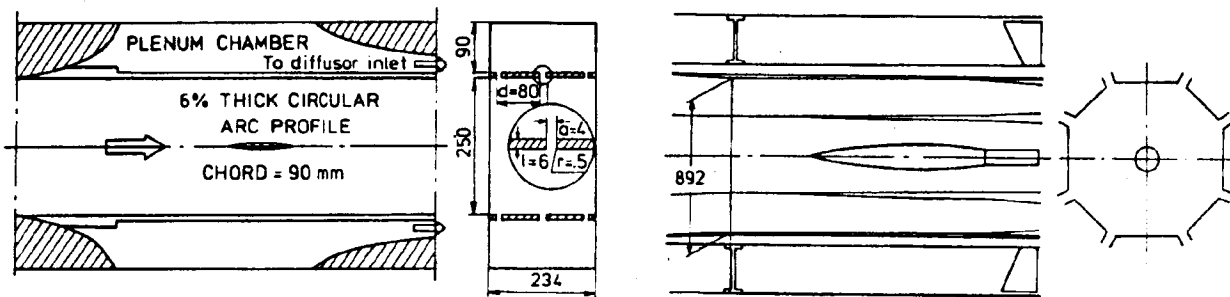
Model: 6% circular-arc profile. Range:  $\alpha = 0$ ,  $M = 0.7-0.9$   
 Pressure distributions: model, side wall, slats, slots, plenum  
 Wall boundary layers: two different thicknesses  
 Total pressures: inside slots and plenum  
 Oil flow pictures: slats, slot walls, symmetry plane of slots

(ii) Axisymmetric flow (Ref. 2)

Models: Parabolic-arc, blockage ratios 0.4 and 2.2%  
 Range:  $\alpha = 0$ ,  $M = 0.90-0.98$   
 Pressure distributions: large model, slats  
 Total pressures: symmetry plane of slots

(iii) Lifting delta wing

Model: Triangular,  $A = 2.7$ , span = 40 % of test section width  
 Range:  $\alpha = 4^\circ - 14^\circ$ ,  $M = 0.8-0.975$   
 Pressure distributions: slats, plenum



(a) Two-dimensional test sections.

(b) Three-dimensional test sections.

Figure 1. Two- and three-dimensional test sections.

ORIGINAL PAGE IS  
 OF POOR QUALITY

Early two-dimensional measurements (Ref. 1) indicated that agreement between the classical slotted-wall formula (including a quadratic cross-flow term) and experiments could be obtained if in the formula were used (1) a reduced slot width (by some 15%) as determined from the boundary layers inside the slot, and (2) a reduced longitudinal velocity in the slot (and correspondingly reduced density) as determined from the total-pressure loss in the plane of symmetry of the slot.

In evaluating the axisymmetric tests in which the viscous effects are stronger, detailed measurements of the slot flow were not available. A cruder version of the correction scheme was therefore adopted. It is postulated that a constant slot width reduction and a constant total-pressure reduction can be used. The width reduction is determined at a position (arrow at  $x \approx 600$  mm in Fig. 2) where the crossflow is dominating, while the total-pressure reduction is determined at a position ( $x \approx 1100$  mm) where the curvature term is strong and the crossflow vanishes. Figure 2 shows the kind of agreement that is obtained. The width reduction in this case is 20%, and the longitudinal velocity reduction is 30%. The theoretical results were obtained by solving the transonic small-perturbation equation with the generalized homogeneous wall boundary condition of Ref. 3, and accounting for the wall boundary layer buildup of the empty test section.

The remaining disagreement, essentially in the shock position, might be due to (1) wall boundary layers, (2) the numerical method, or (3) the wall boundary condition in the shock region.

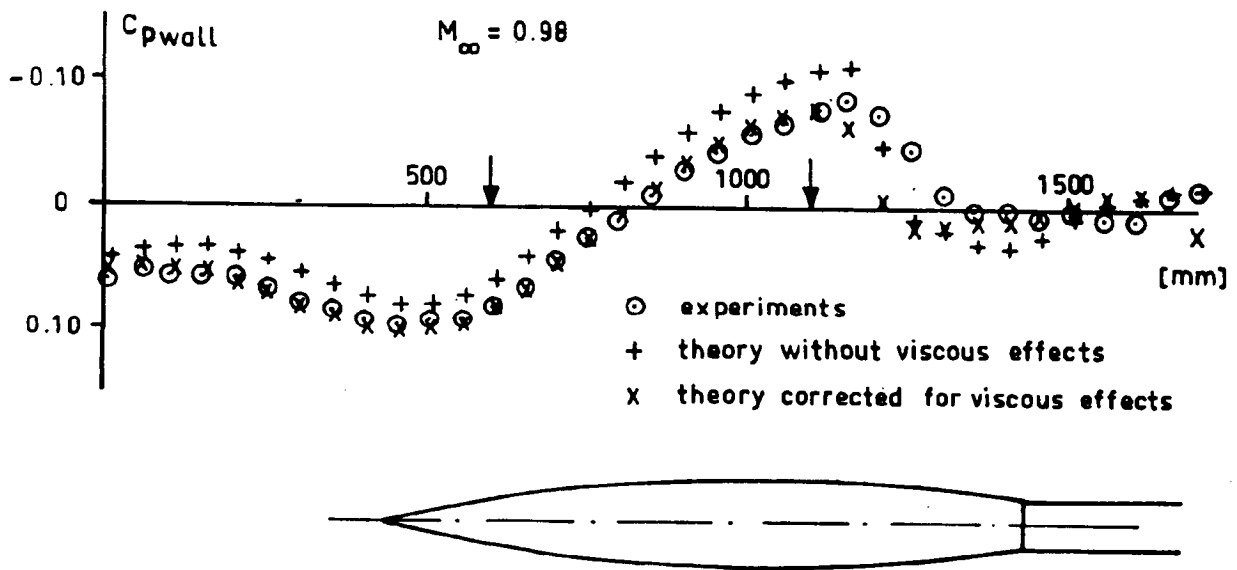


Figure 2. Pressure distributions along slot (large model in forward position, shallow slots).

WALL INTERFERENCE ASSESSMENT FROM NEAR-WALL MEASUREMENTS

A number of two-dimensional assessment methods reported in the literature depend upon measuring pressure distributions at two levels near the wall. In Ref. 4, this approach is analyzed in the situation in which the two levels are located within the influence region of individual slots. Approximating the slots by line sources and locally using the slender-body approximation, the cross flow velocities (Fig. 3) that are needed for an accurate assessment are obtained. Extension to three-dimensional tests is now being considered.

Notation:  $y, z$  cross flow coordinates, wall at  $y = 0$   
 $d$  distance between slots  
 $S_y, S_z$  cross flow velocities in  $y$  and  $z$  directions

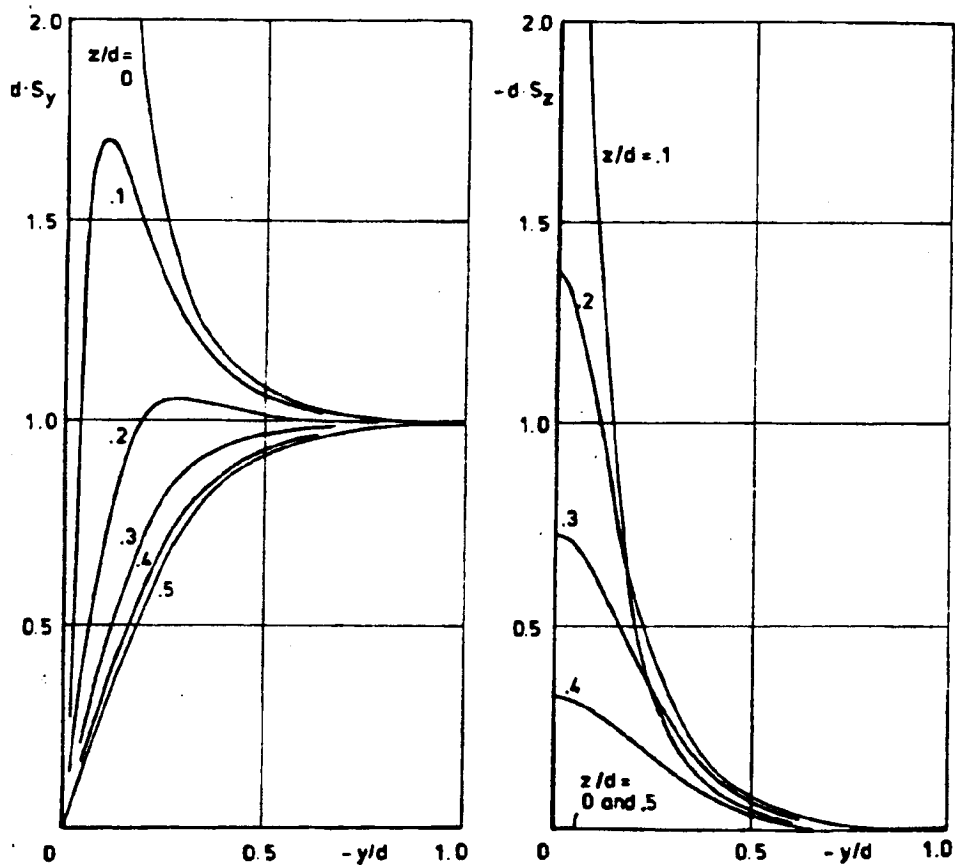


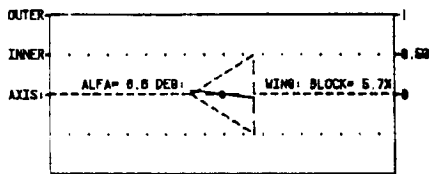
Figure 3. Cross flow velocities at a slotted wall.

INTERFERENCE ON LIFTING DELTA WINGS

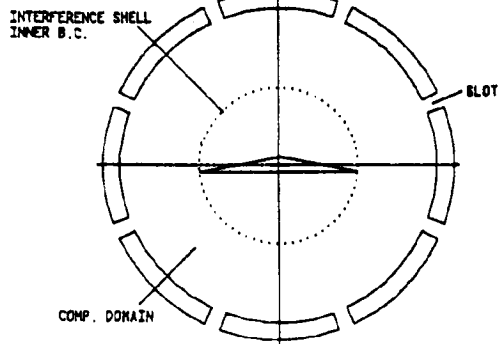
Preliminary theoretical results for slots of constant width have recently been presented by Sedin and Karlsson (Ref. 5). The method is an extension of the method used by them in the axisymmetric case. A few samples are shown in Figs. 4a,b and c. The continued computations are planned to include the cases tested by FFA and numerical experiments to define minimum interference slot geometries.

All the diagrams demonstrate a basic assymetry between the pressure side and the suction side, pointing to the necessity of having wider slots on the pressure side than on the suction side. There is nothing to indicate that even with the larger model (Fig. 4c) the interference cannot be considerably reduced by selecting a proper slot geometry. Fig. 4c demonstrates that the interference in the region of the model can be reduced by lowering the plenum pressure. The number of slots is 8 in all three cases. Cases with 16 slots have also been computed and show very small deviations, indicating that 8 slots will suffice.

MACH=0.95 PLENUM CP= 0.000 SLOT DEPTH=0.11 VENT= 0.2X P= 0.00  
QUALITATIVE INTERFERENCE NUMBERS AT INNER BOUNDARY.  
WING POINTS ONLY. FTIL=-0.04 FTID=-0.05 FTIR= 0.05 FTIP= 0.12

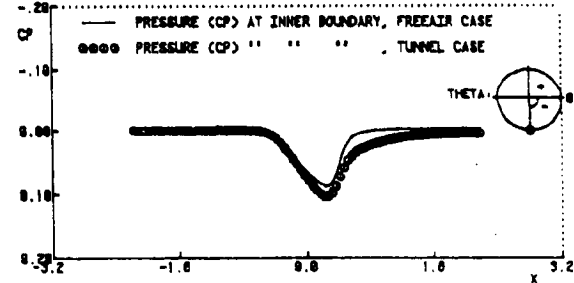
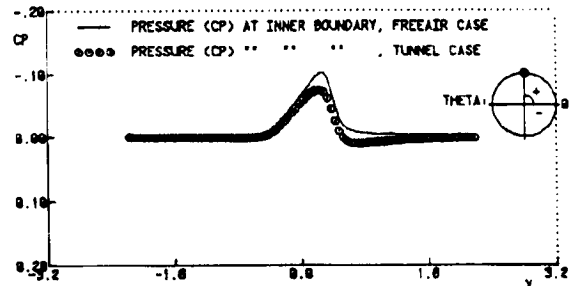


DEF: WING BLOCK=CL+SWING/CROSS



DOUBLET BOUNDARY COND: DELTA-WING, AR=2.5, HSP=.5 \*\*RUN=003

MACH=0.95 PLENUM CP= 0.000 SLOT DEPTH=0.11 VENT= 0.2X P= 0.00

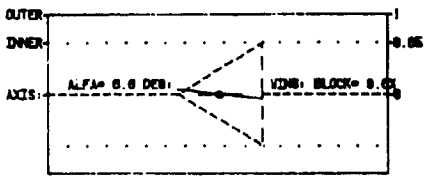


DOUBLET BOUNDARY COND: DELTA-WING, AR=2.5, HSP=.5 \*\*RUN=003

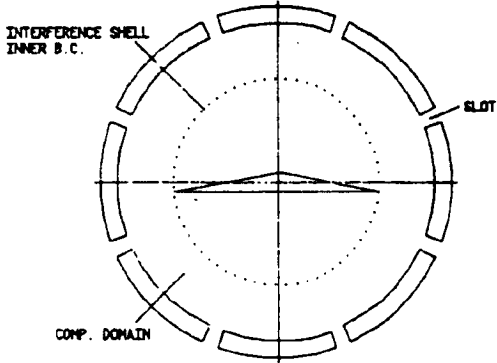
(a)  $M_{\infty} = 0.95$ ,  $\alpha = 6.6^{\circ}$ , span = 50% of tunnel width.

Figure 4. Pressure distributions at inner boundary.

MACH=0.95 PLENUM CP= 0.000 SLOT DEPTH=0.11 VENT= 0.2X P= 0.00  
 QUALITATIVE INTERFERENCE NUMBERS AT INNER BOUNDARY:  
 WING POINTS ONLY: FTIL=0.01 FTID= 0.02 FTIR= 0.01 FTIP= 0.27

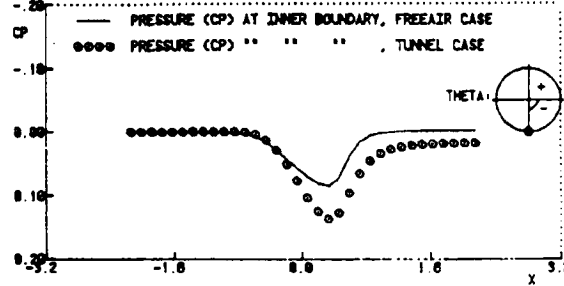
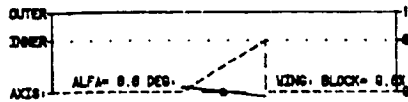
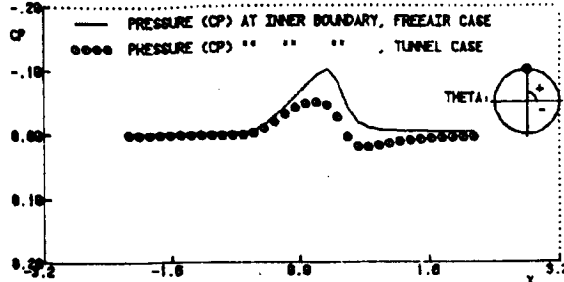


DEF: WING BLOCK=CL+SWING/SCROSS



DOUBLET BOUNDARY COND: DELTA-WING, AR=2.5, HSP=.65 \*\*RUN=022

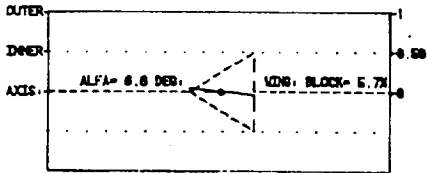
MACH=0.95 PLENUM CP= 0.000 SLOT DEPTH=0.11 VENT= 0.2X P= 0.00



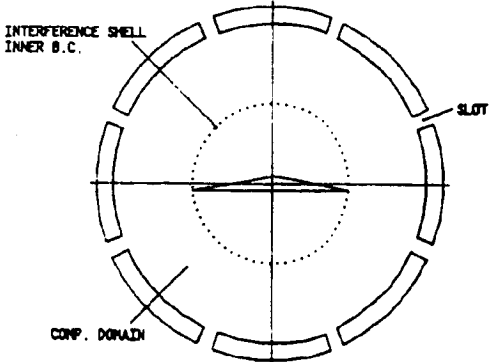
DOUBLET BOUNDARY COND: DELTA-WING, AR=2.5, HSP=.65 \*\*RUN=022

(b)  $M_\infty = 0.95$ ,  $\alpha = 6.6^\circ$ , span = 65% of tunnel width.

MACH=0.95 PLENUM CP=0.020 SLOT DEPTH=0.11 VENT= 0.2X P= 0.00  
 QUALITATIVE INTERFERENCE NUMBERS AT INNER BOUNDARY:  
 WING POINTS ONLY: FTIL=0.05 FTID=0.05 FTIR= 0.05 FTIP= 0.12

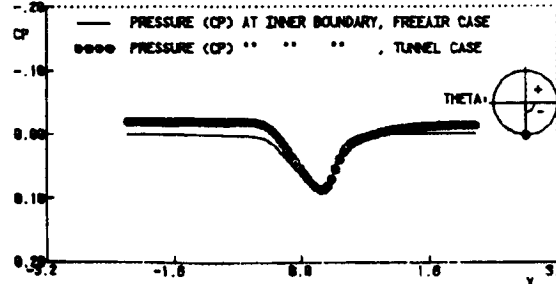
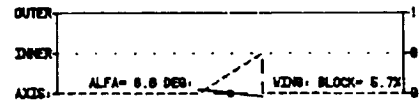
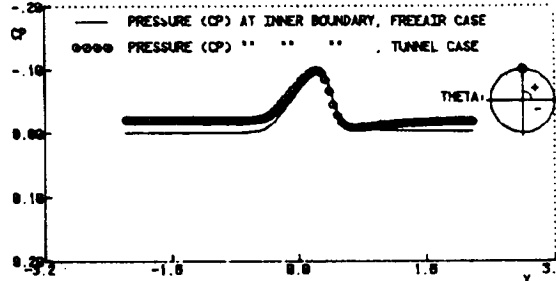


DEF: WING BLOCK=CL+SWING/SCROSS



DOUBLET BOUNDARY COND: DELTA-WING, AR=2.5, HSP=.5 \*\*RUN=011

MACH=0.95 PLENUM CP=0.020 SLOT DEPTH=0.11 VENT= 0.2X P= 0.00



DOUBLET BOUNDARY COND: DELTA-WING, AR=2.5, HSP=.5 \*\*RUN=011

(c)  $M_\infty = 0.95$ ,  $\alpha = 6.6^\circ$ , span = 50% of tunnel width, plenum suction applied.

Figure 4. Concluded.

ORIGINAL MATERIAL  
 OF POOR QUALITY

## REFERENCES

1. Berndt, S. B. and Sörensen, H., Flow properties of slotted walls for transonic test sections. AGARD CP-174, paper no. 17, March 1976, pp. 17-1 - 17-10.
2. Berndt, S. B., Flow properties of slotted-wall test sections. AGARD CP-335, paper no. 6, 1982, pp. 6-1 - 6-7.
3. Berndt, S. B., Inviscid theory of wall interference in slotted test sections. AIAA J., vol. 15, no. 9, Sept. 1977, pp. 1278-1287.
4. Berndt, S. B., Measuring the flow properties of slotted test section walls. FAA Rep. 135, 1982.
5. Sedin, Y. C.-J. and Karlsson, K. R., Some theoretical wall interference calculations in slotted transonic test sections, three-dimensional flows. Proc. Internat. Council Aeronaut. Sci. Congr., 13th, and AIAA Aircraft Systems and Technol. Conf., 1982, pp. 455-466.

N85 12029

D18

WIND TUNNEL WALL INTERFERENCE CORRECTIONS  
FOR AIRCRAFT MODELS

M. H. Rizk and M. G. Smithmeyer  
Flow Industries, Inc.  
Research and Technology Division  
Kent, Washington

E. M. Murman  
Massachusetts Institute of Technology  
Cambridge, Massachusetts

PRECEDING PAGE BLANK NOT REPRODUCED

Preceding page blank

## INTRODUCTION

A model tested in a wind tunnel at a given free-stream Mach number will develop different flow properties at its surface (Mach number and pressure distribution) as compared to those developed by the same model in free air at the same free-stream Mach number. Wall interference correction procedures seek to determine the required changes in certain flow or geometric parameters so that the difference between the flow properties at the model's surface in the tunnel and free air are minimized. A transonic and a linear correction procedure have been developed for aircraft models.

In addition to Mach number and angle-of-attack corrections, the transonic correction procedure provides an estimate of the accuracy of the corrections. Lift, pitching moment and pressure measurements near the tunnel walls are required. Details of the transonic correction procedure are given in Ref. 1. An earlier but less complete version of this work has been presented in Ref. 2. In the present work, the efficiency and accuracy of the correction procedure are improved. Moreover, the present work allows correction of both the wing and tail angles of attack, while the work described in Ref. 2 allows only one angle-of-attack correction.

The above procedure is valid for transonic as well as subcritical flows. However, for subcritical flows further approximations and simplifying assumptions may be made, leading to a very simple and efficient correction procedure. Details of the linear correction procedure are given in Refs. 3 and 4. This procedure is an extension of the two-dimensional method of Ref. 5 to three-dimensional flows.

- **A Procedure is Developed for Post-Test Assessment of Wall Interference Applicable to Wind Tunnel Tests at Transonic Speeds for Three-Dimensional Aircraft Models**
- **The Assessment Results Include Corrections to Mach Number and Angle of Attack and Some Quantitative Indication of the Residual Interference Not Accounted for by the Corrections**
- **The Cost and Complexity of the Procedure is within Limits which Allow its Use as a Practical Tool for Wind Tunnel Test Corrections**
- **For Subcritical Flows Simplifying Assumptions are Introduced Leading to a Highly Efficient Linearized Correction Procedure**
- **Both Correction Procedures are Demonstrated Through Numerical Examples**

## SYMBOLS AND ABBREVIATIONS

c	=	characteristic chord length
L	=	lift/( $P_o c^2$ )
$\ell$	=	lift spanwise distribution/( $P_o c^2$ )
M	=	Mach number
m	=	$\frac{\text{Pitching moment about the axis } x = x_m}{P_o c^3}$
P	=	Pressure
$P_o$	=	total pressure
X	=	x coordinate relative to the wing leading tip
x, y, z	=	Cartesian coordinate system
$x_m$	=	x coordinate of axis about which the model pitching moment is measured
Y	=	y coordinate normalized by the wing semispan
$\alpha$	=	angle of attack
$\Delta M$	=	Mach number correction
$\Delta \alpha$	=	angle-of-attack correction
$\phi$	=	perturbation velocity potential for the tunnel flow

### Subscripts and Superscripts

d	=	model
e	=	measured quantity or experimental condition
F	=	calculated quantity for the equivalent model in an inviscid free-air flow
f	=	corrected condition
s	=	shock wave
T	=	calculated quantity for the equivalent model in an inviscid tunnel flow
t	=	tail
w	=	wing
$\infty$	=	undisturbed condition

## **OBJECTIVE OF WALL INTERFERENCE CORRECTION PROCEDURES**

To match as much as possible the flow properties on the surface of the tested model to those which would develop by the model when tested in free air.

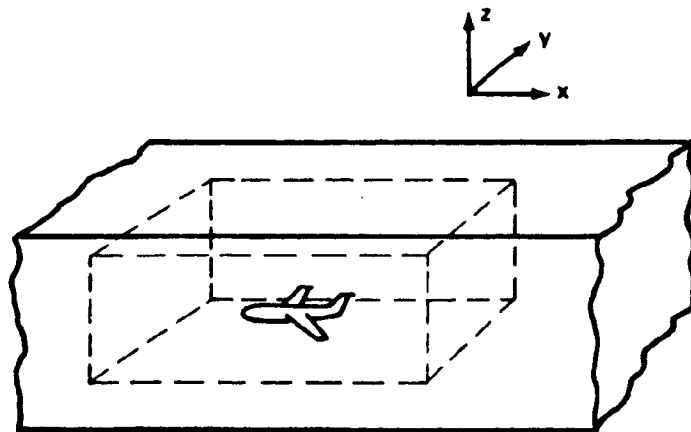
## **METHODS FOR MAKING WALL INTERFERENCE CORRECTIONS**

- **Adaptive Wall Tunnels**
  - Eliminates wall interference by creating free-air conditions
- **Data Corrections**
  - Determines the aerodynamic data which will result if the model is tested in free air at the same tunnel conditions  $\alpha$ ,  $M_\infty$
- **Test Condition Correction**
  - Determines the values of  $\alpha$  and  $M_\infty$  which would produce nearly the same aerodynamic tunnel data if the model is tested in free air

## BASIC REQUIREMENTS FOR THE TEST CONDITION CORRECTION PROCEDURE

- An Estimate of the Flow Properties (e.g. P or M) on the Model Surface in the Wind Tunnel
- An Estimate of the Flow Properties on the Model Surface in Free Air
- Determination of  $\Delta\alpha$  and  $\Delta M_\infty$  Which Will Reduce the Difference Between the Flow Properties in Both Cases as Much as Possible

## GEOMETRICAL CONFIGURATION



## **REQUIRED INPUT**

- **Pressure Measurements at Parallelepiped Boundaries**
- **Free-Stream Mach Number and Wing and Tail Angle of Attacks**
- **Measured Lift Force and Pitching Moment**
- **Model Geometrical Description**

## CORRECTION PROCEDURE

**Step I:** Numerically Simulate the Wind Tunnel Flow ( $M_{\infty T} = M_{\infty e}$ ) About a Simplified Representation of the Experimental Model, and Determine the Angles of Attack  $\alpha_{T,w}$  and  $\alpha_{T,t}$  Such that the Calculated Lift and Pitching Moment are Matched to the Corresponding Measured Values

$$L_{T,d} = L_{e,d} \quad \text{and} \quad m_{T,d} = m_{e,d}$$

**Step II:** Numerically Simulate the Free Air Flow About the Simplified Representation of the Model, and Determine the Angles of Attack  $\alpha_{F,w}$  and  $\alpha_{F,t}$  and Mach Number  $M_{F\infty}$  Such that

$$L_{F,w} = L_{T,w} \quad L_{F,t} = L_{T,t}$$
$$\int (M_F - M_T)^2 dS \text{ is minimized}$$

**Step III:** Calculate Corrections

$$\Delta M = M_{F\infty} - M_{T\infty}$$
$$\Delta \alpha_w = \alpha_{F,w} - \alpha_{T,w}$$
$$\Delta \alpha_t = \alpha_{F,t} - \alpha_{T,t}$$

**Step IV:** Apply Corrections to Data

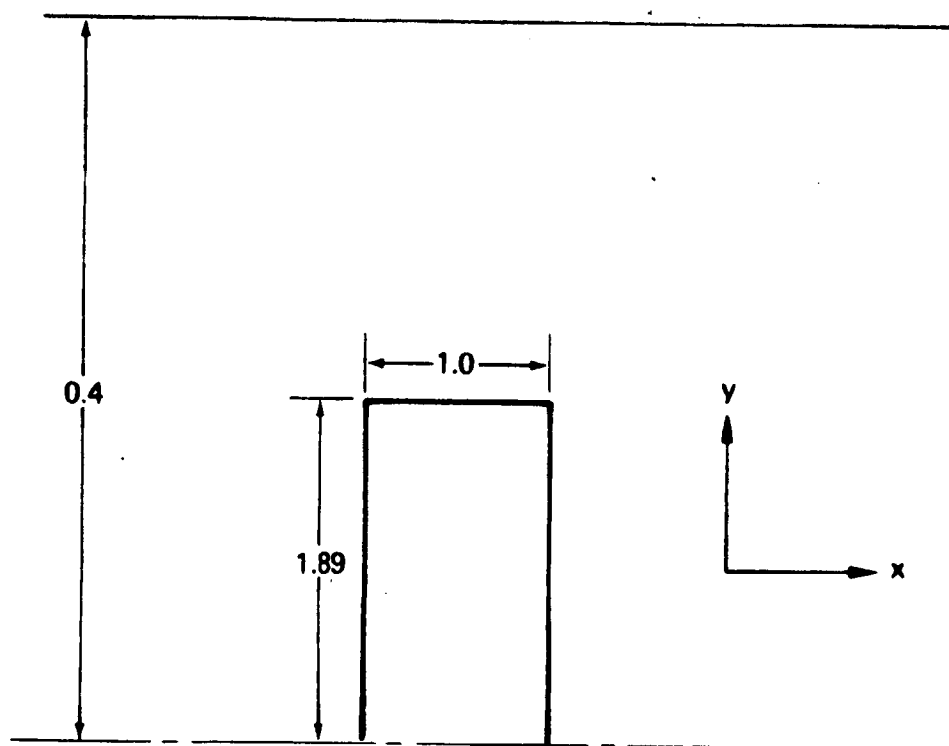
$$M_{f\infty} = M_{e\infty} + \Delta M$$
$$\alpha_{f,w} = \alpha_{e,w} + \Delta \alpha_w$$
$$\alpha_{f,t} = \alpha_{e,t} + \Delta \alpha_t$$

## **NUMERICAL APPROACH**

- **A Standard Line Relaxation Solution is Used to Solve the Potential Equation for  $\phi$**
- **In Addition to Updating the Value of  $\phi$  in Each Iterative Sweep, the Values of  $\alpha_w$  and  $\alpha_t$  are Updated to Reduce the Difference Between the Measured Lift and Pitching Moment Values and the Corresponding Iterative Values, While the Value of  $M_\infty$  is Updated to Reduce the Mach Number Difference on the Model Surface**

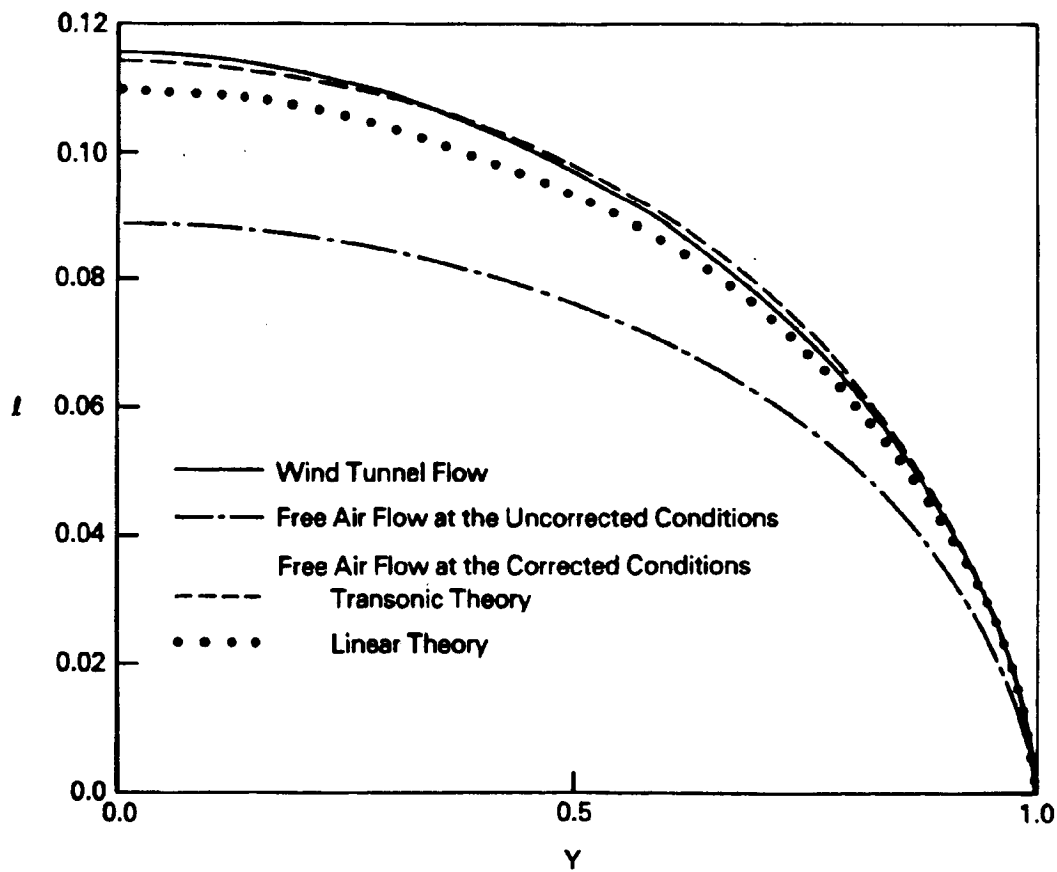
## WING IN TUNNEL

Angle-of-attack and Mach number corrections are calculated for a rectangular wing in a solid-wall wind tunnel. The wing is assumed to be located at mid-distance between the tunnel upper and lower walls. The distance between the walls is 3.26. A NACA 0012 airfoil section is used for the wing. The flow in the wind tunnel is assumed to be inviscid with an undisturbed Mach number value 0.8, while the value of the lift experienced by the wing is assumed to be  $L = 0.343$ . In the case of a model with only one lifting surface, the correction procedure does not require the pitching moment.



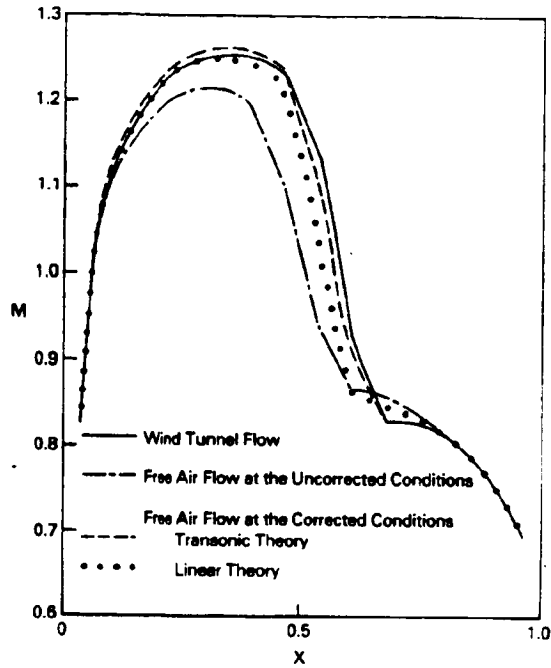
### SPANWISE LIFT DISTRIBUTION

A comparison is presented between the spanwise lift distribution for the wind tunnel flow ( $M_\infty = 0.8$ ,  $\alpha = 2.768^\circ$ ), the free-air flow at the uncorrected conditions ( $M_\infty = 0.8$ ,  $\alpha = 2.768^\circ$ ), the free-air flow at the corrected conditions ( $M_\infty = 0.809$ ,  $\alpha = 3.361^\circ$ ) and the free-air flow at the conditions corrected by linear theory ( $M_\infty = 0.804$ ,  $\alpha = 3.318^\circ$ ).

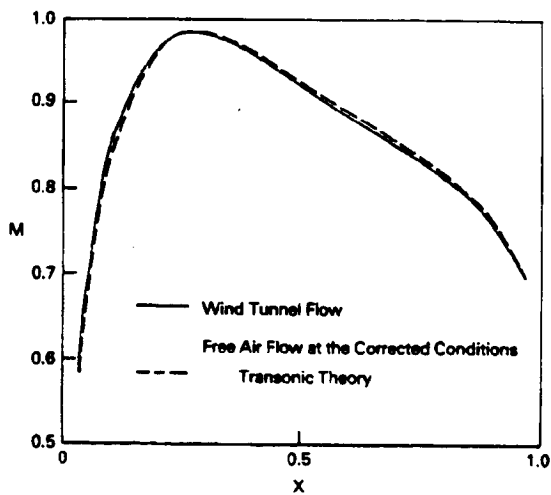


ORIGINAL PAGE IS  
OF POOR QUALITY

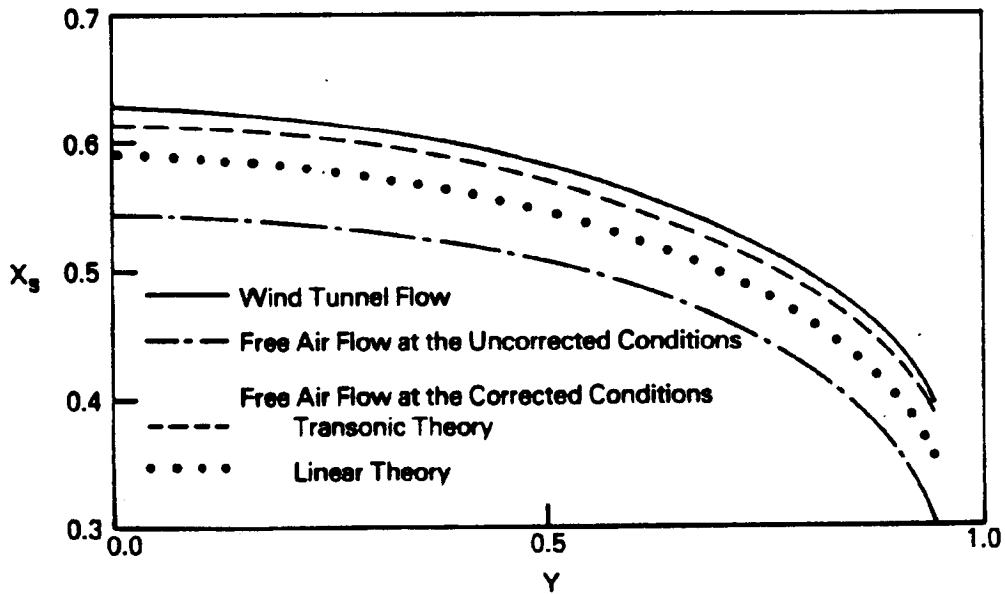
### MACH NUMBER DISTRIBUTION ON WING TOP AT THE MID SEMISPAN STATION



### MACH NUMBER DISTRIBUTION ON WING BOTTOM AT THE MID SEMISPAN STATION



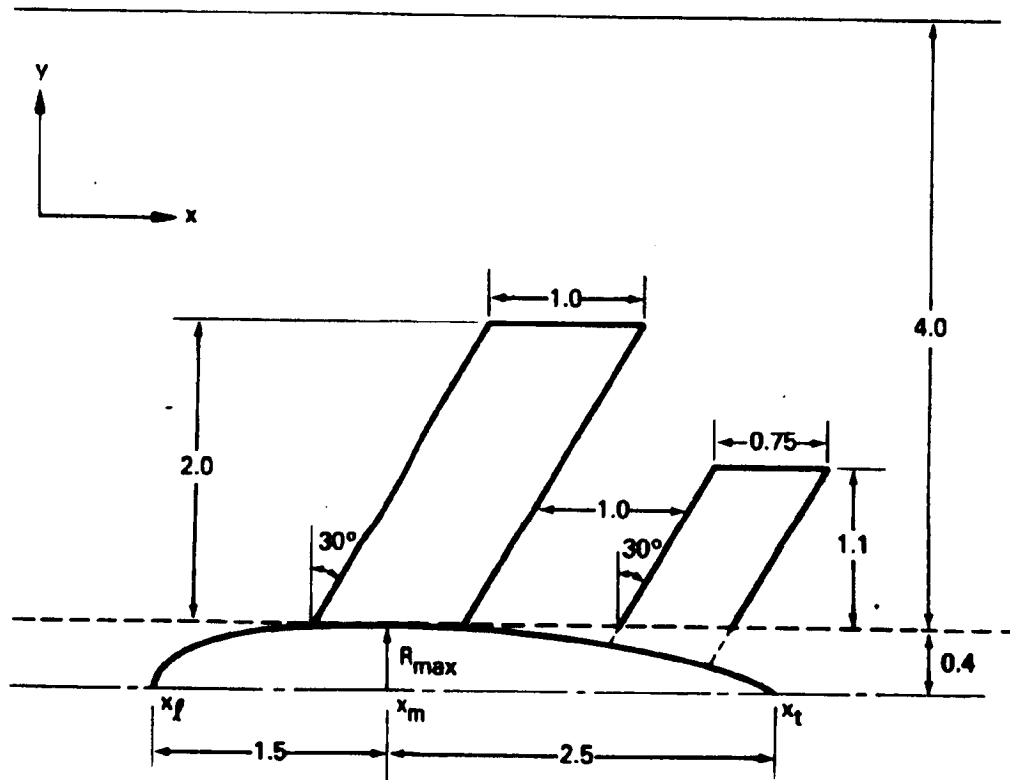
# SHOCK POSITION ON WING TOP



TOP VIEW OF MODEL IN TUNNEL

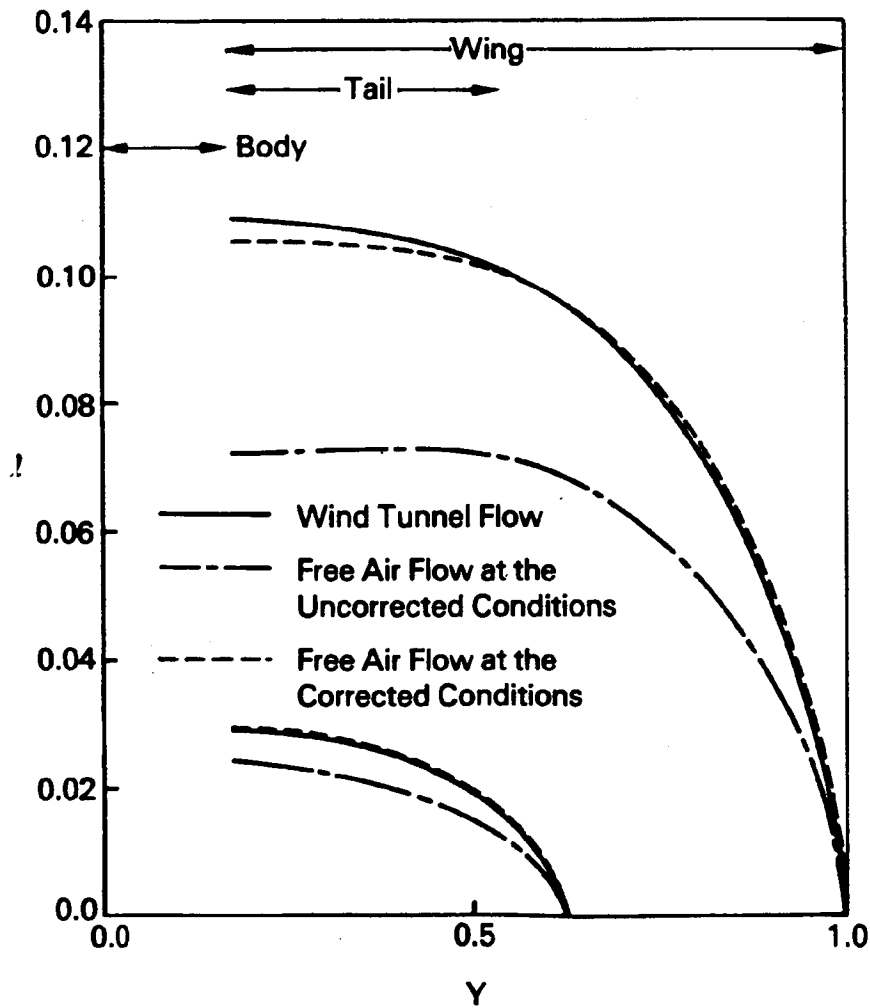
ORIGINAL PAGE IS  
OF POOR QUALITY

The correction procedure is applied to a wing-body-tail model configuration. The geometrical configuration of the model in a solid-wall wind tunnel is shown. The model is assumed to be located at mid-distance between the tunnel upper and lower walls. The distance between the walls is 3.2. A NACA 0012 airfoil section is used for both the wing and tail. The maximum body radius is  $R_{max} = 0.4$ . The undisturbed wind tunnel Mach number is assumed to be 0.77, while  $L_{e,d}$  and  $m_{e,d}$  are assumed to be 0.4 and 1.6, respectively.



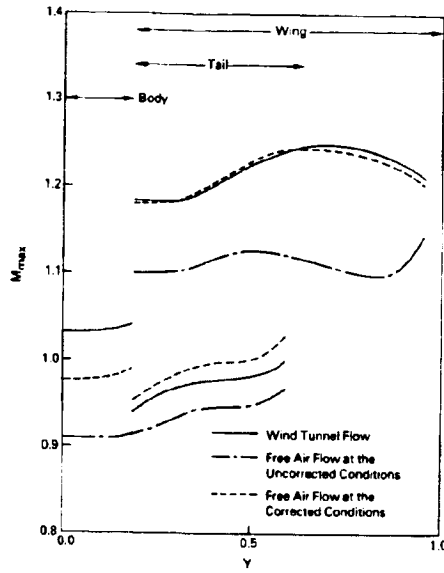
SPANWISE LIFT DISTRIBUTION  
FOR WING AND TAIL

A comparison is given between the spanwise lift distribution for the wind tunnel flow ( $M_\infty = 0.77$ ,  $\alpha_w = 3.296^\circ$ ,  $\alpha_t = 3.780^\circ$ ), the free-air flow at the corrected conditions ( $M_\infty = 0.799$ ,  $\alpha_w = 4.212^\circ$ ,  $\alpha_t = 4.944^\circ$ ) and the free-air flow at the uncorrected conditions ( $M_\infty = 0.77$ ,  $\alpha_w = 3.296^\circ$ ,  $\alpha_t = 3.780^\circ$ ).

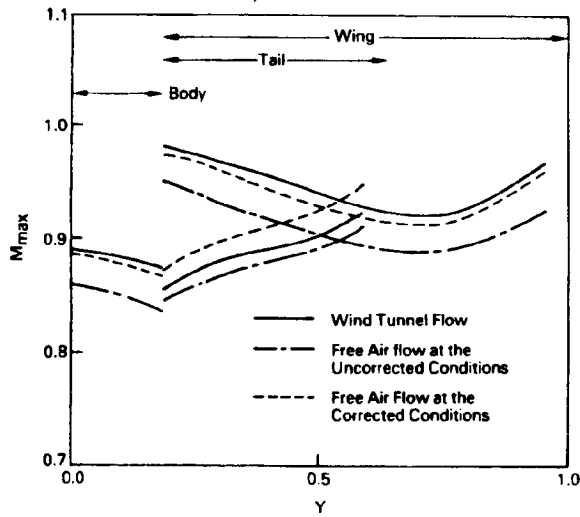


ORIGINAL PAGE IS  
OF POOR QUALITY

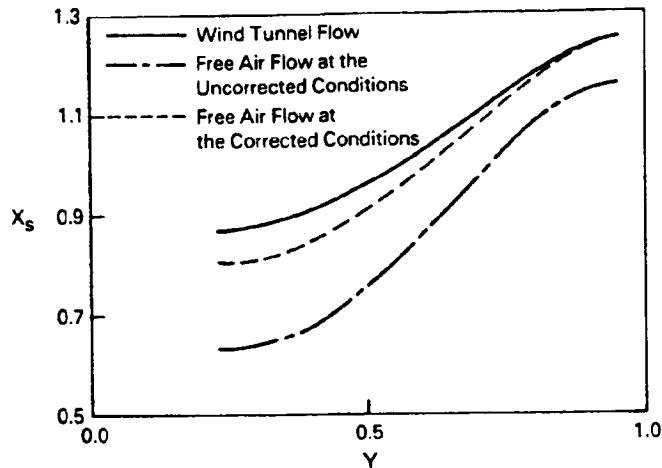
### MAXIMUM MACH NUMBER DISTRIBUTION ALONG WING TOP AND TAIL TOP



### MAXIMUM MACH NUMBER DISTRIBUTION ALONG WING BOTTOM AND TAIL BOTTOM



## SHOCK POSITION ON WING TOP



## SUMMARY OF LINEAR CORRECTION PROCEDURE FOR SUBCRITICAL FLOWS

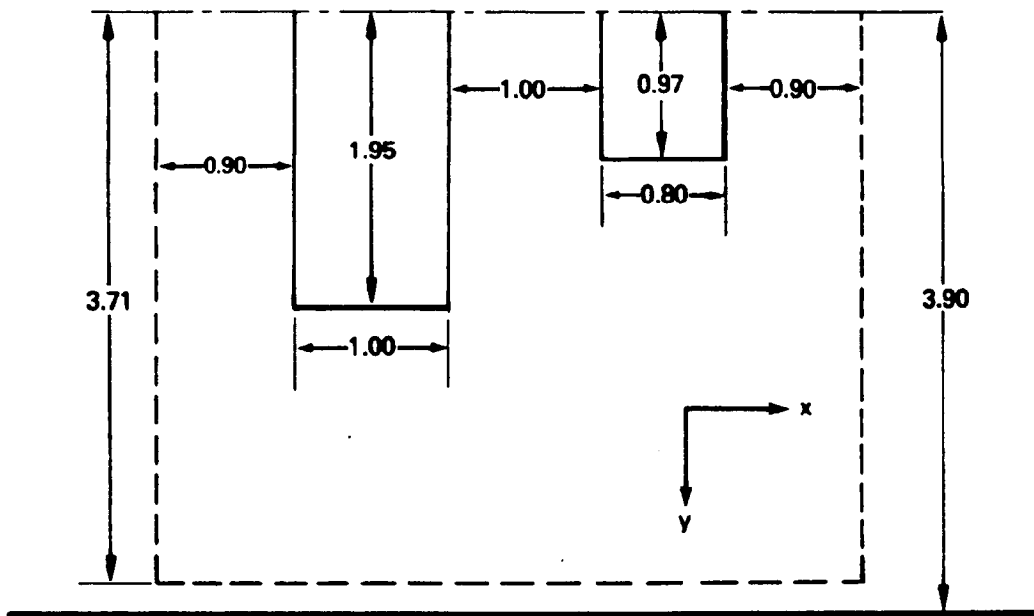
- The Tunnel Flow is Assumed to Satisfy the Prandtl-Glauert Equation; However, a Numerical Simulation of this Flow is Not Required
- The Free Air Flow About a Model With the Same Spanwise Lift Distribution as the Tested Model is Assumed to Satisfy the Prandtl-Glauert Equation; However, a Numerical Simulation of This Flow is Not Required
- The Procedure Requires the Calculation of the Correction Flow Which is the Difference Between the Free Air Flow and the Tunnel Flow

## **LINEAR CORRECTION PROCEDURE (CONT.)**

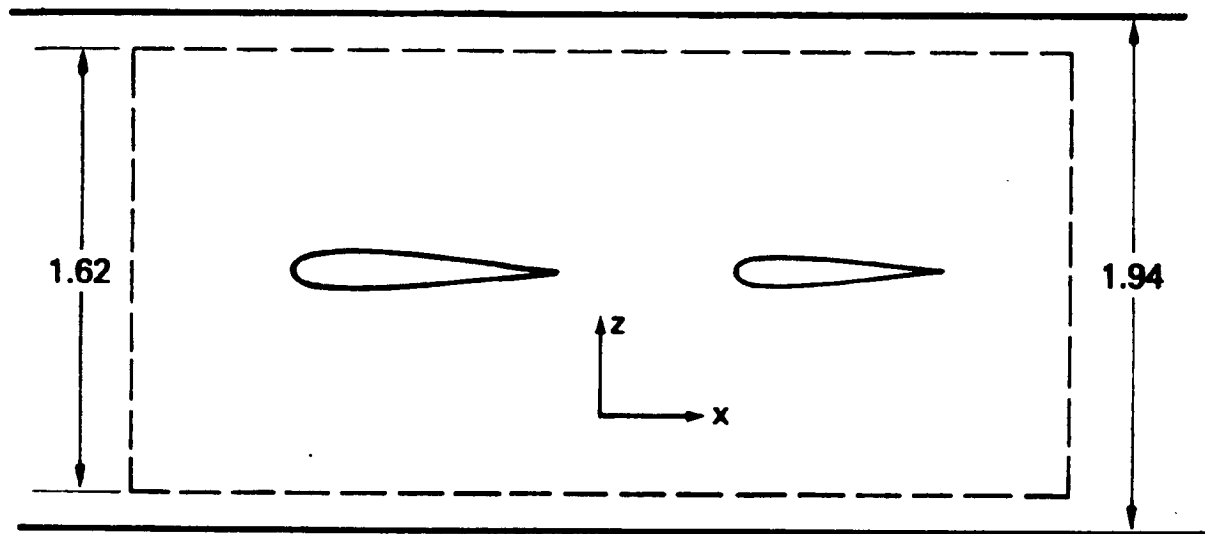
- **Boundary Conditions for the Correction Flow are the Difference Between the Tunnel Flow Boundary Conditions (Obtained from Pressure Measurements Near the Wall) and the Free Air Conditions (Obtained from a Truncated Series Describing the Free-Air Solution)**
- **The Correction Flow Solution is Obtained Through the Use of a Fast Three-Dimensional Laplace Solver, Leading to a Very Efficient Procedure**
- **The Correction Flow Solution Allows the Calculation of Angle of Attack and Mach Number Corrections**
- **The Linear Procedure Does Not Give a Quantitative Indication of the Residual Interference not Accounted for by the Correction**

TOP VIEW OF WING-TAIL IN TUNNEL.

Angle-of-attack corrections are calculated for the wing-tail configuration in a solid-wall wind tunnel. The dashed lines in the figure indicate the boundaries of the boundary value problem for the correction flow. The wing angle of attack is chosen to be  $3^\circ$ , while the tail angle of attack is chosen to be  $4^\circ$ . The undisturbed wind tunnel Mach number  $M_\infty^T$  is taken to be 0.7, and a NACA 0012 airfoil section is used for both the wing and the tail.

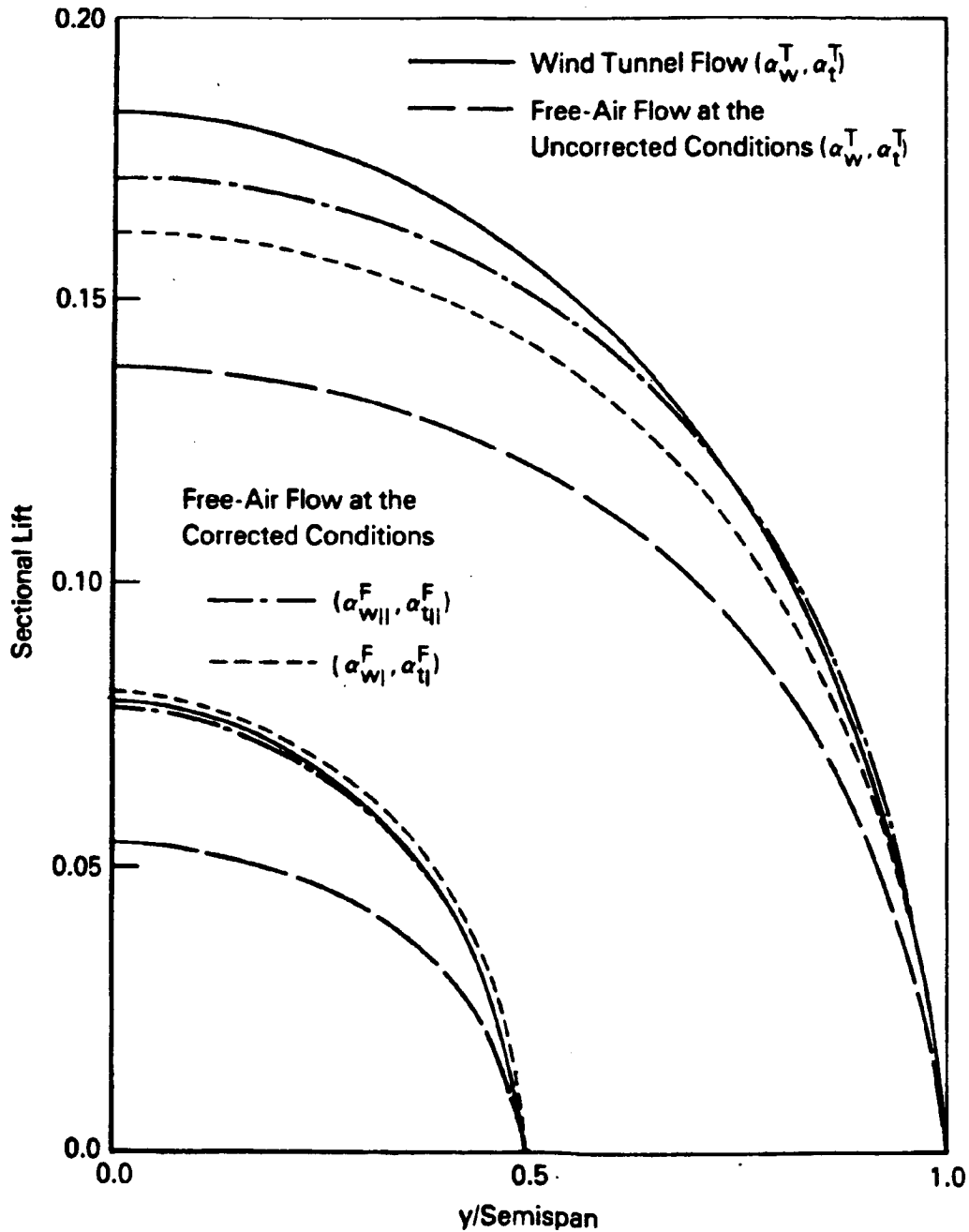


## SIDE VIEW OF WING-TAIL IN TUNNEL



SPANWISE LIFT DISTRIBUTION FOR WING AND TAIL

A comparison is presented between the spanwise lift distribution for the wind tunnel flow ( $\alpha_w = 3^\circ, \alpha_t = 4^\circ$ ), the free-air flow at the corrected conditions derived from first-order theory (Ref. 3) ( $\alpha_{wI}^F = 3.52^\circ, \alpha_{tI}^F = 5.32^\circ$ ), the free-air flow at the corrected conditions derived from second-order theory (Ref. 4) ( $\alpha_{wII}^F = 3.74^\circ, \alpha_{tII}^F = 5.37^\circ$ ), and the free-air flow at the uncorrected conditions ( $\alpha_w = 3^\circ, \alpha_t = 4^\circ$ ).



## **CONCLUDING REMARKS**

- **A Procedure has been Developed for the Evaluation of Wall Interference Corrections for Three-Dimensional Aircraft Configurations in the Transonic Regime**
- **The Procedure Requires an Inviscid Potential Code to Solve the Flow Field About a Suitable Simplification of the Experimental Model**
- **Pressure Measurements Near the Walls and the Model Lift and Pitching Moment are Required Input**
- **For Subcritical Flows Simplifying Assumptions Reduce the Correction Procedure to a Highly Efficient Linear Procedure Which Requires Pressure Measurements Near the Walls and an Approximate Estimate of the Spanwise Lift Distribution**
- **The Procedures have been Applied to Examples with Numerically Generated Test Data with Good Results.**

## REFERENCES

1. Rizk, M. H., and Murman, E. M., "Wind Tunnel Wall Interference Corrections for Aircraft Models in the Transonic Regime," Report No. 244, Research and Technology Division, Flow Industries, Inc., Kent, Washington, December 1982.
2. Rizk, M. H., Hafez, M., Murman, E. M., and Lovell, D., "Transonic Wind Tunnel Wall Interference Corrections for Three-Dimensional Models," AIAA Paper 82-0588, March 1982.
3. Rizk, M. H., and Smithmeyer, M. G., "Wind-Tunnel Wall Interference Corrections for Three-Dimensional Flows," J. Aircraft, Vol. 19, June 1982, pp. 465-472.
4. Rizk, M. H., "Higher-Order Flow Angle Corrections for Three-Dimensional Wind Tunnel Wall Interference," J. Aircraft, Vol. 19, Oct. 1982, pp. 893-895.
5. Mokry, M., and Ohman, L. H., "Application of the Fast Fourier Transform to Two-Dimensional Wind Tunnel Wall Interference," J. Aircraft, Vol. 17, June 1980, pp. 402-408.

N85 12030

019

AN INTERFERENCE ASSESSMENT APPROACH  
FOR A THREE-DIMENSIONAL SLOTTED TUNNEL  
WITH SPARSE WALL PRESSURE DATA

William B. Kemp, Jr.  
Virginia Associated Research Campus  
Newport News, Virginia

## GOALS OF STUDY

The various procedures referred to as wall interference assessment and correction procedures presume the existence of a surface distribution of data (usually static pressure) measured over a surface on or near the tunnel walls for each test point to be assessed. The present study addresses an alternative approach in which a reasonably sophisticated computer model of the test section flow would be fitted parametrically to a sparse set of measured data. For application to the National Transonic Facility, for example, the measurements would provide line distributions of static pressure near the center lines of the top, side and bottom walls. The major goals of the study are noted in figure 1. This paper will show highlights of progress to date toward the first goal, development of a test section model incorporating explicit recognition of discrete slots of finite length with controlled flow reentry into the solid-wall downstream portion of the tunnel.

- DEVELOP HIGH-LEVEL MODEL OF 3-D FINITE LENGTH SLOTTED-WALL TEST SECTION
- FOR WIAC, ADJUST PARAMETERS IN ABOVE MODEL TO MATCH IT TO AVAILABLE PRESSURE DATA
- DEVELOP ALTERNATIVE WIAC PROCEDURE USING KNOWN FLOW AT WALL AND EXTERIOR FLOW SOLUTION

Figure 1

## ELEMENTS USED IN TEST SECTION MODELING

The test section model is being developed initially for subsonic speeds within the framework of a high-order panel method using technology similar to that of reference 1. The author is indebted to James L. Thomas of Langley Research Center for making available the basic panel method program written by him for the CYBER 203 vector processor. As shown in figure 2, the test section and flow are assumed to be symmetrical so that only one half need be modeled. The type of singularity used in each of the various paneled regions is chosen to minimize the perturbation in the fictitious flow outside the panels. Accordingly, doublet panels alone are suitable for modeling solid walls. Combined source and doublet panels are used to implement a homogeneous slotted-wall boundary condition and segmented source lines are added for discrete slot modeling. The upstream and downstream terminations are provided by source panels, the downstream panel being linked with special control points to provide a smooth flow exit regardless of the velocity in the exit duct. For the results shown in this paper, the test model is represented by a point disturbance but a full wing-body-tail representation similar to that used in reference 2 is also available.

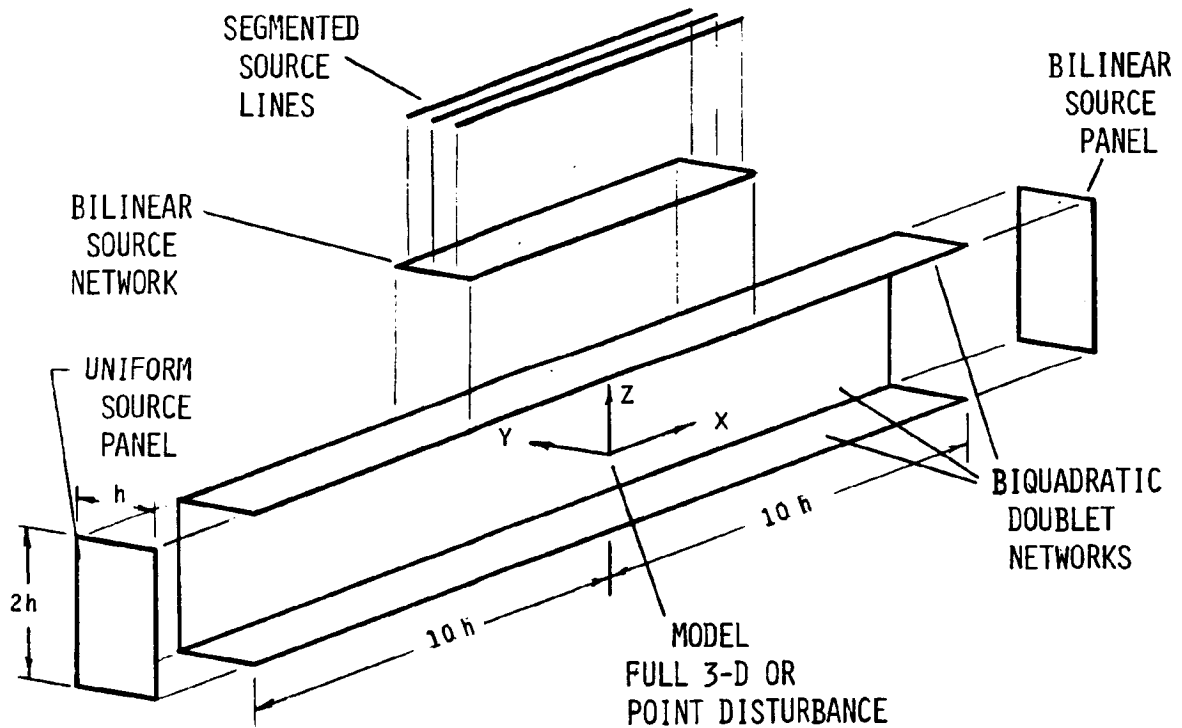


Figure 2

### DISCRETE SLOT REPRESENTATION

A discrete slot representation is used so that the modeled pressures may be matched to data measured directly on the wall between slots. As illustrated schematically in figure 3, the discretely slotted wall flow is represented as a flow which satisfies a homogeneous wall representation plus a perturbation which serves to cancel the wall normal flux between slots and replace it with an equal flux along lines at the slot locations. The discrete slot perturbation is modeled as the influence of a combination of surface and line source distributions. To insure that this influence decays to zero at large distance from the wall, the net source strength associated with the discrete slot perturbation must integrate to zero over a region extending one half of the slot spacing to each side of each slot. The resulting local line source strength is  $-2a v_n$  where  $v_n$  is the outward normal velocity of the homogeneous wall flow.

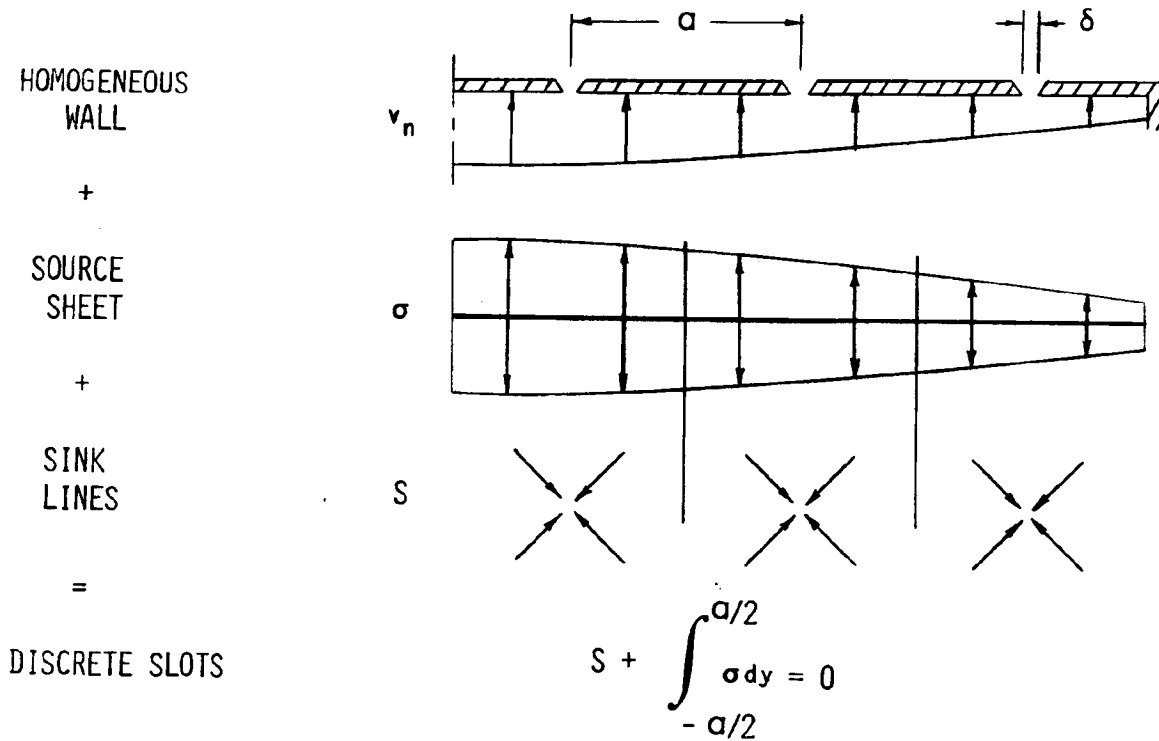


Figure 3

### SLOTTED-WALL BOUNDARY CONDITIONS

The boundary condition used in this study for the homogeneous representation of a slotted wall as well as those used for the discrete slotted wall are given in figure 4. In both cases, provision is made for a non-zero pressure coefficient in the plenum as well as a quadratic term to account for the dynamic pressure of slot flow issuing into the plenum as a jet. The quadratic term (shown in parentheses) has not yet been implemented but will be included in a future iterative solution procedure. For the discrete slot case, the zero normal velocity condition is imposed explicitly at control points between the slots. The condition imposed at the slots is derived from the homogeneous wall condition by using the normal flux equivalence  $S = -2a v_n$ . The longitudinal gradient of  $S$  is expressed in a difference form compatible with the linear strength variation used in each line source segment. Although the source line influence is singular at the line, the longitudinal perturbation velocity  $u$  can be evaluated using a limit form for control points on the line.

#### HOMOGENEOUS REPRESENTATION

$$2U + 2KQ \frac{\partial v_N}{\partial X} = -C_{P,PLEN} - \left( \frac{Q v_N^2}{\delta^2} \right)$$

#### DISCRETE SLOT REPRESENTATION

$$2U - K \frac{\Delta S}{\Delta X} = -C_{P,PLEN} - \left( \frac{S^2}{4\delta^2} \right) \quad \text{AT SLOTS}$$

$$v_N = 0 \quad \text{BETWEEN SLOTS}$$

Figure 4

### LATERAL SURVEY OF FLOW AT TOP WALL

A conceptual error was made when the discrete slot model was first programmed. Results from a fully correct discrete slot case are not yet available. The error was such that the source conservation condition noted on figure 3 was not satisfied although all boundary conditions were correctly satisfied at control points. It is believed that results from this program, a sample of which is shown in figure 5, are adequate to illustrate qualitatively the nature of the discrete slot flow even though the solution is quantitatively in error. Note that on figure 5 the normal velocity component  $w$  has been enlarged by a factor of 100 before plotting to illustrate that the high-order panels achieve a commendable approximation to the zero normal velocity condition not only at control points but also across the entire flat between slots. Although the  $C_p$  variations across the flats are fairly small, it is not yet possible to judge the need for discrete slot modeling in using pressure measurements at wall orifices.

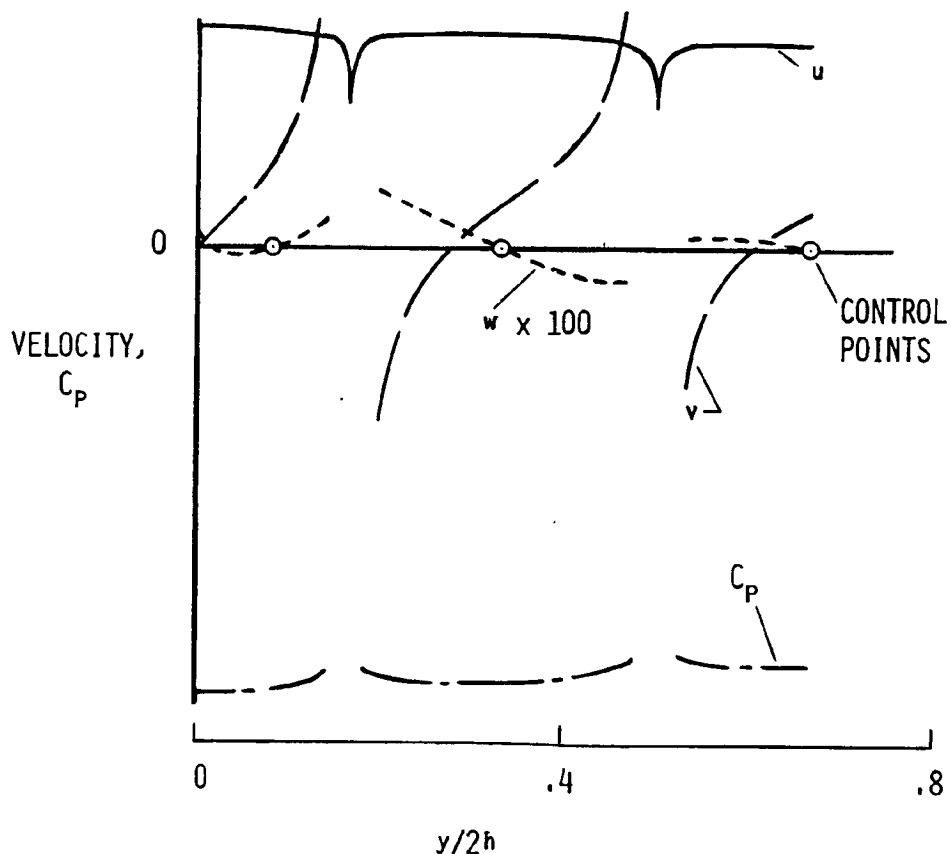


Figure 5

FINITE-LENGTH EFFECTS ON SOLID BLOCKAGE

Tunnel centerline distributions of wall interference velocity and distributions near the top-wall centerline of total longitudinal velocity are shown in figures 6, 7 and 8 for point disturbance models yielding solid blockage, wake blockage and lift interference respectively. All of these results were obtained using the homogeneous representation of slotted top and bottom walls. Interference distributions for solid walls and for infinite-length slotted walls with  $K=3$  are compared with predictions of the value and gradient at the model location from reference 3 and show excellent agreement. The finite-length slotted walls extended from  $1.5 h$  upstream of the model to about  $1.42 h$  downstream.

For the solid-blockage case (figure 6), finite-length slots with zero plenum pressure coefficient resulted in a significant excess velocity in the downstream solid-wall region implying a significant mass transfer from the plenum into the tunnel. A negative value of  $C_{p, plen}$  could be found which eliminated this plenum pumping. The resulting interference velocity distribution is shifted upward from the infinite-length case by about the amount needed to join smoothly the solid-wall interference values at the upstream and downstream ends of the slots.

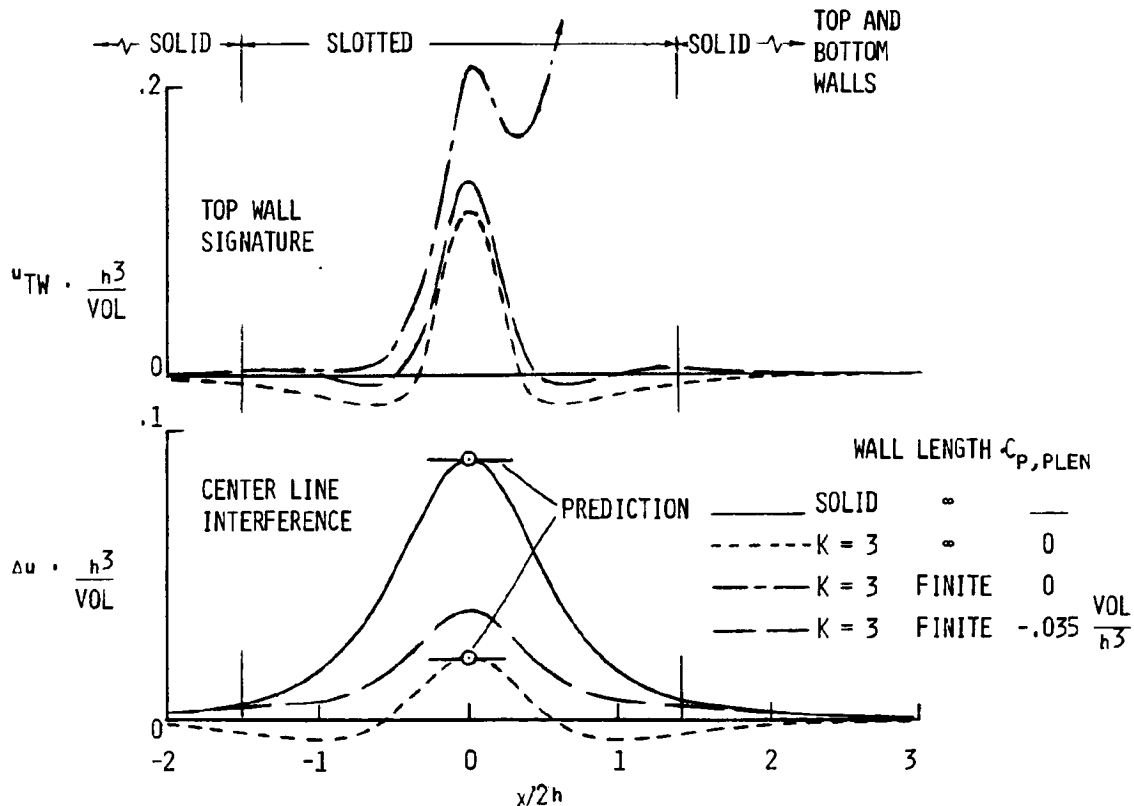


Figure 6

### FINITE-LENGTH EFFECTS ON WAKE BLOCKAGE

The model disturbance for the wake blockage case (figure 7) is a point source in the center of the tunnel. With solid walls, the added mass from the point source causes a higher velocity in the exit duct than that in the entrance duct. With finite-length slots, this downstream velocity could be matched by setting  $C_{p, plen}$  to  $-.072 C_D S/C$ . The resulting wake blockage interference at the model is higher in both magnitude and gradient than that for the infinite-length slotted case. A further reduction in plenum pressure was used to model the case in which the added mass corresponding to wake thickness was removed by suction from the plenum, thereby reducing the velocity perturbation in the exit duct to zero. The resulting wake blockage interference velocity is still higher than that for the infinite-length case but the gradient is now less. These results imply that any other phenomena affecting the velocity entering the exit duct, such as a sting support system and shaping of the diffuser walls, should be accounted for in the test section model.

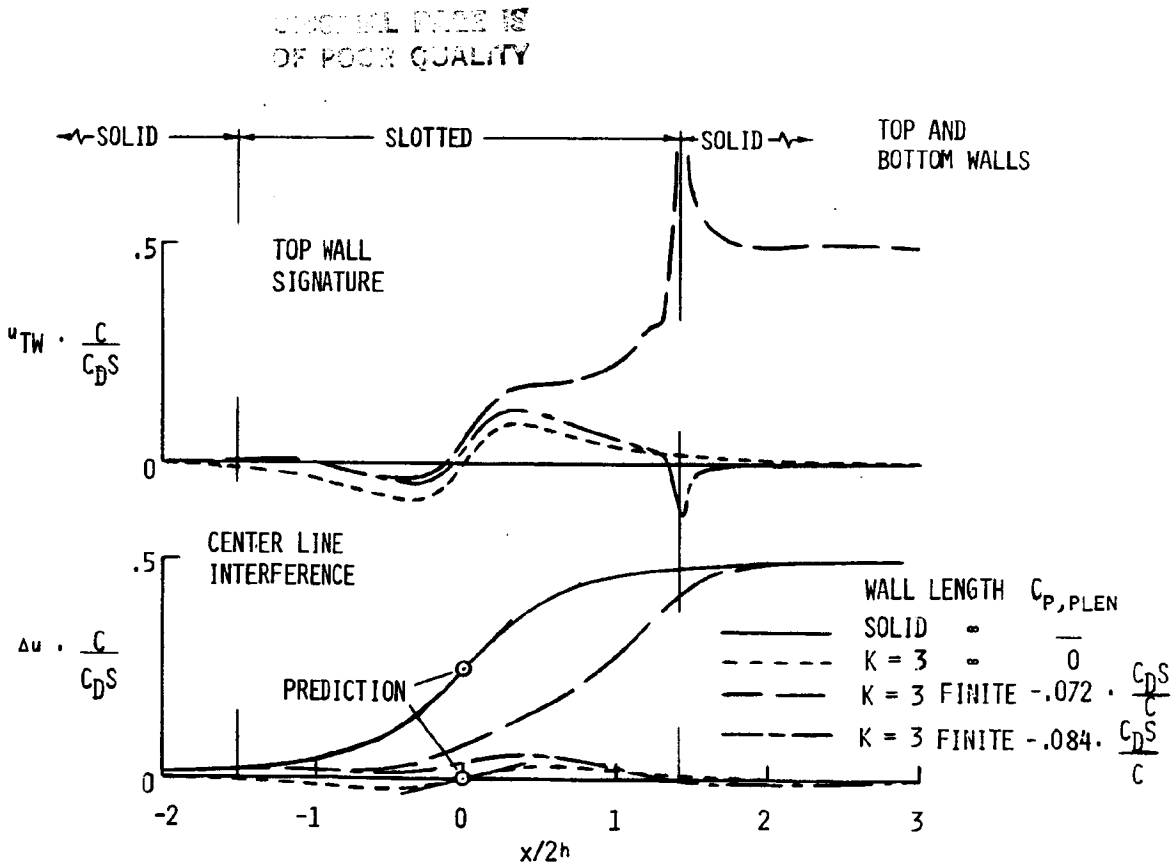


Figure 7

ORIGINAL 17-11-53

FINITE LENGTH EFFECTS ON LIFT INTERFERENCE OF POOR QUALITY

As shown in figure 8, the level of wall-induced upwash downstream of the model is much less for the infinite-length slotted tunnel than for the solid tunnel whose walls must cancel the downwash which occurs naturally behind a lifting system. In the finite-length slotted tunnel, the interference upwash must undergo a transition from the slotted-wall level to the solid-wall level. If the presence of a reentry flap is ignored, this transition is centered around the entrance to the solid-wall exit duct and is not felt at the model. The sudden turning of the flow into the exit duct produces a sharp spike in the upper-wall velocity signature. Most slotted-wall tunnels employ some form of reentry flap to guide the flow smoothly into the exit duct. Such a flap was modeled by prescribing a linear variation of plenum  $C_D$  from zero at the flap leading edge to a value at the end of the slots such that the normal velocity  $w$  at the top and bottom walls approached zero smoothly. The effect on the center line interference was an upstream shift in the transition from slotted wall to solid-wall levels.

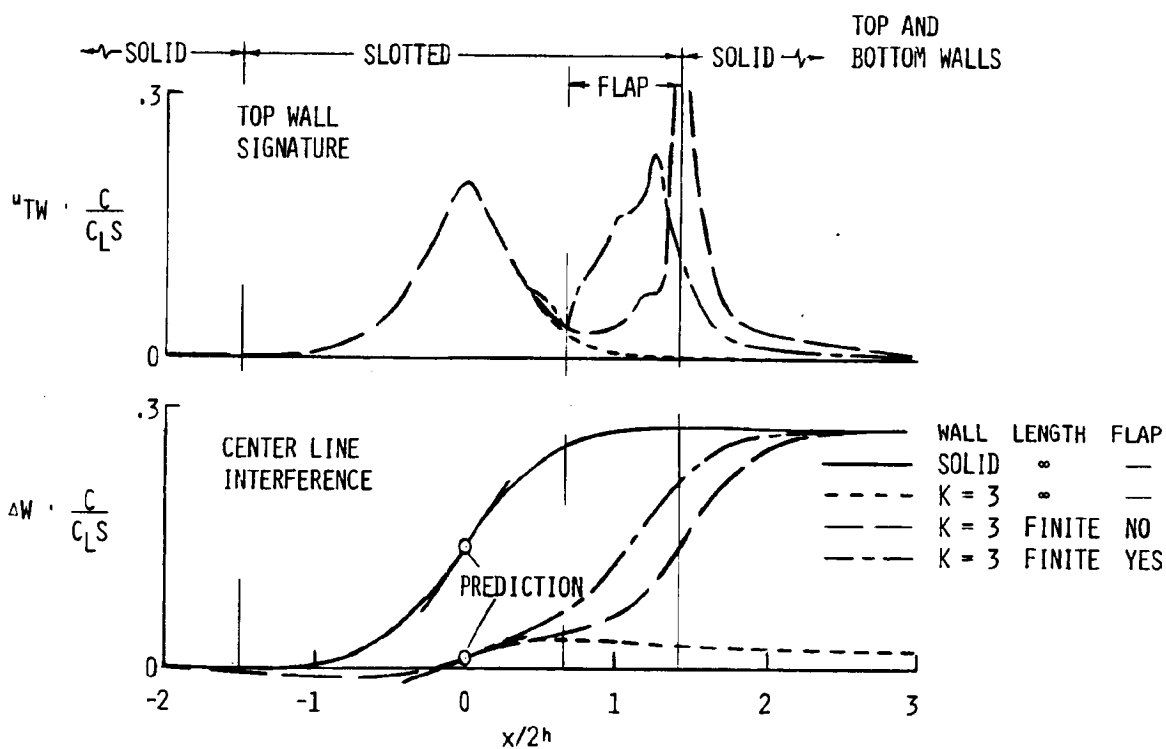


Figure 8

## CONCLUSIONS

The conclusions drawn from the information presented in this paper are summarized in figure 9.

- HIGH-LEVEL MODEL OF SLOTTED TEST SECTION APPEARS FEASIBLE
- PLENUM PRESSURE CONTROLS DIFFUSER ENTRANCE VELOCITY
- REENTRY FLAP EFFECTS CAN BE SIMULATED BY A DISTRIBUTION OF PLENUM PRESSURE
- STING SUPPORT AND DIFFUSER WALL SHAPE SHOULD BE INCLUDED IN TEST SECTION MODEL

Figure 9

## SYMBOLS AND ABBREVIATIONS

$a$	slot spacing
$C$	cross section area of test section
$C_D$	drag coefficient of test model
$C_L$	lift coefficient of test model
$C_P$	pressure coefficient
$C_{p,plen}$	pressure coefficient in plenum surrounding test section
$h$	half height of test section
$K$	slotted-wall parameter normalized by slot spacing
$S$	line source strength, also reference area for lift and drag coefficients
$u, v, w$	perturbation velocity components in x, y and z directions respectively
$VOL$	test model volume
$v_n$	normal velocity at wall
$x, y, z$	Cartesian coordinates
$\delta$	slot width
$\sigma$	source sheet strength
3-D	three-dimensional

#### REFERENCES

1. Johnson, Forrester T.; and Erickson, Larry L.: A General Panel Method for the Analysis and Design of Arbitrary Configurations in Incompressible Flows. NASA CR-3079, June 1979.
2. Rizk, M. H.; and Smithmeyer, M. G.: Wind Tunnel Wall Interference Corrections for Three-Dimensional Flows. J. Aircraft, Vol. 19, June 1982, pp. 465-472.
3. Pindzola, M.; and Lo, C. F.: Boundary Interference at Subsonic Speeds in Wind Tunnels with Ventilated Walls. AEDC TR-69-47, May 1969.

DETERMINATION OF EQUIVALENT MODEL GEOMETRY  
FOR TUNNEL WALL INTERFERENCE ASSESSMENT/CORRECTION\*

C. F. Lo  
Calspan Field Services, Inc./AEDC Division  
Arnold Air Force Station, Tennessee

\*The work reported here was performed by the Arnold Engineering Development Center, Air Force Systems Command. The work and analysis were done by personnel of Calspan Field Services, Inc./AEDC Division, operating contractor for Aerospace Flight Dynamics Testing at AEDC.

## INTRODUCTION

The residual interference must be assessed to determine the wall interference in a conventional tunnel or the degree of convergence of the adaptive-wall procedure. Since there are two variables measured at the interface of an adaptive-wall tunnel, a theoretical procedure can be developed to assess the level of interference with these two variables as known inputs. In general, the equivalent model geometry, including viscous effects, is not known in the tunnel experiments. However, the flow variables measured at the interface contain the influence of such viscous effects in addition to those of the model itself. If one can determine the equivalent model shape based on these variables, this shape then can be used to assess the wall interference.

The present effort, based on two-dimensional subsonic flow, is devoted to deriving a formula for the determination of equivalent model geometry with two variables measured at the interface. It is believed that this predicted model profile is a reasonable initial estimate for transonic flow as long as the sonic region does not reach the interface.

In the presentation, a general formula will be given in two forms. One is in terms of complex variable functions and the other is an integral equation. The complex-function formula has the advantage of using analytic expressions. The integral-equation form requires a numerical solution after assuming the model geometry as a polynomial function. Examples will be given to illustrate the application of the formulas.

## TUNNEL FLOW FIELD

The boundary value problem for the tunnel flow field is described in figure 1. Two techniques are applied to solve the boundary value problem. First, a Fourier transform technique solution is given, followed by an alternate derivation for two-dimensional flow based on the complex velocity.

The solution of the velocity field components is obtained in the Fourier transformed plane:

$$\bar{V}_T(p,y) = i\beta\bar{U}_T(p,h) \frac{\sinh p\beta y}{\cosh p\beta h} + \bar{F}'(p) \frac{\cosh p\beta(h-y)}{\cosh p\beta h} \quad (1)$$

Evaluation of equation (1) at the interface  $y = h$  yields

$$\bar{V}_T(p,h) = i\beta\bar{U}_T(p,h) \tanh p\beta h + \bar{F}'(p)/\cosh p\beta h \quad (2)$$

By eliminating  $\bar{F}'(p)$  in equations (1) and (2), the vertical velocity component is obtained in terms of the measured velocity components at the interface as

$$\bar{V}_T(p,y) = \bar{V}_T(p,h) \cosh p\beta(h-y) - i\beta\bar{U}_T(p,h) \sinh p\beta(h-y) \quad (3)$$

The relationship corresponding to equation (3) in the physical plane can be derived by inverting equation (3) using the Wiener-Hopf technique (ref. 1) to obtain

$$V_T(x,y) = \operatorname{Re} \left\{ V_T[x+i\beta(h-y),h] \right\} + \beta \operatorname{Im} \left\{ U_T[x+i\beta(h-y),h] \right\} \quad (4)$$

#### MODEL PROFILE FORMULA

Equation (4) gives the vertical velocity component inside the tunnel region. The equivalent model profile is assumed to be the vertical velocity along the x-axis; that is, as  $y \rightarrow 0$  for thin airfoils,

$$\begin{aligned} F'(x) &= \lim_{y \rightarrow 0} V_T(x,y) \\ &= \lim_{y \rightarrow 0} \operatorname{Re} \left\{ V_T[x+i\beta(h-y),h] \right\} + \beta \operatorname{Im} \left\{ U_T[x+i\beta(h-y),h] \right\} \end{aligned} \quad (5)$$

This equation indicates that the model geometry can be determined once two components of velocity at the interface are measured. Equation (5) can also be derived using complex velocity with analytic continuation theory, as presented in the next section. However, the Fourier transform technique can be extended to the three-dimensional case but the complex (variable) velocity approach is limited to the two-dimensional problem.

#### MODEL PROFILE EQUATION DERIVED BY COMPLEX FUNCTION

In two-dimensional flow with the Laplace equation as the field equation, the complex-variables approach is the most efficient way to obtain the solution. Let the complex velocity be (dropping all subscripts for convenience)

$$\begin{aligned} U(x,y) - iV(x,y) &= g(x+iy) \\ &= \operatorname{Re} \left\{ g(x+iy) \right\} + i \operatorname{Im} \left\{ g(x+iy) \right\} \end{aligned} \quad (6)$$

Rewriting  $x + iy = x - i(h - y) + ih$  in the expression on the right-hand side (RHS) of equation (6) yields

$$\text{RHS of eq. (6)} = \operatorname{Re} \left\{ g[x-i(h-y)+ih] \right\} + i \operatorname{Im} \left\{ g[x-i(h-y)+ih] \right\}$$

The substitution of  $g = U - iV$  in the above equation yields

$$\begin{aligned} \text{RHS of eq. (6)} &= \text{Re} \{ U[x-i(h-y),h] - iV[x-i(h-y),h] \} \\ &\quad + i \text{Im} \{ U[x-i(h-y),h] - iV[x-i(h-y),h] \} \end{aligned} \quad (7)$$

Thus equation (6) can be rewritten with the form of equation (7) as

$$\begin{aligned} U(x,y) - iV(x,y) &= \text{Re} \{ U[x-i(h-y),h] \} + \text{Im} \{ V[x-i(h-y),h] \} \\ &\quad - i \text{Re} \{ V[x-i(h-y),h] \} + i \text{Im} \{ U[x-i(h-y),h] \} \end{aligned} \quad (8)$$

Hence equating the imaginary part of equation (8) yields

$$V(x,y) = \text{Re} V[x-i(h-y),h] - \text{Im} U[x-i(h-y),h] \quad (9)$$

If  $f(x)$  is a real function, then

$$\begin{aligned} \text{Re} \{ f(z) \} &= \text{Re} \{ f(\bar{z}) \} \\ \text{Im} \{ f(z) \} &= -\text{Im} \{ f(\bar{z}) \} \end{aligned} \quad (10)$$

where  $z = x + iy$  and its conjugate  $\bar{z} = x - iy$ .

Using the relationship of equation (10), we rewrite equation (9) as

$$V(x,y) = \text{Re} \{ V[x+i(h-y),h] \} + \text{Im} \{ U[x+i(h-y),h] \} \quad (11)$$

which is identical to equation (4) as derived by the Fourier transform and Wiener-Hopf techniques (without the  $\beta$  factor).

#### ILLUSTRATIVE EXAMPLES

Examples selected to demonstrate the model profile predicted by equation (5) are given for a general profile in solid-wall and open-jet tunnels and for a circular-arc airfoil in a solid-wall tunnel.

### Solid Wall Tunnel

Assume the interface  $y = h$  located at the tunnel wall; hence  $V_T(x, y) = 0$  for a solid-wall tunnel. We obtain the velocity distribution  $U_T(x, h)$  by taking the inverse transform of equation (2):

$$U_T(x, h) = \frac{-1}{2h\beta^2} \int_{-\infty}^{\infty} F'(\xi) \tanh \frac{\pi}{2\beta h} (\xi - x) d\xi \quad (12)$$

where  $F'(\xi)$  is a general function of model geometry.

Substituting  $U_T(x, h)$  of equation (12) and  $V_T(x, h) = 0$  into the right-hand side of equation (5), we obtain

$$\begin{aligned} & \lim_{y \rightarrow 0} \beta \operatorname{Im} \left\{ U_T[x + i\beta(h-y), h] \right\} \\ &= \frac{-1}{2\beta h} \lim_{y \rightarrow 0} \operatorname{Im} \left\{ \int_{-\infty}^{\infty} F'(\xi) \tanh \frac{\pi}{2\beta h} [\xi - x - i\beta(h-y)] d\xi \right\} \\ &= \frac{-1}{2\beta h} \int_{-\infty}^{\infty} F'(\xi) \lim_{y \rightarrow 0} \operatorname{Im} \left\{ \tanh \frac{\pi}{2\beta h} [(\xi - x) - i\beta(h-y)] \right\} d\xi \end{aligned} \quad (13)$$

It should be noted that for  $\xi - x \neq 0$ ,

$$\begin{aligned} & \lim_{y \rightarrow 0} \operatorname{Im} \left\{ \tanh \frac{\pi}{2\beta h} [(\xi - x) - i\beta(h-y)] \right\} \\ &= \lim_{y \rightarrow 0} \frac{-\sin \frac{\pi}{h} y}{\cosh \frac{\pi}{\beta h} (\xi - x) - \cos \frac{\pi}{h} y} \\ &= 0 \end{aligned}$$

Equation (13) becomes

$$\begin{aligned}
 & \frac{-1}{2\beta h} \int_{-\infty}^{\infty} F'(\xi) \lim_{y \rightarrow 0} \frac{-\sin \frac{\pi}{h} y}{\cosh \frac{\pi}{\beta h} (\xi-x) - \cos \frac{\pi}{h} y} d\xi \\
 &= \frac{-1}{2\beta h} F'(x) \lim_{y \rightarrow 0} \int_{-\infty}^{\infty} \frac{-\sin \frac{\pi}{h} y}{\cosh \frac{\pi}{\beta h} (\xi-x) - \cos \frac{\pi}{h} y} d\xi \\
 &= F'(x) \frac{2}{\pi} \lim_{y \rightarrow 0} \tan^{-1} \left( \frac{\sin \frac{\pi}{h} y}{1 - \cos \frac{\pi}{h} y} \right) \\
 &= F'(x)
 \end{aligned}$$

Thus the right-hand side of equation (5) is equal to  $F'(x)$ . (14)

This result is expected; that is, equation (5) is verified.

#### Open-Jet Tunnel

Again, assume the interface  $y = h$  is located at the tunnel test section boundary and  $U_T(x, h) = 0$  for an open-jet tunnel. The vertical velocity distribution  $V_T(x, h)$  is obtained by taking the inverse transform of equation (2):

$$V_T(x, h) = \frac{1}{2\beta h} \int_{-\infty}^{\infty} F'(\xi) \operatorname{sech} \frac{\pi(\xi-x)}{2\beta h} d\xi \quad (15)$$

Substituting  $V_T(x, h)$  of equation (15) and  $U_T(x, h) = 0$  into the right-hand side of equation (5), we obtain

$$\begin{aligned}
 & \lim_{y \rightarrow 0} \operatorname{Re} \left\{ V_T[x+i\beta(h-y), h] \right\} \\
 &= \frac{1}{2\beta h} \int_{-\infty}^{\infty} F'(\xi) \lim_{y \rightarrow 0} \operatorname{Re} \left\{ \operatorname{sech} \frac{\pi[(\xi-x)-i\beta(h-y)]}{2\beta h} \right\} d\xi
 \end{aligned} \quad (16)$$

It is noted that for  $\xi - x \neq 0$ ,

$$\begin{aligned} & \lim_{y \rightarrow 0} \operatorname{Re} \left\{ \operatorname{sech} \frac{\pi}{2\beta h} [(\xi-x) - i\beta(h-y)] \right\} \\ &= \lim_{y \rightarrow 0} \frac{\cosh \frac{\pi}{2h\beta} (\xi-x) \sin \frac{\pi}{2h} y}{\sinh^2 \frac{\pi}{2h\beta} (\xi-x) + \sin^2 \frac{\pi}{2h} y} \\ &= 0 \end{aligned}$$

Then equation (16) becomes

$$\begin{aligned} & \frac{1}{2\beta h} F'(x) \lim_{y \rightarrow 0} \int_{-\infty}^{\infty} \frac{\cosh \frac{\pi}{2h\beta} (\xi-x) \sin \frac{\pi}{2h} y}{\sinh^2 \frac{\pi}{2h\beta} (\xi-x) + \sin^2 \frac{\pi}{2h} y} d\xi \\ &= \frac{1}{2\beta h} F'(x) \frac{2h\beta}{\pi} \lim_{y \rightarrow 0} \tan^{-1} \frac{\sinh \frac{\pi}{2\beta h} (\eta)}{\sin \frac{\pi}{2h} y} \Bigg|_{-\infty}^{\infty} \\ &= F'(x) \end{aligned}$$

Thus we have verified the profile formula, equation (5).

#### REFERENCE

1. Collins, R. E.: *Mathematical Methods for Physicists and Engineers*. Rheinhold Book Corp., 1968.

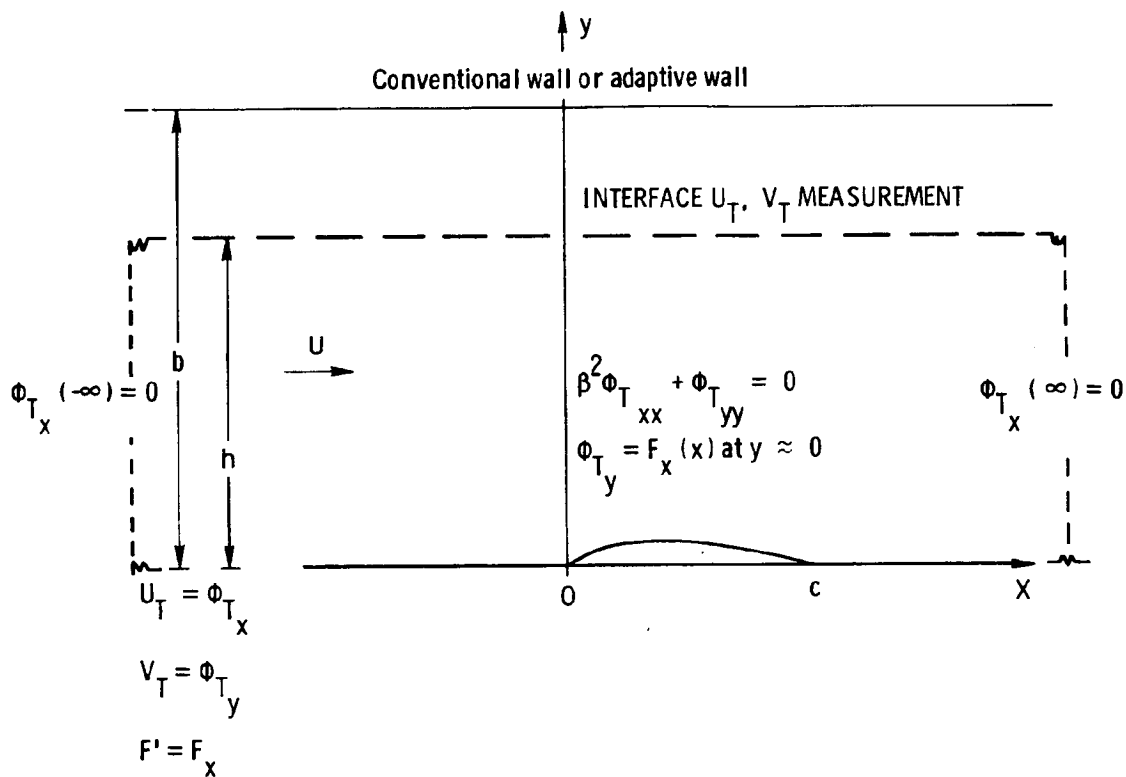


Figure 1.- Boundary value problem of tunnel simulation with boundary measurements.

omit

SESSION Vc

CORRECTION METHODS USING MEASURED BOUNDARY DATA

Chairman: R. L. Bengelink, Boeing

N85 12032

121

EXPERIENCES WITH A HIGH-BLOCKAGE MODEL TESTED  
IN THE NASA AMES 12-FOOT PRESSURE WIND TUNNEL

David W. Coder  
David W. Taylor Naval Ship Research and Development Center  
Bethesda, Maryland

PRECEDING PAGE BLANK NOT FILMED

Preceding page blank

## SUMMARY

Because of the interest in representing the flow around full-scale ships, naval and marine hydrodynamic researchers have turned to subsonic wind tunnels in order to attain Reynolds numbers as high as possible. While the attainment of length Reynolds numbers needed to represent a full-scale ship (above 1000 million) is beyond the capability of present wind tunnels, Reynolds numbers above 100 million are possible and represent an order of magnitude improvement over typical hydro-mechanics facilities. As part of the quest to attain the largest possible Reynolds number for any tunnel facility, large models with high blockage (greater than 1 percent) are used which can result in significant wall interference effects. Some experiences with such a high blockage model (2.6 percent) tested in the NASA Ames 12-Foot Pressure Wind Tunnel are summarized here.

In the Ames experiment, hull static pressure distributions, hull boundary layer flows (velocity profiles), stern flows (velocity components and Reynolds stresses), and resistance of a body of revolution model were measured. The static pressure distribution on the wall of the tunnel and the tunnel wall boundary layer velocity profile (at the mid-model location) were also measured to aid in the assessment of wind tunnel wall interference effects. These tunnel wall measurements were invaluable in interpreting the test results and performing wind tunnel wall corrections. For example, the two methods that were used during the test to calculate the tunnel velocity failed to produce reasonable results for model hull static pressure coefficient over the entire range of test conditions. Reasonable results were obtained (during data analysis after the test) only by developing an alternate method of determining the tunnel velocity using the tunnel wall measurements. Further, comparisons of blockage effects calculated separately from the model hull static pressure distributions and from the tunnel wall static pressure distributions indicated the extent of an interference effect at the stern of the model caused by a downstream strut in the tunnel diffuser. This enabled a tunnel strut interference correction to be made to the measured stern flow and tunnel thrust (horizontal buoyancy) calculations.

The main results of the experiment relating to wind tunnel wall interference effects are as follows:

- The high blockage of the model caused a somewhat higher velocity over the forward part of the model than that predicted for infinite fluid. Measured boundary layer velocity profiles over this part of the model, where the boundary layer is "thin", agreed well with calculated velocity profiles assuming an infinite fluid. Also, no noticeable differences were obtained with the boundary layer calculations whenever the measured hull static pressure distributions were used to represent the in-the-tunnel situation in the calculations.
- The tunnel strut interference caused a lower velocity over the model stern than that predicted for an infinite fluid. Here, the boundary layer may be considered "thick" and developing in an adverse pressure gradient. The measured stern flow velocity profiles were significantly different from those calculated for an infinite fluid. Fair agreement was obtained between the measured profiles and calculated ones whenever measured hull static pressure coefficient distributions were used to represent the in-the-tunnel situation in the calculations.
- The values of the tunnel thrust (horizontal buoyancy) calculated from the model hull static pressure distributions were consistently lower than those obtained from tunnel wall measurements. This is due largely to the strut interference effect that created a pseudo "pressure recovery" at the stern of the model.

### CHARACTERISTICS OF CANDIDATE WIND TUNNELS

The Reynolds number based on length for a full-scale ship can be as large as 1000 million and higher. In order to perform experiments as close to this Reynolds number as possible under controlled conditions, wind tunnels in the United States and Canada (refs. 1 through 5) were considered for subsonic flow (Mach number less than or equal to 0.3) high Reynolds testing of ship models. This led to consideration of the large subsonic, pressure subsonic, and transonic wind tunnels as shown ranked in Figure 1. The tunnels were ranked based on a high Reynolds number figure of merit which is the quoted maximum Reynolds number per length times the square root of the test section cross sectional area. Other characteristics of the tunnels listed in the table are: (a) the ability to change Reynolds number and Mach number independently, (b) the quality of flow (turbulence level), and (c) the availability of the tunnel during the proposed testing period. The National Transonic Facility (NTF, ref. 6) and the NASA Ames 80x120 were not considered for the present test but are recent inclusions for completeness and future consideration. Even though the NASA Ames 40x80 wind tunnel has the largest Reynolds number figure of merit (except for the NTF and the 80x120), the other tunnel characteristics made the NASA Ames 12-Foot Pressure Wind Tunnel more attractive for the present experiment. Also, in the smaller tunnel, the model needed for equivalent Reynolds numbers in the larger tunnel was proportionally smaller. This reduced model construction and transportation costs and made for easier handling.

RANK	TUNNEL	TYPE	$R_N/FT \times 10^{-6}$ AT $M_N \leq 0.3$	$R_N/FT \times \sqrt{A}$ $\times 10^{-6}$	$R_N$ AND $M_N$ INDEP. VARIABLE	TURBULENCE LEVEL SAT.	AVAILABILITY
A	NATIONAL TRANSONIC FACILITY (2.5M x 2.5M)	TRANSONIC	70.7	580	✓	✓	
B	AMES 80 FT x 120 FT	SUBSONIC	2.1	206	X	X	
1	AMES 40 FT x 80 FT	SUBSONIC	2.1	119	X	X	✓
2	AMES 12 FT	SUBSONIC PRESSURE	9	96	✓	✓	✓
3	NAE 5 FT x FT	TRANSONIC	14.6	73	✓	✓	✓
4	UNITED AIRCRAFT 18 FT	SUBSONIC	4.2	67	X	X	
5	LOCKHEED 26 FT x 30 FT	SUBSONIC	2.3	64	X	X	
6	NAE 15 IN. x 60 IN.	TRANSONIC	22.8	57	✓	✓	✓
7	LANGLEY 30 FT x 60 FT	SUBSONIC	1	42	X	X	
8	VERTOL 20 FT x 20 FT	SUBSONIC	2	40	X	X	
9	DOUGLAS 4 FT x 4 FT	TRANSONIC	10*	40	✓	✓	AFTER JAN 79

\*THIS TUNNEL IS BEING MODIFIED FOR CRYOGENIC OPERATION WHICH IS EXPECTED TO INCREASE THE MAXIMUM REYNOLDS NUMBER BY ABOUT 5.0

Figure 1

## HIGH REYNOLDS NUMBER/LOW BLOCKAGE TRADE-OFF

In order to obtain the highest Reynolds number possible in a wind tunnel, the largest possible model should be used. However, the larger the model becomes, the larger the solid blockage and the associated wind tunnel wall effects become. In order to make the trade-off between high Reynolds number and low blockage, Figure 2 was constructed for the subject body of revolution model. The maximum Reynolds number may be calculated as the maximum Reynolds number per length ( $R_n/\text{length}$ ) times the model length ( $L$ ). The solid blockage ( $b$ ) is the model cross sectional area ( $\pi R^2$ ) divided by the tunnel cross sectional area ( $A$ ). Thus for the model in question the maximum Reynolds number equation may be rearranged to yield

$$(R_n/\text{length}) \times (A)^{0.5} = 0.0806 (R_n)/(b)^{0.5}$$

where the left side is the tunnel Reynolds number figure of merit and the right side is composed of the desired experimental parameters of maximum model Reynolds number and model solid blockage. It is seen from Figure 2 that for the NASA Ames 12-Foot Pressure Wind Tunnel (refs. 1 and 2), that a Reynolds number of 100 million can be obtained with a model having less than 1 percent solid blockage. Conversely, it is seen that for 1 percent blockage only two tunnels (excluding the NTF (ref. 6) and the NASA Ames 80x120) can obtain model Reynolds numbers of 100 million. Note that, in the future, full-scale Reynolds numbers of interest (1000 million and above) would be obtainable with a 2 percent solid blockage model in the NTF. For the present experiment a 20-ft-long model with a solid blockage of about 2.6 percent in the NASA Ames 12-Foot Pressure Wind Tunnel was chosen.

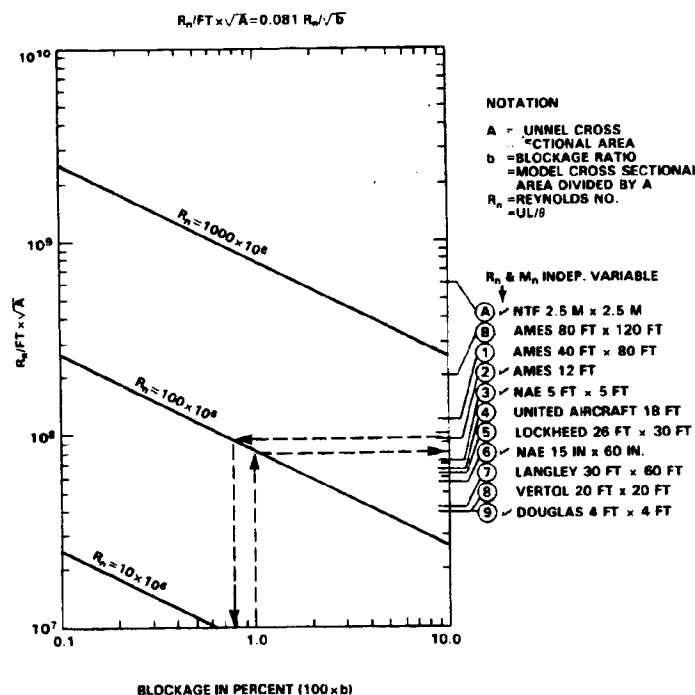


Figure 2

### DEFINITION OF TUNNEL VELOCITY

The ideal wind tunnel would be one in which the blockage would be so small that the velocity of flow near and along the tunnel wall would be essentially the same as the free-stream velocity for the model in infinite flow. However, in a conventional tunnel (solid and straight walled) of finite size as show in Figure 3, the blockage due to the model, support structure, boundary layers on the model and tunnel walls, and the wakes of the model and support structure cause a general increase in velocity of flow around the model compared with that obtained in an infinite fluid. Since the main purpose for the experiment was to determine the flow characteristics around the model in infinite flow, the measurements in the tunnel needed to be corrected for any tunnel effects. In order to make these wind tunnel wall corrections for the present experiment it was considered essential to make measurements of the tunnel wall static pressure distribution and tunnel wall boundary layer profiles. These measurements were not only used to calculate the classical blockage corrections for a solid wall tunnel but also added understanding to all of the measured data. In particular, these wall measurements allowed a more reasonable determination of the tunnel velocity and equivalent infinite-fluid free-stream velocity than what was provided by the standard tunnel method. Further, these measurements together with model measurements provided a means to evaluate the interference effect due to a large strut (used for sting mount models) located in the tunnel diffuser.

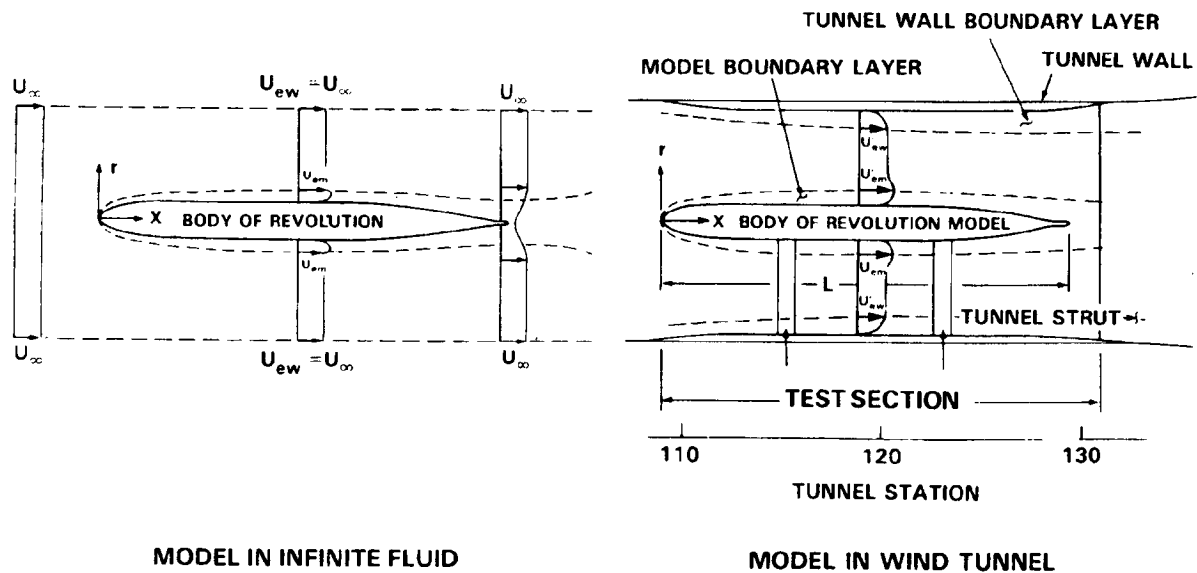


Figure 3

## DETERMINATION OF TUNNEL VELOCITY

For the present experiment the model almost entirely occupied the tunnel test section so that nowhere in the tunnel did there exist a uniform flow that could be considered the infinite fluid free-stream velocity. Thus, the measurement of this velocity was indirect. Two methods of measurement were employed during testing. The first method (ref. 7) was based on measurement of tunnel total pressure and the static wall pressure in the nozzle, known geometry of the tunnel (ref. 8), calculation of the maximum solid blockage, and estimates of the drag coefficients (ref. 9) for the model and support struts. The velocity determined this way is labeled "U<sub>A</sub>". The second method, which was much simpler, was based on the tunnel total pressure and the static pressure in the plenum chamber around the test section. This velocity is labeled "U<sub>A'</sub>". During data analysis after the experiment, a third method was used which made the model hull static pressure distribution results more consistent. Here the velocity at the edge of the tunnel wall boundary layer at the mid-model location (U<sub>mm</sub>) was determined from the tunnel wall static pressure at that location and the tunnel total pressure. This velocity was then divided by the classical blockage factor (ref. 10) determined for that location (1+ε<sub>mm</sub>). These three "tunnel reference velocities" are compared with the theoretically predicted value of infinite fluid free-stream velocity in Figure 4. It is seen that U<sub>mm</sub>/(1+ε<sub>mm</sub>) best represents the predicted free-stream velocity over the range of test conditions. The first methods appear to be adequate for the lower Reynolds number range which occurred under atmospheric tunnel conditions. The discrepancy appears at the higher Reynolds numbers and under pressurized tunnel conditions.

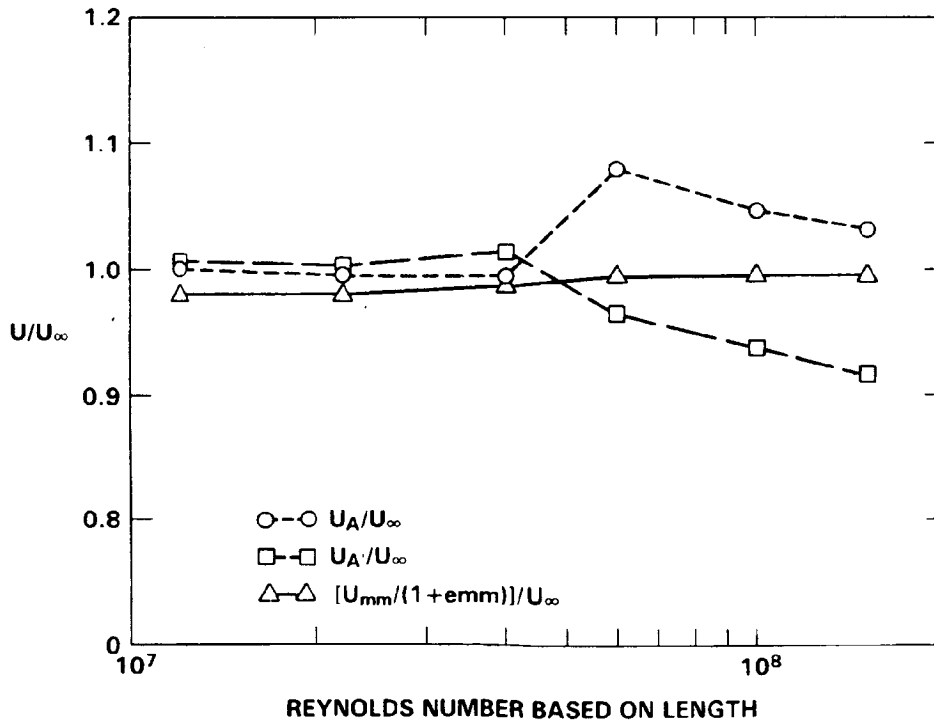


Figure 4

## TUNNEL SOLID BLOCKAGE

A graphical representation of the solid blockage for the present model in the NASA Ames 12-Foot Pressure Wind Tunnel (ref. 8) is shown in Figure 5. The cross section of the tunnel test section is circular with an inside diameter of 12 ft. However, for part of the test section, there are ramped flat plates about 4 ft wide on the floor, ceiling, and both sides that occupy about 4.1 percent of the tunnel cross sectional area. The model was placed such that its nose and tail would span the length of the ramped plates. Thus the model nose was in a slight nozzle area and its tail was in a slight diffuser area but most of the model was in the straight walled part of the test section. The model solid blockage based on the total circular tunnel area was about 2.3 percent and doubled to 4.6 percent at the two model support locations. The tunnel strut, used to support a sting mechanism, is mostly located in the tunnel diffuser so that its blockage is compensated for by the increase in tunnel area. However, part of the strut is in front of the diffuser and causes a solid blockage of about 5.3 percent at the end of the test section. Thus it can be seen that the solid blockage varies significantly throughout the tunnel and is of such a magnitude that wind tunnel wall interaction effects must be considered.

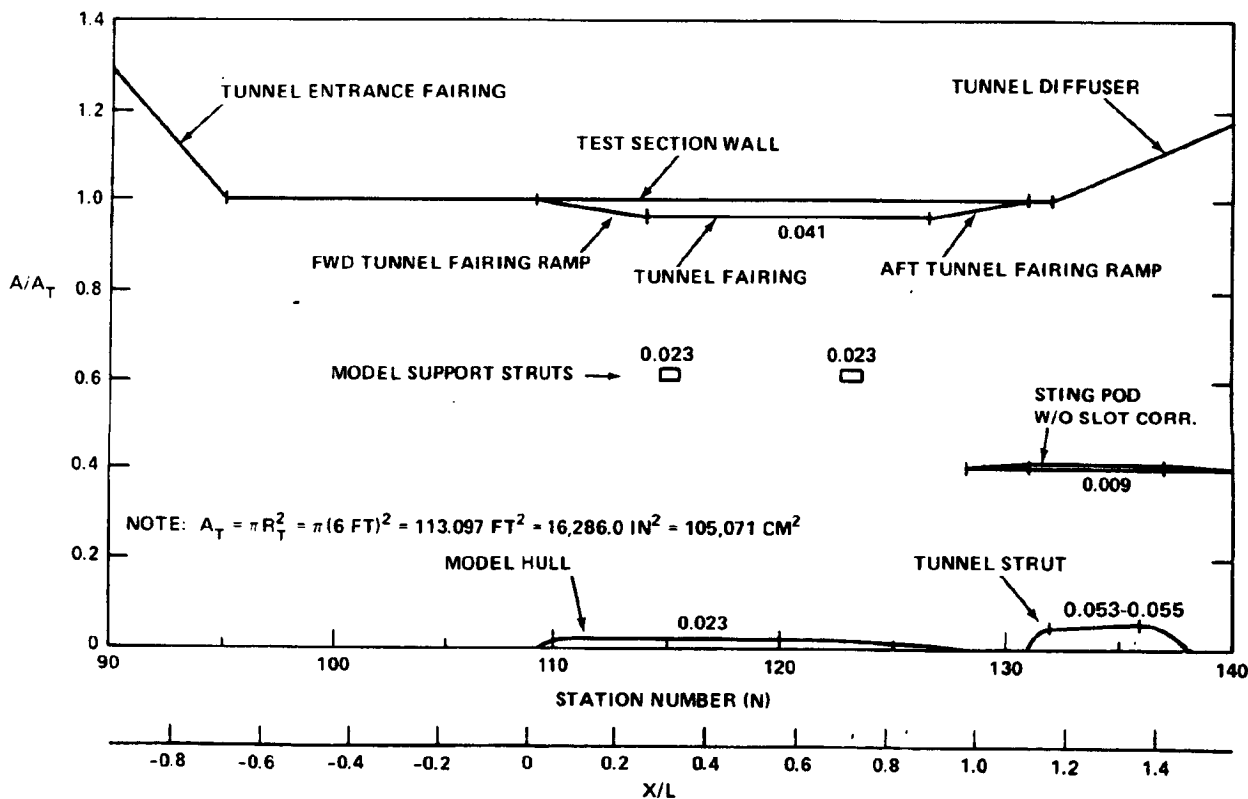


Figure 5

## TYPICAL TUNNEL WALL STATIC PRESSURE DISTRIBUTIONS

Typical distributions of tunnel wall static pressure with no model in the tunnel (ref. 11) and with the model in place are shown in Figure 6. These data were obtained from circumferential static rings (four static pressure taps located in an "X" pattern and hooked together), static pressure taps located 45 deg from the bottom on the port and starboard (left and right looking forward) sides of the tunnel. One additional wall-mounted static tube was added on the port side across from the mid-bow of the model. The data are seen to have a lot of scatter and several trends are noticeable. First of all, since these pressure coefficients are based on  $U_{\text{m}}$ , the average of the port and starboard measurement at mid model ( $X/L = 0.5$ ) is zero. Also, the starboard values are in general lower than the port values. Since all the tunnel wall pressures (except the most forward ring pressure) were measured with a common pressure gage (by use of a Scanni-valve arrangement), this indicated that the flow velocity was not perfectly uniform across the tunnel and was slightly higher on the starboard side. Also observable is a significant dip in the pressure near the rear mounting strut indicating a local increase in velocity. No dip is obvious near the forward mount, perhaps due to the sparseness of measurements. Further, note the rise of pressure near the stern of the model due partly to the decrease in model diameter but mostly due to the disappearance of the side wall plates. Proceeding down the diffuser there is a significant dip and then an increase of pressure. This indicates that the flow was not gently diffused and may indicate an area for possible tunnel improvement.

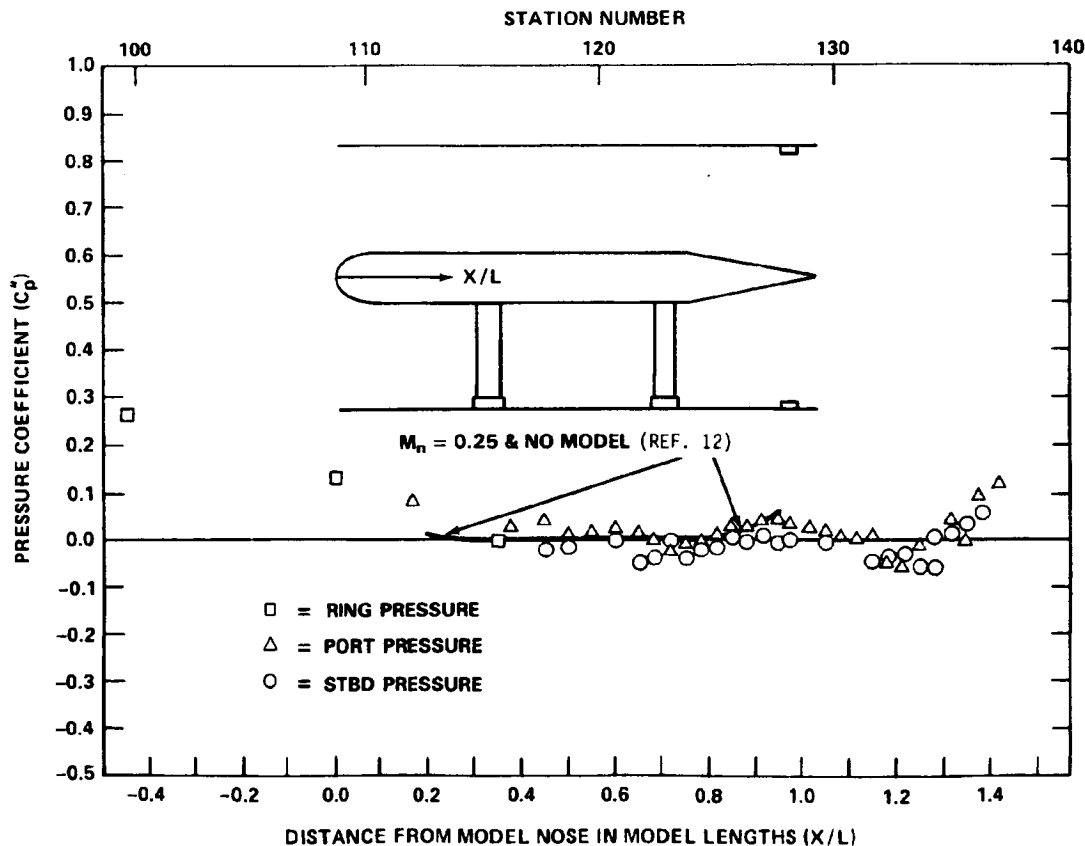


Figure 6

### TYPICAL MODEL SKIN STATIC PRESSURE DISTRIBUTION

A typical set of measurements of model hull static pressure taken along the top of the model (to stay as far away from the model support strut influence as possible) are presented in Figure 7. These data are pressure coefficients based on  $U_{\infty}$ , the velocity near the tunnel wall at the mid-model location. As is to be expected, the velocity accelerates ( $C_p$  decreases) around the bow, becomes almost constant over the parallel middlebody ( $X/L$  from about 0.16 to about 0.62), accelerates over the front half of the stern, and then shows a steady pressure recovery over the back half of the stern. The slight increase in velocity over the parallel middlebody is due to increasing viscous blockage caused by boundary layer growth on the model and the walls of the tunnel. Apparent near the locations of the model support struts are local dips in pressure. These dips were disregarded when the data were hand-smoothed in order to be used for input to an axisymmetric boundary layer code (refs. 12 and 13).

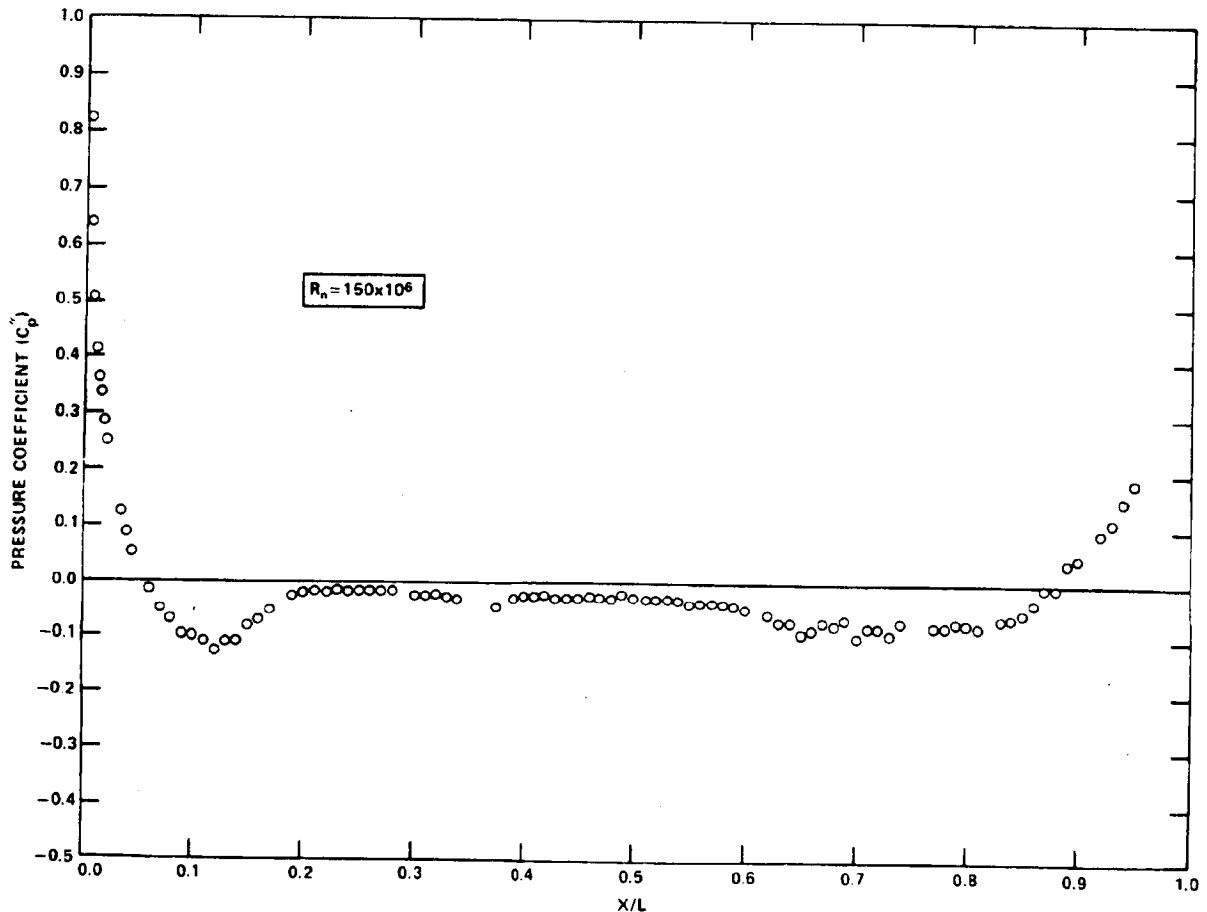


Figure 7

## BLOCKAGE EFFECT ON TUNNEL WALL AND MODEL SKIN

If the boundary layers on the wall of the tunnel and the hull of the model are assumed to be "thin" (no pressure gradient across the layer) and the blockage effect on the boundary layer edge velocity was assumed to be  $Ue' = (1 + e)Ue$  where  $e$  is the local blockage ratio (ref. 10), then the in-the-tunnel measured pressure coefficient based on  $U_{mm}$  and the infinite fluid calculated pressure coefficient based on  $U_{\infty}$  were related as

$$(1 - Cp'')/(1 - Cp) = [(1 + e)/(1 + emm)]^2$$

Thus, the blockage effect was determined from both the tunnel wall measurements of  $Cp''$  ( $Cp$  for the wall is zero) and the measured  $Cp''$  and the calculated  $Cp$  for the model. However when both blockage effects are plotted, as in Figure 8, a discrepancy is observed. The wall values are fairly flat but the model values show an approximate linear drop as the end of the model is approached. These data indicate that at the location of the stern of the model, the flow is significantly different in the center of the tunnel than at the walls. This condition is attributed to the upstream pressure field from the tunnel strut in the diffuser. The effect was considered as a negative blockage effect (slowing of the flow), assumed linear (as shown in Figure 8) as the strut is approached, and used to extrapolate the pressure coefficient to the end of the model.

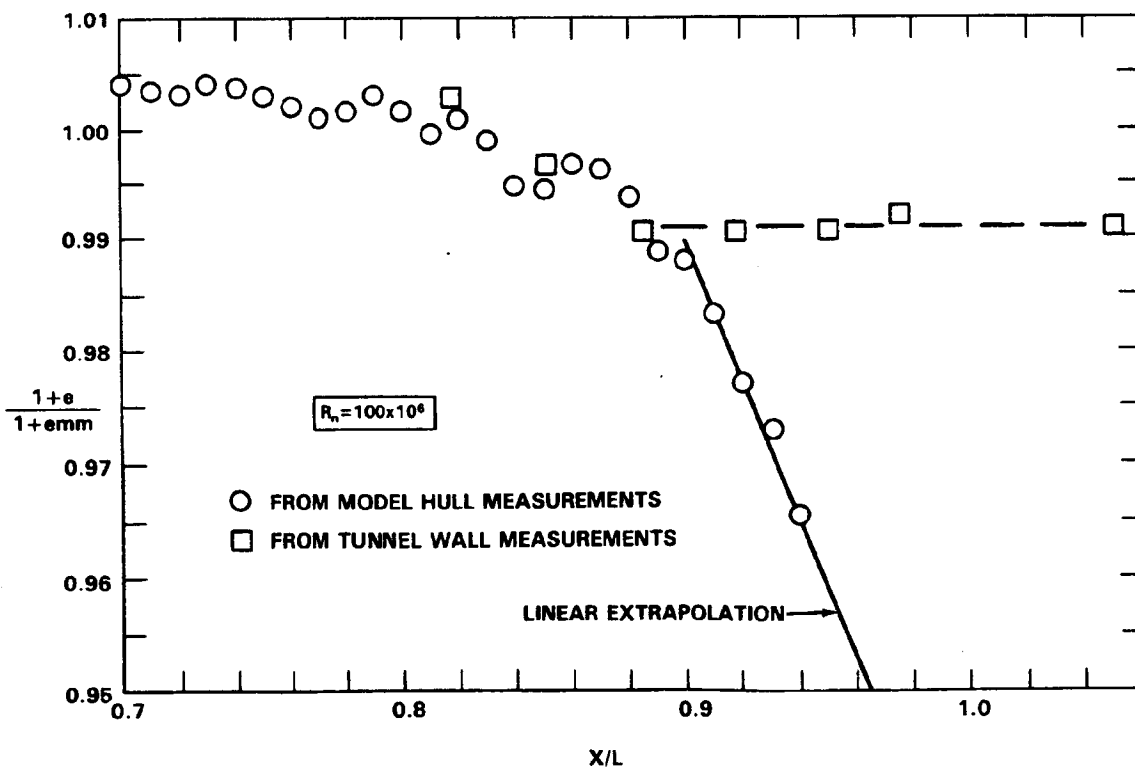


Figure 8

## INTERFERENCE EFFECT OF TUNNEL STRUT

The design of the present experiment included calculations that approximated the interference effect of the strut in the diffuser of the tunnel using uniform, infinite fluid, potential flow past a 2-D section of the strut. It was thought that this would represent a worst case for upstream effects. The results of this analysis, as shown in Figure 9, indicate that at a distance of about 2 ft in front of the strut, the velocity would be slowed down only about 2.5 percent and that the effect decays very little with increasing distance. The rationale for locating the stern measurement plane was to make sure that it was at least 2 ft from the strut. If the analysis indeed represents a worst case, the effects would be less than indicated. Sufficient measurements of wall and model pressures made during the experiment indicate that the strut effect is of the same order as the prediction. Thus, the stern flow was significantly affected and significant corrections had to be applied to these data to convert them to infinite-fluid predictions.

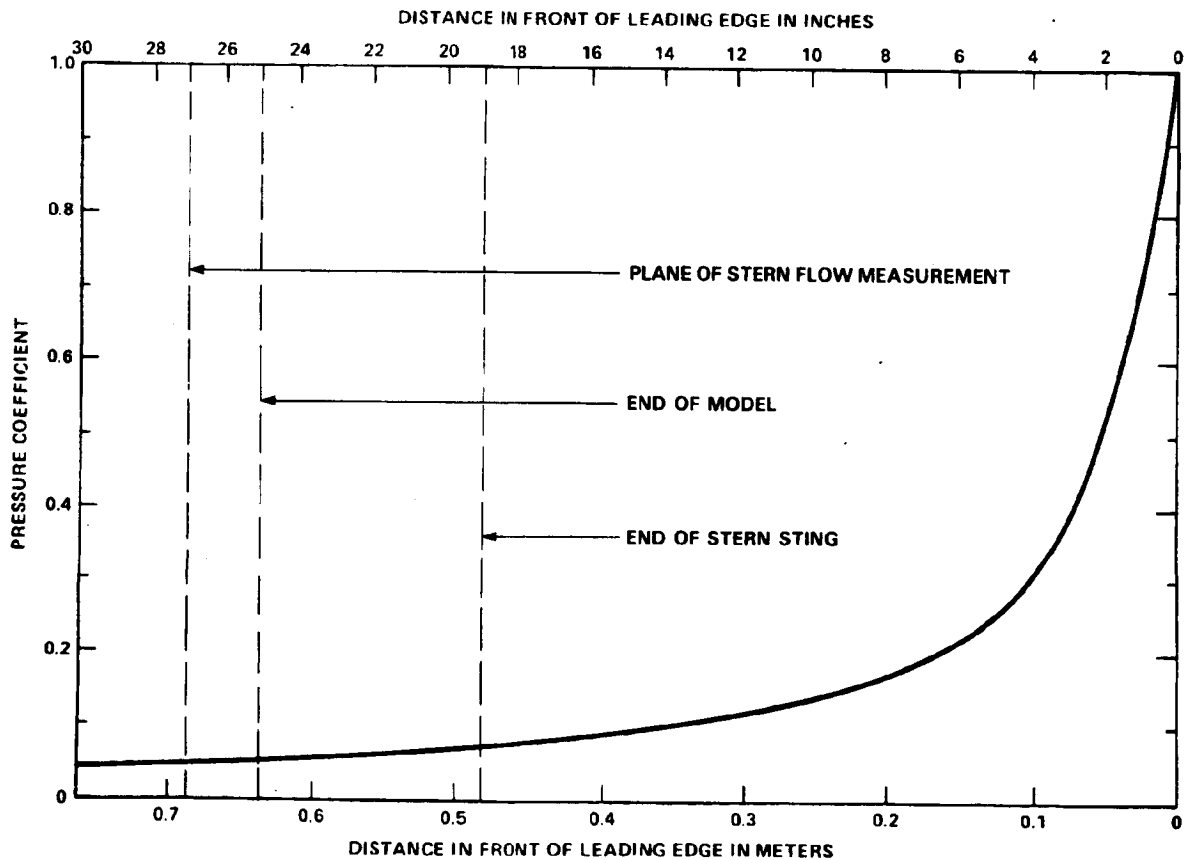


Figure 9

## MEASURED AND CALCULATED MODEL SKIN STATIC PRESSURE DISTRIBUTION

The model hull static pressure coefficient distributions measured in the tunnel and calculated for infinite fluid using an axisymmetric boundary layer code (refs. 12 and 13) for a Reynolds number of 100 million are shown in Figure 10. In general, the velocities measured in the tunnel are lower (higher  $C_p$ ) than the infinite-fluid velocities over the bow of the model and higher (lower  $C_p$ ) over much of the remaining hull except in the region toward the end of the stern. For the stern region aft of about  $X/L$  greater than 0.9, velocities for the measurements in the tunnel are much lower than for infinite fluid. This was attributed to the pressure field created ahead of the large floor-to-ceiling strut permanently installed in the diffuser of the wind tunnel.

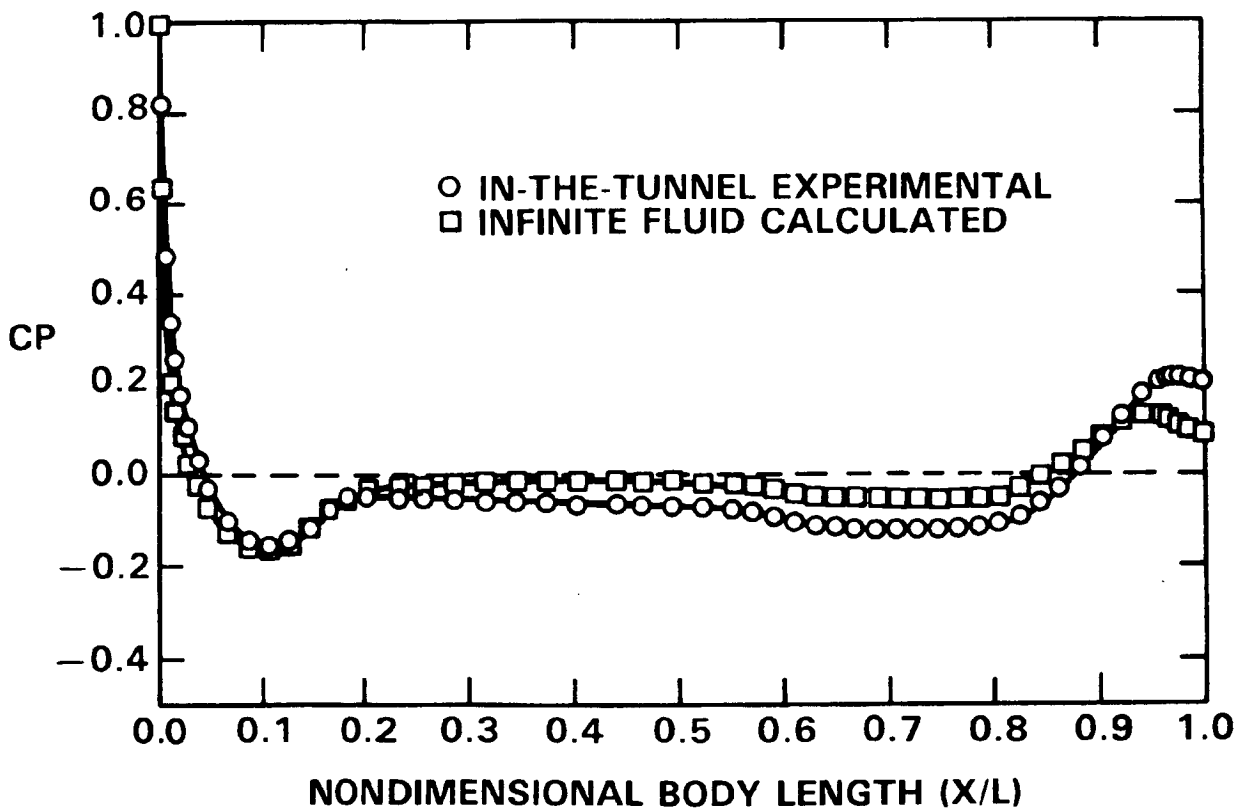


Figure 10

MEASURED AND CALCULATED BOUNDARY LAYER VELOCITY PROFILES

In Figure 11 the in-the-tunnel measured "thin" boundary layer velocity profiles along the length of the model are compared with profiles calculated assuming infinite fluid and measured model hull pressure distributions (ref. 14). The two sets of calculated profiles are not distinguishable from each other (and are shown by a common curve in the figure) even though the static pressure distributions used to calculate them are somewhat different. These calculations indicate that the wind tunnel wall interference effect on thin boundary layer growth for this situation is negligible. Comparing the calculated profiles to the measured ones, it is seen that the calculated profiles are consistently slightly fuller than the experimental ones.

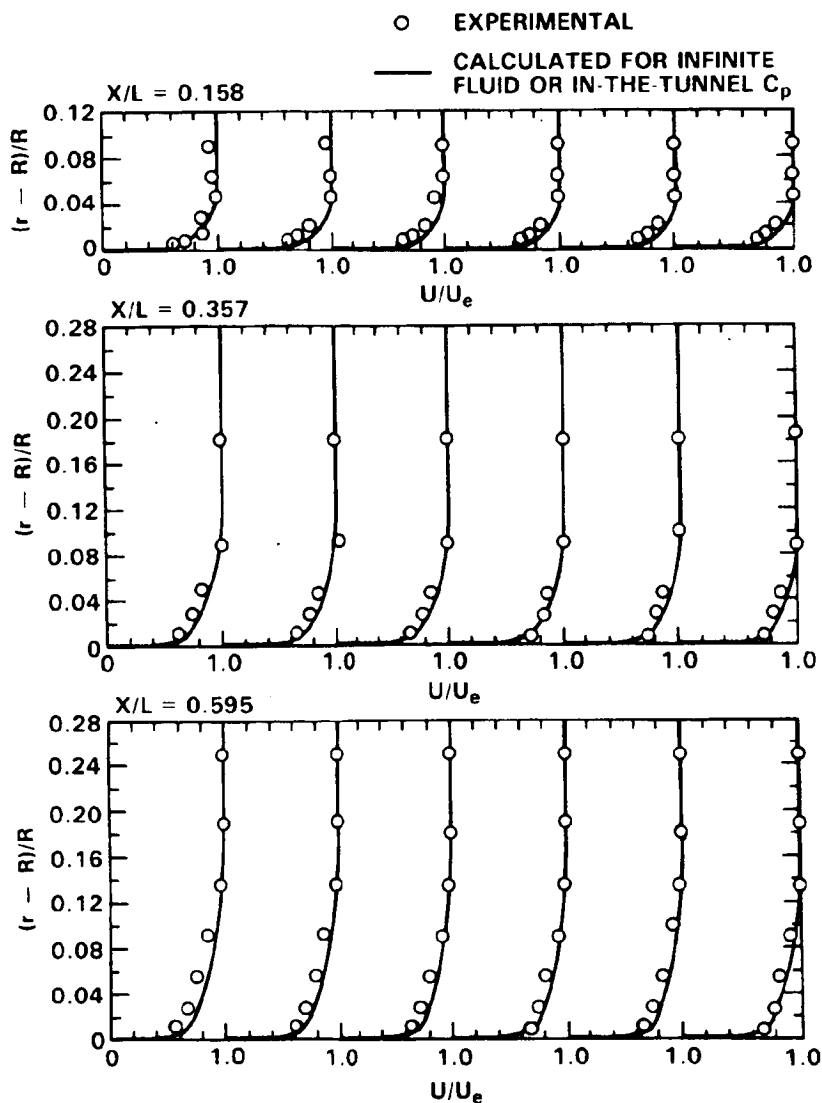


Figure 11

## MEASURED AND CALCULATED STERN FLOW VELOCITY PROFILES

A comparison of the measured and calculated "thick" boundary layer velocity profiles on the stern of the model (from ref. 14) is shown in Figure 12. Here there is a considerable difference between the two calculated profiles depending upon whether infinite fluid or in-the-tunnel measured static pressure distributions are used for the calculations. The stern flow is very sensitive to the distribution of pressure since the boundary layer is thick at the stern and is developing in an adverse pressure gradient. Further it is seen that the calculated results obtained using the measured static pressure distributions are in fair agreement with the measured results. The difference between the two calculated velocity profiles was used as a correction factor that was added to the experimental results to convert them to infinite-fluid predictions.

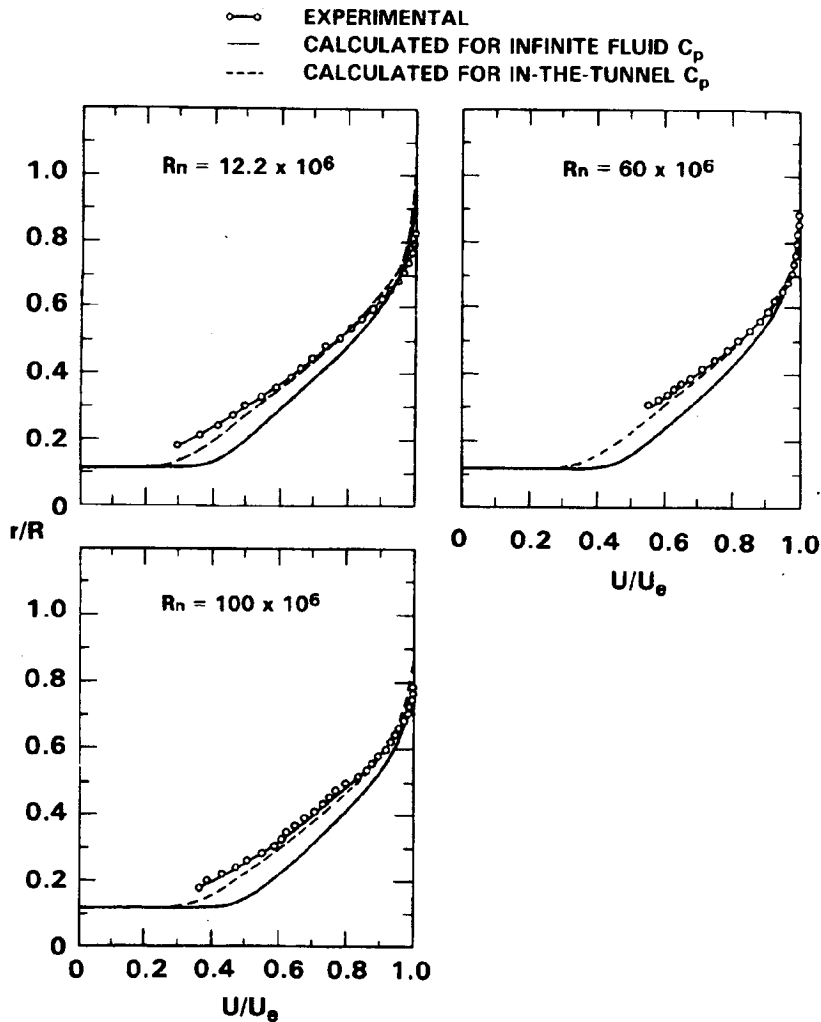


Figure 12

### TUNNEL THRUST CALCULATIONS

As shown in Figure 13, the calculation of the tunnel thrust (horizontal bouyancy) from the experimental data shows that calculations using model hull static pressure distributions are consistently lower than those obtained from tunnel wall measurements. This is due largely to the strut interference effect that created a pseudo "pressure recovery" at the stern of the model.

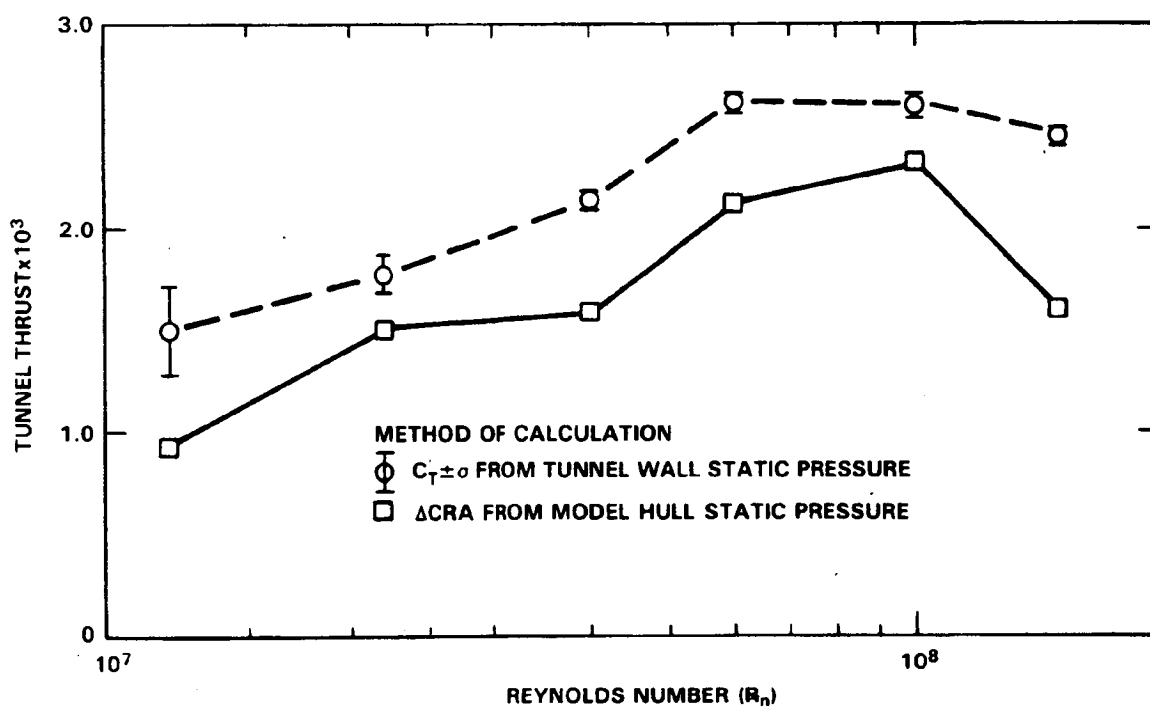


Figure 13

## REFERENCES

1. Characteristics of Six Research Wind Tunnels of the Ames Aeronautical Laboratory. NACA Brochure, 1957.
2. Ames Research Facilities Summary 1974. NASA TM X-69411, 1974.
3. Ohman, L. H., editor: The NAE High Reynolds Number 15 Inch x 60 Inch Two-Dimensional Test Facility, Part I; General Information. NRC-NAE Laboratory Technical Report LTR-HA-4, April 1970.
4. Raddatz, L. A.: The Douglas Aerophysics Laboratory Four-Foot Trisonic Wind Tunnel. Douglas Report DAC-59809, October 1967.
5. Cole, R. M.: Design Problems Associated with the Conversion of a Blow-Down Trisonic Wind Tunnel to Operation at Cryogenic Temperatures. Douglas Aerophysics Laboratory Paper 6610, April 1977.
6. Fuller, D. E.: Guide for Users of the National Transonic Facility. NASA TM-83124, July 1981.
7. Herriot, J. G.: Blockage Corrections for Three-Dimensional-Flow Closed-Throat Wind Tunnels, With Consideration of the Effects of Compressibility. NACA Report 995, 1950.
8. General Arrangement, Test Section and Balance Chamber at Twelve-Foot Pressure Wind Tunnel. NASA Ames Drawing A306-7902-M1, May 1979.
9. Hoerner, S. F.: Fluid-Dynamic Drag; Practical Information on Aerodynamic Drag and Hydrodynamic Resistance, Midland Park, New Jersey, 1957.
10. Pope, A. and Harper, J. J.: Low-Speed Wind Tunnel Testing. John Wiley and Sons, Inc., New York, 1966.
11. Boltz, F. W. et al.: The Boundary-Layer Transition Characteristics of Two Bodies of Revolution, a Flat Plate, and an Unswept Wing in a Low-Turbulence Wind Tunnel. NASA TN D-309, April 1960.
12. Wang, H. T. and Huang, T. T.: User's Manual for Fortran IV Computer Program for Calculating the Potential Flow/Boundary Layer Interaction on Axisymmetric Bodies. DTNSRDC Report SPD-737-01, David W. Taylor Naval Ship Research and Development Center, December 1976.
13. Wang, H. T. and Huang, T. T.: Calculation of Potential Flow/Boundary Layer Interaction on Axisymmetric Bodies. Joint ASME-CSME Applied Mechanics, Fluid Engineering, and Bio-Engineering Conference, Niagara Falls, New York, June 1979.
14. Coder, D. W.: Reynolds Number Scaling of Velocities in Axisymmetric Turbulent Boundary Layers. Presented at Fourteenth Symposium on Naval Hydrodynamics, Ann Arbor, Michigan, August 1982.

N85 12033

4  
22

REVIEW OF THE ADVANCED TECHNOLOGY AIRFOIL  
TEST PROGRAM IN THE 0.3-METER TRANSONIC CRYOGENIC TUNNEL

E. J. Ray and C. L. Ladson  
NASA Langley Research Center  
Hampton, Virginia

## INTERCHANGEABLE TEST SECTIONS IN THE 0.3-M TCT

The original three-dimensional test section was replaced with a two-dimensional test section insert during the summer of 1976, taking advantage of the interchangeable test section feature of the 0.3-m TCT (fig. 1). The two-fold purpose of this extensive modification was to assess the feasibility of two-dimensional testing at cryogenic temperatures and to take additional advantage of the very high unit Reynolds number capability of this relatively small, economical test facility. The two-dimensional insert consisted of a new contraction section, a rectangular pressure plenum encompassing a 20- x 60-cm test section and a new diffuser. The two-dimensional test section provided removable model modules which allow the complete preparation of one model during the testing of another model. In addition, provisions were made to enable computer-driven angle-of-attack and momentum rake systems and a sidewall boundary layer treatment system to be used with the two-dimensional test section. The sidewall treatment is accomplished by "removal" of the boundary layer through porous sidewall inserts.

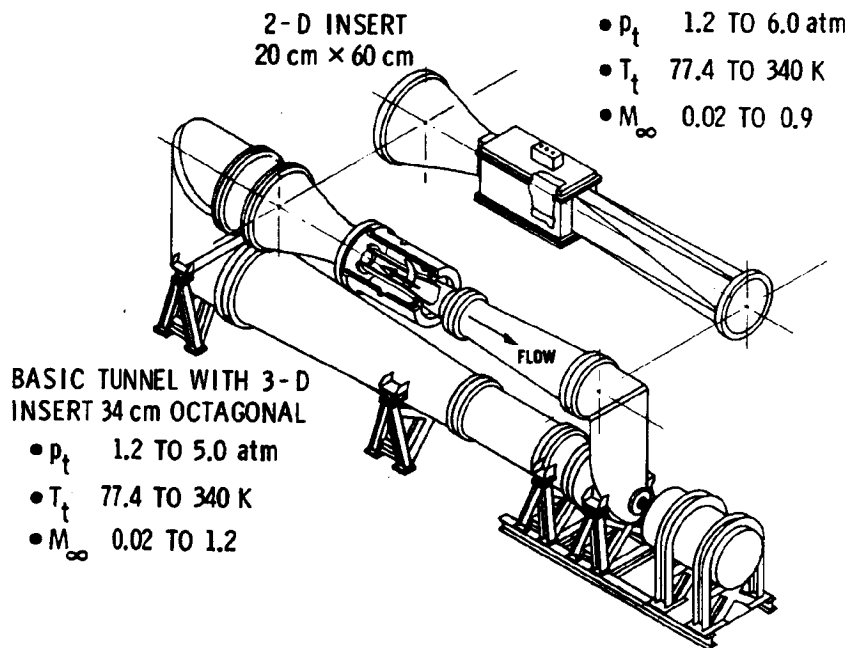


Figure 1

ORIGINAL PAGE IS  
OF POOR QUALITY

THE 0.3-METER TRANSONIC CRYOGENIC TUNNEL

ORIGINAL FACTORY  
OF POOR QUALITY

A photograph of the Langley 0.3-m TCT, in which the test program is being undertaken, is shown below. This tunnel is a continuous-flow fan-driven transonic tunnel which uses nitrogen gas as the test medium. It is capable of operation at Mach numbers from about 0.2 to 0.85 and the maximum Reynolds number (at  $M = 0.85$ ) based on a model chord of 15.24 cm (6.00 in.) is about  $50 \times 10^6$ . The basic tunnel is described in reference 1 and a description of the two-dimensional test section is contained in reference 2. Additional information on instrumentation and calibration results is available in reference 3. Shown in figure 2 are the fan drive section, low-speed diffuser, contraction and screen section, test section, and high-speed diffuser. Liquid-nitrogen injection ports and gaseous-nitrogen exhaust ports for pressure control and sidewall boundary layer bleed are also visible. The 2.2 MW drive motor is located just off the lower right-hand corner of the figure.

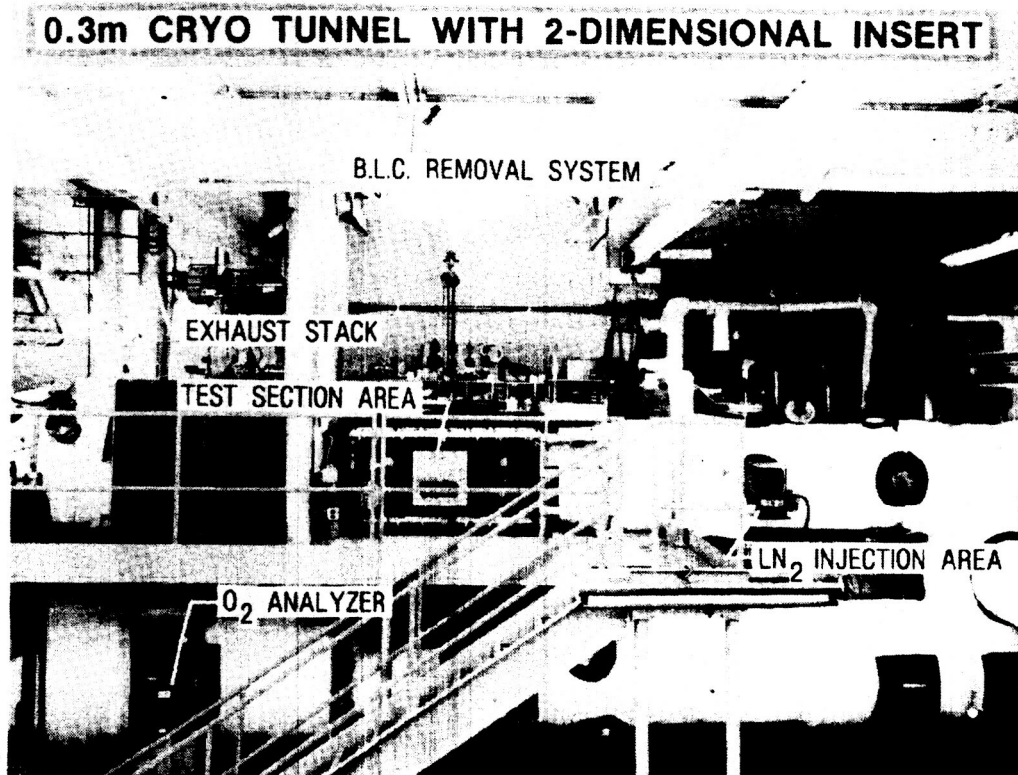


Figure 2

ORIGINAL PAGE IS  
OF POOR QUALITY

TWO-DIMENSIONAL SECTION OF THE 0.3-m TCT

A top view of the Langley 0.3-m TCT test section is shown in figure 3. In this figure the top of the plenum chamber and the top tunnel slotted wall have been removed. Visible in the photograph are the airfoil model, wake survey probe, angle-of-attack position encoder, boxes housing a schlieren system, and the bottom slotted wall. Both the top and bottom walls have two slots with an open-area ratio of 0.05. The test section has removable sidewall inserts just upstream of the model location. The solid inserts can be removed and porous media installed for removal of the tunnel sidewall boundary layer. By use of this mechanism, the wall effects due to sidewall boundary-layer can be investigated and reduced or possibly eliminated. Several studies have been made utilizing the sidewall boundary layer system in the passive mode of operation. Some of the results have been published in reference 4.

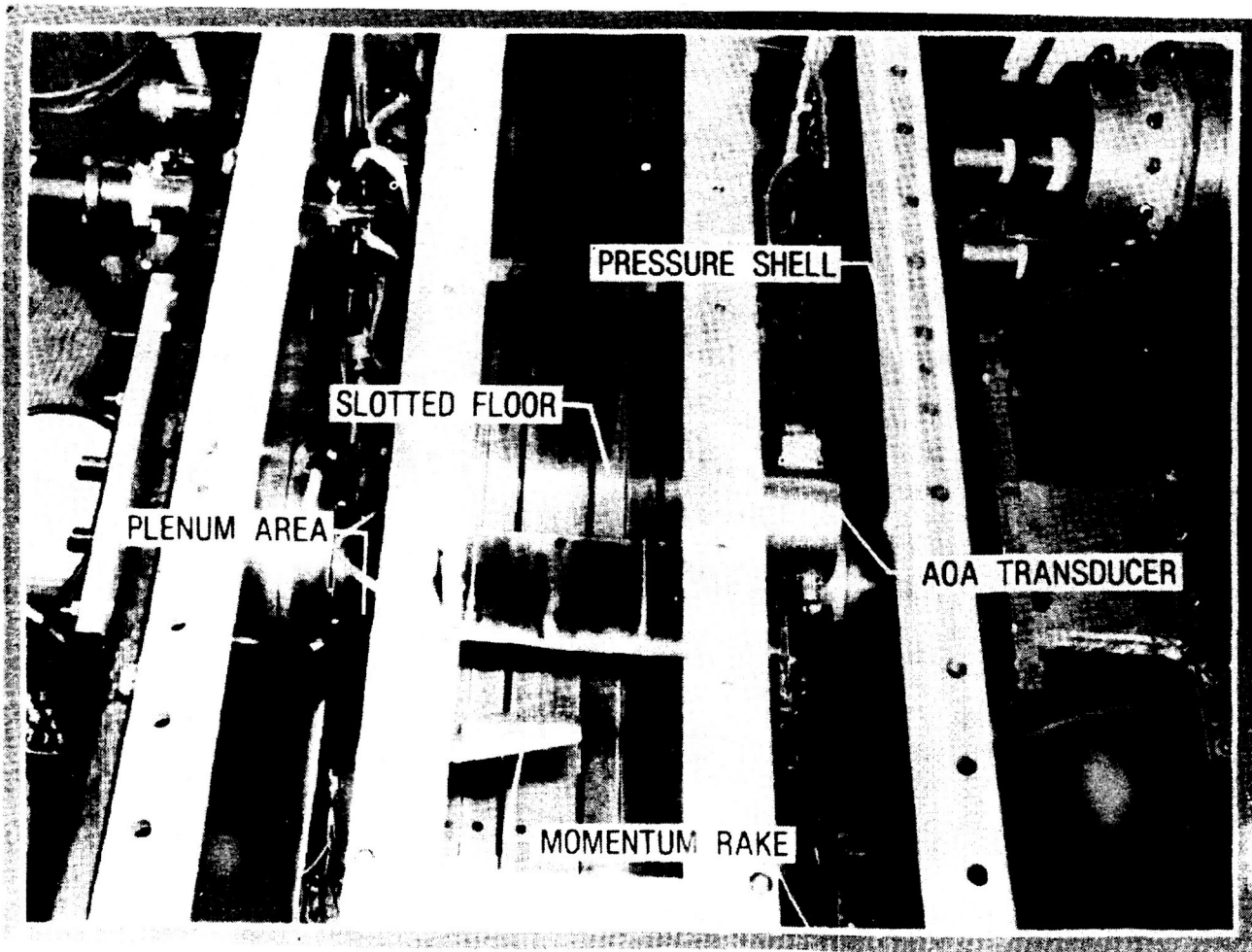


Figure 3

ORIGINAL FILED IN  
OF POOR QUALITY

TYPICAL AIRFOIL INSTALLATION IN THE 0.3-m TCT

Figure 4 below shows a closeup view of the BAC 1 (Boeing) airfoil installed in the two-dimensional test section of the 0.3-m TCT. The models used in the Advanced Technology Airfoil Test Program have been fabricated and finished to a high degree of accuracy. Very small, exact, static pressure orifices were incorporated in all of the airfoils. All of the models were thoroughly measured and checked before and after testing to preclude any unknowns regarding changes in airfoil shape during the cryogenic pressure testing. A description of the BAC 1 model and the results of the 0.3-m TCT study utilizing this particular airfoil are contained in reference 5.

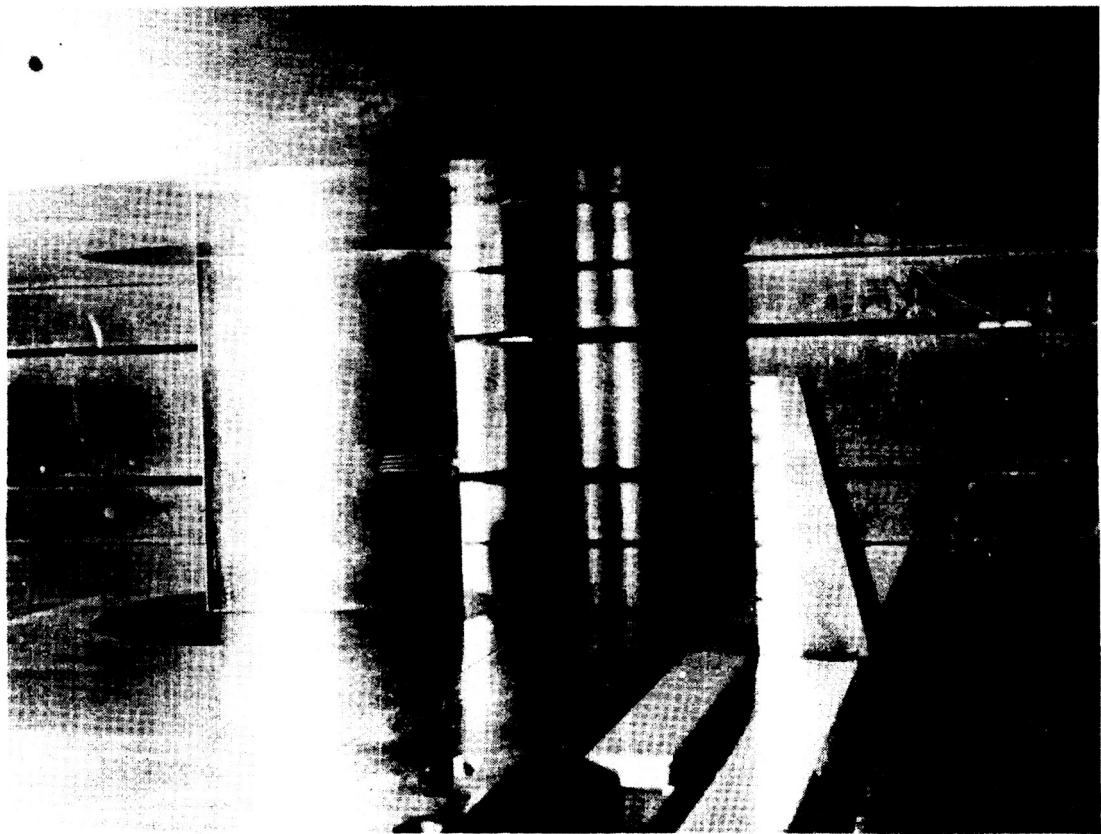


Figure 4

## AIRFOIL CAPABILITY IN THE 0.3-m TCT

The 0.3-m TCT with the two-dimensional test section installed provides one of the foremost airfoil test capabilities in existence. Figure 5 below presents a summary of the two-dimensional 0.3-m TCT Mach number and Reynolds number test capability and the flight Reynolds number airfoil design conditions for several classes of aircraft. The general-aviation design envelope, shown in the low Mach number, low Reynolds number corner of the figure, has not changed significantly over the past several decades. Typical helicopter design conditions have also remained at about the same level for a number of years. The transport-cargo aircraft design trend, however, has changed rapidly and dramatically. The larger transport-cargo types, such as the 747 and C-5, tend to establish the upper requirement for airfoil design considerations. As can be seen from the figure below, the 0.3-m TCT provides an adequate Mach number and Reynolds number capability to simulate the design flight conditions for even the largest of current aircraft.

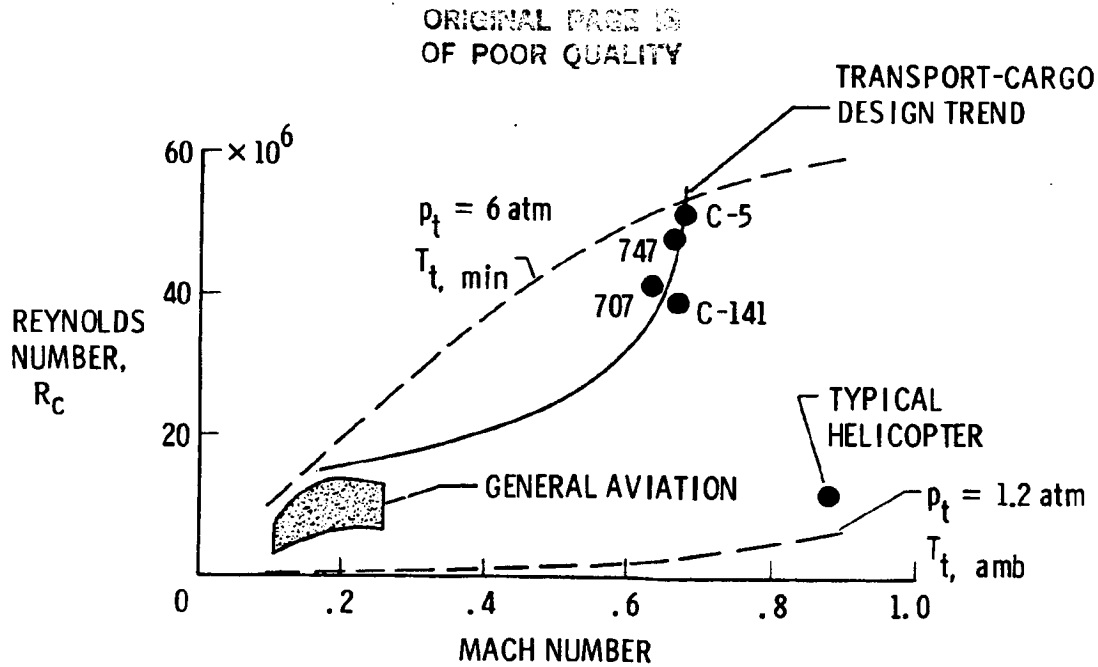


Figure 5

ADVANCED TECHNOLOGY AIRFOIL TEST (ATAT) PROGRAM  
FOR THE 0.3-m TCT

Figure 6 below summarizes the scope and current status of the 0.3-m TCT airfoil program. As shown in this figure, the program includes a series of correlation airfoils as well as advanced NASA, U.S. transport industry, and DFVLR airfoils. Four airfoils are included in the correlation series, two conventional NACA and two NASA supercritical airfoils. Each of the correlation airfoils was selected because of the availability of data from other well-known facilities, including results from other high Reynolds tunnels such as the Lockheed CFWT and the Canadian NAE 5-foot facilities. The advanced NASA airfoil design was selected to provide an indication of the current level of NASA supercritical technology. One of the advanced NASA supercritical airfoils, NASA SC(3)0712A, has been tested, but a post-test validation of airfoil shape revealed that the model had been slightly bowed (in the spanwise direction) and decambered during the cryogenic testing. This airfoil has been redesigned and constructed and a new model, NASA SC(3)0712B, is now available for testing. The industry series of airfoils includes advanced-technology airfoils designed and constructed by the Boeing, Lockheed, and Douglas corporations. In the DFVLR portion of the program, the CAST 10 model was selected due to the unusually high degree of sensitivity of the airfoil to changes in Reynolds number and wall effects. The R-4 represents an advanced technology supercritical airfoil.

<u>CORRELATION</u>	TEST STATUS
NACA 0012	COMPLETE
NACA 65-213	COMPLETE
NASA SC(2)0510	SCHEDULED
NASA SC(2)0714	PENDING
 <u>ADVANCED NASA</u>	
NASA SC(3)0712A	COMPLETE
NASA SC(3)0712B	SCHEDULED
 <u>INDUSTRY PROGRAM</u>	
BAC 1	COMPLETE
BAC 2	50% COMPLETE
DAC	PENDING
LAC 1	COMPLETE
LAC 2	COMPLETE
LAC 3	COMPLETE
 <u>DFVLR PROGRAM</u>	
CAST 10	COMPLETE
CAST 10, c/2	COMPLETE
R-4	COMPLETE

Figure 6

## COOPERATIVE CAST 10 AIRFOIL STUDIES

In addition to the basic ATAT program CAST 10 tests in the Langley 0.3-m TCT, this interesting airfoil has been tested in several European tunnels as well as in the Lockheed CFWT facility. Figure 7 below summarizes some of the major tunnel, model, and test parameters associated with the DFVLR TKG and TWB tunnel tests, the Lockheed CFWT study, and the Langley 0.3-m TCT tests. The primary tunnel-to-model relationships are shown as h/c (ratio of test section height to model chord). The Langley 0.3-m TCT tests will be made with and without boundary layer control. In addition, the overall CAST 10 program includes plans for additional tests in the French ONERA T-2 self-streamlining wall tunnel, the DFVLR TWB tunnel and the Langley self-streamlining wall 0.3-m TCT. The joint NASA/DFVLR/ONERA CAST 10 studies will provide a classic set of experimental results for the overall assessment of wind tunnel wall effects and the evaluation of current corrective techniques.

Tunnel	Model Chord, in	Tunnel Characteristics				Test Conditions			
		h/c	b/c	Type Wall	Poros. $\sigma$ %	M	$\alpha^\circ$	$R_c \times 10^{-6}$	Transition
TKG	7.87	5	5.0	Perf.	6	0.50-0.82	-2 >10	1.3 >4	Fixed & Free ↓
TWB	7.87	3	1.7	Slotted	2.4	0.6,0.7,0.78		3 >14	
CFWT	7.01	4	2.9	Perf.	4	0.60-0.82		4 >31	
0.3-m TCT <sup>1</sup>	6.0	4	1.33	Slotted	5	0.60-0.80		4 >45	
0.3-m TCT <sup>1</sup>	3.0	8	2.66	Slotted	5	↓		4 >20	

<sup>1</sup> with/without BLC

\* : ONERA streamline wall tunnel tests and additional DFVLR tests  
+ NASA follow-on tests

Figure 7

EFFECTS OF REYNOLDS NUMBER ON NORMAL FORCE COEFFICIENT

The effects of Reynolds number on several aerodynamic parameters are presented in figures 8 through 10. Data are shown at lifting conditions for three airfoils: the NACA 0012, the NASA SC(3)0712A, and the BAC 1 airfoils. Data for the NACA 0012 are shown for a normal force coefficient of 0.4, whereas, the remaining airfoils are for 0.6 since the high normal force is above drag rise for this airfoil. The BAC 1 airfoil is about 10 percent thick and would be expected to have different characteristics than the thick airfoils shown.

Plots of normal force coefficient as a function of angle of attack are presented in figure 8 for a Mach number of 0.76. There are no appreciable effects of Reynolds number on the lift curve slope noted for any of the airfoils at this Mach number. However, the two advanced airfoils do exhibit an increase in normal force coefficient as the Reynolds number is increased from the minimum value to  $30 \times 10^6$ . A further increase to about  $40 \times 10^6$  has only little effect.

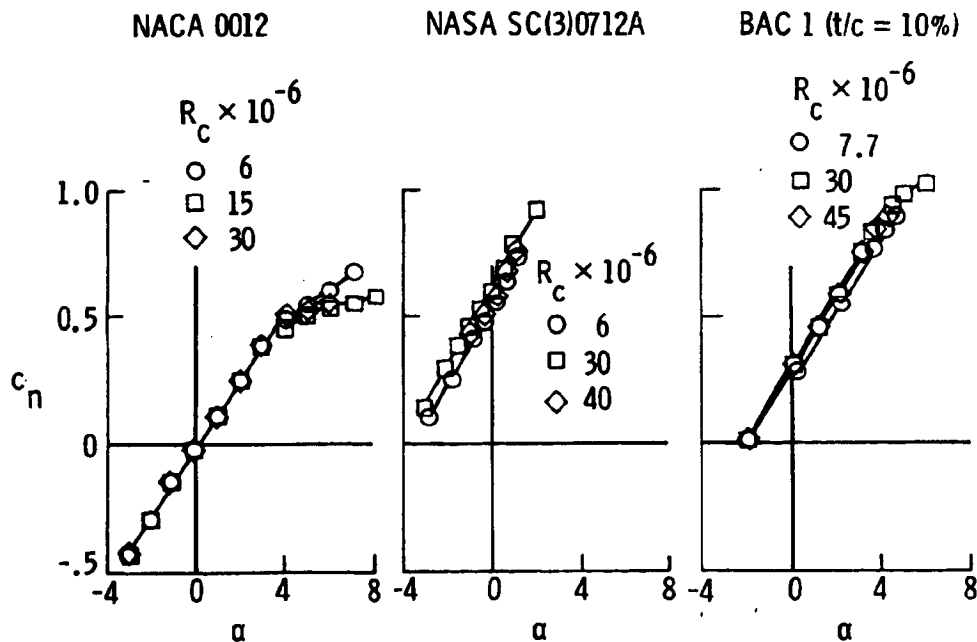


Figure 8

## EFFECTS OF REYNOLDS NUMBER ON CENTER OF PRESSURE

The effects of Reynolds number on the variation of longitudinal location of center of pressure with Mach number is shown in figure 9 for the same three airfoil shapes as the previous figure. The NACA 0012 airfoil shows essentially no effect from Reynolds number, whereas the two advanced airfoil shapes indicate a rearward movement with increasing Reynolds number. The effect of increasing  $R_c$  from 30 to about  $40 \times 10^6$  is very slight, however. Other than the slight rearward shift (about 4 percent chord at the higher Mach number), no effects of  $R_c$  are observed for these test conditions.

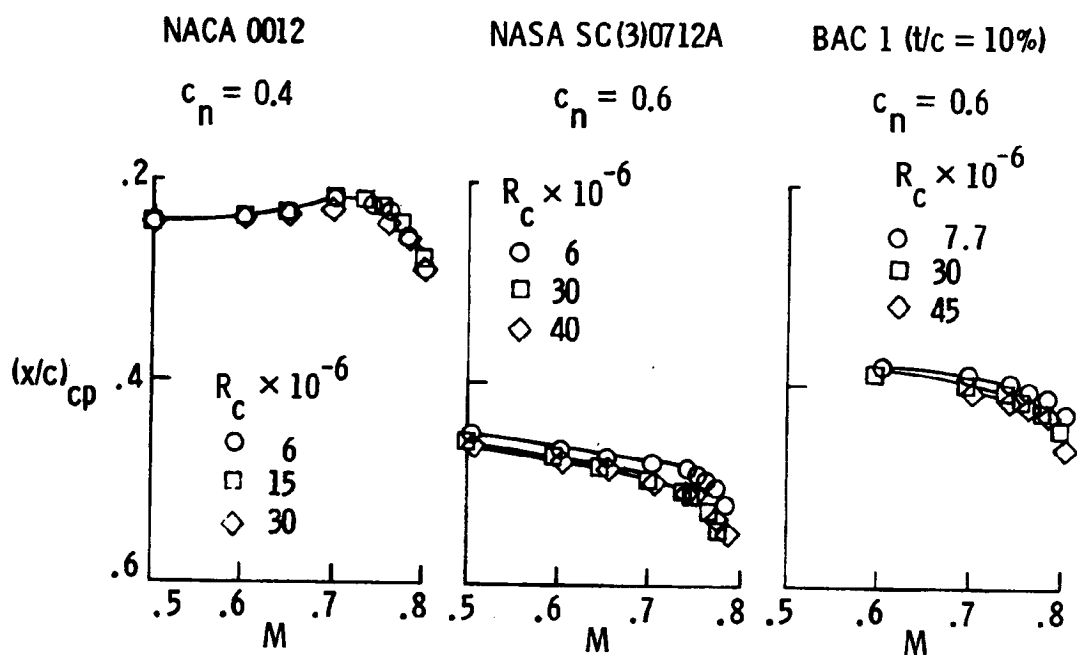


Figure 9

EFFECTS OF REYNOLDS NUMBER ON DRAG COEFFICIENT

The variation of drag coefficient with Mach number and Reynolds number for the three airfoil shapes is shown in figure 10. At the lower Mach number, the drag is constant with Mach number for the NACA 0012, whereas the SC(3)0712A shows a continual gradual rise. This rise (or drag creep) is also evident for the BAC 1 at the lower Reynolds number, but tends to decrease with increasing Reynolds number. There is very little effect of Reynolds number on the drag rise Mach number for the two advanced-technology airfoils.

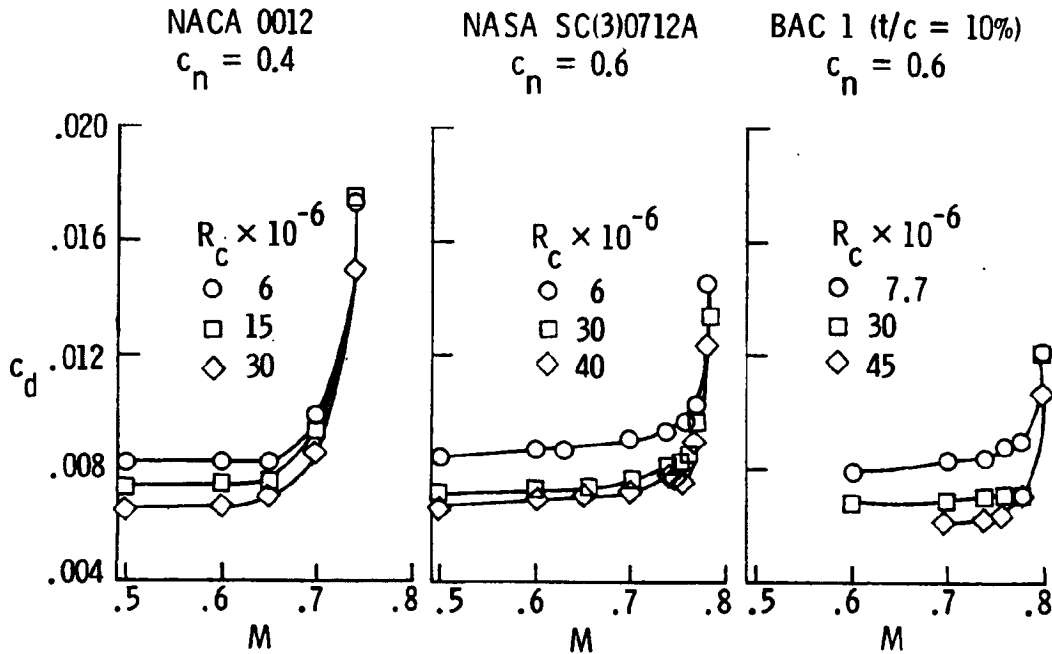


Figure 10

COMPARISON OF EXPERIMENTAL RESULTS WITH THEORY:  
NASA SC(3)0712A STUDY

In the upper left-hand portion of figure 11, a comparison of experimental upper and lower surface pressure coefficient results is shown for the NASA SC(3)0712A airfoil. The shock position for the high Reynolds number case is about 6 percent (of the airfoil chord) more rearward than the low Reynolds number shock position. This comparison of experimental results provides an indication of the sensitivity of the pressure distribution of this class of airfoil to moderate changes in Reynolds number. Figure 11 also includes a comparison of the higher Reynolds number  $M = 0.76$  experimental results with an analytical prediction by a method of Bauer, Garabedian, Korn and Jameson (ref. 6). The degree of agreement as shown in the lower left part of figure 11 is surprisingly good and may be fortuitous considering the fact that the experimental results have not been corrected for the effects of the tunnel walls. If the method of Sewall (ref. 7) were considered for this same condition, there would be an indication that a tunnel sidewall boundary layer correction should be applied to the Mach number. When tunnel sidewall corrections (ref. 7) were applied to the experimental results and the GRUMFOIL theory (ref. 8) was used to predict the pressure characteristics at the corrected Mach number of 0.745, the agreement as shown in the lower right-hand portion of figure 11 between experiment and theory is quite good.

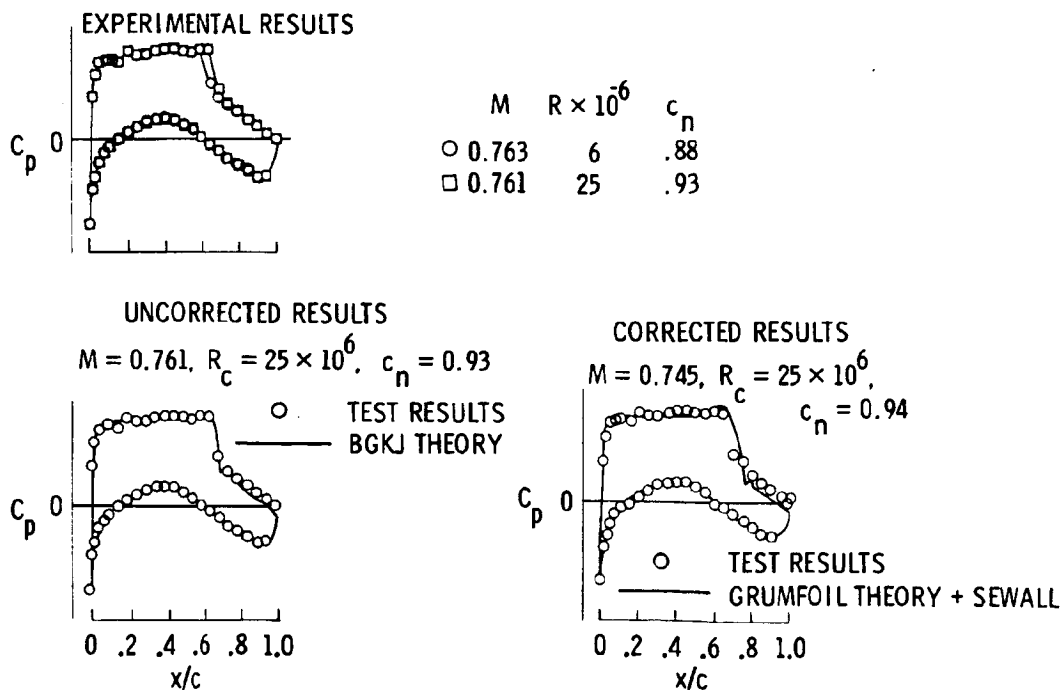


Figure 11

## REFERENCES

1. Kilgore, Robert A.: Design Features and Operational Characteristics of the Langley 0.3-Meter Transonic Cryogenic Tunnel. NASA TN D-8304, 1976.
2. Ray, Edward J.; Ladson, Charles L.; Adcock, Jerry B.; Lawing, Pierce L.; and Hall, Robert M.: Review of Design and Operational Characteristics of the 0.3-Meter Transonic Cryogenic Tunnel. NASA TM-80123, 1979.
3. Ladson, Charles L. and Kilgore, Robert A.: Instrumentation for Calibration and Control of a Continuous-Flow Cryogenic Tunnel. NASA TM-81825, 1980.
4. Murthy, A. V.; Johnson, C. B.; Ray, E. J.; Lawing, P. L.: Recent Sidewall Boundary-Layer Investigations With Suction in the Langley 0.3-m Transonic Cryogenic Tunnel. Presented at the AIAA 20th Aerospace Sciences Meeting, Orlando, Florida, January 11-14, 1982.
5. Johnson, William G., Jr.; Hill, Aquilla S., Ray, Edward J.; Rozendaal, Roger A.; and Butler, Thomas W.: High Reynolds Number Tests of a Boeing BAC 1 Airfoil in the Langley 0.3-Meter Transonic Cryogenic Tunnel. NASA TM-81922, April 1982.
6. Bauer, F.; Garabedian, P.; Korn, D.; and Jameson, A.: Supercritical Wing Section II. Lecture Notes in Economics and Mathematics Systems. M. Beckman and H. P. Lunzi, eds., Springer-Verlag, 1975.
7. Sewall, William G.: The Effects of the Sidewall Boundary Layers on Two-Dimensional Subsonic and Transonic Wind Tunnels. AIAA Journal, Vol. 20, No. 9, September 1982, pp. 1253-1256.
8. Melnik, R. E.; Chow, R.; and Mead, H. R.: Theory of Viscous Transonic Flow Over Airfoils at High Reynolds Number. AIAA 77-680, June 1977.

*Some Experience with Barnwell-Sewall Type  
Correction to Two-Dimensional Airfoil Data*

Rinaldo V. Jenkins  
NASA Langley Research Center  
Hampton, Virginia

PRECEDING PAGE BLANK NOT FILMED

## Introduction

A series of airfoils has been tested in the Langley 0.3-Meter Transonic Cryogenic Tunnel (TCT) at Reynolds numbers from 2 to 50 million. The 0.3-m TCT is equipped with Barnwell slots (ref 1) designed to minimize blockage due to the tunnel floor and ceiling. This design suggests that sidewall corrections for blockage may be needed, and that a lifting airfoil produces a change in angle of attack (ie.  $\Delta \alpha \sim -1.721 c_p$ , ref. 1). Sidewall correction methods have been developed for subsonic (ref. 2) and subsonic-transonic (ref. 3) flow. This paper presents comparisons of theory with experimental data obtained in the 0.3-m TCT for two airfoils, the British NPL 9510 and the German R-4. The NPL 9510 was tested as part of the NASA/United Kingdom Joint Aeronautical Program and R-4 was tested as part of the DFVLR/NASA Advanced Airfoil Research Program. For the NPL 9510 airfoil, only those test points that one would anticipate being difficult to predict theoretically are presented.

Data Comparison with VGK Theory  
NPL 9510 Airfoil

Dr. Robin Lock of RAE/Farnborough, the United Kingdom technical contact for the NPL 9510 airfoil tests, compared the 0.3-m Transonic Cryogenic Tunnel data with VGK theory (ref. 4). This was accomplished with successful agreement for many data points by reducing Mach number until the pressure peak is matched and correcting the lift coefficient by the dynamic pressure ratio, ie :

$$c_{l \text{ cor}} = \frac{q_{\text{mea}}}{q_{\text{cor}}} c_{l \text{ mea}}$$

Data points such as the one presented here were not matched. The suction peak and lower surface pressures are accurately predicted. On the other hand, the upper surface pressures, shock strength and location were *not* well predicted. This approach requires a decrease in Mach number of 0.025 and a lift coefficient increase of 3.7 percent.

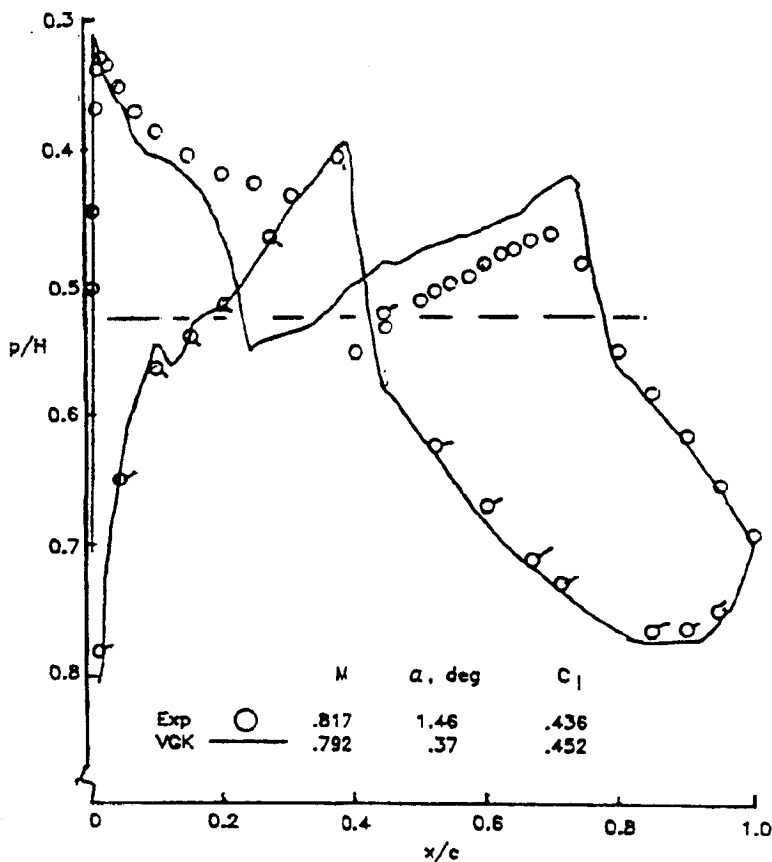


Figure 1.

Sidewall Corrected Data Comparison with GRUMFOIL Theory  
NPL 9510 Airfoil

The data from the previous figure has been corrected by the Sewall sidewall method and compared to GRUMFOIL (ref. 5). The experimental Mach number, lift coefficient, and angle of attack were .817, .436, and 1.5 degrees, respectively. Sewall's sidewall method provides corrected Mach number and lift coefficient of .802 and .441. These values were input to GRUMFOIL and the presented pressure distribution and an angle of attack of .533 degrees were calculated. Note that the measured pressures (symbols) have also been corrected by the Sewall method to account for the 0.015 change in Mach number. The lift coefficient is increased by 1.1 percent and the upper surface pressure distribution forward of the shock location is now better matched, however, the lower surface is not as good.

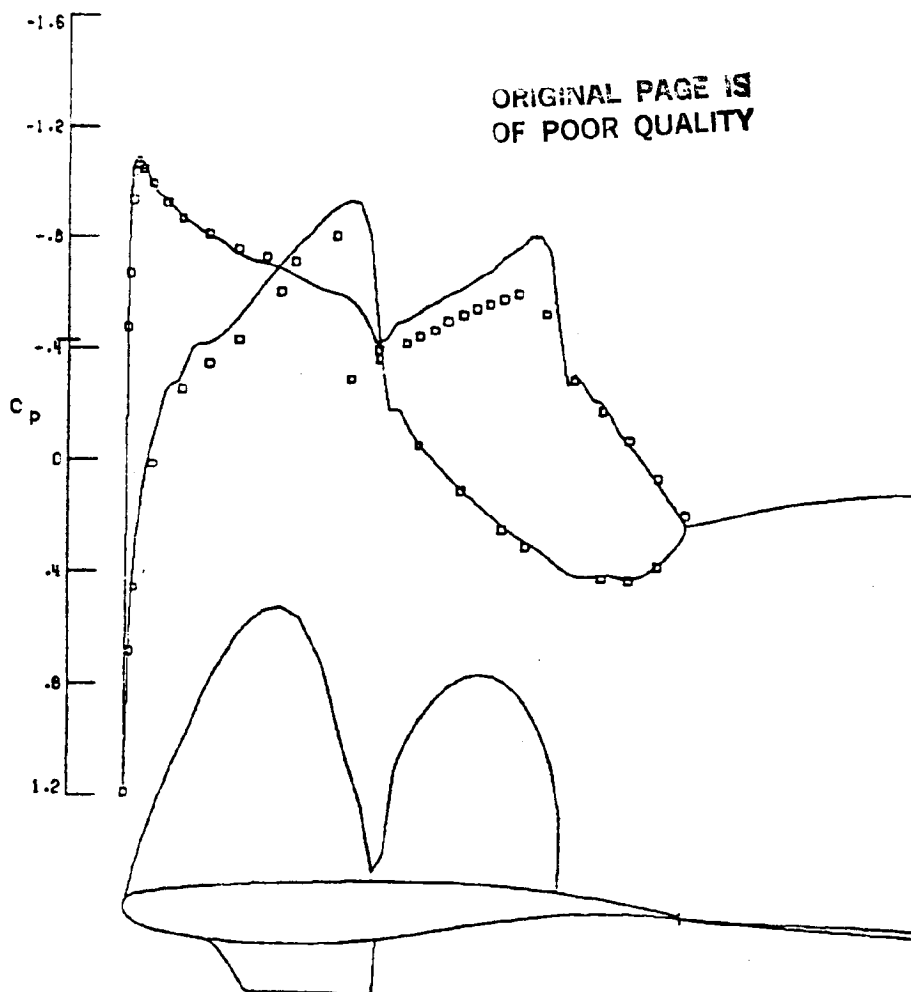


Figure 2.

Uncorrected Data Comparison with GRUMFOIL Theory  
NPL 9510 Airfoil

This is a data point with a pressure distribution similar to the one previously presented. This data, however, has not been corrected by any method and is compared to GRUMFOIL directly. The theoretical and experimental values of Mach number and lift coefficient have the same values of .792 and .551. The experimental angle of attack is 2.2 degrees and GRUMFOIL computes angle of attack as .843 degrees. This procedure results in an over-prediction of the downstream location of the shock wave and a poorly matched pressure distribution.

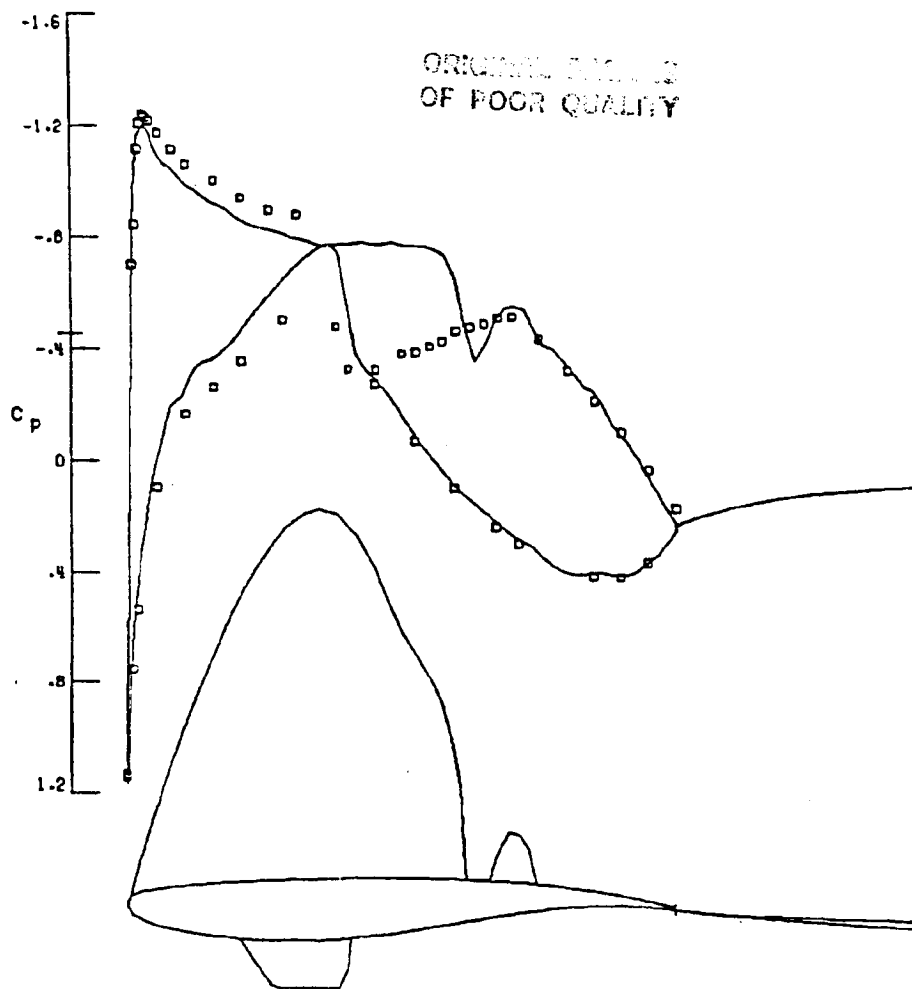


Figure 3.

Sidewall Corrected Data Comparison with GRUMFOIL Theory  
NPL 9510 Airfoil

The data from the previous figure has been corrected by Sewall's sidewall method and compared to GRUMFOIL. The Mach number and lift coefficient are corrected to .777 and .558 and GRUMFOIL now calculates angle of attack as 1.051 degrees. The agreement in the pressure distribution is greatly improved, with a particularly noteworthy forward location for the predicted shock location.

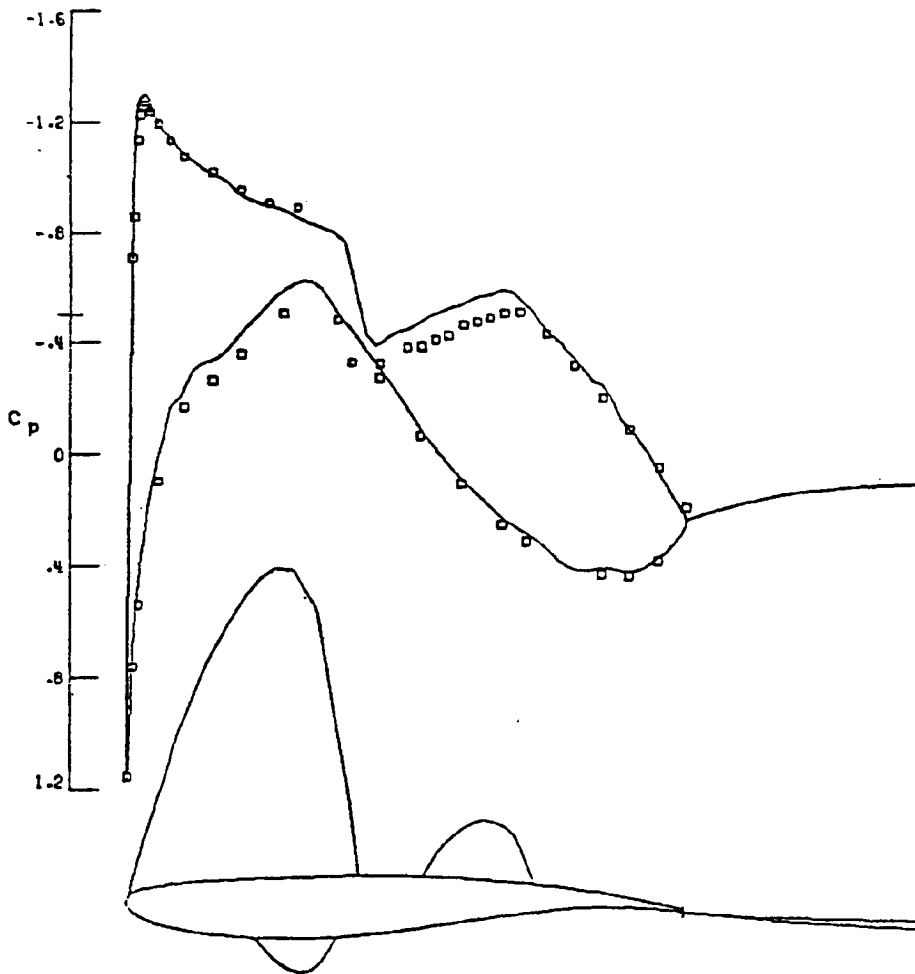


Figure 4.

Uncorrected Data Comparison with BGKJ Theory  
NPL 9510 Airfoil

This is a comparison of an uncorrected pressure distribution with a BGKJ (ref. 6) theoretical prediction. The Mach number and lift coefficient are .736 and .548 respectively, with an experimental angle of attack of 2.47 degrees. The BGKJ prediction gives an angle of attack of 1.72 degrees and the pressure distribution matched rather well.

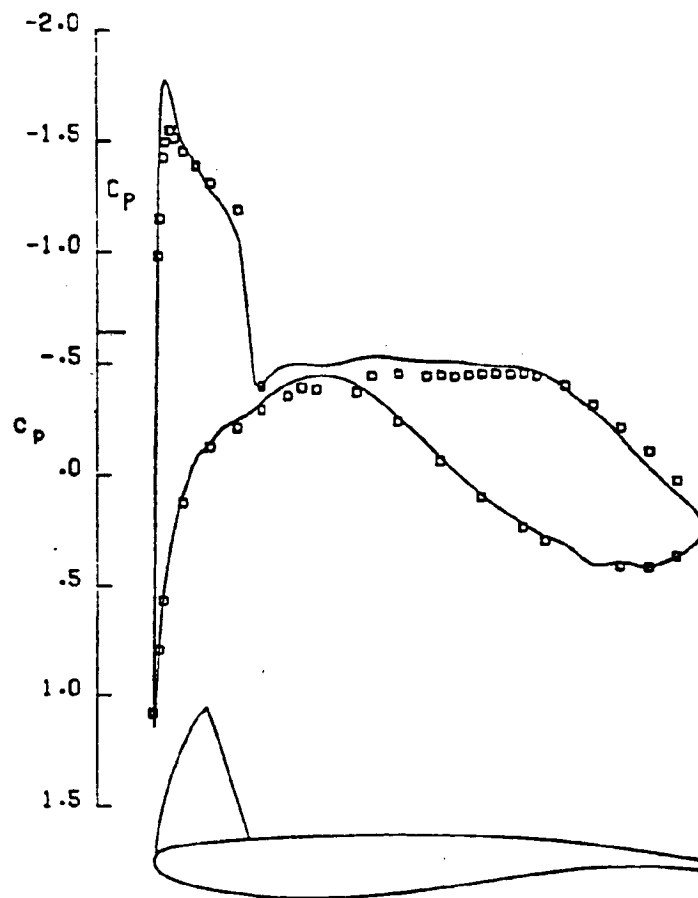


Figure 5.

Uncorrected Data Comparison with GRUMFOIL Theory  
NPL 9510 Airfoil

The good agreement of the BGKJ predicted pressure distribution with the experimental data was not anticipated. The same uncorrected data was then compared to GRUMFOIL with equally as good results as shown below. GRUMFOIL gives a better suction peak prediction and an angle of attack of 1.384 degrees.

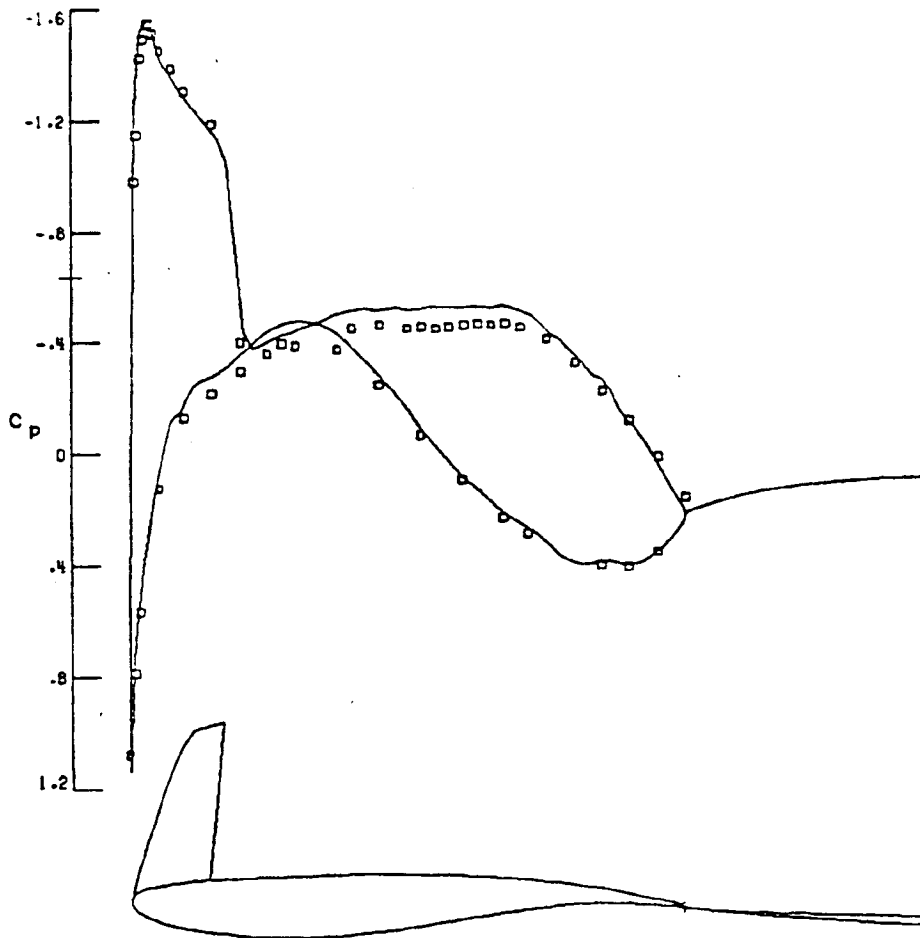


Figure 6.

Sidewall Corrected Data Comparison with GRUMFOIL Theory  
NPL 9510 Airfoil

The results of the previous two figures suggest that the pressure distribution does not change significantly with small changes in Mach number and lift coefficient for this data point. The same data was, thus, corrected by Sewall's method and compared to GRUMFOIL. Sewall's method gives Mach number as .721, lift coefficient as .556, and angle of attack as 1.521 degrees. The prediction still agrees with the experimental pressure distribution although the Mach number decreased by .015 and lift increased by 1.5 percent.

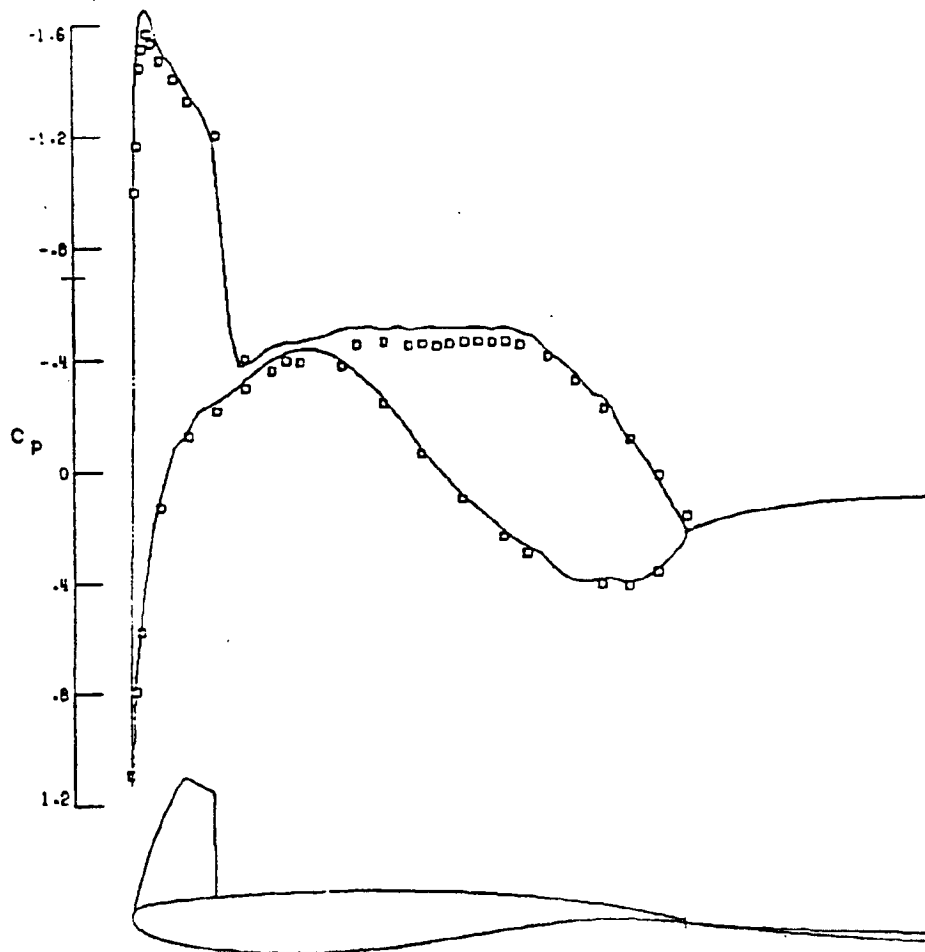


Figure 7.

## DFVLR R-4 Airfoil Drag Results

At this point the DFVLR R-4 airfoil is introduced by way of a plot of its section drag coefficient versus Mach number for a constant lift coefficient of .65. The circular symbol is cross-plotted data and the square symbol represents this cross-plotted data corrected by Sewall's sidewall method. Drag rise Mach number

as determined by the criterion  $\frac{dc_d}{dM} = .1$  is very near the design

Mach number of .73.

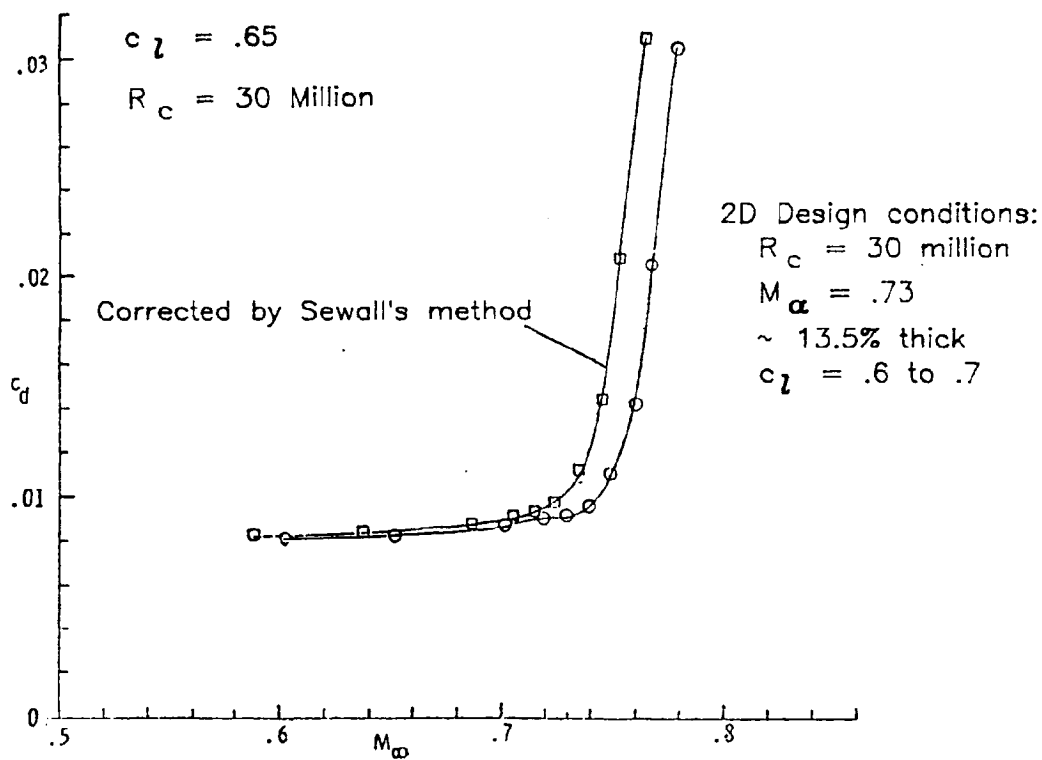


Figure 8.

Pressure Distribution Comparison  
R-4 Airfoil

The next six figures show pressure distributions, for data points from a drag polar near drag rise Mach number for the R-4 which have been corrected by Sewall's method and compared to GRUMFOIL. The experimental Mach number, lift coefficient, and angle of attack are .750, .278, and  $-2.0$  degrees respectively. The sidewall corrected Mach number and lift coefficient are .735 and .281, and GRUMFOIL determines angle as  $-2.363$  degrees.

(a)  $\alpha_T = -2.0$  degrees

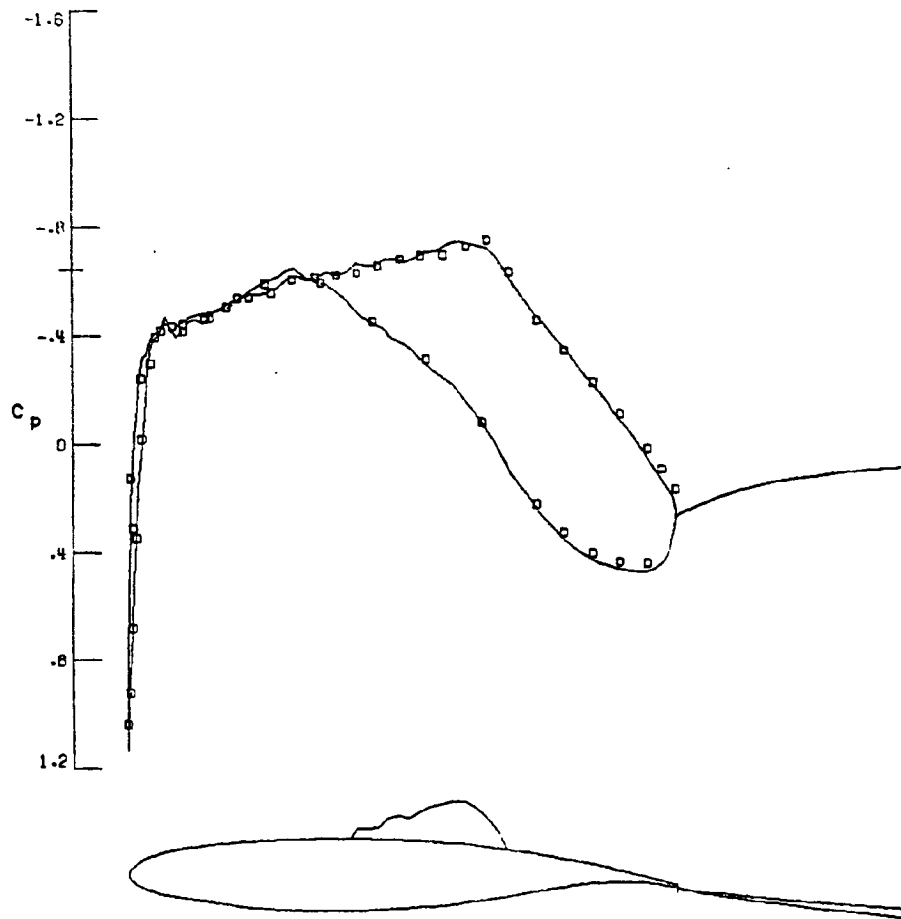


Figure 9.

### Pressure Distribution Comparison R-4 Airfoil

The experimental Mach number, lift coefficient, and angle of attack are .750, .436, and  $-1.0$  degrees. These values are corrected to .735, and .442 for Mach number and lift coefficient and GRUMFOIL gives angle of attack as  $-1.57$  degrees. The pressure distribution is still very well predicted.

(b)  $\alpha_T = -1.0$  degrees

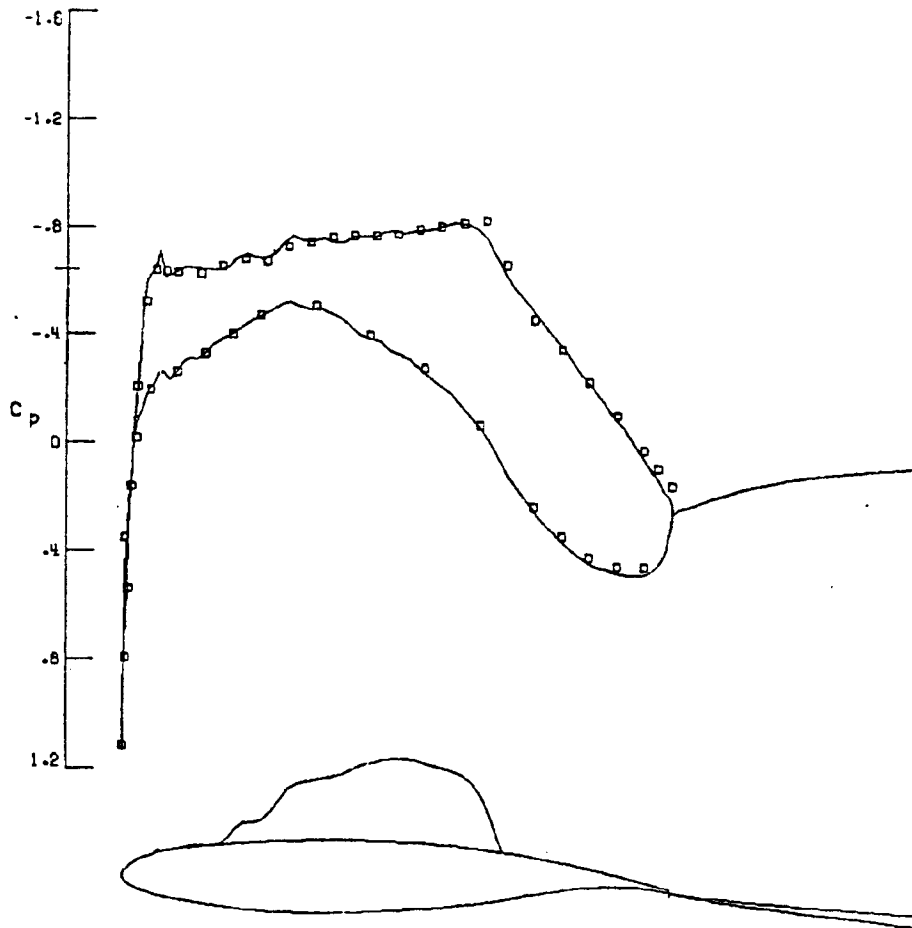


Figure 9. - Continued.

Pressure Distribution Comparison  
R-4 Airfoil

Here the experimental Mach number, lift coefficient, and angle of attack are .748, .596, and 0.0 degrees. The corrected Mach number and lift coefficient are .734, and .604. With these values, GRUMFOIL gives an angle of attack of  $-.818$  degrees and predicts the pressure distribution except for a small wave on the airfoil upper surface.

(c)  $\alpha_T = 0.0$  degrees

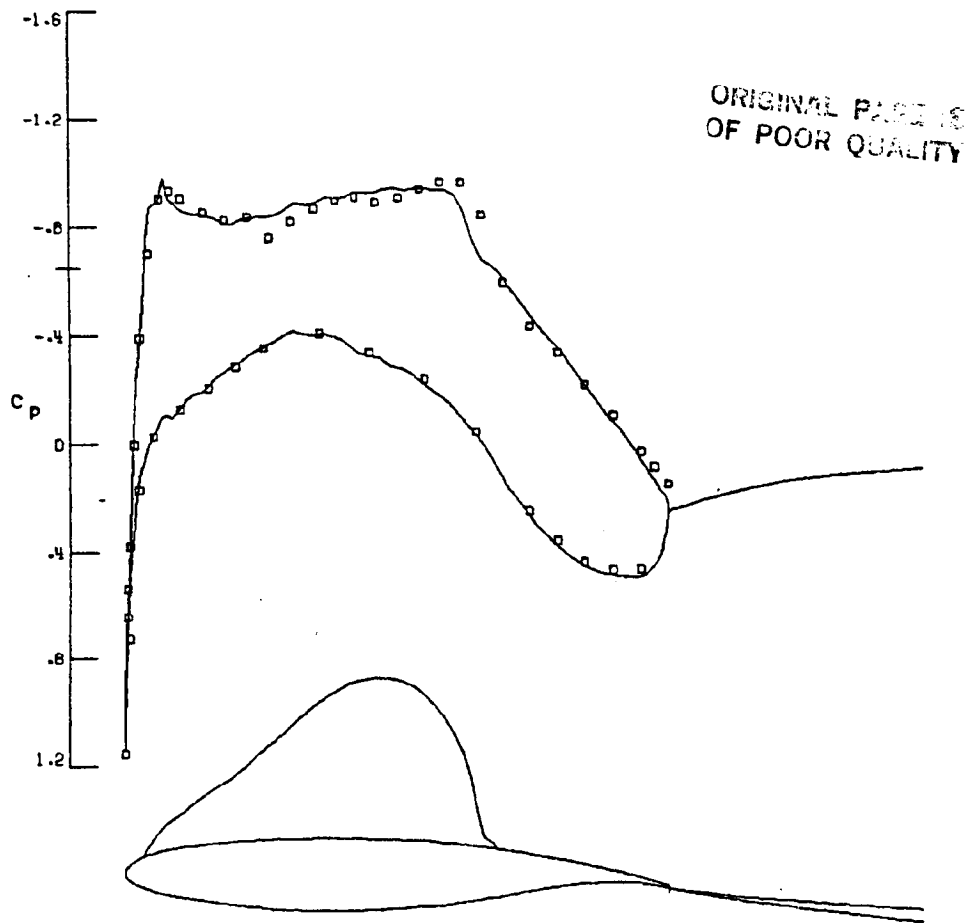


Figure 9. - Continued.

Pressure Distribution Comparison  
R-4 Airfoil

Experimental Mach number, lift coefficient and angle of attack are .750, .685, and 0.5 degrees, respectively. The Sewall method gives .735 for Mach number and .694 for lift coefficient. GRUM-FOIL produces an angle of attack of  $-.45$  degrees and predicts the pressure distribution except for a wave on the upper surface of the airfoil.

(d)  $\alpha_T = 0.5$  degrees

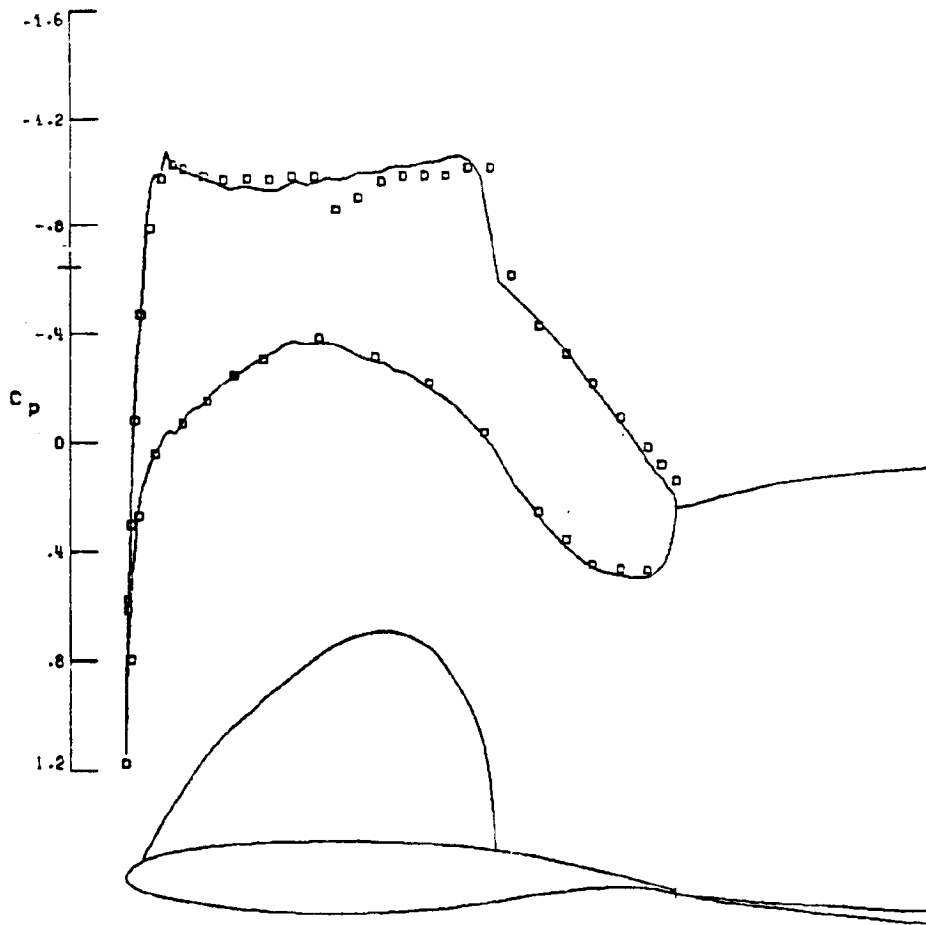


Figure 9. -- Continued.

### Pressure Distribution Comparison R-4 Airfoil

Experimental values of .747, .833 and 1.5 are corrected and computed to a Mach number, lift coefficient, and angle of attack of .732, .845, and .186 degrees. GRUMFOIL is still missing the wave on the upper surface.

(e)  $\alpha_T = 1.5$  degrees

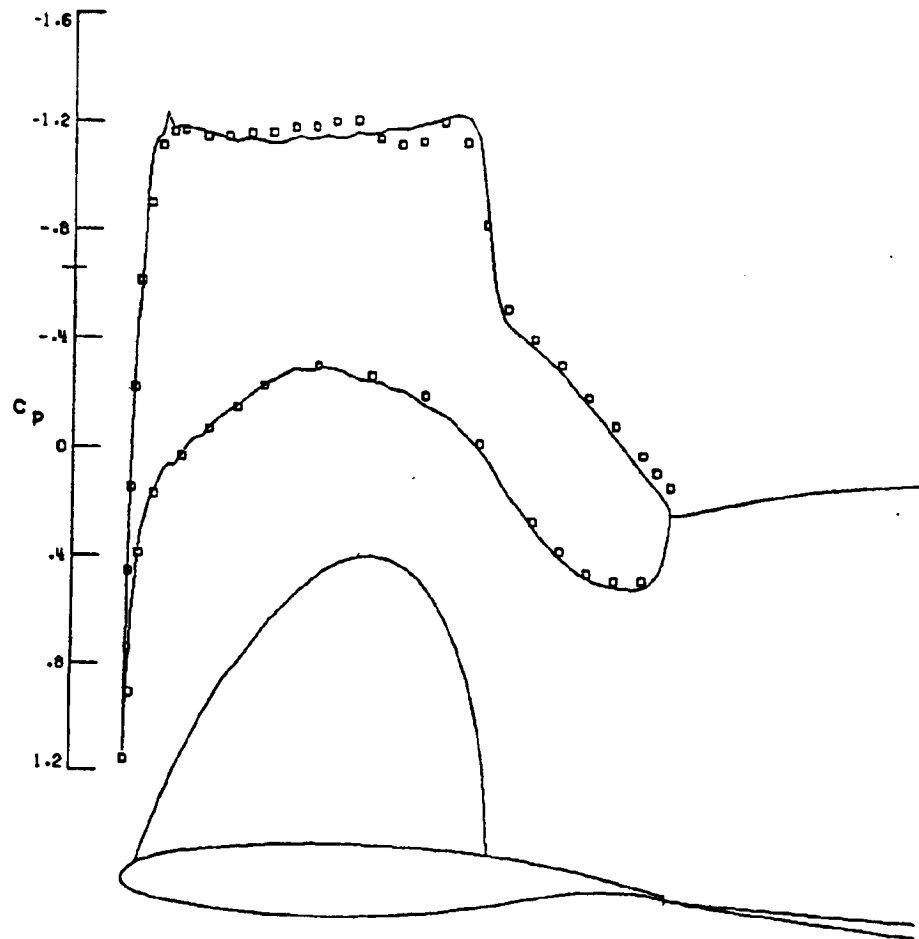


Figure 9. - Continued.

Pressure Distribution Comparison  
R-4 Airfoil

Experimental Mach number, lift coefficient, and angle of attack of .749, .913, and 2.5 degrees are corrected to .734, .926, and .539 degrees. Here the whole upper surface distribution is slightly missed.

(f)  $\alpha_T = 2.5$  degrees

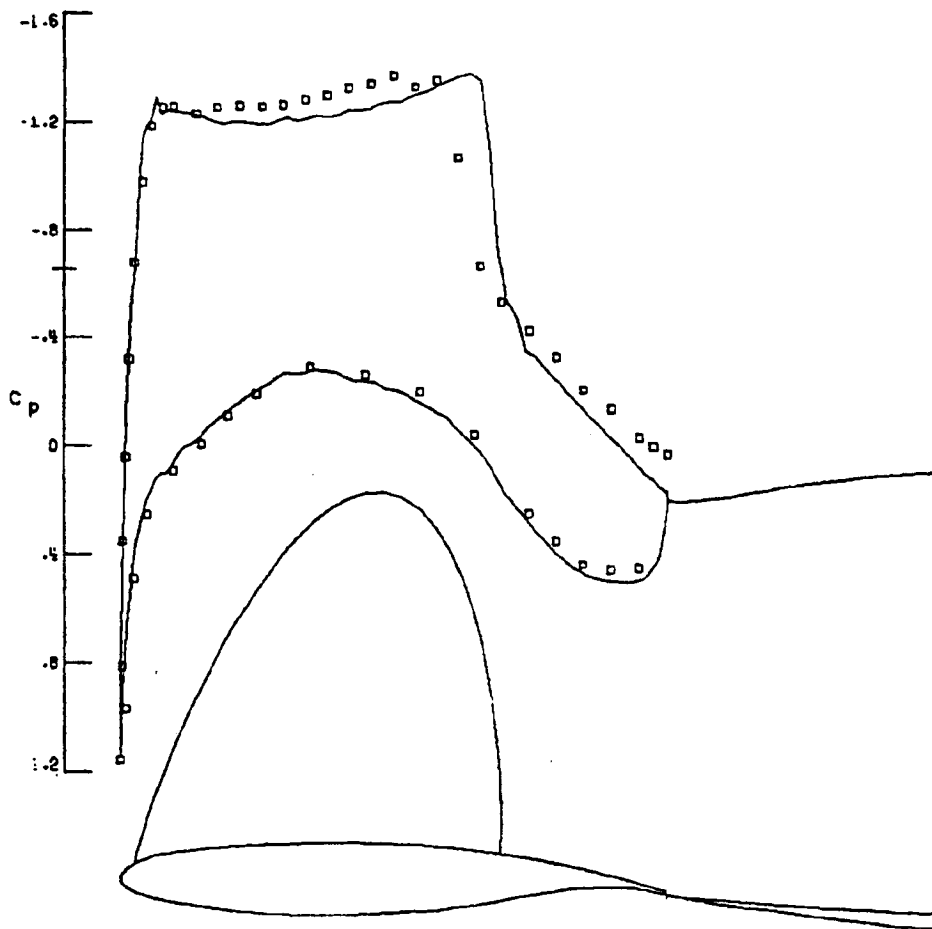


Figure 9. - Concluded.

### Concluding Remarks

Sidewall wall corrections are required for data taken in the 0.3-m TCT at most test conditions. The present results were corrected for blockage effects using the Barnwell-Sewall sidewall-only correction theory (refs. 2 & 3). The adequacy of the correction was assessed with GRUMFOIL free air calculations. These findings indicate the need for further investigation of correction methods, which include an accounting of the response of the sidewall boundary layer to the model pressure field, such as the one proposed in reference 7.

## References

1. Barnwell, Richard W.: Design and Performance Evaluation of Slotted Walls for Two Dimensional Wind Tunnels. NASA TM 79648, February 1978.
2. Barnwell, Richard W.: A Similarity Rule for Compressibility and Sidewall Boundary-Layer Effects in Two-Dimensional Wind Tunnels. AIAA Journal, Vol. 18, No. 9, September 1980, pp 1149-1151.
3. Sewall, William G.: The Effects of Sidewall Boundary Layers in Two-Dimensional Subsonic and Transonic Wind Tunnels. AIAA Journal, Vol. 20, No. 9, September 1982, pp 1253-1256.
4. Lock, Robin C.: A Review of Methods for Predicting Viscous Effects on Aerofoils and Wings at Transonic Speeds. Paper No. 2 of the AGARD Conference Proceeding No. 291. Fluid Dynamics Panel Symposium at the United States Air Force Academy, Colorado Springs, Colorado, USA, Sept. 29-Oct. 1, 1980.
5. Melnik, R. E.: Turbulent Interactions on Airfoils at Transonic Speeds - Recent Developments. Paper No. 10 of the AGARD Conference Proceeding No. 291. Fluid Dynamics Panel Symposium at the United States Air Force Academy, Colorado Springs, Colorado, USA, Sept. 29 - Oct. 1, 1980.
6. Bauer, F.; Garabedian, P.; Korn, D.; and Jameson, A.: Super-critical Wing Section II. Lecture Notes in Economics and Mathematics Systems, M. Beckman and H. P. Lunzi, eds. Springer-Verlag c. 1975.
7. Kemp, William B., Jr.; and Adcock, Jerry B.: Combined Four-Wall Interference Assessment in Two-dimensional Airfoil Tests. AIAA Paper No. 82-0586 presented at the 12th Aerodynamic Testing Conference, Williamsburg, VA, March 21-24, 1982.

N85 12035

D24

ADAPTATION OF A FOUR-WALL INTERFERENCE  
ASSESSMENT/CORRECTION PROCEDURE  
FOR AIRFOIL TESTS IN THE 0.3-m TCT

Clyde R. Gumbert, Perry A. Newman, William B. Kemp, Jr., and Jerry B. Adcock  
NASA Langley Research Center  
Hampton, Virginia

DATA FLOW FOR AUTOMATED, TRANSONIC,  
FOUR-WALL CORRECTIONS

In order to validate a wall-interference assessment/correction (WIAC) method by applying it to many sets of test data, an automated procedure is required. The procedure devised and discussed here is for airfoil test data from the 0.3-m Transonic Cryogenic Tunnel (TCT). This procedure consists of three computer programs: (1) a Data Preprocessor code to preview the data from 0.3-m TCT data tapes and transform it to an input file for the correction code; (2) TWINTAN (ref. 1), a transonic, small-disturbance potential flow code to obtain a four-wall interference correction to the tunnel Mach number and angle of attack; and (3) GRUMFOIL (ref. 2), a 2-D, full-potential transonic analysis code with viscous interaction to independently check the corrections in free air. The data flow through these codes and output are indicated in figure 1. Both the sequential and the unified four-wall correction methods discussed in ref. 1 are included here.

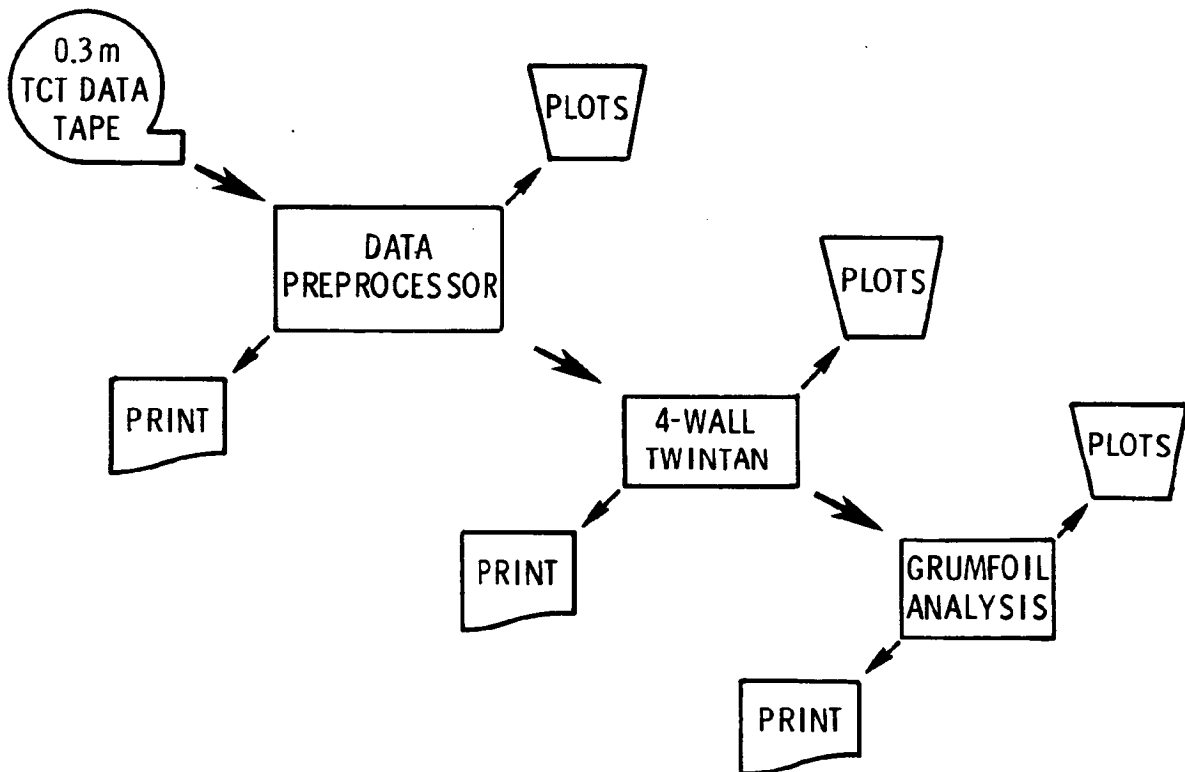


Figure 1

SAMPLE PLOTS OF MEASURED PRESSURE COEFFICIENTS  
FROM DATA PREPROCESSOR PROGRAM

The Preprocessor Program allows the user to preview measured pressures on both the airfoil surface and the top and bottom tunnel walls. Any unreasonable-looking data points can be edited or deleted before corrections are attempted. Three representative plots from the test of a 12-percent-thick supercritical airfoil, the NASA SC(3)0712A, at various tunnel angles of attack,  $\alpha_T$ , are shown in figure 2. The nominal tunnel reference Mach number  $M_T$  is 0.76 while the Reynolds number based on chord,  $Re_c$ , is about six million. All of these pressures are used as boundary conditions in the TWINTAN correction code. An additional boundary condition representing the upstream flow direction near the walls is also required but such values were not measured during the test. Note that for all three cases (figs. 2a,b,c) the most upstream values of  $C_p$  on the walls do not coincide, indicating a possible non-parallel upstream flow. For this tunnel, this is the region in which the tapered slots are opening and ahead of which pressure measurements were not taken.

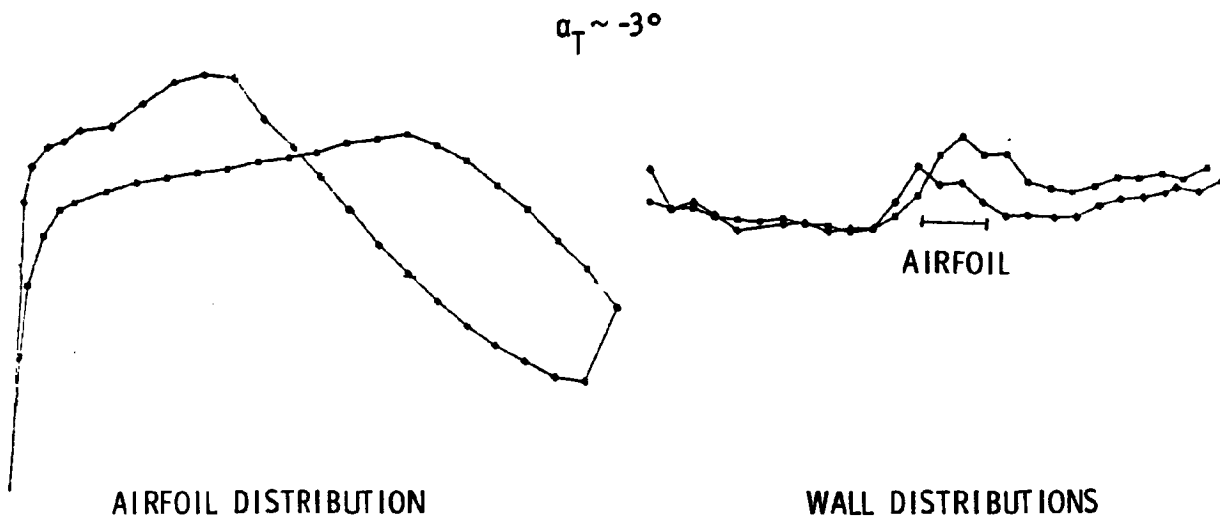


Figure 2(a)

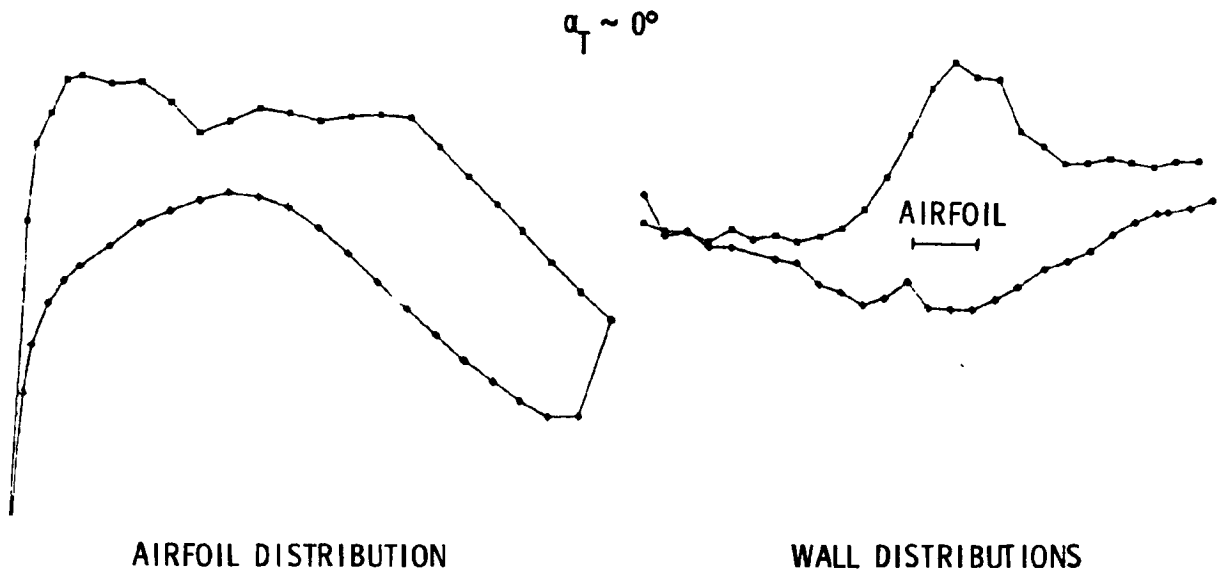


Figure 2(b)

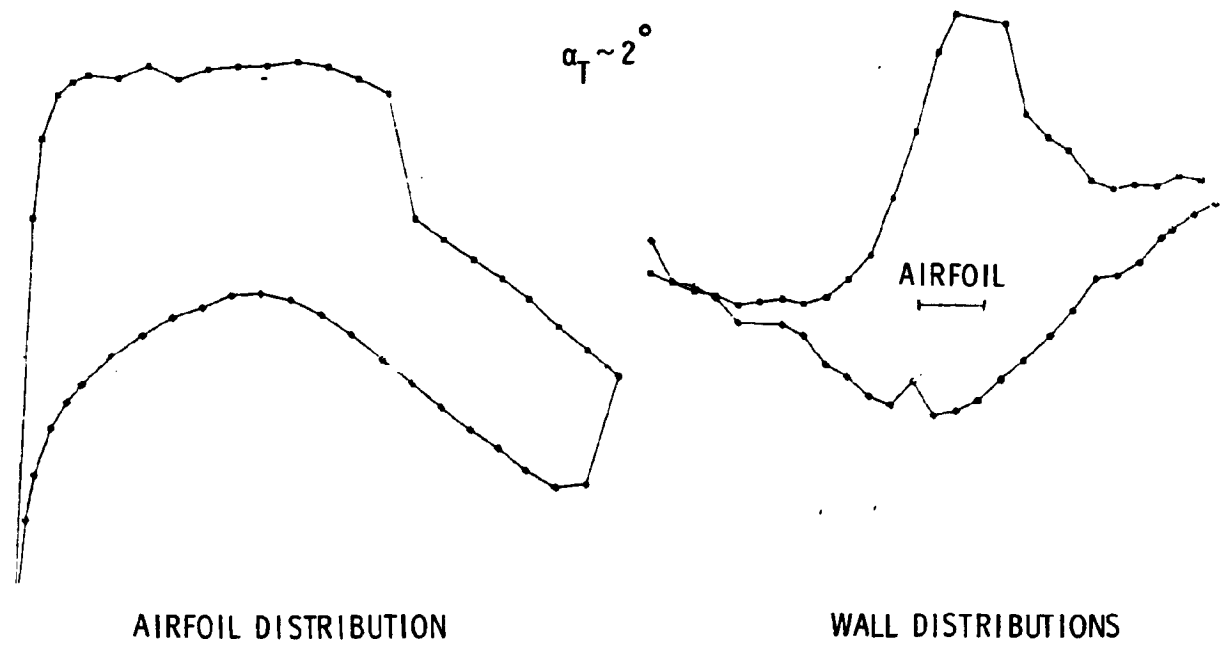


Figure 2(c)

### SAMPLE PLOTS FROM TWINTAN FOUR-WALL CORRECTION PROGRAM

The TWINTAN correction program provides the user with three types of plotted output. Figure 3a compares the hard airfoil geometry and calculated equivalent-body shape; figure 3b shows the wall-induced disturbance velocities along the tunnel centerline; and figure 3c compares measured airfoil pressure coefficients (renormalized by the corrected Mach number) with the free-air solution for the equivalent body at corrected  $M(= M_T + \Delta M)$  and  $\alpha(= \alpha_T + \Delta\alpha)$ . These figures, as well as several to follow, are for the case where  $M_T \sim 0.76$  and  $\alpha_T \sim -3^\circ$ . The comparison of airfoil shapes in figure 3a indicates a slight misalignment which is most noticeable toward the trailing edge. There one would expect the effective inviscid shape to show a boundary layer displacement thickness; however, it is not apparent on the airfoil upper surface.

### TWINTAN AIRFOIL SHAPES

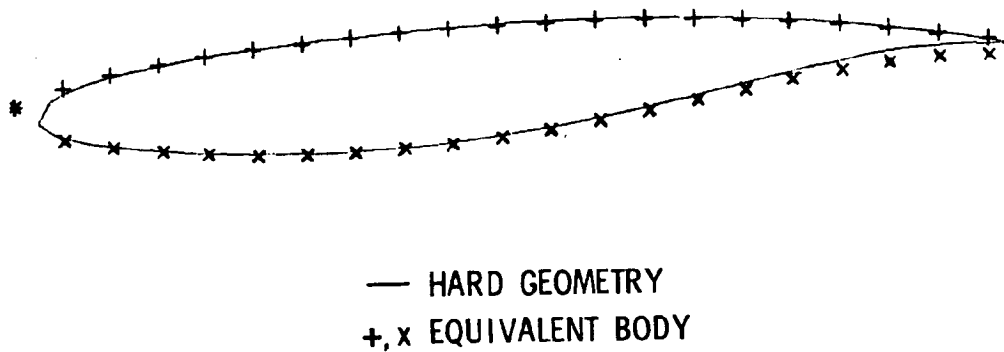


Figure 3(a)

### WALL-INDUCED VELOCITIES

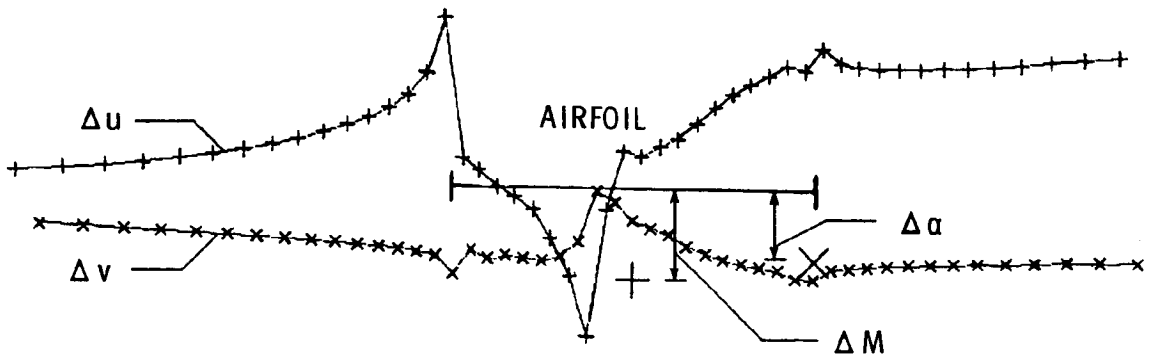


Figure 3(b)

### AIRFOIL PRESSURES

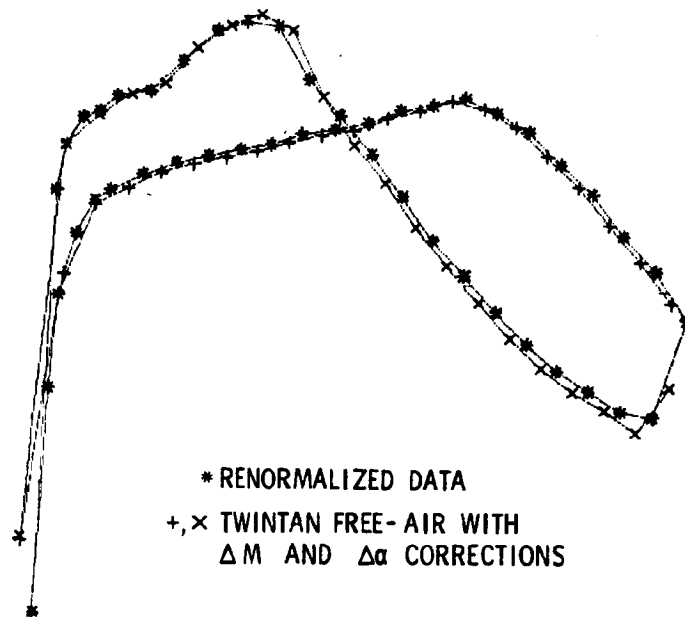


Figure 3(c)

## SAMPLE PLOTS FROM GRUMFOIL FREE-AIR ANALYSIS PROGRAM

The GRUMFOIL free-air analysis program provides the user with a number of plots, three of which are of interest here. Figure 4a compares measured pressure data (renormalized by the corrected Mach number) with the free-air solution for the hard airfoil geometry at the corrected Mach number, lift coefficient and tunnel Reynolds number. Several GRUMFOIL curves are shown on figure 4a: the solid line (easily seen between symbols near the leading edge and through the shock) gives the airfoil surface and mean wake pressures accounting for the strong viscous interaction at the trailing edge. The symbols (+, x) denote inviscid (outer-edge) pressures above and below the airfoil wake viscous regions, respectively. At the trailing edge, the solid line results satisfy the Kutta condition, while the mismatch seen for the symbol results (+, x) indicates the normal pressure gradient across the near wake.

Figures 4b and 4c show detail comparisons of the equivalent inviscid body calculated in the TWINTAN correction code with the effective inviscid shape as obtained from the GRUMFOIL free-air solution boundary layer displacement thicknesses. The increment in effective thickness over that of the hard airfoil shape is shown in figure 4b while the increment in camber is shown in figure 4c. Again this is for the sample case where  $M_T \sim 0.76$  and  $\alpha_T \sim -3$ . In this comparison of magnified camber increments, the misalignment of airfoil shapes is very apparent and is deemed to be caused by the assumed upstream flow direction. It should be pointed out that in TWINTAN, matching the measured drag essentially fixes the equivalent-body thickness increment level near the airfoil trailing edge. However, no such constraint affects the local level of camber increment and it has been shifted slightly in figure 4c so that the slope can be compared easily.

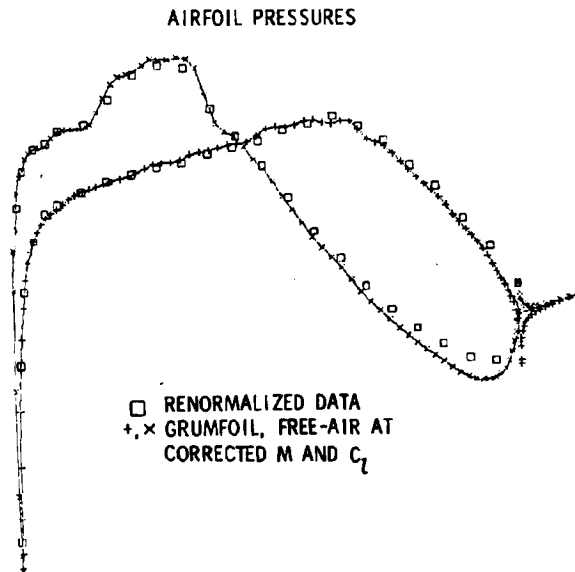
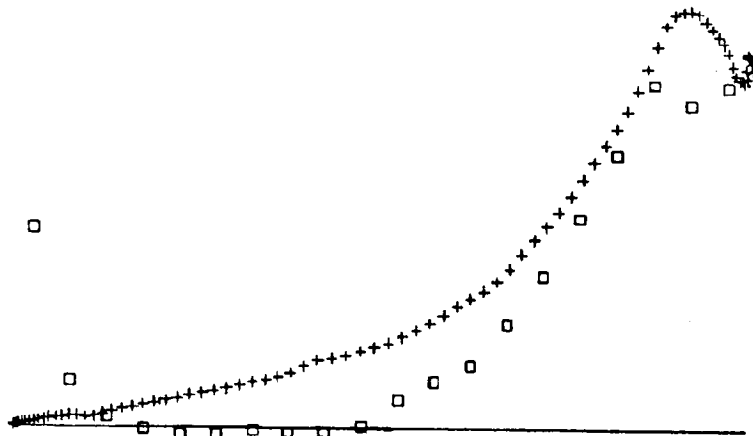


Figure 4(a)

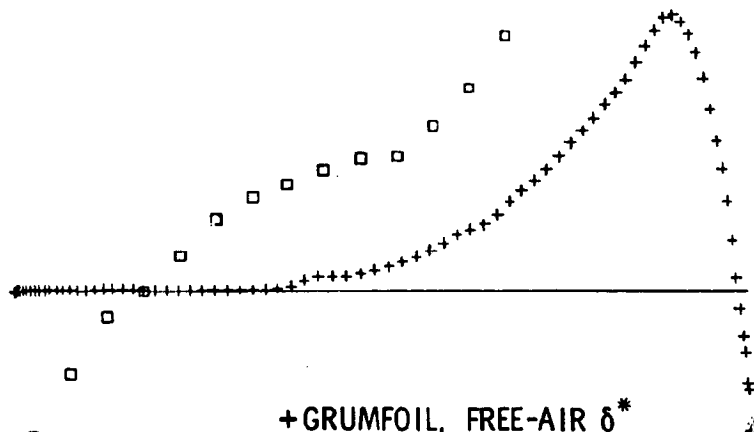
THICKNESS INCREMENTS



+ GRUMFOIL, FREE-AIR  $\delta^*$   
□ TWINTAN, EQUIVALENT BODY

Figure 4(b)

NEGATIVE OF CAMBER INCREMENTS



+ GRUMFOIL, FREE-AIR  $\delta^*$   
□ TWINTAN, EQUIVALENT BODY

Figure 4(c)

## MODIFIED DATA FLOW FOR MULTIPLE WALL CORRECTIONS

This modified procedure allows the user to look at several types of corrections independently and make multiple corrections. The first pass through the correction procedure can be used to assess the upstream flow angularity if it has not been measured. This upstream boundary condition can then be adjusted and used as input for a second pass through the TWINTAN correction program. In addition, the modified procedure allows one to make input files for the free-air GRUMFOIL analysis program at several points in the correction procedure so that various types of corrections can be made and compared. The data flow and feedback are indicated in figure 5. The TWINTAN correction code has also been modified to automatically find the  $\Delta M$  and  $\Delta \alpha$  corrections subject to a best least-squares pressure matching constraint over the airfoil surface (as proposed in ref. 3) rather than the single match point condition originally used in TWINTAN (ref. 4).

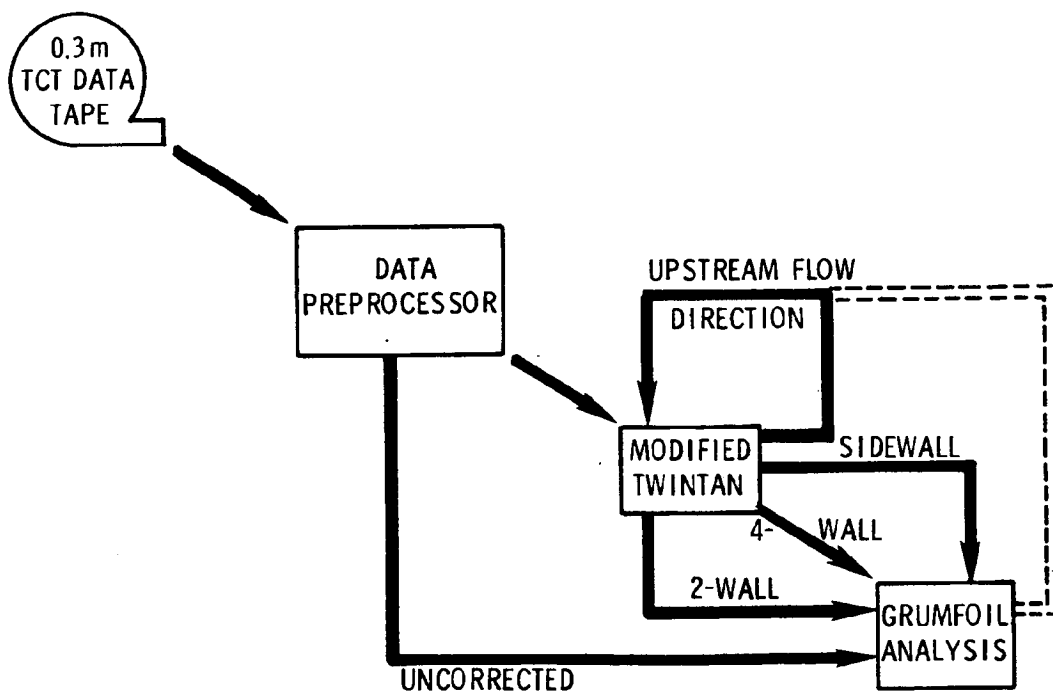


Figure 5

AIRFOIL PRESSURE COEFFICIENT COMPARISONS  
FOR DIFFERENT WALL CORRECTIONS

Free-air results from GRUMFOIL for conditions predicted by several types of wall corrections (as well as uncorrected) are compared with the renormalized tunnel data in figure 6. For this sample case all of the pressure distributions look reasonable. The shock wave on the airfoil lower surface, as predicted by GRUMFOIL, is noticeably downstream for the uncorrected conditions, not present at all for the sidewall-only correction conditions, and reasonably located (with respect to that in the experiment) for the 4-wall correction conditions. These 4-wall results were from the unified procedure, with and without upstream flow direction feedback.

It was suggested in ref. 3 that the pressure distribution calculated in free-air by the assessment/correction procedure be considered as better corrected for higher order interference effects than is the renormalized tunnel data. Ref. 1 reinforced this suggestion by correlating the pressure distribution differences with the nonuniformities in both components of wall-induced velocity. For the present sample case, the pressure comparison shown in figure 3c implies that the higher-order correction would improve the agreement with the GRUMFOIL prediction on the lower part of figure 6. Adoption of such higher order corrections to the airfoil pressure distribution should be considered for future versions of the WIAC procedure.

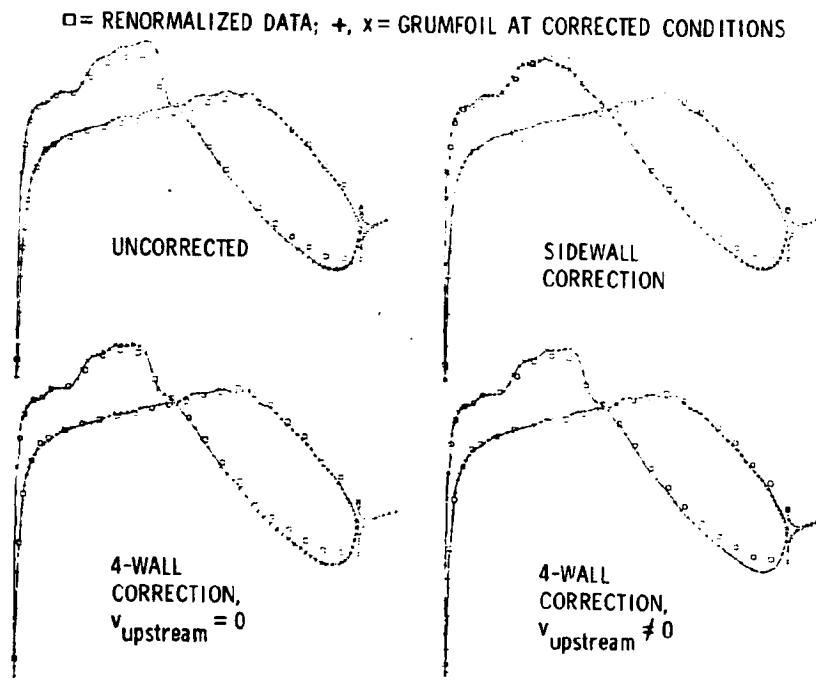


Figure 6

## UPSTREAM FLOW DIRECTION EFFECTS ON EQUIVALENT BODY

The upstream flow direction near the walls is not measured in the 0.3-m TCT airfoil tests. Here it is assumed that it can be linearly decomposed into  $v_{\text{even}}$ , the angularity or lift component, and  $v_{\text{odd}}$ , the divergence or thickness component. This latter component is an indication of flow through the slots into the plenum since the average of the upper- and lower-wall pressures,  $\overline{C_{p, \text{wall}}}$ , at the first wall pressure tap location is higher than the plenum pressure. At the bottom of figure 7a,  $-C_p$  along the walls is plotted and values for  $C_{p, \text{plenum}}$  and  $C_{p, \infty}$  are also shown. To lowest order,  $v_{\text{odd}}$  is  $\sqrt{-\overline{C_{p, \text{wall}}}}$ . Applying this approximate flow divergence at the upstream boundary makes the effective body thinner, as seen at the top of figure 7a. However, this seems to be in the wrong direction for this sample case.

The angularity component is evaluated from the mismatch in the camber increment comparison as indicated on figure 7b. This assessment is done over the forward part of the airfoil where differential upper-to-lower surface boundary layer effects are deemed to be negligible. The GRUMFOIL results for  $\frac{1}{2}(\delta_l^* - \delta_u^*)$  are plotted as (+) on figure 7b. The curve to the right shows the effect of applying the angularity from the first pass as an upstream boundary condition in the second pass. As intended, the mismatch in the slope of the camber increments was reduced, perhaps even overcorrected, in the second pass. The airfoil shapes plotted by TWINTAN and shown in figure 7c also appear to be better aligned.

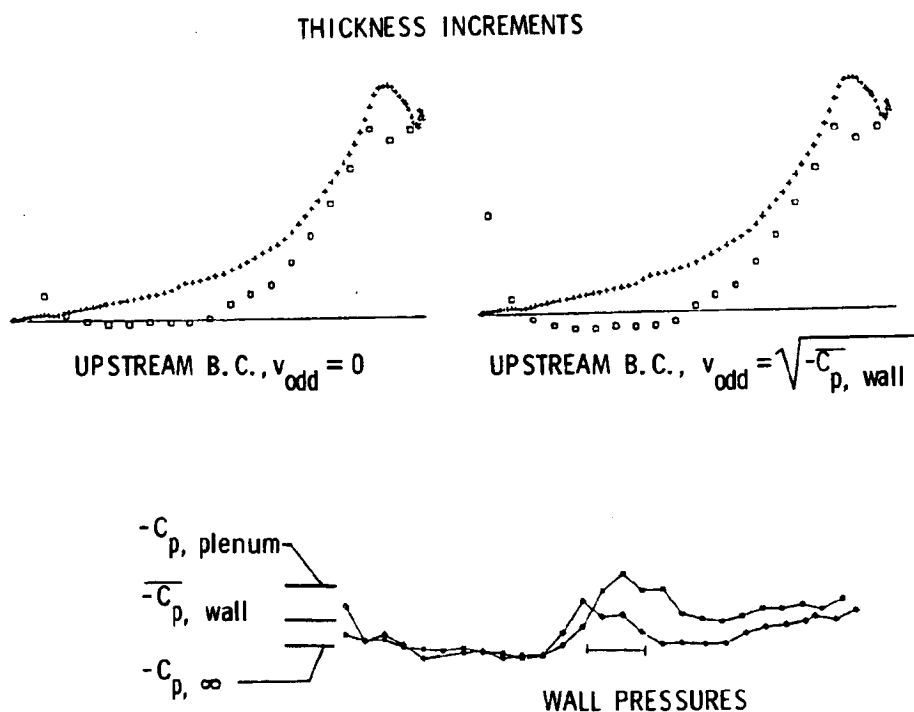
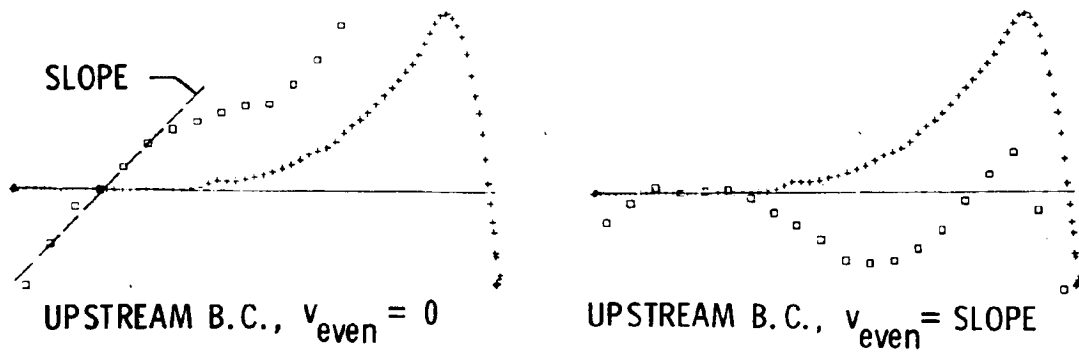


Figure 7(a)

NEGATIVE OF CAMBER INCREMENTS

ORIGINAL PAGE IS  
OF POOR QUALITY



$$\text{SLOPE} = \frac{d(-\Delta c)}{dx}$$

Figure 7(b)

AIRFOIL SHAPES

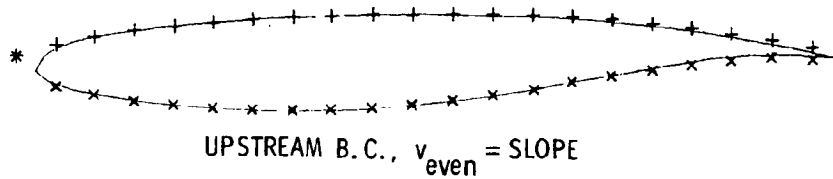
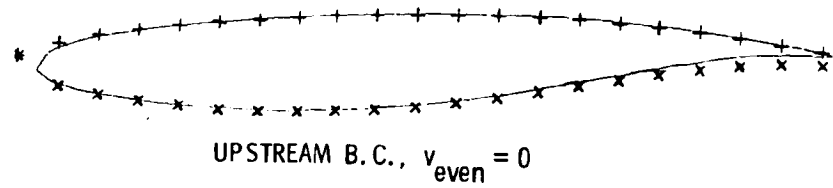


Figure 7(c)

## SLOPE OF EQUIVALENT-BODY CAMBER INCREMENT CURVE

The SLOPE values of TWINTAN first-pass equivalent-body camber increment curves were deduced for several different lift coefficient levels at each of three tunnel Mach numbers. These SLOPE values are shown in figure 8 to be linearly dependent upon the lift coefficient and only mildly dependent upon the Mach number. The sample case previously shown is labeled as  $\alpha_T \sim -3^\circ$ . These SLOPE values are used as upstream boundary conditions in the second-pass TWINTAN correction.

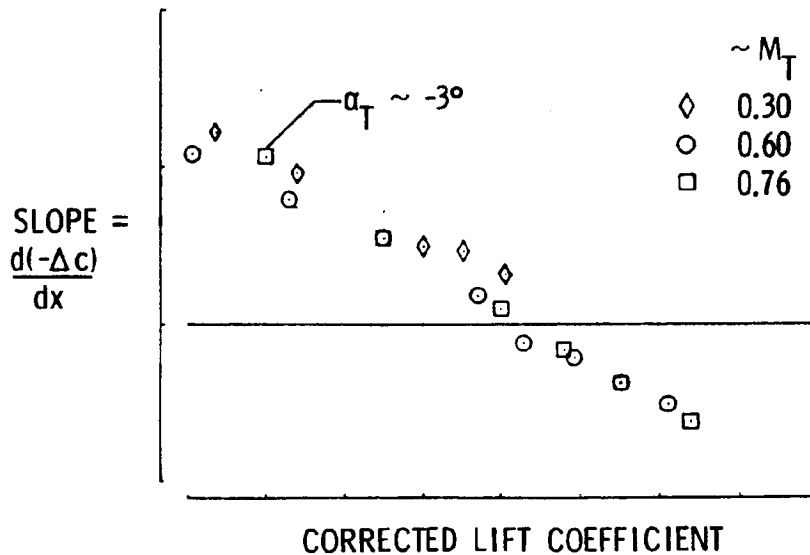


Figure 8

UPSTREAM FLOW DIRECTION EFFECT ON ANGLE-OF-ATTACK CORRECTION

The angle-of-attack corrections for the two passes through the TWINTAN correction code are compared in figure 9. Results for the first pass,  $v_{\text{upstream}} = 0$ , are given by the solid symbols. For the second pass,  $v_{\text{upstream}}$  is derived from SLOPE as shown in figures 7 and 8 and the results are given by the open symbols in figure 9. It is seen that in some cases the angle-of-attack correction even changes sign. It should be pointed out that this cambered airfoil must be near  $\alpha_T = -4^\circ$  for zero lift.

ORIGINAL PAGE IS  
OF POOR QUALITY

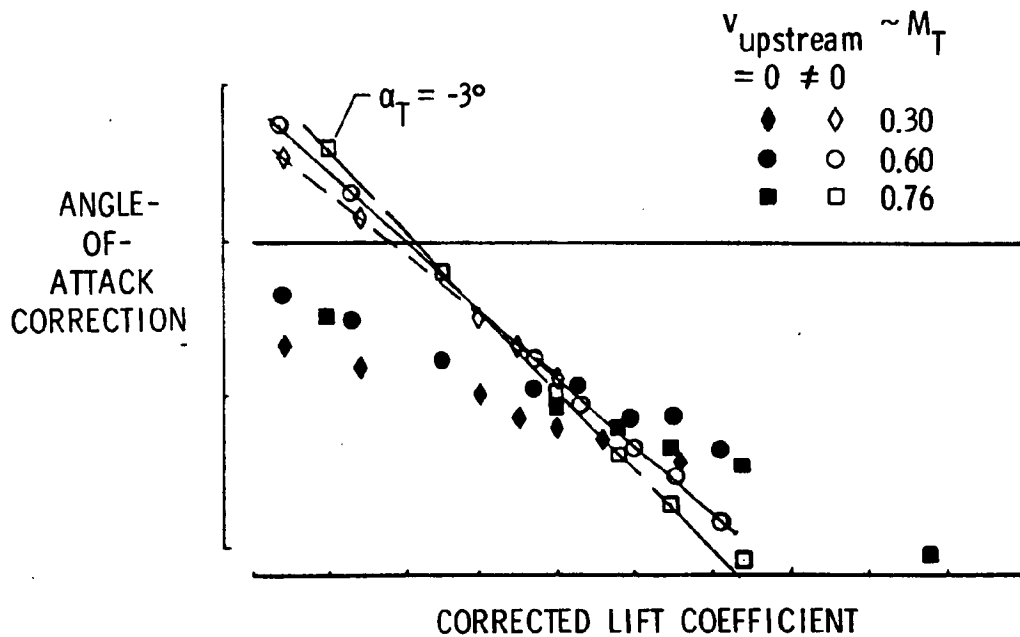


Figure 9

## WALL INTERFERENCE CORRECTION OF LIFT CURVES

Initial results for wall-interference corrections to lift curves ( $c_l$  vs.  $\alpha$ ) for 0.3-m TCT data by several procedures included in the modified, automated procedure are shown in figure 10. Figure 10a is the key while figures 10b and 10c give curves for  $M_T=0.60$  and  $0.76$  respectively. The experimental data is shown by the open squares ( $\square$ ) with a solid line through them. The Barnwell-Sewall (ref. 5) type sidewall-only boundary layer correction does not significantly affect this curve. The data ( $\circ$ ) is shifted slightly upward indicating the magnitude of the renormalization due to the Mach number correction. The lift curve appears to be rotated counterclockwise by only a small amount. Corrections calculated from the first pass through the TWINTAN 4-wall code (+) increase the lift-curve slope but not quite to that of the GRUMFOIL free-air results ( $\Delta, \nabla$ ). Accounting for the upstream flow angularity in the second pass through the 4-wall correction code ( $\times$ ) increases this slope above what GRUMFOIL predicts. It should be noted that the GRUMFOIL free-air analysis is run with the corrected  $M$  and  $c_l$  as input and returns  $\alpha$  as an answer. Since none of the Mach number corrections here are large, the GRUMFOIL results are essentially along one curve, the dashed line. These nonlinear corrections are compared with two classical, linear, angle-of-attack corrections of the experimental data. The Davis-Moore correction is shown as the open diamonds ( $\diamond$ ) while the solid diamonds ( $\blacklozenge$ ) are for the empirically-correlated Davis-Moore (ref. 6). It is encouraging that the 4-wall corrections lie near both the GRUMFOIL free-air results and the empirically correlated linear corrections throughout this moderate lift range.

NASA SC(3)0712A AIRFOIL, 0.3 m TCT,  $Re_c \sim 6 \times 10^6$

- $\square$  UNCORRECTED TUNNEL DATA
- $\circ$  SIDEWALL, BARNWELL-SEWALL CORRECTION
- TWINTAN, 4-WALL, UNIFIED CORRECTIONS:
- +  $v_{\text{upstream}} = 0$
- $\times$   $v_{\text{upstream}} \neq 0$
- GRUMFOIL FREE-AIR ANALYSES:
- $\Delta$  AT UNCORRECTED  $M$  AND  $c_l$
- $\nabla$  AT CORRECTED  $M$  AND  $c_l$
- CLASSICAL CORRECTIONS:
- $\diamond$  DAVIS-MOORE
- $\blacklozenge$  EMPIRICALLY CORRELATED DAVIS-MOORE

Figure 10(a)

ORIGINAL PAGE IS  
OF POOR QUALITY

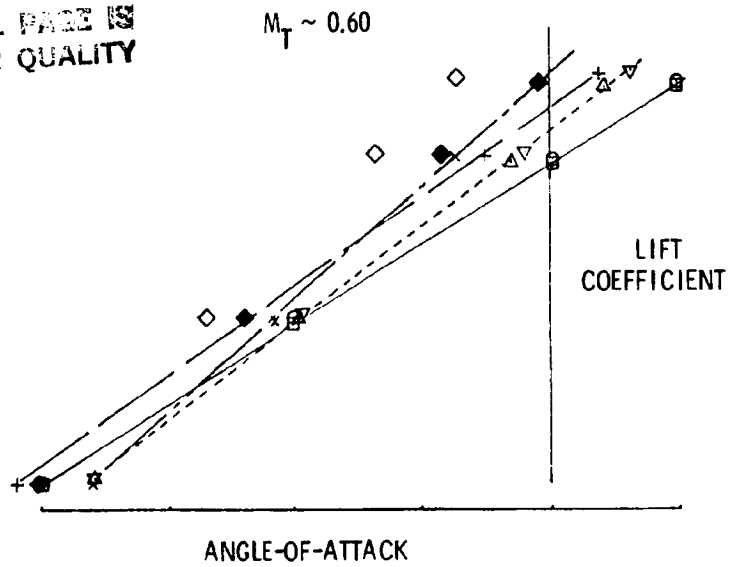


Figure 10(b)

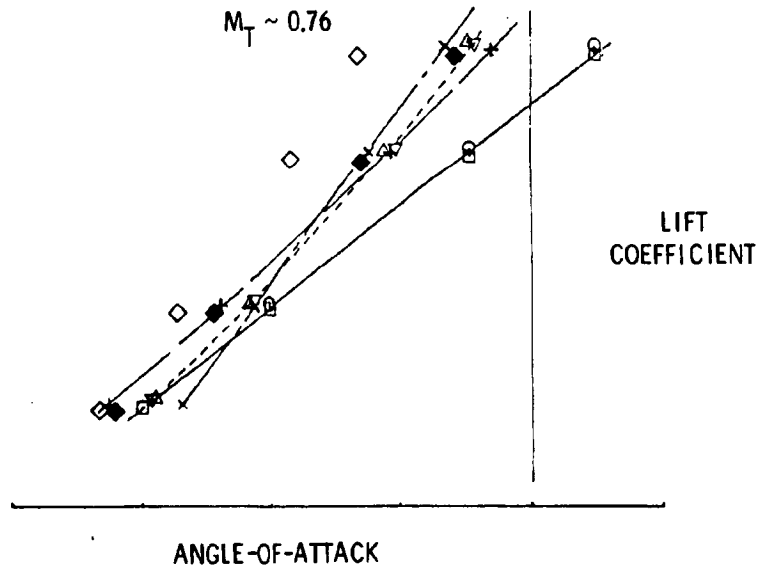


Figure 10(c)

## COMMENTS

Based upon our limited, initial observations of wall interference corrections obtained for one airfoil test, there is a need for assessing the upstream flow direction. If there is no direct measurement then a two-pass correction procedure similar to the one described here is required. Questions have arisen pertaining to the correct interpretation of the pressure coefficients measured on the slats of a slotted tunnel wall, the interpretation of just what the calculated equivalent body encompasses or should include, and what can or should be considered as quantitative criteria for data correctability. Further studies using this modified procedure will address these questions. Hopefully, a meaningful WIAC procedure can be validated for the airfoil tests in the 0.3-m TCT. (See fig. 11.)

INITIAL LOOK AT SOME DATA FROM ONE TEST ONLY

NEED FOR UPSTREAM FLOW DIRECTION ASSESSMENT

OPEN QUESTIONS TO BE ADDRESSED IN VALIDATION WITH MORE DATA:

- INTERPRETATION OF SLAT  $C_p$  FOR SLOTTED WALL
- INTERPRETATION OF EQUIVALENT BODY RESULTS
- QUANTITATIVE MEASURE OF CORRECTABILITY

Figure 11

#### REFERENCES

1. Kemp, W. B., Jr.; and Adcock, J. B.: Combined Four-Wall Interference Assessment in Two-Dimensional Airfoil Tests, AIAA 82-0586, AIAA 12th Aerodynamic Testing Conference (Williamsburg, Virginia), March 1982.
2. Melnik, R. E.; Chow, R.; and Mead, H. R.: Theory of Viscous Transonic Flow Over Airfoils at High Reynolds Number, AIAA 77-680, AIAA 10th Fluid and Plasma Dynamics Conference (Albuquerque, New Mexico), June 1977.
3. Murman, E. M.: A Correction Method for Transonic Wind Tunnel Wall Interference, AIAA 79-1533, AIAA 12th Fluid and Plasma Dynamics Conference (Williamsburg, Virginia), July 1979.
4. Kemp, W. B.; TWINTAN: A Program For Transonic Wall Interference Assessment in Two-Dimensional Wind Tunnels, NASA TM-81819, May 1980.
5. Barnwell, R. W.; and Sewall, W. G.: Similarity Rules for Effects of Sidewall Boundary Layer in Two-Dimensional Wind Tunnels, AGARD CP-335, Fluid Dynamics Panel Specialists' Meeting on Wall Interference in Wind Tunnels (London, U.K.), May 1982.
6. Barnwell, R. W.: Design and Performance Evaluation of Slotted Walls for Two-Dimensional Wind Tunnels, NASA TM-78648, February 1978.

SESSION VI

OPEN FORUM - ASSESSMENT OF ISSUES

Moderator: P. J. Bobbitt, NASA Langley

Editors' Note:

The open-forum session was originally intended to be a one-half-day group discussion session to identify WIAC issues, assess progress to date and suggest future directions. However, as the final program evolved, it was felt that all who had responded to our abstract solicitation should be given an opportunity to participate in this first wall interference assessment/correction workshop, if possible. In addition, since a number of attendees had expressed an interest in seeing the NTF, a tour was included in the program. Furthermore, the workshop attendance was also larger than anticipated. As a consequence, this session was shortened and there was not sufficient time to break up into smaller informal discussion groups prior to an open forum. The end result was a short, directed open-forum discussion with the entire group in which a series of problem areas and questions were posed and comments from the audience solicited. Unfortunately the comments of several people were not recorded. Thus, the following written version of the open forum discussion is limited to the questions raised by the moderator for discussion and to several items suggested for near-term future emphasis. The questions posed have been regrouped and, consequently, are not in the order presented and discussed at the workshop. The discussion generally affirmed that most of these questions are indeed issues and, in many cases, are being worked on.

Preceding page blank

413

PRECEDING PAGE BLANK NOT FILMED

1  
END

**DISCUSSION OF WIND TUNNEL WALL  
INTERFERENCE CORRECTION ISSUES**

**P. J. Bobbitt and P. A. Newman**

**NASA Langley Research Center  
Hampton, Virginia**

PRECEDING PAGE BLANK NOT FILMED

Preceding page blank

## INTRODUCTION

I thought the workshop was excellent, and the reason, aside from the material presented, is that many of the key players in the world of wind tunnel wall interference are here and they represent most of the organizations which one would expect to be interested in the subject. It is a bit surprising that so many came because wind tunnel wall interference is not the number one priority on most laboratories' list of "things to do;" there is, evidently, a continuous but low level effort. Certainly since May 1974, when NASA Langley had a much smaller workshop prior to key NTF decisions, the progress has been steady if not remarkable. We have heard papers on both adaptive and fixed walls of various kinds; some of these adaptive walls (there were three examples in the workshop) are now trying to "work" the 3-D problem. Linear and nonlinear theories have been displayed here in various stages of completeness. Some of the research is just now nearing a point where good results can be obtained and compared to theory and to other cases. Several tunnels have recently added or are in the process of implementing flow field or boundary instrumentation in order to acquire data suitable for validating and implementing correction schemes. Much of the classical data used for comparisons are of little use now because most current methodology requires a great deal more than just wake rake and surface pressure data.

There are a number of formal and informal cooperative arrangements that appear to be very instrumental in providing communication between people in this discipline, in accelerating the formulation of good data bases, and in getting experimentalists and theoreticians to understand each other. Nevertheless, there are a few problems in communication, both in terms of distributing the latest data or theories and in relating to the experiences gained by others. In the past, each group or laboratory has tended to concentrate on a particular airfoil in a particular tunnel with a particular methodology, and this individualistic approach has impeded this transfer of information. Clearly, cooperative efforts should include theory and experiment; one presenter suggested having a runoff with experimental competition or comparison, in addition to theory validations. Test models that can serve now as some "absolute standard" were mentioned and are of interest. In particular we need to have these 3-D cases established where all of these flow field data needed by assessment and correction methods have been taken. The AEDC interference model might be one candidate; Mike Goodyer's interference model was also tested in the NASA Langley 7- by 10-Foot High-Speed Tunnel; Pathfinder I and Pathfinder 1/2 (NTF calibration models) might be additional candidates that could be used to assess these methods and, in fact, could also be tested in different tunnels.

## TUNNEL WALL INTERFERENCE QUESTIONS

I have several viewgraphs which list some particular issues, concerns or questions that came to me before, during and after the presentations. Many of these have been raised in the summary papers. There are quite a few of them and they cover the waterfront, so there is little possibility that your interests have been left out. In addition, if there are things which have not been discussed that are relevant to the material we saw or, more importantly, to what we should be doing next, please bring this up in the discussion.

## Measured Data Aspects

One of the things that a lot of people talked about here was the measurement in the flow field on a reference surface, or the tunnel wall, of various kinds of data; the first viewgraph poses questions related to measured data aspects. It is not clear to me how useful wall pressures are in slotted and porous tunnels. Can we measure P along with U or should we obtain U and W? Should we use a single quantity on two planes or two quantities on one plane? The degree of variability we saw in the presentations makes it all rather confusing. If anyone has light to shed on the "best" combination, please let us know! Also, in many cases, particularly in 3-D, it would seem difficult to measure enough data in a wind tunnel to get the answer that you need for a complicated geometry.

Do we need more experimental research to characterize boundary conditions? We saw several papers that related to this topic. The question then has to be asked: Do we get the data to try to provide an effective homogeneous boundary condition or do we do it to model the finite, variable, boundary condition? Where are we there?

Do we need to know more about what the free-stream conditions are? We make a measurement of the free-stream condition and use it when we provide a correction. It is the number we add to or subtract from. However, the fact is that a lot of times, because of the model size blockage or the length of the test section or whatever, this number may not be what we think it is. It appears that we have to do more work to understand what free-stream condition means both in theory and in experiment.

This gets to the question of whether we have any useful wall interference data and, if so, whether we have enough. The answer to these questions may be a judgemental thing but I think that a lot of the data we previously thought of as being archival or certified would now be judged as unfit for use in the newer methods for evaluating interference. I do not know whether that is a general view, but if it is, we must collectively decide how many kinds of airfoils or thicknesses or configurations we should strive for as well as what types of data and resolution are required. In our 0.3-m TCT, we carried out a cooperative airfoil program with industry mainly to look at high Reynolds number effects, but in the process some wall pressures were obtained. These data may be useful for WIAC applications.

Should we do more with the tunnel-to-tunnel comparisons? The kinds of things we are doing now with CAST-10, such as testing in both slotted and streamline walls and in several different sizes, seem appropriate to really tie things down for one airfoil. We should do this for more airfoil types and also get the associated flow field and wall pressures. In the case of bodies of revolution, we are building several for testing in the NTF to understand blockage. It would be desirable to have other organizations test these models, or similar ones, as an aid in evaluating both the data differences between different tunnels and the interference calculations. Similar tests of other calibration models, such as the AEDC interference model, would also be a beneficial activity.

### Theory/Code Aspects

The second viewgraph deals with theory/code aspects or issues. In regard to the first question listed, there are several aspects. How complicated (accurate) does the geometry have to be if you are using theory to augment experiment? Can we actually substitute theoretically manufactured data? I am not talking here about the interpolation of actual data, but the augmentation of measured data. If you did that, what would that combination be?

We really need to have a hierarchy of codes and this observation stems from a comment that was made earlier. When you are doing production work you may want something that is very fast using a minimum of measurements; that is particularly true if you are involved in parametric work. But if you are really looking for that last drag count, if you are betting millions of dollars on an answer, I think you would be willing to run the tunnel for 10 minutes on a test point to obtain the data that would enable you to make the most accurate correction possible. So you may end up with a linear code and several different types of nonlinear codes that solve various forms of the Navier-Stokes equations as well. In the nonlinear, high-subsonic-speed range, when we try to do assessment/corrections and understand whether data are really correctable, are we going to have to run these 3-D full potential and Euler equation codes? Perhaps when you see how complicated the flow field is, particularly where you have shocks hitting the wall, separated flows, etc., you may get more and more interested in how far you can push linear theory. This question was brought up several times by different speakers and I am not sure whether we have the answer to that yet but I think it is an important one. Most of the theory that we have heard here relates to linear analysis or the nonlinear potential approach. We have seen some remarkable progress, in the last few years, in applying Euler equations to both 2-D and 3-D and the Navier-Stokes, of course, mainly to 2-D. Someone may correct me here, but I have not seen any of that methodology applied to tunnel walls at this workshop. It would seem that there are a lot of conditions at the higher speeds where the shocks do get to be significant and the Euler equations would have an advantage. What do you see as the barriers to going ahead and applying those kinds of equations?

Do we need more theoretical research to characterize tunnel wall boundary conditions? Several papers discussed or used (Bill Kemp's analysis, for instance) representations of finite discrete tunnel wall boundary conditions. Nevertheless, my impression is that we are not very far along in this area and we continue to use the age-old homogeneous boundary conditions even though we do not know how well they represent slotted and perforated walls. In regard to "free-stream" conditions, early 3-D TSDE calculations, including tunnel walls with different kinds of boundary conditions, found results sensitive to the placement of the upstream boundary condition. Norm Malmuth talked about it earlier. There appears to be a need for both theoretical and experimental work in this area. As a point of interest, the NTF was made with a lot longer test section than most transonic tunnels because of this concern.

### WIAC Applicability and Other Aspects

The third viewgraph relates to WIAC applicability and relationship to other aspects concerning flow confinement. We did not talk much here, that I noticed, about high alpha and high  $C_L$  corrections, yet we all test fighter aircraft at high alpha and we want to test airfoils and high-lift systems at high lift as well. The corrections that go with high alpha flows when you have flow separation, vortex flows, etc., require some special treatment and attention. We have done that in a free-air environment and the various theories are published, but I have not seen tunnel walls incorporated in any of these calculations. What are the prospects for extending our methods to deal with separated flows? That is a critical concern; I would appreciate a lot of you giving some thought to it.

What is the combined effect of wall and sting? We saw one application in the workshop where the sting was accounted for and it was a critical element. Conversely, if the sting had not been accounted for the answer would have been worthless. I wonder, when we do all these corrections, how we are going to extract the sting effects. Certainly you can model the sting, but many times that degree of detail is beyond what we want to do or can do. I think we need to look at it as an additive effect, where it is modeled versus where it is not modeled, and try to understand what it does not only to the wind tunnel model itself but to the far-field and/or wall measurements.

How about WIAC applicability to dynamic data? I threw that one in because no one said anything about dynamic motions and how wall effects are accounted for. There are only one or two papers in the literature pertaining to the subject that I know about. It is a real problem if you are doing forced oscillation work or perhaps where you have an oscillating wake. What is the importance of unsteadiness in the wake and can its effect be accounted for, in some way, by a steady one?

There is another effect on wall interference which we must also be able to handle, or even before that, to understand. It is the influence of a shock impinging on a ventilated wall, an old problem that unfortunately happens in situations where the corrections are large. We want to be able to analyze it but I am not sure that any of us understand yet how to do that.

We did not talk about flow quality effects here but I think a number of us realize that at times the wall interference effects get confused with flow quality effects, in the sense that flow quality and tunnel walls can affect the pressure distribution (particularly through shock location), which in turn affects the transition point. Even at high Reynolds numbers you can get significant runs of laminar flow on wings and bodies. You do not want to put a trip strip on them to make comparisons with other tunnels or flight data, but if the flow qualities are different, you have no choice. Furthermore, if you force transition to be at a specific location in order to make a valid comparison, then you had better be sure that those trip strips look alike. People are worried about flow quality more and more and we do lots of things here at Langley in our tunnels to make flow quality better. We do this knowing that it affects drag, pitching moment, lift - the whole thing. Normally in wind tunnel wall interference discussions this subject is not brought up as a source of confusion and error.

As for the last point here, Reynolds number effects are a particular concern at Langley. Typically in the past, when we calibrated older wind tunnels, the Reynolds number range at a given Mach number was so small that we never worried about it in terms of wall interference effect. None of the theories used a dozen years ago concerned that at all. But now, when you can change Reynolds number from a couple of million to 100 million, the thickness of the boundary layer in the test section is going to be very different. The effective width of the wall slots is going to be different, and in that way, the data will be affected. The addition of Reynolds number to the "puzzle" lends added concern in terms of the methodology required.

#### Tunnel and Hardware Aspects

The last viewgraph deals with tunnel and hardware aspects. Will our renewed concentration on the wall interference problem and correction methods lead to improved passive walls? I remember some time ago when Tony Ferri had ideas about some weird-looking wall geometries that seem to have been forgotten. But still, I wonder whether or not porous and slotted walls are the best answer for a passive-wall wind tunnel.

In an airfoil tunnel, what is the "best" approach for sidewall boundary layer control? The observation was made that you have to apply suction around the juncture region. If you do not do it all the way from the roof to the floor, then the boundary layer above this suction region has a different thickness distribution. You have thinned it down over the area where suction was applied. I am wondering if people who use this technique, although it helps the problem of sidewall separation at high angles of attack, really know what is in the tunnel. The sidewall boundary layer becomes a complicated looking flow and we need to do some analysis to define what the total 3-D environment looks like in a so-called 2-D test.

What about partially adaptive strategies? Most flexible walls are solid; that is the way you have to start out. The question that comes to me is whether or not we can combine that idea with a slotted or porous wall to help the interference problem. Some of you know that AFWAL researchers built a flex wall; it had about a dozen different segments (rods) so you could form it differently across the span, from one wall to the other, to get a 3-D effect on the streamlines. That approach was a little bit in the hybrid wall direction. Can we have adaptive walls in one plane? This is the sort of thing Mike Goodyer is trying to do now; you use only the top and bottom walls to eliminate the interference and correct for the rest. Hopefully, if you are lucky, that is 90 percent of it. In fact, there was a theoretical result some years ago by Newman and Klunker indicating that this was the case. Earlier measurements, done at AEDC and NAE, with uniform porosity on the top, bottom, and side walls (but not the same on all walls) indicated that most of the interference could be eliminated with just that simple kind of articulation.

NEAR-TERM FUTURE DIRECTIONS  
SUGGESTED IN OPEN FORUM DISCUSSION

It goes without saying that all the things we intend to do in the near term are high priority, but we want to look beyond that. What should we do collectively? I feel that we should place particular emphasis on cooperative efforts where possible and feasible because these seem to get the job done better. As I said earlier, they promote communication and continued contacts. Efforts should be made to periodically hold workshops or informal meetings, such as this one, to aid in this communication and continually assess the progress.

Specific items for consideration, action or research in the near term, as suggested during the open-forum discussion, were

1. The collection or establishment of both theoretical and experimental data bases suitable for WIAC use, particularly for comparison of procedures; these data would be made generally available without restriction and would include data for two-dimensional, body-of-revolution, and three-dimensional configurations
2. An appraisal of the flow field data measurements suitable for WIAC procedures which can now be routinely made and an assessment of the impact of typical measurement errors associated with them upon WIAC
3. The inclusion of model support system interference effects in WIAC procedures
4. The continued effort to develop a hierarchy of WIAC codes, since questions remain concerning the requirements on degree of flow equation complexity, type and amount of measured boundary data, computational time versus tunnel hardware costs, etc.; requirements will surely vary from facility to facility and test to test in a given facility.

## MEASURED DATA ASPECTS

- What type and amount data required for WIAC?
  - Pressures/ velocities
  - Flow field/ model/ wall
  - How much for 3-D?
- Is there need for experimental research to characterize:
  - Discrete/ homogeneous boundary conditions?
  - "Free-stream" conditions?
- Do we have adequate "absolute" reference data?
- What about tunnel-to-tunnel and flight-to-tunnel comparisons?
  - Airfoils (0012, 65-213, CAST-10, BGK-1, etc)
  - Vehicles (B-O-R, Pathfinder, AEDC Int. model, etc)

## THEORY/CODE ASPECTS

- Can theory be used as partial substitute for data?
- Is there virtue in having available a hierarchy of codes?
  - How far can you push linear theory ideas?
  - Can we run nonlinear codes in parallel with tunnel?
  - Should Euler or Navier-Stokes codes be developed?
- Is there need for theoretical research to characterize:
  - Discrete/ homogeneous boundary conditions?
  - "Free-stream" conditions?

## WIAC APPLICABILITY AND OTHER ASPECTS

- How about WIAC applicability to:
  - High  $\alpha$  / High  $C_l$  ?
  - Sting and support system effects?
  - Dynamic data?
- Do we understand how to handle or separate:
  - Shock impingement on ventilated walls?
  - Flow quality effects?
  - Wall Reynolds number effects, especially for cryo?

## TUNNEL AND HARDWARE ASPECTS

- Do we have the "best" types of passive walls?
- What is the "best" approach for sidewall BLC in 2-D?
- What partially adapted walls are possible?
  - Combined flexible and ventilated?
  - Spatially limited adaptability?

1. Report No. NASA CP		2. Government Accession No.		3. Recipient's Catalog No.	
4. Title and Subtitle WIND TUNNEL WALL INTERFERENCE ASSESSMENT/CORRECTION - 1983				5. Report Date	
7. Author(s) Perry A. Newman and Richard W. Barnwell, Editors				6. Performing Organization Code 505-31-53-12	
9. Performing Organization Name and Address NASA Langley Research Center Hampton, VA 23665				8. Performing Organization Report No. L-15812	
12. Sponsoring Agency Name and Address National Aeronautics and Space Administration Washington, DC 20546				10. Work Unit No.	
15. Supplementary Notes				11. Contract or Grant No.	
16. Abstract  This report is a compilation of papers presented at the Wind Tunnel Wall Interference Assessment/Correction (WIAC) Workshop held January 25 and 26, 1983, at the Langley Research Center. The workshop was to provide an informal technical information exchange focused upon the emerging WIAC techniques applicable to conventional and passively or partially adapted wall transonic wind tunnels. The twenty-five presentations consisted of invited talks summarizing the foreign work on WIAC technology and solicited domestic talks concerning data bases suitable for WIAC validation and the status of WIAC strategies, codes, and applications.				13. Type of Report and Period Covered <u>Conference Publication</u>	
17. Key Words (Suggested by Author(s)) Adaptive walls Transonic wind tunnels Wall interference Wind tunnel corrections				14. Sponsoring Agency Code	
18. Distribution Statement  Unclassified - Unlimited  Subject Category 02					
19. Security Classif. (of this report) Unclassified		20. Security Classif. (of this page) Unclassified		21. No. of Pages 434	22. Price A19